UNIVERSIDADE DE LISBOA
Instituto de Geografia e Ordenamento do Território

# Deglaciation chronology and post-glacial environmental evolution of the Upper Garonne valley (Central Pyrenees)

Marcelo Vieira Fernandes

Orientador(es): Prof. Doutor Marc Oliva i Franganillo
Prof. Doutor Gonçalo Brito Guapo Teles Vieira

Tese especialmente elaborada para obtenção do grau de Doutor em Geografia, especialidade de Geografia Física

2023

UNIVERSIDADE DE LISBOA
Instituto de Geografia e Ordenamento do Território

# Deglaciation chronology and post-glacial environmental evolution of the Upper Garonne valley (Central Pyrenees)

Marcelo Vieira Fernandes

Orientador(es): Prof. Doutor Marc Oliva i Franganillo
Prof. Doutor Gonçalo Brito Guapo Teles Vieira

Tese especialmente elaborada para obtenção do grau de Doutor em Geografia, especialidade de Geografia Física

Júri:
Presidente: Doutor Mário Adriano Ferreira do Vale, Professor Catedrático e Presidente do Conselho Científico do Instituto de Geografia e Ordenamento do Território da Universidade de Lisboa
Vogais:

- *Doctora* Nuria de Andrés de Pablo, *Profesora Titular*
  *Faculdad de Geografia e Historia, Universidad Complutense de Madrid*, Espanha;
- *Doctor* Enrique Serrano Cañadas, *Catedrático d'Universidad*
  *Faculdad de Filosofia y Letras, Universidad de Valladolid*, Espanha;
- *Doutor* Marc Oliva i Franganillo, *Profesor Titular d'Universitat*
  *Facultat de Geografia i Història, Universitat de Barcelona*, orientador;
- Doutora Maria da Conceição Pombo de Freitas, Professora Catedrática
  Faculdade de Ciências da Universidade de Lisboa;
- Doutor José Luís Gonçalves Moreira da Silva Zêzere, Professor Catedrático
  Instituto de Geografia e Ordenamento do Território da Universidade de Lisboa.

Tese financiada por fundos nacionais através da Fundação para a Ciência e a Tecnologia (FCT, I.P.), com a bolsa número SFRH/BD/139568/2018.

2023

À Teresa

This thesis was supported by the Doctoral Program of the Fundação para a Ciência e Tecnologia, I.P., which granted me with the scholarship SFRH/BD/139568/2018.

# Acronyms

AMOC – Atlantic Meridional Overturning Circulation

AMS – Accelerator Mass Spectrometer

B-A – Bølling-Allerød interstadial

CRE – Cosmic-ray exposure

ELA – Equilibrium line altitude

ESR – Electron spin resonance

GI – Greenland Interstadial

GLGM – Global Last Glacial Maximum

GS – Greenland Stadial

HE – Heinrich Stadial

HTM – Holocene Thermal Maximum

IRD – Ice-rafting detritus

LBBB – Loures-Barousse-Barbazan basin

LGC – Last Glacial Cycle

LGM – Last Glacial Maximum

LIA – Little Ice Age

LLGM – Local Last Glacial Maximum

MAAT – Mean annual air temperatures

MIE – Maximum ice extent

MIS – Marine isotope stage

OD – Oldest Dryas stadial

OLS – Optically stimulated luminescence

PGC – Penultimate glacial cycle

SHED – Schmidt Hammer exposure dating

SST – Sea surface temperature

YD – Younger Dryas stadial

# Preamble

The motivation for conducting research in Iberian mountain environments arose before this PhD dissertation during my master's in 2014. The final stage of the master's degree was accomplished with the achievement of a thesis about the geomorphological and environmental evolution of the Upper Garonne basin, Central Pyrenees, since the last glacial cycle. This project ended in the publication of a scientific paper in 2015, showing me the peer-reviewing process to reach scientific value and the approval of the community. Such honest pursuit of the truth to better understand mountain system dynamics during the Late Pleistocene and the passion for extreme environments motivated me to embrace the adventure of doing a PhD in Geography.

This dissertation is under the academic scope of Physical Geography. It is guided by the general goal of reconstructing the chronology of glacial advances during the Late Pleistocene and understanding the subsequent postglacial geomorphological dynamics after the deglaciation of the Upper Garonne basin, Central Pyrenees. To reach this goal, several specific objectives were defined:

- Geomorphological mapping of the landforms existing in the Upper Garonne catchment;
- Identifying the chronology of the Late Pleistocene glacial dynamics by means of cosmic-ray exposure dating;
- Identifying the palaeoglacier' characteristics, palaeoELAS and palaeotemperatures during the Late Pleistocene glacial phases;
- Constraining the chronological framework of the glacial to periglacial transition in the highest cirques of the study area; and
- Identifying the morphological, lithological and geographical factors controlling major slope failures following deglaciation.

The final structure of the article-based PhD thesis encompasses the following sections: introduction, results, and conclusions. The results comprise six main papers in the form of published papers in peer-reviewed international journals, except the last one, which is still under revision:

1. **Fernandes, M.,** Oliva, M., Vieira, G., & Lopes, L. (2022). Geomorphology of the Aran Valley (Upper Garonne Basin, Central Pyrenees). Journal of Maps, 1–13. https://doi.org/10.1080/17445647.2022.2035266. (SCI IF: 2.7; Q1);
2. **Fernandes, M.,** Oliva, M., Vieira, G., Palacios, D., Fernández-Fernández, J. M., Delmas, M., García-Oteyza, J., Schimmelpfennig, I., Ventura, J., Aumaître, G., & Keddadouche, K. (2021). Maximum glacier extent of the Penultimate Glacial Cycle in

the Upper Garonne Basin (Pyrenees): new chronological evidence. Environmental Earth Sciences, 80(24), 796. https://doi.org/10.1007/s12665-021-10022-z. (SCI IF: 3.1; Q2);

3. **Fernandes, M.,** Oliva, M., Vieira, G., Palacios, D., Fernández-Fernández, J. M., García-Oteyza, J., Schimmelpfennig, I., Team, A., & Antoniades, D. (2021). Glacial oscillations during the Bølling–Allerød Interstadial–Younger Dryas transition in the Ruda Valley, Central Pyrenees. Journal of Quaternary Science, 37(1), 42–58. https://doi.org/10.1002/jqs.3379. (SCI IF: 2.8; Q1);
4. Oliva, M., **Fernandes, M.,** Palacios, D., Fernández-Fernández, J. M., Schimmelpfennig, I., Team, A., & Antoniades, D. (2021). Rapid deglaciation during the Bølling-Allerød Interstadial in the Central Pyrenees and associated glacial and periglacial landforms. Geomorphology, 385, 107735. https://doi.org/10.1016/j.geomorph.2021.107735. (SCI IF: 4.5; Q1);
5. **Fernandes, M.,** Oliva, M., & Vieira, G. (2020). Paraglacial slope failures in the Aran valley (Central Pyrenees). Quaternary International, 566–567, 24–38. https://doi.org/10.1016/j.quaint.2020.07.045. (SCI IF: 2.4; Q1);
6. **Fernandes, M.,** Oliva, M., Fernández-Fernández, J. M., Vieira, G., Palacios, D., García-Oteyza, J., Ventura, J., Schimmelpfennig, I., & Team, A. (*submitted*). Geomorphological record of the glacial to periglacial transition in the Central Pyrenees: the Lòcampo Cirque in the regional context. Geomorphology. (SCI IF: 4.5; Q1).

Apart from these scientific articles, throughout the period of elaboration of the dissertation, I also published and submitted book chapters within the topic of the thesis that are attached as annexes; i.e. the reviews of the glacial and periglacial environments of the Pyrenees or other Iberian ranges and the application of the methodological approach based on cosmogenic nuclides:

(i) Oliva, M., Serrano, E., Fernández-Fernández, J. M., Palacios, D., **Fernandes, M.,** García-Ruiz, J. M., López-Moreno, H. I., Pérez-Alberti, A., Antoniades, A. (2022). The Iberian Peninsula. In Oliva, M., Nývlt, D., & Fernández-Fernández J. M. (Eds.), *Periglacial landscapes of Europe* (*2022*). Springer. https://doi.org/10.1007/978-3-031-14895-8_4

(ii) Oliva, M., Gómez-Ortiz, A., Palacios, D., Franch, F. S., Ramos, M., de Sanjosé-Blasco, J. J., **Fernandes, M.**, Fernández-Fernández, J. M., Galindo-Zaldívar, J., García-Oteyza, J., González, L., Hauck, C., Martín-Díaz, J., Nofre, J., de Galdeano, C. S., & Tanarro-García, L. M. (2022). *Ancient and Present-Day Periglacial Environments in the Sierra Nevada*. In Zamora, Z., & Oliva, M. (eds.), *The Landscape of the Sierra Nevada: A Unique Laboratory of Global Processes in Spain* (pp. 115–128). Springer International Publishing. https://doi.org/10.1007/978-3-030-94219-9_8.

(iii) Delmas, M., Oliva, M., Gunnell, Y., **Fernandes, M.,** Reixach, T., Fernández-Fernández, J. M., & Calvet, M. (2023a). The Pyrenees : glacial landforms from the Younger Dryas (12.9-11.7 ka). In D. Palacios, P. Hughes, J. M. García-Ruiz, & N. Andrés (Eds.), *European Glacial Landscapes (II)* (pp. 541–552). Elsevier. https://doi.org/10.1016/B978-0-323-91899-2.00038-3

(iv) Delmas, M., Oliva, M., Gunnell, Y., **Fernandes, M.,** Reixach, T., Fernández-Fernández, J. M., & Calvet, M. (2023b). The Pyrenees: glacial landforms from the Bølling-Allerød Interstadial (14.6-12.9 ka). In D. Palacios, P. Hughes, J. M. García-Ruiz, & N. Andrés (Eds.), *European Glacial Landscapes (II)* (pp. 361–367). Elsevier. https://doi.org/10.1016/B978-0-323-91899-2.00050-4

(v) Delmas, M., Oliva, M., Gunnell, Y., Fernández-Fernández, J. M., Reixach, T., **Fernandes, M.,** & Calvet, M. (*in press*). The Pyrenees: glacial landforms from the Holocene. In D. Palacios, P. Hughes, J. M. García-Ruiz, & N. Andrés (Eds.), *European Glacial Landscapes (III)* (*in press*). Elsevier.

Throughout the dissertation, I kept the local toponomy in the respective French, Catalan and Aranese territories.

# Acknowledgments

First of all, I would like to thank the entities that formally allowed me to do this PhD. To the Center for Geographical Studies of the University of Lisbon for being the host institution and for supporting all my scientific activities in Portugal and abroad. Finally, to the Institute of Geography and Spatial Planning of the University of Lisbon to train me as a geographer.

Secondly, a special thanks to my advisors Marc Oliva and Gonçalo Vieira for their role as supervisors of this PhD thesis. These gentlemen were loyal, worthy pedagogues who did not let me get lost in the wanderings of a doctoral student and ultimately prepared me for the world of science, and despite the science, with whom I could count on, even for a beer. To them, a warm and sincere thank you.

Thirdly, thanks to those who helped me throughout the thesis process with issues such as science, fieldwork and logistics. Many thanks to Luís Lopes and José María Fernández, who were faithful companions; special thanks to David Palacios and Nuria Andrés de Pablo from the Universidad Complutense de Madrid, who received and taught me a lot about the basis of exposure dating using cosmogenic nuclides and its importance to geomorphology research. To Irene Schimmelpfenning from the University of Provence Aix-Marseille who showed me the laboratory processes and age calculation. From this bunch, I must add Leatitia Leanni who also helped me in the lab; Joanna Charton and Tancrede Leger who shared similar cosmogenic interests.

For sharing their time and words of encouragement during this journey, I thank Jorge Rocha, Inês Girão, Cláudia Viana, Luís Encalada, Maurício Santos, Pedro Freitas, Bernardo Silva, Rodrigue Tanguy, Desideria Santella, Diogo Silva, Raquel Fernandes, Márcia Matias, Tiago Silva, Ana Gonçalves, Catarina Sequeira, Luis Miguel Tanarro, Jose Úbeda, Javier de Marcos, Meriem Djellalli, Julia García-Oteyza, Josep Ventura, Xavier Úbeda, Jordí Nofre, Jordi Martín and Rui Filipe Carvalho.

Fourthly, I thank my parents Paulo Fernandes and Mercês Vieira, not only for their emotional support throughout the thesis but fundamentally for giving me the necessary virtues to finish it. To my brothers and their spouses, Cristiana, Manuel Gil, Francisca and Daniel for being my daily inspiration. To Teresa's parents, Mendo Castro Henriques and Branca Braga de Macedo, for all the direct and indirect support they gave me during

this time. To my brothers-in-law, António, Jorge and Francisco, for the thoughtful conversations about my concerns. And finally, even though 2000 km apart Cilgia and Walter who have always been close and attentive.

Finally, a special word to the girls in my life. To my oldest daughter Branca, thank you for every effort to get out of bed earlier so I could get to work earlier and I'm sorry for the times that you called for me from your room window while I was away. To Vera, my newborn, who came right on time for this labour. Last but not least, to Teresa, words are not enough to thank you for all you have done for me during this time, I would not be writing the final pages of this thesis without your help. I could not have been able to achieve the fundamental tasks of this PhD that had to do with my absences in Portugal. To you, I must also apologise for the bad mood that I may have had as a result of this hard work. Finally, thank you for being the mother of my daughters and for your unconditional presence every day during these four years.

# Abstract

This PhD dissertation focuses on the Upper Garonne basin, Central Pyrenees. The study area ranges from the highest peaks at >2800-3000 m to the lowest moraine deposits located in the Loures Barousse Barbazan basin (LBBB) at 400-500 m. This catchment hosted the largest Quaternary glacier in the Pyrenees, although little was known about its glacial chronology.

An accurate geomorphological analysis and mapping of the distribution of glacial and periglacial phenomena in the study area revealed the existence of a wide variety of landforms indicative of the occurrence of several periods of intense glacial and periglacial activity. The moraine distribution indicates that glaciers formed three moraine complexes at (1) moraines at the glacial terminal basin (420-820 m), (2) moraines at the mountain slopes and high valleys (1000-2100 m) and moraines at the glacial cirques (>2100 m).

In the foreland of the Pyrenees, we find the LBBB, which includes the lowest moraine system of the Upper Garonne basin at 80 km from the headwaters of the catchment. Here, the external moraine (ca. 420 m) was dated by means of cosmic-ray exposure (CRE) and yielded an age of 128.5 ± 9.1 ka. This age constitutes the most solid chronological record of glacier advance in the Pyrenees during the Last Glacial Cycle and suggests that the past Equilibrium Line Altitude (palaeoELA) at that time was set at 1705 m and summer temperatures were ca. 9.3 ºC lower than the current values. The Garonne palaeoglacier must have also reached the LBBB during the Last Glacial Cycle (LGC), as confirmed by lake sediments from the Barbazan lake, although CRE results from boulders in the internal moraine system reported very scattered ages (73.1 ± 4.6 to 17.1 ± 1.8 ka). Such a large extension of the Garonne palaeoglacier during the global Last Glacial Maximum (GLGM) is also suggested by two CRE ages from the polished surfaces near the Marignac basin (7 km south of the LBBB). These ages of 24.2 ± 2.1 and 20.7 ± 1.2 ka indicate that this palaeoglacier was retreating during the GLGM while in Northern Europe, glaciers were still growing or at their maximum.

The long-term recession was interrupted by brief periods of glacier expansion. No evidence has been dated yet of a glacial advance during the Oldest Dryas in this valley. Warm temperatures prevailing during the first half of the Bølling-Allerød (B-A) favoured a massive glacial retreat, with glaciers mostly disappearing from the highest catchments from 16.0 ± 1.0 to 13.5 ± 0.8 ka. During the late B-A and early Younger Dryas (YD), short episodes of lower temperatures and higher precipitation promoted glacial expansion and moraine formation, with 4.5 to 0.5-km-long glaciers advancing towards the high valley bottoms by 13.5 ± 0.9, 13.2 ± 1.1 and 13.0 ± 0.8 ka. These moraines are indicative of palaeoELAs up to 2461-2505 m and summer palaeotemperatures of 4.2-3.9 ºC lower than present-day.

During the cold YD, small glaciers developed in the highest northern and western cirques by 12.8 ± 0.5 and 12.6 ± 1.3 ka. However, the increasing aridity during this stadial promoted their disappearance from larger cirques below 2800 m by 12.8 ± 0.8 and 12.7 ± 0.8 ka. During this short event, palaeoELAs were located at 2504-2571 m and summer palaeotemperatures of 3.4-3 ºC lower than today.

The deglaciation of the cirques and mountain slopes favoured paraglacial adjustment, triggering widespread slope failures and generating rock glaciers. In the Upper Garonne basin, paraglacial dynamics were largely controlled by lithology, as shown by the occurrence of large rock failures in the slates and lutites with limestones and rock glaciers in granitoids. The application of the CRE dating in rock glaciers showed that the glacial to periglacial transition was underway by 13.6 ± 0.9 ka, when rock glaciers started developing. These features stabilised soon after their formation and became relict by 11.9 ± 0.7 ka.

During the cold phases of the Holocene, glaciers could have formed within sheltered areas in the highest cirques of the Central Pyrenees forming moraines above 2500 m, although no evidence has been found yet in the study area.

**Keywords**: Geomorphology, Late Quaternary; Deglaciation; Cosmic-ray exposure dating, Upper Garonne

# Resumo

O alto Vale do rio Garona (AVRG) está situado na margem setentrional dos Pirenéus Centrais. A sua bacia inclui picos que ultrapassam os 3000 m (por ex.: 3219 m no pico do Perdiguero), a partir dos quais descem vales com uma clara morfologia glaciária em U, entalhados em batólitos. À medida que a altitude diminui, as suas linhas de festo, talhadas em metassedimentos paleozóicos afastam-se e as vertentes tornam-se mais retilíneas, denunciando uma maior influência fluvial. As temperaturas médias anuais do ar sobem de 2,7 ºC a 9,6 ºC entre as estações de Bonaigua, a 2266 m, e Vielha, a 980 m de altitude. A precipitação reflete a orografia, com os valores anuais a decrescerem de cerca de 1100 para 900 mm entre ambas as estações. Já no sopé da cordilheira, as largas bacias colmatadas por sedimentos quaternários, atingem os 450 m de altitude e assentam nos relevos de costeira talhados em rochas do Mesozóico. Neste limite inferior do AVRG, a temperatura média anual do ar é de 12 ºC e a precipitação anual acumulada é de 850 mm na estação de Clarac, a 401 m.

A presente dissertação tem como principal objetivo reconstruir cronologicamente as fases de avanço glaciário no AVRG e de ajustamento do relevo ao desaparecimento dos glaciares durante o Plistocénico Superior e Holocénico. Para atingir este objetivo, cinco objetivos específicos foram definidos: i) identificação e mapeamento dos complexos morénicos no AVRG, nomeadamente na bacia de Loures-Barousse-Barbazan (LBBB) e na cabeceira do rio Garona, no Vale de Ruda; ii) identificação da cronologia dos avanços glaciários durante o Plistocénico Superior com base em datações por isótopos cosmogénicos ($^{10}$Be); iii) reconstituição da extensão e superfície dos glaciares no AVRG, bem como as Altitudes das Linhas de Equilíbrio (ELAs) e as temperaturas durante os avanços glaciários; iv) criação de um modelo cronológico para a fase de transição entre as dinâmicas glaciária e periglaciária nos circos glaciários da áreas de estudo; e vi) avaliar os fatores morfológicos, litológicos e geográficos que condicionaram a dinâmica de vertentes no Vale de Aran durante a fase paraglaciária.

O mapa geomorfológico de pormenor na escala 1:25000 revela a existência de uma enorme variedade de evidências glaciárias e periglaciárias que indicam a períodos passados de intensa atividade glaciária e periglaciária (Artigo 1). A distribuição das evidências glaciárias e respetiva interpretação mostram três momentos importantes na evolução glaciária na bacia do AVRG, testemunhados por complexos morénicos: i) o complexo da bacia de LBBB composto pelos sistemas morénicos externo, a 420-720 m, e interno, a 460-820 m de altitude; ii) o complexo de moreias nas vertentes dos altos tributários entre 1000 e 2100 m; e iii) as moreias de circo acima de 2100 m.

No sopé da cordilheira, dois sistemas morénicos de baixa altitude na AVRG encontram-se na bacia de LBBB. Durante a formação do sistema morénico externo, o glaciar do Garona atingiu a sua máxima extensão, apresentando 80 km de comprimento. Durante essa fase, as evidências geomorfológicas sugerem a presença de um glaciar com espessura máxima de cerca de 800 m no vale principal. Esta espessura permitiu a ligação de línguas glaciárias nas partes mais altas, através transfluências em portelas com altitudes inferiores à superfície de gelo, formando um campo de gelo. Após a Extensão Máxima de Gelo (MIE), o glaciar do Garona sofreu um recuo assinalável. No entanto, esse recuo generalizado foi interrompido por várias fases de reavanço ou estabilização glaciária. Durante a primeira fase, os glaciares de vale formaram moreias que se encontram preservadas nas vertentes montanhosas, entre 1000 e 1950 m, e na base dos altos tributários, a 2000-2100 m de altitude. Depois desta fase, os glaciares voltaram a recuar, deixando áreas livre de gelo com depósitos sedimentares, suscetíveis a serem transportados para os fundos de vale, que hoje se encontram colmatados. Mais tarde, os glaciares voltaram a avançar, formando dois sistemas morénicos preservados dentro dos circos glaciários a 2400-2500 m e acima dos 2500 m. Com a deglaciação dos circos, as paredes descobertas de gelo começaram a fornecer grandes quantidades de blocos para o fundo dos circos, formando diversos glaciares rochosos. Por último, os glaciares recuaram para os circos mais altos, com picos que ultrapassam os 3000 m, onde ainda persistem acima de 2750 m, juntamente com glaciares rochosos ativos que surgem acima de 2600 m. Contudo, a atual posição da ELA no Pirenéus Centrais, a 3140 m, ameaça a continuidade dos últimos glaciares do AVRG.

Um dos maiores desafios das ciências do Quaternário na atualidade, é registar cronologicamente as glaciações anteriores à Última Glaciação, ou seja, do Plistocénico Médio. Nos Pirenéus, os glaciares responderam às condições frias globais do MIE do Penúltimo Ciclo Glaciário (PGC), correspondente ao Estádio Isotópico Marinho 6 (MIS-6). Este registo foi demonstrado pela idade da moreia externa da LBBB, que resultou numa idade de exposição de 128,5 ± 9,1 ka (Artigo 2). Esta idade constitui o primeiro registo cronológico sólido do avanço dos glaciares nos Pirenéus durante o MIS-6. Contudo, outros *proxies* também confirmaram a presença de glaciações durante o Plistocénico Médio, nomeadamente na datação de um bloco errático no Vale do Ariège com uma idade de exposição de 133,9 ± 5,3 ka (Delmas et al., 2011) e de uma moreia externa no Vale de Aragón com uma idade de enterramento (*optically stimulated luminescence*: OSL) de 171 ± 22 ka (García-Ruiz et al., 2013). No MIS-6 o glaciar do Garona atingiu 80 km de comprimento e tinha uma ELA a cerca de 1700 m com temperaturas de verão 9,3 ºC inferiores às atuais.

As condições frias da fase terminal do Último Ciclo Glaciário (LCG) forçaram o avanço do glaciar do Garona até à LBBB, no sopé da cordilheira. Esta afirmação é sustentada pelos trabalhos prévios sobre os sedimentos lacustres do Lago de Barbazan, alojado entre as moreias

internas de La Serre e Labroquère-Valcabrère. As características destes sedimentos indicam que foram acumulados num ambiente proglaciário entre 40,7/32,3 e 31,6/30,1 ou 29,9/27,2 cal ka BP. A origem da água de fusão do glaciar encontrava-se, possivelmente, na moreia mais proximal do sistema, a de Labroquère-Valcabrère. Esta evidência sugere que as moreias distais do sistema morénico interno (moreias de La Serre, Burs e Barbazan), se desenvolveram antes da formação do lago. No entanto, as idades de exposição dos blocos nas moreias de Burs e Barbazan revelaram resultados muito dispersos cronologicamente (73,1 ± 4,6 a 17,1 ± 1,8 ka) que não permitiram comprovar esta hipótese (Artigo 2).

Durante Último Máximo Glaciário Global (GLGM), os glaciares nos vales pirenaicos, influenciados pelo clima atlântico, já estavam numa fase de recuo, enquanto na Europa, ainda avançavam ou estavam a atingir a MIE (ex.: calote de gelo Escandinava há 22 ka). Esta hipótese é sugerida pelas idades de exposição de duas superfícies polidas localizadas 7 km a sul da LBBB, perto de Marignac, que mostraram idades de 24,2 ± 2,1 e 20,7 ± 1,2 ka (Artigo 2). O recuo glaciário registado na bacia de Marignac é correlativo do início da sedimentação siltosa e de matéria orgânica a 29,9-27,2 cal ka BP no Lago Barbazan. Esta cronologia sugere que a LBBB já estava livre de gelo durante o GLGM e que a deglaciação do vale do Garona já se encontrava em marcha. Este comportamento pode sugerir uma possível influência do anticiclone estacionário que transportava massas de ar secas de leste, impedindo a manutenção dos glaciares e levando ao seu recuo na fachada atlântica da Europa.

Durante e após o GLGM, o retrocesso generalizado dos glaciares para as partes mais altas das montanhas foi interrompido por vários avanços glaciários associados às principais oscilações climáticas do Hemisfério Norte. Durante o primeiro desses avanços, os glaciares formaram moreias nas vertentes montanhosas dos altos tributários e nas pequenas bacias laterais do AVRG e tinham entre 23 a 2 km de comprimento, respetivamente. Contudo, não foram encontrados blocos no vale principal do Garona adequados para datar este avanço glaciário, possivelmente correspondendo a um estádio. Depois desta fase, as condições quentes que prevaleceram durante a primeira metade do *Bølling–Allerød* (B-A), favoreceram o recuo glaciário nos altos vales e baixos circos. Este comportamento foi apoiado pelas 14 datações de exposição em superfícies polidas e blocos erráticos, que mostraram idades entre 16,0 ± 1,0 e 13,5 ± 0,8 ka nas partes altas do AVRG (Artigo 3 e 4). Estes resultados mostram uma concordância com os baixos valores do $\delta^{18}O_{ice}$ medidos nos carotes de gelo da Gronelândia, que são frequentemente usados para indicar condições quentes durante o B-A, no Hemisfério Norte.

A tendência de retrocesso glaciário durante no B-A foi interrompida por curtos períodos frios durante a segunda parte do B-A, que terão registado mais precipitação nival, promovendo o avanço glaciário nos altos tributários. Estes avanços sucederam-se com glaciares de 0,5 a 4 km

de comprimento, formando moreias cujos blocos preservam uma concentração de $^{10}$Be que permitiu estimar idades de exposição de 13,5 ± 0,9, 13,2 ± 1,1 e 13,0 ± 0,8 ka no ALRG (Capítulos 3 e 6). Estas moreias tinham as ELAs a 2461 e 2505 m e correspondem a temperaturas do ar de verão 3,9 a 4,2 ºC inferiores às atuais.

Durante o Dryas Recente (YD), as condições frias favoreceram um novo avanço glaciário nos altos circos abrigados e orientados a norte e oeste. Este comportamento foi demonstrado pelas moreias frontais datadas de 12,8 ± 0,8 e 12,6 ± 1,3 ka (Capítulos 3 e 4). Este avanço glaciário constituiu a última fase com glaciação nos circos com picos inferiores a 2700 m. A ELA situava-se a 2504 e a 2571 m e as temperaturas de verão foram 3 e 3,4 ºC, inferiores às atuais, respetivamente. Contudo, a aridez associada a este estádio provocou o retrocesso glaciário em algumas áreas, como foi o caso dos grandes circos pouco abrigados. De facto, as idades das superfícies polidas sugerem um recuo glaciário durante o YD (12,8 ± 0,8 e 12,7 ± 0,8 ka). Este comportamento também pode ter sido condicionado por fatores topoclimáticos, que por um lado causaram elevados níveis de ablação nival provocada pela intensidade do vento nos circos amplos, e por outro, promoveram a persistência de neve e gelo nos circos mais sombrios e protegidos.

Durante a deglaciação, os altos tributários e os circos glaciários do AVRG registaram um intenso ajustamento paraglaciário, promovendo a sua instabilização por processos de *debuttressing*. Como resultado, vários tipos de processos foram desencadeados dentro da área que tinha estado glaciada: deslizamentos catastróficos, movimentos de massa profundos, desabamentos e deslizamentos. A litologia condicionou a sua ocorrência, como demostrado nos afloramentos de ardósias ou lutitos e calcários, onde se encontram mais evidências (Artigo 5). No entanto, ainda não existem idades disponíveis para perceber a resposta temporal da paisagem após a deglaciação nas vertentes do AVRG. O ajustamento paraglaciário também afetou os circos glaciários, onde inúmeros glaciares rochosos se formaram, principalmente setores de rocha magmática. A forma como estas evidências geomorfológicas ocorrem no terreno, sugere uma transição rápida de ambientes glaciários para ambientes periglaciários, durante a segunda metade do B-A, ou mesmo sincrónica à deglaciação. Esta transição está registada nas idades de exposição sequenciais obtidas entre uma moreia de circo e um glaciar rochoso no circo de Lòcampo. Os resultados mostraram que, logo após o abandono da moreia pelo glaciar, há 13,2 ± 1,1 ka, formou-se um glaciar rochoso, datado de há 13,6 ± 0,9 ka (Artigo 6). Contudo, a estabilização definitiva deste, só terá ocorrido após 2 a 3 ka, pois o isolamento provocado pelo manto de detritos atrasou a fusão do gelo intersticial. Este comportamento foi sugerido pelas idades de exposição do glaciar rochoso, que mostram que a estabilização definitiva ocorreu no início do Holocénico, há 11.9 ± 0.7 ka.

Nos circos mais altos da cabeceira do vale principal do Garona não foram encontradas mais moreias com blocos ideais a datar por isótopos cosmogénicos. Contudo, noutros altos tributários onde os picos ultrapassam os 3000 m, existem moreias preservadas acima de 2500 m que podem revelar idades mais jovens do que o YD, nomeadamente do Máximo Glaciário do Holocénico (e.g. Neoglaciar, Pequena Idade do Gelo).

**Palavras-chave**: Geomorfologia; Quaternário Superior; Deglaciação; datações por isótopos cosmogénicos, alto Vale do rio Garona

# Table of Contents

# List of Figures of the Section 1

# List of Tables of the Section 1

# Section 1: Introduction

# 1. Geographical framework

## 1.1. Geographical and geological setting Pyrenees

In the *Encyclopaedia Geographica*, the Roman geographer Strabo (64 BC-21 AD) described the Iberian Peninsula as an ox-hide-shaped territory whose neck is constituted by a mountain range called the Pyrenees, dividing the westernmost peninsula from the rest of the known world. As described by mythological tales, the Pyrenees was named after the Spanish princess *Pyrene* that died after giving birth to a snake. In the woods where she died, Heracles piled up a set of boulders to build her tomb that formed the chain.

Geographically, the range is located between 2ºW-3ºE longitude and 42º-43ºN latitude and constitutes the isthmus between the Iberian Peninsula and the Eurasian landmass, dividing also the Mediterranean Sea and the Atlantic Ocean. This piece of land stretches from ESE to WNW and is ca. 450-km-long and ca. 75-150-km-wide. The highest elevations exceed 3000 m a.s.l. are mainly located along the Central Axis, with the Aneto Peak as the highest of the range (3404 m). Considering a regional lapse rate of 0.55-0.65 ºC/100 m, the current regional 0 ºC isotherm is roughly placed between 2950 and 3150 m, with the lowest values located in the northern slope of the range (López-Moreno et al., 2016). In the northern slope of the highest massifs in the Central Pyrenees, there are still 19 glaciers of reduced size (2-95 ha). All of them retreated since the LIA, with some phases of advance and stabilisation within the long-term recession; recently, the shrinking trend accelerated, with an average 0.7 $m^{-1}$ from 2010 to 2020, (Rico et al., 2017; Vidaller et al., 2021).

The Pyrenean range forces the squeezing of the transition zone between the Atlantic- and the Mediterranean-influenced climates that result in a rapid shift between cold/wet northern valleys – influenced by the westerlies that discharge abundant precipitations (especially in winter) – and warm/dry southern valleys – where the Azores anticyclone dictates the atmospheric stability (especially in summer). These climatic asymmetries imply changes in the hydrology of the Pyrenean catchments, as considerable amounts of water are discharged down valley through the Garonne catchment (annual average of 630-700 $m^3/s$; Lescure et al., 2015); compared with the south slope where water is less abundant in the Ebro catchment (annual average of 430 $m^3/s$; Batalla et al., 2014). Such interaction between relief and climate at a regional scale discloses the Pyrenees as a complex range, commonly divided into three parts: the Western or Atlantic, the Eastern or Mediterranean, and the Central Pyrenees, in between. This dissertation focuses on the Central Pyrenees, taking the Upper Garonne basin area as the focus of the study (Fig. 1.1).

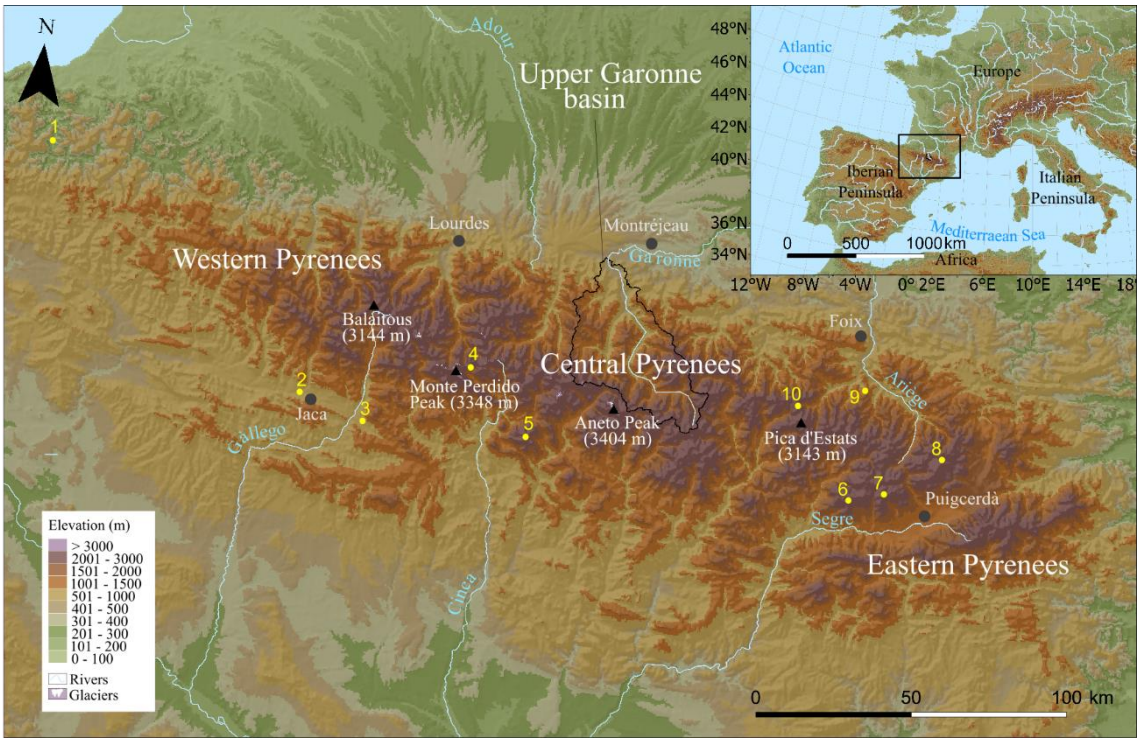


Figure 1.1. Relief of the Pyrenees and inset showing its location in Europe. Discussed sites in this chapter are highlighted in yellow: 1 – Ostolo Cave; 2 – Villanúa basin; 3 – Sabiñánigo basin; 4 – Marboré cirque; 5 – Basa de la Mora Lake; 6 – La Pera cirque; 7 – Malniu cirque; 8 – Carlit massif; 9 – Niaux-Lombrives-Sabart caves; 10 - Médecourbe cirque.

The Pyrenees constitute a borderland, dividing seas, climates, and also geologies. The North Pyrenean Fault is the limit between the European and the Iberian plates (Fig. 1. 2; Fitzgerald et al., 1999). This discontinuity splits the range into two units: the North Pyrenean Zone, mainly composed of Mesozoic outcrops, and the Axial Zone, which encompasses the Hercynian basement composed of Palaeozoic metasediments that have been intruded by batholiths and plutons (Espurt et al., 2019; Muñoz, 1992). From the Axial Zone southwards, there is a third geological unit, the South Pyrenean Zone that is formed by Mesozoic and Cenozoic sequences. These three units compose the Pyrenean range, flanked by Cenozoic sedimentary covers in the Aquitaine and the Ebro basins.

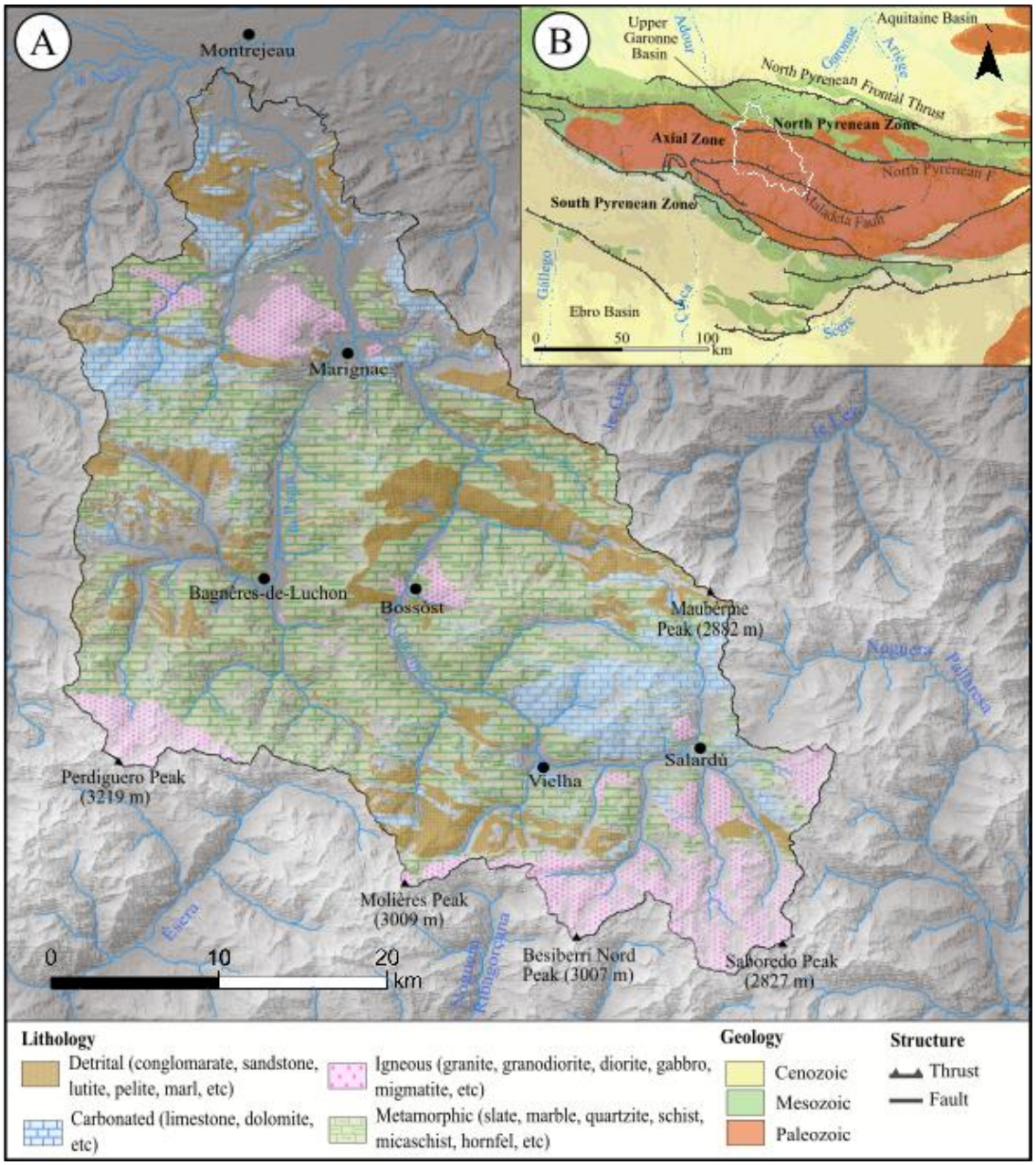


Figure 1.2. Simplified geological framework of the Pyrenees (B) and main lithological units existing in the Upper Garonne basin (A).

The whole Pyrenean range emerged from the Alpine orogenic lifting of the Hercynian basement (García-Sansegundo et al., 2013). During the Palaeozoic, the tectonic stability of the Cambrian-Early-Ordovician (>470 Ma) was followed by an uplift episode during the Early-Mid-Ordovician (470-458 Ma; Fig. 1.3A). This phase was succeeded by the extensional pulse during the Late-Ordovician responsible for depositing the Jujols Formation (458-444 Ma; Casas et al., 2019). This instability was subsequently substituted by the widespread sedimentation between the Silurian and Devonian, including the deposition of black carboniferous shales on a poorly oxygenated sea (444-359 Ma; Casas et al., 2019). Thereafter, during the end of the Carboniferous Period, the collision between the Laurussia and the Gondwana continents resulted in the lifting of the Hercynian Mountain range – from Morocco to Central Europe (320-290 Ma; Cochelin, 2017).

These sedimentary sequences were metamorphosed during the deformation events, especially during the intrusion of batholiths, such as in Bossòst by 338 Ma and Maladeta-Lys Caillaouas by 302-300 Ma (Fig. 1.3-C; Quesada and Oliveira, 2019a). During the Permian (299-251 Ma), the Pangea break-up opened the Tethys Ocean and dismantled the Hercynian Mountain range. This extensional regime formed grabens in the Pyrenees, then filled with Palaeozoic sediments by fluvial, alluvial and marine processes (Paris et al., 1970; Quesada and Oliveira, 2019b). Afterwards, during the Alpine orogeny, the collision with subduction of the Iberian plate against the European one lifted and deformed those sedimentary basins, progressively above sea level, as a consequence of the compressional deformation during the Late-Cretaceous (100-66 Ma; Calvet et al., 2021; Choukroune, 1992; DeFelipe et al., 2019; Teixell et al., 2018). Such collision reactivated the Hercynian faults and shortened by ∼150 km the range between the Early-Cretaceous to the Early-Miocene (84-20 Ma; Muñoz, 1992). This N-S deformation forced the north-dipping Alpine thrusts to form an antiformal stack relief (Cochelin, 2017; Muñoz, 1992). The major Pyrenean morphostructural units exist since the Palaeogene (<66 Ma; Calvet et al., 2021), with some post-orogenic changes in the foreland during the Neogene (23-2.6 Ma), such as the accumulation of large megafans; this occurred, for instance, in the Lannemezan Formation at the Neste basin that aggraded about 120-170 m of sediment thickness, most possibly during a warm climate period (Taillefer, 1951). During the Quaternary (<2.6 Ma), these deposits became dissected by changes in fluvial regime patterns until ca. 300 ka, as demonstrated by $^{10}$Be exposure dating on alluvial terraces (Mouchené et al., 2017). Finally, in this deposit, the presence of erratic boulders triggered the discussion about the magnitude and timing of the Quaternary glaciations in the northern Pyrenean foreland (Boule, 1895; Menteath, 1868; Piette, 1874).

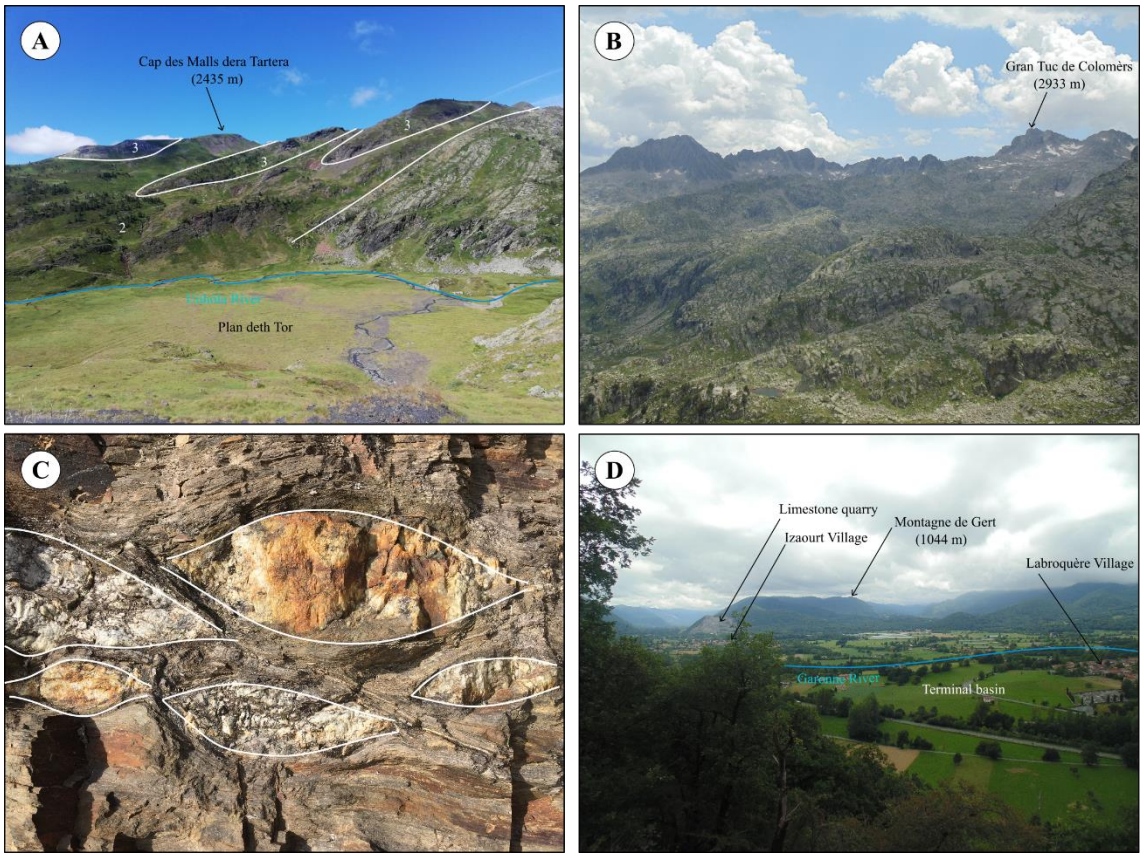


Figure 1.3. Chronologically organised examples of several geological units of the Upper Garonne basin: A) lithological sequence from the Cambrian to the Devonian in the synclinal of the Aran Valley: (1) the Júpols Formation composed of sandstones and lutites of the Cambro-Ordovician, (2) black slates intercalated with grey limestone from the Silurian-Devonian, (3) limestones and black slates from Silurian-Devonian age; B) granodiorites from the Carboniferous-Permian in the eastern margin of the Maladeta Batholith, Aiguamòg tributary; C) geological evidence located south from Bossòst Village showing evidence of extensional tectonics (*boudinage*), likely from Late-Ordovician age; D) Small hills composed of limestone and dolomites from the Late-Jurassic – Early-Cretaceous surrounding the glacial terminal basin of the Upper Garonne catchment.

During the Quaternary Period (2.6 Ma), glaciers became one of the most important agents reshaping the landscape, mainly by catchment denudation (Calvet et al., 2021). The past glacier distribution in the Pyrenees has been studied for the last two centuries, starting with the identification of glacial evidence and the delineation of the ice extent which demonstrated a previous larger glaciation with significant asymmetries (Fig. 1.4; Calvet, 2004; Calvet et al., 2011; Delmas, 2015; Delmas et al., 2022a, 2022b; Hérail and Jalut, 1986; Penck, 1883; Taillefer, 1966). However, the low intensity of glacial and fluvial processes left behind a pre-glacial relief that is still preserved, as shown by the flatness of mountain-tops within the glaciated areas of the Pyrenees. Such flat tops are found mainly in the Eastern flank of the range but also occur punctually in the Central part, such as in the Upper Garonne basin at 2000-2200 m: Porèra, Montromies, Era Cauva and Planhèth Dera Montanha (Calvet et al., 2021). An alternative interpretation postulate these surfaces as remnants from a previous peneplain formed at sea level with subsequent Late Miocene rise (Bosch et al., 2016). This hypothesis agrees with the reconstructed post-orogenic uplift (0.08-0.19 mm $y^{-1}$) of the Maladeta Fault since the Late Miocene based on

the estimation made in faceted spurs of the Aran Valley (Ortuño Candela, 2008; Ortuño Candela et al., 2013).

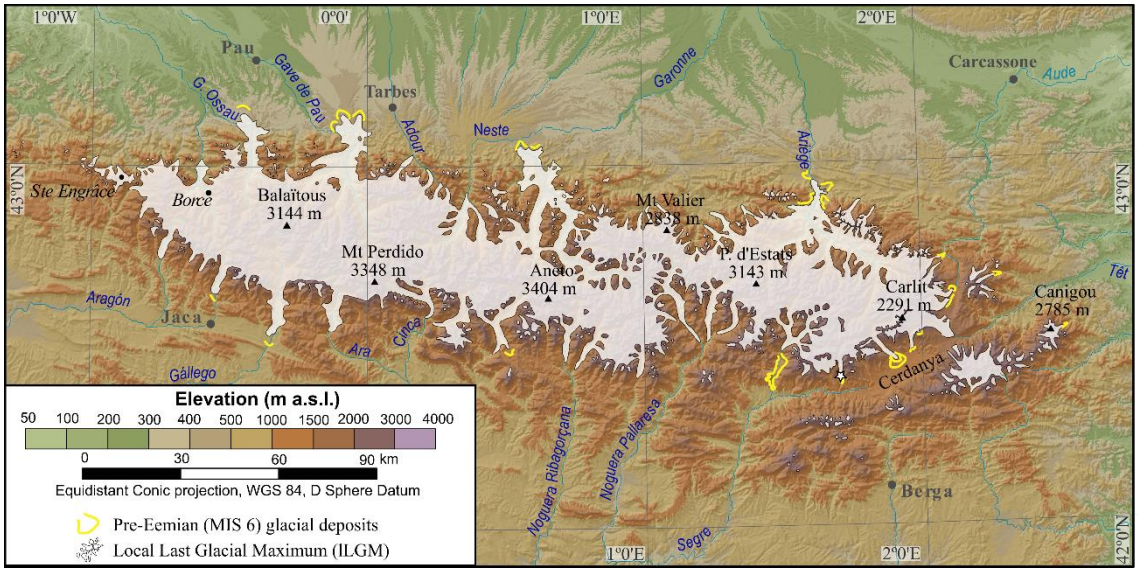


Figure 1.4. Approximate distribution of the Pyrenean glaciers extent the LLGM (adapted from Delmas et al., 2022a).

## 1.2. The Upper Garonne basin: Physical and human setting

Taking into account the objective of this research, the Upper Garonne basin is defined as the area stretching along 40 km straight north into the Aquitanian basin, which encompasses a fluvial catchment of 1261 km$^2$ that represents only 2.3% of the total catchment (55000 km$^2$). Geographically, it is located between the Perdiguero Peak (3219 m; 42º41'N-0º31'E), the Saboredo Peak (2827 m; 42º36'N-0º58'E) and the LBBB (~420 m; 43º03'N-0º33'E). At the backbone of the Axial Zone, the highest summits are increasingly lower from west to east; Perdiguero Peak, Maupás Peak (3111 m), Molières Peak (3009 m), Besiberri Nord Peak (3007 m), Gran Tuc de Colomèrs (2933 m), Saboredo Peak. Herein, the MAAT isotherm of 0 ºC lies at 2950 m. Present-day temperatures favour precipitation in the form of snow between October and May above 2000 m (López-Moreno et al., 2019). However, the elevation of the ELA has increased over the last years in response to a warming climate, and glaciers have accelerated mass losses (López-Moreno et al., 2016, 2015; Rico et al., 2017; Serrat and Ventura, 1993; Vidaller et al., 2021). The ELA of present-day glaciers, including several small features existing within the Garonne catchment, is found well above the glaciated environment at 2750 m, which explains its shrinking trend (Serrano, 2022). Most glaciers are located at the northern cirques towered by the Perdiguero and Maupas peaks (Table 1.1). The upper N-facing tributaries of the Garonne River are divided by the eastern (Aran Valley, Spain) and the western ones at the la Pique River (Haute-Garonne, France). From these altitudes down to ca. 500 m, both the Garonne and la Pique rivers drain northwards, joining at the Marignac basin. The lowest part of the Upper Garonne basin is defined by the northernmost preserved glacial deposits from the Late-Pleistocene, at 440-420 m

in the LBBB, south of Montrèjeau. Along the valley, the MAAT rises with decreasing altitudes from 3 ºC at Bonaigua (2266 m) to 10 ºC at Vielha (980 m) and 12 ºC at Clarac (401 m) stations and the annual precipitation decreases from ca. 1100 mm in Bonaigua to ca. 900 mm in Vielha and ca. 850 mm in Clarac (2000-2020 series). This dissertation focuses on the main valley of the Garonne palaeoglacier, from the Ruda Valley to the LBBB.

Table 1.1. Comparison of the glaciers from the Upper Garonne basin between the end of the LIA and 2020.

| Glacier | Peak (m) | Exposure | 1850* | | 2020* | |
|---|---|---|---|---|---|---|
| | | | Lower limit (m) | Size (ha) | Lower limit (m) | Size (ha) |
| Seil de la Baque | Seil de la Baque (3076) | N | 2580 | 139 | 2860 | 7.9 |
| Portillon | Perdiguèro (3219) | N | | | 2900 | 1.5 |
| Lézat N | Lézat (3107) | NE | 2785 | 5 | - | 0 |
| Lézat E | Lézat (3107) | NE | 2750 | 5 | - | 0 |
| Litérole inf. W | Crabioules (3110) | NW | 2900 | 2 | - | 0 |
| Crabioules | Crabioules (3110) | N | 2560 | 91 | - | 0 |
| Maupas W | Maupas (3011) | NW | 2547 | | - | 0 |
| Maupas E | Maupas (3011) | NE | 2846 | 45 | 2850 | 4 |
| Boum | Boum (2987) | NW | | | | |
| Mail Barrat | Mail Barrat (2984) | N | 2530 | | 2760 | 2.3 |
| Graouès | Mail Barrat (2984) | N | 2630 | 11 | - | 0 |
| Besiberri Nord | Besiberri Nord (3007) | N | 2700 | ~ 4 | - | snow patch |
| Baraque des mineurs | Mail de Bulard (2751) | W | 2345 | 1 | - | snow patch |
| Arcouzan | Mont Valier (2838) | W | 2200 | 6 | 2300 | 1.9 |

* Based on the values from Delmas et al. (2023)

### 1.2.1. The morphostructure

The landscape of the Upper Garonne basin may be described as having three main units where particular geomorphological processes and vegetation belts occur: i) the highest peaks and cirques at ca. 3000-2100 m (Fig. 1.5-B); ii) the mountain slopes and high valleys between 2100 and 1100 m (Fig. 1.5-A); and the valley bottoms and forelands from 1100 to 500 m (Fig. 1.5-C).

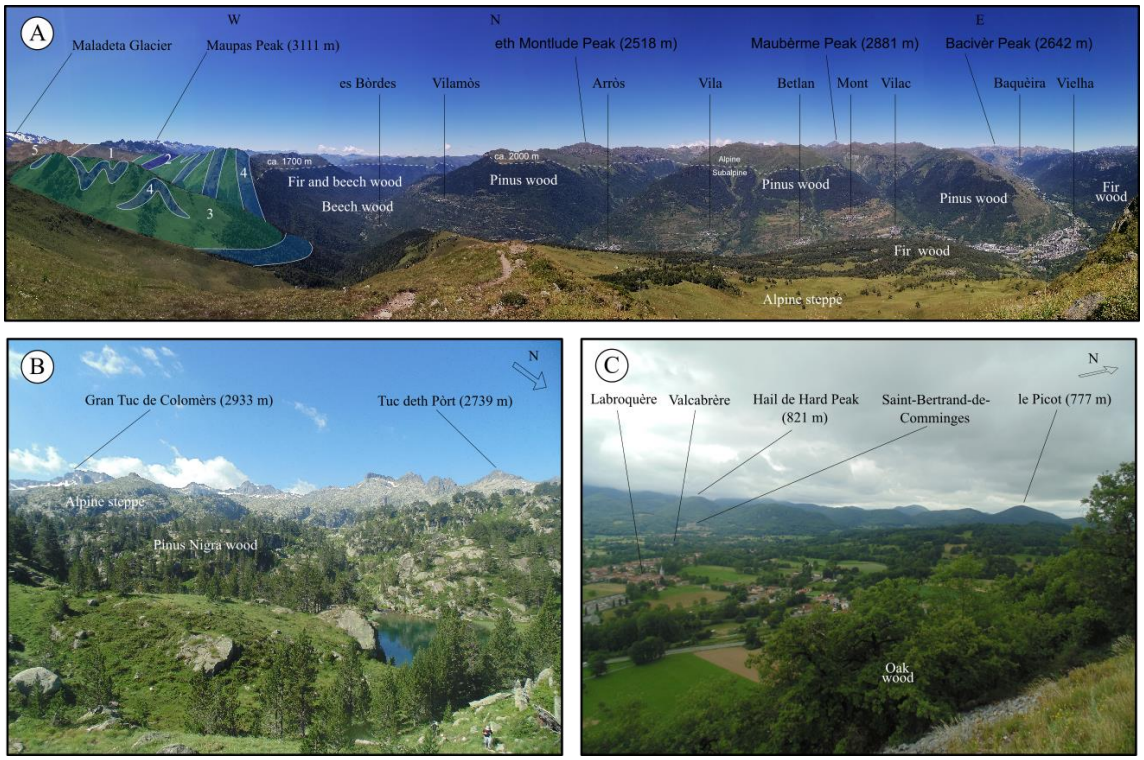


Figure 1.5. Examples of the three landscape units of the Upper Garonne basin: A) Panoramic view of the glacial main Garonne Valley showing the main landscape elements: geology (1- lutites in the Júpols Formation, 2 - intercalations of Silurian-Devonian limestones with lutites, 3 - intercalations of Devonian slates with limestones, 4 - Devonian limestones, 5 - intercalations of Carboniferous sandstones with lutites), vegetation and villages distribution; B) Colomèrs cirque located at the Carboniferous Maladeta batholith; C) small mountains from the Late Jurassic-Early Cretaceous surrounding the Quaternary LBBB.

The highest peaks and cirques (ca. 3000-2100 m) are mainly located in the backbone of the Axial Zone, in the Carboniferous granitoids (Cochelin, 2017; Esteban et al., 2015; Garcia-Sansegundo, 2004). The differential erosion resulting from the interaction between exogenous processes and lithology favoured the towering of the highest summits (>2900 m) in the resistant crystalline granitoids. The most paradigmatic example is the Maladeta Batholith that corresponds to the headwaters of the Garonne River, specifically in eastern N-facing tributaries, i.e. Ruda, Aiguamòg, Valarties and Nere valleys. In the western margin of the basin, the Dome of Lys-Caillaouas encompasses the highest lands of the l'One and d'Enfer valleys (Fig. 1.2). There are other minor intrusions, such as the Marimanha Pluton (2642 m; Tuc de Bacivèr), and the Bossòst Dome (2518 m; Eth Montlude Peak). However, the highest peaks and cirques are not limited to the Pyrenean batholiths. The lowest limit of this group is defined by the bottom of the cirques that coincides with hard metasediments (marbles, hornfels, slates and quartzites) and sedimentary rocks (limestones and conglomerates) that stand today on top of the landscape at 2300-2100 m (e.g. Samont or Armèros cirques).

Within this highest unit, the prevailing periglacial conditions trigger different geomorphological processes depending on the relief configuration. In steep slopes, frost shattering prevails on bare rocks precluding vegetation development, especially above 2600 m,

where permafrost occasionally occurs (Fernandes et al., 2017; Serrano et al., 2011). Pattern ground processes also occur in the highest lands, particularly in flat surfaces or gentle slopes. Slopes are intensely influenced by seasonal snow dynamics that trigger snow avalanches (Fernandes et al., 2017). Indeed, the harsh climate conditions are one the most important factors in determining the scarcity of vegetation in the subnival (>2800 m) and Alpine belts (2800-2400 m). The first is characterised by the absence of vegetation in the most unstable areas (e.g. steep slopes or active rock glaciers) or the occurrence of lichens and mosses in the most stable deposits. The lower includes gentler slopes within the glacial cirques where fine sediments are preserved (e.g. till or fluvial sediments), promoting the development of organic soil and allowing alpine grasslands to colonise. Here, xerophilous grasslands dominate the Alpine belt with *Oxytropis halleri* and *Oxytropis foucaudii* in basic soils and *Festuca airoides* in acidic ones (Ninot et al., 2017). In contrast, in some high overdeepened basins, peatlands show hygrophilous communities. Solifluction landforms represent the most widespread periglacial phenomena in these relatively flat areas. Finally, from 2400 to 2100 m, the first evidence of trees occurs with small isolated *Pinus nigra* growing on rock fractures, defining the timberline and the onset of the subalpine belt (Ninot et al., 2017).

The landscape from the headwaters downwards (2100-1100 m) is mainly composed of mountain slopes and high valleys from the tributaries of the Axial Zone. High valleys are carved on sedimentary (sandstones, lutites, limestones, conglomerates) and metamorphic (marbles, schists, slates, hornfels, and quartzites) rocks from the Cambrian to the Devonian (Kleinsmiede, 1960; Mapa geològic 1:50 000, 2017). Structurally, this unit coincides with W-E folded infrastructure (Cantabrian-Ordovician) and suprastructure (Silurian-Devonian) affected by metamorphisation and deformation during the Hercynian orogeny (Cochelin, 2017; García-Sansegundo, 1996; Sitter and Zwart, 1962; Zwart, 1979). However, the intensity of Quaternary weathering and their relationship with lithology and structure have dictated complex processes to develop the current arrangement of the slopes and valleys of this unit. On the one hand, during the Quaternary, glaciers flowed from the backbone of the Axial Zone northwards, carving classical U-shaped S-N valley oriented. These are perpendicular to the lithostructure organisation showing no conditioning from the pre-relief: e.g. Joèu, la Pique. On the other hand, at lower positions, the considerable number of tributaries parallelly oriented with lithostructure might show the importance of rock hardness and predominance of W-E faults (e.g. Bossòst Fault). The millions of years of weathering of the Palaeozoic metasediments facilitated the Quaternary glacier carving, fluvial incision and gravitational processes in a prevailing W-E orientation. These are the cases of the Salient, Varradòs, Toran, Ruisseau de Maudan, le Portet and la Pique valleys that are parallelly oriented with the lithological boundaries and structure (W-E faults: e.g. Bossòst). Besides, these valleys have more rectilinear slopes, and water divides are far from each other,

showing that glaciations were not as intense as those north-oriented (Martí-Soler, 1988). The exception to this unit is the N-S Unhòla catchment, surrounded by mountain ridges that obstruct northern humid air masses from entering the valley and force the dominance of grasslands instead of forest that only occurs near the main Garonne Valley. In fact, the absence of forest shows the lower limit of the Alpine steppe belt varying according to exposure, continentality, human activities and geomorphological processes. Snow persists annually for several months in the mountain slopes as the winter 0 ºC isotherm likely goes down valley to the foot of the slopes at 1600 m (López-Moreno, 2005). The snow avalanches play an important role in opening slope corridors with absence of trees that coincide with ravines frequently affected by debris flows and rockfalls damaging roads and infrastructures (e.g. Valarties in 2018 or Saut deth Pish, 2020; Fig. 1.6). On the other hand, the most stable areas are suitable to soil processes that favour forest development. Such transition seals the onset of the subalpine belt at 2100 m that goes down to 1600 m, where slopes are colonised by coniferous woods dominated by *Pinus nigra* (*Pinus uncinata*) and fir (*Abies alba*) (Bolòs and Vigo, 1984; Rivas-Martínez and Costa, 1998).

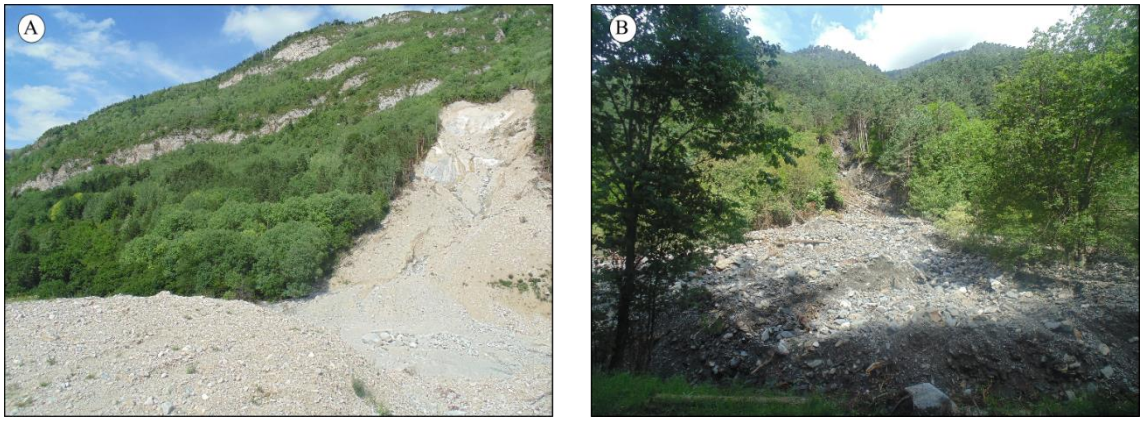


Figure 1.6. Examples of debris flows in the Aran Valley: A) the event occurred in 2018 in the Valarties Valley and reworked the slope and till deposits at the right margin of the valley; B) the event occurred in 2020 near the Saut deth Pish on the right slope of Varradòs Valley and transported essentially sediments and vegetation debris.

The third landscape unit is located at the valley bottoms and forelands from 1100 to 500 m in the LBBB and its surrounding mountains. This unit comprises Quaternary deposits on the valley bottoms seated along the Palaeozoic basement and northern Mesozoic basin (Fig. 1.2). In addition, the small mountains (<1100 m) surrounding the LBBB encompass Mesozoic rocks (limestones, conglomerates, sandstones, dolomites, breccia, flysch, marls, siltstones, hornfels, ophiolites, and quartzites) from the Jurassic-Cretaceous periods distributed across the piggyback relief that lifted during the Alpine orogeny (Paris et al., 1970; Barrère et al., 1984; Muñoz, 1992; Handy et al., 2010). Along this unit, flat areas with fluvial terraces occur parallel to the Garonne and la Pique rivers resulting from the glacial, lacustrine and fluvial sediment aggradation of overdeepened basins during the paraglacial phase. This aggradation phase occurred during the intense sediment transport during cold climate stages of the Last Deglaciation (Lambs et al., 2014;

Nivière et al., 2016). Fluvial incision occurred during the warm phases, estimated to be from 0.68 to 1.56 mm $y^{-1}$ at the upper valleys (Victoriano et al., 2016). In present day, incision has been mainly linked to catastrophic events occurring every 30 to 50 years that affect the alluvial plain and are highly influenced by snow melting events and heavy rainfall (Victoriano et al., 2016). At the margins of the plain, numerous alluvial fans are fed with the material produced from the slopes by debris flows, alluvial processes and snow avalanches (Fernandes et al., 2017). Near the Pyrenean foreland, where the basins become wider, ice thickness was increased by glacial merging, such as in the Marignac basin, with an estimated maximum sediment thickness of 300 m (Perrouty et al., 2015). At the LBBB, above the glaciofluvial plain, glacial remnants are preserved at the bottom of the basin in the form of lateral and frontal moraines (Boule, 1895; Depéret, 1923 and thereafter). At the top of the surrounding mountains, there are other much more degraded moraine remnants (Leymerie, 1881; Pic, 1933; Piette, 1874 and thereafter). These areas are commonly covered with a mixed forest of the montane belt (1600-900 m) dominated by beech (*Fagus sylvatica*) and coniferous woods (*Pinus sylvestris*) that occur predominantly in the highest and sunny areas. Besides that, fir woods (*Abies alba*) also appear in the shadiest and sheltered slopes and oak woods (*Quercus petraea*) in the bare outcrops (Rivas-Martínez and Costa, 1998). The environmental conditions, such as temperature, humidity, soil composition, and solar radiation, in the submontane belt (under 900 m) lead to a dominance of mixed deciduous forest of oak forests (*Quercus robur and Quercus petraea*) (Brus et al., 2012). Besides, alongside the Garonne River, the riparian gallery is settled on the margins of the flood plain resisting mean discharges of 200 $m^3/s$ and peaks of 4000 $m^3/s$ during floods events (Steiger et al., 1998; Weng et al., 2003). Finally, the composition of fine sediments at the LBBB favours the anthropic land use mainly to produce cereals. In fact, human presence in the Upper Garonne basin, especially in this lower unit since the palaeolithic (Rusch et al., 2019).

### 1.2.2. The human occupation

During the Late Pleistocene, groups of Neanderthals in the Aquitaine basin avoided the Garonne basin, at 300-500 m, particularly during cold phases on account of harsh environments (Bruxelles and Jarry, 2011). This was also validated by the archaeological findings of lithic assemblages exchanged between the western Pyrenees and the Bay of Biscay; however, in the Garonne River plain, no sites with this evidence were found (Minet et al., 2021). The Neanderthals remained in these areas until ca. 40 ka, whereas modern humans started to occupy it since 42 ka, suggesting both groups' coexistence (Djakovic et al., 2022). During the Last Glacial Cycle (LGC), humans have inhabited the Upper Garonne basin during onset of the GLGM (28-25 cal ka BP), when cold conditions forced them to shelter in caves as demonstrated by the hand paintings, engraved panels, and fauna fossils found in the Gargas Cave, 2 km north from the Jaunac Village (Foucher, 2015; Foucher et al., 2008). In the upper tributaries, the vegetation taxa from the Basa

Nere, at the Aiguamòg valley, suggests that humans have been grazing since 7.3 cal ka BP ka and producing cereals since 5.2 cal ka BP (Garcés-Pastor et al., 2017b). *In situ* findings of human settlement in granite shelters at the Aigüestortes i Estany de Sant Maurici National Park also agree with sediment records by suggesting grazing, hunting, and agriculture since the Holocene Thermal Maximum (HTM) at ca. 8-7 ka. In the case of the Upper Garonne Valley and nearby areas, concavities below moraine boulders with evidence of fire activity were found in the cirques of Saboredo, at 2345 m, and Ratera, at 2322 m, with preserved coal dated at the Mid-Holocene (Neolithic and Chalcolithic), at 4.9-4.6 and 4.8-4.5 cal ka BP, respectively (Gassiot et al., 2014). During the last millennia, the sediments from the Basa Nera show that terrestrial systems responded to the centennial climate events, notwithstanding being highly influenced by anthropic activities such as grazing (Garcés-Pastor et al., 2017a). This activity dominated until recent times, when a clear shift towards the tertiarisation of the economy occurred by developing tourism mostly related to the creation of snow resorts (e.g. Baqueira-Beret, Luchon-Superbagnères). These changes were triggered by the construction of the Vielha tunnel in 1948, connecting the Aran Valley with large urban areas in the south, such as Barcelona (Sabiron i Herrero, 1994). Today, the population of the Upper Garonne Valley is around 15000 people (ca. 10000 in Aran and ca. 5000 in Bagnères-de-Luchon); they live mostly in the main Garonne Valley and are distributed along the flood plain, at localities such as Vielha, Les, Bossòst, Bagnères-de-Luchon, as well as on the most stable slopes, including small villages such as Vilamòs, Canejan and Cazarilh.

## 1.3. Glacial studies in the Upper Garonne basin

Since the 18$^{th}$ and 19$^{th}$ centuries transition, European researchers have considered the Upper Garonne basin a case study to understand the glacial evolution in the Pyrenees. During these ca. 200 years, a set of sedimentological, pedological, palynological, chemical, geomorphological, dating and modelling studies were conducted in this area based on the features left by the largest glacier in the Pyrenees to reconstruct and better understand the past Quaternary glaciations.

### 1.3.1. Evolution of the glacial knowledge

The existence of Quaternary glaciers in the Pyrenees is an old and accepted statement. After the first doctrines about the previous glaciation in the Alps, it took around 100 years for the first complete glacial interpretation in the Pyrenees (Obermaier, 1906; Penck, 1883; Penck and Brückner, 1909). The hypothetical explanations of erratic boulders of granite lying on the limestone of the Jura mountains were first alluded by the father of Geology, James Hutton (1726-1797), and then proliferated by the naturalists Jean de Charpentier (1783-1855), Karl Schimper (1803-1867), and Louis Agassiz (1807-1873), among others. Those ideas were spreading across

the academy and replicated in other mountains resulting in the first Pyrenean study on glaciers (Carbonnières, 1792). Carbonnières supported its insights on comparisons with the Alps, admitting that glaciers were dynamic and stating that they advanced down valleys to places close to villages – by that time, glaciers were possibly near the LIA moraines. During the following years, the first glacier database encompassing the largest Pyrenean glaciers was described, including those from the Upper Garonne basin, such as Crabioules, which by that time had similar dimensions to the Maladeta glacier (Charpentier, 1823). However, the first descriptions of previous, and larger, glaciations in the Upper Garonne basin were done in the second half of the 19$^{th}$ century: the glacial features observed across the Garonne Valley were similar to those existing below the contemporary glaciated landscapes in the Alps by the end of the LIA (Leymerie, 1855; Menteath, 1868). Once the previous glaciation was recognised, identifying large erratic boulders and external moraines became a technique to the pioneer researchers for delineating the distribution of the palaeoglaciers. In fact, after that it was easier to speculate about glacial origin of the new findings of erratic boulders and moraine deposits, even if they were far from the headwaters. At an external position in the terminal basin, between the Garonne and Nest rivers, boulders embedded in a 20 m high crest indicate the existence of a moraine at Boucoulan, in the left margin of the basin (Piette, 1874). However, the interpretation of the origin of this outmost deposit remained inconclusive due to the lack of glacial abrasion erratics. He also documented the best preserved moraine in the terminal basin, the La Serre moraine, naming it Labroquère moraine, which is the only preserved moraine left of the three lobes of the Garonne palaeoglacier, i.e. northern (La Serre), western (where the Garonne River is currently draining) and eastern (Barbazan). On top of the eastern flat-topped mountain, another moraine composed of metric boulders of granite was documented near the Burs Village, lying 200 m above the basin floor on limestone outcrops (Leymerie, 1881). Leymerie studied the erratic boulders across the Spanish and French valleys and pointed the Aran Valley as the place where they were more common. Moreover, he acknowledged the scary but helpful hypothesis of a 700-800-m thick glacier in la Pique Valley in order to explain the transport and accumulation of the few granite boulders out the level of the Cazaril Village. From these preliminary findings and further extensive moraine identification across the Pyrenean valleys, the German geographer Albrecht Penck and his disciple Hugo Obermaier formulated the first map of the MIE in the Pyrenees, including the Garonne catchment (Fig. 1.7; Obermaier, 1906; Penck, 1883).

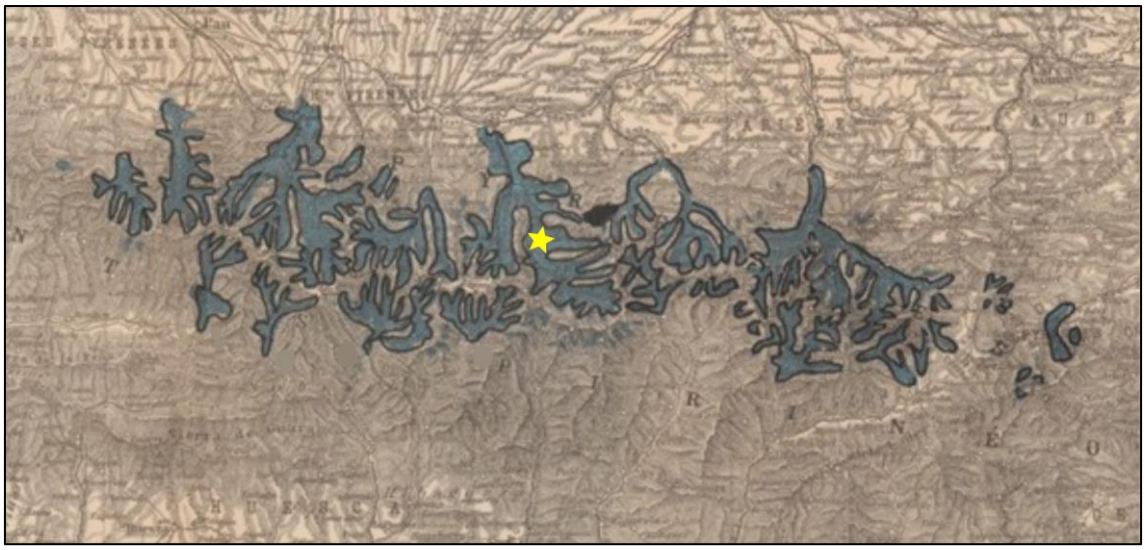

Figure 1.7. Penck's interpretation of the first complete MIE of the LGC in the Pyrenees in 1883. The Garonne palaeoglacier is highlighted with a yellow star.

The sedimentary terraces composed of cobles and pebbles above the current flood plain were classically related to aggradation phases of heavy discharge associated with glacial advances. In the Upper Garonne basin, staggered terraces were first identified at the foreland by geologists (Leymerie, 1855, 1881; Boule, 1895; Denizot, 1922; Depéret, 1923; Pic, 1933; Breuil, 1937). However, interpreting the complex state of preservation and distribution (e.g. height above the riverbed) of those terraces was not trivial. It led to ambiguous interpretations about the timing of formation (Goron, 1941). The first detailed description of those terraces was made by Boule (1895) at 15 (T1) and 50 m (T2) above the riverbed (Fig. 1.8). The lower terrace was found next to the riverbed (e.g. Montréjeau and Sant-Gaudens) and is composed of cobles and a minor fraction of pebbles and sand; the highest terrace (T2), mainly located in Sant-Gaudens, has a similar composition but with rusty yellow colour and covered by an oxidised loess layer of a reddish colour. The lowest terrace (T1) was associated with the Labroquère moraine due to its morphological correlation, similar altitudes and faceted cobbles (Boule, 1895; Depéret, 1923). Whereas the T2 had no such obvious correlation because of the highly weathered state of the moraines at the external position (Pic, 1933). The intermediate terrace, or T3, is well preserved in the left margin of the Garonne River and between Montréjeau and Saint-Gaudens (Alimen, 1964; Paris et al., 1970). Finally, the T4 lies 80 m high up from the riverbed and forms a straight bed highly eroded and just below the Lannemezan megafan (Paris et al., 1970). The identification of depressions commonly occupied by lakes or peatland within the moraine limits or polished rock surfaces also allowed to reinforce the hypothesis of glacial dynamics (Penck, 1894; Depéret, 1923).

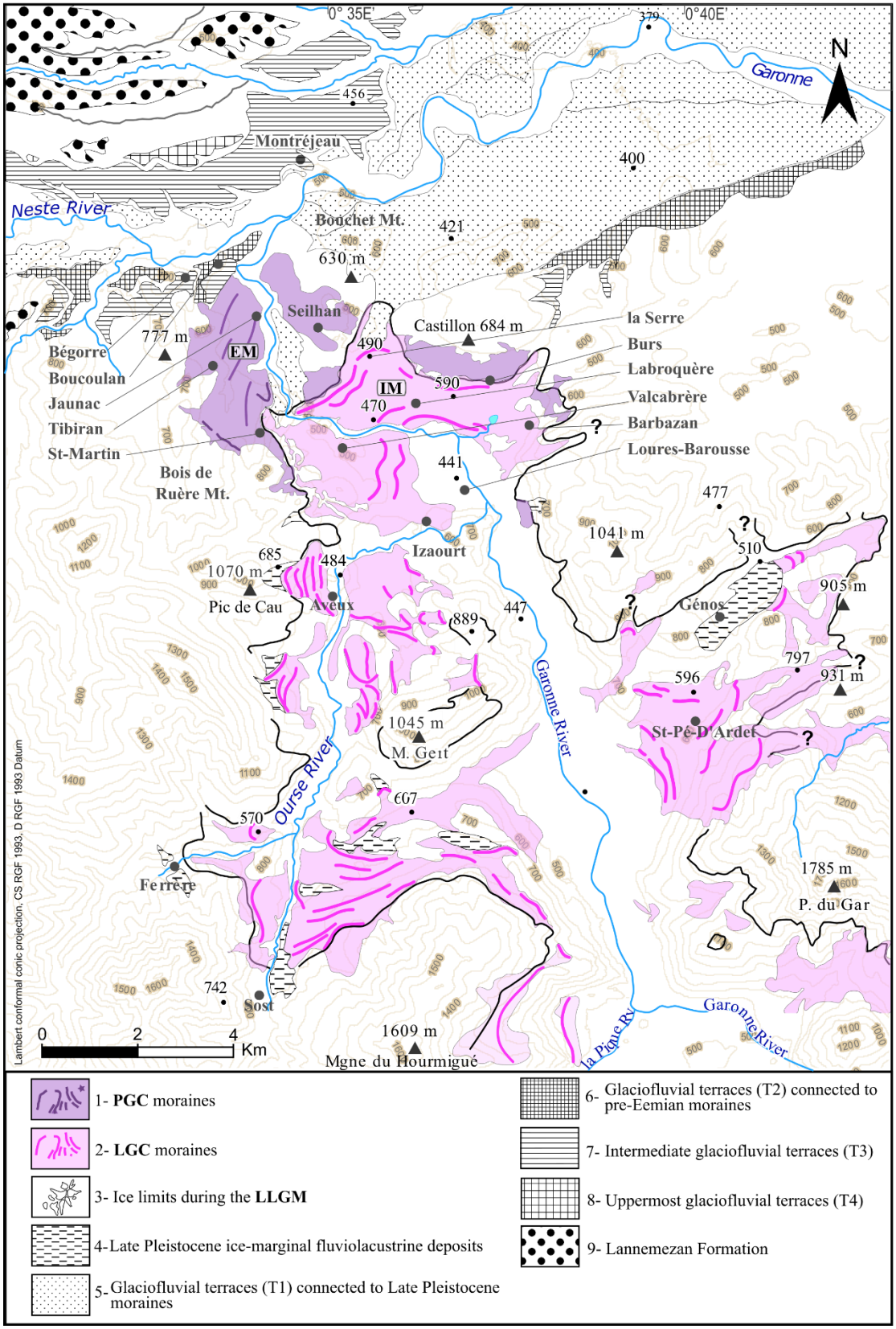


Figure 1.8. Moraine deposits and terraces in the LBBB adopted from Delmas et al., 2022b.

The glacial evidence in the terminal basin supported the reconstruction of the Garonne palaeoglacier at the multiple stages of glacial advance. Moreover, erratic boulders and moraines on the margins of the ice field allowed reconstructing the glacier's thickness (Boule, 1895;

Leymerie, 1881; Piette, 1874). In fact, the distribution of erratic boulders on slopes of the upper lands has been used to make several proposals of ice thickness during its maximum extent in different sectors of the basin: 700-800 m at Bagnères-de-Luchon (Leymerie, 1881); 1200 m at Les, 800 m at Bossòst, 600 m at Frontignan, and 200 m at Loures-Barousse by (Mianes, 1955); 800 m in Varicauva (Bordonau, 1985); 400-500 m near Vielha by (Kleinsmiede, 1960) or 700 m near Arties (Martí-Soler, 1988). Based on these findings, the first glacial handmade model for the Aran Valley was drawn by Bordonau (1985) proposing an ice thickness of 400-500 m at the bottom of the upper tributaries (Aiguamòg, Valarties and Nere) and 800 m in the main Garonne basin. More recently, considering the most external moraines of the LBBB, Fernandes et al. (2017) reconstructed the whole Garonne palaeoglacier, showing that 72% of the area was glaciated, with a total ice volume of 260 $km^3$ and a maximum ice thickness of 835 m. This model showed was validated with glacial sedimentological evidence (i.e. erratic boulders) and to the topography, as glaciers flowed into watershed breaches (cols), forming glacial transfluences in the eth Portillon (Bossòst), Bonaigua, Beret, Colhada de Varradòs, headwaters of the Joèu.

However, the assessment of the glacial evolution of the Upper Garonne basin needs to incorporate the sedimentological and erosional landforms distribution within the catchment.

### 1.3.2. Sedimentological features

The aforementioned introductory study of the moraine deposits in the Upper Garonne basin considers three moraine complexes described below. These features were deposited during the entire Late Pleistocene and cover 10% of the surface (Clin et al., 1989; Paris et al., 1970).

1. Phase 1 - Moraine systems of the glacial terminal basin (420-820 m).
   In the LBBB, several detailed surveys showed a set of moraines from the basin floor at 420 m to the surrounding mountain slopes up to 820 m (Andrieu et al., 1988; Andrieu, 1991a; Barrère et al., 1984; Chaput, 1924, 1927; Denizot, 1922, 1925; Depéret, 1923; Fernandes et al., 2017; Hubschman, 1984; Pic, 1933; Stange et al., 2014; Taillefer, 1945, 1953, 1965). The geological map at the scale 1:50.000 divides this moraine complex in the external system between Jaunac and Saint-Martin villages and the internal one between Labroquère and Loures-Barouse villages (Paris et al., 1970):
   1.a. The poorly defined ridges at the outermost part of the LBBB plain and surrounding mountains are included in the external moraine system (Fig. 1.8). Here, the Garonne River divides the moraine ridges at the left margin and the sparse till existing on the right one. The northernmost ridge, previously called Boucoulan or Bégorre moraine, shows SW-NE alignment at 480-490 m with smooth topography and embedded boulders; it was considered by Depéret (1923) as having two lobes. Further south, two more crests display an oblique feature (SW-NE) between Jaunac and Tibiran villages at the same altitude

(Fig. 1.8). Near the St-Martin Village, 300 m southwards, another ridge at 480 m (Fig. 1.9-A), with embedded boulders on top, connects the Bois de Ruère hill with the basin, previously called Barsous moraine (Goron, 1941). At the opposite margin of the Garonne River, there is a relatively flat area from Seilhan to the foot of Bouchet Mountain. Some opened sections with crystalline boulders within a poorly sorted matrix are considered the remaining till of the corresponding right crests (Pic, 1933). At the right side of the LBBB, no moraines are preserved, whereby it is reasonable to think that the thin exit at the Bazert Village formed a barrier where the postglacial dynamics would rapidly rework glacial sediments. The flat hilltops at the surrounding mountains of the LBBB contain glacial evidence at 600-720 m (i.e., 180-300 m above the basin floor). Southwards from the Izaourt Village, the sparse granite boulders lay 230 m above the basin floor on the bedrock of Cretaceous limestone may correspond to this phase (Fig. 1.9-B). On the other side, south of Barbazan, at the top of the hill, exposed sections are opened in this moraine system that shows sub-angular to sub-rounded boulders supported in a poorly sorted matrix. There are no well-defined ridges near the Burs Village, but boulders and glacial-fluvial cobbles are embedded in the sandy matrix (Leymerie, 1881).

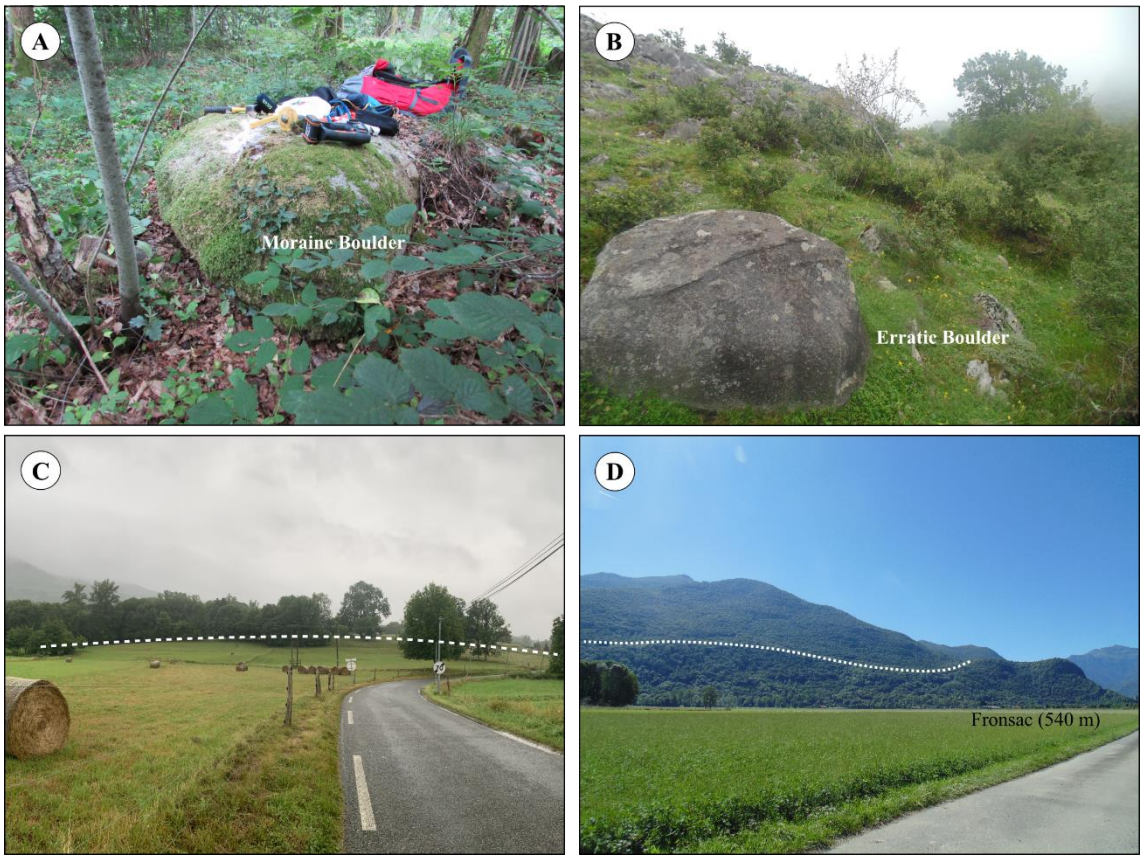


Figure 1.9. Examples of glacial deposits distributed in the LBBB and valley sides of the Upper Garonne basin: A) moraine boulder at the innermost ridge of the external moraine system (1a); B) igneous erratic boulder lying on limestone outcrop near Izaourt village; C) La Serre moraine; D) moraine crest from the 1b moraine complex at the right valley side near the Fronsac Village, 9 km upvalley from the LBBB.

1.b. The internal moraine system is composed of a series of ridges across the innermost part of the LBBB and at the valleys sides of the glacial catchment, from 550 to 820 m. In this system, two sets of discontinuous arches and ridges define the palaeoglacier limits on the frontal and lateral margins. From north to south, at the LBBB floor, SE from the Seilhan Village, there is the most preserved lobate crest – La Serre arch (Boule, 1895) – easily identified by the topography due to its 30 m high (491 m); it was called by previous authors the Camarroux or Labroquère moraine (Denizot, 1922; Pic, 1933). This moraine stretches until the basin's margins, reaching the foot slopes of the hills (Fig. 1.9-C). It closes the distal part of the Barbazan Lake on the east side and ends south of St-Martin on the west side. Here, this moraine is cut by the Garonne River at the Borde de Garonne. The same happened to two other moraine crests between Valcabrère and Loure-Barousse villages, previously called Barbazan-Coumanié-Labroquère moraine (Andrieu et al., 1988). This two-crest moraine closes the proximal part of the Barbazan Lake and is the innermost moraine of the LBBB. From the exit of the LBBB upvalley, there are lateral moraines on the valley sides located 7 km south from the innermost moraine (Fig. 1.9-D). Some rare boulders are embedded in the moraines between 580 to 800 m at the left

margin (Sost and Ferrère villages) and 530 to 780 m at the right side (Lourde, Saint-Pé-d'Ardet and Génos villages).

1.c. Some authors have also ascribed the moraines existing in the lowest glacial cirques of the upper valleys to this phase. This is the case of the moraines located in the Corilha ravine at 1800-2000 m, right margin of the main Garonne Valley, where a small frontal moraine is preserved (Martí-Soler, 1988). However, these assumptions are yet to be demonstrated.

Following the abandonment of these moraines, the Garonne palaeoglacier retreated upvalley from the LBBB and valley sides position. This retreat was interrupted by glacial advances that developed moraines in the upper tributaries, forming four other moraine complexes (Fernandes et al., 2017):

2. Phase 2 - Moraine systems on the mountains slopes and high valleys (ca. 1000-2100 m; Fig. 1.10).

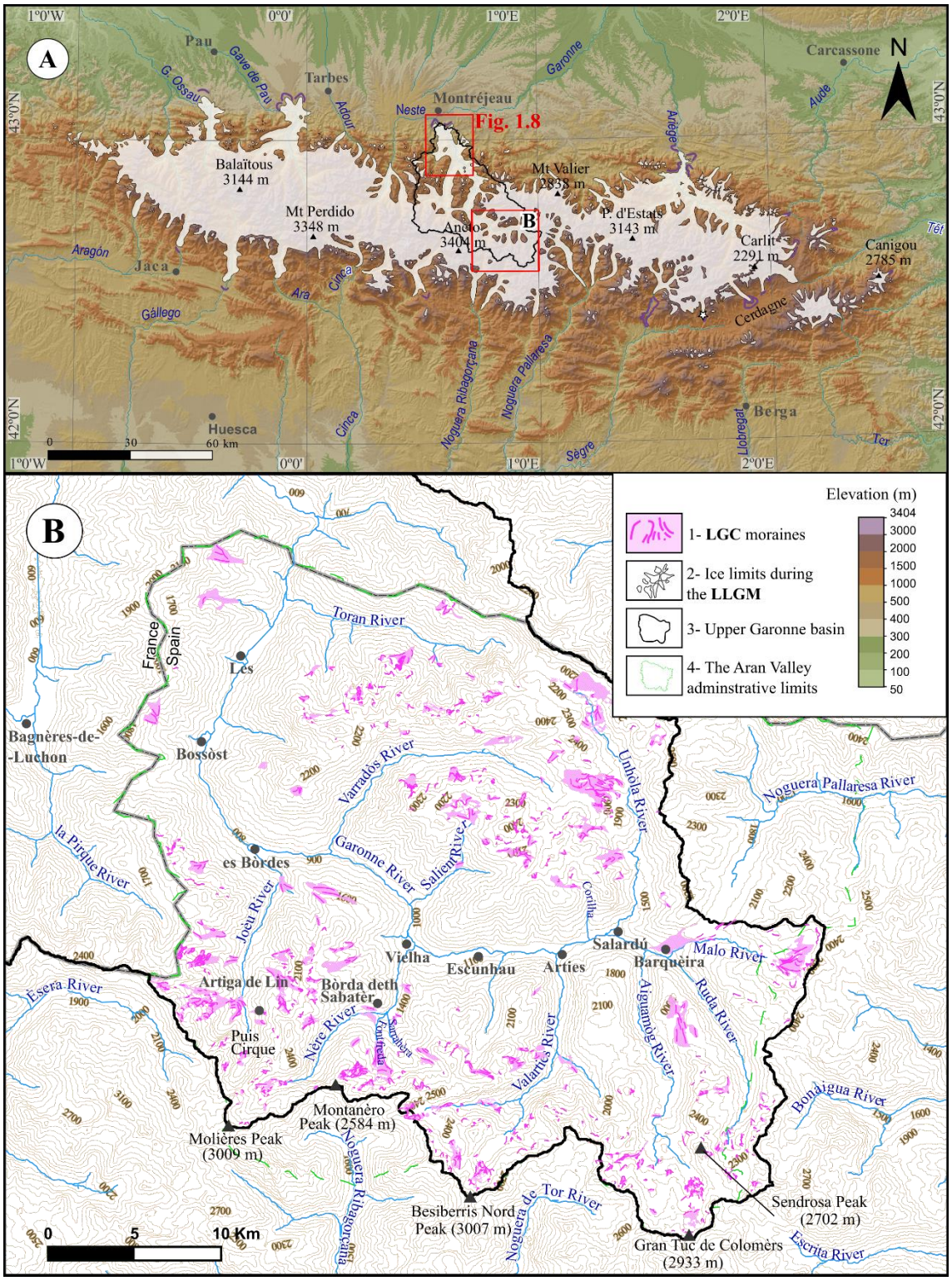


Figure 1.10. Distribution of glaciers during the MIE in the Pyrenees (A; adopted from Delmas et al., 2022c), along with the moraine deposits in the highest tributaries of the Upper Garonne basin (B).

2.a. In the northern tributaries, there are frontal and lateral moraines located within the valleys that represent the valley glacier phase. At the left margin of the Nère Valley, there is a lateral left moraine at 1340 m called Bòrda deth Sabatèr moraine and a latero-frontal moraine stretching from 1620 to 1950 m in Fontfreda lateral catchment (Bordonau, 1985). In the Joèu Valley, there are two overdeepened basins where one frontal moraine and one

lateral moraine develop at 1440-1460 m near Artiga de Lin (Bordonau, 1985; Fig. 1.11-A). In the main Garonne Valley, a considerable proportion of subrounded granite boulders within the poorly sorted sandy matrix occur between the Escunhau Village, at 1000 m, and the Baqueira resort, at 1850 m, implying glaciers with 23-12-km-long (Fernandes et al., 2017). In this deposit, clear crests only occur at the upper section of the deposit, in the Beret plateau. The distribution of these moraines implies that the lower moraine near Escunhau was formed by a glacier fed from the Unhòla, Ruda, Aiguamòg and Valarties valleys. In contrast, during the formation of the upper moraine at the Beret plateau, glaciers were already disconnected from the main Garonne Valley.

2.b. At the upper part of the high valleys, there are frontal and lateral moraines distributed across the valley bottom. In the Ruda Valley, frontal moraines are found down to 2050 m (e.g. Bacivèr and Ruda valleys), immediately below the glacial cirques, and suggest the occurrence of a glacial phase with 2.6-4.5-km-long glaciers (Fernandes et al., 2017). Similarly, in the Unhòla Valley, a moraine at 2080 m was documented in the south-facing Liat basin (Martí-Soler, 1988; Fig. 1.11-B).

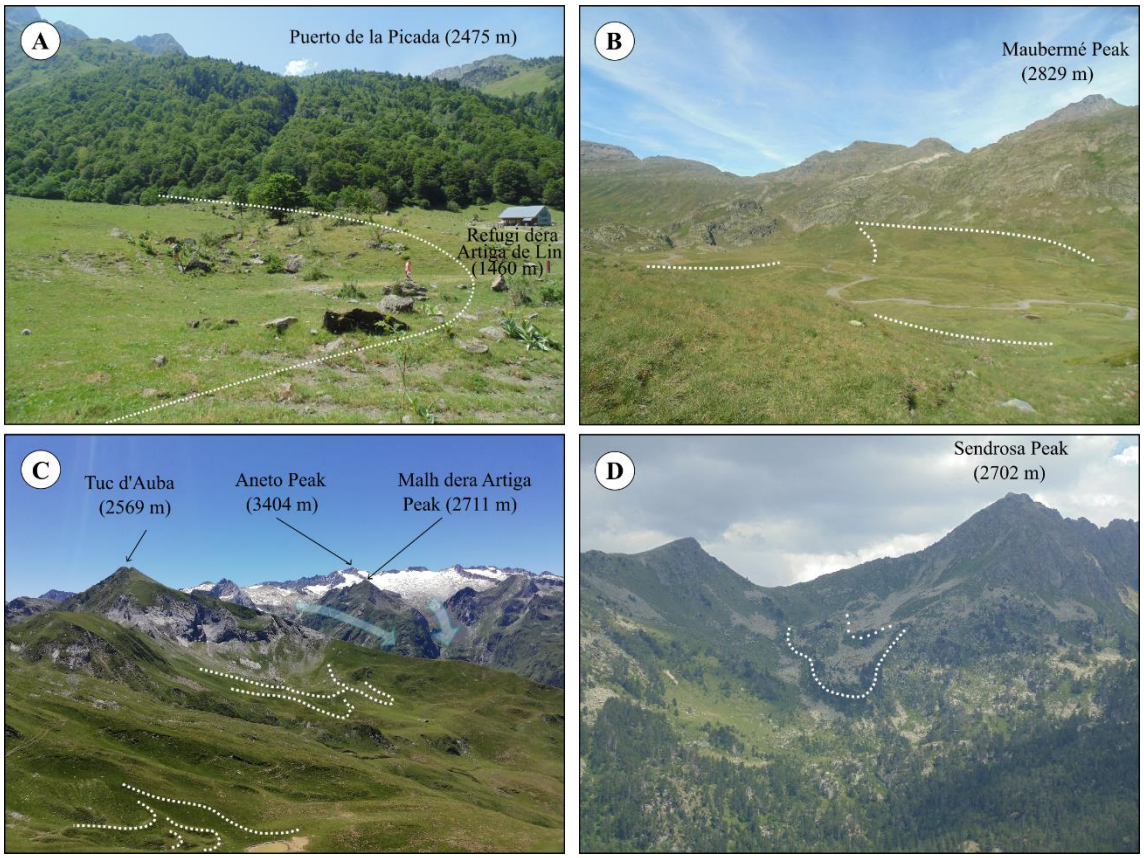


Figure 1.11. Examples of glacial deposits distributed across the valleys and cirques of the Upper Garonne basin: A) moraine crest from the 2a moraine system at Artiga de Lin, Joèu Valley; B) Moraine system 2b at Liat basin, Unhòla Valley; C) view to the Aneto Peak facing the Auba cirque where two moraine systems are preserved in the Joèu Valley from the moraine complex 3. This picture C also shows two arrows evidencing the transfluence of glacial ice from the Ésera catchment into the Garonne basin during the MIE; D) moraine system 3b closing a rock glacier within the NW glacial cirque at the foot of the Sendrosa Peak.

3. Phase 3 - Moraine systems within the glacial cirques (above 2100 m).

3.a. In low glacial cirques with peaks at 2600 m, other documented moraines are located in altitudes of ca. 2200 m. These are the cases of the Sarrahèra cirque, at 2150 m, Montanèro cirque, at 2250 m, and Sèrra des Neres cirque, at 2350 m, in the Nère Valley, Puis cirque, at 2000 m, in the Joèu Valley (Fig. 1.11-C), and in the Samont Peak, at 2250 m, in the Salient Valley (Bordonau, 1985; Martí-Soler, 1988).

3.b. In glacial cirques with summits above 2700 m, several moraines were mapped above 2400 m, which are indicative of ancient small cirque glaciers (Fernandes et al., 2017). This is the case of the Sendrosa cirques (Fig. 1.11-D), where moraines are located at 2450-2500 m in the eastern and western cirques.

3.c. In the peaks exceeding 3000 m, unvegetated moraines with fresh surfaces occur at elevations between 2500 and 2800 m. This is mainly the case of Maupas and Perdiguero, where moraines located at 2580 and 2730 m are preserved next to the cirque walls or below the current glaciers (Paris et al., 1970). In the small hollows of the headwaters of Valarties and Aiguamòg valleys, there are moraines at ca. 2500-2700 m within the Colomèrs and Besiberri cirques (Serrat et al., 1994).

### 1.3.3. Erosional landforms

Alongside the previously described glacial deposits, erosional landforms also confirm the occurrence of widespread past glacial dynamics in the Upper Garonne basin (Fig. 1.12). At the bottom of the valleys, erosional imprints are mainly shown as overdeepened basins and U-shaped valleys (Bordonau, 1985; Fernandes et al., 2017; Lopes et al., 2018; Martí-Soler, 1988; Serrat et al., 1994). The largest overdeepened basins likely reflect intense glacial carving during the coldest phases of the different Late-Pleistocene glacial cycles. These are the cases of the LBBB, Marignac, Arlos, Fos, Bagnères-de-Luchon, Les, Bossòst and Vielha, located from 400 to 1000 m. On the other hand, at the highest tributaries, there are well preserved glacial cirques, hanging valleys, *roche mountonées*, striations, subglacial channels, and *riegels*. In the Aran Valley, 119 glacial cirques mainly NE-oriented, with altitudes of the cirque floor at 2200-2400 m were mapped (Lopes et al., 2018; Serrat et al., 1994). The analysis of the distribution of these landforms showed their formation, characteristics and that they are intimately controlled by lithology (Lopes et al., 2018). Indeed, glacial cirques in soft lithologies (e.g. as schists, sandstones, slates) tend to be strongly carved, whereas others in hard rocks (e.g. marble and quartzite) show a poorer development (Martí-Soler, 1988).

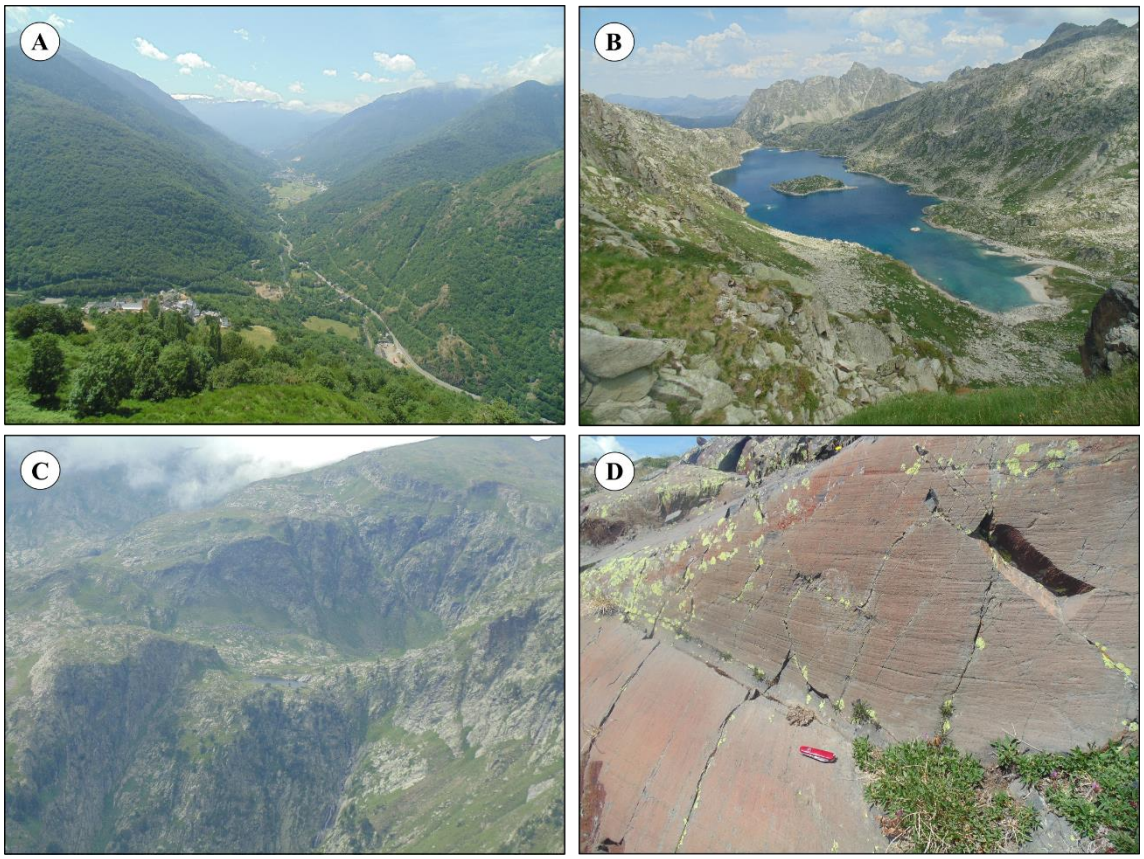


Figure 1.12. Glacial erosional features in the highest valleys of the Upper Garonne basin: A) and B) overdeepened basins near the Les Village filled with Quaternary sediments and waters at the Estany de Mar (headwaters of the Valarties Valley), respectively; C) *riegel* closing a glacial cirque at the Sèrra de Pica Palomera, Varradòs Valley; D) striations on slates indicating subglacial flow at the Maubèrme cirque, Unhòla Valley.

Up to the present study, no detailed geomorphological map in the Upper Garonne basin includes the distribution of the glacial deposits and erosional landforms of glacial origin. Such mapping of the broad spectrum of landforms generated during and glacier presence will be assessed in this dissertation. The Paper 1 of this dissertation will be dedicated to introduce the results of the geomorphological map of the Aran Valley at the scale 1:25000. Finally, this information supports further geochronological reconstructions of glacial and post glacial dynamics and can also be beneficial to spatial planning purposes.

# 2. Chronology and uncertainties of the glacial response to climate variability in the Pyrenees during the Mid-Late Pleistocene

## 2.1. Introduction

The Quaternary (last 2.6 Ma) was the period with the most significant planetary changes in the last 60 Ma (Bradley, 2015). After the final closure of the Panama seaway by ca. 2.7 Ma, the geological history of the Earth since the onset of the Quaternary was marked by repeated climatic fluctuations including glacial and interglacial cycles with a periodicity of ca. 41-ka during the Early Pleistocene (2.6-0.8 Ma) and 100-ka during the Mid-Late Pleistocene (Ehlers et al., 2018; Haug and Tiedemann, 1998; Hughes and Gibbard, 2018). Largely triggered by orbital dynamics, the occurrence of these cycles forced global impacts that included major changes in the atmosphere, oceans, land and vegetation (Benn and Evans, 2010; Ruddiman, 2006). During the cold cycles, the low insolation reaching high latitudes and efficient water vapour supply from the ocean determined the reduced energy available on Earth and the subsequent growth of the Northern Ice Sheets (Haug et al., 2005; Hays et al., 1976). The larger ice masses and sea ice expansion caused high albedo that amplified the cooling trend and forced atmospheric readjustments: the anticyclones over the North polar region were enhanced and the polar front migrated towards lower latitudes (ca. 40º); moisture availability was reduced and wind fluxes loaded with considerable amounts of dust (10x higher than the present day) were reinforced (Chylek et al., 2001; Lambert et al., 2008). Such atmospheric reorganisation, mainly driven by SST reduction, also involved impacts within the Tropics through the shrinking of the Intertropical Convergence Zone in 3º latitude (from 30º to 27º in the north and south Hemispheres) and the weakening of the Asian Monson (Chylek et al., 2001; Rind, 2009). During this phase, there was a reduction of the AMOC – responsible for heat transport to Europe – trapping $CO_2$ in the Southern Hemisphere (see Palacios et al., 2021). These colder conditions also limited biomass production and reduced the vegetation cover over the continents (Sánchez-Goñi, 2022a). This positive feedback cascade ended during the MIE that coincided with the minimum sea level dropping about 100-130 m (Clark et al., 2009). During the MIE of glacial phases, global temperatures lowered by ca. 8-10 ºC, covering 30% of the Earth's surface with ice, mostly over the high latitudes and mountain ranges. *Sensu lato*, this global scenario that occurred successively 41 times over the Pleistocene with more or less intensity, was interrupted by the Terminations (or Deglaciations) and subsequent occurrence of Interglacials, such as the current one (Ehlers et al., 2011).

The distribution of glaciers during the glacial cycles was controlled by the combination of temperature and precipitation, which are largely determined by latitude, altitude and proximity

to the ocean (Benn and Evans, 2010). During the MIE of each glaciation, glaciers reached the sea level in the polar regions (Ehlers et al., 2018). In contrast, in low-latitude mountain ranges, they may have stayed above 3000 m, and in Mediterranean mountains glaciers extended over elevations of 1000 to >3000 m (Hughes and Woodward, 2017; Fig. 1.13). In fact, Mediterranean glaciers were highly sensitive to Late Pleistocene climate oscillations, responding synchronously to a reduction in temperature (as it occurred globally) but asynchronously to precipitation shifts (Hughes et al., 2022). In addition, the wide spectrum of orientation and altitudes in the Mediterranean mountain ranges influences the distribution of moisture derived from the predominant winds, which conditioned a large variety of glacial systems, sizes and termini (Oliva et al., 2022c); i.e. those glaciers facing the cold north slopes tended to be larger than those facing the sunny south slopes.

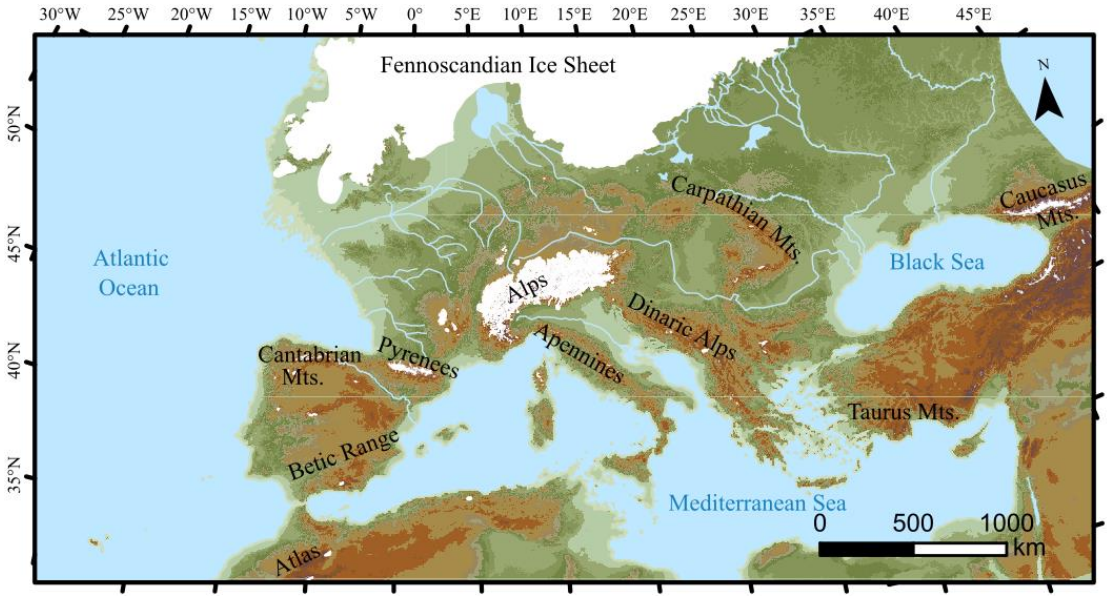


Figure 1.13. Simplified model of glacier distribution during the GLGM in Europe (Becker et al., 2015).

One of the current scientific challenges in glacial reconstruction is to track evidence from glaciations older than the LGC (Hughes et al., 2022). The high marine sedimentation rates (10-20 cm/1 $ka^{-1}$) at the bottom of the margin of the Iberian Peninsula allowed the most detailed reconstructions of glacial cycles in the North Hemisphere (Martrat et al., 2007). This natural archive allows assessing direct glacier discharges since the onset of the Quaternary by identifying IRD transported by icebergs (Ehlers et al., 2018). By contrast, in the continents, the impact of mountain glaciations can be studied by direct surveys based on geomorphological features, although it is essentially applied to the LGC and previous glacial phases are much less studied. In the mountains surrounding the Mediterranean basin, the oldest glacial evidence ever dated allowed to infer glacial advances during the MIS 14, 12, 10, 8, 5d-2 (Adamson et al., 2013). However, as glaciers during the MIE of the last glaciation reached similar positions to previous glacial phases, most sedimentary and erosive records have been erased and only a few older

remnants are still preserved mainly outside their margins (Hughes et al., 2020). The timing of the glacial evidence has been defined based on dating techniques ($^{14}$C, cosmic-ray exposure, optically stimulated luminescence, among others) that allowed constraining chronologically their period of formation during the Mid and Late Pleistocene (Hughes and Woodward, 2017). In order to correlate with the chronology of other mountain ranges in the Iberian Peninsula, glacial cycles discussed in this dissertation follow the climatostratigraphic system of the MIS, which defines boundary events, including glacial expansion periods (Vázquez-Riveiros et al., 2022).

## 2.2. Geographical and climatic factors controlling the glaciations in the Pyrenees

During the GLGM, about 60 x $10^6$ km$^2$ of glacial ice covered the surface of the North Hemisphere (24%). Most of it corresponded to two ice masses: the Laurentide Ice Sheet in America, and the Scandinavian Ice Sheet in Europe (Benn and Evans, 2010). Sourced in snowy areas, these ice sheets flowed southwards reaching 40º and 50ºN, respectively. Such differences between the Laurentide and Scandinavian Ice Sheets showed the importance of heat transport from the Gulf Stream to explain reduced dimensions of glaciers in Europe (Oliva et al., 2022c). The altitude of the Pyrenees at 42º N allowed the development of an ice field that represented the double (ca. 7600 km$^2$) of all Iberian glaciated area (Oliva et al., 2022c). In this sense, the 250-km-long main ice field formed a spatially unique ice mass, situated in the transition between the Northern Ice Sheets and the isolated ice-cap domes, or singular valley glaciers, common in the Southern Mediterranean mountains (Adamson et al., 2013; Benn and Evans, 2010; Hughes et al., 2006).

The Pyrenees are the European smallest land area dividing the Atlantic Ocean and the Mediterranean Sea, thus constituting a unique place to preserve evidence of the past dynamics of both basins connected by the Gibraltar Strait. Besides the maritime influence, the mid-latitude position of the Pyrenees, aligned with the current westerlies corridor, allows recording shifts in the position of the subpolar cyclone and of the Azores anticyclone, which influence the position of the polar front (Hughes and Woodward, 2017). Glacial simulations during the GLGM have shown that the Pyrenees constitute one of the best places to study climatic shifts during the Quaternary, namely the position of the westerlies or polar front (Višnjević et al., 2020). Finally, alongside the importance of the Pyrenees to glacial surveys during the Quaternary, this range also contributed as biotic refuges to further colonisation of the Northern Europe during the interglacials (Hewitt, 2000).

During the Late Pleistocene maximum ice extension, the Pyrenean ice field included an interconnected glacial system composed of piedmont and valley glaciers (Calvet et al., 2021). At the upper lands, however, glaciers were divided by peaks and ridges protruding above the ice

(nunataks), with some cols holding glacier transfluences. This was the example of the Malh dera Artiga in the headwaters of Joèu Valley, from where the Maladeta glacier projected two glacier tongues into the Garonne catchment (Fig. 1.11-C). This system of sinuous glaciers was much more complex in the northern valleys where ice thickness facilitated the glacier's interconnection between different basins. The northern valleys represented 2/3 of the Pyrenean ice field, showing a strong asymmetry between slopes (Calvet et al., 2011b). In the Northern and Western Pyrenees, glaciers reached 50-80-km in length with 600-800 m of thickness, forming perfect U-shaped valleys (Oliva et al., 2019). On this slope, glacier fronts reached 300-400 m a.s.l., developing piedmont moraines in the biggest valleys where the ELA was located at 1200-1600 m (Delmas et al., 2022c; Taillefer, 1952; Table 1.2). On the other hand, in the eastern and southern face of the range, glaciers were confined in their upper catchments to a length of 10-40 km, with their terminal moraines at 700-900 m. The low glacial incision was also marked by the higher ELA at 2100-2200 m and by thin glaciers that had one of the world's lowest glacial erosion rates (Hérail et al., 1987, Calvet, 2004; Calvet et al., 2021, 2011b, 2011a; Delmas et al., 2022b, 2022c, 2022a, 2009). The N-S gradient in the Pyrenees has been in place since, at least, the end of the LGM, as shown by palaeoglaciological reconstructions (Reixach et al., 2021). It is worth mentioning that smaller massifs and valleys were also glaciated outside the main ice field, such as the Carançà, Cadí, Canigó, Madrès, or Tabe, in the Eastern Pyrenees, or Ori, in the Western margin (Fig. 1.4).

Table 1.2. Main characteristics of the largest Late Pleistocene glaciers of the Pyrenees.

| | Basin | Nearest settlement | Glacier length (km) | Alt. of the glacier front (m) | First significant reference |
|---|---|---|---|---|---|
| Northern valleys | Ariège | Foix | 65 | 380 | Taillefer (1977) |
| | Garonne | Loures-Barrouse | 78 | 440 | Goron, (1941) |
| | Gave de Pau | Lourdes | 53 | 370 | Taillefer (1948) |
| | Gave d'Ossau | Arudy | 38 | 370 | Taillefer, (1948) |
| Southern valleys | Valira | Sant Julià de Lòria | 43 | 770 | (Turu, 1994) |
| | Noguera Pallaresa | Sort | 63 | 700 | Martí-Bono and García-Ruiz (1994) |
| | Noguera Ribagorçana | Villaler | 26 | 930 | Vilaplana (1983) |
| | Ésera | Bisaurri | 38 | 860 | Martínez De Pisón (1989) |
| | Ara | Sarvisé | 38 | 755 | Martí-Bono and García-Ruiz (1994) |
| | Gállego | Sabiñánigo | 43 | 800 | Martí-Bono and García-Ruiz (1994) |
| | Aragón | Castiello de Jaca | 25 | 880 | Llopis-Lladó (1947) |

The Pyrenees are currently the westernmost glaciated range in Europe due to the extensive land surface situated above 2500 m (1409 km$^2$) and the high Atlantic precipitation reaching 3000 mm in the wettest western areas (García-Ruiz and Serrano, 2022). Despite its southern position, the Pyrenees still host 19 glaciated massifs, with small ice masses mostly

located in north-exposed cirques under peaks of >3000 m (Rico et al., 2017). The Pyrenees are currently affected by the regional asymmetries of sharp N-S gradients dictated by the W-E alignment of the range to the predominant winds. These winds condition the snow source and accumulation. The smooth W-E gradient is influenced by the vicinity of the Atlantic Ocean and the Mediterranean Sea (Calvet et al., 2021; Oliva et al., 2019; Taillefer, 1952). This interface results in a dichotomy between the Atlantic valleys – colder (10 - -2.5 ºC; <2000 h/year of sunshine) and wetter (1800-3000 mm; <125 rainy days) – and the Mediterranean valleys – warmer (12.5 - 2.5 ºC; 2750 h/year of sunshine) and drier (1000-1400 mm; >150 rainy days) (1971-2000; Herrera and Serrão, 2011). Besides that, there is also a W-E gradient across the Axial Zone of the Pyrenees, as suggested by the climate data from stations located above 2200 m, such as Bonaigua (Central Pyrenees: MAAT of 3 ºC and annual precipitation of ~1100 mm) and Malniu (Eastern Pyrenees: MAAT of 5 ºC and annual precipitation of ~1000 mm) (series 2000-2019; *Servei Meteorològic de Catalunya*: https://www.meteo.cat/). Remarkably, it should be highlighted that in some areas along the Central Axis, air masses penetrate trough depressed zones (such as cols below 2000-2200 m) allowing to extend the Atlantic-climate influence to the southern valleys and *vice versa* (Delmas et al., 2022c).

## 2.3. Mid-Late Pleistocene glaciations in the Pyrenees

### 2.3.1. Introduction

Only a few proxies showed that the Pyrenees were glaciated during the Mid-Late Pleistocene (i.e. older than MIS-4/2). Ground-breaking studies based on the speleothems from the Niaux-Lombrives-Sabart caves (Ariège catchment), showed the possibility of previous glaciations from the LGC, as they showed several periods of karst stability during the MIS-16, MIS-14, MIS-8, MIS-6, MIS-4 and MIS-2, intercalated with reactivation during interglacials (Bakalowicz et al., 1984; Sorriaux, 1982). Notwithstanding this work ending the debate among monoglacialists and polyglacialists, no robust chronology emerged from direct glacial features in order to validate these glacier advance hypotheses.

### 2.3.2. Glaciations prior to the Last Glacial Cycle

The PGC occurred between ~190 and 130 ka (i.e. MIS-6 Hughes, 2022), and its global maximum took place during the highest values of dust, recorded in Antarctica at 140 ka, when the lower deuterium-derived temperature was ca. 10 ºC lower than the current values (Colleoni et al., 2016; Lambert et al., 2008; Martrat et al., 2007). The PGC is known to have been the most massive glaciation during the Quaternary in Northern Europe, as suggested by the position of the glaciers during its maximum (Hughes and Gibbard, 2018). This extensive MIE was, possibly, driven by warmer North Atlantic temperatures (SST of 15.6 ºC), when compared to MIS-2 (11.2 ºC), which provided more moisture to grow the glaciers (Colleoni et al., 2016; Hughes and

Gibbard, 2018; Naafs et al., 2013). However, most of the glacial evidence from the PGC was erased because of the glacier erosion during the LGC; this is the case of the Northern Hemisphere Ice Sheets and the eastern part of the Mediterranean basin (Romania, Turkey) where glacial evidence from the Mid Pleistocene is absent (Hughes, 2022). On the contrary, these landforms are still preserved in the Western Mediterranean; thus, the Pyrenees are a preferential range to study such periods (Hughes et al., 2022). The available chronologies showed that the MIE of the Northern Ice Sheets (Laurentide and European) were synchronous during the PGC, as it was for the last four glaciations. However, the external moraines in the mountains from the Southern Europe were formed by glacial advances previous to the global maximum of each glacial cycle (Hughes et al., 2022). This asynchronism is called local maximum.

For more than ca. 100 years, researchers have tried to find a consensus on the glacial limits and their respective chronology in the Pyrenees. The pursuit of evidence of glacial activity before the LGC was done essentially through the identification of direct or indirect glacial landforms with traces of older ages, such as: i) composition, comparison of the altitude and weathering degree of glaciofluvial terraces above the riverbed; ii) relative position, weathering degree and soil development on top the most external moraines in the terminal basins (Leymerie, 1881; Boule, 1895; Penck, 1883; Penck and Brückner, 1909; Mengaud, 1910; Depéret, 1923; Panzer, 1926; Faucher, 1937; Goron, 1941; Llopis-Lladó, 1947; Fontboté, 1948; Alimen, 1964; Hubschman, 1984). By the end of the XX century, Jacques Hubschman and Michel Icole – supported by the weathering state of such features in distal and proximal positions at the terminal basins – proposed a model of development of the glaciofluvial terraces and moraines during the Penultimate Glaciation (Hubschman, 1975a, 1984; Icole, 1974). The onset of the radiometric studies allowed to reinforce that hypothesis by the pivotal study on speleothems dated by U-Th, which suggested that during several glacial phases, the Ariège palaeoglacier blocked the entrance to the Niaux-Lombrives-Sabart cave (Bakalowicz et al., 1984; Sorriaux, 1982; Sorriaux et al., 2016). In the same catchment, the glaciofluvial terrace (T2), seated next to Foix, was correlated with glacial evidence 50-100 m above the LLGC moraines and ascribed to the MIS-6 (Delmas, 2011; Hubschman, 1975a, 1975b, 1975c). This glacial evidence was described as a degraded deposit where an erratic boulder resting near Caraybat yielded a $^{10}$Be exposure age of 122.2 ± 4.9 ka (recalculated to 133.9 ± 5.3 ka by Delmas et al., 2022b). The only radiometric study based on PGC moraines in the Pyrenees was carried out in the most external moraine of the Aragón catchment, on the southern slopes of the Pyrenees, where the application of OSL yielded an age of 171 ± 22 ka (MIS-6) (García-Ruiz et al., 2013). Other dating techniques were applied to track the glacial dynamics, such as the ESR in glaciofluvial terraces. In the Têt catchment, the deposition of the glaciofluvial terrace T2 occurred during the MIS-6, as showed ESR burial dating near Escatllars at 174 ± 44 ka (Delmas et al., 2018). In Aragón, the glaciofluvial terraces at 60

and 20 m above the riverbed related to two main frontal moraines (M1 and M2) were, respectively, ascribed to the last two glaciations (Panzer, 1926 and thereafter). Notwithstanding, the burial ages validated the initial proposal to the M2 (68 ± 7 ka), the oldest 60-m terrace was deposited by 263 ± 21 ka (MIS-8?) and the M1 by 171 ± 22 ka (MIS-6), suggesting different periods of deposition (García-Ruiz et al., 2013). In the parallel catchments of Cinca and Gállego rivers, robust OSL datasets helped to reconstruct glacier outwash dynamics by dating the Sabiñánigo glaciofluvial terrace at 46-72 m above the riverbed, by 151 ± 11 ka, and the Belver glaciofluvial terrace at 178 ± 21 ka, respectively (Lewis et al., 2009; Peña-Monné et al., 2004). In spite of no solid direct chronological datasets available from the PGC, several erratic boulders and till deposits several km outside the limits of the LGC glacial limits have already been documented (García-Ruiz and Serrano, 2022; Salvador-Franch et al., 2022; Ventura and Turu, 2022). The isolated ages from glacial landforms and high uncertainty range hampers a solid interpretation of the PGC in the Pyrenees, a gap this dissertation tries to solve.

In the Upper Garonne basin, following the ancient chronostratigraphic assumption of the four Quaternary glaciations – Günz, Mindel, Riss, Würm (Penck and Brückner, 1909) – researchers strived to find similarities between glaciofluvial terraces and moraines from the Alps and the Pyrenean ranges and ascribing them a glacial period. However, the application of this chronological model in the Pyrenees was not conclusive in Penck's work (1883). Further detailed analyses of the terminal basin allowed better assumptions based on relative criteria (morphological, palaeontological and archaeological) albeit with little consensus about the oldest glaciations. The Günz (MIS-16?) and Mindel glaciations (MIS-12/MIS-10?) in the terminal basin were ascribed to glaciofluvial terraces 4 and 3 with no connection to moraines (Alimen, 1964; Paris et al., 1970). The first is the T4, which is located 80 m above the riverbed, almost without crystalline boulders and a pH of 5; whereas the second is the T3 has a pH of 6-7 within a reddish palaeosoil (loess deposit) on top of the 60 m high terrace (Icole, 1974; Fig. 1.8). In T2, research pioneers were not able to connect this feature with external moraines, as shown by the conservative position of the Boucoulan moraine whose relation to a pre-LGC glaciation is vaguely considered (Boule, 1895; Pic, 1933; Goron, 1941). Such interpretation was readjusted by attributing various external moraine ridges of the basin floor between the St-Martin and Jaunac villages to older glaciations (Fig. 1.14; Chaput, 1924; Denizot, 1922; Depéret, 1923). This hypothesis was assessed through pedological surveys on soil profiles and weathering indicators in glaciofluvial terraces and moraines (Cavaillé, 1953; Hubschman, 1984, 1975a; Icole, 1974). However, the current absolute dataset based on the Barbazan sedimentary sequence showed only LGC ages (Andrieu, 1991a).

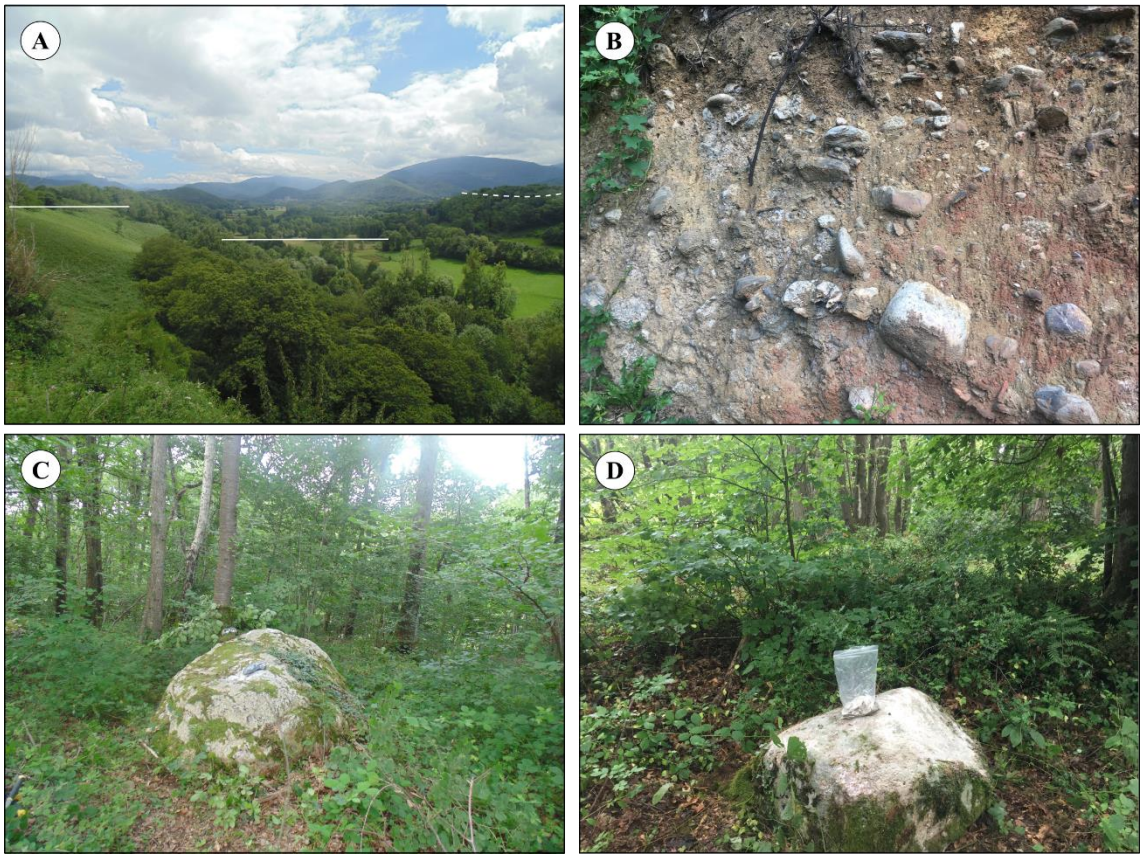

Figure 1.14. Examples of different geomorphological features in the LBBB: A) Glaciofluvial terrace on the right side of the Garonne River; B) open section in exposed till, 2 km north from Seilhan likely correlated with the moraines of the PGC; C) and D) scattered boulders on the moraine crest correlated with the external moraine system (1a) near the Saint-Martin and Jaunac, respectively.

### 2.3.3. The glacial advance during the Local Last Glacial Maximum

The beginning of the LGC started with the end of the Eemian (MIS-5e) at 115 ka and ended before the current interglacial, at 11.7 ka (Palacios et al., 2022). During the transition between the MIS-5 and 4 (ca. 71-60 ka), the reduced summer insolation in boreal regions and low $CO_2$ concentrations entailed glacial inception (Ganopolski et al., 2016). Such favourable conditions for glacier growth led glaciers to develop in some mid-latitude mountains, reaching their MIE before the GLGM (Hughes and Gibbard, 2018; Sánchez-Goñi, 2022a). In fact, the LLGM is commonly attributed to the last maximum in the mid-latitude mountains of the Northern Hemisphere (Gillespie and Molnar, 1995; Thackray et al., 2008). The general cooling continued throughout the MIS-4 and 3 (ca. 60-30 cal ka BP) causing the sea level to drop 80 m in relation to current levels (Waelbroeck et al., 2002). In spite of the general cooling, the superimposed temperature variability was marked by rapid events of temperature increase (interstadials) and decrease (stadials). Throughout this unstable phase, episodes of colder temperatures (12-16 ºC of SST reduction) named Heinrich Events (HE) were linked with several episodes of iceberg discharges every 10-7 ka (Sánchez-Goñi and Harrison, 2010). These episodes were intercalated by warming episodes named Dansgaard-Oeschger Events (D-O) characterised by an initial temperature rise of SST 8-16 ºC and followed by a cooling (Sánchez-Goñi et al., 2008). In the

Mediterranean Region, the reconstructions of vegetation from deep-sea sediments showed considerable shifts during these periods; forests developed south of 40ºN during the D-O events, while herbaceous open landscapes prevailed during the HE (Sánchez-Goñi, 2022a). In the offshore of the Iberian Peninsula, SST derived from planktonic foraminifera during these events oscillated between 4 and 16 ºC (Martrat et al., 2007, 2004; Sánchez-Goñi et al., 2013).

In general, the considerable inputs of freshwater by iceberg discharges onto the North Atlantic Ocean precluded the heat from reaching northern latitudes and forced temperatures to decrease in North Europe (Sánchez-Goñi, 2022b). This context brought the most favourable conditions to positive mass balances and glacial development in the Iberian mountains before the GLGM (Moreno et al., 2012b). In the Pyrenees, the MIE occurred asynchronously during the MIS-4 and 3 where several moraines constrain the LLGM at 65-55 ka in the Central Pyrenees and at 45-30 ka in the Eastern Pyrenees (Oliva et al., 2019). The book European Glacial Landscapes dedicated one of the review chapters led by Delmas et al. (2022b) to the glacial evidence before the GLGM. This scientific work allowed us to easily understand the importance of ice-marginal fluvio-lacustrine deposits behind the internal moraines of the terminal basins; the sediments collected were dated by means of $^{14}C$ showing the timing of sediment accumulation after the glaciers retreated. This proxy shows the onset of the glacial retreat and the subsequent palaeoenvironmental evolution and suggests the closest period to the moraine formation to have been between 48.3-39.7 and 34.2-29.7 cal ka BP in the northern valleys (Andrieu, 1987; Andrieu et al., 1988; Jalut et al., 1988; Mardones and Jalut, 1983) and between 35.6-34.6 and 25.9-24.2 cal ka BP in the southern ones (García-Ruiz et al., 2003; Montserrat-Martí, 1992). In spite of this radiometric method suggesting a minimum age for the glacial advance, it has inherent limitations, such as: i) the impossibility of yielding older ages than the MIS-3; ii) overestimated ages by hard water effect from underlying mineral carbon contamination (Pallàs et al., 2006); iii) unknown time between the moraine formation and the onset of sediment accumulation at the proglacial lake.

In the beginning of the 21$^{st}$ century, OSL dating allowed to constrain chronologically well-sorted sediments in glaciofluvial terraces from glacial outwash from older glaciations than the GLGC (Peña-Monné et al., 2003; Lewis et al., 2009; García-Ruiz et al., 2013). One of the most complete examples comes from the Gállego Valley, where OSL results suggest the outermost Aurín moraine formation by 85 ± 5 ka; it was succeeded by the formation of the middle Sabiñánigo glaciofluvial terrace (preserved downvalley; Fig. 1.1) at 68 ± 7 ka; and finally the formation of the Senegüé moraine (2 km upvalley) before 36 ± 3 ka, as postglacial dynamics in the upper tributaries occurred during this age (Peña-Monné et al., 2003; Lewis et al., 2009; Guerrero et al., 2018).

During the last decade, CRE dating techniques have helped geomorphologists to move forward the chronological history of the Pyrenees in a significant way (Table 1.3); this method allowed to infer the timing when glacier retreat exposed a rock surface (sediment or outcrop). Furthermore, this method was applied to study the glacial phases during the LLGM (i.e. external moraines), mainly in the Eastern Pyrenees. This is the example of the Ariège basin, where an erratic boulder at the altitude of the LLGM moraine and the boulder on the LLGM moraine yielded a recalculated exposure age of 87.4 ± 4 ka (original age = 79.9 ± 14.3 ka; Delmas et al., 2011, 2022b). Similar ages were detected in the Malniu catchment, where moraine boulder ages were recalculated to 84.2 ± 2.2 and 52.2 ± 1.4 ka (original age = 76.5 ± 2.0 and 49.2 ± 1.3 ka; Pallàs et al., 2010; Delmas et al., 2022a). The scattering of the ages suggests that several glacial advances reached similar positions and created a polygenic moraine. Finally, SHED measurements calibrated with CRE ages performed in the moraines of the Têt basin confirm exposure ages during the MIS-3 glacial advance by 40.9 ± 1.1 ka (Tomkins et al., 2018).

Table 1.3. Glacial setting and available ages for the LLGM in the Pyrenees (adapted from Delmas et al., 2022a).

| | Basin | ELA during the LLGM (m) | Chronology (ka) | Method | Significant reference |
|---|---|---|---|---|---|
| Northern valleys | Ariège | 1600-1800 | 87.4 ± 4 | CRE* | (Delmas et al., 2011) |
| | Garonne | 1500-1600 | 40.7-32.3 cal BP | Radiocarbon ($^{14}$C)** | (Mardones and Jalut, 1983) |
| | Gave de Pau | 1400-1500 | 48.3-39.7 cal BP | Radiocarbon ($^{14}$C) | (Andrieu et al., 1988) |
| | Gave d'Ossau | 1400 | 34.2-29.7 cal BP | Radiocarbon ($^{14}$C) | (Andrieu et al., 1988) |
| Southern valleys | Aragón | 1900 | 51 ± 4.5 | OSL | (García-Ruiz et al., 2013) |
| | Gállego | 1900-2000 | 85 ± 5-36 ± 3 | OSL | (García-Ruiz et al., 2003) |
| | Cinca | 2100-2200 | 64 ± 11 | OSL | (Lewis et al., 2009) |
| | Ara | 2100-2200 | 49 ± 8 | OSL | (Sancho et al., 2018a) |
| | Ésera | 2100-2200 | ? | - | - |
| | Noguera Ribagorçana | 2100-2200 | ? | - | (Bordonau et al., 1993) |
| | Noguera Pallaresa | 2200-2300 | ? | ? | (Ventura and Turu, 2022) |
| | Valira | 2300 | 42 ± 8 | OSL | (Turu et al., 2022) |
| | Aránser | 2200-2300 | ? | - | (Andrés et al., 2018; Palacios et al., 2015b) |
| | Llosa | 2200-2300 | ? | - | (Andrés et al., 2018; Palacios et al., 2015b) |
| | Duran | 2200-2300 | ? | - | (Andrés et al., 2018; Palacios et al., 2015b) |
| | Malniu | 2200-2300 | 81.2 ± 2-52.2 ± 2.3 | CRE | (Pallàs et al., 2010) |
| | Querol | 2100-2200 | ? | - | (Pallàs et al., 2010) |
| | Têt | 2000-2100 | 40.9 ± 1.1 | CRE | (Tomkins et al., 2018) |

*CRE ages have been recalculated using the CRONUScal

**Radiocarbon ages were calibrated using CALIB 7.1 or OXCAL programs

In the terminal LBBB, assumptions of glacial advances during the LGC were first supported by well-developed terminal moraines containing palaeontological fossils from cold environments (e.g. cave bears) and archaeological records of human evidence in the Gargas cave (Boule, 1895). Even if it is challenging to infer different glacial phases within the LGM without absolute numerical ages, several moraine crests have been already ascribed to distinct glacial advances from the LLGM and GLGM (Taillefer, 1957). Some authors have distinguished PGC from LGC moraines based on the weathering state of moraines. Such relative criterion was applied to compare the weathering rind from granite cobbles within the moraines of the LBBB (Stange et al., 2014). This study showed a differentiable degree of degradation between the external and internal moraine systems and proposed the LLGM to be the oldest deposit. The first radiometric study developed on the sediments from the Barbazan Lake suggested the onset of the lake formation during the LLGM (Andrieu et al., 1988; Andrieu, 1991a; Delmas et al., 2022a). In fact, considering the Barbazan Lake position between the external and internal moraines of complex 1.b, the La Serre, Burs and Barbazan moraines were already abandoned when the lake was formed (Andrieu, 1991b). The basal unit of the Barbazan sequence was constituted by glaciolacustrine rhythmites and diamictons, suggesting a deposition within a proglacial lake environment, by 40.7-32.3 cal ka BP (22.7-22.6 m depth). During the proglacial sedimentation of the lake, organic content was lower than 1% and herbaceous pollen taxa dominated by *Poaceae* with few tree taxa of *Pinus* indicated an open landscape and a possible cold continental climate with <250 mm (<60 rainy days) of precipitation totals (Jalut et al., 1992). Following this phase, at 9.6-9.5 m depth, the carbonated and organic-rich silts show that the Garonne palaeoglacier stopped the meltwater supply at 30.1-30.6 cal ka BP, probably leaving the LBBB from the Labroquère-Valcabrère moraine position. In addition, the left moraine on the valley sides, 6 km up the valley from the LBBB, closes a peak bog near the village of Sost from where inferences based on pollen records suggested an age of the basal unit at >45 ka (Hérail and Jalut, 1986). In the upper tributaries, the sedimentary complex of Soberado on the right slope of the Joèu Valley, at 120-160 m above the riverbed, is composed of an upper unit with ca. 40 m thick, interpreted as a deposit of basal till accumulated during the MIE of the LGC (Bordonau, 1985). However, this hypothesis needs to be validated as the glacier thickness during the LLGM and GLGM should be similar (400 m) leaving few changes to preserve such a thick deposit.

### 2.3.4. The global Last Glacial Maximum

As any Mid-Late Pleistocene glaciation, the culmination of each glacial cycle is defined by the maximum ice extent at a global scale, and the last one (GLGM) occurred between 26 and 19 ka (Clark et al., 2009). This phase is constrained in the first half of the MIS-2 and is defined by the lowest reconstructed sea level at ~130 m and the maximum of benthic $\delta^{18}O$ that have been widely used to determine the GLGM (Clark et al., 2009; Shackleton, 1967). This peak was likely

driven by the minima of summer insolation, SST in the Pacific Ocean, and atmospheric $CO_2$, as assessed by more than 4000 ages that define the time window of the GLGM (Clark et al., 2009). In spite of the GLGM being mainly based on the in the Northern Ice Sheets ice maximum, mid-latitude glaciers responded also with large advances. During this phase, conditions in Southern Europe were generally dryer and colder than today, with large regional asymmetries (Allen et al., 2008; Toucanne et al., 2022). Temperature reconstructions from mid-latitude mountains revealed MAAT values significantly lower than present-day, of 6-9 ºC in the Iberian mountains (Moreno et al., 2012a), 9-15 ºC in the Alps (Peyron et al., 1998) and 10-12 ºC in the Romanian Carpathians (Obreht et al., 2014). In the Iberian Peninsula, the glacier chronology shows a complex response to this event. Some moraines indicate that glaciers were highly sensitive to this thermal minimum as they reached their maximum extent (e.g. Iberian and Central ranges) and others only got positions behind LLGM moraines (e.g. Sierra Nevada, Cantabrian Mountains; Delmas et al., 2022c; Oliva et al., 2022a, 2022b; Vieira et al., 2021).

In the Pyrenees, the previous interpretations about the glacial advance that occurred during the GLGM based on radiocarbon ages from the ice-marginal fluviolacustrine sediments in the terminal basins were validated by CRE dating on glacially-transported boulders (Table 1.4; Delmas, 2015). However, this validation occurred mainly in the Mediterranean valleys of the Pyrenees. In the Eastern Pyrenees, the robust $^{10}$Be CRE datasets from the Têt, Querol, Malniu, Duran, La Llosa and Aránser catchments show glacial advances occurring during the GLGM. In the Têt Valley, three moraine boulders from the recessional standstill behind the LLGM moraine revealed recalculated $^{10}$Be ages between 21.6 ± 2.7 and 20.4 ± 0.4 ka (Delmas et al., 2008). In Querol and Malniu, the glacial advances almost reached the LLGM moraines. They were dated and recalculated by the average $^{10}$Be ages of 24.6 ± 0.6 ka and 27-24 ka, respectively (Delmas et al., 2022b; Pallàs et al., 2010). Further southeast, in the Duran, La Llosa, and Aránser valleys, Late Pleistocene glacial advances were constrained topographically in the valleys and forced the development of either polygenic or parallel moraine crests with no clear features. However, $^{36}$Cl ages from these moraines support the hypothesis of several small advances during the GLGM between 23 and 20 ka (Andrés et al., 2018; Palacios et al., 2015b). In the south part of the Central Pyrenees, $^{10}$Be recalculations of two moraines from the Artigalonga-Llestui system, Noguera Ribagorçana, showed similar exposure ages; the ice margin deposit at ca. 1300 m, ca. 300 m above Ginaste, yielded an average age of 26.3 ± 5.3 ka and the moraine at ca. 1700 m, ca. 500 m above Senet, was dated at 22.5 ± 1.2 ka (Delmas et al., 2022b; Pallàs et al., 2006). This age shows an early glacial advance during the GLGM that is in agreement with the glaciolacustrine sequence of Llestui, the basal unit being dated and recalculated at 23.5-20.7 cal ka BP (Bordonau et al., 1993; Vilaplana, 1983). At the Northern and Western parts of the Pyrenees, dated moraines showed no clear evidence of glacial advances during the GLGM. The frontal moraines from the

Garrabet, Bompas-Arignac and Bernière were interpreted to have developed during the GLGM. However, the $^{10}$Be dataset showed only minimum ages between 20.8 ± 1.3 and 16.5 ± 0.8 ka (Delmas et al., 2015, 2011). Further west, in the Gállego Valley, the absence of moraines behind the Senegüe moraine (OSL age of 36 ± 3 ka) and the upper sedimentary sequences dated by means of the $^{14}$C suggest that these areas were already ice-free during the GLGM. In fact, following the glacial retreat, the overdeepened basins were progressively filled with postglacial sediments dated at the Paúl Búbal by 25.9-24.2 cal ka BP (1110 m; Montserrat, 1992) and Tramacastilla Lake by 25.3-24.4 cal ka BP (1670 m; García-Ruiz et al., 2003). This glacial recession favoured also widespread slope processes during the paraglacial environmental readjustment. In the Gállego Valley, several landslides above ca. 1500 m dammed palaeolakes that were by means of $^{14}$C and OSL before the GLGM (García-Ruiz et al., 2003; Guerrero et al., 2018). In the northern valleys of the Western Pyrenees, despite the absence of available CRE dates of glacial features, recalculated ages from fluvio-lacustrine sediments in the Gave de Pau and Gave d'Ossau showed that glaciers retreated from the terminal positions during the GLGM; this is the case of Lourdes sequence (Gave de Pau) by 24.6-23.8 cal ka BP and the Estarrès sequence (Gave d'Ossau) by 31.0-27.1 ca ka BP (Andrieu, 1987; Jalut et al., 1988; Reille and Andrieu, 1995).

Table 1.4. Glacier setting and available ages for the GLGC in the Pyrenees (adapted from Delmas et al., 2022b).

| | Basin | ELA during the LLGM (m) | Chronology (ka) | Method (recalculation) | First significant reference |
|---|---|---|---|---|---|
| Northern valleys | Ariège | 1600-1800 | 20.8 ± 1.3 | CRE* | (Delmas et al., 2011) |
| | Garonne | ? | ? | - | - |
| | Gave de Pau | ? | 24.6-23.8 cal BP | Radiocarbon ($^{14}$C)** | (Reille and Andrieu, 1995) |
| | Gave d'Ossau | ? | - | - | - |
| Southern valleys | Aragón | ? | ? | - | - |
| | Gállego | 2000 | 25.9-24.2 cal BP | Radiocarbon ($^{14}$C) | (García-Ruiz et al., 2003) |
| | Cinca | ? | ? | - | - |
| | Ara | ? | ? | - | - |
| | Ésera | ? | ? | - | - |
| | Noguera Ribagorçana | 2100-2200 | ca. 25 – 27.9-24.0 cal BP | CRE and radiocarbon ($^{14}$C) | (Pallàs et al., 2006) |
| | Noguera Pallaresa | ? | ? | - | - |
| | Aránser | ? | ? | - | - |
| | Llosa | 2200-2300 | 20.8 ± 1.9 | CRE | (Andrés et al., 2018; Palacios et al., 2015b) |
| | Duran | 2200-2300 | 21.9 ± 2.6 – 20.9 ± 2.0 | CRE | (Andrés et al., 2018; Palacios et al., 2015b) |
| | Malniu | 2200-2300 | 27.2 ± 0.7 – 23.9 ± 0.7 | CRE | (Pallàs et al., 2010) |
| | Querol | 2100-2200 | 27.2 ± 0.7 – 23.9 ± 0.7 | CRE | (Pallàs et al., 2010) |
| | Têt | 2000-2100 | 24.3 ± 3.8 | CRE | (Tomkins et al., 2018) |

*CRE ages have been recalculated using the CRONUScal

**Radiocarbon ages were calibrated using CALIB 7.1 or OXCAL programs

The distance between the Pyrenean LLGM and GLGM moraines shows that they are closer in the eastern part (300 m) than in the western (<20 km) (Tomkins et al., 2018), which may be associated with changing moisture patterns during the LGC. Indeed, it may suggest that during the GLGM, glacial feeding and subsequent glacier advance from Mediterranean-influence at the eastern valleys was more important than Atlantic one on the western valleys (Delmas et al., 2022b). This regional pattern reveals that during the prevailing dry and cold conditions of the GLGM, the Mediterranean cyclones would nourish the eastern glaciers in contrast with the Atlantic-influenced mountains. In the latter, climate conditions were driven by a stationary high-pressure system that would favour lower accumulation rates, which is the exact opposite of the current climate.

The content of limestone and feldspar in a moraine is indicative of the relative age deposition, as they dissolve after being exposed. In the LBBB, the high content of limestones and feldspar in the moraine system 1b when compared the 1a supported its relation to the LGC (Hubschman, 1984). In the Barbazan Lake, the glaciofluvial rhythmites and diamictons existing between 22.6 and 9.5 m depth suggest that the glacier was nearby, possibly at the position of the Labroquère-Valcabrère moraine, or even in contact with lake between 40.7-32.3 and 31.6-30.1 cal ka BP (Andrieu, 1991b, 1991a; Andrieu et al., 1988; Jalut et al., 1992). After this, the glacier retreated upvalley, a fact which supports that glaciers in Atlantic-influenced valleys of the Pyrenees were not in the terminal basins during the GLGM. The comparison of weathering rinds on granite cobbles within the La Serra and Labroquère-Valcabrère moraines showed no relevant differences (Stange et al., 2014); however, the external position of the La Serre moraine reinforced the hypothesis that it formed during the GLGM whereas the Labroquère-Valcabrère moraines during a pulsation thereafter (Fig. 1.8). In the upper main Garonne Valley, the cirque located at the lateral Barranc de Corillha preserves a moraine formed at 1800 m that was ascribed to a period of glacial stabilisation after the MIE of the LGC (Martí-Soler, 1988), although this has not been yet validated. During the LLGM and GLGM, the landscape beyond the glaciers was characterised by braided rivers and proglacial lakes within a periglacial environment (Andrieu, 1991b, 1987; Jalut et al., 1992). The poorly vegetated environment was covered only with 10-30% of steppe vegetation with herbaceous plants (*Poaceae, Artemisia*, *Chenopodiaceae, Helianthemum* and *Compositae* sp.) and few tree taxa (dominance of *Pinus* with others such as *Fagus*, *Abies* and *Picea* sp.).

## 2.4. The Termination-1

### 2.4.1. The climate variability in the Pyrenees

Following the culmination of each glacial cycle, the Terminations took place with the most brutal global environmental shifts within a short period of ca. 10 ka (Sarnthein and

Tiedemann, 1990). The last deglaciation was the Termination-1, spanning between the end of the GLGM and the onset of the Holocene; i.e. between 20-19 and 11.7 ka (Naughton et al., 2023). These periods have been also used to assess the onset and end of the Quaternary glaciations as they are a good indicator of the limit of glacial expansions and collapses (Hughes and Gibbard, 2018). As this period started after the rise of summer temperatures, the northern marine-based ice sheets from the GLGM became unstable, which resulted in massive iceberg discharges into the Atlantic Ocean (Denton et al., 2010). Such considerable input of water promoted sea level rise by 80 m until the onset of the Holocene (Carlson and Clark, 2012). However, paradoxically, following the onset of the T-1, the freshwater input also triggered the ocean cooling and the weakening of the AMOC leading to the onset of a new stadial (Naughton et al., 2022). This stadial, which is chronologically constrained from 18.2 to 14.6 ka, is named differently according to the geographical setting: OD in the European continent, HE-1 in the North Atlantic ocean and GS-2a in the Greenland Ice Sheet (Rasmussen et al., 2014). In fact, during this phase, the freshwater input from icebergs that travelled south to latitudes of the Iberian Peninsula also transported embedded sediments that accumulated at the bottom of the Atlantic Ocean. This process of IRD was repeated several times throughout the T-1 and is the indicator of cold conditions (Hodell et al., 2017). The sequence of these sediments allows the reconstruction of millennial cold and dry events (HE) that influenced the Iberian climate with a reduction of 2-3 ºC of SST (Martrat et al., 2007; Rodrigues et al., 2010). These cold conditions were interrupted by the intensification of the AMOC that transported heat to Europe (Cacho, 2022). Therefore, after the GS-2a, warm conditions prevailed during the so-called B-A (or GI-1) that is constrained between 14.6 and 12.9 ka (Rasmussen et al., 2014). This new oceanic and atmospheric reorganisation likely led to the rise of $CO_2$ concentrations and SST of 4 ºC over the Iberian Peninsula margin (Cacho et al., 2001; Denton et al., 2010). Finally, once again, cold and dry conditions resumed during the YD (GS-1: 12.9-11.7 ka) with SST decreasing of 2-3 ºC.

The T-1 represents the period with more palaeoclimatic information and glacial evidence available, which provides a good comprehension of the impacts of climate variability on the various natural systems of the Pyrenees (Oliva et al., 2022d). A large variety of independent fluvial, lacustrine, karstic and marine proxies reconstructed local and regional patterns over the Pyrenees and supported assumptions about past glacial dynamics. The values of $\delta^{18}O$ throughout the T-1 from the Ostolo cave imply a maximum MAAT increase of ca. 9 ºC from the end of the LGM to the Early Holocene based on the corrected temperature dependence of 0.47-0.52‰/ºC (Bartolomé et al., 2015; Bernal-Wormull et al., 2021). This increment in temperature forced the widespread development of scrubs (*Juniperus*) and arboreous (*Pinus* and Birch) that colonised the landscape in 60 to 80% (Jalut et al., 1992). However, the reduction of $\delta^{18}O$ values during the OD (-8.92‰) and YD (-5.83‰) from the Seso and Ostolo speleothems suggests a maximum

decrease in the MAAT of ca. 6 ºC and 5 ºC, respectively (Fig. 1.15; Bartolomé et al., 2015; Bernal-Wormull et al., 2021). The general rise of biostasia conditions was interrupted by these cold spells with low biological production and strong influence from glacier meltwaters, as suggested by low organic matter and high carbonate values from the Pyrenean sequences (González-Sampériz et al., 2006; Jalut et al., 1992; Millet et al., 2012). During these periods, cold-climate conditions forced a considerable increase of steppe vegetation (e.g. *Artemisia*) and a retreat of tree taxa, as shown by pollen records from the sedimentary sequences in the Central Pyrenees (González-Sampériz et al., 2017; Jalut et al., 1992). Finally, between OD and the YD, the B-A took place with a MAAT increase of 7.5 ºC in a few decades, according to the high-resolution karst proxies (Bernal-Wormull et al., 2021). From the sedimentary sequence in the Ech palaeolake, Western Pyrenees, chironomid-based summer air temperatures showed an increase of 6 ºC during the B-A (Millet et al., 2012). Such a period was characterised by warm and humid conditions forcing the development of forest taxa (e.g. Birch) in the Northern Pyrenean foreland (Jalut et al., 1992).

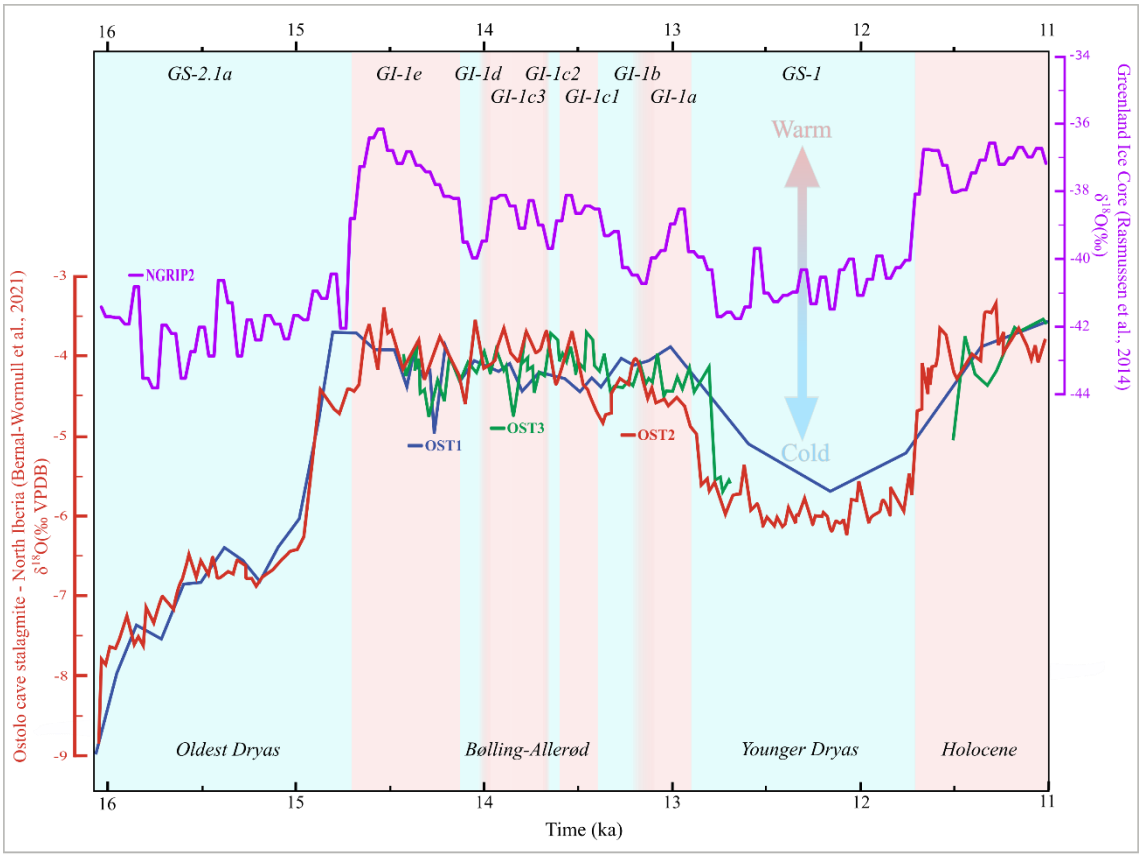


Figure 1.15. Temperature reconstruction based on $\delta^{18}O$ record from the NGRIP ice core and the evolution of the $\delta^{18}O$ record from tree stalagmite in the Ostolo cave, Western Pyrenees. The curves are plotted in the time periods based on the Greenland stratigraphic climate history at the top and in the respective periods in in the European records at the bottom.

## 2.4.2. Glacier fluctuations during the Termination-I in the Pyrenees

During the T-1 glaciers responded in the Pyrenees to climate forcing changes in the North Hemisphere (Oliva et al., 2022d). The sedimentary interpretations and CRE dating of glacial

evidence were used to reconstruct the glacial dynamics during the T-1 in the Pyrenees (Table 1.5), showing strong asymmetries between northern and southern valleys (Reixach et al., 2021). Glacier retreat started by 18 ka, as detected by exposure ages on polished surfaces of the Eastern Pyrenees, mainly in the Cerdanya area (Palacios et al., 2015b). This early retreat was confirmed with $^{14}$C age of 20-19 cal ka BP of the lower unit of the buried peatland of La Grave-amout in the Carlit Cirque, Têt Valley (Delmas, 2005; Delmas et al., 2008). However, this long-term glacial retreat was interrupted by periods of glacial advance (Delmas et al., 2023a, 2023b, 2023c; Oliva et al., 2019; Reixach et al., 2021). In the most recent synthesis on glacial evolution during the T-1, three standstills, or glacial advances within the glacial valleys are revealed by CRE ages during the OD, B-A and YD (Delmas et al., 2023a, 2023c, 2023b). The OD glacial advance was confirmed in the Ariège, Eastern Pyrenees, where a robust dataset from the moraines at the Aix-les-Thermes (900 m) and Mérens-les-Vals (1100 m) yielded CRE ages of 17.3 ± 0.5 and 15.7 ± 0.5 ka, respectively (Delmas et al., 2011; Pallàs et al., 2010; Reixach et al., 2021). In the Gállego and Èsera valleys, Central Pyrenees, several moraines at 1400 to 2400 m were dated by means of CRE dating, showing ages of 17.5 and 14.5 ka related to glaciers located in the highest valleys (Crest et al., 2017; Palacios et al., 2017). Following this glacial advance, milder conditions prevailing during the B-A over the Pyrenees triggered glacial recession; for example, the ELAs rose up to 2200-2500 m in the eastern valleys impeding glacial accumulation below this altitude (Reixach et al., 2021). CRE ages from polished surfaces validated this regional glacial recession during the OD/B-A transition (i.e. 15 to 13.5 ka) and showed that glaciers likely abandoned the valleys (Palacios et al., 2020). However, some examples of moraine development during the second half of the B-A suggest that particular topographical conditions favoured glacier persistence within the glacial cirques (Delmas et al., 2023b). This is the example of the moraines dated by 13.6 ± 0.9 ka in the Perafita cirque, Aränser, or by 13.2 ± 0.9 ka in the Médecourbe cirque, Ariège (Crest et al., 2017; Palacios et al., 2015b; Tomkins et al., 2018). During the cold and dry conditions of the YD, glacier advances occurred within the glacial cirque limits in the Pyrenees (García-Ruiz et al., 2016). This glacial advance did not override the evidence of the B-A one. In the Eastern Pyrenees, a glacier persisted in the Médecourbe cirque, Ariège, forming a moraine yielding a CRE age of 12.4 ± 0.4 ka (Jomelli et al., 2020). Another moraine was dated 15 km southwards in the Mouscadous cirque and ascribed to the YD (Crest et al., 2017). Herein, initially two moraine boulders embedded in the lateral right moraine showed an age of 11.8 ± 1.1 and 11.4 ± 0.8 ka that were later recalculated to 12.3 ± 0.2 ka (Reixach et al., 2021). In the Central Pyrenees, the innermost moraine of the three-moraine Renclusa system (Maladeta Cirque) showed $^{10}$Be age of 12.1 ± 0.4 ka and was related to the YD (Crest et al., 2017). Finally, palaeoprecipitation and palaeotemperature reconstructions based on the modelled ELA from the Eastern Pyrenees allowed reinforcing the idea that the OD (-62 ± 8%) was dryer than the YD (-44 ± 16 %) (Reixach et al., 2021).

Table 1.5. The most significant dates from each Pyrenean basin during the for the T-1 (adapted from Delmas et al., 2023a, 2023b, 2023c).

| | Basin | OD evidence and chronology (ka) | B-A evidence and chronology (ka) | YD evidence and chronology (ka) | Significant reference |
|---|---|---|---|---|---|
| Northern valleys | Ariège | Ax-les-Thermes by 19-18 | Médecourbe by 14-13 | Vicdessos 13-12 | (Crest et al., 2017; Delmas et al., 2011; Jomelli et al., 2020) |
| | Garonne | ? | ? | ? | - |
| | Gave de Pau | ? | ? | ? | - |
| | Gave d'Ossau | ? | ? | ? | - |
| Southern valleys | Aragón | ? | ? | ? | (García-Ruiz et al., 2013) |
| | Gállego | Caldarés by 17-16 | Above 2600 (no glaciers) | Below 2800 (no glaciers) | (Palacios et al., 2017, 2015a) |
| | Cinca | ? | ? | ? | - |
| | Ara | ? | ? | ? | - |
| | Ésera | ? | Aigualluts by 16-14 | ? | (Crest et al., 2017) |
| | Noguera Ribagorçana | Santet by 17-16 | ? | Mulheres by 13 | (Bordonau et al., 1993; Pallàs et al., 2006) |
| | Noguera Pallaresa | ? | ? | ? | - |
| | Valira | ? | ? | ? | - |
| | Aránser | Aránser by 17-16 | Tossa Plana (no glaciers) | No glaciers | (Andrés et al., 2018; Palacios et al., 2015b) |
| | Llosa | ? | ? | ? | - |
| | Duran | ? | ? | ? | - |
| | Malniu | ? | Camcardós (No glaciers) | No glaciers | (Pallàs et al., 2010) |
| | Querol | ? | Orri by 15-14 | ? | (Pallàs et al., 2010) |
| | Têt | Grave by 17-16 | Grave by 14-13 | Grave by 13-12 | (Delmas et al., 2008; Reixach et al., 2021; Tomkins et al., 2018) |

In the Upper Garonne basin, the distribution of the moraines suggests that the Last Deglaciation was characterised by massive glacial retreat upvalley that left several glacial deposits mainly in flat areas – such as plateaus and the bottom of glacial cirques – where postglacial dynamics had no time and intensity to dismantle them, yet. Glacial deposits, such as moraines, till, kame terraces, and erratic boulders have been mapped to reconstruct the ice limits during the deglaciation (Martí-Soler, 1988; Bordonau, 1992; Serrat et al., 1994; Fernandes et al., 2017). However, there are no ages from moraines in the upper tributaries. The glacier recession also reduced the sediment load of the Garonne River and led to river incision and abandonment of flood plains, as suggested by the Plaine de Rivière glaciofluvial terrace (25-16 m above the riverbed) formed after the MIS-2 (Stange et al., 2014). The Barbazan Lake in the LBBB showed lacustrine sedimentation without the influence of the Garonne meltwaters and the development of organic matter between 15.2 ± 1.2 and 13.4 ± 0.6 cal ka BP, suggesting warming conditions (Andrieu et al., 1988). In the upper valleys of the Upper Garonne basin, the moraines documented in the Aran Valley were attributed to different phases of glacial advance during the deglaciation

(Bordonau, 1985; Martí-Soler, 1988; Table 1.6). These authors have mapped moraines within the valleys and cirques assuming they were formed during the deglaciation process, as proposed in other valleys where sedimentary sequences indicated cold periods favourable to glacial advances (Vilaplana, 1983). Therefore, after the glaciers left the LBBB (stage 1), a glacier advanced within the valleys and formed moraines at 1000-2100 m (stage 2); this is the example of the moraines located in the Artiga de Lin, Joèu, at 1440-1460 m or in the Liat basin, Unhòla, at 2080 m (Fig. 1.11-B). Lastly, the glaciers advanced again within the cirques forming moraines at 2350-2500 m (stage 3); this is the example of the moraines in Fontfreda cirque, Nere, at 2100-2200 m (Fig. 1.16-C).

Table 1.6. Geographic distribution of the main moraine systems identified in the Upper Garonne basin.

| Glacial phase | Glacial system | Glacial type | Elevation of the moraines (m) | Distance from the headwaters (km) | ELA* |
|---|---|---|---|---|---|
| 1 | M-1 | Piedmont | 420-820 | 80 | 1532 |
| 2 | M-2 | Alpine | 1000-2100 | 23-2 | 1982 |
| 3 | M-3 | Cirque | >2100 | 4.5-0.4 | 2336-2408 |

*ELA elevation results from the AABR and AAR mean values

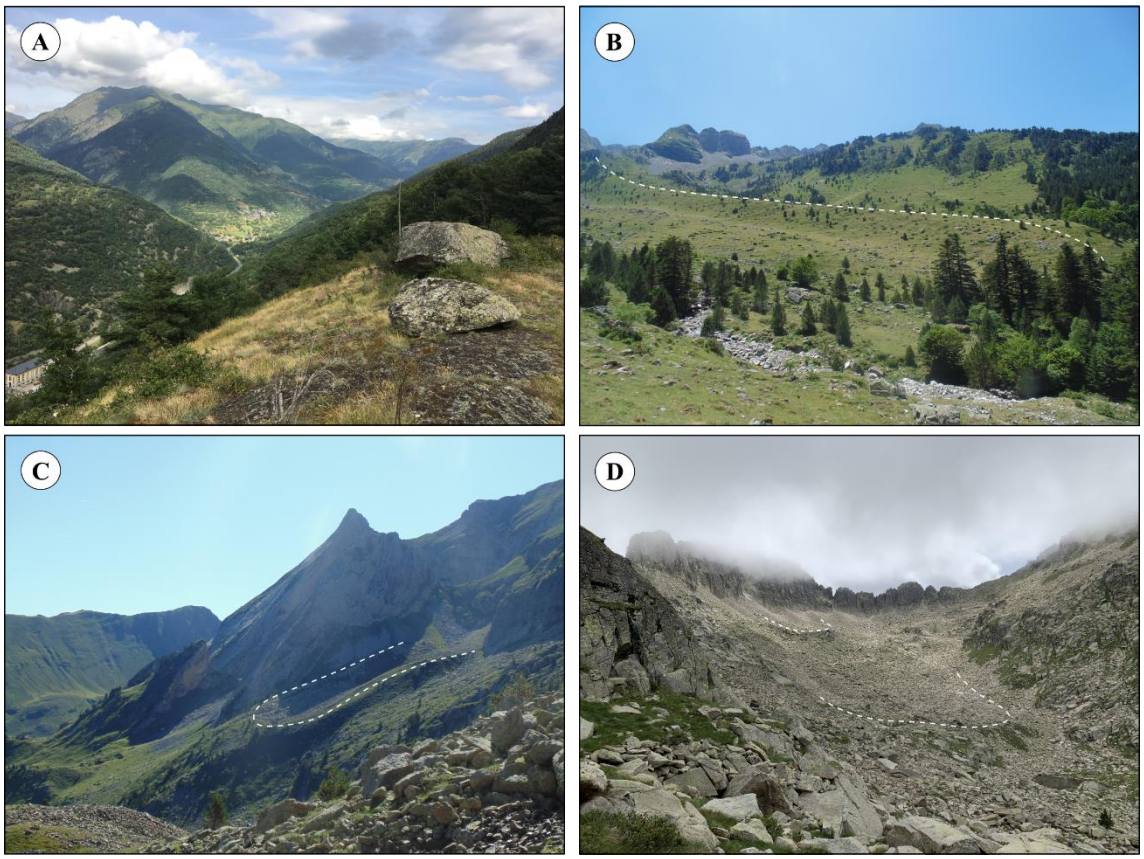


Figure 1.16. Examples of glacial features in the upper valleys of the Upper Garonne basin: A) erratic granitic boulder placed on slates between the Joèu and Garonne valleys; B) and C) latero-frontal left moraine between 1620 and 1950 m at the Fontfreda cirque and frontal moraine between 2100 and 2200 m, respectively; D) moraine from a debris-covered between 2430 and 2500 m and a moraine from a debris-free glacier at 2550 m in the Aiguamòg Valley.

However, the timing of the glacial stages was inferred based on moraines dated by means of CRE with similar settings and characteristics within other Iberian Peninsula ranges (Fernandes et al., 2017). Considering the ages available at the LBBB (Andrieu et al., 1988), these moraines must have formed during the LGM or Termination-1. This dissertation will provide the chronological framework for these moraine systems and fill this knowledge gap in the Paper 3 and 4).

## 2.5. The Holocene

### 2.5.1. The climate variability in the Pyrenees

The current interglacial started with the onset of the stratigraphic Holocene Epoch (meaning totally recent), by 11.7 ka, which is divided in three stages: Early (11.7-8.2 ka), Middle (8.2-4.3 ka) and Late (4.3-nowdays; Walker et al., 2018, 2012). At the onset of the Holocene, SST rose by ca. 4-6 ºC in the western and eastern margins of the Pyrenees (Cacho et al., 2001; Català et al., 2019; Martrat et al., 2014; Mary et al., 2017). After the initial warming during the onset of the Early Holocene, the climate became progressively colder superimposed by strong climate variability (Cacho, 2022).

Following the onset of the Early Holocene, the freshwater melting from the ice sheet remnants might have weakened the AMOC favouring colder conditions that forced the MIE of the Holocene in the mountain glaciers of the Northern Hemisphere by ca. 10 ka (Jomelli et al., 2022). During this phase, the maximum summer insolation in the Northern Hemisphere likely triggered a significant increase of temperatures that lead in the one hand to glacier reduction and another to the onset of the HTM, albeit with substantial temporal and regional variations (Renssen et al., 2012). In the Central Pyrenees, the timing of HTM was defined in the Basa de la Mora Lake sequence at between 8 and 6.2 cal ka BP based on increase of chironomid-derived summer air temperatures (Tarrats et al., 2018). This time-span largely correlates with pollen records of forest development (Cunill et al., 2013; Leunda et al., 2017), maximum lake levels (Morellón et al., 2008; Pellicer et al., 2016), and the peak of river discharge (Eynaud et al., 2022; Frigola et al., 2007). The Mid-Holocene started with the sudden but short-lasting 8.2 ka cold event that forced a 2 ºC decrease of summer temperatures, as demonstrated by $\delta^{18}$O-derived SST in Mesolithic shell exploitation in a cave from the north of the Iberian Peninsula (García-Escárzaga et al., 2022). The following general cooling likely represents the onset of the so-called Neoglaciation, which is a time-transgressive period constrained between 6.5 and the LIA (Davis et al., 2009; Denton and Porter, 1970; Porter, 1971). From this phase onwards, the link between vegetation and climate since the Mid-Holocene is challenging as part of pollen taxa may result from human impact through grazing and forest opening (Cunill et al., 2013; Pérez-Díaz et al., 2015; Pérez-Sanz et al., 2013). However, other non-vegetation proxies showed a general reduction of 1 ºC in summer air temperatures (chironomid-derived) together with the lowest lake levels, which suggest a reinforcement of the aridity trend in the Central Pyrenees during the first half of the Late-Holocene (4.2-2.0 ka) (Tarrats et al., 2018). Over the last 2 ka, the climate became progressively warmer (ca. +2 ºC) as documented by changes in $\delta^{18}$O in the speleothems from the Central Pyrenees (Sancho et al., 2018b). However, this phase was highly variable as it included several centennial climate events, fluctuating between warm (Roman Warm Period: 0-5th centuries; Medieval Warm Period: 9-14th centuries; and Industrial Period: 19th century-nowadays) and cold episodes (Dark Ages Cold Period: 5-9th; and LIA: 14-19th; González-Sampériz et al., 2017). During the Industrial Period, 32 series of instrumental data recorded temperatures between 1959 and 2010 show an increase of 0.2 ºC per decade over the Pyrenees (ca. 1 ºC in total; OPCC-CT, 2018).

### 2.5.2. Holocene glacial dynamics

During the Holocene, the Pyrenean range was almost ice-free, and glaciers have only expanded occasionally with very limited dimensions. The glaciers responded following the prevailing climate variability with two advances during the Early Holocene and Neoglacial phases that interrupted the long-term retreat until nowadays. The highest massifs in the Central Pyrenees

are the only areas including Holocene glacial geomorphological evidence. During the Early Holocene, glaciers formed moraines in the Médécourbe cirque, Ariège, where two boulders embedded on the moraine at 2600 m were dated at 9.6 ± 0.4 ka (Jomelli et al., 2020) and in the Grave cirque, Têt, a moraine at 2200 m was dated by means of calibrated SHED at 9.4 ± 0.6 ka (Tomkins et al., 2018). In the Southern and Southeastern parts of the Pyrenees, the last glacial phase occurred during the Early Holocene (Salvador-Franch et al., 2022). This assumption was supported by CRE ages in polished surfaces at the bottom of the glacial cirques above 2100 m (Pallàs et al., 2010). In this sector, particularly in Aránser Valley, rock falls triggered by the deglaciation process promoted the formation of rock glaciers. The application of the CRE dating on boulders from rock glacier suggests the moment of stability towards the relict state where the youngest one – normally at the upper lobe – is indicative of the final stabilisation (Fernández-Fernández et al., 2020). This is the case of the Perafita rock glacier, where the upper lobe (at 2500 m) yielded a recalculated exposure age of 8.6 ± 1.1 ka (Andrés et al., 2018; original age of 10.4 ± 0.7 ka: Palacios et al., 2015b). Further west, a robust dataset of CRE ages in the Noguera Ribagorçana Valley, Central Pyrenees, revealed that moraines in the eastern cirque of the Molières Peak stabilized by 10.4 ± 1.0 ka (1700 m), in the Pleta Naua by 10.2 ± 0.7 ka (2200 m) and in the eastern cirque of the Besiberri Peak at 10.1 ± 0.6 ka (2700 m) (Pallàs et al., 2006). In the Gállego Valley, polished surfaces showed glacial retreat during the Early Holocene between 2100 to 2800 m (Palacios et al., 2017). There, the disappearance of glaciers was also confirmed by the formation of rock glaciers, which were dated by means of CRE. In the Piniecho and Catieras cirques (Gállego), several boulders on the lobes of rock glaciers, at 2200-2400 m, showed exposure ages from the Early Holocene (Palacios et al., 2015a). However, the insulation effect caused by the debris mantle on buried ice favoured ice persistence in the north-facing cirques until the HTM. This is supported by the study cases where the uppermost boulders of rock glaciers showed younger exposure ages than the front ones, such as in Ariège by 7.2 ± 0.3 ka (2400 m; Jomelli et al., 2020) or in Gállego by 6.3 ± 0.4-5.6 ± 0.3 ka (2400 m; Palacios et al., 2017). The HTM was followed by the cooling trend that reactivated glaciers during the onset of the Neoglaciation and during the Dark Ages (García-Ruiz and Serrano, 2022; Sancho et al., 2018a, 2018b). In the Pyrenees, the Neoglaciation advances were only recorded in the Central Pyrenees. In the Troumouse Cirque, Gave de Pau Valley, two glacial advances possibly caused silt accumulation in the peatland just below the moraines from where the sediments were collected and dated by 6.0/5.6-5.5/5.3 and 6.0/5.6-5.5/5.3 cal ka BP (Gellatly et al., 1992). However, the best direct glacial record preserved in the Pyrenees during this period is at the Marboré cirque (Cinca Valley). There, after the glacial retreat during the Early Holocene, several glacial advances occurred at 6.9 ± 0.8 ka, the Dark Ages and the LIA, which interrupted glacial retreat at 3.4 ± 0.2, 2.5 ± 0.1 and 1.1 ± 0.1 ka (García-Ruiz et al., 2020, 2014). These periods of glacial advances are likely correlated with high rates of cave ice accumulation from ca. 6.1 to 1.9 cal ka BP (Sancho

et al., 2018b). Throughout the Holocene, glacial advances were likely synchronous with the rest of Europe (García-Ruiz et al., 2020). During this period, the coldest phases occurred in the transition between the 17-18th and 18-19th centuries, with important environmental shifts in the Pyrenees, including glacier advances (Oliva et al., 2018; Serrano, 2022). Up to 52 glaciers advanced by 1850, encompassing a variety of sizes between 5 and 250 ha and a total area of 2060 ha (González-Trueba et al., 2008; Rico et al., 2017). Since then, an average of 11 ha of ice melted every year until 2000 and 18 ha since then. In fact, the temperature increase since the Industrial Period forced glaciers to shrink by ca. 90% of its LIA dimensions (2060 to 242 ha; Rico et al., 2017). Today, only 19 glaciers persist in sheltered northern cirques under steep rock walls of peaks above 2800-3000 m (Rico et al., 2017).

In the Upper Garonne basin, the glacial and periglacial evolution during the Holocene has been poorly studied. In the Basa Nere peatland, at 1900 m, the pollen taxa dominated by herbs (mainly *Poaceae* and *Artemisia*), together with low carbon content and wetland communities between 10.2 and 1.01 cal ka BP suggest the occurrence of a steppe environment frequently flooded by meltwaters (Garcés-Pastor et al., 2017b). A period of forest development (including deciduous species) and the general increase of organic content suggest a rise of warm conditions between 10.2 to 5.8 cal ka BP. The degradation of these conditions occurred between 5.8 and 3.9 cal ka BP. Sedimentological properties, with a sharp decrease in organic matter content, suggest a trend towards colder conditions. However, from this phase onwards, the intensification of human presence suggested by the rise of fires and grazing precludes the differentiation between natural and anthropic signals (Cacho, 2022). The only direct glacial record in the Garonne catchment is based on geomorphological maps suggesting, in relation to other dated moraines, that fresh moraines at 2260-2590 m might correspond with a glacial advance during the coldest phase of the Holocene (Fig. 1.17; Fernandes et al., 2017). However, no dates are yet available and this thesis will provide new information about the onset of the Holocene glacial dynamics in the Papers 4 and 6.

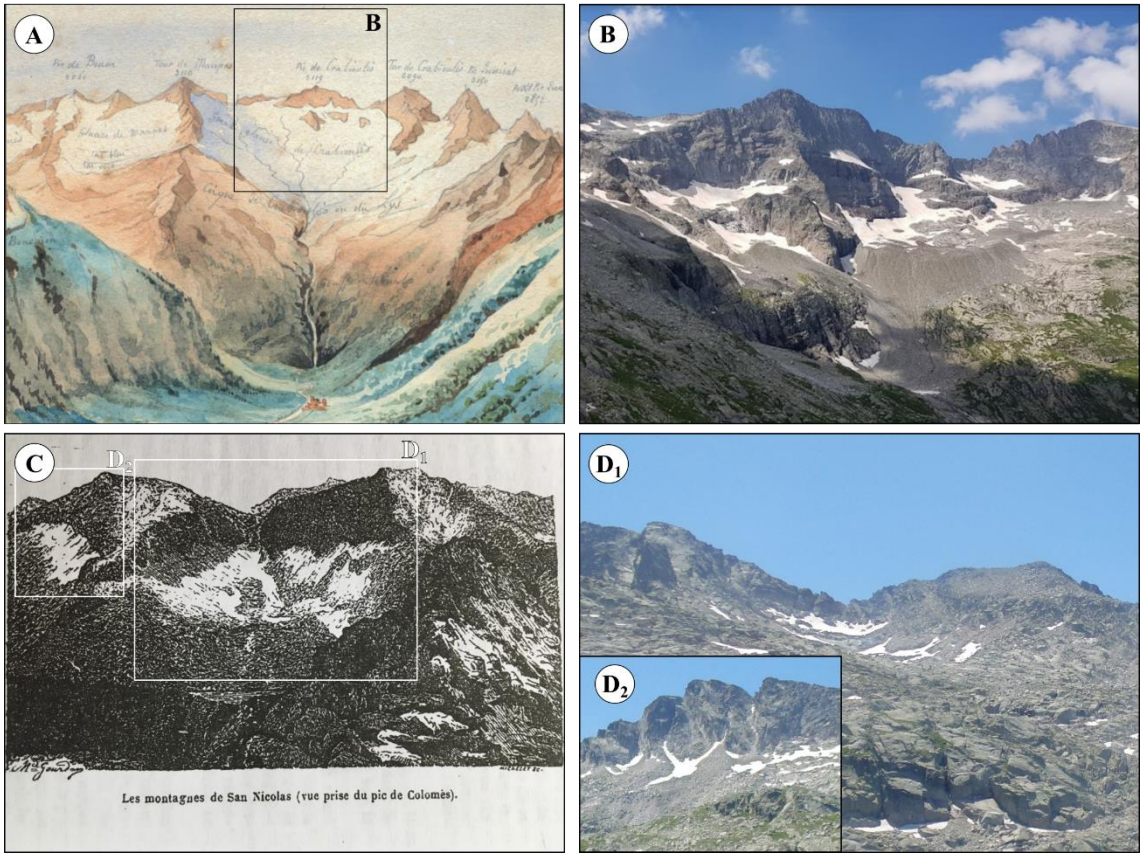

Figure 1.17. Examples of glaciers existing during the Late Holocene in the upper tributaries of the Upper Garonne basin: A) and B) comparison of Ramond's painting of the Crabioules glacier during the onset of the 19st and in the summer of 2019, respectively (credits to Juan Areta); C) and D) comparison of the Colomèrs glacier in 1884 (credits to Maurice Gourdon) and in the summer of 2019, respectively.

## 2.6. The paraglacial readjustment

Following the glacier retreat in high mountain environments, the terrain becomes unstable resulting in the transfer of sediments from the high land to the low terrain. During the Last Deglaciation, the ice thinning and recession forced a readjustment period, called the paraglacial phase (Ballantyne, 2002). This glacial-nonglacial transition period results in overdeepened basins infill, slope instability, and unconsolidated sediment reworking, controlled by fluvial, lacustrine, gravitational and periglacial processes (Ballantyne, 2002). In deglaciated areas, following the paraglacial phase, the degradation of permafrost and periglacial landscapes can also trigger a readjustment period named the paraperiglacial phase, especially during ongoing warm episodes (Mercier, 2008).

There are few studies about the paraglacial dynamics in the Pyrenees. The postglacial readjustment phase following glacial retreat has been studied mostly focusing onthe on slope failures and overdeepened basin infill. This is the case of valley infill in several northern and southern Pyrenean catchments where hundreds of meters of sediments were deposited in the valley floors during the paraglacial phase (Perrouty et al., 2015). This is the case of the Esterri d'Aneu basin, Noguera Pallaresa, where resistivity surveys suggested a sedimentary infill of 400

m (Bordonau, 1992). As glaciers were confined to the highest lands, slopes became unstable and favoured widespread slope failures. This is the case of the Gállego Valley, where downslope displacement of large landslides blocked the drainage forming lakes upstream; from the fine sediments accumulated at the lakes, radiocarbon and OSL dating yielded ages of 41.5 ± 3.9 to 15.1 ± 0.3 ka (Guerrero et al., 2018). In the western part of the French Pyrenees, the Cristallere deep-seated landslide was dated at 1.3 ± 0.06 ka, and was possibly triggered by the Lavedan earthquake around 1380 (Lebourg et al., 2014). The biggest landslide dataset corresponds to the eastern catchments of the Pyrenees, where the distribution of large-scale rock slope failures was linked with specific lithologies, such as Silurian shales and faults (Jarman et al., 2014). This study also evidences the contribution of paraglacial processes in eliminating pre-glacial relief. In the upper tributaries and cirques, smaller basins filled by lakes or peatlands have been widely used to model palaeoenvironmental reconstructions since the T-1 (Montserrat-Martí, 1992 and thereafter). In these basins where glacial cirques are clearly featured, the deglaciation of crystalline lithologies forced large rockfalls that, once deposited, formed and nourished rock glaciers above 1700 m (Fernandes et al., 2018). In the Central Pyrenees, part of these rock glaciers are still active showing permafrost above 2600 and 2800 in the north and south faces of the range, respectively (e.g. Palacios et al., 2017; Serrano et al., 2011).

Since the Garonne palaeoglacier retreated from the lower areas of the basin, the overdeepened basins functioned as sediment reservoirs. That is the case of the Marignac basin at ca. 500 m, which is the deepest basin of the catchment where gravimetric data collected enabled the estimation of a maximum postglacial infill 300 m thick, with 3.3 $km^3$ of sediments (Perrouty et al., 2015). Smaller basins at higher areas in the main Garonne Valley contain proglacial sediments with soil units, till, and lacustrine sediments with a depth between 11 m in the Lez Village (ca. 650 m a.s.l.) and 23 m in the Baquèira Village, at ca. 1400 m a.s.l.. At the slopes of the upper valleys, there are basins originated from glacial carving or deep-seated deformations. In the Bassa d'Oles, in the Varicauva forest (main Garonne Valley), at 1630 m, a resistivity survey showed a depth of 5 m filled by slope deposits and peat sediments (Bordonau et al., 1989). Indeed, these basins were filled with postglacial, lacustrine, alluvial, and fluvial processes transporting material from upland sources of unconsolidated glacial sediments and rock slope failures. There are several large rock slope failures in the Upper Garonne basin mapped in the upper tributaries (Fig. 1.18; Bordonau, 1985; Martí-Soler, 1988). In the slopes of the Nere and Garonne valleys, two slope deformations (Sèrra d'Horno and Varicauva forest, respectively) are associated with the stress release resulting from glacial debuttressing (Bordonau, 1985). Slope features can also be correlated to the ravines, from where debris flows formed two generations of alluvial fans at the foot of the slopes (Victoriano et al., 2016). Such postglacial processes also triggered rockfalls and rock avalanches that fed the foot slopes of the glacial cirques where permafrost-related

landforms – rock glaciers and protalus lobes – developed after the deglaciation (Fernandes et al., 2018). In the Aran Valley, such features are distributed essentially at the glacial cirques with a mean altitude of 2200 m and mainly NW, N, and NE oriented, and are commonly associated with periods of rapid deglaciation during T-1 (Fernandes et al., 2018). This dissertation will show in the Paper 6, the first chronological data in the north part of the Central Pyrenees of the glacial to periglacial transition of a glacial cirque, including the final stabilisation of a rock glacier.

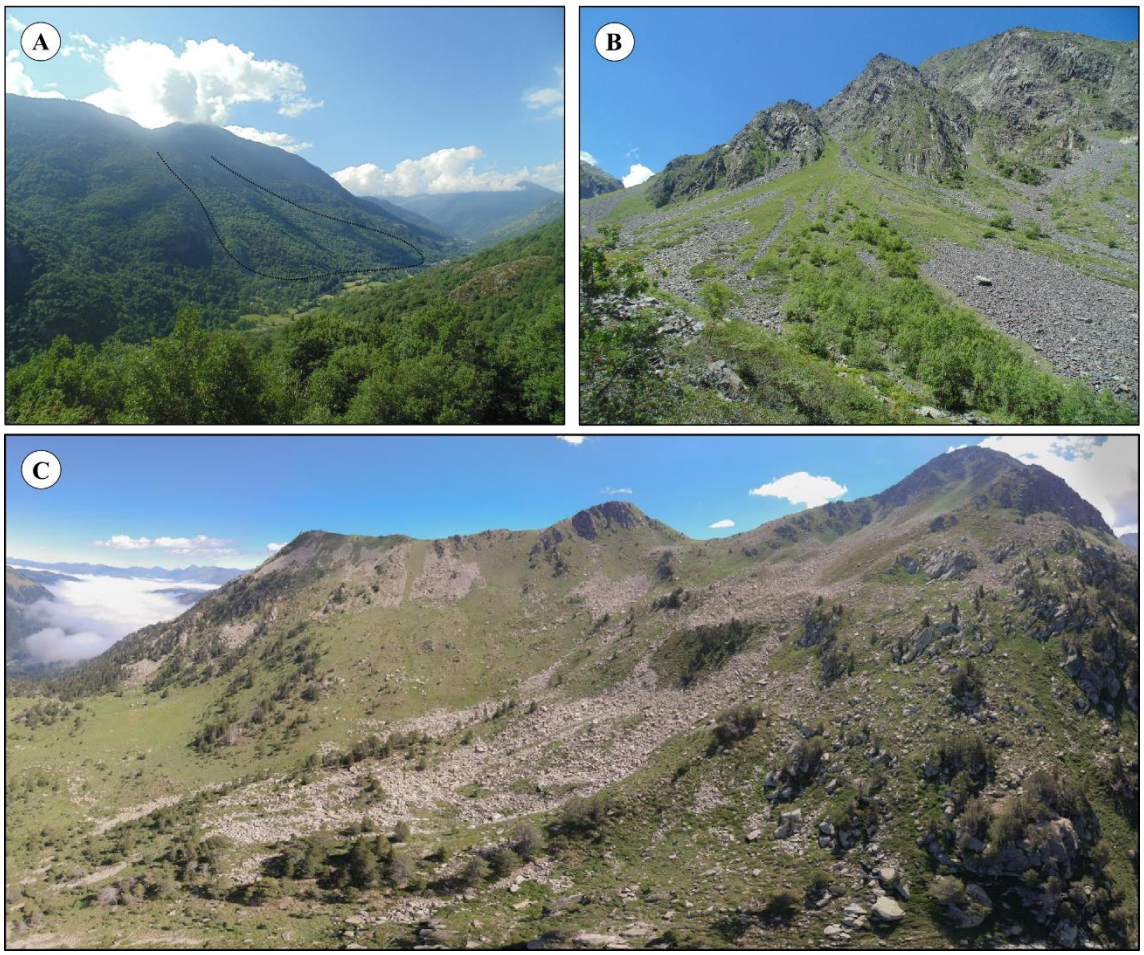


Figure 1.18. Examples of postglacial features in the upper tributaries of the Upper Garonne basin: A) rock failure near the Lez Village; B) debris cone in the Nere Valley; C) rock glacier in the Sendrosa western cirque (credits to Julia García-Oteyza).

# 3. Methods: geomorphology and geochronology

The understanding of Late Pleistocene glacier dynamics in the Upper Garonne basin was supported by a methodological approach commonly used in the field of Physical Geography. In this sense, the first approach on geomorphological mapping was carried out in order to construct a hypothesis of the deglaciation chronology in the entire Upper Garonne basin. The sequence of glacial phases based on the distribution of the moraine systems, which was validated in the field, allowed the formulation of hypotheses about the glacial evolution. The most stable and preserved features of each moraine system were selected to be dated by means of surface exposure dating using the $^{10}$Be-isotope in order to unveil an estimated age of the moraine's formation. Finally, the palaeoglaciers and palaeoELAs from each glacial phase were reconstructed in GIS environments using semi-automatic tools.

## 3.1. Geomorphological mapping

The landscape is the thin layer on top of the landmasses that results from the interaction between the physical or/and anthropic domains (Griffiths et al., 2011). To understand it, geomorphological mapping received revolutionary attention from Earth science researchers in the 1950-60s in order to emphasise and explain their morphology, morphogenesis, evolution, activity and related deposits (Paron and Claessens, 2011). The geomorphological maps were drawn from several perspectives, such as both air and ground in order to adjust into small (<1:1.000.000) and large (>1:10.000/5.000) scales, respectively (Dramis and Bisci, 1998; Peña-Monné et al., 1997). Such tool brought light on the understanding of the natural evolution at the various time scales; i.e. macro (million), meso (thousands) and microscales (including present-day; Baker, 1986). Therefore, the geomorphological map synthesises the distribution of landforms giving a comprehensive picture to formulate theoretical assumptions of the triggers, forces, processes and constrainers within an interconnected landscape system.

In this dissertation, the reconnaissance of geomorphological features within the GIS environment and systematic validation in the field were carried out to create a detailed geomorphological map of the highest parts of the Upper Garonne basin, namely the Aran Valley (Chandler et al., 2018; Dramis et al., 2011). The details of the characteristics and sources used to identify landforms are described in the Paper 1 of this dissertation. The results of this work, especially concerning the glacial and periglacial landforms, supported the formulation of hypotheses about the natural evolution of the Upper Garonne valley, including glacial extent at the various glacial phases, permafrost distribution and paraglacial adjustment. The distribution of the moraines supported a chronosequence of glacial evolution that allowed the best identification possible of the potential sites to collect samples for CRE dating purposes.

## 3.2. Chronology of the glacial landscapes

The geochronology consists in collecting relative or numerical (radioisotopic, palaeomagnetic, chemical, biological) data from climate-driven natural archives: marine and lacustrine sediments, loess, ice, speleothems, biological material and geomorphological features (Bradley, 2015). Dating accurately a specific landform, sediment or organic material is of fundamental importance. Without it, it is impossible to formulate a solid hypothesis about the previous processes or propose any assumptions about palaeoclimatic and palaeoenvironmental events. Therefore, numerical methods represent the most reliable source to establish an absolute age to a certain landform, sediment, or organic content and to correlated it to a stratigraphic meaning at the various scales (local, regional, hemispheric or global). The most suitable method depends on the period of activity of geomorphic process we are looking for, the precision needed to constrain this process, and the available material.

In this sense, as a basis for palaeoglacier reconstructions, CRE dating has been widely used due to its precision and to the broad presence of cosmogenic nuclides in nature (Dunai, 2000). This technique has been used to study glacial oscillations, for instance, in the mountains surrounding the Mediterranean Basin, representing 77% of all radiometric ages reported in literature (Allard et al., 2021). Not surprisingly, the Pyrenees are the most studied range with 20% of all the ages out of the 18 major mountains. However, the distribution of the dated features is mainly centred on the Eastern side of the Pyrenees, and the glacial chronology of the Atlantic-influenced basins is still poorly studied. This dissertation provides further new dated features about the glacial and periglacial dynamics since the Mid-Late Pleistocene in the Atlantic-influenced areas of the Pyrenees, and results will be assessed and compared with available data in the Mediterranean-influenced valleys.

### 3.2.1. Principles of cosmogenic dating and Cosmic-Ray Exposure dating

The foundation of cosmogenic science was established more than 50 years ago and its application for CRE dating in Earth Sciences has exponentially increased during the last 20 years (Balco, 2011; Dunai and Lifton, 2014). The production of cosmogenic nuclides relies on the principle that the Earth's surface is continuously bombarded by cosmic radiation (high-energy particles originated outside the solar system) inducing nuclear reactions in the minerals of a rock surface (Balco, 2011; Gosse and Phillips, 2001; Lal and Peters, 1967). These reactions are mainly (98%) driven by spallation from secondary cosmic rays produced in the atmosphere and dominate cosmogenic nuclide production. However, this production is highly variable over time and setting: the detailed process is explained in detail in Gosse and Phillips (2001), Balco (2008) and Dunai (2010). The use of cosmogenic isotopes for dating has a variety of applications, such as exposure,

burial, erosion and uplift rates (Dunai, 2010). This can be applied to a wide range of scientific fields, such as can also be used for archaeological and sedimentological studies, soil production, soil residence studies, and growth rate of marine crusts, etc. In the case of the CRE, hundreds of nuclides can be formed from these interactions. However, only six ($^{10}$Be, $^{26}$Al, $^{36}$Cl, $^{14}$C, $^{3}$He, and $^{21}$Ne) are suitable for geomorphological processes, such as glacial dynamics (Ivy-Ochs and Kober, 2008). Extraordinary conditions are needed to a specific nuclide to be useful for understanding Earth surface dynamics: long half-lives in order to preserve isotope concentrations within the period of the process (e.g. $^{10}$Be is 1.4 Ma; Korschinek et al., 2010), nuclide is being rare enough to be distinguished from similar isotopes and finally being detectable within common minerals (Balco, 2020).

Over the last 10 years, the use of CRE dating for past glacial reconstructions has witnessed a revolutionary increase (Allard et al., 2021). Glacial landforms are suitable to be dated by CRE as short-length waves of cosmic rays cannot pass through the ice. Therefore, theoretically, the moment of ice retreat from a rock surface is the year zero of counting nuclide concentration (Davies, 2022). Hence, today's rock surfaces within previous ice limits yield an isotope concentration that is function of the time it has been exposed. Importantly, these CRE ages provide a direct age of the moraine formation or ice retreat rather than, for instance, radiocarbon, that gives the ages of the organic matter death after the deglaciation (Balco, 2011). Besides the numerical exposure time, an accurate dating also depends on the confidence that this period is glacial-derived and not affected by other processes (Balco, 2020). This last ingredient theoretically lies on the premise that inherited nuclides – i.e. concentration from previous exposure periods – were eliminated by glacial erosive dynamics, which tend to characterise the temperate glaciers of the mid-latitudes (Davies, 2022). Several works have shown overestimated ages due to nuclide inheritance, especially near rock walls (Applegate et al., 2012; Çiner et al., 2017). On the other hand, glacial-derived rock surfaces must be preserved from post-glacial dynamics to avoid underestimated exposure ages, as demonstrated by periods of landform stabilisation, rock surfaces buried by sediments or eroded by landslides resulting in nuclide concentrations that are not from the moment of glacial retreat (Briner et al., 2005; Palacios et al., 2019).

### 3.2.2. Sampling strategy

CRE dating can be applied to track Late Pleistocene glacial dynamics in the Pyrenees following a specific sampling strategy. Moraine boulders, erratic boulders and polished surfaces are the most common glacial landforms for CRE dating, although their geomorphological significance is different in each case. Dating moraine boulders is essential, as they indicate the periods of the maximum glacier advance favourable to build moraines and subsequent moraine stabilization. In fact, CRE ages on moraine boulders typically indicate the moment of moraine

stabilisation right after the glacial advance/stabilisation throughout a cold period (Davies, 2022). To better constrain the moraine age, large boulders should be selected as they tend to show better age clustering than smaller boulders, because their pronounced topography preclude post-glacial shielding (Heyman et al., 2016). On the other hand, erratics and polished surfaces reveal horizontal retreat and vertical thinning of the ice masses (Corbett et al., 2011; Fernández-Fernández et al., 2021). In practice, erratic boulders or polished surfaces suggest the timing of exposure after the glacier shrinking. In areas where no suitable erratic boulders are available, the bedrock is widely vegetated or covered with sediments, and inheritance is highly possible, smaller cobbles or pebbles with evidence of glacial transport can be used for cosmogenic dating (Dong et al., 2016; Hein et al., 2011; Rhee et al., 2022). In addition, attention is needed when applying this method to older surfaces than the GLGM, as this glaciation was large enough to delete most of the previous evidence and also because mountains passed through a destabilisation period – paraglacial phase – that eroded or covered most of the glacial surfaces. Besides that, other surfaces such as those from limestone outcrops are constantly dissolving, which is a major challenge to have accurate exposure ages (Hughes et al., 2022). Therefore, $^{10}$Be is one the most used isotopes to date glacial landforms as quartz is widely found and very resistant to weathering (Davies, 2022). Finally, the CRE dating allow us to understand the timing of the glacier footprint and the subsequent response to the climate oscillations that can be used to reveal the palimpsest of the palaeoclimate and palaeoenvironment during the Late Pleistocene in the mid-latitude mountain ranges.

The Central Pyrenees encompass granitoids rich in quartz minerals (23-25%; Kleinsmiede, 1960) allowing the extraction of the $^{10}$Be nuclide. From the backbone of the Central Pyrenees, glaciers have transported asymmetrical amounts of crystalline boulders down to the terminal basins of the MIE of the LGC (Goron, 1941). In the b, we collected 49 samples during the summer campaigns of 2016, 2019 and 2020 from polished surfaces, erratic and moraine boulders, as well as from rock glaciers for CRE dating (Fig. 1.19). We used a hammer and chisel to minimise the environmental and visual impact (Davies, 2022). To understand the chronology of the entire deglaciation of this catchment, boulders were collected from the terminal basin, from 420-440 m, up to the headwaters of the Garonne River, in the Ruda Valley, at 2400-2500 m (Table 1.7). The sampling strategy considered the results of the geomorphological mapping and field evidence. We attempted to collect a minimum of 3 to 5 samples per moraine, however the absence of suitable boulders in some of the moraines did not allow to collect such number of samples (Putkonen and Swanson, 2003). To be sure that boulders have been stable since the last glacial deposition, we targeted well-anchored and meter-sized boulders as they are more likely to yield well-clustered ages (Davies, 2022). The polished bedrock selected to be sampled stood out from the surroundings, minimising the risk of burial after glacier retreat. The erratic boulders selected

to be sampled had metric sizes and were located in stable areas far from the slopes, to reduce the risk of post-glacial transport or burial. In the case of rock glaciers, samples were collected from boulders far from the slopes and on the edge of the rock glacier's crests, avoiding the risk of being affected by paraglacial readjustment (Mercier, 2008). Each sample encompassed ca. 1 kg from the 3-5 cm of superficial rock extracted in flat or gentle top surfaces to guarantee the best layer of terrestrial cosmogenic production (Gosse and Phillips, 2001).

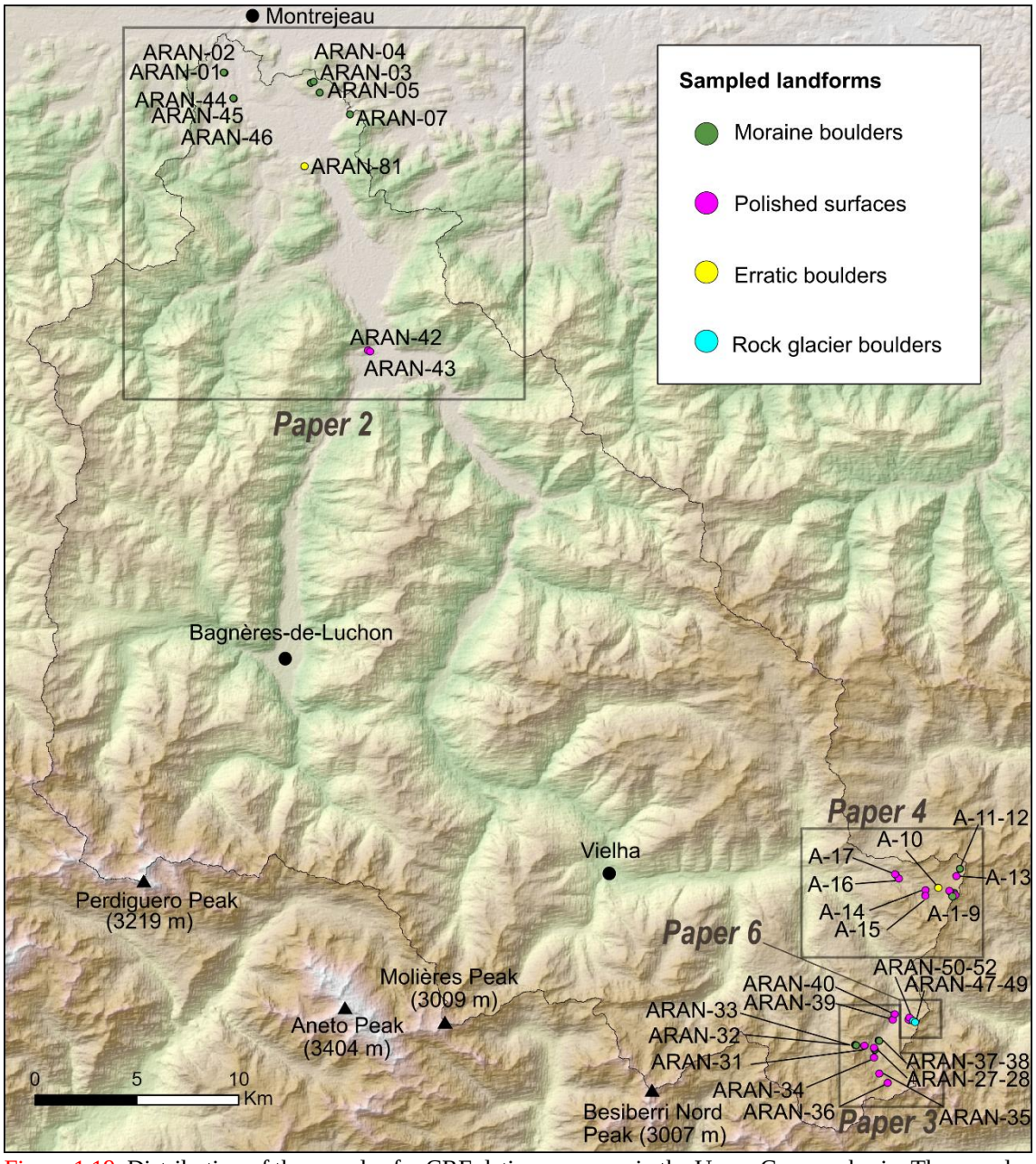


Figure 1.19. Distribution of the samples for CRE dating purposes in the Upper Garonne basin. The samples are clustered within the paper they are presented. Considering the scale of the map, some of the samples can not be clearly distinguished; although they can be checked in the respective paper.

Table 1.7. Main characteristics of the samples collected for CRE dating.

| Sample name | Landform | Latitude (DD) | Longitude (DD) | Elevation (m a.s.l.) | Geomorphological setting | Stratigraphic sequence of features | Lithology |
|---|---|---|---|---|---|---|---|
| ARAN-01 | Moraine boulder | 43.0537 | 0.5502 | 477 | Pyrenean foreland | | Quartzite |
| ARAN-02 | Moraine boulder | 43.0538 | 0.5497 | 481 | Pyrenean foreland | | Quartzite |
| ARAN-44 | Moraine boulder | 43.0388 | 0.5598 | 475 | Pyrenean foreland | | Aplite |
| ARAN-45 | Moraine boulder | 43.0389 | 0.5598 | 475 | Pyrenean foreland | Piedmont moraine (1a) | Quartzite |
| ARAN-46 | Moraine boulder | 43.0389 | 0.5598 | 474 | Pyrenean foreland | | Quartzite |
| ARAN-81 | Erratic boulder | 43.0098 | 0.6036 | 680 | Pyrenean foreland | | Granite |
| ARAN-03 | Moraine boulder | 43.0466 | 0.6060 | 674 | Pyrenean foreland | | Quartzite |
| ARAN-04 | Moraine boulder | 43.0473 | 0.6078 | 658 | Pyrenean foreland | | Quartzite |
| ARAN-05 | Moraine boulder | 43.0425 | 0.6114 | 576 | Pyrenean foreland | | Granite |
| ARAN-07 | Moraine boulder | 43.0332 | 0.6301 | 590 | Pyrenean foreland | Piedmont moraine (1b) | Granite |
| ARAN-42 | Polished surface | 42.9291 | 0.6454 | 541 | Pyrenean foreland | | Quartzite |
| ARAN-43 | Polished surface | 42.9287 | 0.6459 | 525 | Pyrenean foreland | | Quartzite |
| ARAN-40 | Polished surface | 42.6416 | 0.9713 | 1862 | Ruda Valley | | Granodiorite |
| ARAN-39 | Polished surface | 42.6393 | 0.9701 | 1900 | Ruda Valley | | Granodiorite |
| ARAN-38 | Moraine boulder | 42.6296 | 0.9624 | 2079 | Ruda Valley | Valley moraine (2b) | Granite |
| ARAN-37 | Moraine boulder | 42.6299 | 0.9620 | 2075 | Ruda Valley | | Granite |
| ARAN-28 | Polished surface | 42.6263 | 0.9593 | 2188 | Ruda Valley | | Granite |
| ARAN-27 | Moraine boulder | 42.6257 | 0.9599 | 2184 | Ruda Valley | | Granite |
| ARAN-36 | Polished surface | 42.6111 | 0.9681 | 2360 | Saboredo Cirque | | Granite |
| ARAN-35 | Polished surface | 42.6152 | 0.9630 | 2316 | Saboredo Cirque | | Granite |
| ARAN-34 | Polished surface | 42.6224 | 0.9596 | 2266 | Saboredo Cirque | Cirque moraine (3a) | Granite |
| ARAN-31 | Polished surface | 42.6274 | 0.9536 | 2378 | Saboredo Cirque | | Granite |
| ARAN-33 | Moraine boulder | 42.6275 | 0.9487 | 2470 | Sendrosa Cirque | | Granite |
| ARAN-32 | Moraine boulder | 42.6277 | 0.9480 | 2467 | Sendrosa Cirque | | Granite |
| ARAN-47 | Moraine boulder | 42.6399 | 0.9802 | 2236 | Lòcampo Cirque | | Granodiorite |
| ARAN-48 | Moraine boulder | 42.6398 | 0.9802 | 2236 | Lòcampo Cirque | | Granodiorite |
| ARAN-49 | Moraine boulder | 42.6397 | 0.9805 | 2240 | Lòcampo Cirque | Cirque moraine (2b) | Granodiorite |
| ARAN-53 | Moraine boulder | 42.6385 | 0.9836 | 2334 | Lòcampo Cirque | | Granodiorite |
| ARAN-54 | Moraine boulder | 42.6385 | 0.9836 | 2332 | Lòcampo Cirque | | Granodiorite |
| ARAN-50 | Rock glacier boulder | 42.6396 | 0.9797 | 2224 | Lòcampo Cirque | | Granodiorite |
| ARAN-51 | Rock glacier boulder | 42.6393 | 0.9803 | 2236 | Lòcampo Cirque | Periglacial transition | Granodiorite |
| ARAN-52 | Rock glacier boulder | 42.6391 | 0.9818 | 2266 | Lòcampo Cirque | | Granodiorite |
| A-16 | Polished surface | 42.7017 | 0.9717 | 1998 | Bacivèr Cirque | | Granodiorite |
| A-17 | Polished surface | 42.7033 | 0.9700 | 1949 | Bacivèr Cirque | | Granodiorite |
| A-14 | Polished surface | 42.6968 | 0.9880 | 2215 | Bacivèr Cirque | | Granodiorite |
| A-15 | Polished surface | 42.6946 | 0.9879 | 2179 | Bacivèr Cirque | | Granodiorite |
| A-10 | Erratic boulder | 42.6980 | 0.9956 | 2322 | Bacivèr Cirque | Cirque moraine (3a) | Granite |
| A-3 | Polished surface | 42.6950 | 1.0047 | 2436 | Bacivèr Cirque | | Granite |
| A-4 | Polished surface | 42.6948 | 1.0046 | 2438 | Bacivèr Cirque | | Granite |
| A-8 | Polished surface | 42.6961 | 1.0031 | 2371 | Bacivèr Cirque | | Granite |
| A-9 | Polished surface | 42.6967 | 1.0023 | 2353 | Bacivèr Cirque | | Granite |

| | | | | | | |
|---|---|---|---|---|---|---|
| A-13 | Polished surface | 42.7034 | 1.0063 | 2371 | Bacivèr Cirque | Granite |
| A-1 | Moraine boulder | 42.6959 | 1.0052 | 2431 | Bacivèr Cirque | Granite |
| A-2 | Moraine boulder | 42.6959 | 1.0052 | 2431 | Bacivèr Cirque | Granite |
| A-11 | Moraine boulder | 42.7034 | 1.0062 | 2371 | Bacivèr Cirque | Granite |
| A-12 | Moraine boulder | 42.7067 | 1.0083 | 2437 | Bacivèr Cirque | Granite |
| A-5 | Moraine boulder (Debris-covered) | 42.6945 | 1.0042 | 2437 | Bacivèr Cirque | Granite |
| A-6 | Moraine boulder (Debris-covered) | 42.6943 | 1.0043 | 2435 | Bacivèr Cirque | Granite |
| A-7 | Moraine boulder (Debris-covered) | 42.6945 | 1.0041 | 2434 | Bacivèr Cirque | Granite |

### 3.2.3. Laboratory analysis of the CRE samples

In accordance with the quartz-rich lithology of the study area, *in situ* produced cosmogenic nuclide $^{10}$Be concentration was quantified in the AMS. The procedure of $^{10}$Be preparation samples consists of two steps: isolation of quartz and isotope extraction (Gosse and Phillips, 2001).

The first step, or the physical processing, consists of crushing and sieving the samples to 125-500 µm fraction to easily get individual grain minerals, including pure quartz. This step was carried out at the Physical Geography Laboratory (Universidad Complutense de Madrid, Spain) in November-December 2019. Subsequently, in September-October 2020, minerals were separated with a magnetic separator (Frantz Magnetic Separator) at the Laboratoire National des Nucléides Cosmogéniques (LN2C) of the Centre Européen de Recherche et d'Enseignement des Géosciences de l'Environnement (CEREGE; Aix-en-Provence, France). The resulting non-magnetic fraction was chemically attacked with concentrated hydrochloric (1/3 HCl) and hexafluorosilicic (2/3 $H_2SiF_6$) acids aiming to dissolve the non-quartz fraction. Finally, the atmospheric $^{10}$Be was eliminated with four successive partial leaches of concentrated hydrofluoric acid (HF) (Kohl and Nishiizumi, 1992). This process of quartz purification should guarantee ca. 20 g of sample to young-expected age samples (<10 ka) and ca. 10 g to older ones.

In cases where isotopes contain low concentrations such as $^{10}$Be, a $^{9}$Be carrier is added before the total dissolution to ensure further detection of the $^{10}$Be/$^{9}$Be ratio by the AMS measurements (Dunai, 2010). In this sense, once the purification was completed, a spike of 150 µL of an in-house manufactured $^{9}$Be carrier solution was added to the samples (concentration: 3025 ± 9 µgg−1; Merchel et al., 2008). Thereafter, total dissolution was administered with 48% concentrated HC leaching (3.6 mL per gram of quartz + 30 mL). As a result, solutions of quartz were totally evaporated and then recovered with HCl (7.1 Mol). After that, ammonia was added ($NH_3$) to the samples allowing the precipitation of the samples to beryllium hydroxide ($Be(OH)_2$) at pH of 9. After that, 1.5 mL of HCL at 1 Mol was added to the samples in order to dissolve the Be (in a form of natant). The separation of Be from other elements was carried out by means of

resin columns; i.e. the Dowex 1 × 8 anionic exchange column was used to remove elements such as Fe, Mn and Ti, and the Dowex 50WX8 cationic exchange column was used to discard B and recover Be (Merchel and Herpers, 1999). Finally, the eluted Be was precipitated, dried and then oxidised to BeO at 700 ºC, the result of which was mixed with niobium powder at similar proportions into copper cathodes (Fig. 1.20).

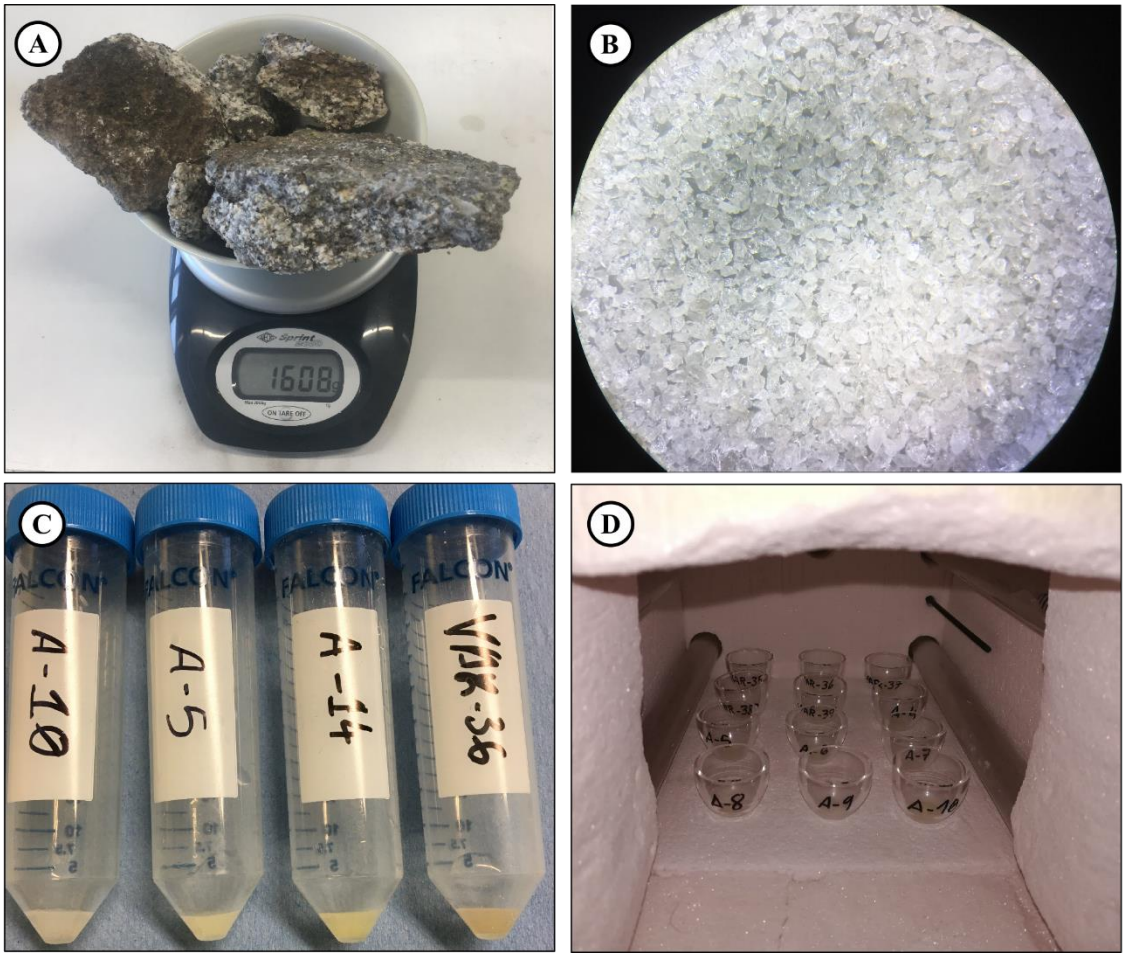


Figure 1.20. Illustration of the steps followed during the sample processing: A) original state; B) the pure-quartz fraction at the microscope; C) the state of precipitated Be inside of the centrifuge tubes; D) BeO after the oxidation in the oven.

The concentration of $^{10}$Be from each target is calculated from the $^{10}$Be/$^{9}$Be ratio measured at the Accelerator pour les Sciences de la Terre, Environnement et Risques (ASTER) National AMS facility at CEREGE. The AMS measurements were calibrated against the in-house standard STD-11 with an assigned $^{10}$Be/$^{9}$Be ratio of (1.191 ± 0.013) × $10^{-11}$ (Braucher et al., 2015). The analytical part of the uncertainties at 1σ result from the AMS uncertainties counting statistics, the external 0.5% AMS error (Arnold et al., 2010), and uncertainties related with the chemical blank correction.

## 3.2.4. Exposure age calculation, scaling schemes and uncertainties

A set of online calculators is available to calculate exposure ages, including the CRONUS-Earth (Balco et al., 2008; Phillips et al., 2016), CREp (Martin et al., 2017) and IceTEA

tools (Jones et al., 2019). At the latitudes of the Pyrenees and the altitude of the samples, no major differences are to be expected from the different calculators (Balco et al., 2008). However, in order to compare with other published CRE ages, we have used the CREp calculator (https://crep.otelo.univ-lorraine.fr/#/). This semi-automatic calculation requires a set of variables organised in an excel spreadsheet available on the website: ID, latitude, longitude, altitude, $^{10}$Be concentration (at/g), shielding corrector, rock density, sample thickness (cm), measured uncertainty, erosion rate.

Production rate and scaling factors support any reliable exposure age calculation from cosmogenic nuclide concentration (Dunai, 2010). The production rates from any isotope can be defined in several ways, where the most common derive from its concentration measurement at a rock surface whose exposure history is already known from another independent proxy (Gosse and Phillips, 2001). The isotope with more local production rates is the $^{10}$Be (e.g. Balco et al., 2008; Small and Fabel, 2015). However, because no local production rate for $^{10}$Be is available from the Pyrenees, I used the worldwide mean production rate at sea level high latitude (SLHL) of 3.98 ± 0.22 atoms $g^{-1}$ $yr^{-1}$ that is available in the CREp tool (Martin et al., 2017). This reference occurs at high latitudes because cosmic-ray fluxes are stable over long time scales, as it does not change with geomagnetic field shifts (Dunai and Lifton, 2014).

On the other hand, the *in situ* cosmogenic nuclide production depends on the variability of cosmic-ray flux at altitude, latitude and time, called scaling factors (Darvill, 2013). They aim to model all the effects of the cosmic-ray flux in the production rate at a specific location (Desilets and Zreda, 2003; Dunai, 2000; Lal, 1991; Lifton et al., 2005; Stone, 2000); e.g. cosmogenic isotope production rate doubles every 1000 m of altitude increase (Dunai, 2010) or changes in climate dynamics at synoptic scale may influences around 10% of the production rates over glacial cycles (Dunai, 2010). Moreover, the geomagnetic field also influences production rates in time and space. Secondary cosmic-flux and production rates of terrestrial cosmogenic nuclides increase with geomagnetic latitude due to the penetration of a broad spectrum of rays at the atmosphere through poles within the last 10 ka (15-35% changes in the production rate; Dunai, 2001). Empirical studies suggest that production rates are time-dependency on long-term scales (Gosse and Phillips, 2001). Between 10 and 100 ka, the dipole geomagnetic field changed significantly, causing shifts of about 3% in production rates (Desilets and Zreda, 2003; Dunai, 2001; Lifton et al., 2005). In addition, cosmic-ray fluxes tend to be higher during periods of high solar modulation, which is intimately related to solar activity, affecting ca. 18% of cosmogenic-nuclide production at high latitudes (Desilets and Zreda, 2003; Dunai, 2010; Lifton et al., 2005). Therefore, these claims grounded our following choices in the settings of the CREp tool: LSD (Lifton-Sato-Dunai) elevation/latitude scaling scheme (Lifton et al., 2014), ERA40 atmospheric model (Uppala et al., 2005) and geomagnetic database based on the LSD framework (Lifton et

al., 2014). In any case, I have always used the same factors to make more accessible the comparison of the resulting CRE ages.

The relief also affects cosmogenic nuclide concentrations as it can block the cosmic-flux to reach an exposure of rock surfaces reducing nuclide production (Darvill, 2013; Gosse and Phillips, 2001). Commonly, in mountain environments, the impact of the topographical shielding on the nuclide production rate can be modelled based on the geometry of the surrounding slopes (Dunne et al., 1999). In a GIS environment, this effect is measured and quantified by an index (0-1) whose technical details are described in Li, (2018).

The exposure ages can be affected by other sources of error, such as rock erosion rates and snow shielding. The superficial layer of glacially modulated rock surfaces is altered by post-glacial weathering that can be measurable from 0.2 to 5 mm $ka^{-1}$, depending on the lithology (André, 2002). In this dissertation, we have adopted the 0.2- and 1-mm $ka^{-1}$ to better fit in the crystalline rock outcrops from the batholiths of Garonne's headwater (Steinemann et al., 2020; Zasadni et al., 2020). In the same train of thought, winter snow cover attenuates the radiation that reaches the rock surfaces (Gosse and Phillips, 2001). In the case of the Central Pyrenees, we have assumed the current annual average of snow cover of 7.5 months at 2200 m and a thickness of 100 cm with 0.2 g $cm^{-3}$ of density (Styllas et al., 2018). In this dissertation, in spite of all CRE ages are calculated with and without correction (Paper 2, 3, 4, 6), the ones without are selected in order to compare with other published ages (Oliva et al., 2022c). Oliva et al. (2023c) demonstrated that in the Iberian Mountains, most of the published ages contain no correction, therefore, I have used CRE ages without correction throughout this dissertation (Papers 2, 3, 4, 6) in order to compare with other study cases.

Uncertainties must be considered to assess the validity of interpretations based on the CRE measurements. In the CRE dating, uncertainty comes from different sources: i) analytical, ii) methodological and iii) natural (Dunai, 2010). The analytical uncertainty results from the sample treatment, counting from the sample collection until the AMS measurement, which can lead to a 1-6% of error. This uncertainty is numerically presented in the form of external/full (1σ; derived from analytical and production rate uncertainties) and internal/analytical uncertainties. Throughout the discussion, only full uncertainties are used in order to compare with other ages, including from other nuclides or methods (Balco et al., 2008). The methodological source of error is related to the production rates, scaling factors, half-lives, and mass attenuation, resulting in a 5-15% error (Dunai, 2010). This parameter can be important if the local production rate is available as it reduces the full uncertainties (Balco, 2011). Finally, the last errors result from the intrinsic geomorphological history of the sample: post-glacial burial, inheritance or shielding history. This source of error can determine the validity of the age; for instance, an age that is much

younger than the rest of the dataset, with the samples showing possible traces of having being buried (e.g. site of the sampling is at the surface level or show signs of fresh surface compared to the rest of the samples) should be excluded from the set of ages.

### 3.2.5. Identification of outliers and dataset consistency

Interpretation of CRE ages and their association with other climate proxies depends on the scattering of the age dataset that should be assessed before defining an age to a rock surface. Therefore, as soon as the ages are calculated, Earth scientists try to identify outliers with the various available tools (Balco, 2011). The most common is based on the statistical method of the chi-squared test that identifies whether scatting is only a source of uncertainty or if there is another geomorphological process affecting that age (Ward and Wilson, 1978). If it is only a matter of well-distributed uncertainties among the dataset, the mean age yields a more accurate landform age than a single age alone. On the other hand, if scattering is caused by other processes, outliers should be eliminated in order to apply the mean age (Davies, 2022). However, giving an age to a moraine from a CRE dataset can also derive from selecting the youngest age or the oldest. The selection of the best choice is related to the glacial and postglacial dynamics of the study area. Age datasets from regions controlled by cold-based glaciers normally contain inheritance problems resulting in old biased ages. In these cases, the closest age to the true history is by selecting the youngest age of the dataset. On the contrary, in temperate-based glacier regions, post-glacial dynamics also cause incomplete exposure history due to surface erosion, exhumation, and moraine degradation, especially to ages prior to the last glacial cycle, resulting in scattered ages (Davies, 2022). In these cases, the biased young age could be solved by selecting the oldest age and considering it the minimum age for the deglaciation (Heyman et al., 2011).

## 3.3. Palaeoglaciers and palaeoELAS reconstruction

The relationship between summer temperatures and annual precipitation with the position of the current Equilibrium Line Altitude (ELA) has been empirically demonstrated (Ohmura et al., 1992). Hence, knowing previous glacier positions based on geomorphology evidence, it is possible to infer the respective climates (Pearce et al., 2017; Vieira, 2008). Therefore, modelling precisely the geometry of palaeoglaciers is essential to better reconstruct such palaeoELAs, and glacial dynamics related to different climatic contexts (Benn and Evans, 2010; Carr et al., 2010).

In this dissertation, palaeoglacier reconstruction was carried out for each dated moraine and, therefore, all glacial phases. The position of the frontal moraine allows the geomorphologically-based palaeoglacier reconstructions using the semi-automatic GlaRE toolbox (Pellitero et al., 2016). As glacier ice behaviour is defined by slow deformed viscous fluid, this model assumes perfect plastic rheology (Cuffey and Paterson, 2010). This glacial deformation, or creep, is modelled with the physical equation of Schilling and Hollin (1981) based

on the following variables: basal shear stress (kPa), shape factor index, ice density (900 kg $m^{-3}$), gravitational acceleration (9.81 m $s^{-2}$), step length (m) and ice thickness (m). Van der Veen (1999) improved this equation, solving the problem when ice thickness equals 0. The tool proposed by Pellitero et al. (2015) requires a Digital Elevation Model (DEM; 5 m of spatial resolution from the official national hypsometry in France (https://www.geoportail.gouv.fr/carte) and Spain http://www.ign.es/iberpix/visor)), a shapefile with the approximated palaeoglacier geometry and a flowline are required. Glacial modelling was organised in three steps: basal shear stress, shape factor (F factor) and interpolation. Nodes defined the basal shear stress along the flowline from the terminal moraine to the headwaters, including tributaries connected with the main trunk (Paterson, 1994). The ice thickness was calculated in each node by using a shear stress of 100 kPa, which is a common value in temperate valley glaciers (Cuffey and Paterson, 2010). Subsequently, the ice thickness was improved with the F factor that basically provides the glacier lateral drag generated by valley slopes that significantly reduces the error associated with <10% in volume and ca. 6% in surface (Nye, 1952). This step was given by cross-sections along the valley sectors (Benn and Hulton, 2010). Once the ice thickness values were improved, the interpolation was processed to extract the resulting DEM of the palaeoglacier surface. Such workflow was repeated for each glacier phase document in this dissertation.

The ELA represents the position of the zero-mass balance of the glacier and the climate conditions to glacier persistence (Nesje, 1992; Ohmura et al., 1992). The supra mentioned palaeoglacier tool allows calculating the palaeoELA from each reconstructed model using the automatic tool developed by Pellitero et al. (2015). The selected methods were the Accumulation Area Ratio (Porter, 1975) and the Area Altitude Balance Ratio (Osmaston, 2005). Further technical considerations are described in the research articles included in Papers 2, 3 and 4 of this dissertation.

# 4. References


Adamson, K.R., Hughes, P.D., Woodward, J.C., 2013. Pleistocene glaciation of the Mediterranean Mountains. Quat. Newsl. 131, 2–15.

Alimen, H., 1964. Le Quaternaire des Pyrénées de la Bigorre, Mémoire du Service de la Carte Géologique.

Allard, J.L., Hughes, P.D., Woodward, J.C., 2021. Earth-Science Reviews A radiometric dating revolution and the Quaternary glacial history of the Mediterranean mountains. Earth-Science Rev. 223, 103844. https://doi.org/10.1016/j.earscirev.2021.103844

Allen, R., Siegert, M.J., Payne, A.J., 2008. Reconstructing glacier-based climates of LGM Europe and Russia - Part 2: A dataset of LGM precipitation/temperature relations derived from degree-day modelling of palaeo glaciers. Clim. Past 4, 249–263. https://doi.org/10.5194/cp-4-249-2008

André, M.F., 2002. Rates of Postglacial rock weathering on glacially scoured outcrops (Abisko-Riksgränsen area, 68°N). Geogr. Ann. Ser. A Phys. Geogr. 84, 139–150. https://doi.org/10.1111/j.0435-3676.2002.00168.x

Andrés, N., Gómez-Ortiz, A., Fernández-Fernández, J.M., Tanarro, L.M., Salvador-Franch, F., Oliva, M., Palacios, D., 2018. Timing of deglaciation and rock glacier origin in the southeastern Pyrenees: a review and new data. Boreas 47, 1050–1071. https://doi.org/10.1111/bor.12324

Andrieu, V., 1991a. Dynamique du paléoenvironnement de la vallée montagnarde de la Garonne (Pyrénées Centrales, France) dela fin des temps glaciaires à l'actuel. University of Toulouse, Toulouse-2.

Andrieu, V., 1991b. Paysages de la haute Garonne depuis les temps glaciaires. Rev. Geogr. Pyren. Sud. Ouest. 62, 95–99. https://doi.org/10.3406/rgpso.1991.3241

Andrieu, V., 1987. Le paléoenvironnement du piémont nord-pyrénéen occidental de 27 000 BP au Postglaciaire: la séquence d'Estarrès (Pyrénées Atlantiques, France) dans le bassin glaciaire d'Arudy. Comptes-Rendus l'Académie des Sci. 304, 103–108.

Andrieu, V., Hubschman, J., Jalut, G., Hérail, G., 1988. Chronologie de la déglaciation des Pyrénées françaises . Dynamique de sédimentation et contenu pollinique des paléolacs; application à l ' interprétation du retrait glaciaire. Bull. l'Association française pour l'étude du Quat. 25, 55–67. https://doi.org/doi.org/10.3406/quate.1988.1866

Applegate, P.J., Urban, N.M., Keller, K., Lowell, T. V., Laabs, B.J.C., Kelly, M.A., Alley, R.B., 2012. Improved moraine age interpretations through explicit matching of geomorphic process models to cosmogenic nuclide measurements from single landforms. Quat. Res. 77, 293–304. https://doi.org/10.1016/j.yqres.2011.12.002

Arnold, M., Merchel, S., Bourlès, D.L., Braucher, R., Benedetti, L., Finkel, R.C., Aumaître, G., Gottdang, A., Klein, M., 2010. The French accelerator mass spectrometry facility ASTER: Improved performance and developments. Nucl. Instruments Methods Phys. Res. Sect. B Beam Interact. with Mater. Atoms 268, 1954–1959. https://doi.org/10.1016/j.nimb.2010.02.107

Bakalowicz, M., Sorriaux, P., Ford, D., 1984. Quaternary glacial events in the Pyrenees from U-series dating of speleothems in the Niaux-Lombrives-Sabart caves, Ariège, France. Nor. Geogr. Tidsskr. 38, 193–197. https://doi.org/10.1080/00291958408552125

Baker, V., 1986. Introduction: regional landform analysis, in: Short, N.M., Blain Jr., R.W. (Eds.), Geomorphology From Space: A Global Overview of Regional Landforms. pp. 1–26.

Balco, G., 2020. Glacier Change and Paleoclimate Applications of Cosmogenic-Nuclide Exposure Dating. Annu. Rev. Earth Planet. Sci. 48, annurev-earth-081619-052609. https://doi.org/10.1146/annurev-earth-081619-052609

Balco, G., 2011. Contributions and unrealized potential contributions of cosmogenic-nuclide exposure dating to glacier chronology, 1990-2010. Quat. Sci. Rev. 30, 3–27. https://doi.org/10.1016/j.quascirev.2010.11.003

Balco, G., Stone, J.O., Lifton, N.A., Dunai, T.J., 2008. A complete and easily accessible means of calculating surface exposure ages or erosion rates from 10Be and 26Al measurements. Quat. Geochronol. 3, 174–195. https://doi.org/10.1016/j.quageo.2007.12.001

Ballantyne, C.K., 2002. Paraglacial Geomorphology. Encycl. Quat. Sci. Second Ed. 21, 553–565. https://doi.org/10.1016/B978-0-444-53643-3.00089-3

Barrère, P., Bouquet, C., Debroas, E.J., Pelissonnier, H., Peybernes, B., Soulé, J.C., Souquet, P., Ternet, Y., 1984. BRGM Geological map 1/50 000 - Arreau.

Bartolomé, M., Moreno, A., Sancho, C., Stoll, H.M., Cacho, I., Spötl, C., Belmonte, Á., Edwards, R.L., Cheng, H., Hellstrom, J.C., 2015. Hydrological change in Southern Europe responding to increasing North Atlantic overturning during Greenland Stadial 1. Proc. Natl. Acad. Sci. 112, 6568–6572. https://doi.org/10.1073/pnas.1503990112

Batalla, R.J., Vericat, D., Tena, A., 2014. The fluvial geomorphology of the lower Ebro (2002-2013): bridging gaps between management and research. Cuad. Investig. Geográfica 40, 29–52. https://doi.org/10.18172/cig.2569

Becker, D., Verheul, J., Zickel, M., Willmes, C., 2015. LGM paleoenvironment of Europe - Map. CRC806-Database. https://doi.org/10.5880/SFB806.15

Benn, D.I., Evans, D.J.A., 2010. Glaciers and Glaciation, Second edi. ed, Hodder Education. London. https://doi.org/10.5860/CHOICE.35-6240

Benn, D.I., Hulton, N.R.J., 2010. An Excel™ spreadsheet program for reconstructing the surface profile of former mountain glaciers and ice caps. Comput. Geosci. 36, 605–610. https://doi.org/10.1016/j.cageo.2009.09.016

Bernal-Wormull, J.L., Moreno, A., Pérez-Mejías, C., Bartolomé, M., Aranburu, A., Arriolabengoa, M., Iriarte, E., Cacho, I., Spötl, C., Edwards, R.L., Cheng, H., 2021. Immediate temperature response in northern Iberia to last deglacial changes in the North Atlantic. Geology 49, 999–1003. https://doi.org/10.1130/G48660.1

Bolòs, O. de, Vigo, J., 1984. Flora dels països catalans. Editorial Barcino, Barcelona.

Bordonau, J., 1992. Els complexos glàcio-lacustres relacionats amb el darrer cicle glacial als Pirineus. Universitat de Barcelona.

Bordonau, J., 1985. Estudi geomorfològic del sector sudoccidental de la Vall d'Aran. L'evolució Quaternària de les valls dels rius Joeu i Nere. Tesis de Licenciatura.

Bordonau, J., Manuel Vilaplana, J., Fontugne, M., 1993. The Glaciolacustrine complex of Llestui (Central Southern Pyrenees): a key-locality for the chronology of the last glacial cycle in the Pyrenees. Comptes-Rendus l'Académie des Sci. des Sci. II, 807–813.

Bordonau, J., Pous, J., Queralt, P., Vilaplana, J.M., 1989. Geometría y depósitos de las cubetas glaciolacustres del Pirineo. Estud. Geol. 45, 71–79. https://doi.org/10.3989/egeol.89451-2482

Bosch, G., Van Den Driessche, J., Babault, J., Robert, A., Carballo, A., Le Carlier, C., Loget, N., Prognon, C., Wyns, R., Baudin, T., 2016. Peneplanation and lithosphere dynamics in the Pyrenees. Comptes Rendus Geosci. 348, 194–202.

https://doi.org/10.1016/j.crte.2015.08.005

Boule, M., 1895. Le plateau de Lannemezan et les alluvions anciennes des hautes vallées de la Garonne et de la Neste. Bull. du Serv. la Cart. géologique la Fr. 6.

Bradley, R.S., 2015. Paleoclimatology. Reconstructing climates of the Quaternary, Third. ed. Elsevier.

Braucher, R., Guillou, V., Bourlès, D.L., Arnold, M., Aumaître, G., Keddadouche, K., Nottoli, E., 2015. Preparation of ASTER in-house 10Be/9Be standard solutions. Nucl. Instruments Methods Phys. Res. Sect. B Beam Interact. with Mater. Atoms 361, 335–340. https://doi.org/https://doi.org/10.1016/j.nimb.2015.06.012

Breuil, H., 1937. Terrasses et quartzites taillés de la Haute-Vallée de la Garonne. Bull. la Société préhistorique Fr. 34, 104–130. https://doi.org/10.3406/bspf.1937.4519

Briner, J.P., Kaufman, D.S., Manley, W.F., Finkel, R.C., Caffee, M.W., 2005. Cosmogenic exposure dating of late Pleistocene moraine stabilization in Alaska. Geol. Soc. Am. Bull. 117, 1108–1120. https://doi.org/10.1130/B25649.1

Brus, D.J., Hengeveld, G.M., Walvoort, D.J.J., Goedhart, P.W., Heidema, A.H., Nabuurs, G.J., Gunia, K., 2012. Statistical mapping of tree species over Europe. Eur. J. For. Res. 131, 145–157. https://doi.org/10.1007/s10342-011-0513-5

Bruxelles, L., Jarry, M., 2011. Climatic conditions, settlement patterns and cultures in the Paleolithic: The example of the Garonne Valley (southwest France). J. Hum. Evol. https://doi.org/10.1016/j.jhevol.2011.05.009

Cacho, I., 2022. Quaternary ice ages in the Iberian Peninsula, in: Oliva, M., Palacios, D., Fernández-Fernández, J.M. (Eds.), Iberia, Land of Glaciers. Elsevier B.V, Amsterdam, pp. 13–35.

Cacho, I., Grimalt, J.O., Canals, M., Sbaffi, L., Shackleton, N.J., Schönfeld, J., Zahn, R., 2001. Variability of the western Mediterranean Sea surface temperature during the last 25,000 years and its connection with the Northern Hemisphere climatic changes. Paleoceanography 16, 40–52. https://doi.org/10.1029/2000PA000502

Calvet, M., 2004. The Quaternary glaciation of the Pyrenees. Dev. Quat. Sci. 2, 119–128. https://doi.org/10.1016/S1571-0866(04)80062-9

Calvet, M., Delmas, M., Gunnell, Y., Braucher, R., Bourlès, D., 2011a. Recent Advances in Research on Quaternary Glaciations in the Pyrenees, in: Developments in Quaternary Science. pp. 127–139. https://doi.org/10.1016/B978-0-444-53447-7.00011-8

Calvet, M., Delmas, M., Gunnell, Y., Braucher, R., Bourlès, D.L., 2011b. Recent advances in research on quaternary glaciations in the pyrenees. Dev. Quat. Sci. 15, 127–139. https://doi.org/10.1016/B978-0-444-53447-7.00011-8

Calvet, M., Gunnell, Y., Laumonier, B., 2021. Denudation history and palaeogeography of the Pyrenees and their peripheral basins: an 84-million-year geomorphological perspective. Earth-Science Rev. 215, 103436. https://doi.org/10.1016/j.earscirev.2020.103436

Carbonnières, R. de, 1792. Voyage et observations faites dans les Pyrénées.

Carlson, A.E., Clark, P.U., 2012. Ice sheet sources of sea level rise and freshwater discharge during the last deglaciation. Rev. Geophys. 50.

Carr, S.J., Lukas, S., Mills, S.C., 2010. Glacier reconstruction and mass-balance modelling as a geomorphic and palaeoclimatic tool 1115, 1103–1115. https://doi.org/10.1002/esp.2034

Casas, J.M., Álvaro, J.J., Clausen, S., Padel, M., Puddu, C., Sanz-López, J., Sánchez-García, T.,

Navidad, M., Castiñeiras, P., Liesa, M., 2019. Palaeozoic Basement of the Pyrenees, in: Quesada, C., Oliveira, J.T. (Eds.), The Geology of Iberia: A Geodynamic Approach (The Variscan Cycle). Springer, pp. 229–259. https://doi.org/10.1007/978-3-030-10519-8_8

Català, A., Cacho, I., Frigola, J., Pena, L.D., Lirer, F., 2019. Holocene hydrography evolution in the Alboran Sea: A multi-record and multi-proxy comparison. Clim. Past 15, 927–942. https://doi.org/10.5194/cp-15-927-2019

Cavaillé, A., 1953. Formation, évolution et classification des sols du département de Tarn et Garonne. Bull. l'Association française pour l'étude du sol 2–18.

Chandler, B.M.P., Lovell, H., Boston, C.M., Lukas, S., Barr, I., Benediktsson, Í.Ö., Benn, D.I., Clark, C.D., Darvill, C.M., Evans, D.J.A., Ewertowski, M.W., Loibl, D., Margold, M., Otto, J.C., Roberts, D.H., Stokes, C.R., Storrar, R.D., Stroeven, A.P., 2018. Glacial geomorphological mapping: A review of approaches and frameworks for best practice. Earth-Science Rev. 185, 806–846. https://doi.org/10.1016/j.earscirev.2018.07.015

Chaput, E., 1927. Recherches sur l'évolution des terrasses de l'Aquitaine. Bull. la Société d'Histoire Nat. Toulouse XVI, 17–100.

Chaput, E., 1924. L'origine des terrasses de la Garonne. Bull. la Société Géologique Fr. 4º, 449–461.

Charpentier, J.G.F. von, 1823. Essai sur la constitution géognostique des Pyrénées.

Choukroune, P., 1992. Tectonic evolution of the Pyrenees. Annu. Rev. Earth Planet. Sci. Vol. 20 143–158. https://doi.org/10.1146/annurev.ea.20.050192.001043

Chylek, P., Lesins, G., Lohmann, U., 2001. Enhancement of dust source area during past glacial periods due to changes of the Hadley circulation. J. Geophys. Res. Atmos. 106, 18477–18485.

Çiner, A., Sarıkaya, M.A., Yıldırım, C., 2017. Misleading old age on a young landform? The dilemma of cosmogenic inheritance in surface exposure dating: Moraines vs. rock glaciers. Quat. Geochronol. 42, 76–88. https://doi.org/10.1016/j.quageo.2017.07.003

Clark, P.U., Dyke, A., Shakun, J.D., Carlson, A.E., Wohlfarth, B., Mitrovica, J., Hostetler, S., McCabe, A., 2009. The Last Glacial Maximum. Science (80-. ). 325, 710–714. https://doi.org/10.1126/science.1172873

Clin, M., Taillefer, F., Pouchan, P., Muller, A., 1989. La carte géologique à 1/50000 Bagnères-de-Luchon. Bur. Rech. GÉOLOGIQUES MINIÈRES 1–80.

Cochelin, B., 2017. Champ de déformation du socle paléozoïque des Pyrénées. University of Toulouse 3.

Colleoni, F., Wekerle, C., Näslund, J., Brandefelt, J., Masina, S., 2016. Constraint on the penultimate glacial maximum Northern Hemisphere ice topography (~140 kyrs BP). Quat. Sci. Rev. 137, 97–112. https://doi.org/10.1016/j.quascirev.2016.01.024

Corbett, L.B., Young, N.E., Bierman, P.R., Briner, J.P., Neumann, T.A., Rood, D.H., Graly, J.A., 2011. Paired bedrock and boulder 10 Be concentrations resulting from early Holocene ice retreat near Jakobshavn Isfjord , western Greenland. Quat. Sci. Rev. 30, 1739–1749. https://doi.org/10.1016/j.quascirev.2011.04.001

Crest, Y., Delmas, M., Braucher, R., Gunnell, Y., Calvet, M., 2017. Cirques have growth spurts during deglacial and interglacial periods: Evidence from 10Be and 26Al nuclide inventories in the central and eastern Pyrenees. Geomorphology 278, 60–77. https://doi.org/10.1016/j.geomorph.2016.10.035

Cuffey, K.M., Paterson, W.S.B., 2010. The Physics of Glaciers, Fourth. ed. Elsevier.

Cunill, R., Soriano, J.M., Bal, M.C., Pèlachs, A., Rodriguez, J.M., Pérez-Obiol, R., 2013. Holocene high-altitude vegetation dynamics in the Pyrenees: A pedoanthracology contribution to an interdisciplinary approach. Quat. Int. 289, 60–70. https://doi.org/10.1016/j.quaint.2012.04.041

Darvill, C.M., 2013. Cosmogenic nuclide analysis. Br. Soc. Geomorphol. Geomorphol. Tech. 4, 10.

Davies, B.J., 2022. Cryospheric Geomorphology: Dating Glacial Landforms II: Radiometric Techniques, in: Treatise on Geomorphology. Elsevier, pp. 249–280. https://doi.org/10.1016/B978-0-12-818234-5.00040-7

Davis, P.T., Menounos, B., Osborn, G., 2009. Holocene and latest Pleistocene alpine glacier fluctuations: a global perspective. Quat. Sci. Rev. 28, 2021–2033. https://doi.org/10.1016/j.quascirev.2009.05.020

DeFelipe, I., Pedreira, D., Pulgar, J.A., van der Beek, P.A., Bernet, M., Pik, R., 2019. Unraveling the Mesozoic and Cenozoic Tectonothermal Evolution of the Eastern Basque-Cantabrian Zone–Western Pyrenees by Low-Temperature Thermochronology. Tectonics 38, 3436–3461. https://doi.org/10.1029/2019TC005532

Delmas, M., 2015. The last maximum ice extent and subsequent deglaciation of the Pyrenees: an overview of recent research. Cuad. Investig. Geográfica 41, 359. https://doi.org/10.18172/cig.2708

Delmas, M., 2011. La déglaciation dans le massif du Carlit (Pyrénées orientales): approches géomorphologique et géochronologique nouvellesThe deglaciation in the Carlit massif: news geomorphological and geochronological insights. Quaternaire 16, 45–55. https://doi.org/10.4000/quaternaire.198

Delmas, M., 2005. LA DÉGLACIATION DANS LE MASSIF DU CARLIT (Pyrénées orientales): APPROCHES GÉOMORPHOLOGIQUE ET GÉOCHRONOLOGIQUE NOUVELLES. Quaternaire 45–55.

Delmas, M., Braucher, R., Gunnell, Y., Guillou, V., Calvet, M., Bourlès, D.L., 2015. Constraints on Pleistocene glaciofluvial terrace age and related soil chronosequence features from vertical 10Be profiles in the Ariège River catchment (Pyrenees, France). Glob. Planet. Change 132, 39–53. https://doi.org/10.1016/j.gloplacha.2015.06.011

Delmas, M., Calvet, M., Gunnell, Y., 2009. Variability of Quaternary glacial erosion rates - A global perspective with special reference to the Eastern Pyrenees. Quat. Sci. Rev. 28, 484–498. https://doi.org/10.1016/j.quascirev.2008.11.006

Delmas, M., Calvet, M., Gunnell, Y., Braucher, R., Bourlès, D.L., 2011. Palaeogeography and 10Be exposure-age chronology of Middle and Late Pleistocene glacier systems in the northern Pyrenees: Implications for reconstructing regional palaeoclimates. Palaeogeogr. Palaeoclimatol. Palaeoecol. 305, 109–122. https://doi.org/10.1016/j.palaeo.2011.02.025

Delmas, M., Calvet, M., Gunnell, Y., Voinchet, P., Manel, C., Braucher, R., Tissoux, H., Bahain, J.-J., Perrenoud, C., Saos, T., 2018. Terrestrial 10Be and electron spin resonance dating of fluvial terraces quantifies quaternary tectonic uplift gradients in the eastern Pyrenees. Quat. Sci. Rev. 193, 188–211. https://doi.org/10.1016/j.quascirev.2018.06.001

Delmas, M., Gunnell, Y., Braucher, R., Calvet, M., Bourlès, D.L., 2008. Exposure age chronology of the last glaciation in the eastern Pyrenees. Quat. Res. 69, 231–241. https://doi.org/10.1016/j.yqres.2007.11.004

Delmas, M., Gunnell, Y., Calvet, M., Reixach, T., Oliva, M., 2023a. The Pyrenees: environments and landforms in the aftermath of the LGM (18.9-14.6 ka), in: Palacios, D., Hughes, P., García-Ruiz, J.M., Andrés, N. (Eds.), European Glacial Landscapes. Elsevier, Amsterdam.

Delmas, M., Gunnell, Y., Calvet, M., Reixach, T., Oliva, M., 2022a. The Pyrenees: glacial landforms prior to the Last Glacial Maximum, in: Palacios, D., Hughes, P., García-Ruiz, J.M., Andrés, N. (Eds.), European Glacial Landscapes. Elsevier, pp. 295–307. https://doi.org/10.1016/B978-0-12-823498-3.00020-0

Delmas, M., Gunnell, Y., Calvet, M., Reixach, T., Oliva, M., 2022b. The Pyrenees: glacial landforms from the Last Glacial Maximum, in: Palacios, D., Hughes, P., García-Ruiz, J.M., Andrés, N. (Eds.), European Glacial Landscapes. Elsevier, pp. 461–472. https://doi.org/10.1016/B978-0-12-823498-3.00035-2

Delmas, M., Gunnell, Y., Calvet, M., Reixach, T., Oliva, M., 2022c. Glacial landscape of the Pyrenees, in: Palacios, D., Hughes, P., García-Ruiz, J.M., Andrés, N. (Eds.), European Glacial Landscapes. Elsevier, Amsterdam, pp. 123–128.

Delmas, M., Oliva, M., Gunnell, Y., Fernandes, M., Reixach, T., Fernández-Fernández, J.M., Calvet, M., 2023b. The Pyrenees: glacial landforms from the Bølling-Allerød Interstadial (14.6-12.9 ka), in: Palacios, D., Hughes, P., García-Ruiz, J.M., Andrés, N. (Eds.), European Glacial Landscapes. Elsevier, Amsterdam, pp. 361–367.

Delmas, M., Oliva, M., Gunnell, Y., Fernandes, M., Reixach, T., Fernández-Fernández, J.M., Calvet, M., 2023c. The Pyrenees: glacial landforms from the Younger Dryas (12.9-11.7 ka), in: Palacios, D., Hughes, P., García-Ruiz, J.M., Andrés, N. (Eds.), European Glacial Landscapes. Elsevier, Amsterdam, pp. 541–552.

Denizot, G., 1925. L'origine des terrasses de la Garonne d'après M. Charput. Compte rendu Somm. des séances la Société géologique Fr. 130–178.

Denizot, G., 1922. Terrasses alluviales du bassin de la Garonne en amont de Toulouse. Bull. Com. des Trav. Hist. Sci. Sect. Géographie XXXVII, 47–53.

Denton, G.H., Anderson, R.F., Toggweiler, J.R., Edwards, R.L., Schaefer, J.M., Putnam, A.E., 2010. The Last Glacial Termination. Science (80-. ). 328, 1652–1656. https://doi.org/10.1126/science.1184119

Denton, G.H., Porter, S.C., 1970. Neoglaciation. Sci. Am. 222, 100–109.

Depéret, C., 1923. Les glaciations des vallées pyrénéennes françaises et leurs relations avec les terrasses fluviales. Gauthier-Villars.

Desilets, D., Zreda, M., 2003. Spatial and temporal distribution of secondary cosmic-ray nucleon intensities and applications to in situ cosmogenic dating. Earth Planet. Sci. Lett. 206, 21–42. https://doi.org/10.1016/S0012-821X(02)01088-9

Djakovic, I., Key, A., Soressi, M., 2022. Optimal linear estimation models predict 1400–2900 years of overlap between Homo sapiens and Neandertals prior to their disappearance from France and northern Spain. Sci. Rep. 12, 15000. https://doi.org/10.1038/s41598-022-19162-z

Dong, G., Huang, F., Yi, C., Liu, X., Zhou, W., 2016. Mid-late Pleistocene glacial evolution in the Grove Mountains, East Antarctica, constraints from cosmogenic 10Be surface exposure dating of glacial erratic cobbles. Quat. Sci. Rev. 145, 71–81. https://doi.org/10.1016/j.quascirev.2016.05.030

Dramis, F., Bisci, C., 1998. Cartografia Geomorfologica: Manuale di Introduzione al Rilevamento ed alla Rappresentazione Degli Aspetti Fisici del Territorio. Pitagora Editrice Bologna.

Dramis, F., Guida, D., Cestari, A., 2011. Nature and Aims of Geomorphological Mapping, in: Smith, M.J., Paron, P., Griffiths, J.S. (Eds.), Geomorphological Mapping Methods and Applications2. Elsevier, pp. 39–64.

Dunai, T.J., 2010. Cosmogenic Nuclides: Principles, Concepts and Application in the Earth Surface Sciences. Cambridge University Press, Edinburgh. https://doi.org/10.1016/j.quageo.2009.1004.1003 B.1

Dunai, T.J., 2001. Influence of secular variation of the geomagnetic field on production rates of in situ produced cosmogenic nuclides. Earth Planet. Sci. Lett. 193, 197–212. https://doi.org/10.1016/S0012-821X(01)00503-9

Dunai, T.J., 2000. Scaling factors for production rates of in situ produced cosmogenic nuclides: A critical reevaluation. Earth Planet. Sci. Lett. 176, 157–169. https://doi.org/10.1016/S0012-821X(99)00310-6

Dunai, T.J., Lifton, N.A., 2014. The nuts and bolts of cosmogenic nuclide production. Elements 10, 347–350. https://doi.org/10.2113/gselements.10.5.347

Dunne, J., Elmore, D., Muzikar, P., 1999. Scaling factors for the rates of production of cosmogenic nuclides for geometric shielding and attenuation at depth on sloped surfaces. Geomorphology 27, 3–11. https://doi.org/10.1016/S0169-555X(98)00086-5

Ehlers, J., Gibbard, P., Hughes, P.D., 2011. Quaternary Glaciations – Extent and Chronology: A Closer Look 15.

Ehlers, J., Gibbard, P.L., Hughes, P.D., 2018. Quaternary Glaciations and Chronology, in: Past Glacial Environments. Elsevier Ltd, pp. 75–102. https://doi.org/10.1016/B978-0-08-100524-8.00003-8

Espurt, N., Angrand, P., Teixell, A., Labaume, P., Ford, M., de Saint Blanquat, M., Chevrot, S., 2019. Crustal-scale balanced cross-section and restorations of the Central Pyrenean belt (Nestes-Cinca transect): Highlighting the structural control of Variscan belt and Permian-Mesozoic rift systems on mountain building. Tectonophysics 764, 25–45. https://doi.org/10.1016/j.tecto.2019.04.026

Esteban, J.J., Aranguren, A., Cuevas, J., Hilario, A., Tubía, J.M., Larionov, A., Sergeev, S., 2015. Is there a time lag between the metamorphism and emplacement of plutons in the Axial Zone of the Pyrenees? Geol. Mag. 152, 935–941. https://doi.org/10.1017/S001675681500014X

Eynaud, F., Verdin, F., Mary, Y., Beaudouin, C., López-Romero, E., Penaud, A., Colin, C., Culioli, C., 2022. Holocene climate dynamics on the European scale: Insights from a coastal archaeological record from the temperate Bay of Biscay (SW France). Quat. Int. 613, 46–60. https://doi.org/10.1016/j.quaint.2021.09.018

Faucher, D., 1937. Le glacier de l'Ariège dans la basse vallée montagnarde. Rev. Geogr. Pyren. Sud. Ouest. 8, 335–349.

Fernandes, M., Oliva, M., Palma, P., Ruiz-Fernández, J., Lopes, L., 2017. Glacial stages and post-glacial environmental evolution in the Upper Garonne valley, Central Pyrenees. Sci. Total Environ. 584–585, 1282–1299. https://doi.org/10.1016/j.scitotenv.2017.01.209

Fernandes, M., Palma, P., Lopes, L., Ruiz-Fernández, J., Pereira, P., Oliva, M., 2018. Spatial distribution and morphometry of permafrost-related landforms in the Central Pyrenees and associated paleoclimatic implications. Quat. Int. 470. https://doi.org/10.1016/j.quaint.2017.08.071

Fernández-Fernández, J.M., Oliva, M., Palacios, D., Garcia-oteyza, J., Navarro, F., Schimmelpfennig, I., Léanni, L., ASTER Team, 2021. Ice thinning on nunataks during the glacial to interglacial transition in the Antarctic Peninsula region according to Cosmic-Ray Exposure dating: Evidence and uncertainties. Quat. Sci. Rev. 264, 107029. https://doi.org/10.1016/j.quascirev.2021.107029

Fernández-Fernández, J.M., Palacios, D., Andrés, N., Schimmelpfennig, I., Tanarro, L.M., Brynjólfsson, S., López-Acevedo, F.J., Sæmundsson, Þ., Team, A., 2020. Constraints on the timing of debris-covered and rock glaciers: An exploratory case study in the Hólar area, northern Iceland. Geomorphology 361, 107196. https://doi.org/10.1016/j.geomorph.2020.107196

Fitzgerald, P.G., Muñoz, J.A., Coney, P.J., Baldwin, S.L., 1999. Asymmetric exhumation across the Pyrenean orogen: Implications for the tectonic evolution of a collisional orogen. Earth Planet. Sci. Lett. 173, 157–170. https://doi.org/10.1016/S0012-821X(99)00225-3

Fontboté, J.M., 1948. La Ribera de Biescas. Pirineos 7, 39–88.

Foucher, P., 2015. Flint economy in the Pyrenees: A general view of siliceous raw material sources and their use in the Pyrenean Gravettian. J. Lithic Stud. 2. https://doi.org/10.2218/jls.v2i1.1306

Foucher, P., Juan-foucher, C.S., Oberlin, C., 2008. Les niveaux d'occupation gravettiens de Gargas (Hautes-Pyrénées): nouvelles données chronostratigraphiques. Société préhistorique française 373–385.

Frigola, J., Moreno, A., Cacho, I., Canals, M., Sierro, F.J., Flores, J.A., Grimalt, J.O., Hodell, D.A., Curtis, J.H., 2007. Holocene climate variability in the western Mediterranean region from a deepwater sediment record. Paleoceanography 22, 1–16. https://doi.org/10.1029/2006PA001307

Ganopolski, A., Winkelmann, R., Schellnhuber, H.J., 2016. Critical insolation-CO2 relation for diagnosing past and future glacial inception. Nature 529, 200–203. https://doi.org/10.1038/nature16494

Garcés-Pastor, S., Cañellas-boltà, N., Clavaguera, A., Calero, M.A., Vegas-vilarrúbia, T., 2017a. Vegetation shifts, human impact and peat bog development in Bassa Nera pond (Central Pyrenees) during the last millennium. The Holocene 27, 553–565. https://doi.org/10.1177/0959683616670221

Garcés-Pastor, S., Cañellas-Boltà, N., Pèlachs, A., Soriano, J.M., Pérez-Obiol, R., Pérez-Haase, A., Calero, M.A., Andreu, O., Escolà, N., Vegas-Vilarrúbia, T., 2017b. Environmental history and vegetation dynamics in response to climate variations and human pressure during the Holocene in Bassa Nera, Central Pyrenees. Palaeogeogr. Palaeoclimatol. Palaeoecol. 479, 48–60. https://doi.org/10.1016/j.palaeo.2017.04.016

García-Escárzaga, A., Gutiérrez-Zugasti, I., Marín-Arroyo, A.B., Fernandes, R., Núñez de la Fuente, S., Cuenca-Solana, D., Iriarte, E., Simões, C., Martín-Chivelet, J., González-Morales, M.R., Roberts, P., 2022. Human forager response to abrupt climate change at 8.2 ka on the Atlantic coast of Europe. Sci. Rep. 12, 1–14. https://doi.org/10.1038/s41598-022-10135-w

García-Ruiz, J.M., Martí-Bono, C., Peña-Monné, J.L., Sancho, C., Rhodes, E., Valero-Garcés, B.L., González-Sampériz, P., Moreno, A., 2013. Glacial and Fluvial Deposits in the Aragón Valley, Central-Western Pyrenees: Chronology of the Pyrenean Late Pleistocene Glaciers. Geogr. Ann. Ser. A Phys. Geogr. 95, 15–32. https://doi.org/10.1111/j.1468-0459.2012.00478.x

García-Ruiz, J.M., Palacios, D., Andrés, N., López-Moreno, J.I., 2020. Neoglaciation in the Spanish Pyrenees: a multiproxy challenge. Mediterr. Geosci. Rev. https://doi.org/10.1007/s42990-020-00022-9

García-Ruiz, J.M., Palacios, D., de Andrés, N., Valero-Garcés, B.L., López-Moreno, J.I., Sanjuán, Y., 2014. Holocene and 'Little Ice Age' glacial activity in the Marboré Cirque, Monte Perdido Massif, Central Spanish Pyrenees. Holocene 24, 1439–1452.

https://doi.org/10.1177/0959683614544053

García-Ruiz, J.M., Palacios, D., González-Sampériz, P., de Andrés, N., Moreno, A., Valero-Garcés, B.L., Gómez-Villar, A., 2016. Evidencias de actividad glaciar durante el Dryas Reciente (12,9-11,7 ka BP) en la Península Ibérica. Cuaternario y Geomorfol. 30, 9–21. https://doi.org/10.17735/cyg.v30i1-2.39250

García-Ruiz, J.M., Serrano, E., 2022. The glaciers of the Central-Western Pyrenees, in: Oliva, M., Palacios, D., Fernández-Fernández, J.M. (Eds.), Iberia, Land of Glaciers: How the Mountains Were Shaped by Glaciers. Elsevier, pp. 123–155.

García-Ruiz, J.M., Valero-Garcés, B.L., Martí-Bono, C., González-Sampériz, P., 2003. Asynchroneity of maximum glacier advances in the central Spanish Pyrenees. J. Quat. Sci. 18, 61–72. https://doi.org/10.1002/jqs.715

Garcia-Sansegundo, J., 2004. Estructura varisca de los Pirineos. Geol. España 254–258.

García-Sansegundo, J., 1996. Hercynian structure of the Axial Zone of the Pyrenees: The Aran Valley cross-section (Spain-France). J. Struct. Geol. 18, 1315–1325. https://doi.org/10.1016/S0191-8141(96)00050-8

García-Sansegundo, J., Merino, J.R., Santisteban, R.R., Leyva, F., 2013. Canejan-Vielha Mapa geologico 1:50 000, Instituto Geologico y Minero de España. Madrid.

Gassiot, E., Antón, D., Mañosa, A.P., Obiol, R.P., Brugués, R., Marie-Claude, B.-S., Mazzucco, N., 2014. La alta montaña durante la Prehistoria: 10 años de investigación en el Pirineo catalán occidental. Trab. Prehist. 71, 261–281. https://doi.org/10.3989/tp.2014.12134

Gellatly, A.F., Grove, J.M., Switsur, V.R., 1992. Mid-Holocene glacial activity in the Pyrenees. Holocene 2, 266–270. https://doi.org/10.1177/095968369200200309

Gillespie, A., Molnar, P., 1995. Asynchronous maximum advances of mountain and continental glaciers. Rev. Geophys. 33, 311. https://doi.org/10.1029/95RG00995

González-Sampériz, P., Aranbarri, J., Pérez-Sanz, A., Gil-Romera, G., Moreno, A., Leunda, M., Sevilla-Callejo, M., Corella, J.P., Morellón, M., Oliva, B., Valero-Garcés, B.L., 2017. Environmental and climate change in the southern Central Pyrenees since the Last Glacial Maximum: A view from the lake records. Catena 149, 668–688. https://doi.org/10.1016/j.catena.2016.07.041

González-Sampériz, P., Valero-Garcés, B.L., Moreno, A., Jalut, G., García-Ruiz, J.M., Martí-Bono, C., Delgado-Huertas, A., Navas, A., Otto, T., Dedoubat, J., 2006. Climate variability in the Spanish Pyrenees during the last 30,000 yr revealed by the El Portalet sequence. Quat. Res. 66, 38–52.

González-Trueba, J.J., Martín-Moreno, R., Martínez De Pisón, E., Serrano, E., 2008. "Little ice age" glaciation and current glaciers in the Iberian Peninsula. Holocene 18, 551–568. https://doi.org/10.1177/0959683608089209

Goron, L., 1941. Les vallums morainiques et les terrasses des dernières glaciations dans la région prépyrénéenne et son avant-pays (suite et fin). Rev. Geogr. Pyren. Sud. Ouest. 12, 5–429. https://doi.org/10.3406/rgpso.1941.4499

Gosse, J.C., Phillips, F.M., 2001. Terrestrial in situ cosmogenic nuclides: theory and application. Quat. Sci. Rev. 20, 1475–1560.

Griffiths, J.S., Paron, P., Mike, S., 2011. Introduction to Applied Geomorphological Mapping, in: Smith, M.J., Paron, P., Griffiths, J.S. (Eds.), Geomorphological Mapping Methods and Applications. Elsevier, pp. 3–8.

Guerrero, J., Gutiérrez, F., García-Ruiz, J.M., Carbonel, D., Lucha, P., Arnold, L.J., 2018.

Landslide-dam paleolakes in the Central Pyrenees, Upper Gállego River Valley, NE Spain: timing and relationship with deglaciation. Landslides 15, 1975–1989. https://doi.org/10.1007/s10346-018-1018-9

Handy, M.R., M. Schmid, S., Bousquet, R., Kissling, E., Bernoulli, D., 2010. Reconciling plate-tectonic reconstructions of Alpine Tethys with the geological-geophysical record of spreading and subduction in the Alps. Earth-Science Rev. 102, 121–158. https://doi.org/10.1016/j.earscirev.2010.06.002

Haug, G.H., Ganopolski, A., Sigman, D.M., Rosell-Mele, A., Swann, G.E.A., Tiedemann, R., Jaccard, S.L., Bollmann, J., Maslin, M.A., Leng, M.J., Eglinton, G., 2005. North Pacific seasonality and the glaciation of North America 2.7 million years ago. Nature 433, 821–825. https://doi.org/10.1038/nature03332

Haug, G.H., Tiedemann, R., 1998. Effect of the formation of the Isthmus of Panama on Atlantic Ocean thermohaline circulation. Nature 393, 673–676. https://doi.org/10.1038/31447

Hays, J.D., Imbrie, J., Shackleton, N.J., 1976. Variations in the Earth's Orbit: Pacemaker of the Ice Ages: For 500,000 years, major climatic changes have followed variations in obliquity and precession. Science (80-. ). 194, 1121–1132.

Hein, A.S., Dunai, T.J., Hulton, N.R.J., Xu, S., 2011. Exposure dating outwash gravels to determine the age of the greatest Patagonian glaciations. Geology 39, 103–106. https://doi.org/10.1130/G31215.1

Hérail, G., Hubschman, J., Jalut, G., 1987. Quaternary glaciation in the French Pyrenees. Quat. Sci. Rev. 5, 397–402. https://doi.org/10.1016/0277-3791(86)90203-9

Hérail, G., Jalut, G., 1986. L'obturation de Sost (Haute Garonne): données nouvelles sur le paléoenvironnement de la phase de progression du glacier würmien dans les Pyrénées centrales. Comptes Rendus l'Académie des Sci. Paris 303, 743–748.

Herrera, R., Serrão, A., 2011. Atlas climático ibérico/ Iberian climate atlas, Agencia Estatal de Meteorología, Ministerio de Medio Ambiente y Medio Rural y Marino, Madrid.

Hewitt, G., 2000. The genetic legacy of the Quaternary ice ages. Nature 405.

Heyman, J., Applegate, P.J., Blomdin, R., Gribenski, N., Harbor, J.M., Stroeven, A.P., 2016. Boulder height - exposure age relationships from a global glacial 10Be compilation. Quat. Geochronol. 34, 1–11. https://doi.org/10.1016/j.quageo.2016.03.002

Heyman, J., Stroeven, A.P., Harbor, J.M., Caffee, M.W., 2011. Too young or too old: Evaluating cosmogenic exposure dating based on an analysis of compiled boulder exposure ages. Earth Planet. Sci. Lett. 302, 71–80. https://doi.org/10.1016/j.epsl.2010.11.040

Hodell, D.A., Nicholl, J.A., Bontognali, T.R.R., Danino, S., Dorador, J., Dowdeswell, J.A., Einsle, J., Kuhlmann, H., Martrat, B., Mleneck-Vautravers, M.J., Rodríguez-Tovar, F.J., Röhl, U., 2017. Anatomy of Heinrich Layer 1 and its role in the last deglaciation. Paleoceanography 32, 284–303. https://doi.org/10.1002/2016PA003028

Hubschman, J., 1984. Glaciaire ancien et glaciaire récent: analyse comparée de l'altération de moraines terminals nord-pyrénéennes. Mont. Piémonts R.G.P.S.O. 313–332.

Hubschman, J., 1975a. Morphogénèse et pédogénèse quaternaires dans le piémont des Pyrénées garonnaises et ariégeoises. University of Toulouse.

Hubschman, J., 1975b. L' évolution des nappes alluviales antérissiennes de la Garonne, dans l' avant-pays molassique. Bull. l'Association française pour l'étude du Quat. 12, 149–169. https://doi.org/doi.org/10.3406/quate.1975.1262

Hubschman, J., 1975c. Les terrasses récentes de la Garonne et leur évolution. Bull. l'Association

française pour l'étude du Quat. 12, 137–147. https://doi.org/doi.org/10.3406/quate.1975.1261

Hughes, P.D., 2022. Concept and global context of the glacial landforms prior to the Last Glacial Maximum, in: European Glacial Landscapes. Elsevier, pp. 197–199. https://doi.org/10.1016/B978-0-12-823498-3.00057-1

Hughes, P.D., Gibbard, P.L., 2018. Global glacier dynamics during 100 ka Pleistocene glacial cycles. Quat. Res. (United States) 90, 222–243. https://doi.org/10.1017/qua.2018.37

Hughes, P.D., Oliva, M., Sarıkaya, M.A., 2020. Holocene and earlier glaciations in the Mediterranean Mountains. Mediterr. Geosci. Rev. 2, 1–4. https://doi.org/10.1007/s42990-020-00025-6

Hughes, P.D., Palacios, David, García-Ruiz, J.M., Andrés, N., 2022. The European glacial landscapes prior to the Last Glacial Maximum - synthesis, in: Palacios, D., Hughes, P., García-Ruiz, J.M., Andrés, N. (Eds.), European Glacial Landscapes. Elsevier, Amsterdam, pp. 341–351. https://doi.org/10.1016/B978-0-12-823498-3.00009-1

Hughes, P.D., Woodward, J.C., 2017. Quaternary glaciation in the Mediterranean mountains: a new synthesis. Geol. Soc. London, Spec. Publ. 433, 1–23. https://doi.org/10.1144/sp433.14

Hughes, P.D., Woodward, J.C., Gibbard, P., 2006. Late Pleistocene glaciers and climate in the Mediterranean. Glob. Planet. Change 50, 83–98. https://doi.org/10.1016/j.gloplacha.2005.07.005

Icole, M., 1974. Géochimie des altérations dans les nappes d'alluvions du piémont occidental nord-pyrénéen. Essai de paléopédologie quaternaire. Université Louis Pasteur de Strasbourg.

Ivy-Ochs, S., Kober, F., 2008. Surface exposure dating with cosmogenic nuclides. Eiszeitalter und Gegenwart Quat. Sci. J. 57, 1–2.

Jalut, G., Andrieu, V., Delibrias, G., Fontugne, M., 1988. Palaeoenvironment of the valley of Ossau (Western French Pyrenees) during the last 27,000 years. Pollen et spores 30, 357–394.

Jalut, G., Marti, J.M., Fontugne, M., Delibrias, G., Vilaplana, J.M., Julia, R., 1992. Glacial to interglacial vegetation changes in the northern and southern Pyrénées: Deglaciation, vegetation cover and chronology. Quat. Sci. Rev. 11, 449–480. https://doi.org/10.1016/0277-3791(92)90027-6

Jarman, D., Calvet, M., Corominas, J., Delmas, M., Gunnell, Y., 2014. Large-scale rock slope failures in the eastern pyrenees: Identifying a sparse but significant population in paraglacial and parafluvial contexts. Geogr. Ann. Ser. A Phys. Geogr. 96, 357–391. https://doi.org/10.1111/geoa.12060

Jomelli, V., Chapron, E., Favier, V., Rinterknecht, V., Braucher, R., Tournier, N., Gascoin, S., Marti, R., Galop, D., Binet, S., Deschamps, C., Tissoux, H., Aumaître, G., Bourlès, D.L., Keddadouche, K., 2020. Glacier fluctuations during the Late Glacial and Holocene on the Ariège valley, northern slope of the Pyrenees and reconstructed climatic conditions. Mediterr. Geosci. Rev. https://doi.org/10.1007/s42990-020-00018-5

Jomelli, V., Swingedouw, D., Vuille, M., Favier, V., Goehring, B., Shakun, J., Braucher, R., Schimmelpfennig, I., Menviel, L., Rabatel, A., Martin, L.C.P., Blard, P.-H., Condom, T., Lupker, M., Christl, M., He, Z., Verfaillie, D., Gorin, A., Aumaître, G., Bourlès, D.L., Keddadouche, K., 2022. In-phase millennial-scale glacier changes in the tropics and North Atlantic regions during the Holocene. Nat. Commun. 13, 1419. https://doi.org/10.1038/s41467-022-28939-9

Jones, R.S., Small, D., Cahill, N., Bentley, M.J., Whitehouse, P.L., 2019. iceTEA: Tools for plotting and analysing cosmogenic-nuclide surface-exposure data from former ice margins. Quat. Geochronol. 51, 72–86. https://doi.org/10.1016/j.quageo.2019.01.001

Kleinsmiede, W.F.J., 1960. Geology of the Valle de Aran.

Kohl, C.P., Nishiizumi, K., 1992. Chemical isolation of quartz for measurement of in-situ - produced cosmogenic nuclides. Geochim. Cosmochim. Acta 56, 3583–3587. https://doi.org/10.1016/0016-7037(92)90401-4

Korschinek, G., Bergmaier, A., Faestermann, T., Gerstmann, U.C., Knie, K., Rugel, G., Wallner, A., Dillmann, I., Dollinger, G., von Gostomski, C.L., Kossert, K., Maiti, M., Poutivtsev, M., Remmert, A., 2010. A new value for the half-life of 10Be by Heavy-Ion Elastic Recoil Detection and liquid scintillation counting. Nucl. Instruments Methods Phys. Res. Sect. B Beam Interact. with Mater. Atoms 268, 187–191. https://doi.org/10.1016/j.nimb.2009.09.020

Lal, D., 1991. Cosmic ray labeling of erosion surfaces: in situ nuclide production rates and erosion models: Earth and Planetary Science Letters. Earth Planet. Sci. Lett. 104, 424–439.

Lal, D., Peters, B., 1967. Cosmic ray produced radioactivity on the Earth. Handb. der Phys. 551–612.

Lambert, F., Delmonte, B., Petit, J.R., Bigler, M., Kaufmann, P.R., Hutterli, M.A., Stocker, T.F., Ruth, U., Steffensen, J.P., Maggi, V., 2008. Dust-climate couplings over the past 800,000 years from the EPICA Dome C ice core. Nature 452, 616–619. https://doi.org/10.1038/nature06763

Lambs, L., Loudes, J.-P., Berthelot, M., 2014. The use of the stable oxygen isotope (18O) to trace the distribution and uptake of water in riparian woodlands.

Lebourg, T., Zerathe, S., Fabre, R., Giuliano, J., Vidal-Romaní, J.R., 2014. A Late Holocene deep-seated landslide in the northern French Pyrenees. Geomorphology 208, 1–10. https://doi.org/10.1016/j.geomorph.2013.11.008

Lescure, S., Arnaud-Fassetta, G., Le Coeur, C., Colin, A., Faravel, S., Mathé, V., Montenegro, M.-E., Carozza, J.-M., 2015. Évolution hydrogéomorphologique holocène de la Garonne maritime - Focus sur les sites de Langoiran et de l'Isle-Saint-Georges (Gironde, France). Géomorphologie Reli. Process. Environ. 21, 57–72. https://doi.org/10.4000/geomorphologie.10860

Leunda, M., González-Sampériz, P., Gil-Romera, G., Aranbarri, J., Moreno, A., Oliva-Urcia, B., Sevilla-Callejo, M., Valero-Garcés, B., 2017. The Late-Glacial and Holocene Marboré Lake sequence (2612 m a.s.l., Central Pyrenees, Spain): Testing high altitude sites sensitivity to millennial scale vegetation and climate variability. Glob. Planet. Change 157, 214–231. https://doi.org/10.1016/j.gloplacha.2017.08.008

Lewis, C.J., McDonald, E. V., Sancho, C., Peña-Monné, J.L., Rhodes, E.J., 2009. Climatic implications of correlated Upper Pleistocene glacial and fluvial deposits on the Cinca and Gállego Rivers (NE Spain) based on OSL dating and soil stratigraphy. Glob. Planet. Change 67, 141–152. https://doi.org/10.1016/j.gloplacha.2009.01.001

Leymerie, A., 1881. Description géologique et paléontologique des Pyrénées de la Haute-Garonne, Toulouse : ed. Toulouse.

Leymerie, A., 1855. Du phénomène diluvien dans la vallée de la Haute-Garonne, in: Bulletin de La Société Géologique. p. 1299.

Li, Y., 2018. Determining topographic shielding from digital elevation models for cosmogenic nuclide analysis: a GIS model for discrete sample sites. J. Mt. Sci. 15, 939–947.

https://doi.org/10.1007/s11629-018-4895-4

Lifton, N.A., Bieber, J.W., Clem, J.M., Duldig, M.L., Evenson, P., Humble, J.E., Pyle, R., 2005. Addressing solar modulation and long-term uncertainties in scaling secondary cosmic rays for in situ cosmogenic nuclide applications. Earth Planet. Sci. Lett. 239, 140–161. https://doi.org/10.1016/j.epsl.2005.07.001

Lifton, N.A., Sato, T., Dunai, T.J., 2014. Scaling in situ cosmogenic nuclide production rates using analytical approximations to atmospheric cosmic-ray fluxes. Earth Planet. Sci. Lett. 386, 149–160. https://doi.org/10.1016/j.epsl.2013.10.052

Llopis-Lladó, N., 1947. El relieve del Alto Aragón. Pirineos 5, 81–166.

Lopes, L., Oliva, M., Fernandes, M., Pereira, P., Palma, P., Ruiz-Fernández, J., 2018. Spatial distribution of morphometric parameters of glacial cirques in the Central Pyrenees (Aran and Boí valleys). J. Mt. Sci. 15. https://doi.org/10.1007/s11629-018-4873-x

López-Moreno, J.I., 2005. Recent variations of snowpack depth in the central Spanish Pyrenees. Arctic, Antarct. Alp. Res. 37, 253–260. https://doi.org/10.1657/1523-0430(2005)037[0253:RVOSDI]2.0.CO;2

López-Moreno, J.I., Alfonso-González, E., Monserrat, O., Del Río, L.M., Otero, J., Lapazaran, J., Luzi, G., Dematteis, N., Serreta, A., Rico, I., Serrano, E., Bartolomé, M., Moreno, A., Buisan, S., Revuelto, J., 2019. Ground-based remote-sensing techniques for diagnosis of the current state and recent evolution of the Monte Perdido Glacier, Spanish Pyrenees. J. Glaciol. 65, 85–100. https://doi.org/10.1017/jog.2018.96

López-Moreno, J.I., Revuelto, J., Rico, I., Chueca-Cía, J., Julián-Andrés, A., Serreta, A., Serrano, E., Vicente-Serrano, S.M., Azorín-Molina, C., Alonso-González, E., García-Ruiz, J.M., 2016. Thinning of the Monte Perdido Glacier in the Spanish Pyrenees since 1981. Cryosphere 10, 681–694. https://doi.org/10.5194/tc-10-681-2016

López-Moreno, J.I., Revuelto, J., Rico, I., Chueca-Cía, J., Julián-Andrés, A., Serreta, A., Serrano, E., Vicente-Serrano, S.M., Azorín-Molina, C., Alonso-González, E., García-Ruiz, J.M., 2015. Accelerated wastage of the Monte Perdido Glacier in the Spanish Pyrenees during recent stationary climatic conditions. Cryosph. Discuss. 9, 5021–5051. https://doi.org/10.5194/tcd-9-5021-2015

Mapa geològic 1:50 000, 2017. Base de dades geològiques de Catalunya 1:50.000 v1.0.

Mardones, M., Jalut, G., 1983. La tourbiere de Biscaye (alt. 409 m, Hautes Pyrenees): Approche paleoecologique des 45.000 dernières annees. Pollen et spores 25, 163–212.

Martí-Bono, C., García-Ruiz, J.M., 1994. El Glaciarismo Surpirenaico: Nuevas Aportaciones. Geoforma Ediciones, Logroño.

Martí-Soler, M., 1988. Estudi geomorfològic del massis central de la Vall d'Aran (Pirineu Central). (Bachelor thesis) University of Barcelona.

Martin, L.C.P., Blard, P.-H., Balco, G., Lavé, J., Delunel, R., Lifton, N.A., Laurent, V., 2017. The CREp program and the ICE-D production rate calibration database: A fully parameterizable and updated online tool to compute cosmic-ray exposure ages. Quat. Geochronol. 38, 25–49. https://doi.org/10.1016/j.quageo.2016.11.006

Martínez De Pisón, E., 1989. Morfología glaciar del valle de Benasque (Pirineo Aragonés). Eria 18, 51–64.

Martrat, B., Grimalt, J.O., Lopez-Martinez, C., Cacho, I., Sierro, F.J., Flores, J.A., Zahn, R., Canals, M., Curtis, J.H., Hodell, D.A., 2004. Abrupt temperature changes in the Western Mediterranean over the past 250,000 years. Science (80-. ). 306, 1762–1765.

https://doi.org/10.1126/science.1101706

Martrat, B., Grimalt, J.O., Shackleton, N.J., De Abreu, L., Hutterli, M.A., Stocker, T.F., 2007. Four climate cycles of recurring deep and surface water destabilizations on the Iberian margin. Science (80-. ). 317, 502–507. https://doi.org/10.1126/science.1139994

Martrat, B., Jimenez-Amat, P., Zahn, R., Grimalt, J.O., 2014. Similarities and dissimilarities between the last two deglaciations and interglaciations in the North Atlantic region. Quat. Sci. Rev. 99, 122–134. https://doi.org/10.1016/j.quascirev.2014.06.016

Mary, Y., Eynaud, F., Colin, C., Rossignol, L., Brocheray, S., Mojtahid, M., Garcia, J., Peral, M., Howa, H., Zaragosi, S., Cremer, M., 2017. Changes in Holocene meridional circulation and poleward Atlantic flow: the Bay of Biscay as a nodal point. Clim. Past 13, 201–216. https://doi.org/10.5194/cp-13-201-2017

Mengaud, L., 1910. Notice géologique sur les Pyrénées ariégeoises et luchonnaises et le Pays toulousain, in: 39º Congrès de La Association Française Pour l'avancement Des Sciences. pp. 76–102.

Menteath, S., 1868. Sur les évidences d'une époque glaciaire miocène considérée spécialement dans les Pyrénées. Bull. la Société Géologique Fr. 2, 694–708.

Merchel, S., Arnold, M., Aumaître, G., Benedetti, L., Bourlès, D.L., Braucher, R., Alfimov, V., Freeman, S.P.H.T., Steier, P., Wallner, A., 2008. Nuclear Instruments and Methods in Physics Research B Towards more precise 10 Be and 36 Cl data from measurements at the 10 À 14 level : Influence of sample preparation Be / B e. Nucl. Inst. Methods Phys. Res. B 266, 4921–4926. https://doi.org/10.1016/j.nimb.2008.07.031

Merchel, S., Herpers, U., 1999. An Update on Radiochemical Separation Techniques for the Determination of Long-Lived Radionuclides via Accelerator Mass Spectrometry. Radiochim. Acta 84, 215–219. https://doi.org/10.1524/ract.1999.84.4.215

Mercier, D., 2008. Paraglacial and paraperiglacial landsystems: concepts, temporal scales and spatial distribution. Géomorphologie Reli. Process. Environ. 14, 223–233.

Mianes, A., 1955. Les anciens glaciers des Pyrénées garonnaises. Pirineos 35, 5–71.

Millet, L., Rius, D., Galop, D., Heiri, O., Brooks, S.J., 2012. Chironomid-based reconstruction of Lateglacial summer temperatures from the Ech palaeolake record (French western Pyrenees). Palaeogeogr. Palaeoclimatol. Palaeoecol. 315–316, 86–99. https://doi.org/10.1016/j.palaeo.2011.11.014

Minet, T., Deschamps, M., Mangier, C., Mourre, V., 2021. Lithic territories during the Late Middle Palaeolithic in the central and western Pyrenees: New data from the Noisetier (Hautes-Pyrénées, France), Gatzarria (Pyrénées-Atlantiques, France) and Abauntz (Navarre, Spain) caves. J. Archaeol. Sci. Reports 36, 102713. https://doi.org/10.1016/j.jasrep.2020.102713

Montserrat-Martí, J.M., 1992. Evolución glaciar y postglaciar del clima y la vegetación en la vertiente sur del Pirineo: estudio palinológico. Monogr. del Inst. Piren. Ecol. Actas. Instituto Pirenaico de Ecología.

Morellón, M., Valero-Garcés, B., Moreno, A., González-Sampériz, P., Mata, P., Romero, O., Maestro, M., Navas, A., 2008. Holocene palaeohydrology and climate variability in northeastern Spain: The sedimentary record of Lake Estanya (Pre-Pyrenean range). Quat. Int. 181, 15–31. https://doi.org/10.1016/j.quaint.2007.02.021

Moreno, A., González-Sampériz, P., Morellón, M., Valero-Garcés, B.L., Fletcher, W.J., 2012a. Northern Iberian abrupt climate change dynamics during the last glacial cycle: A view from lacustrine sediments. Quat. Sci. Rev. 36, 139–153.

https://doi.org/10.1016/j.quascirev.2010.06.031

Moreno, A., Pérez, A., Frigola, J., Nieto-Moreno, V., Rodrigo-Gámiz, M., Martrat, B., González-Sampériz, P., Morellón, M., Martín-Puertas, C., Corella, J.P., Belmonte, Á., Sancho, C., Cacho, I., Herrera, G., Canals, M., Grimalt, J.O., Jiménez-Espejo, F., Martínez-Ruiz, F., Vegas-Vilarrúbia, T., Valero-Garcés, B.L., 2012b. The Medieval Climate Anomaly in the Iberian Peninsula reconstructed from marine and lake records. Quat. Sci. Rev. 43, 16–32. https://doi.org/10.1016/j.quascirev.2012.04.007

Mouchené, M., van der Beek, P., Mouthereau, F., Carcaillet, J., 2017. Controls on Quaternary incision of the Northern Pyrenean foreland: Chronological and geomorphological constraints from the Lannemezan megafan, SW France. Geomorphology 281, 78–93. https://doi.org/10.1016/j.geomorph.2016.12.027

Muñoz, J.A., 1992. Evolution of a continental collision belt: ECORS-Pyrenees crustal balanced cross-section. Thrust Tectonics 235–246. https://doi.org/10.1007/978-94-011-3066-0_21

Naafs, B.D.A., Hefter, J., Stein, R., 2013. Millennial-scale ice rafting events and Hudson Strait Heinrich(-like) Events during the late Pliocene and Pleistocene: A review. Quat. Sci. Rev. 80, 1–28. https://doi.org/10.1016/j.quascirev.2013.08.014

Naughton, F., Sánchez-Goñi, M.F., Landais, A., Rodrigues, T., Vazquez-Riveiros, N., Toucanne, S., 2023. Introduction to the Last Deglaciation climate, in: European Glacial Landscapes. pp. 33–36. https://doi.org/10.1016/B978-0-323-91899-2.00030-9

Naughton, F., Sánchez-Goñi, M.F., Landais, A., Rodrigues, T., Vázquez-Riveiros, N., Toucanne, S., 2022. The Bølling-Allerød Interstadial, in: Palacios, D. (Ed.), European Glacial Landscapes. pp. 0–7. https://doi.org/https://doi.org/10.1016/B978-0-323-91899-2.00015-2

Nesje, A., 1992. Topographical effects on the equilibrium-line altitude on glaciers. GeoJournal 27, 383–391. https://doi.org/10.1007/BF00185102

Ninot, J.M., Carrillo, E., Ferré, A., 2017. The Pyrenees, in: Loidi, J. (Ed.), The Vegetation of the Iberian Peninsula. Elsevier, pp. 323–366.

Nivière, B., Lacan, P., Regard, V., Delmas, M., Calvet, M., Huyghe, D., Roddaz, B., 2016. Evolution of the Late Pleistocene Aspe River (Western Pyrenees, France). Signature of climatic events and active tectonics. Comptes Rendus - Geosci. 348, 203–212. https://doi.org/10.1016/j.crte.2015.07.003

Nye, J.F., 1952. The Mechanics of Glacier Flow. J. Glaciol. 2, 82–93. https://doi.org/10.3189/s0022143000033967

Obermaier, H., 1906. Beitrâge zur Kenntniss des Quartârs in den Pyrenâen. Arch. fur Anthropol. 299–310.

Obreht, I., Buggle, B., Catto, N., Markovič, S.B., Bösel, S., Vandenberghe, D.A.G., Hambach, U., Svirčev, Z., Lehmkuhl, F., Basarin, B., Gavrilov, M.B., Jović, G., 2014. The Late Pleistocene Belotinac section (southern Serbia) at the southern limit of the European loess belt: Environmental and climate reconstruction using grain size and stable C and N isotopes. Quat. Int. 334–335, 10–19. https://doi.org/10.1016/j.quaint.2013.05.037

Ohmura, A., Kasser, P., Funk, M., 1992. Climate at the equilibrium line of glaciers. J. Glaciol. 38, 397–411.

Oliva, M., Fernández-Fernández, J.M., Palacios, D., 2022a. The Iberian Mountains: glacial landforms from the Last Glacial Maximum, in: Palacios, D., Hughes, P., García-Ruiz, J.M., Andrés, N. (Eds.), European Glacial Landscapes. Elsevier, Amsterdam, pp. 473–480. https://doi.org/10.1016/B978-0-12-823498-3.00029-7

Oliva, M., Fernández-Fernández, J.M., Palacios, D., 2022b. The Iberian Mountains: glacial landforms from the Last Glacial Maximum, in: Palacios, D., Hughes, P., García-Ruiz, J.M., Andrés, N. (Eds.), European Glacial Landscapes. Elsevier, pp. 473–478.

Oliva, M., Palacios, D., Fernández-Fernández, J.M., 2022c. Iberia, land of glaciers: How The Mountains Were Shaped By Glaciers. Elsevier.

Oliva, M., Palacios, D., Fernández-Fernández, J.M., 2022d. Iberia: land of the ancient glaciers, in: Oliva, M., Palacios, D., Fernández-Fernández, J.M. (Eds.), Iberia, Land of Glaciers: How the Mountains Were Shaped by Glaciers. Elsevier, Amsterdam, pp. 555–589.

Oliva, M., Palacios, D., Fernández-Fernández, J.M., Rodríguez-Rodríguez, L., García-Ruiz, J.M., Andrés, N., Carrasco, R.M., Pedraza, J., Pérez-Alberti, A., Valcárcel, M., Hughes, P.D., 2019. Late Quaternary glacial phases in the Iberian Peninsula. Earth-Science Rev. 192, 564–600. https://doi.org/10.1016/j.earscirev.2019.03.015

Oliva, M., Ruiz-Fernández, J., Barriendos, M., Benito, G., Cuadrat, J.M., Domínguez-Castro, F., García-Ruiz, J.M., Giralt, S., Gómez-Ortiz, A., Hernández, A., López-Costas, O., López-Moreno, J.I., López-Sáez, J.A., Martínez-Cortizas, A., Moreno, A., Prohom, M., Saz, M.A., Serrano, E., Tejedor, E., Trigo, R., Valero-Garcés, B.L., Vicente-Serrano, S.M., 2018. The Little Ice Age in Iberian mountains. Earth-Science Rev. 177, 175–208. https://doi.org/10.1016/j.earscirev.2017.11.010

OPCC-CT, 2018. Climate change in the Pyrenees: Impacts, vulnerabilities and adaptation. Bases of knowledge for the future climate change adaptation strategy in the Pyrenees.

Ortuño Candela, M., 2008. Deformación activa en el Pirineo Central: La falla Norte de la Maladeta y otras fallas activas. University of Barcelona.

Ortuño Candela, M., Martí, A., Martín-Closas, C., Jiménez-Moreno, G., Martinetto, E., Santanach, P., 2013. Palaeoenvironments of the late miocene prüedo basin: Implications for the uplift of the central pyrenees. J. Geol. Soc. London. 170, 79–92. https://doi.org/10.1144/jgs2011-121

Osmaston, H., 2005. Estimates of glacier equilibrium line altitudes by the Area×Altitude, the Area×Altitude Balance Ratio and the Area×Altitude Balance Index methods and their validation. Quat. Int. 138–139, 22–31. https://doi.org/10.1016/j.quaint.2005.02.004

Palacios, D., Andrés, N., López-Moreno, J.I., García-Ruiz, J.M., 2015a. Late Pleistocene deglaciation in the upper Gállego Valley, central Pyrenees. Quat. Res. (United States) 83, 397–414. https://doi.org/10.1016/j.yqres.2015.01.010

Palacios, D., García-Ruiz, J.M., Andrés, N., Schimmelpfennig, I., Campos, N., Léanni, L., Aumaître, G., Bourlès, D.L., Keddadouche, K., 2017. Deglaciation in the central Pyrenees during the Pleistocene–Holocene transition: Timing and geomorphological significance. Quat. Sci. Rev. 162, 111–127. https://doi.org/10.1016/j.quascirev.2017.03.007

Palacios, D., Gómez-Ortiz, A., Alcalá-Reygosa, J., Andrés, N., Oliva, M., Tanarro, L.M., Salvador-Franch, F., Schimmelpfennig, I., Fernández-Fernández, J.M., Léanni, L., 2019. The challenging application of cosmogenic dating methods in residual glacial landforms: The case of Sierra Nevada (Spain). Geomorphology 325, 103–118. https://doi.org/10.1016/j.geomorph.2018.10.006

Palacios, D., Gómez-Ortiz, A., Andrés, N., Vázquez-Selem, L., Salvador-Franch, F., Oliva, M., 2015b. Maximum extent of Late Pleistocene glaciers and last deglaciation of La Cerdanya mountains, Southeastern Pyrenees. Geomorphology 231, 116–129. https://doi.org/10.1016/j.geomorph.2014.10.037

Palacios, D., Hughes, P.D., García-Ruiz, J.M., Andrés, N., 2022. European Glacial Landscapes: Maximum extent of glaciations. Elsevier, Amsterdam.

Palacios, D., Oliva, M., Gómez-Ortiz, A., Andrés, N., Fernández-Fernández, J.M., Schimmelpfennig, I., Léanni, L., Team, A.S.T.E.R., 2020. Climate sensitivity and geomorphological response of cirque glaciers from the late glacial to the Holocene, Sierra Nevada, Spain. Quat. Sci. Rev. 248. https://doi.org/10.1016/j.quascirev.2020.106617

Pallàs, R., Rodés, Á., Braucher, R., Bourlès, D.L., Delmas, M., Calvet, M., Gunnell, Y., 2010. Small, isolated glacial catchments as priority targets for cosmogenic surface exposure dating of Pleistocene climate fluctuations, southeastern Pyrenees. Geology 38, 891–894. https://doi.org/10.1130/G31164.1

Pallàs, R., Rodés, Á., Braucher, R., Carcaillet, J., Ortuño Candela, M., Bordonau, J., Bourlès, D.L., Vilaplana, J.M., Masana, E., Santanach, P., 2006. Late Pleistocene and Holocene glaciation in the Pyrenees: a critical review and new evidence from 10Be exposure ages, south-central Pyrenees. Quat. Sci. Rev. 25, 2937–2963. https://doi.org/10.1016/j.quascirev.2006.04.004

Panzer, W., 1926. Talentwicklung und Eiszeitklima im nor- dostlichen Spanien. Abhandlungen der Secken- bergischen Naturforschenden Gesellschaft. Naturforschenden Gesellschaft 1–15.

Paris, J.., Icole, M., Tegyey, G., Monciardini, C., Andreieff, P., Collignon, M., 1970. Carte géologique détaillée de la France au 1/50000: Montréjeau. Orléans.

Paron, P., Claessens, L., 2011. Makers and Users of Geomorphological Maps, Geomorphological Mapping Methods and Applications. Elsevier B.V. https://doi.org/10.1016/B978-0-444-53446-0.00004-5

Paterson, W.S.B., 1994. The Physics of Glaciers, 3rd Editio. ed. Elsevier, London. https://doi.org/10.1016/C2009-0-14802-X

Pearce, D.M., Ely, J.C., Barr, I., Boston, C.M., 2017. Glacier Reconstruction, in: Cook, S., Clarke, L., Nield, J. (Eds.), Geomorphological Techniques. British Society for Geomorphology.

Pellicer, X.M., Corella, J.P., Gutiérrez, F., Roqué, C., Linares, R., Carbonel, D., Zarroca, M., Guerrero, J., Comas, X., 2016. Sedimentological and palaeohydrological characterization of Late Pleistocene and Holocene tufa mound palaeolakes using trenching methods in the Spanish Pyrenees. Sedimentology 63, 1786–1819. https://doi.org/10.1111/sed.12290

Pellitero, R., Rea, B.R., Spagnolo, M., Bakke, J., Hughes, P.D., Ivy-Ochs, S., Lukas, S., Ribolini, A., 2015. A GIS tool for automatic calculation of glacier equilibrium-line altitudes. Comput. Geosci. 82, 55–62. https://doi.org/10.1016/j.cageo.2015.05.005

Pellitero, R., Rea, B.R., Spagnolo, M., Bakke, J., Ivy-Ochs, S., Frew, C.R., Hughes, P.D., Ribolini, A., Lukas, S., Renssen, H., 2016. GlaRe, a GIS tool to reconstruct the 3D surface of palaeoglaciers. Comput. Geosci. 94, 77–85. https://doi.org/10.1016/j.cageo.2016.06.008

Peña-Monné, J.L., Lozano, M.V., Sánchez, M., Chueca-Cía, J., Julián-Andrés, A., Pellicer, F., Calvet, J., Muñoz, J., Herrero, M., Echeverría, M., Sancho, C., 1997. Cartografía Geomorfológica básica y aplicada.

Peña-Monné, J.L., Sancho, C., Lewis, C.J., McDonald, E. V., 2004. Datos cronológicos de las morrenas terminales del glaciar del Gállego y su relación con las terrazas fluvioglaciares (Pirineo de Huesca). Geogr. Física Aragón. Asp. Gen. y temáticos 71–84.

Peña-Monné, J.L., Sancho, C., Lewis, C.J., McDonald, E. V., Rhodes, E., 2003. Las morrenas terminales de dos valles del Gallego y Cinca.pdf. Boletín Glaciológico Aragon. 4, 91–109.

Penck, A., 1894. Studien über das Klima Spaniens während der jüngeren Tertiärperiode und der Diluvialperiode, SONDERABDRUCK AUS DER ZEITSCHRIFT DER GESELLSCHAFT FÜR ERDKUNDE ZU BERLIN XXIX.

Penck, A., 1883. La période glaciaire dans les Pyrénées. Bull. la Société d'histoire Nat. Toulouse 19, 105–200.

Penck, A., Brückner, E., 1909. Die Alpen im eiszeitalter, Chr. Herm. ed. Taunitz, Leipzig.

Pérez-Díaz, S., López-Sáez, J.A., Galop, D., 2015. Vegetation dynamics and human activity in the Western Pyrenean Region during the Holocene. Quat. Int. 364, 65–77. https://doi.org/10.1016/j.quaint.2014.10.019

Pérez-Sanz, A., González-Sampériz, P., Moreno, A., Valero-Garcés, B.L., Gil-Romera, G., Rieradevall, M., Tarrats, P., Lasheras-Álvarez, L., Morellón, M., Belmonte, Á., Sancho, C., Sevilla-Callejo, M., Navas, A., 2013. Holocene climate variability, vegetation dynamics and fire regime in the central Pyrenees: The Basa de la Mora sequence (NE Spain). Quat. Sci. Rev. 73, 149–169. https://doi.org/10.1016/j.quascirev.2013.05.010

Perrouty, S., Moussirou, B., Martinod, J., Bonvalot, S., Carretier, S., Gabalda, G., Monod, B., Hérail, G., Regard, V., Remy, D., 2015. Geometry of two glacial valleys in the northern Pyrenees estimated using gravity data. Comptes Rendus Geosci. 347, 13–23. https://doi.org/10.1016/j.crte.2015.01.002

Peyron, O., Guiot, J., Cheddadi, R., Tarasov, P., Reille, M., De Beaulieu, J.L., Bottema, S., Andrieu, V., 1998. Climatic Reconstruction in Europe for 18,000 YR B.P. from Pollen Data. Quat. Res. 49, 183–196. https://doi.org/10.1006/qres.1997.1961

Phillips, F.M., Argento, D.C., Balco, G., Caffee, M.W., Clem, J., Dunai, T.J., Finkel, R., Goehring, B., Gosse, J.C., Hudson, A.M., Jull, A.J.T., Kelly, M.A., Kurz, M., Lal, D., Lifton, N.A., Marrero, S.M., Nishiizumi, K., Reedy, R.C., Schaefer, J., Stone, J.O.H., Swanson, T., Zreda, M.G., 2016. The CRONUS-Earth Project: A synthesis. Quat. Geochronol. 31, 119–154. https://doi.org/10.1016/j.quageo.2015.09.006

Pic, R., 1933. Les terrasses de la Neste-Garonne (suite). Rev. Geogr. Pyren. Sud. Ouest. 4, 472–489. https://doi.org/10.3406/rgpso.1933.4111

Piette, M., 1874. Glacier quaternaire de la Garonne. Bull. la Société géologique 3, 498–519.

Porter, S.C., 1975. Equilibrium-line altitudes of late Quaternary glaciers in the Southern Alps, New Zealand. Quat. Res. 5, 27–47. https://doi.org/10.1016/0033-5894(75)90047-2

Porter, S.C., 1971. Holocene Eruptions of Mauna Kea Volcano, Hawaii 375–377.

Putkonen, J., Swanson, T., 2003. Accuracy of cosmogenic ages for moraines. Quat. Res. 59, 255–261.

Quesada, C., Oliveira, J., 2019a. The Geology of Iberia: A Geodynamic Approach (The Variscan Cycle), Regional Geology Reviews. Springer International Publishing, Cham. https://doi.org/10.1007/978-3-030-10519-8

Quesada, C., Oliveira, J., 2019b. The Geology of Iberia: A Geodynamic Approach (The Alpine Cycle).

Rasmussen, S.O., Bigler, M., Blockley, S.P., Blunier, T., Buchardt, S.L., Clausen, H.B., Cvijanovic, I., Dahl-Jensen, D., Johnsen, S., Fischer, H., Gkinis, V., Guillevic, M., Hoek, W.Z., Lowe, J., Pedro, J.B., Popp, T., Seierstad, I.K., Steffensen, J.P., Svensson, A.M., Vallelonga, P., Vinther, B.M., Walker, M.J.C., Wheatley, J.J., Winstrup, M., 2014. A stratigraphic framework for abrupt climatic changes during the Last Glacial period based on three synchronized Greenland ice-core records: Refining and extending the INTIMATE event stratigraphy. Quat. Sci. Rev. 106, 14–28. https://doi.org/10.1016/j.quascirev.2014.09.007

Reille, M., Andrieu, V., 1995. The late Pleistocene and Holocene in the Lourdes Basin, Western

Pyrenees, France: new pollen analytical and chronology data. Veg. Hist. Archaeobot. 4, 1–21.

Reixach, T., Delmas, M., Calvet, M., 2021. Climatic conditions between 19 and 12 ka in the eastern Pyrenees, and wider implications for atmospheric circulation patterns in Europe. Quat. Sci. Rev. 260. https://doi.org/10.1016/j.quascirev.2021.106923

Renssen, H., Seppä, H., Crosta, X., Goosse, H., Roche, D.M., 2012. Global characterization of the Holocene Thermal Maximum. Quat. Sci. Rev. 48, 7–19. https://doi.org/10.1016/j.quascirev.2012.05.022

Rhee, H.-H., Yeong-Bae, S., Ju-Sun, W., Changhwan, O., Byung-Yong, Y., 2022. Reconstructing the post-LGM deglacial history of Hollingsworth Glacier on Ricker Hills , Transantarctic Mountains , Antarctica 19, 1217–1230. https://doi.org/doi.org/10.1007/s11629- 022-7338-1

Rico, I., Izagirre, E., Serrano, E., López-Moreno, J.I., 2017. Current glacier area in the Pyrenees: an updated assessment 2016. Pirineos 172, 10–3989.

Rind, D., 2009. Atmospheric Circulation During the Last Glacial Maximum BT - Encyclopedia of Paleoclimatology and Ancient Environments, in: Gornitz, V. (Ed.), . Springer Netherlands, Dordrecht, pp. 57–61. https://doi.org/10.1007/978-1-4020-4411-3_15

Rivas-Martínez, S., Costa, M., 1998. Datos sobre la vegetación y el bioclima del Valle de Arán. Acta Bot. Barcinonensia 473–499.

Rodrigues, T., Grimalt, J.O., Abrantes, F., Naughton, F., Flores, J.-A., 2010. The last glacial–interglacial transition (LGIT) in the western mid-latitudes of the North Atlantic: Abrupt sea surface temperature change and sea level implications. Quat. Sci. Rev. 29, 1853–1862. https://doi.org/10.1016/j.quascirev.2010.04.004

Ruddiman, W.F., 2006. Orbital changes and climate. Quat. Sci. Rev. 25, 3092–3112. https://doi.org/10.1016/j.quascirev.2006.09.001

Rusch, L., Gregoire, S., Pois, V., Moigne, A.-M., 2019. Neanderthal and carnivore occupations in unit II from the Upper Pleistocene site of Ramandils Cave, (Port-la-Nouvelle, Aude, France). J. Archaeol. Sci. Reports 28, 102038. https://doi.org/10.1016/j.jasrep.2019.102038

Sabiron i Herrero, B., 1994. Atles dera Val d'Aran.

Salvador-Franch, F., Andrés, N., Gómez-Ortiz, A., Palacios, D., 2022. The glaciers of the Southeastern Pyrenees, in: Oliva, M., Palacios, D., Fernández-Fernández, J.M. (Eds.), Iberia, Land of Glaciers: How the Mountains Were Shaped by Glaciers. Elsevier, pp. 61–85.

Sánchez-Goñi, M.F., 2022a. The climatic and environmental context of the Late Pleistocene, in: Updating Neanderthals. Elsevier, pp. 17–38. https://doi.org/10.1016/B978-0-12-821428-2.00017-2

Sánchez-Goñi, M.F., 2022b. An overview of the Last Glacial Cycle, in: Palacios, D., Hughes, P., García-Ruiz, J.M., Andrés, N. (Eds.), European Glacial Landscapes. Elsevier, pp. 163–169.

Sánchez-Goñi, M.F., Bard, E., Landais, A., Rossignol, L., D'errico, F., 2013. Air-sea temperature decoupling in western Europe during the last interglacial-glacial transition. Nat. Geosci. 6, 837–841. https://doi.org/10.1038/ngeo1924

Sánchez-Goñi, M.F., Harrison, S.P., 2010. Millennial-scale climate variability and vegetation changes during the Last Glacial: Concepts and terminology. Quat. Sci. Rev. 29, 2823–2827. https://doi.org/10.1016/j.quascirev.2009.11.014

Sánchez-Goñi, M.F., Landais, A., Fletcher, W.J., Naughton, F., Desprat, S., Duprat, J., 2008.

Contrasting impacts of Dansgaard–Oeschger events over a western European latitudinal transect modulated by orbital parameters. Quat. Sci. Rev. 27, 1136–1151. https://doi.org/10.1016/j.quascirev.2008.03.003

Sancho, C., Arenas, C., Pardo, G., Peña-Monné, J.L., Rhodes, E.J., Bartolomé, M., García-Ruiz, J.M., Martí-Bono, C., 2018a. Glaciolacustrine deposits formed in an ice-dammed tributary valley in the south-central Pyrenees: New evidence for late Pleistocene climate. Sediment. Geol. 366, 47–66. https://doi.org/10.1016/j.sedgeo.2018.01.008

Sancho, C., Belmonte, Á., Bartolomé, M., Moreno, A., Leunda, M., López-Martínez, J., 2018b. Middle-to-late Holocene palaeoenvironmental reconstruction from the A294 ice-cave record (Central Pyrenees, northern Spain). Earth Planet. Sci. Lett. 484, 135–144. https://doi.org/10.1016/j.epsl.2017.12.027

Sarnthein, M., Tiedemann, R., 1990. Younger Dryas-Style Cooling Events at Glacial Terminations I-VI at ODP Site 658: Associated benthic δ 13 C anomalies constrain meltwater hypothesis. Paleoceanography 5, 1041–1055. https://doi.org/10.1029/PA005i006p01041

Schilling, D.H., Hollin, J.T., 1981. Numerical reconstructions of valley glaciers and small ice caps, in: Denton, G.H., Hughes, T.J. (Eds.), The Last Great Ice Sheets. Wiley, New York, pp. 207–220.

Serrano, E., 2022. The existing glaciers of the Iberian Peninsula, in: Oliva, M., Palacios, D., Fernández-Fernández, J.M. (Eds.), Iberia, Land of Glaciers: How the Mountains Were Shaped by Glaciers. Elsevier, pp. 525–554.

Serrano, E., González-Trueba, J.J., Sanjosé-Blasco, J.J., 2011. Dynamic, evolution and structure of Pyrenean rock glaciers. Cuad. Investig. Geogr. 37. https://doi.org/https://doi.org/10.18172/cig.1260

Serrat, D., Martí, M., Bordonau, J., 1994. Geologia, Geomofologia e Risques, em: Geografia Física, em: Atlas comarcau de Catalunya-Val d'Aran. Inst. Cart. Catalunya. Cons. Generau d'Aran.

Serrat, D., Ventura, J., 1993. Glaciers of Europe - Glaciers of the Pyrenees, Spain and France. Satell. Image Atlas Glaciers world E49–E61.

Shackleton, N.J., 1967. Oxygen Isotope Analyses and Pleistocene Temperatures Re-assessed. Nature 215, 15–17.

Sitter, L.U., Zwart, H.J., 1962. Geological Map of the Paleozoic of the Central Pyrenees. Leidse Geol. Meded. 33, 191–254.

Small, D., Fabel, D., 2015. A Lateglacial 10Be production rate from glacial lake shorelines in Scotland. J. Quat. Sci. 30, 509–513. https://doi.org/10.1002/jqs.2804

Sorriaux, P., 1982. Contribution à l'étude de la sédimentation en milieu karstique. Le système de Niaux-Lombrives-Sabart (Pyrénées Ariégeoises). Université Toulouse 3.

Sorriaux, P., Delmas, M., Calvet, M., Gunnell, Y., Durand, N., Edwige, P., 2016. Relations entre karst et glaciers depuis 450 ka dans les grottes de Niaux-Lombrives-Sabart (Pyrénées ariégeoises) Nouvelles datations U/Th dans la grotte de Niaux. Karstologia 67, 3–16.

Stange, K.M., van Balen, R.T., Kasse, C., Vandenberghe, J., Carcaillet, J., 2014. Linking morphology across the glaciofluvial interface: A 10Be supported chronology of glacier advances and terrace formation in the Garonne River, northern Pyrenees, France. Geomorphology 207, 71–95. https://doi.org/10.1016/j.geomorph.2013.10.028

Steiger, J., James, M., Gazelle, F., 1998. CHANNELIZATION AND CONSEQUENCES ON

FLOODPLAIN SYSTEM FUNCTIONING ON THE GARONNE RIVER , SW FRANCE. Regul. RIVERS Res. Manag. 14, 13–23.

Steinemann, O., Reitner, J.M., Ivy-Ochs, S., Christl, M., Synal, H.A., 2020. Tracking rockglacier evolution in the Eastern Alps from the Lateglacial to the early Holocene. Quat. Sci. Rev. 241, 106424. https://doi.org/10.1016/j.quascirev.2020.106424

Stone, J.O., 2000. Air pressure and cosmogenic isotope production. J. Geophys. Res. 105, 753–759.

Styllas, M.N., Schimmelpfennig, I., Benedetti, L., Ghilardi, M., Aumaître, G., Bourlès, D.L., Keddadouche, K., 2018. Late-glacial and Holocene history of the northeast Mediterranean mountains - New insights from in situ-produced 36Cl-based cosmic ray exposure dating of paleo-glacier deposits on Mount Olympus, Greece. Quat. Sci. Rev. 193, 244–265. https://doi.org/10.1016/j.quascirev.2018.06.020

Taillefer, F., 1977. Le glacier de l'Ariège dans le bassin de Tarascon. Rev. Geogr. Pyren. Sud. Ouest. 48, 269–286.

Taillefer, F., 1966. Quaternaire et géomorphologie sur le versant nord des Pyrénées centrales, d'après H. Alimen. Rev. Geogr. Pyren. Sud. Ouest. 37, 47–57. https://doi.org/10.3406/rgpso.1966.4814

Taillefer, F., 1965. La carte géologique de Grenade-sur-Garonne : Carte géologique détaillée de la France au 1 / 50 000 . Grenade-sur-Garonne , par A . Cavaillé 161–163.

Taillefer, F., 1957. Glaciaire pyrénéen: versant nord et versant sud. Rev. Geogr. Pyren. Sud. Ouest. 28, 221–244. https://doi.org/10.3406/rgpso.1957.1459

Taillefer, F., 1953. La morphologie de la Moyenne Garonne et les données pédologiques. [d'après Albert Cavallié, Formation, évolution et classification des sols au département de Tarn-et-Garonne]. Rev. Geogr. Pyren. Sud. Ouest. 24, 159–162. https://doi.org/10.3406/rgpso.1953.1373

Taillefer, F., 1952. Le piémont des Pyrénées françaises. Inf. Geogr. 16, 34–37.

Taillefer, F., 1951. Le piémont des Pyrénées françaises. University of Toulouse.

Taillefer, F., 1948. Les bassins glaciaires d'Arudy et de Lourdes et le détournement des Gaves d'Ossau et de Pau. Mélanges géographiques D. Faucher 449–465.

Taillefer, F., 1945. L'évolution du relief à l'Ouest des Petites Pyrénées de la Haute-Garonne. Rev. Geogr. Pyren. Sud. Ouest. 16–17, 302–320.

Tarrats, P., Heiri, O., Valero-Garcés, B., Cañedo-Argüelles, M., Prat, N., Rieradevall, M., González-Sampériz, P., 2018. Chironomid-inferred Holocene temperature reconstruction in Basa de la Mora Lake (Central Pyrenees). Holocene 28, 1685–1696. https://doi.org/10.1177/0959683618788662

Teixell, A., Labaume, P., Ayarza, P., Espurt, N., de Saint Blanquat, M., Lagabrielle, Y., 2018. Crustal structure and evolution of the Pyrenean-Cantabrian belt: A review and new interpretations from recent concepts and data. Tectonophysics 724–725, 146–170. https://doi.org/10.1016/j.tecto.2018.01.009

Thackray, G.D., Owen, L.A., Yi, C., 2008. Timing and nature of late quaternary mountain glaciation. J. Quat. Sci. 23, 503–508. https://doi.org/10.1002/jqs.1225

Tomkins, M.D., Dortch, J.M., Hughes, P.D., Huck, J.J., Stimson, A.G., Delmas, M., Calvet, M., Pallàs, R., 2018. Rapid age assessment of glacial landforms in the Pyrenees using Schmidt hammer exposure dating (SHED). Quat. Res. 90, 26–37. https://doi.org/10.1017/qua.2018.12

Toucanne, S., Landais, A., Naughton, F., Rodrigues, T., Riveiro, N.V., Sánchez-Goñi, M.F., 2022. The Global Last Glacial Maximum: the Eastern North Atlantic (marine sediments) and the Greenland Ice Sheet climatic signal, in: Palacios, D., Hughes, P., García-Ruiz, J.M., Andrés, N. (Eds.), European Glacial Landscapes. Elsevier, pp. 189–194.

Turu, V., 1994. Datos para la determinación de la máxima extensión glaciar en los valles de Andorra (Pirineo Central), in: Arnáez-Vadillo, J., García-Ruiz, J.M. (Eds.), Geomorfología En España: III Reunión de Geomorfología. Sociedad Espanola de Geomorfologia, Logrono, pp. 265–273.

Turu, V., Chevalier, M., Sciences, E., Ventura, J., 2022. Glacial-Interglacial cycles in the south-central and southeastern Pyrenees since ≈ 180 ka (NE Spain - Andorra - S France). https://doi.org/10.1017/qua.2022.68

Uppala, S.M., Kållberg, P.W., Simmons, A.J., Andrae, U., da Costa Bechtold, V., Fiorino, M., Gibson, J.K., Haseler, J., Hernandez, A., Kelly, M.A., Li, X., Onogi, K., Saarinen, S., Sokka, N., Allan, R.P., Andersson, E., Arpe, K., Balmaseda, M.A., Beljaars, A.C.M., van de Berg, L., Bidlot, J., Bormann, N., Caires, S., Chevallier, F., Dethof, A., Dragosavac, M., Fisher, M., Fuentes, M., Hagemann, S., Hólm, E., Hoskins, B.J., Isaksen, L., Janssen, P.A.E.M., Jenne, R., McNally, A.P., Mahfouf, J.F., Morcrette, J.J., Rayner, N.A., Saunders, R.W., Simon, P., Sterl, A., Trenberth, K.E., Untch, A., Vasiljevic, D., Viterbo, P., Woollen, J., 2005. The ERA-40 re-analysis. Q. J. R. Meteorol. Soc. 131, 2961–3012. https://doi.org/10.1256/qj.04.176

Vázquez-Riveiros, N., Toucanne, S., Rodrigues, T., Landais, A., Naughton, F., Sánchez-Goñi, M.F., 2022. Definition of the Last Glacial Cycle marine stages and chronology, in: Palacios, D., Hughes, P., García-Ruiz, J.M., Andrés, N. (Eds.), European Glacial Landscapes. Elsevier B.V, pp. 171–173. https://doi.org/https://doi.org/10.1016/B978-0-12-823498-3.00023-6

Ventura, J., Turu, V., 2022. The glaciers of the Central-Eastern Pyrenees, in: Oliva, M., Palacios, D., Fernández-Fernández, J.M. (Eds.), Iberia, Land of Glaciers: How the Mountains Were Shaped by Glaciers2. Elsevier, pp. 87–121.

Victoriano, A., García-Silvestre, M., Furdada, G., Bordonau, J., 2016. Long-term entrenchment and consequences for present flood hazard in the Garona River (Val d'Aran, Central Pyrenees, Spain). Nat. Hazards Earth Syst. Sci. 16, 2055–2070. https://doi.org/10.5194/nhess-16-2055-2016

Vidaller, I., Revuelto, J., Izagirre, E., Rojas-Heredia, F., Alonso-González, E., Gascoin, S., René, P., Berthier, E., Rico, I., Moreno, A., Serrano, E., Serreta, A., López-Moreno, J.I., 2021. Toward an Ice-Free Mountain Range: Demise of Pyrenean Glaciers During 2011–2020. Geophys. Res. Lett. 48. https://doi.org/10.1029/2021GL094339

Vieira, G., 2008. Combined numerical and geomorphological reconstruction of the Serra da Estrela plateau icefield, Portugal. Geomorphology 97, 190–207. https://doi.org/10.1016/j.geomorph.2007.02.042

Vieira, G., Palacios, D., Andrés, N., Mora, C., Vázquez-Selem, L., Woronko, B., Soncco, C., Úbeda, J., Goyanes, G., 2021. Penultimate Glacial Cycle glacier extent in the Iberian Peninsula: New evidence from the Serra da Estrela (Central System, Portugal). Geomorphology 388, 107781. https://doi.org/10.1016/j.geomorph.2021.107781

Vilaplana, J.M., 1983. Estudi del glaciarisme quaternari de les altes valls de la Ribagorça. TDX (Tesis Dr. en Xarxa). Universitat de Barcelona.

Višnjević, V., Herman, F., Prasicek, G., 2020. Climatic patterns over the European Alps during the LGM derived from inversion of the paleo-ice extent. Earth Planet. Sci. Lett. 538. https://doi.org/10.1016/j.epsl.2020.116185

Waelbroeck, C., Labeyrie, L., Michel, E., Duplessy, J.C., McManus, J.F., Lambeck, K., Balbon, E., Labracherie, M., 2002. Sea-level and deep water temperature changes derived from benthic foraminifera isotopic records. Quat. Sci. Rev. 21, 295–305. https://doi.org/10.1016/S0277-3791(01)00101-9

Walker, M., Head, M.J., Berkelhammer, M., Björck, S., Cheng, H., Cwynar, L., Fisher, D., Gkinis, V., Long, A., Lowe, J., Newnham, R., Rasmussen, S.O., Weiss, H., 2018. Formal ratification of the subdivision of the Holocene Series/ Epoch (Quaternary System/Period): Two new Global Boundary Stratotype Sections and Points (GSSPs) and three new stages/ subseries. Episodes 41, 213–223. https://doi.org/10.18814/epiiugs/2018/018016

Walker, M.J.C., Berkelhammer, M., Björck, S., Cwynar, L.C., Fisher, D.A., Long, A.J., Lowe, J., Newnham, R.M., Rasmussen, S.O., Weiss, H., 2012. Formal subdivision of the Holocene Series/Epoch: A Discussion Paper by a Working Group of INTIMATE (Integration of ice-core, marine and terrestrial records) and the Subcommission on Quaternary Stratigraphy (International Commission on Stratigraphy). J. Quat. Sci. 27, 649–659. https://doi.org/10.1002/jqs.2565

Ward, G.K., Wilson, S.R., 1978. Procedures for comparing and combining radiocarbon age determination: a critique. Archaeometry 20, 19–31. https://doi.org/10.1111/j.1475-4754.1978.tb00208.x

Weng, P., Sánchez-Pérez, J.M., Sauvage, S., Vervier, P., Giraud, F., 2003. Assessment of the quantitative and qualitative buffer function of an alluvial wetland : hydrological modelling of a large floodplain ( Garonne River , France ). Hydrol. Process. 17, 2375–2392. https://doi.org/10.1002/hyp.1248

Zasadni, J., Kłapyta, P., Broś, E., Ivy-Ochs, S., Świąder, A., Christl, M., Balážovičová, L., 2020. Latest Pleistocene glacier advances and post-Younger Dryas rock glacier stabilization in the Mt. Kriváň group, High Tatra Mountains, Slovakia. Geomorphology 358. https://doi.org/10.1016/j.geomorph.2020.107093

Zwart, H.J., 1979. The geology of the Central Pyrenees. Leidse Geol. Meded. 90, 1–74.

# Section 2: Results

# 1. Geomorphology of the Aran Valley (Upper Garonne Basin, Central Pyrenees)

Fernandes, M., Oliva, M., Vieira, G., & Lopes, L. (2022). Geomorphology of the Aran Valley (Upper Garonne Basin, Central Pyrenees). *Journal of Maps*, 1–13. https://doi.org/10.1080/17445647.2022.2035266

JOURNAL OF MAPS
https://doi.org/10.1080/17445647.2022.2035266

SCIENCE

OPEN ACCESS Check for updates

# Geomorphology of the Aran Valley (Upper Garonne Basin, Central Pyrenees)

M. Fernandes [a], M. Oliva [b], G. Vieira [a] and L. Lopes [c]

[a]Centre of Geographical Studies – IGOT, University of Lisbon, Lisbon, Portugal; [b]Department of Geography, University of Barcelona, Barcelona, Spain; [c]Centre for Applied Ecology "Professor Baeta Neves" (CEABN), InBIO, School of Agriculture, University of Lisbon, Lisbon, Portugal

**ABSTRACT**

Geomorphological mapping in mountain regions is key for a better understanding of past and present environmental dynamics. Here, we present a 1:25000 scale geomorphological map covering 553 km$^2$ of the Aran Valley, Upper Garonne Basin (Central Pyrenees). The map identifies 44 different geomorphological units classified under glacial, periglacial, nival, karst, slope, alluvial, and fluvial categories. The area includes geomorphic evidence of past Quaternary glaciations reconstructed based on the distribution of moraines from the valley floor to the highest cirques. Following deglaciation of the valley, the landscape was mainly reshaped by periglacial, slope, alluvial and fluvial processes. In addition to paleoenvironmental reconstruction, the map can also be used to promote geoheritage and geoconservation, as well as for planning. As such, it is of relevance for areas exposed to natural hazards, since present-day slope failures and debris flows frequently impact the villages and infrastructures across the valley floor.

**ARTICLE HISTORY**
Received 18 June 2021
Revised 28 December 2021
Accepted 3 January 2022

**KEYWORDS**
Aran Valley; Upper Garonne Basin; geomorphological map; glaciations; deglaciation

## 1. Introduction

Geomorphological mapping in mountains has significantly advanced over the last decades in parallel to the development of survey techniques and availability of aerial and satellite images (Chandler et al., 2018), as well as of airborne LiDAR surveys (Oguchi et al., 2012). A better understanding of present-day geomorphological processes allows improved territorial management in areas exposed to natural hazards (Paron & Claessens, 2011). Accurate geomorphological maps of alpine regions can be used to reconstruct their past environmental histories and to promote the inventorying and classification of geoheritage (Coratza & de Waele, 2012). As such, geomorphological maps are important tools, leading to the implementation of geoconservation measures that may be applied to promote regional development policies.

Geomorphological maps have been used as a scientific tool since the 1960s, developing into more complex maps on glaciated landscapes of mountains, piedmonts, and glacial forefields at the beginning of the twenty-first century (Knight et al., 2011). Several geomorphological maps have been recently published for mid-latitude mountains, such as the Iberian mountains (González-Gutiérrez et al., 2017; Pellitero, 2014) and the Alps (Coratza et al., 2019; Lambiel et al., 2016), or for areas such as the Tibetan Plateau (Lindholm & Heyman, 2016; Schneider et al., 2021). In the Pyrenees, besides the geomorphological maps by the 'Instituto Geológico y Minero de España' at 1:50000, detailed geomorphological mapping has mostly focused on (i) National Parks, such as Ordesa-Monte Perdido (García-Ruiz & Martí-Bono, 2001) and Aigüestortes-Estany de Sant Maurici (Martínez-Rius, 2010), (ii) some large valleys, such as Benasque (García-Ruiz et al., 1992) or Andorra (Copons, 2005), (iii) singular landscape features for all valleys of the southern part of the range, such as glacial landforms (Martí-Bono & García-Ruiz, 1994), or (iv) in small valleys and glacial cirques, where geomorphological sketches and maps supported various research topics, mainly on glacial, periglacial or slope dynamics (e.g. Andrés et al., 2018; Fernandes et al., 2017; Jarman et al., 2014; Serrano et al., 2020). To date, a detailed map including the wide range of geomorphological features existing in the Aran Valley is still missing.

This work focuses on the Aran Valley, one of the longest glacial valleys in the Pyrenees, which showed a ca. 80 km long valley glacier at the maximum ice extent of the last glacial cycle (Fernandes et al., 2017). The geomorphological and paleogeographical richness of the area has resulted in several publications (Fernandes et al., 2021b, 2021a, 2018, 2017; Lopes et al., 2018; Oliva et al., 2021). The valley has ca.

CONTACT M. Fernandes marcelo.fernandes@campus.ul.pt Centre for Geographical Studies – IGOT, University of Lisbon, Rua Branca Edmée Marques, Lisbon 1600-276, Portugal

Supplemental map for this article is available online at https://doi.org/10.1080/17445647.2022.2035266.

10,000 inhabitants distributed in 33 settlements and infrastructures are widespread both in the valley floor and mountain slopes. Hence, an accurate identification and analysis of the geomorphological features become important for a better spatial planning, for the mitigation of natural hazards and for the implementation of geoconservation measures and promoting geoconservation. To present, the existing geomorphological coverage of the Aran Valley is incomplete and not systematic, consisting of: (i) a low-resolution map from the early 1990s focussing on the main glacial features (Serrat et al., 1994), (ii) a geomorphological map of the northern part of the Aran Valley including only the Toran, Varradòs and Unhòla tributaries (Martí-Soler, 1988), (iii) a map of glacial and postglacial features of the SW area of Aran, namely the Joèu and Nère valleys (Bordonau, 1985), and (iv) the geomorphological map of the Ruda Valley (Fernandes et al., 2017).

The objectives of this work are to: (i) improve the existing geomorphological maps, which covered only 200 km$^2$ and expand the survey to the entire 553 km$^2$ of the Aran Valley, and (ii) offer the local authorities a high-resolution geomorphological map, that may be used as a tool for spatial planning purposes.

## 2. Study area

The Aran Valley is the northwesternmost district of Catalonia within Spanish administrative territory (Figure 1). The headwaters are on the central axis of the Pyrenees, with elevations above 3000 m a.s.l. (Molières Peak, 3009 m asl; Besiberri Nord Peak, 3007 m), whereas the valley floor, near the French border, is at ca. 600 m. The Aran Valley constitutes the headwaters of the Upper Garonne Basin at its easternmost flank (Figure 1).

The current climate in the Aran Valley is dominated by wet and cool Atlantic air masses. Annual precipitation in the valley floor is ca. 900 mm at Vielha village (980 m), and increases to 1232 mm at the Port de la Bonaigua water divide (2266 m). Annual air temperatures (MAAT) at these two sites are 9.6°C and 2.7°C, respectively. The regional 0°C isotherm is at 2950 m asl in the Central Pyrenees (López-Moreno et al., 2016), with only the highest summits recording negative MAATs. The Aran Valley shows typical Euro-Siberian vegetation, with flat-leaf, deciduous forests in the lower elevations and conifers up to ca. 2200–2300 m asl, where they are replaced by alpine meadows (Bolòs & Vigo, 1984).

The Aran Valley is part of the Paleozoic basement of the Central Pyrenees that was uplifted during the Alpine orogeny (García-Sansegundo et al., 2013; Quesada & Oliveira, 2019). The rise of the Pyrenees formed several thrusts organized in two structural domains: the first is mainly located in the northern part of the Aran Valley with E-W direction subhorizontal structures, and the second constitutes the central part of the valley and mainly includes E-W subvertical folds (Sitter & Zwart, 1962; Zwart, 1979). Both were intruded by granitoids, such as the Maladeta Batholith and the Dome of Bossòst (García-Sansegundo, 2004). Bedrock in the north and central valley slopes is composed of metamorphic (slates, schists and marbles) and sedimentary rocks (limestones, lutites, conglomerates and sandstones) from the Cambrian to the Devonian periods (Geològic de Catalunya, 2017). The highest areas are mostly composed of igneous rocks (granites) that intruded during the Carboniferous period (Martínez et al., 2016; Mezger & Gerdes, 2016). Quaternary deposits are located along the narrow valley bottoms, floors and footslopes of the glacial cirques and in parts of the slopes.

Similar to other areas of the Pyrenees, the Aran Valley was extensively glaciated during Quaternary glacial cycles (Oliva et al., 2019). A ca. 80-km long glacier descended along the main Garonne Valley until the glacial basin near Montrejeau at 400–500 m asl, where it formed a series of frontal moraine ridges, both at ca. 130 ka and prior to 24–21 ka (Fernandes et al., 2021b). At those periods, the equilibrium line altitude (ELA) was located at ca. 1500 m (Fernandes et al., 2017).

The Aran Valley presents a U-shaped cross-section and a prevailing S-N direction, turning E-W between the villages of Baquèira and Vielha (Figure 1). The relief may be divided into three major units: (i) interfluves (peaks, ridges and summit plateaus) and glacial cirques, (ii) mountain slopes, and (iii) gently sloping floors of the Garonne Valley and its tributaries (Aiguamòg, Valarties, Nère, etc.). The landscape was extensively shaped by Quaternary glaciers, although the chronological framework of glacial oscillations in the northern slope of the Central Pyrenees is yet to be established (Fernandes et al., 2021a; Oliva et al., 2019). Postglacial dynamics has been mainly driven by periglacial and nival processes in the highest areas, with the occurrence of frequent permafrost-related features, such as rock glaciers and protalus lobes (Fernandes et al., 2018), as well as by hillslope and alluvial processes across the slopes and valley floor (Fernandes et al., 2020). Warmer temperatures during the Holocene promoted soil development, slope stabilization and forest expansion (González-Sampériz et al., 2017; Tejedor-Rodríguez et al., 2021). Since the Neolithic/Chalcolithic periods, and particularly since 4 ka cal BP, humans have significantly modified the landscape. Initially the impacts were associated with forest clearing to expand transhumance practices, that triggered hydrologic and erosion changes (García-Ruiz et al., 2020; Tejedor-Rodríguez et al., 2021). Over the last millennium, particularly since 1.1 ka cal BP, human settlements grew and agriculture and grazing expanded across the valley floor (Garcés-Pastor et al., 2017). Since the latest twentieth century, a tourism-

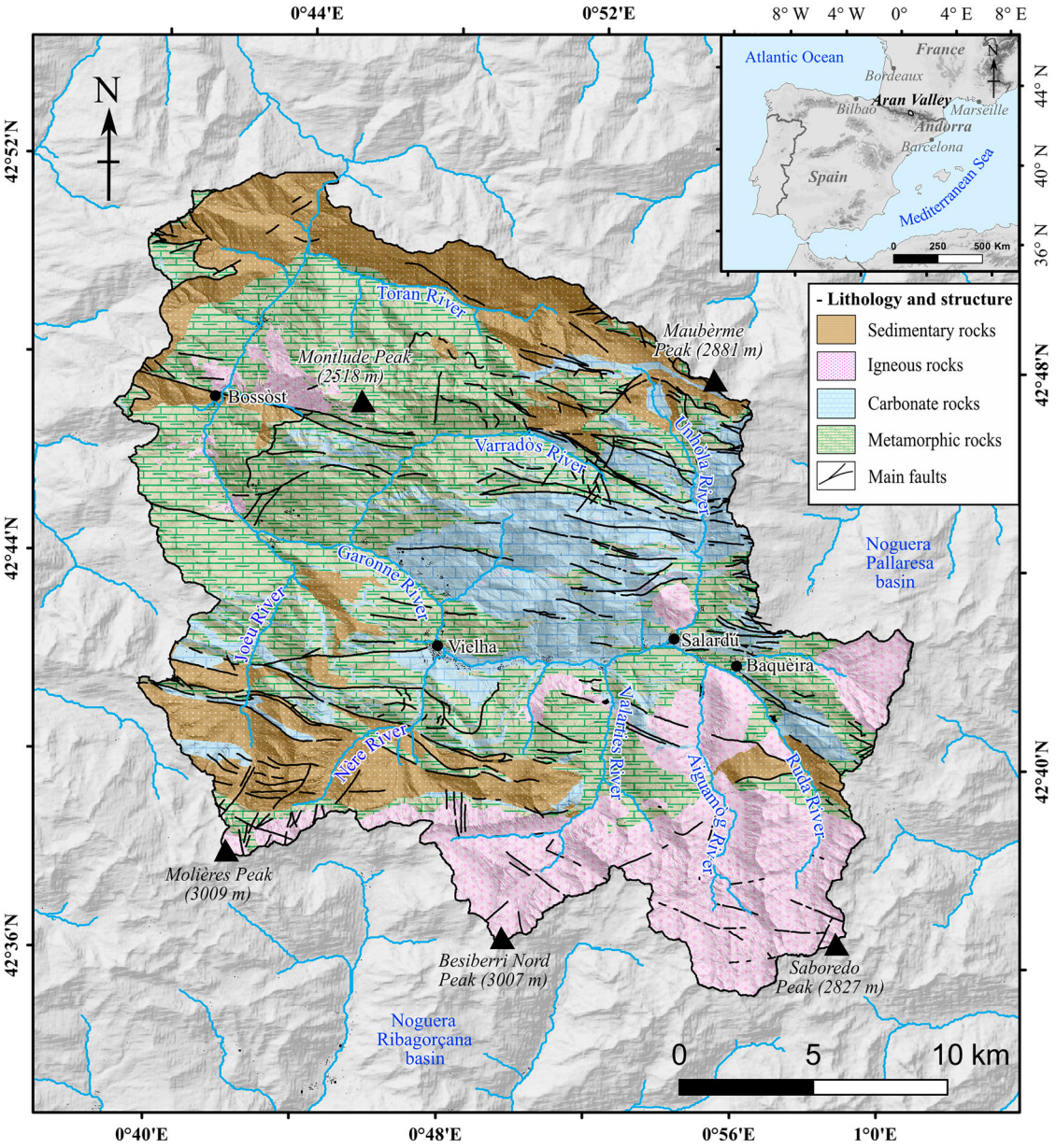


**Figure 1.** Location of the Aran Valley within the Pyrenean range, including the main lithological units of the study area.

driven economy has dramatically changed the landscape, with the construction of infrastructures and the expansion of settlements, mainly across the valley floor.

## 3. Methodology

The elaboration of the geomorphological map of the Aran Valley at 1:25000 scale was based on:

(i) extensive bibliographical and cartographic review, including georeferencing of existing geomorphological maps by Bordonau (1985), Martí-Soler (1988) and Serrat et al. (1994),
(ii) remote sensing data interpretation, including the analysis of LiDAR-derived terrain models (digital elevation model, hillshade and slope), digital orthophotomaps and very high-resolution Google Earth imagery (Table 1),
(iii) systematic field surveys during the summers of 2015, 2019, 2020 and 2021 for reconnaissance, landform identification and validation (Figure 2(C)), and
(iv) editing in GIS environment (ArcGIS) and the final map layout (Illustrator).

The geomorphological map main focus is on landforms and processes, with Table 2 synthesizing the criteria used for their mapping. They were outlined and symbolized according to Joly (1997) and Lambiel et al. (2013) and grouped following criteria on glacial, periglacial, slope, alluvial, fluvial, nival and karst features. The symbolization uses lines for the linear landforms (e.g. moraine crests), points for the isolated landforms or deposits (e.g. erratics), and polygons for larger non-linear features (e.g. fluvial plain). Additional information includes the main faults (Geològic de Catalunya, 2017), pre-Quaternary geology (1:50000; Geològic de

**Table 1.** Attributes of the remote sensing products used for the geomorphological map.

| Product | Source | Characteristics and spatial resolution | Information |
|---|---|---|---|
| Orthophotomaps | Institut Cartogràfic i Geològic de Catalunya (ICGC) (http://www.icc.cat/appdownloads/index.html?c=fmeof25c) | RGB, 25 cm/pixel | Terrain characteristics (e.g. vegetation cover, outcrops, deposits, etc) |
| Lidar data | ICGC (http://www.icc.cat/appdownloads/?c=dlfxlidar) | Collected in 2011. Point cloud density of 0.5-2.7 $m^2$ | Ground surface characteristics (e.g. flat surfaces, furrows, crests, etc) and delimitation of landforms |
| Stereoscopic viewer | Instituto Geográfico Nacional (IGN; http://www.ign.es/3d-stereo/) | Photograms of the Plan Nacional de Ortofotografia Aérea. Variable resolution (22-45 cm/pixel) | Characteristics of the ground surface morphology |
| 3D models satellite images | Browser of Google Earth (https://earth.google.com/web/) | IGN imagery (large scale) and Landsat imagery (small scale). NASA SRTM Digital Elevation dataset (30 m) with the IGN imagery (25x25 cm) and Landsat imagery (30x30 m) | Validation of the ground and terrain characteristics and a broader framework of geomorphological features |

Catalunya, 2017), rivers and lakes (*Institut Cartogràfic i Geològic de Catalunya* ICGC), 100 m contours (derived from the Advanced Spaceborne Thermal Emission and Reflection Radiometer – ASTER DEM), main peaks (*Instituto Geográfico Nacional de España*; IGN), and main infrastructures (ICGC).

All landforms were validated during the summer when the snow-free landscape allowed for the identification of geomorphological features. Most landforms were identified in LiDAR-derived models, online anaglyph map viewer (https://www.ign.es/iberpix2/visor/), satellite imagery, and orthophotomaps, with only the small-size features having been identified in the field.

## 4. Results

### 4.1 Glacial landforms

Abundant erosional and depositional glacial landforms occur from the highest areas to the Aran Valley floor. The highest areas show glacial cirques (Figure 3(D)), where ice accumulated before filling the valleys with a maximum thickness of ca. 800 m (Fernandes et al., 2017). The main valley as well as its tributaries display well-preserved U-shaped sections. Glacial erosion shaped overdeepened basins along the valley bottoms (e.g. Valarties Valley), that are occupied by lakes, peatlands (e.g. Ruda Valley; Figure 3(C)) and fluvial plains

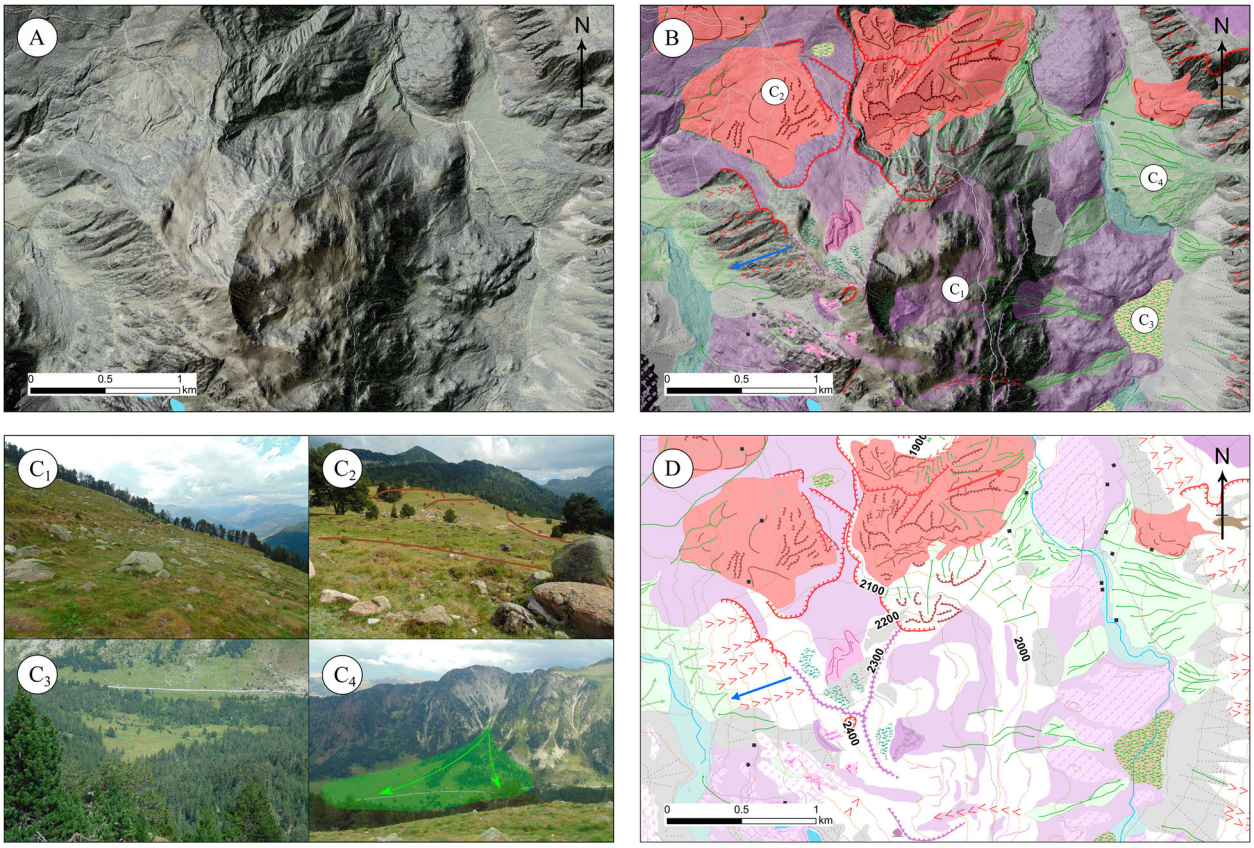


**Figure 2.** Steps followed during the elaboration of the geomorphological map; (A) combination of hillshade (40% transparent) with orthophotomaps; (B) first draft of the geomorphological map; (C) field validation of the first geomorphological draft with pictures, such as till cover ($C_1$), superficial deformation of till cover at the plateau ($C_2$), peat area ($C_3$), and alluvial fan ($C_4$). (D) final geomorphological map respecting the Main map legend.

**Table 2.** Location and morphological characteristics of the landforms and processes drew in the Main map.

| Categories | Landforms and processes | Geomorphological setting | Morphological criteria | Mapping identification criteria | Reference |
|---|---|---|---|---|---|
| Glacial | Cirque | Headwaters of the valleys | Amphitheatre-like basin surrounded by steep walls | Steep walls displaying a concave area with a (semi)elliptical morphology | Joly (1997); Lambiel et al. (2013) |
| | Ridge (or *arêtes*) | Water divide between glacial cirques/valleys | Truncated spur dividing adjacent glacial cirques or valleys | Sharp and narrow rock alignments | Giles et al. (2017) |
| | U-shaped valley | Trunk and tributary valleys shaped by glaciers | U-shaped transverse valley section with concave slopes | Parabolic cross-profile (steep-sided and flat bottom) | Evans (2013) |
| | Rock step (>50°) | Polished surface in glacial cirques/valleys | Slope rupture with a rounded shape and asymmetric up/down valley faces | Higher slope degrees in lee's bare rocks | Joly (1997); Giles et al. (2017) |
| | Watershed breach | Headwaters of the valleys (cols) | Concave water divide eroded by past glacial diffluence | Lower areas within an elevated alignment, able to connect two opposite valleys containing bare rocks and/or boulders | Joly (1997); Giles et al. (2017) |
| | Overdeepened basin | Depressed area in glacial cirques/valleys | (Semi)circular depression surrounded by polished surfaces or glacial deposits | Current flat areas frequently include lakes or peatlands | Joly (1997); Lambiel et al. (2013) |
| | Hanging valley | Lateral glacial valley hanging above the main glacial valley floor | Glacially eroded valley floor standing above the adjacent valley | Different base levels between lateral valleys and the tributary/main valley | Joly (1997); Giles et al. (2017) |
| | Riegel | Bottom of glacial cirques/valleys | Upstanding transverse ridge with polished surfaces | Rock barrier across the bottom of the glaciated valley/cirque with or without a narrow exit | Lambiel et al. (2013); Giles et al. (2017) |
| | Roche moutonnée | Bottom of glacial cirques/valleys | Convex surfaces showing polished surfaces upstream and quarrying downstream | Bare surfaces with a smooth up-facing slope and steep down-facing slope | Lambiel et al. (2013); Giles et al. (2017) |
| | Polished surface | Slope or bottom of glacial cirques/valleys | Relatively horizontal glacially abraded bedrock | Bare rocks with a smooth surface | Giles et al. (2017) |
| | Striation | Polished rock surface in glacial cirques/valleys | Millimetric to metric long scratches or grooves commonly on stoss side of the polished rock surfaces | Only identifiable in field observations | Lambiel et al. (2013); Giles et al. (2017) |
| | Debris-free glacier moraine | Bottom and slopes of glacial cirques/plateaus/valleys | One or several crests with subangular to subrounded boulders and with a depression upvalley | Elongated ridges with smooth surfaces | Joly (1997); Lambiel et al. (2013) |
| | Debris-covered glacier moraine | Bottom and slopes of glacial cirques | Supraglacial till with angular boulders showing frequent longitudinal furrows and crests | Parallel ridges with supraglacial boulders on top or surfaces with collapses (minor-closed depressions) and debris thickness increasing towards the glacier front | Evans (2005) |
| | Till | Wide range of settings affected by past glaciations (summit surfaces, slopes, plateaus, valley bottoms) | Unsorted glacial sediment | Soft surfaces covered with unsorted sediments and embedded boulders where commonly vegetation colonized the fine fraction of the deposit | Lambiel et al. (2013); Benn and Evans (2010) |
| | Till collapse | Till deposits | Depression on till cover | Closed depressions | – |
| | Kame terrace | Sides of glacial valleys | Relatively horizontal deposit generated by meltwater streams along the side of a glacial valley | Smooth and flat (table-like) surfaces | Joly (1997); Lambiel et al. (2013) |
| | Erratic boulder | Widespread deposit across formerly glaciated areas | Isolated boulder lying on the surface | Large boulders needing of field validation | Joly (1997); Lambiel et al. (2013) |
| Periglacial | Rock glacier | At the foot slope and bottom of glacial cirques | Large accumulation of boulders displaying perpendicular ridges and furrows and a steep front | Large boulders with different vegetation matureness and morphological changes ridges-like | Joly (1997); Kääb (2013) |
| | Protalus lobe | At the foot of talus slopes in glacial cirques/valleys | Accumulation of boulders with one lobate ridge at the front | Large boulders with different vegetation matureness and morphological changes ridge-like | French (2007); Kääb (2013) |
| | Block stream | Slopes of glacial cirque/valleys | Linear accumulation of coarse angular boulders | Angular boulders with scarce vegetation flowing downslope | French (2007); Knight and Harrison (2009) |
| | Patterned ground | Relatively flat surfaces or gentle slopes, generally at high altitudes | Geometric landforms composed of sorted/non-sorted circles (flat | Only identifiable in field observations | Joly (1997); French (2007) |

(*Continued*)

**Table 2.** Continued.

| Categories | Landforms and processes | Geomorphological setting | Morphological criteria | Mapping identification criteria | Reference |
|---|---|---|---|---|---|
| | | | surfaces) and stripes (downslope). | | |
| | Block field | Relatively flat surfaces or gentle slopes at the summit level | Accumulation of *in-situ* boulders on the mountaintops | Only identifiable in field observations | Giles et al. (2017) |
| | Solifluction lobe | Slopes of glacial cirques/valleys | Tongue-shaped landforms or *terrassettes* occurring in vegetation and sediments | Only the biggest lobated structures are identified on vegetation and sediments | Joly (1997); Giles et al. (2017) |
| | Ploughing boulder | Gentle slope of glacial valleys | Boulder showing downslope displacement with a linear depression upslope | Boulder's pathway is recorded in vegetation and topography | Joly (1997) |
| Nival | Late-lying snow patch | Hollows of glacial cirques | Semi-permanent snow field | Snow patches | Joly (1997); Lambiel et al. (2013) |
| | Avalanche corridor | Steep slope of glacial cirques/ valleys | Corridor of frequent avalanche occurrence | Linear areas with no arboreous strata along the slope | Joly (1997) |
| | Protalus rampart | At the foot of slopes in glacial cirques/valleys | Accumulation of well-sorted sediments transversal to slope and at the foot of late-lying snow patches | Difficult to identify with remote sensing products | Joly (1997); Lambiel et al. (2013) |
| Karst | Doline | Outcrop of limestones | Isolated closed depression | Dots identified as topographic depressions | Joly (1997) |
| | Uvala | Outcrop of limestones | Set of coalescent dolines next to each other | Set of dots connected with each other identified as one topographic depression | Joly (1997) |
| | Karst window | Contact between limestone and silt-grained bedrock | Depression where a stream falls into a karst aquifer | Only identifiable in field observations | – |
| Slope | External scar | Slopes or interfluves of glacial cirques/valleys | Delineation of the slope failure origin | Steep areas of downslope ruptures | Lambiel et al. (2013) |
| | Internal scar/ antiscar | Surface of rock slope failures in glacial cirques/valleys | Downslope or upslope scar | Steep areas of perpendicular and linear ruptures on the mass movement. The position of the highest degrees on the rupture defines if is downslope or upslope | – |
| | Talus slope | At the foot of rock walls in glacial cirques/valleys | Irregular and angular rock debris covering the valley sides | Large boulders forming a talus or cone morphology | Joly (1997); Giles et al. (2017) |
| | Rock slope failure | Slopes of glacial cirques/valleys | Break of slope caused by mass movements | Steep downslope scars with irregular displaced body surface and steep front | Joly (1997); Giles et al. (2017) |
| | Rock fall | At the foot of the rock wall of glacial cirques/valleys | Non-sorted deposit of large angular boulders | Large boulders showing a chaotic distribution on foot slopes | Lambiel et al. (2013) |
| | Gully/Ravine | Slopes of glacial cirques/valleys | Narrow runoff channels eroding the bedrock/soil. | Abrupt channels directly affecting the bedrock | Rapp (1960); Lambiel et al. (2013) |
| | Debris flow | Slopes of glacial cirques/valleys | Channel, levée margin and sometimes lobate feature on the terminal areas of talus slopes | Narrow channels on sediments | Joly (1997); Lambiel et al. (2013) |
| | Lobate front | Foot slopes of glacial cirques/ valleys | Prominent toe of the rock slope failures | Arched morphologies facing downslope | – |
| Alluvial | Alluvial fan | Foot slopes of glacial valleys | Triangular-shaped deposits of gravels and fine-grained sediments | Triangular-shape morphologies | Joly (1997) |
| | Alluvium | Flat area on the slopes of glacial valley | Alluvium defined by a relatively horizontal surface | Soft and flat surfaces covered with herbs | Parry (2011) |
| | Mudflow | Slope of glacial cirques/valleys | Silty-rich deposit with lobate morphology in the distal section | Poorly defined morphologies with fan-shaped and lobate terminus | Matsuoka et al. (2005) |
| | Peatland/wetland | Depressed area of glacial cirques/valleys | Dense vegetation cover with poor drainage within overdeepened basins | Relatively horizontal surfaces covered with peat sediments | Joly (1997) |
| Fluvial | Gorge | Bottom of glacial valleys | Deep fluvial incision on bedrock | Longitudinal deeply incised bedrock | Joly (1997); Lambiel et al. (2013) |
| | Plain | Bottom of glacial valleys | Relatively horizontal surface formed by fluvial sediments | Relatively soft and flat surface parallel to the riverbed | Joly (1997) |
| | Terrace | Bottom of glacial valleys | Lateral staggered level of fluvial sediments | Staggered flat levels constrained by steep slopes, parallel to the main axis of the river | Joly (1997); Lambiel et al. (2013) |
| Hydrology | River/stream | Bottom of glacial cirques/ valleys | | Linear water bodies | |

(*Continued*)

**Table 2.** Continued.

| Categories | Landforms and processes | Geomorphological setting | Morphological criteria | Mapping identification criteria | Reference |
|---|---|---|---|---|---|
| | | | Linear water body that is permanent (river) or ephemeral (stream) | | Joly (1997); Lambiel et al. (2013) |
| | Lake | Bottom of glacial cirques/ valleys | Permanent water body with irregular shape | Water bodies from natural origin, coinciding with overdeepened basins or landslide obstructions/ scars | Joly (1997); Lambiel et al. (2013) |

(e.g. main Garonne Valley). Intense glacial erosion is also shown in smaller landforms, such as roches moutonneés and glacially polished surfaces – including striations – along the valleys (e.g. next to the Maubèrme Peak). A significant part of the glacially eroded material was transported downvalley and accumulated as terminal and lateral moraines (e.g. Nère Valley; Figure 3(A)), till or scattered erratics (e.g. main Garonne Valley; Figure 3(B)). Moraines accumulated during different periods of advance or standstills during glacial retreat and are distributed in a wide elevation range: from the highest cirques at 2400 to 2600 m asl (e.g. Aiguamòg Valley) to the valley floors at 1300 m asl (e.g. Nère Valley), or even on the marginal and elevated plateaus including deposits located 500 m above the riverbed (e.g. between Ruda and Aiguamòg valleys).

### 4.2 Periglacial landforms

The frozen ground has promoted the development of numerous landforms, some of which are still active under current climate conditions. Rock glaciers (Figure 4(A)) and protalus lobes (Figure 4(B)) provide evidence for the past occurrence of permafrost (Fernandes et al., 2018), with only one active rock glacier having been identified in the area (Serrano et al., 2011). Above ca. 2300 m asl, smaller landforms associated with seasonal frost show traces of activity. In relatively flat summit surfaces, there are block fields (e.g. between Joèu and Nère valleys) and patterned ground features (e.g. next to the Maubèrme Peak; Figure 4(D)), while in gentle slopes, there are block streams (e.g. Ruda Valley; Figure 4(C)) and solifluction lobes (e.g. Salient Valley).

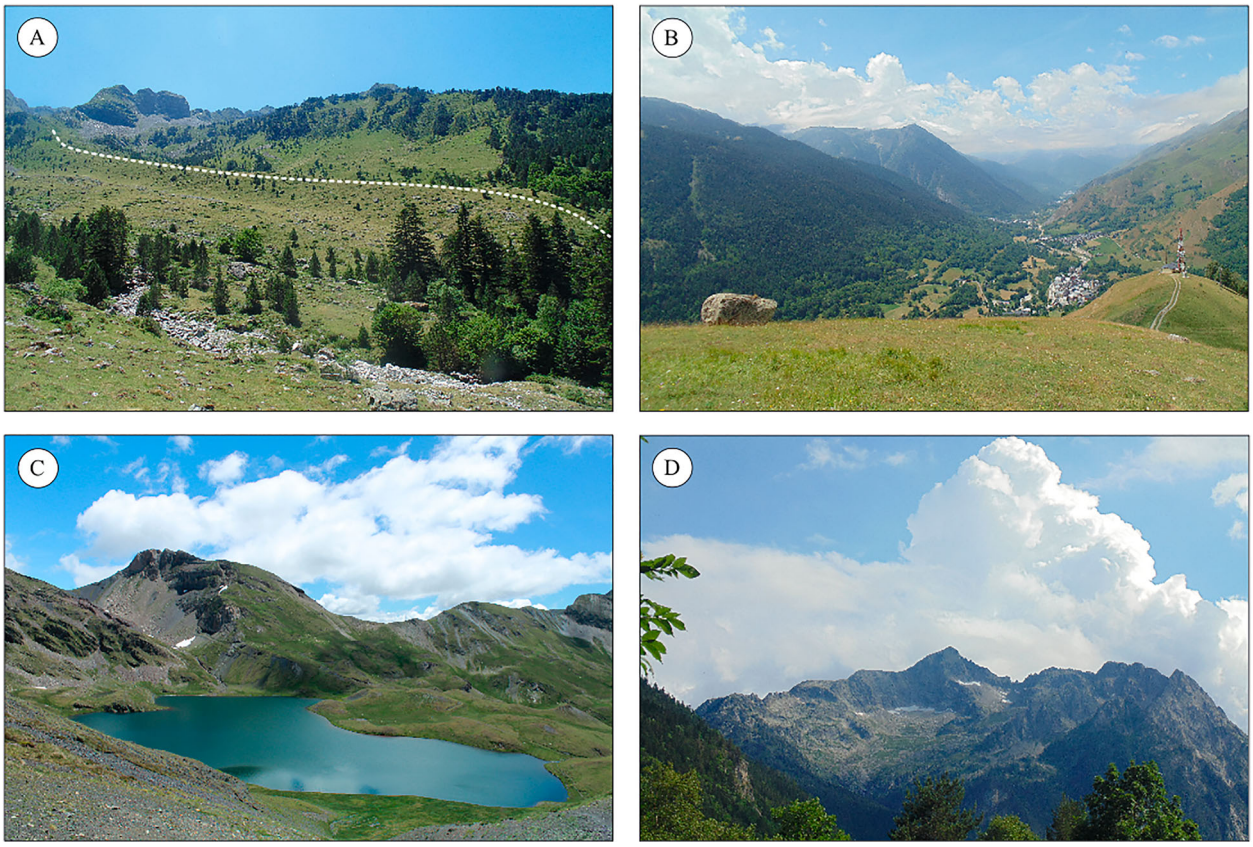


**Figure 3.** Examples of the different glacial landforms identified in the area: (A) lateral moraine around 1600 m at the Nère Valley; (B) E-W perspective of the main Garonne Valley with an erratic boulder of granite distributed on a slate outcrop above Salardú village; (C) glacial lake distributed in an overdeepened basin at the Unhòla Valley; (D) glacial cirque of the Montardo Peak at the Valarties Valley.

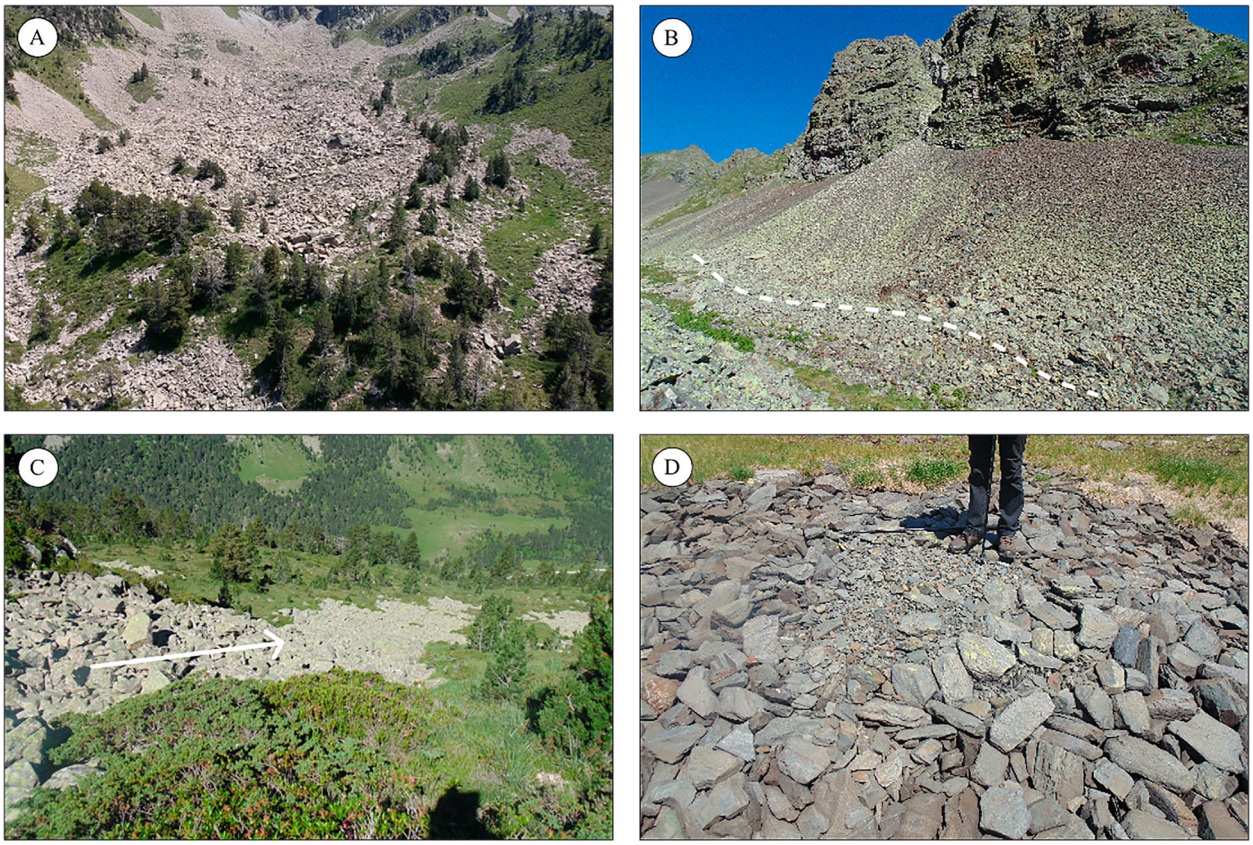


**Figure 4.** Examples of the different periglacial landforms identified in the area: (A) relict rock glacier distributed across the glacial cirque floor of Locampo, Ruda Valley; (B) active talus slope with protalus lobes at the Nère Valley; (C) relict block stream at 2200 m in the Ruda Valley; (D) inactive sorted cirques at 2480 m in the Mauberme cirque, Unhòla Valley.

### 4.3 Nival landforms

Under current climate conditions, snow remains for 6–8 months/year above 2000–2200 m asl with nival dynamics affecting upper slopes. Snow avalanches are relevant on steep slopes (e.g. Valarties Valley) and in shady areas of the cirques and high valleys, snow-patches can persist during most of the year (Figure 5(A)), triggering the formation of protalus ramparts (e.g. Nère Valley).

### 4.4 Karst landforms

Karst morphologies occur in limestone terrain, especially at the Unhòla valley, between the Armeròs and Maubèrme peaks. In these sectors, glaciers and dissolution have originated a glacio-karst landscape (Figure 5(B)) with dolines, uvalas and karst windows.

### 4.5 Slope landforms and processes

The elevation difference of ca. 2500 m from the highest peaks to the lowest valley floors in the Aran results in very active slope processes, particularly in slopes between 25 and 35°. Past slope dynamics occurred mostly during the paraglacial stage consisted of catastrophic rock slope failures, rock slope deformations, rockfalls and landslides (Figure 5(C)) (Fernandes et al., 2020). Postglacial gravitational processes generated thick debris mantles covering the slopes (e.g. main Garonne Valley). Talus cones and talus slopes, particularly those located at lower elevations (e.g. Nère Valley), have gradually become inactive, allowing for soil development and forest expansion. Some of them show traces of deep incision, following debris flows and gully erosion (e.g. Varradòs Valley). These processes also occur on fine-grained sedimentary rocks, such as lutites or shales.

### 4.6 Alluvial landforms and processes

Alluvial fans (Figure 5(D)) are found at the contact between steep slopes and the valley floors, forming triangular-shaped features of fine sediments of variable sizes (e.g. main Garonne Valley). Depending on the prevailing lithology, alluvial fans can be also reshaped by debris flows, mudflows or rockfalls (e.g. main Garonne Valley). These are particularly intense during heavy rainfall or snow-melt episodes. Sediments can also accumulate in overdeepened basins in the valley heads (e.g. Ruda Valley), infilling ancient lakes and promoting the development of peatlands (e.g. Unhòla Valley).

### 4.7 Fluvial landforms

Rivers and streams flowing to the Garonne River show a high capacity to mobilize sediments, particularly during the snow-melting period. Whereas in some

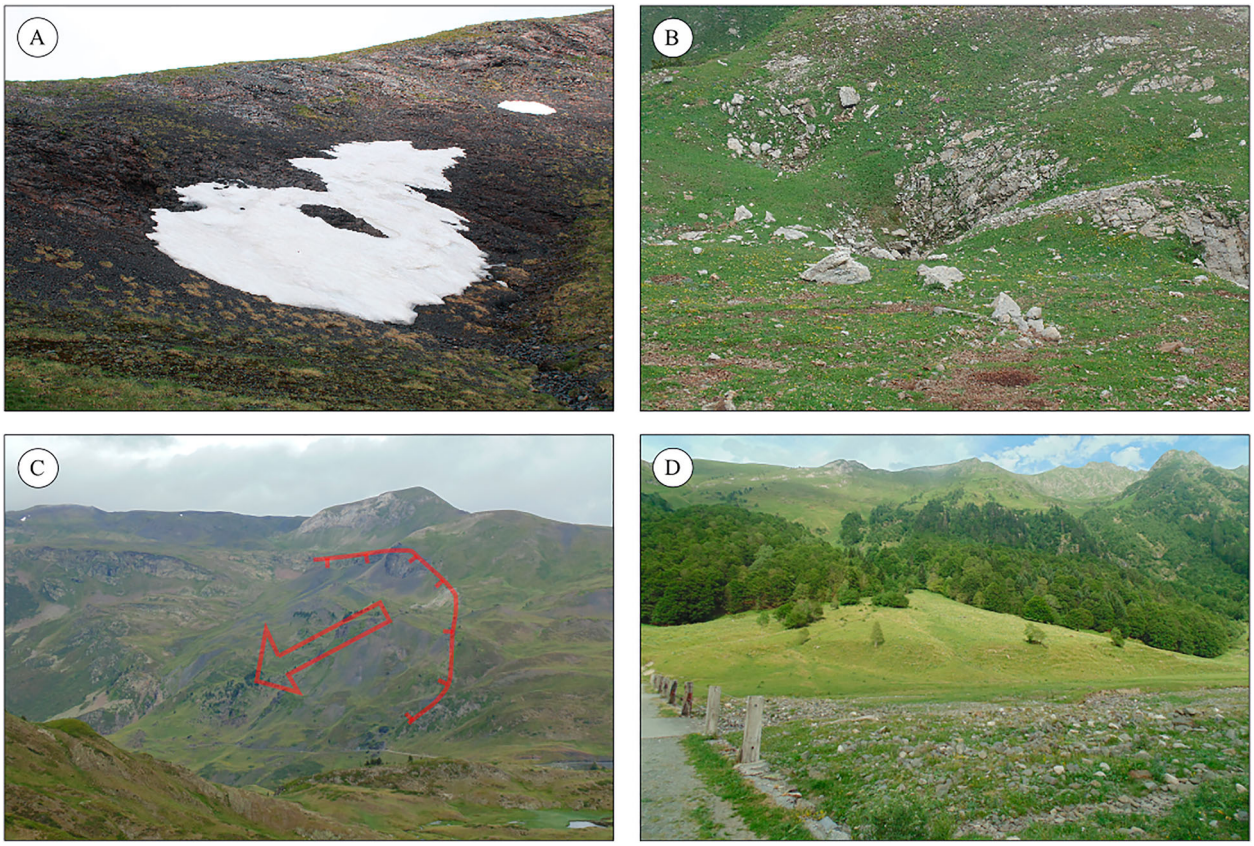


**Figure 5.** Examples of other geomorphological landforms identified in the area: (A) long-lying snow patch at 2350 m, in the north face of the Armèros Peak; Unhòla Valley (B) dolines located in the Sascorjada glacial cirque, Toran Valley; (C) Rock slope deformation at the Varradòs Valley; (D) alluvial fan connected with the fluvial plain at the Joèu Valley.

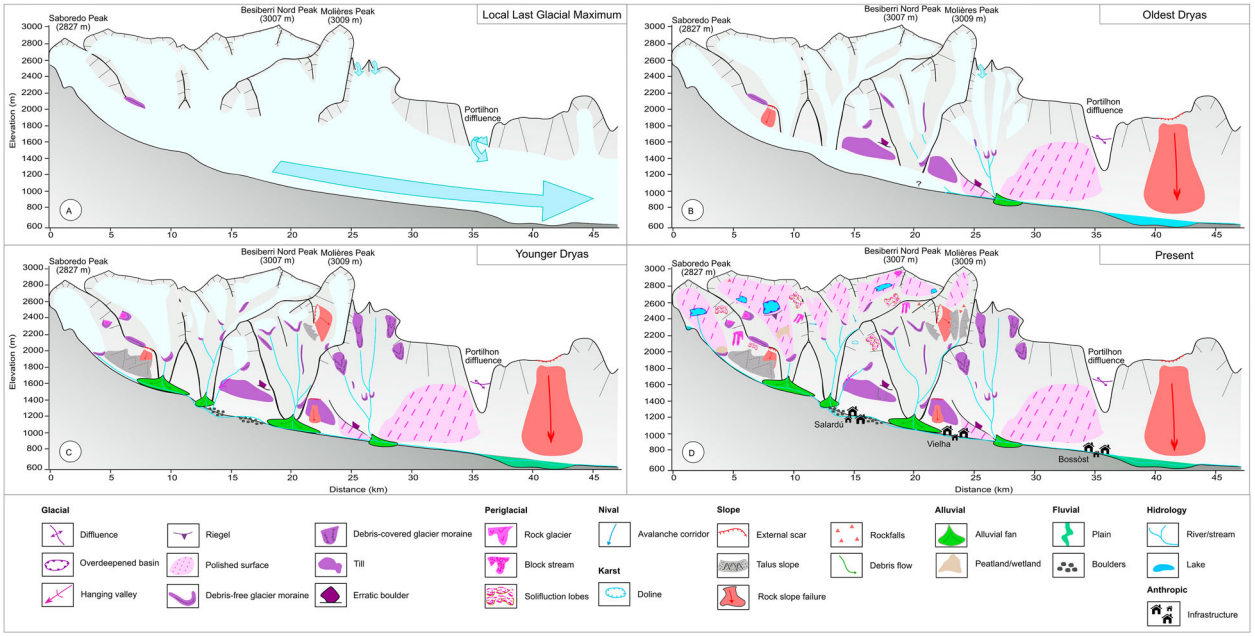


**Figure 6.** Sequence of environmental phases shaping the landscape of the Aran Valley: (A) maximum ice extent of the last glacial cycle; (B) glacial tongues flowing downvalleys during a glacial advance/standstill (Oldest Dryas) within the long-term glacial retreat of the Garonne paleoglacier that favored also intense slope readjustment; (C) alpine and cirque glaciers (Younger Dryas) with very intense postglacial slopes dynamics, and the occurrence of permafrost that promoted the formation of rock glaciers; (D) deglaciated cirques with periglacial processes prevailing at higher elevations (inactive rock glaciers), and slope, alluvial and fluvial processes at lower elevations.

areas the rivers flow through gorges (e.g. Unhòla Valley), in others the valley presents a large flood plain that is used for agriculture and grazing purposes (e.g. Nère Valley). In the Aran Valley, there are more than 700 lakes of glacial origin distributed between 1566 and 2711 m asl with a 0.5 $m^2$ ha mean size (Main map). In the Aran Valley, 80% of the lakes are located above 2000m asl, mostly in overdeepened basins in the granitic bedrock. At lower areas, the lakes are smaller and show infill of peat and proglacial sediments.

## 5. Discussion

The geomorphological map of the Aran Valley shows evidence that almost the entire valley was glaciated during the last glacial cycle, and only the peaks and rock ridges (<8% of the area) protruded above the ice as nunataks (Main map). Given the prevalence of glacial erosional landforms supporting basal sliding, the broad spectrum of periglacial, slope and alluvial phenomena existing in the area must have formed following deglaciation of the valley.

The chronology of the maximum ice extent of the last glacial cycle is still not well-known in the Central Pyrenees (Oliva et al., 2019). However, recent studies shed light on the chronological frame of the terminal basins. Glacial features associated with the Garonne paleoglacier in the Loures-Barousse-Barbazan basin at 470–680 m asl show an advance during the marine isotope stage (MIS)-6 and retreat during MIS-2 (Fernandes et al., 2021a). The presence of discontinuous morainic steps on the slopes above the main Garonne Valley suggests that glaciers reached an ice thickness of ca. 600–800 m during the maximum Pleistocene ice expansion (Figure 6). The intensity of postglacial slope, alluvial and fluvial dynamics must have destroyed glacial evidence in the lowest areas of the Aran Valley, where no terminal moraines are preserved. Erosional (e.g. polished surfaces) and accumulation glacial landforms (e.g. moraines) are widespread in the upper parts of the valley. Indeed, exposure ages from polished surfaces showed glacier recession at 15–14 and at 12.7 ka. Moraines located in glacial cirques at 2080–2190 m and 2430–2470 m asl show ages of 13.5–13.0 and 12.9–12.6 ka, respectively. These relate to glacial advances or standstills in the Bølling-Allerød, as well as in the Bølling-Allerød to Younger Dryas transition (Fernandes et al., 2021b; Oliva et al., 2021). Such glacial landforms are a legacy from past processes and environments. The wide range of glacial landforms, its degree of preservation, as well as its singularity within southern Europe constitute key elements of the natural heritage and geodiversity of the Aran Valley.

As glaciers disappeared from glacial cirques, periglacial morphogenesis became the prevailing process shaping the highest land surfaces. Indeed, rock glaciers and protalus lobes present in most cirques show evidence of permafrost in formerly glaciated cirques (Fernandes et al., 2018). In the Pyrenees, these periglacial features developed following glacial retreat at the end of both the Oldest and Younger Dryas cold events under paraglacial debuttressing of cirque slopes (Andrés et al., 2018; García-Ruiz et al., 2016; Palacios et al., 2017). The readjustment to new glacier-free conditions favored widespread slope failure events affecting both the bedrock and unconsolidated glacial sediments. Fernandes et al. (2020) show that more than 90% of the 135 large slope failures identified in the Aran Valley occurred within the glaciated domain of the last glacial cycle (Figures 5(C) and 6).

Since the onset of the Holocene, climate variability ranged within ± 2°C compared to present conditions in mid-latitude regions (Mayewski et al., 2004; Wanner et al., 2015). The current periglacial zone in the Aran Valley is located above ca. 2300 m asl (Fernandes et al., 2017) and thus seasonal frost processes should have affected elevations between ca. 2000 and 2500 m asl, with permafrost existing at the summit levels only during the coldest phases (Oliva et al., 2018). Holocene periglacial processes have reshaped slopes with widespread development of talus cones and slopes, as well as solifluction landforms, whereas patterned ground and block fields formed in flat or low gradient hillsides (e.g. Nère and Unhòla valleys – Main map). Climatic changes during the Holocene together with transhumance practices during the Mid-Late Holocene promoted vegetation shifts in the periglacial environment that enhanced or diminished hydrological and geomorphic dynamics (García-Ruiz et al., 2020).

Frequent high-intensity events, such as snow avalanches (e.g. Valarties Valley), debris flows (e.g. Varradòs Valley) or mudflows (e.g. Bargadera Valley), dominate the glacial landscape from the cirques and valley heads to the valley floors, where they contributed to the development of several generations of alluvial fans (e.g. Unhòla; Victoriano et al., 2016). These are the major natural hazards currently affecting the Aran Valley, particularly debris flows that cause annual infrastructure damage, such as in the road network. An example occurred in the Valarties Valley, where a debris flow in May 2018 mobilized 50,000 $m^3$ of sediments, destroying the local road (Perdices Cos, 2019). Intense rainfall and snow-melting episodes lead to frequent flood events that trigger intense fluvial erosion in the highest sectors and accumulation of sediments in the flood plains of the lowest areas, such as in June 2013 where a flash flood in the Upper Garonne Basin caused damage to infrastructure exceeding 100 million euros (Balasch et al., 2019; Victoriano et al., 2016). Therefore, this high-resolution geomorphological map identifying landforms

associated with natural hazards can be used by local authorities to better predict the location of hazards and their impacts.

## 6. Conclusions

Accurate mapping of geomorphological processes and landforms of the Aran Valley at 1:25000 scale allows a better understanding of the processes that have shaped the alpine landscape of this valley. The glacial landforms are diverse and widespread from the summits to the Garonne riverbed, and reveal that glacial, periglacial, nival, karst, slope, alluvial and fluvial processes have played a role in shaping the landscape of the entire valley. Once glaciers started retreating and thinning following the Last Glacial Maximum, periglacial processes dominated in the exposed ice-free terrain, accompanied by intense slope, alluvial and fluvial dynamics. In specific areas, nival and karstic processes also contributed to reshape the formerly glaciated environment.

Today, the steep slopes surrounding the main valley floor favor the occurrence of slope failures and frequent snow avalanches. In addition, sudden snow-melting episodes and torrential rains trigger also floods. Mapping these processes at a high-resolution improves the precision of the available tools and consequently enhances spatial planning, such as by validating susceptibility maps of geohazards or by promote geoheritage protection and assess geosite management.

## Software

The geomorphological map was developed using ArcGIS 10.7.1 (ESRI) software. The final map was improved with Illustrator 16.3.

## Disclosure statement

No potential conflict of interest was reported by the author (s).

## Funding

Marcelo Fernandes is funded by a PhD fellowship (SFRH/139569/2018) from the Fundação para a Ciência e Tecnologia of Portugal. Field work was supported by the Centro de Estudos Geográficos - University of Lisbon (FCT - UIDB/00295/2020 and UIDP/00295/2020). Marc Oliva is supported by the Research scientist, Ramon y Cajal program (RYC-2015-17597) and the Research Group ANTALP (Antarctic, Arctic, Alpine Environments; 2017-SGR-1102) funded by the Government of Catalonia through the AGAUR agency. Luis Lopes is a PhD fellow funded by the FCT (PT/BD/142963/2018), under the SUSFOR – Sustainable Forests and Products Doctoral Programme. This research is framed within the College on Polar and Extreme Environments (Polar2E) of the University of Lisbon, and it complements the study topics of the PALEOGREEN (CTM2017-87976-P) project of the Ministry of Economy of Spain.

## Data availability statement

The data described in this article are openly available at the ZENODO data repository (https://doi.org/10.5281/zenodo.4644265).

## ORCID

*M. Fernandes* http://orcid.org/0000-0001-6840-4317
*M. Oliva* http://orcid.org/0000-0001-6521-6388
*G. Vieira* http://orcid.org/0000-0001-7611-3464
*L. Lopes* http://orcid.org/0000-0002-5132-9258

## References

Andrés, N., Gómez-Ortiz, A., Fernández-Fernández, J. M., Tanarro García, L. M., Salvador-Franch, F., Oliva, M., & Palacios, D. (2018). Timing of deglaciation and rock glacier origin in the southeastern Pyrenees: A review and new data. *Boreas*, *47*(4), 1050–1071. https://doi.org/10.1111/bor.12324

Balasch, J. C., Tuset, J., Furdada, G., Porras, L., Castelltort, X., Barriendos, M., & Pino, D. (2019). The Upper Garonne flood series from discharge gauging data (Bossost, Val d'Aran, Spain) and reconstruction of historical floods (Saint-Béat, France), in: EGU General Assembly 2019.

Benn, D. I., & Evans, D. J. A. (2010). *Glaciers and glaciation*. Hodder Education.

Bolòs, O. d., & Vigo, J. (1984). *Flora dels països Catalans*. Editorial Barcino.

Bordonau, J. (1985). Estudi geomorfològic del sector sudoccidental de la Vall d'Aran. L'evolució Quaternària de les valls dels rius Joeu i Nere. Tesis de Licenciatura.

Chandler, B. M. P., Lovell, H., Boston, C. M., Lukas, S., Barr, I. D., Benediktsson, Í. Ö., Benn, D. I., Clark, C. D., Darvill, C. M., Evans, D. J. A., Ewertowski, M. W., Loibl, D., Margold, M., Otto, J.-C., Roberts, D. H., Stokes, C. R., Storrar, R. D., & Stroeven, A. P. (2018). Glacial geomorphological mapping: A review of approaches and frameworks for best practice. *Earth-Science Reviews*, *185*, 806–846. https://doi.org/10.1016/j.earscirev.2018.07.015

Copons, R. (2005). *Mapa geomorfològic d'Andorra 1:50.000*. Centre de Recerca en Ciències de la Terra. Govern d'Andorra.

Coratza, P., & de Waele, J. (2012). Geomorphosites and natural hazards: Teaching the importance of geomorphology in society. *Geoheritage*, *4*(3), 195–203. https://doi.org/10.1007/s12371-012-0058-0

Coratza, P., Ghinoi, A., Marchetti, M., & Soldati, M. (2019). Geomorphology of the Rio Cisles basin (Odle Group, Dolomites, Italy). *Journal of Maps*, *15*(2), 546–554. https://doi.org/10.1080/17445647.2019.1633426

Evans, D. J. A. (2005). *Glacial landsystems, glacial landsystems*. Hodder Arnold.

Evans, D. J. A. (2013). *Glacial landsystems. Encyclopedia of quaternary sciences*. Elsevier.

Fernandes, M., Oliva, M., Palma, P., Ruiz-Fernández, J., & Lopes, L. (2017). Glacial stages and post-glacial environmental evolution in the Upper Garonne valley, Central

Pyrenees. *Science of The Total Environment*, *584–585*, 1282–1299. https://doi.org/10.1016/j.scitotenv.2017.01.209

Fernandes, M., Oliva, M., & Vieira, G. (2020). Paraglacial slope failures in the Aran Valley (Central Pyrenees). *Quaternary International*, *566–567*, 24–38. https://doi.org/10.1016/j.quaint.2020.07.045

Fernandes, M., Oliva, M., Vieira, G., Palacios, D., Fernández-Fernández, J. M., Delmas, M., García-Oteyza, J., Schimmelpfennig, I., Ventura, J., & Team, A. (2021a). Maximum glacier extent of the penultimate glacial cycle in the Upper Garonne Basin (Pyrenees): new chronological evidence. *Environmental Earth Sciences*, https://doi.org/10.21203/rs.3.rs-788888/v1

Fernandes, M., Oliva, M., Vieira, G., Palacios, D., Fernández-Fernández, J. M., García-Oteyza, J., Schimmelpfennig, I., Team, A., & Antoniades, D. (2021b). Glacial oscillations during the Bølling–Allerød Interstadial–Younger Dryas transition in the Ruda Valley. *Journal of Quaternary Science*, 1–17. https://doi.org/10.1002/jqs.3379

Fernandes, M., Palma, P., Lopes, L., Ruiz-Fernández, J., Pereira, P., & Oliva, M. (2018). Spatial distribution and morphometry of permafrost-related landforms in the Central Pyrenees and associated paleoclimatic implications. *Quaternary International*, *470*, https://doi.org/10.1016/j.quaint.2017.08.071

French, H. (2007). *The periglacial environment* (Third ed). John Wiley & Sons, Ltd.

Garcés-Pastor, S., Cañellas-Boltà, N., Pèlachs, A., Soriano, J. M., Pérez-Obiol, R., Pérez-Haase, A., Calero, M. A., Andreu, O., Escolà, N., & Vegas-Vilarrúbia, T. (2017). Environmental history and vegetation dynamics in response to climate variations and human pressure during the Holocene in Bassa Nera, Central Pyrenees. *Palaeogeography, Palaeoclimatology, Palaeoecology*, *479*, 48–60. https://doi.org/10.1016/j.palaeo.2017.04.016

García-Ruiz, J. M., Bordonau, J., Martínez de Pisón, E., & Vilaplana, J. M. (1992). *Mapa geomorfológico de Benasque (M.T.N. 180)*. Geoforma Ediciones.

García-Ruiz, J. M., & Martí-Bono, C. (2001). *Mapa geomorfológico del parque nacional de ordesa y monte Perdido*. Organismo Autónomo de Parques Nacionales.

García-Ruiz, J. M., Palacios, D., González-Sampériz, P., De Andrés, N., Moreno, A., Valero-Garcés, B. L., & Gómez-Villar, A. (2016). Mountain glacier evolution in the Iberian peninsula during the younger dryas. *Quaternary Science Reviews*, *138*, 16–30. https://doi.org/10.1016/j.quascirev.2016.02.022

García-Ruiz, J. M., Tomás-Faci, G., Diarte-Blasco, P., Montes, L., Domingo, R., Sebastián, M., Lasanta, T., González-Sampériz, P., López-Moreno, J. I., Arnáez, J., & Beguería, S. (2020). Transhumance and long-term deforestation in the subalpine belt of the central Spanish Pyrenees: An interdisciplinary approach. *Catena*, *195*, 104744. https://doi.org/10.1016/j.catena.2020.104744

García-Sansegundo, J. (2004). *Estructura varisca de los Pirineos*. Geol. España. 254–258

García-Sansegundo, J., Merino, J. R., Santisteban, R. R., & Leyva, F. (2013). *Canejan-Vielha Mapa geologico 1:50 000*. Instituto Geologico y Minero de España.

Geològic de Catalunya. (2017). Base de dades geològiques de Catalunya 1:50.000 v1.0.

Giles, D. P., Griffiths, J. S., Evans, D. J. A., & Murton, J. B. (2017). Chapter 3 geomorphological framework: Glacial and periglacial sediments, structures and landforms. *Geological Society, London, Engineering Geology Special Publications*, *28*(1), 59–368. https://doi.org/10.1144/EGSP28.3

González-Gutiérrez, R. B., Santos-González, J., Gómez-Villar, A., Redondo-Vega, J. M., & Prieto-Sarro, I. (2017). Geomorphology of the Curueño River headwaters, Cantabrian mountains (NW Spain). *Journal of Maps*, *13*(2), 382–394. https://doi.org/10.1080/17445647.2017.1316217

González-Sampériz, P., Aranbarri, J., Pérez-Sanz, A., Gil-Romera, G., Moreno, A., Leunda, M., Sevilla-Callejo, M., Corella, J. P., Morellón, M., Oliva, B., & Valero-Garcés, B. L. (2017). Environmental and climate change in the southern Central Pyrenees since the last glacial maximum: A view from the lake records. *Catena*, *149*, 668–688. https://doi.org/10.1016/j.catena.2016.07.041

Jarman, D., Calvet, M., Corominas, J., Delmas, M., & Gunnell, Y. (2014). Large-scale rock slope failures in the eastern pyrenees: Identifying a sparse but significant population in paraglacial and parafluvial contexts. *Geografiska Annaler: Series A, Physical Geography*, *96* (3), 357–391. https://doi.org/10.1111/geoa.12060

Joly, F. (1997). Glossaire de géomorphologie. Base de donnés sémiologiques pour la cartographie, Masson/Arm. ed. Paris.

Kääb, A. (2013). Rock glaciers and protalus forms. In E. Scott, & C. Mock (Eds.), *Encyclopedia of quaternary science* (pp. 535–541). Elsevier.

Knight, J., & Harrison, S. (2009). Periglacial and paraglacial environments: A view from the past into the future. *Geological Society, London, Special Publications*, *320*(1), 1–4. https://doi.org/10.1144/SP320.1

Knight, J., Mitchell, W. A., & James, R. (2011). Geomorphological field mapping. In M. J. Smith, P. Paron, & J. S. Griffiths (Eds.), *Geomorphological mapping methods and applications* (pp. 151–188). Elsevier.

Lambiel, C., Maillard, B., Kummert, M., & Reynard, E. (2016). Geomorphology of the Hérens valley (Swiss Alps). *Journal of Maps*, *12*(*1*), 160–172. https://doi.org/10.1080/17445647.2014.999135

Lambiel, C., Maillard, B., Regamey, B., Martin, S., Kummert, M., Schoeneich, P., Ondicol, R. P., & Reynard, E. (2013). Adaptation of the geomorphological mapping system of the University of Lausanne for ArcGIS. In 8th International Conference on Geomorphology (IAG). Paris (p. 1176). https://doi.org/10.1016/j.geomorph.2010.03.00

Lindholm, M.S., Heyman, J. (2016). Glacial geomorphology of the Maidika region, Tibetan Plateau. *Journal of Maps*, 12, 797–803. https://doi.org/10.1080/17445647.2015.1078182

Lopes, L., Oliva, M., Fernandes, M., Pereira, P., Palma, P., & Ruiz-Fernández, J. (2018). Spatial distribution of morphometric parameters of glacial cirques in the Central Pyrenees (Aran and Boí valleys). *Journal of Mountain Science*, *15*(10), https://doi.org/10.1007/s11629-018-4873-x

López-Moreno, J. I., Revuelto, J., Rico, I., Chueca-Cía, J., Julián-Andrés, A., Serreta, A., Serrano, E., Vicente-Serrano, S. M., Azorín-Molina, C., Alonso-González, E., & García-Ruiz, J. M. (2016). Thinning of the Monte Perdido glacier in the Spanish Pyrenees since 1981. *The Cryosphere*, *10*(2), 681–694. https://doi.org/10.5194/tc-10-681-2016

Martí-Bono, C., & García-Ruiz, J. M. (1994). *El glaciarismo surpirenaico: Nuevas aportaciones*. Geoforma Ediciones.

Martínez, F. J., Dietsch, C., Aleinikoff, J., Cirés, J., Arboleya, M. L., Reche, J., & Gómez-Gras, D. (2016). Provenance,

age, and tectonic evolution of Variscan flysch, southeastern France and northeastern Spain, based on zircon geochronology. *Geological Society of America Bulletin*, *128*(5-6), 842–859. https://doi.org/10.1130/B31316.1

Martínez-Rius, A. (2010). *Parque Nacional de Aigüestortes i Estany de Sant Maurici. Guía geológica*. Editorial Everest.

Martí-Soler, M. (1988). Estudi geomorfològic del massis central de la Vall d'Aran (Pirineu Central) [Bachelor thesis]. University of Barcelona.

Matsuoka, N., Ikeda, A., & Date, T. (2005). Morphometric analysis of solifluction lobes and rock glaciers in the Swiss Alps. *Permafrost and Periglacial Processes*, *16*(1), 99–113. https://doi.org/10.1002/ppp.517

Mayewski, P. A., Rohling, E. E., Stager, J. C., Karlén, W., Maasch, K. A., Meeker, L. D., Meyerson, E. A., Gasse, F., van Kreveld, S., Holmgren, K., Lee-Thorp, J., Rosqvist, G., Rack, F., Staubwasser, M., Schneider, R. R., & Steig, E. J. (2004). Holocene climate variability. *Quaternary Research*, *62*(3), 243–255. https://doi.org/10.1016/j.yqres.2004.07.001

Mezger, J. E., & Gerdes, A. (2016). Early Variscan (Visean) granites in the core of central Pyrenean gneiss domes: Implications from laser ablation U-Pb and Th-Pb studies. *Gondwana Research*, *29*(1), 181–198. https://doi.org/10.1016/j.gr.2014.11.010

Oguchi, T., Yuichi, H., & Thad, W. (2012). Data sources. In S. Mike, P. Paolo, & G. James (Eds.), *Geomorphological mapping methods and applications* (pp. 189–224). Elsevier.

Oliva, M., Fernandes, M., Palacios, D., Fernández-Fernández, J. M., Schimmelpfennig, I., Team, A., & Antoniades, D. (2021). Rapid deglaciation during the Bølling-Allerød Interstadial in the Central Pyrenees and associated glacial and periglacial landforms. *Geomorphology*, 107735, https://doi.org/10.1016/j.geomorph.2021.107735

Oliva, M., Palacios, D., Fernández-Fernández, J. M., Rodríguez-Rodríguez, L., García-Ruiz, J. M., Andrés, N., Carrasco, R. M., Pedraza, J., Pérez-Alberti, A., Valcárcel, M., & Hughes, P. (2019). Late quaternary glacial phases in the Iberian peninsula. *Earth-Science Reviews*, *192*, 564–600. https://doi.org/10.1016/j.earscirev.2019.03.015

Oliva, M., Žebre, M., Guglielmin, M., Hughes, P. D., Çiner, A., Vieira, G., Bodin, X., Andrés, N., Colucci, R. R., García-Hernández, C., Mora, C., Nofre, J., Palacios, D., Pérez-Alberti, A., Ribolini, A., Ruiz-Fernández, J., Sarıkaya, M. A., Serrano, E., Urdea, P., Valcárcel, M., Woodward, J. C., & Yıldırım, C. (2018). Permafrost conditions in the Mediterranean region since the Last Glaciation. *Earth-Science Reviews*, *185*, 397–436. https://doi.org/10.1016/j.earscirev.2018.06.018

Palacios, D., García-Ruiz, J. M., Andrés, N., Schimmelpfennig, I., Campos, N., Léanni, L., Aumaître, G., Bourlès, D. L., & Keddadouche, K. (2017). Deglaciation in the central Pyrenees during the Pleistocene–Holocene transition: Timing and geomorphological significance. *Quaternary Science Reviews*, *162*, 111–127. https://doi.org/10.1016/j.quascirev.2017.03.007

Paron, P., & Claessens, L. (2011). Makers and users of geomorphological maps. In M. J. Smith, P. Paron, & J. S. Griffiths (Eds.), *Geomorphological mapping methods and applications* (Vol. 15, pp. 75–106). Elsevier B.V. https://doi.org/10.1016/B978-0-444-53446-0.00004-5

Parry, S. (2011). The Application of geomorphological mapping in the assessment of landslide hazard in Hong Kong. In M. J. Smith, P. Paron, & J. S. Griffiths (Eds.), *Geomorphological mapping methods and applications* (pp. 413–442). Elsevier B.V.

Pellitero, R. (2014). Geomorphology and geomorphological landscapes of Fuentes Carrionas. *Journal of Maps*, *10*(*2*), 313–323. https://doi.org/10.1080/17445647.2013.867822

Perdices Cos, P. (2019). *Análisis de un deslizamiento en el Valle de Arán y simulación mediante el método del punto*. Polytechnic University of Catalunha.

Quesada, C., & Oliveira, J. (2019). *The geology of Iberia: A geodynamic approach: The Variscan cycle*. Springer.

Rapp, A. (1960). Talus slopes and mountain walls at Tempelfjorden, Spitsbergen. Skrifter, 125.

Schneider, R. A. A., Blomdin, R., Fu, P., Xu, X. K., & Stroeven, A. P. (2021). Paleoglacial footprint and fluvial terraces of the Shaluli Shan, SE Tibetan Plateau. *Journal of Maps*, https://doi.org/10.1080/17445647.2021.1946443

Serrano, E., González-Trueba, J. J., & Sanjosé, J. (2011). Dynamic, evolution and structure of Pyrenean rock glaciers. Cuadernos de Investigación Geográfica, *37*, https://doi.org/10.18172/cig.1260

Serrano, E., López-Moreno, J. I., Gómez-Lende, M., Pisabarro, A., Martín-Moreno, R., Rico, I., & Alonso-González, E. (2020). Frozen ground and periglacial processes relationship in temperate high mountains: A case study at Monte Perdido-Tucarroya area (The Pyrenees, Spain). *Journal of Mountain Science*, *17*(5), 1013–1031. https://doi.org/10.1007/s11629-019-5614-5

Serrat, D., Martí, M., & Bordonau, J. (1994). *Geologia, geomofologia e risques, em: Geografia física, em: Atlas comarcau de catalunya-Val d'Aran*. Inst. Cart. Catalunya and Conselh Generau d'Aran, Val d'Aran.

Sitter, L. U., & Zwart, H. J. (1962). Geological map of the Paleozoic of the Central Pyrenees. *Leidse Geologische Mededelingen*, *33*, 191–254.

Tejedor-Rodríguez, C., Moreno-García, M., Tornero, C., Hoffmann, A., García-Martínez de Lagrán, Í, Arcusa-Magallón, H., Garrido-Pena, R., Royo-Guillén, J. I., Díaz-Navarro, S., Peña-Chocarro, L., Alt, K. W., & Rojo-Guerra, M. (2021). Investigating Neolithic caprine husbandry in the Central Pyrenees: Insights from a multi-proxy study at Els Trocs cave (Bisaurri, Spain). *PLoS One*, *16*(1), e0244139. https://doi.org/10.1371/journal.pone.0244139

Victoriano, A., García-Silvestre, M., Furdada, G., & Bordonau, J. (2016). Long-term entrenchment and consequences for present flood hazard in the Garona River (Val d'Aran, Central Pyrenees, Spain). *Natural Hazards and Earth System Sciences*, *16*(9), 2055–2070. https://doi.org/10.5194/nhess-16-2055-2016

Wanner, H., Mercolli, L., Grosjean, M., & Ritz, S. P. (2015). Holocene climate variability and change; a data-based review. *Journal of the Geological Society*, *172*(2), 254–263. https://doi.org/10.1144/jgs2013-101

Zwart, H. J. (1979). The geology of the Central Pyrenees. *Leidse Geologische mededelingen*, 90(1), 1–74.

# 2. Maximum glacier extent of the Penultimate Glacial Cycle in the Upper Garonne Basin (Pyrenees): new chronological evidence

Fernandes, M., Oliva, M., Vieira, G., Palacios, D., Fernández-Fernández, J. M., Delmas, M., García-Oteyza, J., Schimmelpfennig, I., Ventura, J., & ASTER, team. (2021). Maximum glacier extent of the Penultimate Glacial Cycle in the Upper Garonne Basin (Pyrenees): new chronological evidence. *Environmental Earth Sciences*, *80*(24), 796. https://doi.org/10.1007/s12665-021-10022-z

Environmental Earth Sciences (2021) 80:796
https://doi.org/10.1007/s12665-021-10022-z

THEMATIC ISSUE

# Maximum glacier extent of the Penultimate Glacial Cycle in the Upper Garonne Basin (Pyrenees): new chronological evidence

Marcelo Fernandes[1] · Marc Oliva[2] · Gonçalo Vieira[1] · David Palacios[3] · José María Fernández-Fernández[1] · Magali Delmas[4] · Julia García-Oteyza[2] · Irene Schimmelpfennig[5] · Josep Ventura[2] · ASTER Team[5]

Received: 5 August 2021 / Accepted: 30 September 2021


## Abstract

The Upper Garonne Basin included the longest glacier in the Pyrenees during the Late Pleistocene. During major glacial advances, the Garonne palaeoglacier flowed northwards along ~ 80 km from peaks of the axial Pyrenees exceeding 2800–3000 m until the foreland of this mountain range at the Loures–Barousse–Barbazan basin (LBBb), at 420–440 m. Here, the palaeoglacier formed a terminal moraine complex that is examined in this work. Based on geomorphological observations and a 12-sample data set of $^{10}$Be Cosmic-Ray Exposure (CRE) ages, the timing of the maximum glacial extent was constrained as well as the onset of the deglaciation from the end of the Last Glacial Cycle (LGC). Chronological data shows evidence that the external moraines in this basin were abandoned by the ice at the end of the Penultimate Glacial Cycle (PGC) and the onset of the Eemian Interglacial, at ~ 129 ka. No evidence of subsequent glacial advances or standstills occurred during the LGC in this basin were found, as the few existing datable boulders provided in the internal moraine showed inconsistent ages, thus probably being affected by post-glacial processes. The terminal basin was already deglaciated during the global Last Glacial Maximum at 24–21 ka, as revealed by exposure ages of polished surfaces at the confluence of the Garonne-La Pique valleys, 13 km south of the entrance of the LBBb. This study introduces the first CRE ages in the Pyrenees for the glacial advance occurred during the PGC and provides also new evidence that glaciers had already significantly shrunk during the LGM.

**Keywords** Central Pyrenees · Upper Garonne Basin · Penultimate Glacial Cycle · Cosmic-ray exposure dating · Moraines · Polished bedrock

ASTER Team—Consortium: Georges Aumaître, Karim Keddadouche.

This article is part of a Topical Collection in Environmental Earth Sciences on Earth Surface Processes and Environment in a Changing World: Sustainability, Climate Change and Society, guest edited by Alberto Gomes, Horácio García, Alejandro Gomez, Helder I. Chaminé.

✉ Marcelo Fernandes
marcelo.fernandes@live.com

[1] Centre for Geographical Studies, Instituto de Geografia E Ordenamento Do Território, Universidade de Lisboa, Rua Branca Edmée Marques, 1600-276 Lisbon, Portugal

[2] Department of Geography, Universitat de Barcelona, Barcelona, Catalonia, Spain

[3] Department of Geography, Universidad Complutense de Madrid, Madrid, Spain

[4] UMR 7194, HNHP, Université de Perpignan Via Domitia, Perpignan, France

[5] Aix-Marseille Université, CNRS, IRD, INRAE, Coll. France, UM 34 CEREGE, Aix-en-Provence, France

## Introduction

High and middle mountain landscapes in mid-latitude ranges have been mostly shaped by glaciers during Pleistocene glacial cycles. Large valleys, glacial cirques, truncated spurs, hanging valleys (large-scale erosional landforms) and till or moraines (accumulation landforms) constitute the legacy of the past glaciations in the highest massifs (Benn and Evans 2010). Such invaluable glacial footprints can provide a better understanding of past environmental and climatic changes (Pearce et al. 2017).

The widespread glacial features existing in mid-latitude and Mediterranean mountains have been increasingly used to reconstruct the timing, magnitude and extent of the glacial oscillations during past glacial cycles (Ehlers et al. 2011; Adamson et al. 2013). The study of glacial advances and retreats has mostly focused on the Late Pleistocene (or Last Glacial Cycle, LGC), from the end of the Eemian Interglacial (129–114 ka) to the Holocene (11.7 ka to present;

Published online: 23 November 2021

Dahl-Jensen et al. 2013; Rasmussen et al. 2014). Glacial studies have resulted in an increase in the number and accuracy of regional and global palaeoclimate records, which generally show a good coupling between cold phases and glacial advances (Bernal-Wormull et al. 2021; González-Sampériz et al. 2006; Morellón et al. 2009; Lisiecki and Raymo 2005; Rasmussen et al. 2014). In the Pyrenees, where this research focuses on, currently available data indicate that the most extensive Pyrenean glaciation of the Late Pleistocene occurred prior to the global Last Glacial Maximum (gLGM: 26–19 ka; Clark et al. 2009). This outermost stadial position (local Last Glacial Maximum; lLGM) was reached not just once, but several times between MIS 5b (or MIS 4) and MIS 3 (Fig. 1a; Mardones and Jalut 1983; Andrieu et al. 1988; García-Ruiz et al. 2003, 2013; Lewis et al. 2009; Pallàs et al. 2010; Delmas et al. 2011; Turu et al. 2016; Sancho et al. 2018; Tomkins et al. 2018; Synthesis in Delmas et al. 2021a). The dimensions of Pyrenean glaciers at the time of the gLGM are well established in the eastern part of the range, where $^{10}$Be, $^{36}$Cl and Schmidt hammer exposure ages have been obtained from boulders embedded in moraines and from ice-scoured rock steps protruding from valley floors (Fig. 1a; Pallàs et al. 2006, 2010; Delmas et al. 2008; Palacios et al. 2015a; Andrés et al. 2018; Tomkins et al. 2018; Synthesis in Delmas et al. 2021b). By contrast, in the westernmost valleys of the Pyrenees, glacier dimensions at the time of the gLGM remain imprecisely defined, because age constraints are mainly provided by glaciolacustrine deposits (Andrieu 1987 1991; Andrieu et al. 1988; Jalut et al. 1988; Montserrat 1992; Reille and Andrieu 1995; García-Ruiz et al. 2003; Synthesis in Delmas et al. 2021b). Besides, other periods of glacial advance and retreat during Termination I are also well-known for northern and southern valleys (Copons and Bordonau 1996; Pallàs et al. 2006,

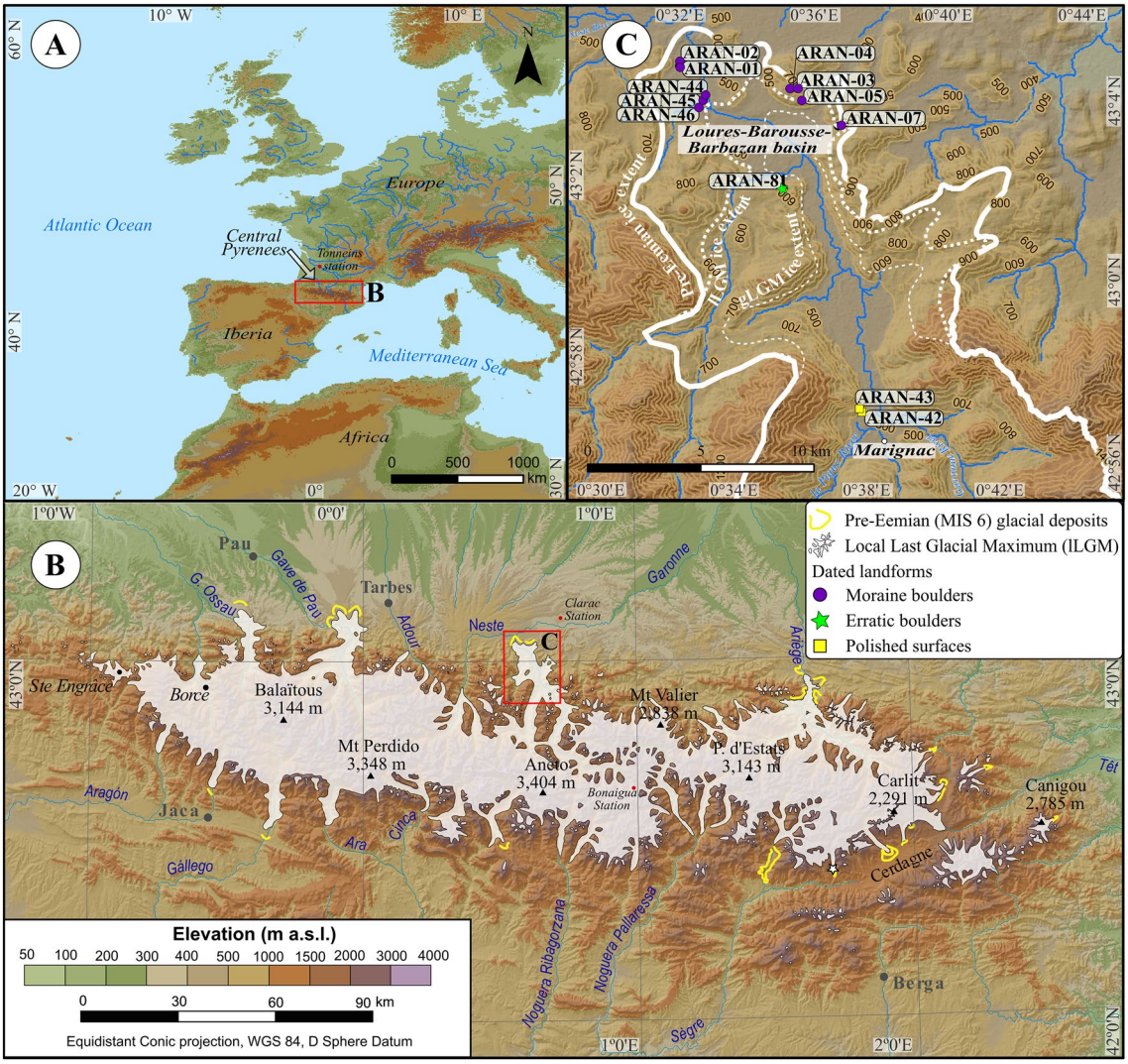


**Fig. 1** Location of the terminal basin of the Loures–Barousse–Barbazan (**C**) in the Pyrenees (**B**) and Europe (**A**)

2010; Delmas et al. 2008, 2011; Palacios et al. 2015a,b, 2017; Crest et al. 2017; Andrés et al. 2018; Tomkins et al. 2018; Fernandes et al. 2021; Oliva et al. 2021; Reixach et al. 2021).

Middle Pleistocene glaciations in the Pyrenees remain poorly documented (Fig. 1a; Synthesis in Delmas et al. 2021a). Most chronological evidence concerning ice-margin fluctuations prior to the Late Pleistocene glacial cycle is known thanks to U–Th ages in cave systems of limestone massifs (Bakalowicz et al. 1984; Quinif and Maire 1998; Sorriaux et al. 2016) and TCN profiles, OSL, ESR ages on glaciofluvial terraces (Turu and Peña-Monné 2006; Turu et al. 2007; Lewis et al. 2009; García-Ruiz et al. 2013; Delmas et al. 2015, 2018). Only one $^{10}$Be exposure age at 133.9 ± 5.3 ka has been obtained from an erratic boulder abandoned by the Ariège Glacier at Caraybat (Delmas et al. 2011). This age also validates the post-depositional weathering criteria to differentiate those glacial deposits from older than MIS 5e and MIS 5d-MIS 2 (Gourinard 1971; Hubschman 1975, 1984; Hétu and Gangloff 1989; Gangloff et al. 1991; Hétu et al. 1992; Calvet 1996).

During the last two glacial cycles, the Central Pyrenees included large ice fields from where composite glaciers flowed downvalley for several tens of km forming piedmont features in the northern foreland and valley glaciers in the southern slope (Fig. 1B). The Upper Garonne Valley hosted the longest Pyrenean palaeoglacier, with an ice tongue following northwards for ~ 80 km down to the Loures–Barousse–Barbazan basin (LBBb) and reaching an elevation of 420–440 m a.s.l. (Andrieu 1991; Calvet et al. 2011). Previous studies based on the degree of soil development and on the state of the weathering of granite cobbles and boulders contained within the glacial sediments revealed the presence of two main morainic complexes in that area: (i) the outermost one surrounding the external northern fringe of the basin is supposed to correspond to the Penultimate Glacial Cycle (PGC; i.e., ~192–135 ka; Obrochta et al. 2014), while (ii) the moraine ridges distributed across the internal part of the basin were associated with the LGC (Hubschman 1975, 1984; Stange et al. 2014). Radiocarbon ages obtained within the Barbazan glaciolacustrine sequence confirmed this relative chronology (Andrieu 1991; Andrieu et al. 1988), even if these ages are controversial, as potential problems associated with hard water effect in the carbon content were raised by other authors (Pallàs et al. 2006).

To shed light on the glacial chronology of the largest expansion of the PGC and LGC glaciers in the northern slope of the Pyrenees, new Cosmic-Ray Exposure (CRE) ages are presented from glacial landforms distributed across the LBBb aiming to answer the following questions:

- When did Pleistocene glaciers reach their maximum extent in the Central Pyrenees?
- Are there glacial remnants from the PGC as previously inferred from post-depositional weathering intensity criteria?
- When did glaciers start retreating and abandoned the Loures–Barousse–Barbazan terminal basin during the LGC?
- Is the timing of glacial oscillations similar to that of the other Pyrenean, Iberian and European mountain ranges?

## Study area

The Pyrenees stretch from the Mediterranean Sea to the Bay of Biscay across ~ 450 km long and ~ 100 km width and divide the Iberian and European tectonic plates. The geographical centre of the range coincides with the highest peaks and a major hydrographic divide, where several rivers drain towards the northern (Aquitaine Basin) and the southern (Ebro Basin) slopes.

The Upper Garonne constitutes one of the largest glacial catchments of the northern Central Pyrenees (1260 km$^2$; Fernandes et al. 2017). It exceeds an elevation of 3000 m in several peaks (e.g., Perdiguero Peak, 42°41′31″N-0°31′08″, 3219 m; Maupas Peak, 3111 m; Molières Peak, 3009 m; Besiberri Nord Peak, 3007 m) and reach 420–440 m at the frontal position of the PGC and LGC palaeoglaciers. The Ruda Valley, located in the Aran Valley (Fig. 1B), constitutes the headwaters of the Garonne River that receives several other tributaries downvalley to become one of the largest rivers of the Pyrenees; at the Tonneins River gauging station, for example, the Garonne River reports an annual average discharge of 603 m$^3$ s$^{-1}$ (1913–2013 series). The abundant discharge results from the Atlantic climate regime, with high precipitation and moderate to cool temperatures. Mean annual air temperature and annual precipitation range from 3 °C and 1122 mm at the Bonaigua station (2266 m; 2000–2020 series) to 12 °C and 852 mm at Clarac (401 m; 2000–2020 series). The precipitation rising and temperature dropping at higher elevations is controlled by the topography of the north face of the range. The elevation difference (~ 2800 m) of the catchment determines a wide range of snow regimes: whereas snow remains in the ground over 8–10 months in the highest areas, the LBBb records scarce snow fall (ANR SCAMPEI: http://www.umr-cnrm.fr/scampei/presentation_scampei/index.php).

The current landscape of the Pyrenees results from both tectonic dynamics and Pleistocene climatic oscillations that have reshaped the environment through glacial, periglacial, alluvial, fluvial and slope processes (Oliva et al. 2019). The LBBb is located at the foreland of the Pyrenees and it is flanked in the northern side by the alluvial megafans of the Lannemezan Formation, which were built by the Neste River during the Late Neogene (~ 10 Ma; Calvet et al. 2021). The

margins of the basin are surrounded by small hills composed of Jurassic–lower Cretaceous limestones standing 200–300 m above the basin floor, such as Picon Garros Peak (631 m), Castillon Peak (684 m), Mail de Mau Bourg Peak (746 m), and le Picon Peak (777 m) (Fig. 1B). The headwaters of the Garonne Valley are located in the Maladeta batholith, of Carboniferous age (granites and granodiorites), while in the lower areas, there are Cambrian to Devonian sedimentary (conglomerates, limestones, lutites, sandstones) and metamorphic rocks (marbles, slates, schists, quartzites, hornfels; ICGC 2017; Quesada and Oliveira. 2019). Up waters, the Garonne Valley narrows and the river flows through steep river gorges until the Marignac basin (490 m), which is surrounded by peaks up to 1600 m (e.g., Cap de Pouy de Hourmigué Peak 1609 m). Currently, deciduous forest extends over most of the LBBb, particularly across the surrounding hills and moraine ridges distributed on the basin floor. In the forest-free areas across the bottom of the basin, cultivated fields and dispersed villages occupy the terraces built up by the Garonne River.

## Methodology

The reconstruction of past glacial oscillations in the Upper Garonne Valley integrates geomorphological observations, geochronological data, and palaeoglacier reconstructions. Field work was conducted during the summer seasons of 2019 and 2020 to better identify the main geomorphological features and directly sample glacial landforms for CRE dating.

### Geomorphological mapping

Based on visual interpretation of satellite imagery from Google Earth®, ortophotomaps (0.5 cm resolution), 10-m resolution digital elevation model (DEM) from the 'Institut National de L'information Geographique et Forestière', the recent overviews of past glaciations in the Pyrenees (Delmas et al. 2021a,b) and on the *Carte géologique* 1:50,000 1054 N, BRGM (https://www.geoportail.gouv.fr/), a geomorphological map was produced focused on the glacial landforms extending across the area from the LBBb to the Marignac basin. This map was in situ validated and complemented with further field observations.

### Sampling strategy related to CRE datings

After the geomorphological survey, 12 samples were collected from the main units highlighted in the aforementioned map for CRE dating following the standard procedures outlined in Gosse and Phillips (2001). Well-anchored moraine boulders of quartzite, granite and aplite and glacially polished bedrock surfaces (quartzite), were sampled for CRE dating. Sampling was restricted to flat-topped features and gentle surfaces (Table 1). Geometric correction of the

**Table 1** Sample and field data

| Sample name | | Landform | Latitude (DD) | Longitude (DD) | Elevation (m a.s.l.)[a] | Topographic shielding factor | Thickness (cm) | Lithology |
|---|---|---|---|---|---|---|---|---|
| *Outermost moraines (EM)* | | | | | | | | |
| ARAN-01 | (EM-2) | Moraine boulder | 43.0537 | 0.5502 | 477 | 0.9995 | 2.0 | Quartzite |
| ARAN-02 | | Moraine boulder | 43.0538 | 0.5497 | 481 | 0.9995 | 2.0 | Quartzite |
| ARAN-44 | (EM-4) | Moraine boulder | 43.0388 | 0.5598 | 475 | 0.9871 | 3.0 | Aplite |
| ARAN-45 | | Moraine boulder | 43.0389 | 0.5598 | 475 | 0.9994 | 2.8 | Quartzite |
| ARAN-46 | | Moraine boulder | 43.0389 | 0.5598 | 474 | 0.9972 | 4.5 | Quartzite |
| *Highest erratic boulder (EM)* | | | | | | | | |
| ARAN-81 | | Erratic boulder | 43.0098 | 0.6036 | 680 | 0.9996 | 3.0 | Granite |
| *Highest moraines of the EM* | | | | | | | | |
| ARAN-03 | | Moraine boulder | 43.0466 | 0.6060 | 674 | 1.0000 | 4.0 | Quartzite |
| ARAN-04 | | Moraine boulder | 43.0473 | 0.6078 | 658 | 0.9966 | 4.0 | Quartzite |
| *Internal moraines (IM)* | | | | | | | | |
| ARAN-05 | (IM-1) | Moraine boulder | 43.0425 | 0.6114 | 576 | 0.9989 | 4.0 | Granite |
| ARAN-07 | | Moraine boulder | 43.0332 | 0.6301 | 590 | 0.9915 | 5.0 | Granite |
| *Polished surfaces* | | | | | | | | |
| ARAN-42 | | Polished surface | 42.9291 | 0.6454 | 541 | 0.9758 | 4.5 | Quartzite |
| ARAN-43 | | Polished surface | 42.9287 | 0.6459 | 525 | 0.9785 | 2.5 | Quartzite |

[a] Elevations derived from the 5 m Digital Elevation Model from the Spanish "Instituto Geográfico Nacional" and the French "l'Institut national de l'information géographique et forestière" are subjected to a vertical accuracy of ± 5 m

topographic shielding by the surrounding topography was calculated throughout the ArcGIS toolbox based on the digital elevation model of 5 m resolution, which was devised by Li (2018).

## Laboratory procedures and CRE age calculation

After field work, samples were crushed and sieved to the 125–500 µm fraction, and subsequently, > 200 g of it were chemically processed at the 'Laboratoire National des Nucléides Cosmogéniques' ($LN_2C$) of the 'Centre Européen de Recherche et d'Enseignement des Géosciences de l'Environnement' (CEREGE; Aix-en-Provence, France). According to the quartz-rich lithology, samples were processed for the extraction of the in-situ-produced cosmogenic nuclide $^{10}$Be.

First, the magnetic minerals of the samples were discarded through magnetic separation conducted in a "Frantz LB-1" magnetic separator. After that, chemical attacks with a concentrated mixture of hydrochloric (1/3 HCl) and hexafluorosilicic (2/3 $H_2SiF_6$) acids and successive partial dissolutions with concentrated hydrofluoric acid (HF). Purified quartz was spiked with 150 µL of an in-house manufactured (from a phenakite crystal) $^9$Be carrier solution (3025 ± 9 µg $^9$Be g$^{-1}$; Merchel et al. 2008), then totally dissolved through a HF leaching, and finally Be was isolated using ion exchange columns (Merchel and Herpers 1999).

Final BeO targets were mixed with niobium powder and loaded in copper cathodes. Their $^{10}$Be/$^9$Be ratios were measured in the 'Accelerator pour les Sciences de la Terre, Environnement et Risques' (ASTER) national AMS facility at CEREGE, from which the $^{10}$Be concentrations were inferred (Table 2). AMS measurements were calibrated against the in-house standard STD-11 with an assigned $^{10}$Be/$^9$Be ratio of $(1.191 \pm 0.013) \times 10^{-11}$ (Braucher et al. 2015).

$^{10}$Be exposure ages were calculated using the CREp online calculator (Martin et al. 2017; http://crep.crpg.cnrs-nancy.fr/#/) with the following settings: LSD (Lifton-Sato-Dunai) elevation/latitude scaling scheme (Lifton et al. 2014), ERA40 atmospheric model (Uppala et al. 2005) and geomagnetic database based on the LSD framework (Lifton et al. 2014). The 'world mean' production rate derived from the ICE-D online calibration data set (Martin et al. 2017; available online at: http://calibration.ice-d.org/) was chosen, which yielded a sea level high-latitude (SLHL) $^{10}$Be production rate of 3.98 ± 0.22 atoms g$^{-1}$ yr$^{-1}$. Exposure ages and 1σ full and analytical uncertainties of the samples are shown in Table 2. The uncertainties discussed throughout

**Table 2** Analytical data and calculated $^{10}$Be exposure ages

| Sample name | | Quartz weight (g) | mass of carrier ($^9$Be mg) | ASTER AMS cathode number | $^{10}$Be/$^9$Be ($10^{-14}$) | Blank correction (%) | [$^{10}$Be] ($10^4$ atoms g$^{-1}$) | Age (ka) |
|---|---|---|---|---|---|---|---|---|
| *External frontal moraines (EM)* | | | | | | | | |
| ARAN-01 | EM-2 | 11.41 | 0.459 | CHAU | 25.54 ± 0.96 | 0.77 | 68.17 ± 2.57 | 123.8 ± 7.8 (4.5) |
| ARAN-02 | | 11.66 | 0.464 | CHAV | 8.96 ± 0.59 | 2.20 | 23.32 ± 1.57 | *41.6 ± 3.4 (2.6)*[a] |
| ARAN-44 | EM-4 ($n$=3) | 18.70 | 0.443 | IGNJ | 43.71 ± 1.46 | 0.44 | 68.85 ± 2.30 | 127.9 ± 8.0 (4.2) |
| ARAN-45 | 124.1 ± 9.6 | 20.45 | 0.441 | IGNK | 44.37 ± 2.80 | 0.43 | 63.63 ± 4.04 | 116.4 ± 9.4 (7.1) |
| ARAN-46 | (5.5) ka | 20.76 | 0.440 | IGNL | 48.89 ± 2.29 | 0.39 | 68.95 ± 3.24 | 128.5 ± 9.1 (6.0) |
| *Highest erratic boulder (EM)* | | | | | | | | |
| ARAN-81 | | 19.23 | 0.438 | IGNU | 5.97 ± 0.57 | 3.34 | 8.79 ± 0.86 | *13.9 ± 1.5 (1.3)* |
| *Highest moraines of the EM* | | | | | | | | |
| ARAN-03 | | 11.19 | 0.455 | CHAW | 17.9 ± 0.55 | 1.93 | 47.65 ± 1.49 | *73.1 ± 4.6 (2.3)* |
| ARAN-04 | | 11.61 | 0.454 | CHAX | 7.90 ± 0.34 | 4.49 | 19.77 ± 0.91 | *31.1 ± 2.1 (1.4)* |
| *Internal moraines* | | | | | | | | |
| ARAN-05 | IM-1 | 10.88 | 0.457 | CHAY | 4.54 ± 2.62 | 8.04 | 11.78 ± 7.35 | *20.3 ± 12.7 (12.7)* |
| ARAN-07 | | 11.44 | 0.460 | CHAZ | 4.01 ± 0.36 | 9.10 | 9.89 ± 0.96 | *17.1 ± 1.8 (1.6)* |
| *Polished surfaces* | | | | | | | | |
| ARAN-42 | | 21.36 | 0.432 | IGNH | 8.58 ± 0.29 | 2.33 | 11.34 ± 0.39 | 20.7 ± 1.2 (0.7) |
| ARAN-43 | | 18.38 | 0.436 | IGNI | 8.67 ± 0.60 | 2.29 | 13.42 ± 0.95 | 24.2 ± 2.1 (1.6) |

**Chemistry blank details**

| Blank name | Processed with | mass of carrier ($^9$Be mg) | ASTER AMS cathode number | $^{10}$Be/$^9$Be ($10^{-14}$) | [$^{10}$Be] ($10^4$ atoms) | | |
|---|---|---|---|---|---|---|---|
| BK-1 | ARAN-3, 4, 5, 7 | 0.46 | CHAT | 0.34 ± 0.04 | 10.30 ± 1.24 | - | - |
| BK-3 | ARAN-1, 2 | 0.46 | IGHI | 0.20 ± 0.03 | 5.98 ± 0.93 | - | - |
| ARAN-BK | ARAN-42, 43, 44, 45, 46, 81 | 0.43 | IGNV | 0.20 ± 0.03 | 5.65 ± 0.84 | - | - |

[a] The exposure ages in grey and italics were considered as outliers based on statistical (chi2-test) and geomorphological criteria. Such exposure ages are therefore not included in the interpretation.

$^{10}$Be/$^9$Be ratios were inferred from measurements at the ASTER AMS facility. Individual ages are shown with their full uncertainties (including analytical AMS uncertainty and production rate uncertainty) and analytical uncertainty only within brackets. Arithmetic mean ages are given with their full uncertainties (including standard deviation and production rate uncertainty) and standard deviations only in brackets

the text include analytical and production rate error unless otherwise stated.

To evaluate the potential impact of the erosion on the exposure ages, the same corrections outlined in Oliva et al. (2021) was implemented, which resulted in older ages by ~ 1% and ~ 8% for the 0.2 and 1 mm $ka^{-1}$ scenarios (André 2002), respectively. However, aiming to enable comparisons with other areas the non-corrected ages was retained along the text. Snow cover is at present close to zero in the LBBb and is thus considered negligible. The high external and internal errors of the samples ARAN-05 and ARAN-81, linked to low current values during the AMS measurement implies that such samples and their derived exposure ages must be rejected. The chi-squared test was applied using the iceTEA tool (http://ice-tea.org/en/tools/remove-outliers/; Jones et al. 2019) to detect potential outliers within the targeted geomorphic units; thus, the exposure age of the sample ARAN-02 was excluded due to the statistical inconsistence.

### Palaeoglaciers and palaeoELAs reconstruction

A three-dimensional palaeoglacier reconstruction was carried out for the different glacial phases using the 'GLaRe' ArcGIS toolbox developed by Pellitero et al. (2016) and a 10-m resolution DEM, which implements a perfect-plasticity physical-based numerical model (Van der Veen 1999; Benn and Hulton 2010) that reconstructs past ice thickness assuming an average shear stress of 100 kPa along a set of flowlines (Paterson 1994; Benn and Hulton 2010). And finally, equilibrium-line altitudes (ELAs) were calculated using the automatic toolbox developed by Pellitero et al. (2015) through the methods Accumulation Area Ratio (Porter 1975; AARs: $0.6 \pm 0.05$) and the Area Altitude Balance Ratio (AABR; Osmaston 2005). For more details on glacier reconstruction and ELA calculation protocols, the reader is referred to Oliva et al. (2021) and the original publications from which the aforementioned toolboxes were derived.

## Results

The distribution of the glacial landforms preserved in the LBBb evidence several glacial advances and retreats during the Pleistocene (Fig. 2). Their timing is constrained by the $^{10}$Be exposure ages obtained from moraine boulders and polished surfaces (Tables 2, 3).

### Glacial geomorphological setting

Glacial deposits located in the LBBb have been largely transformed by historical human practices (e.g., agriculture) and by a dense network of infrastructures that have affected the natural landscapes and the preservation of glacial landforms. In addition, the entire area—particularly the slopes—is extensively forested, which makes even more challenging the interpretation of glacial features as well as the identification of appropriate samples for CRE dating (Figs. 3, 4).

Nonetheless, based on our field work observations and on previous geomorphological mapping (*Carte géologique* 1:50,000 1054 N, BRGM; Delmas et al. 2021a), two main glacial systems were identified (Fig. 3):

#### The external moraine system (EM)

There are only well-preserved deposits in the terminal zone of the palaeoglacier, downstream the villages of Izaourt and Tibiran–Jaunac. It consists of the highest moraines of the EM in the internal and eastern parts of the basin and four moraine ridges in the western side of the basin floor (Fig. 4). The highest moraines of the EM are distributed on the slopes and hilltops of the internal part of the basin (Fig. 2b). At elevations between 600 and 720 m (i.e., 160–280 m above the basin floor) there are exposed sections opened on this moraine showing subangular to subrounded meter-sized granite and quartzite boulders embedded in a poorly sorted matrix. At the same altitude but close to Izaourt, several erratic granite boulders rest on a limestone bedrock that may correspond to the same phase (Fig. 3).

Further north, at lower altitudes (600–670 m), the highest moraines of the EM on the hilltop surface of the Castillon Peak do not define well-preserved moraine ridges, but patches of till deposits are located towards the eastern edge of the basin. Here, there are also sparse boulders and glaciofluvial sediments embedded in a sandy matrix. At the western side of the basin floor, moraines form aligned discontinuous ridges at 460–490 m (i.e., up to 40–70 m height), with well-developed soils and sparse boulders across the surface. These features are extensively forested. Up to four moraine ridges were identified in this system (Figs. 3, 4A):

EM-1—located at the northernmost part of the basin floor and represents the most peripheral moraine ridge preserved in the study area;
EM-2—stretching between the Tibiran and Jaunac villages, this ridge displays an oblique feature with regards to the palaeo ice-flow;
EM-3—located 500 m to the south from the outer ridge, and turns from SW–NE to S–N towards Jaunac village;
EM-4—located 300 m north from the St-Martin village.

To validate the connection between the highest moraines close to the Castillon Peak and the external ridges near Tibiran–Jaunac villages, the area was extensively surveyed to identify potential boulders suitable for CRE dating. Hubschman (1984) attributed those frontal moraines to glacial advances prior to the Eemian Interglacial. To test this

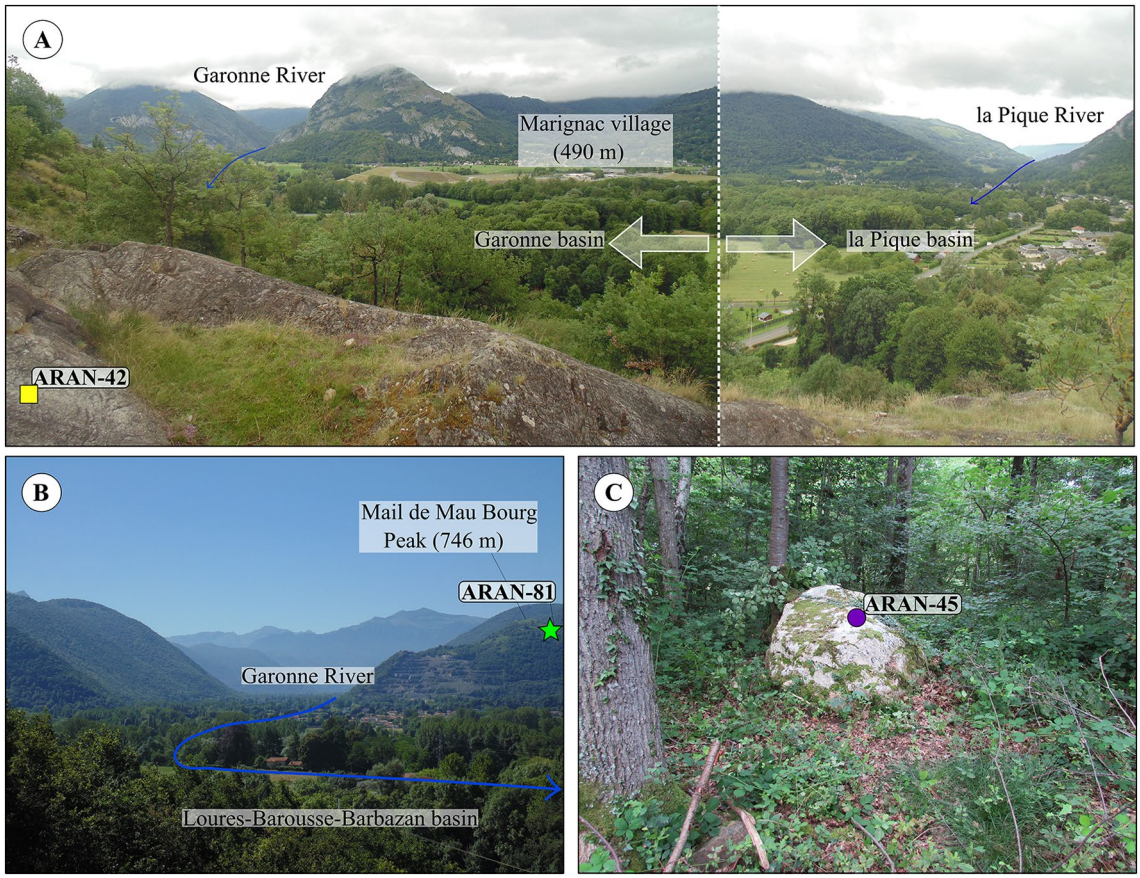


**Fig. 2** Examples of the samples collected from the polished surface in the Marignac basin (**A**; ARAN-42), and the erratic boulder (**B**; ARAN-81) and moraine boulder (**C**; ARAN-45) from the Loures–Barousse–Barbazan basin

**Table 3** Exposure ages according to different erosion scenario corrections

| Sample name | | Exposure ages (arithmetic mean, in ka) | | |
|---|---|---|---|---|
| | | No correction | Erosion correction (0.2 mm/ka) | Erosion correction (1 mm/ka) |
| *Outermost moraines (EM)* | | | | |
| ARAN-1 | EM-2 | 123.8 ± 7.8 (4.5) | 127.1 ± 8.2 (4.7) | 143.4 ± 9.7 (5.6) |
| ARAN-2 | | *41.6 ± 3.4 (2.6)* | *42.0 ± 3.4 (2.7)* | *43.4 ± 3.6 (2.8)* |
| ARAN-44 | | 127.9 ± 8.0 (4.2) | 131.4 ± 8.3 (4.4) | 149.3 ± 9.7 (5.1) |
| ARAN-45 | EM-4 | 116.4 ± 9.4 (7.1) | 119.3 ± 9.6 (7.3) | 133.0 ± 11.1 (8.5) |
| ARAN-46 | | 128.5 ± 9.1 (6.0) | 132.0 ± 9.4 (6.2) | 150.1 ± 11.0 (7.2) |
| *mean* | | *124.1 ± 9.6 (5.5)* | *127.8 ± 11.7 (6.0)* | *144.1 ± 14.4 (6.9)* |
| *Highest moraines* | | | | |
| ARAN-3 | | *73.1 ± 4.6 (2.3)* | *74.3 ± 4.7 (2.3)* | *79.3 ± 5.0 (2.5)* |
| ARAN-4 | | *31.1 ± 2.1 (1.4)* | *31.2 ± 2.1 (1.4)* | *32.0 ± 2.1 (1.4)* |
| *Highest erratic boulder* | | | | |
| ARAN-81 | | *13.9 ± 1.5 (1.3)* | *14.0 ± 1.5 (1.3)* | *14.1 ± 1.5 (1.3)* |
| *Innermost moraines (IM)* | | | | |
| ARAN-7 | (IM-1) | *17.1 ± 1.8 (1.6)* | *17.2 ± 1.8 (1.6)* | *17.4 ± 1.9 (1.6)* |
| *Polished surfaces* | | | | |
| ARAN-42 | | 20.7 ± 1.2 (0.7) | 20.8 ± 1.2 (0.7) | 21.1 ± 1.3 (0.7) |
| ARAN-43 | | 24.2 ± 2.1 (1.6) | 24.3 ± 2.1 (1.6) | 24.8 ± 2.1 (1.7) |

[a] The exposure ages in grey and italics were considered as outliers based on statistical (chi2-test) and geomorphological criteria. Such exposure ages are therefore discarded across the text.

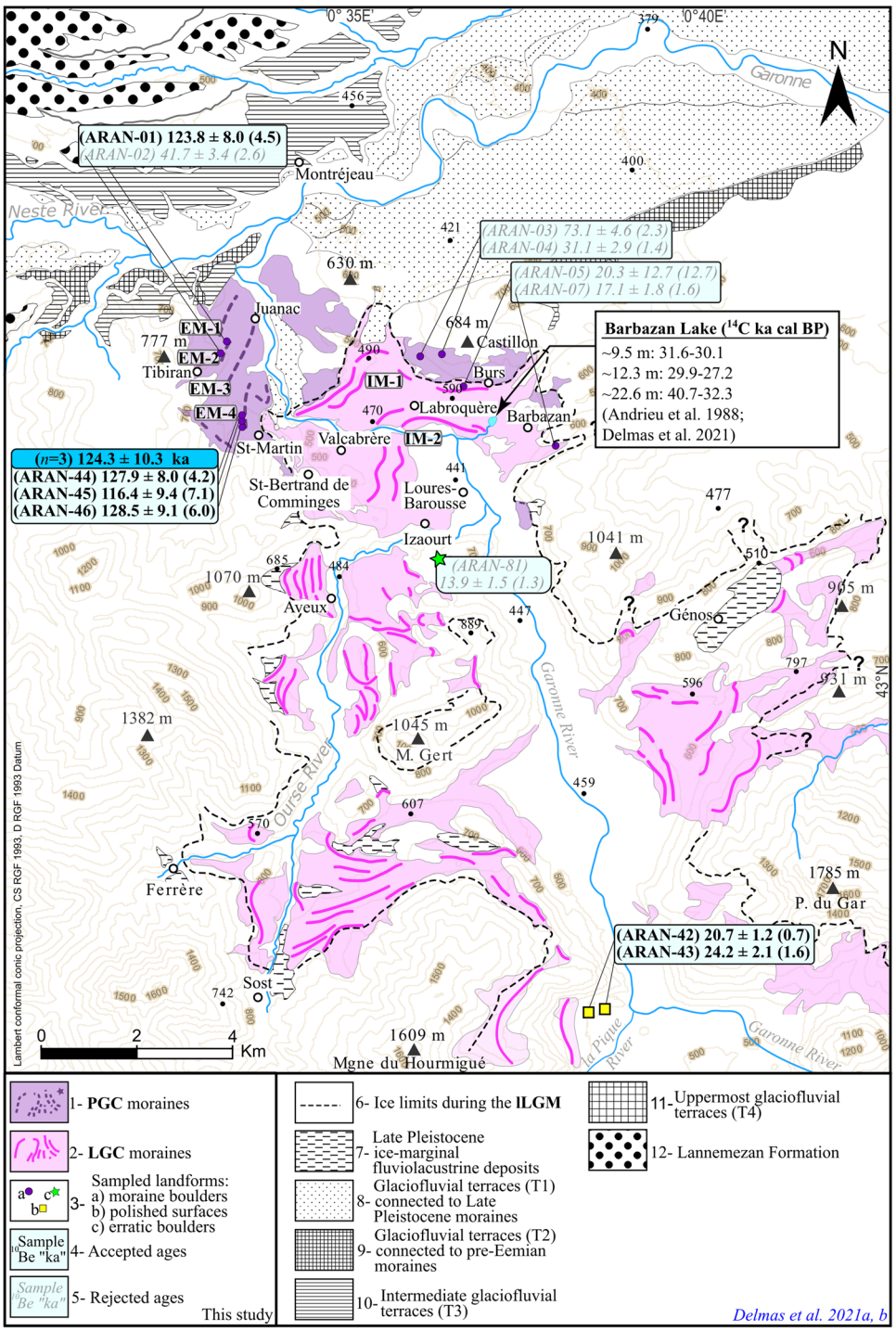


**Fig. 3** Geomorphological map of the study area modified from Delmas et al. (2021a,b)

hypothesis, seven samples were collected from scattered moraine boulders belonging to the following units: the highest moraines of the EM (ARAN-03, ARAN-04), EM-2 (ARAN-01, ARAN-02) and EM-4 (ARAN-44, ARAN-45, ARAN-46). The few boulders found on EM-1 and EM-3 moraine ridges were not adequate for CRE dating as they had seemingly been disturbed from their original position, and therefore, no samples were collected.

### The internal moraine system (IM)

A series of moraine ridges are distributed across the internal part of the LBBb floor at 460–590 m and the valley sides of the glacial catchment, at 550–820 m (Fig. 3), forming discontinuous ridges in the margins of the palaeoglacier. This well-preserved moraine system is composed of two sets of arches that are distributed on the LBBb and connects with

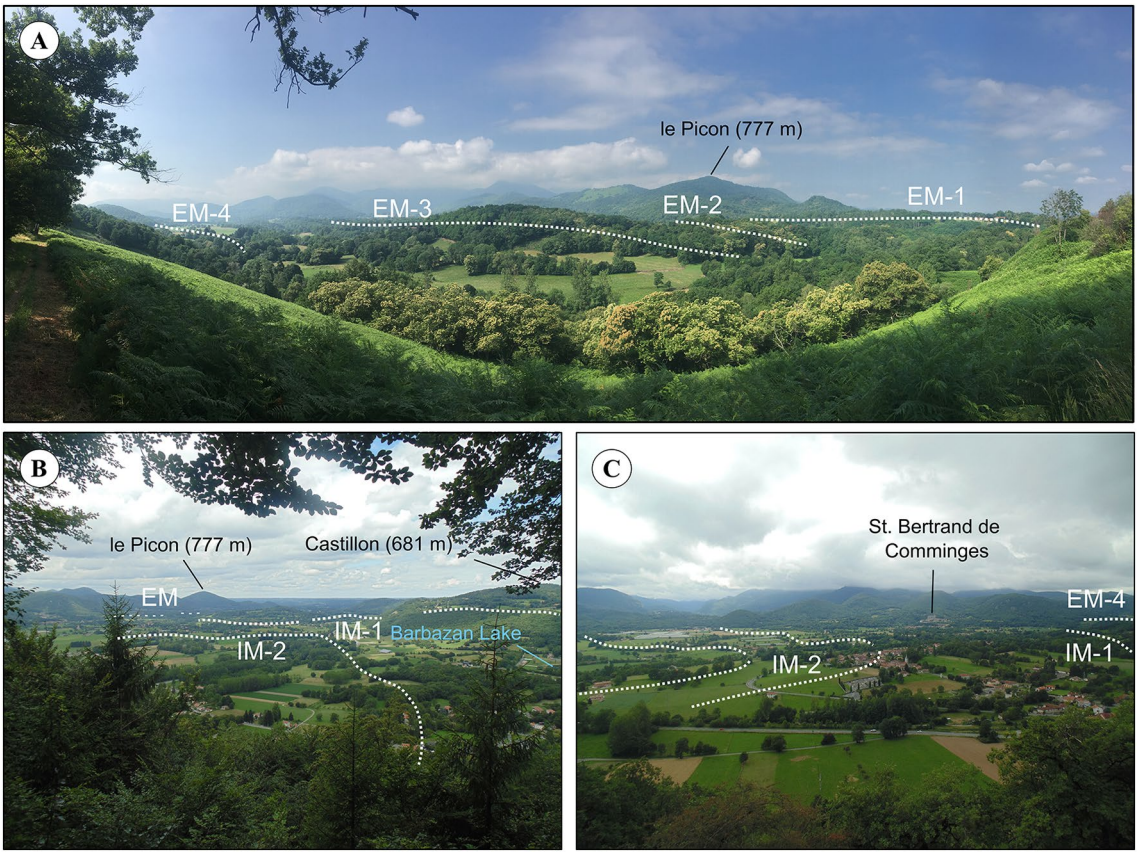


**Fig. 4** Moraine complex in the Loures–Barousse–Barbazan basin: **A** Panoramic view of the northernmost part of the basin and moraine ridges of the external moraine system; **B** moraine ridge IM-1 seen from the southernmost part of the basin; **C** moraine ridges IM-2 viewing from the Burs village

lateral moraine ridges. Those moraine ridges are indicative of the frontal termination of the Garonne palaeoglacier in the LBBb and of the lateral margins, where glacial deposits (ablation moraines and fluviolacustrine obturations) delineate large glacial diffluences that the Garonne palaeoglacier spread across the structural hills framed by the Jurassic–lower Cretaceous limestones of the North Pyrenean zone. Sedimentological, palynological and radiocarbon data obtained in the Barbazan glaciolacustrine sequence allow two main units to be distinguished within the LGC moraine system of the Garonne palaeoglacier (Fig. 3). Thus, two units were considered in the internal moraine system (Fig. 3):

IM-1—In the terminal zone of the LBBb, IM-1 corresponds to a 5 km-long moraine preserved between Burs and St-Martin. Metric-size and well-anchored granite boulders were found in the Eastern margin of the moraine, lying on the foot slopes of Barbazan. Near Burs, the ridge rapidly decreases in elevation (from 590 to 490 m) towards the central part of the basin, connecting with a ~30-m-high arcuate frontal ridge at La Serre. In this section, and especially on the slope between Burs and the Barbazan paleolake, several sedimentary sequences contain meter-sized subrounded to rounded boulders of granite and quartzite, embedded in a sand and silt matrix. From the La Serre arch, the ridge turns westwards and ends 500 m next to the EM-4 ridge. In this section, several scattered boulders were detected at the north margin of the river and in south part of the St-Marti village. Only two samples were collected from the IM-1 ridge near Burs and Barbazan villages (ARAN-05, ARAN-07), at similar altitudes of 580 and 590 m (Table 1). On the lateral left moraine system, ~2 km upvalley from the LBBb, there are lateral ridges close to Aveux and Sacoué villages that are indicative of the palaeoglacier margins at the glacial diffluence. Further south, 6 km upvalley from the LBBb, frontal and lateral moraines lying between 620 and 800 m at the Sost-Ferrère glacial villages are also part of this moraine system. Finally, at the right moraine complex of the palaeoglacier margin, there are several lateral and frontal ridges distributed between 610 and 780 m near Lourde-St-Pé-d'Ardet-Génos villages;

IM-2—In the innermost part of the terminal zone of the LBBl, the IM-2 consists on two parallel moraine ridges (10 m high) located close to the current basin floor between Valcabrère, Labroquère and Loures-Barousse villages. Further south, in the moraine system of Sost-Ferrère, the most internal ridges standing at 580–600 m might correspond to the palaeoglacier margins of the IM-2. In the opposite side, this phase can be represented by lateral and frontal ridges at 530–610 m at the Lourde-St-Pé-d'Ardet-Génos. Despite these lobate ridges surrounding the basin define well-preserved features, they have been intensely disturbed by agriculture activities. Therefore, no suitable boulders for CRE dating were found in the area as they were probably not in the original place, where the ice left them.

Up-valley from the LBBb, the main valley narrows and no glacial features prone for CRE dating were found until the Marignac basin, 13 km upvalley, where the Garonne and la Pique rivers converge (Fig. 2). Hubschman (1984) attributed the IM-1 and IM-2 to glacial advances occurred during the LGC. At the left margin of the main Garonne Valley, there are polished surfaces on granite bedrock, at 18 km from the EM-1 ridge. To validate Hubschman's interpretation, two samples were collected from these surfaces 50 and 30 m above the riverbed (ARAN-42, ARAN-43), as representative of the age of the withdrawal of the palaeoglacier from the terminal basin, of the lateral moraine complexes and of the individualization of the Garonne and la Pique palaeoglaciers within their respective valleys.

## CRE results

The 10 CRE samples collected from the LBBb yielded ages spanning from 128.5 ± 9.1 to 13.9 ± 1.5 ka (Table 2).

From the four moraine ridges integrating the EM moraine system, two samples were obtained from EM-2 (ARAN-01, ARAN-02) with inconsistent ages of 123.8 ± 8.0 and 41.7 ± 3.4 ka, respectively (Table 2). At the EM-4 ridge, three samples (ARAN-44, ARAN-45, ARAN-46) yielded consistent ages of 127.9 ± 8.0, 116.4 ± 9.4 and 128.5 ± 9.1 ka (mean age 124.3 ± 10.3 ka; $n = 3$) (Figs. 3, 5).

At the southern part of the LBBb, an erratic boulder located 240 m above the basin floor (ARAN-81) yielded an age of 13.9 ± 1.5 ka. Due to the bad AMS measurement this age will not be further discussed. The highest moraine of the EM loses altitude northwards, and at 230 and 220 m above the basin floor two other samples were collected (ARAN-03 and ARAN-04) within a forest area near the Castillon Peak, yielding again inconsistent exposure ages of 73.1 ± 4.6 and 31.1 ± 2.9 ka, respectively (Fig. 3).

One sample collected from the IM-1 ridge, close to the Burs village (ARAN-05), reported an exposure age of 20.3 ± 12.7 ka. This age will not be further discussed. At the foot of the slopes surrounding the basin, another sample (ARAN-07) was obtained near the Barbazan village and yielded an age of 17.1 ± 1.8 ka.

The exposure ages of two samples (ARAN-42, ARAN-43) obtained from polished surfaces in the overdeepened basin surrounding the Marignac village, are 20.7 ± 1.2 and 24.2 ± 2.1 ka, respectively.

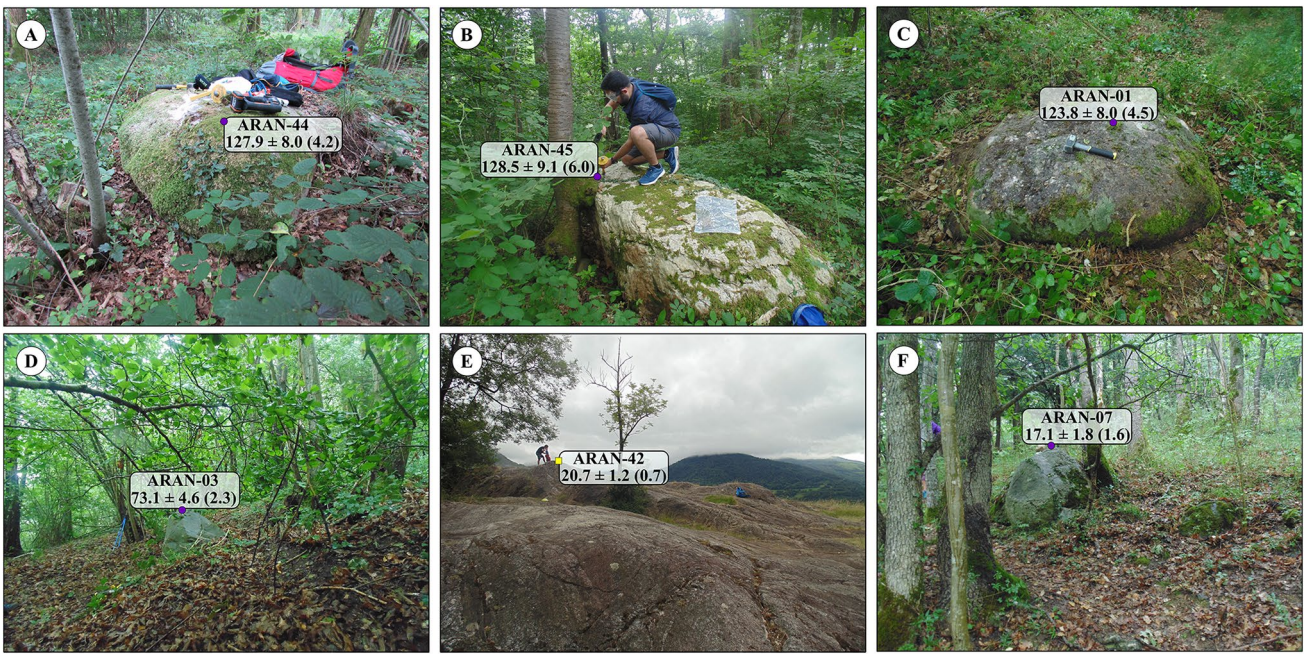


**Fig. 5** CRE ages of the different moraine systems from the terminal basin of the Loures–Barousse–Barbazan and polished surfaces upvalley

## Discussion

The reconstruction of the glacial evolution in the LBBb is based on geomorphological surveying and mapping, and $^{10}$Be exposure ages obtained from moraine boulders and polished surfaces. Data confirms Hubschman's proposal that the most weathered moraine (EM) was formed during a glacial advance prior the Eemian Interglacial, as well as the onset of the final retreat of the Garonne Glacier during the gLGM.

### Interpretation of the CRE results

The sequence of CRE ages from the terminal moraine system of the Upper Garonne Valley is constrained by the long time since the penultimate deglaciation of the area and subsequent postglacial environmental dynamics, which together with land use changes caused by humans within the last millennia in the LBBb, have affected the preservation of the glacial records. Therefore, the reconstruction of the glacial history in the area is challenging, and our study needs to be complemented with other environmental proxies and glacial chronological data from the region.

The exposure ages of the samples (ARAN-01, ARAN-44, ARAN-45 and ARAN-46) from boulders distributed on the moraine ridges EM-2 and EM-4 (123.8 ± 8.0 ka and 124.3 ± 10.3 ka, respectively) show statistical consistence based on the Chi-2 test. They support the hypothesis that the oldest moraine system existing in the glacial terminal basin of the Upper Garonne Valley corresponds to the PGC. These dates confirm the deposit of those moraines during a glacial advance before the Eemian Interglacial period, as postulated in previous studies (Hubschman 1984; Andrieu et al. 1988).

The exposure ages from the samples taken from the highest moraines of the EM (ARAN-03 and ARAN-04) yielded 73.1 ± 4.6 and 31.1 ± 2.9 ka, respectively, showing a lack of consistency between them. These two ages suggest that these moraines might correspond to polygenic features that formed over a long time period when the glacier occupied the top of the Castillon Peak and finally shrunk by 31.1 ± 2.9 ka before the onset of the Barbazan Lake infill, located 1.5 km south (Fig. 4B; Andrieu et al. 1988). However, it is also likely that our boulders had shifted from their original position by subsequent glacial advances or had been exhumated by postglacial erosion processes occurring on the slopes of the Castillon Peak. Therefore, more data is needed to confirm one of the scenarios and verify the link with the maximum glacial advance. Thus, given this uncertainty, for the reconstruction of the glacial history in the area, these samples were excluded.

The exposure age of 17.1 ± 1.8 ka (ARAN-07) obtained from the IM-1 moraine ridge near Burs must be excluded due to its mismatch with the Barbazan Lake records located upvalley, which indicates an older retreat than our exposure ages (Andrieu et al. 1988):

(i) A radiocarbon age of 31.160 ± 1.700 yr BP (40.7–32.3 cal ka BP) at 2263–2274 cm (base of the core) within the basal unit (glaciolacustrine rhythmites and diamictons). Given the location of the Barbazan paleolake with respect to the IM-1, the area of the lake was covered by the ice when IM-1 was formed. Hence, this proglacial lake may only have infilled after the Garonne Glacier retreated from the IM-1. Hence, IM-1 should be older than 40.7–32.3 cal ka BP.

(ii) The sedimentary frame of the glaciolacustrine sequence shows that the Garonne ice margin was close to the paleolake (probably at IM-2) until the interruption of glacial meltwater supply. This interruption occurred at 26.600 ± 460 yr BP (31.6–30.1 cal ka BP; Andrieu 1991), or just after 23.980 ± 680 yr BP (29.9–27.2 cal ka BP). It is, however, possible that the moraine boulders from the IM-1 ridge have been affected by reworking following lLGM glacial retreat and provide thus younger ages than expected.

New CRE ages from polished surfaces on the left margin of the Marignac basin (ARAN-42: 20.7 ± 1.2 ka and ARAN-43: 24.2 ± 2.1 ka) allow us to locate the terminal position of the Garonne palaeoglacier upstream of Marignac at the time of the gLGM.

### Chronology of the glacial advances in the Upper Garonne Valley

Several smooth moraine ridges were mapped within the external moraine system of the LBBb, and ascribed to the oldest glacial advance in the area (Hubschman 1984; Andrieu 1991; Stange et al. 2014; Fernandes et al. 2017). Our CRE dates reveal two moraine ridges deposited prior to the LGC in the Upper Garonne Valley at 123.8 ± 8.0 and 124 ± 9.6 ka. Thus, four CRE dates from the EM-2 and EM-4 ridges provided evidence of moraine stabilization during a time interval spanning from 128.5 ± 9.1 to 116.4 ± 9.4 ka (Table 2). Isotopic inheritance is likely to be absent for moraines far from the source (~ 20–80 km); however, the youngest ages might have been exhumated following the onset of moraine stabilization (Briner et al. 2005). Therefore, the oldest age of these units most likely marks the time of moraine stabilization following the MIS 6 largest glacial advance at ~ 129 ka. As temperatures increased during the transition toward the Eemian Interglacial (Helmens 2013), the Garonne Glacier started receding and moraines

stabilized. This PGC glacial advance must have covered the entire glacial terminal basin of the Upper Garonne Valley with an ice thickness ranging between 200 to 50 m (Fig. 6). According to our results, during this phase, the main Upper Garonne Glacier was ~ 78 km long and covered ~ 900 km$^2$. Considering the position of the frontal moraine ridge EM-2 at 480 m, and the derived palaeoglacier reconstruction, the ELA was located at 1711 ± −65/55 m (AAR), 1719 ± −95/60 m (global AABR) and 1704 ± −105/70 m (mid-latitude AABR), with an average of 1711 m. This altitude suggests a reduction of 9.3 °C with respect of current ELA at 3139 m and assuming no change in the summer precipitation (Campos et al. 2021). As expected, these results show that glaciers had similar extents in the terminal basin during the MIS 6 and lLGM glacial advances and thus climate conditions were probably similar (Fernandes et al. 2017).

No solid chronological data are available to support a straightforward interpretation of the glacial advance during the PGC. The lack of available boulders for CRE dating in the EM-1 ridge impeded establishing the timing of the maximum extent during the PGC in the Upper Garonne Valley, whose external position on the moraine suggest that it may also belong to the PGC (Fig. 6). Indeed, there is evidence indicating that the Pyrenees were extensively glaciated during this period. In the Eastern Pyrenees, a stalagmitic flowstone stemmed from the onset of karst activity by 124.6 ± 6.9 to 121.4 ± 9.4 ka at the Niaux–Lombrives–Sabart cave occurred after the MIS 6 cold period (Sorriaux et al. 2016). In the same catchment, other age obtained from an erratic boulder located 50–100 m above the LGC moraines, reinforced the hypothesis of a previous glaciation that took place in the Ariège Valley at 133.9 ± 5.3 ka (Delmas et al. 2011). In the southern slope of the Pyrenees, an older age from the PGC has also been reported in the Aragón Valley, where the outermost moraine, 80 m above the present-day riverbed, was dated at 171.0 ± 22.0 ka (García-Ruiz et al. 2013).

Geomorphological evidence from the LGC in the LBBb must thus be located in the internal part of the basin and foot slopes close to the Barbazan village. Here, the La Serre and the Burs ridges (IM-1) were generated by a piedmont glacier covering the basin during the lLGM of the LGC. The only available ages correspond to the Barbazan Lake sequence, where the onset of the proglacial lake infill, behind this moraine, started before 40.7–32.3 cal ka BP (Hubschman 1984; Andrieu 1991). In several valleys of the southern slope of the Pyrenees, glacial evidence suggests that the lLGM occurred during the MIS 4 and MIS 3, namely, at 65–55 ka and 45–30 ka (Oliva et al. 2019). However, the chronology

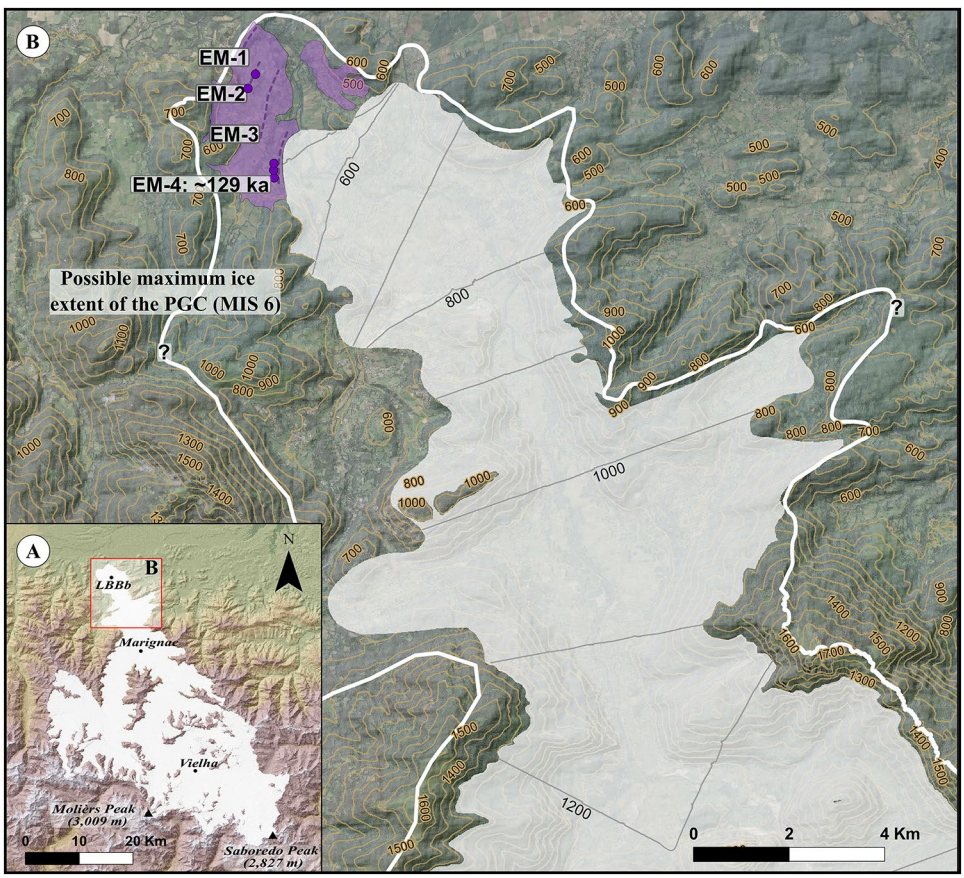


**Fig. 6** Terminal position of the Garonne palaeoglacier during the glacial advance of the MIS 6

of the lLGM glacial advances in the southern slope is not as robust as in the northern slope. In the Ariège Valley, a CRE age from an erratic boulder located on the hilltop between Tarascon and Foix-Montgaillard basins yielded 79.9 ± 14.3 ka and a boulder from a lateral moraine on the confluence between the Aston and Ariège valleys yielded an exposure age of 35.3 ± 8.6 ka (Delmas et al. 2011). In addition, radiocarbon dating of the first organic remnants from the bottom of the ice-marginal deposits behind such moraines has shown the onset of the post-lLGM deglaciation between 48 and 24 ka, namely, at the Estarrès Lake, Gave d'Ossau (34.2–29.7 cal ka BP; Andrieu 1987; Andrieu et al. 1988; Jalut et al. 1988), at the Biscaye peatbog, Gave de Pau (48.3–39.7 cal ka BP; Mardones and Jalut 1983), and at the Freychinède sequence, Ariège Valley (27.3–24.0 cal ka BP; Jalut et al. 1982; Reille and Andrieu 1995). Therefore, the lLGM glacial advance of the LGC in the LBBb is necessarily older than the onset of the sedimentation at the Barbazan Lake, as the glaciolacustrine rhythmites and diamictons at the base of the core sequence accumulated after the glacial retreat that followed the previous glacial advance, which likely coincided with the formation of the IM-1 moraine. Glacial advances during the MIS 3 are more evident in the Eastern Pyrenees, where moraines from Têt Valley were dated at 40.86 ± 1.9 ka (Tomkins et al. 2018) or those in the Malniu area that yielded 51.1 ± 4.8–42.6 ± 4.1 ka (Pallàs et al. 2010).

After the lLGM recession, a moraine-dammed lake formed between the IM-1 ridge and the glacier front blocked the meltwater discharges and filled the Barbazan proglacial lake (Andrieu 1991). The same author indicated that the glaciolacustrine rhythmites and diamictons at the bottom of the sequence (40.7–32.3 cal ka BP) was transported from a nearby source, probably synchronously with the formation of the moraine IM-2. However, no chronological data are yet available to discriminate whether the moraine was formed during a pulsation after the lLGM or as a result of the gLGM advance. It can only be hypothesized that the ages must be older than 31.6–30.1 cal ka BP, because sediments and pollen records showed the progressive glacial abandonment of the terminal basin, with a transition from glaciolacustrine to lacustrine sediments, a reduction of freshwater inputs from the glacier, as well as the decline of the forest coverage (e.g., *Fagus* sp.) and the recovery of herbaceous species (Andrieu et al. 1988; Jalut et al. 1992).

The slopes surrounding the Marignac basin were ice-free during the gLGM, as demonstrated by the exposure ages obtained from polished surfaces at 50 and 30 m above the basin floor. At 24–21 ka, the glacier would have abandoned the terminal basin and split into two individualized glacier tongues constrained within the Garonne and la Pique valleys as the ice shrank. At this time, the palaeoglacier of the Upper Garonne Valley flowed down 60 km along the main valley. In parallel, glacial recession was also underway during the gLGM in the Ariège Valley, where polished surfaces were dated to 18.7 ± 3.8 ka at 20 m above the gLGM Bompas moraine (490 m) (Delmas et al. 2011). In this case the gLGM was depicted with glacial advances leaving several well-preserved moraines (Garrabet, Bernière, Bompas-Arignac): a boulder from the Bernière frontal moraine, ~ 7 km from the lLGM ice limits was dated at 18.8 ± 1.3 ka (Delmas et al. 2011). Subsequently, after the gLGM, glaciers in the Upper Garonne Valley underwent a massive retreat upvalley, reaching the mouth of the highest cirques by ~ 15–14 ka (Oliva et al. 2021; Fernandes et al. 2021).

## Mid-Late Pleistocene glacial dynamics in the Central Pyrenees in the context of European mid-latitude regions

In Eurasia, climatic models have shown that the glacial maximum of the PGC was the most extensive of the last 400 ka (Colleoni et al. 2016). This glacial maximum occurred at 140 ka (MIS 6) based on Antarctic ice core records (Winograd et al. 1992; Colleoni et al. 2016), which is also confirmed by the minimum sea level (likely −150 m) dated at 155–140 ka (Grant et al. 2014; Wekerle et al. 2016). The Greenland ice core recorded the Eemian Interglacial from 129 to 114 ka with a warming peak occurring at 126 ka (Dahl-Jensen et al. 2013). These records correspond to a sea-level stabilization at 130–119 ka, reaching up to 6–9 m above the current level (Hearty et al. 2007). According to the Greenland ice cores, this interglacial was up to 8 ± 4 °C warmer than the last millennium (Dahl-Jensen et al. 2013). The beginning of the Eemian caused a massive ice discharge from Northern Hemisphere ice sheets, when glaciers flowed into the ocean leaving icebergs that drifted debris (> 150 µm) southwards as far as ~ 55°N at 128 ka (McManus et al. 1999; Fig. 7). In fact, disintegration of the northern ice sheets occurred during the end of the PGC, which coincided with the Heinrich Stadial 11 (~ 136–129; Menviel et al. 2019).

According to marine sediments from the Iberian margins, a rapid warming with an increase of annual sea surface temperatures of ~ 10 °C followed the MIS 6 (Martrat et al. 2007). The comparison between the deep-sea cores in the Portuguese margins and European pollen records showed that in southwestern Iberia the warmest and driest period of this interglacial occurred between 126 and 117 ka (Sánchez-Goñi et al. 2005). Such warm conditions after the MIS 6 suggests non-favourable conditions to glacial development in the Iberian Peninsula. Consequently, it is likely that mid-latitude mountain glaciers, such as those existing in the Pyrenees, underwent a massive retreat leaving their terminal basins and probably the lowest peaks.

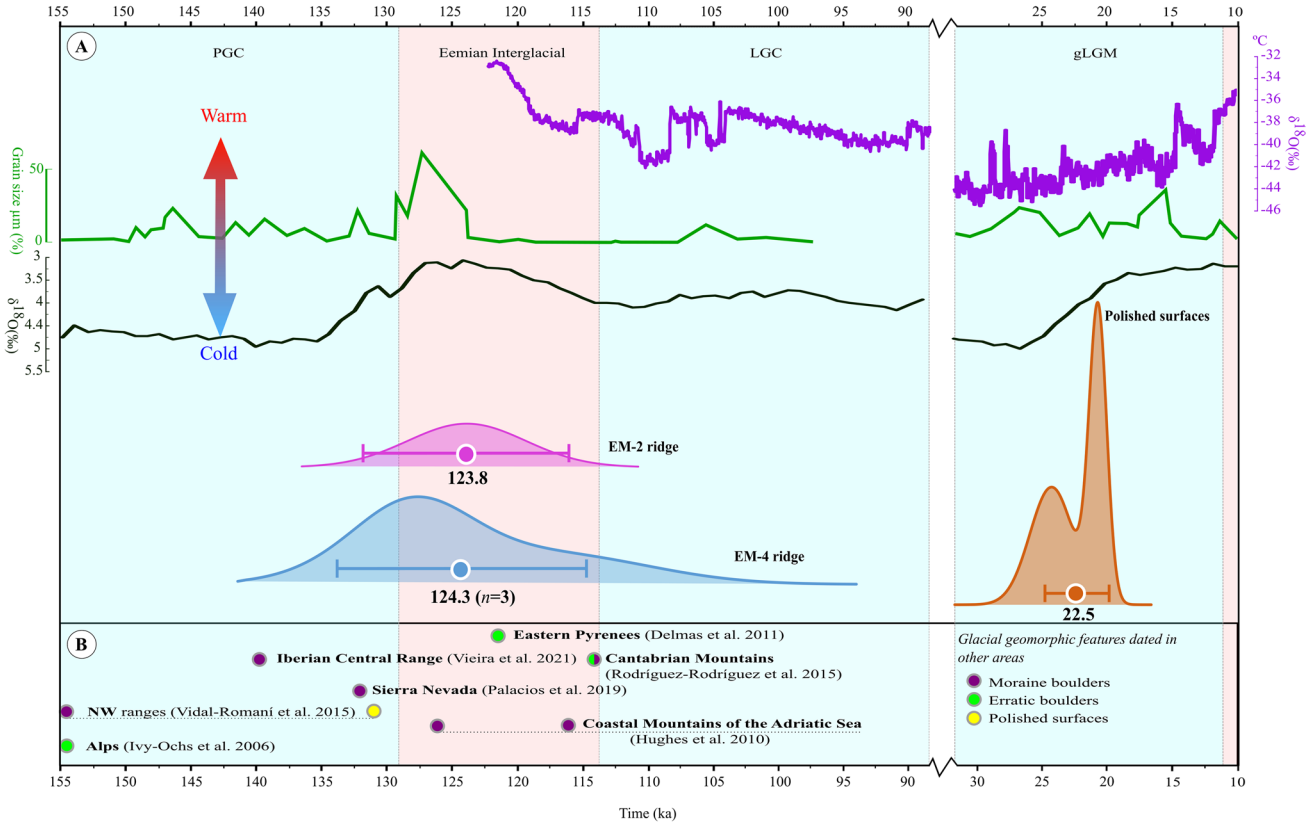


**Fig. 7** Normalized probability distribution functions (PDF) of the $^{10}$Be CRE exposure ages vs. **A** Temperature evolution from the MIS 6 to the gLGM based on the $\delta^{18}$O record from the NGRIP ice core from Greenland (time periods are defined after Rasmussen et al. (2014)); percentage of grain size (> 150 μm) per sample in ice-rafted debris (IRD) from ocean sediments cores (McManus et al. 1999); benthic $\delta^{18}$O record from global distribution (Lisiecki and Raymo 2005); and **B** other CRE dated glacial landforms. The plots of the units result from the sum of the individual PDF of the samples belonging to them. Cold (warm) phases are represented by the blue (red) bands

No robust chronological data on glacial records have been obtained so far to confirm the MIS 6 glaciation in the Pyrenees. Indeed, the wide temporal range (170–120 ka) of exposure ages and associated uncertainties do not let us to have a clear idea about the maximum of the PGC in the Pyrenees. In any case, in this work, the first $^{10}$Be CRE data set from moraine boulders was introduced in Pyrenees that reveal the occurrence of a large glaciation during the MIS 6 in the Upper Garonne Valley. At that time, the ice covered the terminal basin and the glacial system was more extensive than during the lLGM advance. The onset of the penultimate deglaciation started at ~ 129 ka, when the Garonne Glacier abandoned the two moraine ridges (EM-2 and EM-4) located at 480 m and they stabilized.

Intense postglacial geomorphic dynamics (glacial, periglacial, slope and alluvial) have eroded glacial landforms left by previous glaciations, and therefore, the glacial evidence from MIS 6 in the Pyrenees can be only found in a few valleys. The glacial deposits beyond the limits of the LGC in this mountain range have been only recently ascribed to the PGC and gradually confirmed by optically stimulated luminescence (OSL) and CRE dating techniques (Oliva et al. 2019). These deposits, which are highly degraded, presenting only few scattered boulders suitable to CRE dating, are normally located in flat areas far from slope, periglacial and alluvial processes. Several studies have been published showing the glacial and karst evidence from the PGC in the Pyrenees and interpreted from the MIS 6 (Delmas et al. 2011; García-Ruiz et al. 2013; Sorriaux et al. 2016). Within the uncertainties, these evidences are also supported by a fluvial aggradation episode at 178 and 151 ka based on the existence of fluvial and fluvioglacial sediments in fluvial terraces of the Cinca and Gállego valleys, respectively (Lewis et al. 2009).

Available dates of glacial processes during the PGC elsewhere in the Iberian Peninsula are also scarce. Similarly to what has happened with the LGC (Oliva et al. 2019), the increasing application of CRE methods is showing that the most extensive glaciers developed at the end of the PGC. CRE ages between 140 and 120 ka have been reported in several mountain regions regarding the most external moraines. This is the case of Sierra Nevada, where the lowest moraine

was dated at 130–135 ka; Serra da Estrela, where the highest right lateral moraine was developed by ~ 140 ka; and even in the NW ranges, where a push moraine and a polished surface were dated at 155 and 131 ka (Table 4).

Glacial evidence of the PGC has also been detected in other European mountains confirming the maximum glacial advance of the PGC during the MIS 6. This pattern occurred in the Alps, where one erratic boulder in the Jura Mountains was dated using two cosmogenic nuclides, $^{21}$Ne and $^{10}$Be, yielding 128 and 106 ka, respectively (Ivy-Ochs et al. 2006). In the Austrian Alps, OSL was applied to glaciofluvial, fluviolacustrine and eolian sediments showing a culmination of the PGC during the late MIS 6 (149–135 ka) (Bickel et al. 2015). Further south, very similar ages were obtained from U-series in the coastal mountains of the Adriatic Sea revealing cold conditions during the MIS 6, with moraine development starting at 125 ka in the Bijela Gora plateau (Hughes et al. 2010) and at 131 ka for the moraines from the Mount Tymphi, at the northern slope of the Pindus Mountains (Hughes et al. 2006).

During the gLGM, the terminal LBBb was ice free with the glaciers retreating towards headwaters at 24–21 ka. This is supported by exposures ages from polished surfaces, at 18 km southwards the EM-1 ridge, on the lower slopes of the Marignac overdeepened basin that became ice-free by that time (Fig. 7). Therefore, our results also introduce new chronological data about glacial dynamics occurring during the gLGM in the Central Pyrenees. In other valleys of this range, glaciers showed contrasting patterns of glacial advance or retreat during the gLGM. In the Eastern Pyrenees, a glacial advance occurred synchronous with the gLGM, that was noticed in the Têt Valley, where a moraine at ~ 1,690 m was dated to 25 ka (Tomkins et al. 2018); and in the La Llosa and Duran valleys, where moraines at 1520 m and at 1830 m were dated to 20 and 21 ka, respectively (Andrés et al. 2018). In the southern slope of the Pyrenees, glacial retreat was deduced in the upper sector of the Gállego Valley based on a paleolake located at ~ 1500 m dammed by landslide by 20 ka (García-Ruiz et al. 2003).

In the Iberian Peninsula, a general glacial advance occurred at 22–19 ka followed by a massive recession (Oliva et al. 2019). In the central and northern part of the Iberia, other valleys also recorded glacial advances, such as in the Iberian Range, where the end of the gLGM was recorded based on lacustrine sediments in the Sierra de Neila was recorded prior to 21 ka (Vegas Salamanca 2007) or in NW ranges, where the glacier front in the Tera Valley also remained stable until 22 cal ka BP (Rodríguez-Rodríguez et al. 2011). In the southern Iberian Peninsula, glaciers advanced during the gLGM in the Serra Nevada, where moraine stabilization in the San Juan Valley occurred at 21–19 ka (Palacios et al. 2016). In other European mountains, such as the Alps (Ivy-Ochs et al. 2008) or the at the Tatra Mountains (Engel et al. 2015), glaciers reached their maximum position of the LGC at 26–21 ka and undergone a subsequence massive retreat afterwards, at 20–19 ka. This suggests that the Garonne Glacier was already retreating when $CO_2$ concentrations in the atmosphere were still low (180–200 ppm; Shakun et al. 2015).

## Conclusions

The Pyrenees hosted large ice fields during Quaternary glacial phases, with extensive alpine glaciers descending from the highest peaks of the axis of this mountain range. Those glaciers shaped the landscape and left a wide range of geomorphological features of glacial origin, both within the mountain range as well as in the surrounding lowlands of the northern slope. This is the case of the northern foreland of the Central Pyrenees at the LBBb. Here, the longest Late Pleistocene glacier in the Pyrenees that flowed northwards

**Table 4** Comparison of the glacial chronology of the Penultimate Glaciation in the northern valleys of the Pyrenees

| Range | Valley | Age | Geomorphological unit | Dating method | Reference |
|---|---|---|---|---|---|
| Pyrenees (Northern slope) | Ariège Valley | 122 ka | Erratic boulder lying on bedrock | CRE ($^{10}$Be) | Delmas et al. (2011) |
| Pyrenees (Southern slope) | Aragón Valley | 171 ka | Frontal moraine | OSL | García-Ruiz et al. (2013) |
| Central Range (Serra da Estrela) | Zêzere Valley | 140 ka | Lateral moraine | CRE ($^{36}$Cl) | Vieira et al. (2021) |
| Betic Range (Sierra Nevada) | Naute Valley | 130–135 ka | Terminal moraine | CRE ($^{10}$Be) | Palacios et al. (2019) |
| Cantabrian Mountains | Porma Valley | 114 ka | Erratic boulders and ground moraine at the terminal zone | CRE ($^{10}$Be) | Rodríguez-Rodríguez et al. (2016) |
| NW ranges (Serra de Queixa-Invernadoiro) | Conso Valley | 155 ka | Push moraine boulder | CRE ($^{21}$Ne) | Vidal-Romaní et al. (2015) |
| NW ranges (Serra Gerês-Xurés) | Portela da Amoreira divide | 131 ka | Polished surface | CRE ($^{21}$Ne) | Vidal-Romaní et al. (2015) |

along ~ 80 km formed a terminal moraine system at only 420 m on its terminal position.

We present a 10-sample data set of $^{10}$Be CRE dating providing ages for the Late Quaternary maximum ice extent as well as the extent of the Garonne glacier at the time of the gLGM. The long time passed, since last deglaciation has favoured postglacial erosive processes and only a few stable boulders suitable for the application of CRE dating were found. Four boulders from the external moraine ridges confirm that the largest palaeoglacier in the Upper Garonne Valley developed before the LGC, at ~ 129 ka. These are the first CRE ages reporting a period of glacial expansion in the Pyrenees during the PGC, as also observed in other Iberian mountain ranges (e.g., Sierra Nevada, Central Range, NW Ranges), where the largest glacial advance during the MIS 6 was followed by a period of moraine stabilization at ~ 129 ka. However, boulders from the internal moraine system of the glacial terminal basin did not yield consistent geochronological results. Therefore, no data of glacial advance or retreat during the LGC is available in LBBb. Exposure ages from glacially polished bedrock surfaces located at the confluence Garonne-la Pique valleys—18 km to the south of the external moraines—reported ages of 24–21 ka, confirming that the terminal basin was already ice-free during the gLGM.

A better understanding of glacial oscillations during glacial cycles prior to the last one is of major importance to assess whether the spatial and temporal trends of the last glaciation followed the same pattern observed in previous glaciations or they constitute a singular case during the Quaternary. Future research must provide further evidence of the occurrence of this glacial phase in the Pyrenees and couple it with environmental dynamics in the lowlands. The application of individual dating techniques does not resolve the full chronological sequence of the glacial oscillations during the PGC. Future research should address the combination of several data sources (fluvial, glacial, eolian, lacustrine, karst and archeological) and complement them with different chronological methods such as OSL and CRE dating to avoid the intrinsic limitations of each technique and circumvent the uncertainties associated with the occurrence of postglacial processes in such a dynamic environment.

**Acknowledgements** The authors sincerely thank the Dr. Ramón Pellitero for his help to the construction of the Garonne palaeoglacier. We also thank to anonymous reviewers for the constructive revision of an earlier draft of the manuscript. The authors are grateful to Dr. Augusto Pérez-Alberti for his guidance and wise advices during his prolific scientific career. ASTER Team: Georges Aumaître, Karim Keddadouche.

**Author contributions** MF Laboratory tasks (sample processing), collection and handling of aerial photo imagery, geomorphological mapping and writing of a first draft of the manuscript. MO Coordination of the research, funding acquisition, field work, geomorphological analysis, sampling, data processing and contributing to the writing and final revision of the manuscript. GV Geomorphological analysis, discussion of results, contribution to the writing and final revision of the manuscript. DP Fieldwork, geomorphological analysis, discussion of the results, and contribution to the writing and final revision of the manuscript. JMF-F Laboratory tasks (sample processing, exposure age calculations), contribution to the writing and final revision of the manuscript. MD Geomorphological analysis, discussion of results, contribution to the final revision of the manuscript. JG-O Laboratory tasks (sample processing, exposure age calculations), contribution to the writing and final revision of the manuscript. IS Supervision of the whole process of the sample processing and interpretation of the results, contribution to the writing and final revision of the manuscript. JV Fieldwork, geomorphological analysis, discussion of results, contribution to the writing and final revision. ASTER Team. Supervision of the AMS measurements of the $^{36}$Cl samples.

**Funding** This research was financially supported by the Research Group ANTALP (Antarctic, Arctic, Alpine Environments; 2017-SGR-1102) funded by the Government of Catalonia and the Centro de Estudos Geográficos/IGOT—University of Lisbon (FCT I.P. UIDB/00295/2020 and UIDP/00295/2020). The study topics complement those of the project PALEOGREEN (CTM2017-87976-P) funded by the Spanish Ministry of Economy and Competitiveness and the project NUNANTAR funded by the Fundação para a Ciência e Tecnologia of Portugal (02/SAICT/2017—32002). Marcelo Fernandes currently holds a PhD fellowship of the Fundação para a Ciência e Tecnologia of Portugal (FCT—SFRH/139569/2018); Marc Oliva is supported by the Ramón y Cajal Program (RYC-2015-17597) and José M. Fernández-Fernández is supported by a postdoctoral grant within the NUNANTAR project. $^{10}$Be measurements were performed at the ASTER AMS national facility (CEREGE, Aix-en-Provence), which is supported by the INSU/CNRS and the ANR through the "Projets thématiques d'excellence" program for the "Equipements d'excellence" ASTER-CEREGE action and IRD. This work is also framed within the College on Polar and Extreme Environments (Polar2E) of the University of Lisbon.

**Availability of data and materials** The data presented in this article are openly available in this website: http://alpine.ice-d.org/

**Code availability** The geomorphological map was developed using ArcGIS 10.7.1 (ESRI) software based on the UTM projection and the ETRS89 zone 31N coordinate system. The layouts were improved with the Inkscape 1.0 software.

## Declarations

**Conflict of interest** The authors declare that they have no known competing financial interests or personal relationships that could have appeared to influence the work reported in this paper.

**Ethics approval** Not applicable.

**Consent to participate** Not applicable.

**Consent for publication** Not applicable.

## References

Adamson K, Hughes P, Woodward J (2013) Pleistocene glaciation of the Mediterranean Mountains. Quat Newsl 131:2–15

Andrés N, Gómez-Ortiz A, Fernández-Fernández JM, Tanarro García LM, Salvador-Franch F, Oliva M, Palacios D (2018) Timing of deglaciation and rock glacier origin in the southeastern Pyrenees: a review and new data. Boreas 47:1050–1071. https://doi.org/10.1111/bor.12324

Andrieu V (1987) Le paléoenvironnement du piémont nord-pyrénéen occidental de 27 000 BP au Postglaciaire: la séquence d'Estarrès (Pyrénées Atlantiques, France) dans le bassin glaciaire d'Arudy. Comp Rend Acad Sci 304:103–108

Andrieu V (1991) Dynamique du paléoenvironnement de la vallée montagnarde de la Garonne (Pyrénées centrales, France) de la fin des temps glaciaires à l'actuel. Dissertation. Toulouse 2

Andrieu V, Hubschman J, Jalut G, Hérail G (1988) Chronologie de la dégladation des Pyrénées françaises. Dynamique de sédimentation et contenu pollinique des paléolacs ; application à l'interprétation du retrait glaciaire. Bull Assoc Fran Quat 25:55–67

Bakalowicz M, Sorriaux P, Ford D (1984) Quaternary glacial events in the Pyrenees from U-series dating of speleothems in the Niaux-Lombrives-Sabart caves, Ariège, France. Nor Geogr Tidsskr 38:193–197. https://doi.org/10.1080/00291958408552125

Benn DI, Evans DJA (2010) Glaciers and glaciation, 2nd edn. Hodder Education, London. https://doi.org/10.5860/CHOICE.35-6240

Benn DI, Hulton NRJ (2010) An Excel$^{TM}$ spreadsheet program for reconstructing the surface profile of former mountain glaciers and ice caps. Comput Geosci 36:605–610. https://doi.org/10.1016/j.cageo.2009.09.016

Bernal-Wormull JL, Moreno A, Bartolomé M, Aranburu A, Arriolabengoa M, Iriarte E, Cacho I, Spötl C, Edwards RL, Cheng H (2021) Immediate temperature response in northern Iberia to last deglacial changes in the North Atlantic. Geology XX. https://doi.org/10.1130/G48660.1

Bickel L, Lüthgens C, Lomax J, Fiebig M (2015) The timing of the penultimate glaciation in the northern Alpine Foreland: new insights from luminescence dating. Proc Geol Assoc 126:536–550. https://doi.org/10.1016/j.pgeola.2015.08.002

Braucher R, Guillou V, Bourlès DL, Arnold M, Aumaître G, Keddadouche K, Nottoli E (2015) Preparation of ASTER in-house 10Be/9Be standard solutions. Nucl Instrum Methods Phys Res B Beam Interact Mater Atoms 361:335–340. https://doi.org/10.1016/j.nimb.2015.06.012

Briner J, Kaufman D, Manley W, Finkel R, Caffee M (2005) Cosmogenic exposure dating of late Pleistocene moraine stabilization in Alaska. Geol Soc Am Bull 117:1108–1120. https://doi.org/10.1130/B25649.1

Calvet M (1996) Morphogenèse d'une montagne méditerranéenne: Les Pyrénées Orientales. Dissertation. University of Orléans

Calvet M, Delmas M, Gunnell Y, Braucher R, Bourlès D (2011) Recent advances in research on quaternary glaciations in the pyrenees. Dev Quat Sci 15:127–139. https://doi.org/10.1016/B978-0-444-53447-7.00011-8

Calvet M, Gunnell Y, Laumonier B (2021) Denudation history and palaeogeography of the Pyrenees and their peripheral basins: an 84-million-year geomorphological perspective. Earth Sci Rev 215:103436. https://doi.org/10.1016/j.earscirev.2020.103436

Campos N, Alcalá-Reygosa J, Watson S, Kougkoulos I, Quesada-Román A, Grima N (2021) Modeling the retreat of the Aneto Glacier (Spanish Pyrenees) since the Little Ice Age, and its accelerated shrinkage over recent decades. Holocene 31:1315–1326. https://doi.org/10.1177/09596836211011678

Colleoni F, Wekerle C, Näslund JO, Brandefelt J, Masina S (2016) Constraint on the penultimate glacial maximum Northern Hemisphere ice topography (≈140 kyrs BP). Quat Sci Rev 137:97–112. https://doi.org/10.1016/j.quascirev.2016.01.024

Copons R, Bordonau J (1996) El registro sedimentario del Cuaternario Reciente en el lago Redó d'Aigüestortes (Pirineos Centrales). In: Grandal A, Pagés J (eds) IV Reunión de Geomorfología. Sociedad Española de Geomorfología

Crest Y, Delmas M, Braucher R, Gunnell Y, Calvet M (2017) Cirques have growth spurts during deglacial and interglacial periods: evidence from 10Be and 26Al nuclide inventories in the central and eastern Pyrenees. Geomorphology 278:60–77. https://doi.org/10.1016/j.geomorph.2016.10.035

Dahl-Jensen D, Albert MR, Aldahan A, Azuma N, Balslev-Clausen D, Baumgartner M, Berggren AM, Bigler M, Binder T, Blunier T, Bourgeois JC, Brook EJ, Buchardt SL, Buizert C, Capron E, Chappellaz J, Chung J, Clausen HB, Cvijanovic I, Davies SM, Ditlevsen P, Eicher O, Fischer H, Fisher DA, Fleet LG, Gfeller G, Gkinis V, Gogineni S, Goto-Azuma K, Grinsted A, Gudlaugsdottir H, Guillevic M, Hansen SB, Hansson M, Hirabayashi M, Hong S, Hur SD, Huybrechts P, Hvidberg CS, Iizuka Y, Jenk T, Johnsen SJ, Jones TR, Jouzel J, Karlsson NB, Kawamura K, Keegan K, Kettner E, Kipfstuhl S, Kjær HA, Koutnik M, Kuramoto T, Köhler P, Laepple T, Landais A, Langen PL, Larsen LB, Leuenberger D, Leuenberger M, Leuschen C, Li J, Lipenkov V, Martinerie P, Maselli OJ, Masson-Delmotte V, McConnell JR, Miller H, Mini O, Miyamoto A, Montagnat-Rentier M, Mulvaney R, Muscheler R, Orsi AJ, Paden J, Panton C, Pattyn F, Petit JR, Pol K, Popp T, Possnert G, Prié F, Prokopiou M, Quiquet A, Rasmussen SO, Raynaud D, Ren J, Reutenauer C, Ritz C, Röckmann T, Rosen JL, Rubino M, Rybak O, Samyn D, Sapart CJ, Schilt A, Schmidt AMZ, Schwander J, Schüpbach S, Seierstad I, Severinghaus JP, Sheldon S, Simonsen SB, Sjolte J, Solgaard AM, Sowers T, Sperlich P, Steen-Larsen HC, Steffen K, Steffensen JP, Steinhage D, Stocker TF, Stowasser C, Sturevik AS, Sturges WT, Sveinbjörnsdottir A, Svensson A, Tison JL, Uetake J, Vallelonga P, Van De Wal RSW, Van Der Wel G, Vaughn BH, Vinther B, Waddington E, Wegner A, Weikusat I, White JWC, Wilhelms F, Winstrup M, Witrant E, Wolff EW, Xiao C, Zheng J (2013) Eemian interglacial reconstructed from a Greenland folded ice core. Nature 493:489–494. https://doi.org/10.1038/nature11789

Delmas M, Gunnell Y, Braucher R, Calvet M, Bourlès D (2008) Exposure age chronology of the last glaciation in the eastern Pyrenees. Quat Res 69:231–241. https://doi.org/10.1016/j.yqres.2007.11.004

Delmas M, Calvet M, Gunnell Y, Braucher R, Bourlès D (2011) Palaeogeography and 10Be exposure-age chronology of Middle and Late Pleistocene glacier systems in the northern Pyrenees: implications for reconstructing regional palaeoclimates. Palaeogeogr Palaeoclimatol Palaeoecol 305:109–122. https://doi.org/10.1016/j.palaeo.2011.02.025

Delmas M, Braucher R, Gunnell Y, Guillou V, Calvet M, Bourlès D (2015) Constraints on Pleistocene glaciofluvial terrace age and related soil chronosequence features from vertical $^{10}$Be profiles in the Ariège River catchment (Pyrenees, France). Glob Planet Change 132:39–53. https://doi.org/10.1016/j.gloplacha.2015.06.011

Delmas M, Calvet M, Gunnell Y, Voinchet P, Manel C, Braucher R, Tissoux H, Bahain JJ, Perrenoud C, Saos T (2018) Terrestrial $^{10}$Be and electron spin resonance dating of fluvial terraces quantifies quaternary tectonic uplift gradients in the eastern Pyrenees. Quat Sci Rev 193:188–211. https://doi.org/10.1016/j.quascirev.2018.06.001

Delmas M, Gunnell Y, Calvet M, Reixach T, Oliva M (2021a) The Pyrenees: glacial landforms prior to the Last Glacial Maximum. In: Palacios D, Hughes P, García-Ruiz JM, Andrés N (eds) European glacial landscapes: maximum extent of glaciations. Elsevier, Amsterdam

Delmas M, Gunnell Y, Calvet M, Reixach T, Oliva M (2021b) The Pyrenees: glacial landforms from the Last Glacial maximum. In: Palacios D, Hughes P, García-Ruiz JM, Andrés N (eds) European

glacial landscapes: maximum extent of glaciations. Elsevier, Amsterdam
Ehlers J, Gibbard PL, Hughes PD (2011) Quaternary glaciations—extent and chronology: a closer look. In: Developments in quaternary science, vol 15. Elsevier, Amsterdam
Engel Z, Mentlík P, Baucher R, Minár J, Léanni L, Aster Team (2015) Geomorphological evidence and $^{10}$Be exposure ages for the last glacial maximum and deglaciation of the Velká and Malá Studená dolina valleys in the High Tatra Mountains, central Europe. Quat Sci Rev 124:106–123. https://doi.org/10.1016/j.quascirev.2015.07.015
Fernandes M, Oliva M, Palma P, Ruiz-Fernández J, Lopes L (2017) Glacial stages and post-glacial environmental evolution in the Upper Garonne valley, Central Pyrenees. Sci Total Environ 584–585:1282–1299. https://doi.org/10.1016/j.scitotenv.2017.01.209
Fernandes M, Oliva M, Vieira G, Palacios D, Fernández-Fernández JM, Garcia-Oteyza J, Schimmelpfennig I, ASTER Team, Antoniades D (2021) Glacial oscillations during the Bølling-Allerød Interstadial-Younger Dryas transition in the Ruda Valley. J Quat Sci, Central Pyrenees. https://doi.org/10.1002/jqs.3379
Gangloff P, Hetu B, Courchesne F (1991) Présence d'un dépôt glaciaire sous la terrasse moyenne d'Agnos, vallée d'Aspe (Pyrénées-Atlantiques). Quaternaire 2:131–133. https://doi.org/10.3406/quate.1991.1962
García-Ruiz JM, Valero-Garcés BL, Martí-Bono C, González-Sampériz P (2003) Asynchroneity of maximum glacier advances in the central Spanish Pyrenees. J Quat Sci 18:61–72. https://doi.org/10.1002/jqs.715
García-Ruiz JM, Martí-Bono C, Peña-Monné J, Sancho C, Rhodes E, Valero-Garcés BL, González-Sampériz P, Moreno A (2013) Glacial and fluvial deposits in the Aragón Valley, Central-Western Pyrenees: chronology of the Pyrenean Late Pleistocene Glaciers. Geogr Ann Ser A Phys Geogr 95:15–32. https://doi.org/10.1111/j.1468-0459.2012.00478.x
González-Sampériz P, Valero-Garcés BL, Moreno A, Jalut G, García-Ruiz JM, Martí-Bono C, Delgado-Huertas A, Navas A, Otto T, Dedoubat J (2006) Climate variability in the Spanish Pyrenees during the last 30,000 yr revealed by the El Portalet sequence. Quat Res 66:38–52. https://doi.org/10.1016/j.yqres.2006.02.004
Gosse J, Philips F (2001) Terrestrial in situ cosmogenic nuclides: theory and application. Quat Sci Rev 20:1475–1560. https://doi.org/10.1016/S0277-3791(00)00171-2
Gourinard Y (1971) Les moraines de la basse vallée du Carol entre Latour et Puicerda (Pyrénées orientales franco-espagnoles). Comp Rend Acad Sci 272:3112–3115
Grant KM, Rohling EJ, Bronk Ramsey C, Cheng H, Edwards RL, Florindo F, Heslop D, Marra F, Roberts AP, Tamisiea ME, Williams F (2014) Sea-level variability over five glacial cycles. Nat Commun. https://doi.org/10.1038/ncomms6076
Hearty PJ, Hollin JT, Neumann AC, O'Leary MJ, McCulloch M (2007) Global sea-level fluctuations during the last interglaciation (MIS 5e). Quat Sci Rev 26:2090–2112. https://doi.org/10.1016/j.quascirev.2007.06.019
Hétu B, Gangloff P (1989) Dépôts glaciaires du Pléistocène inférieur sur le piémont des Pyrénées Atlantiques. Zeitschr Geomorphol 33:384–403
Hétu B, Gangloff P, Courchesne F (1992) Un till de déformation du Pléistocène inférieur à la basé de la Formation du Lannemezan (Piémont des Pyrénées Atlantiques, France). Quaternaire 3:53–61
Hubschman J (1975) Conclusion : evolution pédo-géochimique et interprétation paléobioclimatique de piémont quaternaire garonnais. Bull Assoc Fran Quat 12:211–216
Hubschman J (1984) Glaciaire ancien et glaciaire récent: analyse comparée de l'altération de moraines terminals nord-pyrénéennes. Mont Piémonts RGPSO, pp 313–332
Hughes PD, Woodward JC, Gibbard PL, Macklin MG, Gilmour MA, Smith GR (2006) The glacial history of the Pindus Mountains, Greece. J Geol 114:413–434. https://doi.org/10.1086/504177
Hughes P, Woodward JC, van Calsteren PC, Thomas AL, Adamson KR (2010) Pleistocene ice caps on the coastal mountains of the Adriatic Sea. Quat Sci Rev 29:3690–3708. https://doi.org/10.1016/j.quascirev.2010.06.032
ICGC (2017) Base de dades geològiques de Catalunya 1:50.000 v1.0
Ivy-Ochs S, Kerschner H, Reuther A, Maisch M, Sailer R, Schaefer J, Kubik PW, Synal H, Schlüchter C (2006) The timing of glacier advances in the northern European Alps based on surface exposure dating with cosmogenic 10Be, 26Al, 36Cl, and 21Ne. Geol Soc Am Spec Pap 415:43–60. https://doi.org/10.1130/2006.2415(04)
Ivy-Ochs S, Kerschner H, Reuther A, Preusser F, Heine K, Maisch M, Kubik P, Schluchter C (2008) Chronology of the last glacial cycle in the European Alps. J Quat Sci 22:559–573. https://doi.org/10.1002/jqs.1202
Jalut G, Delibrias G, Dagnac J, Mardones M, Bouhours M (1982) A palaeoecological approach to the last 21 000 years in the pyrenees: the peat bog of Freychinède (Alt. 1350 m, Ariège, South France). Palaeogeogr Palaeoclimatol Palaeoecol 40:321–359. https://doi.org/10.1016/0031-0182(82)90033-5
Jalut G, Andrieu V, Delibrias G, Fontugne M (1988) Palaeoenvironment of the valley of Ossau (Western French Pyrenees) during the last 27,000 years. Pollen Spores 30:357–394
Jalut G, Monserrat-Marti J, Fontugne M, Delibrian G, Vilaplana J, Rosen J (1992) Glacial to interglacial vegetation changes in the northern and southern Pyrénées: deglaciation, vegetation cover and chronology. Quat Sci Rev 11:449–480
Jones RS, Small D, Cahill N, Bentley MJ, Whitehouse PL (2019) iceTEA: tools for plotting and analysing cosmogenic-nuclide surface-exposure data from former ice margins. Quat Geochronol 51:72–86. https://doi.org/10.1016/j.quageo.2019.01.001
Lewis CJ, McDonald EV, Sancho C, Peña JL, Rhodes EJ (2009) Climatic implications of correlated Upper Pleistocene glacial and fluvial deposits on the Cinca and Gállego Rivers (NE Spain) based on OSL dating and soil stratigraphy. Glob Planet Change 67:141–152. https://doi.org/10.1016/j.gloplacha.2009.01.001
Li Y (2018) Determining topographic shielding from digital elevation models for cosmogenic nuclide analysis: a GIS model for discrete sample sites. J Mt Sci 15:939–947. https://doi.org/10.1007/s11629-018-4895-4
Lifton N, Sato T, Dunai T (2014) Scaling in situ cosmogenic nuclide production rates using analytical approximations to atmospheric cosmic-ray fluxes. Earth Planet Sci Lett 386:149–160. https://doi.org/10.1016/j.epsl.2013.10.052
Lisiecki L, Raymo M (2005) A Pliocene-Pleistocene stack of 57 globally distributed benthic δ 18O records. Paleoceanography 20:1–7. https://doi.org/10.1029/2004PA001071
Mardones M, Jalut G (1983) La tourbiere de Biscaye (alt. 409 m, Hautes Pyrenees): approche paleoecologique des 45.000 dernières annees. Pollen Spores 25:163–212
Martin LCP, Blard PH, Balco G, Lavé J, Delunel R, Lifton N, Laurent V (2017) The CREp program and the ICE-D production rate calibration database: a fully parameterizable and updated online tool to compute cosmic-ray exposure ages. Quat Geochronol 38:25–49. https://doi.org/10.1016/J.QUAGEO.2016.11.006
Martrat B, Grimalt JO, Shackleton NJ, De Abreu L, Hutterli MA, Stocker TF (2007) Four climate cycles of recurring deep and surface water destabilizations on the Iberian margin. Science 317:502–507. https://doi.org/10.1126/science.1139994
McManus JF, Oppo DW, Cullen JL (1999) A 0.5-Million-year record of millennial-scale climate variability in the North Atlantic. Science 283:971–975. https://doi.org/10.1126/science.283.5404.971

Menviel L, Capron E, Govin A, Dutton A, Tarasov L, Abe-Ouchi A, Drysdale RN, Gibbard PL, Gregoire L, He F, Ivanovic RF, Kageyama M, Kawamura K, Landais A, Otto-Bliesner BL, Oyabu I, Tzedakis PC, Wolff E, Zhang X (2019) The penultimate deglaciation: protocol for paleoclimate modelling intercomparison project (PMIP) phase 4 transient numerical simulations between 140 and 127 ka, version 1.0. Geosci Model Dev 12:3649–3685. https://doi.org/10.5194/gmd-12-3649-2019

Merchel S, Herpers U (1999) An update on radiochemical separation techniques for the determination of long-lived radionuclides via accelerator mass spectrometry. Radiochim Acta 84:215–219. https://doi.org/10.1524/ract.1999.84.4.215

Merchel S, Arnold M, Aumaître G, Benedetti L, Bourlès DL, Braucher R, Alfimov V, Freeman SPHT, Steier P, Wallner A (2008) Towards more precise 10Be and 36Cl data from measurements at the 10–14 level: influence of sample preparation. Nucl Instrum Methods Phys Res B 266:4921–4926. https://doi.org/10.1016/j.nimb.2008.07.031

Montserrat J (1992) Evolución glaciar y postglaciar del clima y la vegetación en la vertiente sur del Pirineo: estudio palinológico. Monogr. del Inst. Piren. Ecol. Actas. Instituto Pirenaico de Ecología

Morellón M, Valero-Garcés B, Vegas-Vilarrúbia T, González-Sampériz P, Romero Ó, Delgado-Huertas A, Mata P, Moreno A, Rico M, Corella JP (2009) Lateglacial and Holocene palaeohydrology in the western Mediterranean region: the Lake Estanya record (NE Spain). Quat Sci Rev 28:2582–2599. https://doi.org/10.1016/j.quascirev.2009.05.014

Obrochta S, Crowley T, Channell J, Hodell D, Baker P, Seki A, Yokoyama Y (2014) Climate variability and ice-sheet dynamics during the last three glaciations. Earth Planet Sci Lett 406:198–212. https://doi.org/10.1016/j.epsl.2014.09.004

Oliva M, Palacios D, Fernández-Fernández JM, Rodríguez-Rodríguez L, García-Ruiz JM, Andrés N, Carrasco RM, Pedraza J, Pérez-Alberti A, Valcárcel M, Hughes P (2019) Late quaternary glacial phases in the Iberian Peninsula. Earth Sci Rev 192:564–600. https://doi.org/10.1016/j.earscirev.2019.03.015

Oliva M, Fernandes M, Palacios D, Fernández-Fernández JM, Schimmelpfennig I, Team ASTER, Antoniades D (2021) Rapid deglaciation during the Bølling-Allerød Interstadial in the Central Pyrenees and associated glacial and periglacial landforms. Geomorphology. https://doi.org/10.1016/j.geomorph.2021.107735

Osmaston H (2005) Estimates of glacier equilibrium line altitudes by the area×altitude, the area×altitude balance ratio and the area×altitude balance index methods and their validation. Quat Int 138–139:22–31. https://doi.org/10.1016/j.quaint.2005.02.004

Palacios D, Andrés N, López-Moreno JI, García-Ruiz JM (2015a) Late Pleistocene deglaciation in the upper Gállego Valley, central Pyrenees. Quat Res (USA) 83:397–414. https://doi.org/10.1016/j.yqres.2015.01.010

Palacios D, Gómez-Ortiz A, Andrés N, Vázquez-Selem L, Salvador-Franch F, Oliva M (2015b) Maximum extent of Late Pleistocene glaciers and last deglaciation of La Cerdanya mountains, Southeastern Pyrenees. Geomorphology 231:116–129. https://doi.org/10.1016/j.geomorph.2014.10.037

Palacios D, Gómez-Ortiz A, Andrés N, Salvador-Franch F, Oliva M (2016) Timing and new geomorphologic evidence of the last deglaciation stages in Sierra Nevada (southern Spain). Quat Sci Rev 150:110–129. https://doi.org/10.1016/j.quascirev.2016.08.012

Palacios D, García-Ruiz JM, Andrés N, Schimmelpfennig I, Campos N, Léanni L, Aumaître G, Bourlès DL, Keddadouche K (2017) Deglaciation in the central Pyrenees during the Pleistocene-Holocene transition: timing and geomorphological significance. Quat Sci Rev 162:111–127. https://doi.org/10.1016/j.quascirev.2017.03.007

Pallàs R, Rodés Á, Braucher R, Carcaillet J, Ortuño M, Bordonau J, Bourlès D, Vilaplana JM, Masana E, Santanach P (2006) Late Pleistocene and Holocene glaciation in the Pyrenees: a critical review and new evidence from 10Be exposure ages, south-central Pyrenees. Quat Sci Rev 25:2937–2963. https://doi.org/10.1016/j.quascirev.2006.04.004

Pallàs R, Rodés Á, Braucher R, Bourlès D, Delmas M, Calvet M, Gunnell Y (2010) Small, isolated glacial catchments as priority targets for cosmogenic surface exposure dating of Pleistocene climate fluctuations, southeastern Pyrenees. Geology 38:891–894. https://doi.org/10.1130/G31164.1

Paterson WSB (1994) The physics of glaciers, 3rd edn. Elsevier, London

Pearce D, Ely J, Barr I, Boston C (2017) Glacier reconstruction. In: Cook S, Clarke L, Nield J (eds) Geomorphological techniques. British Society for Geomorphology, UK

Pellitero R, Rea BR, Spagnolo M, Bakke J, Hughes P, Ivy-Ochs S, Lukas S, Ribolini A (2015) A GIS tool for automatic calculation of glacier equilibrium-line altitudes. Comput Geosci 82:55–62. https://doi.org/10.1016/j.cageo.2015.05.005

Pellitero R, Rea BR, Spagnolo M, Bakke J, Ivy-Ochs S, Frew CR, Hughes P, Ribolini A, Lukas S, Renssen H (2016) GlaRe, a GIS tool to reconstruct the 3D surface of palaeoglaciers. Comput Geosci 94:77–85. https://doi.org/10.1016/j.cageo.2016.06.008

Porter SC (1975) Equilibrium-line altitudes of late Quaternary glaciers in the Southern Alps, New Zealand. Quat Res 5:27–47. https://doi.org/10.1016/0033-5894(75)90047-2

Quesada C, Oliveira J (2019) The geology of Iberia: a geodynamic approach. In: The Variscan cycle

Quinif Y, Maire R (1998) Pleistocene deposits in Pierre Saint-Martin cave, French Pyrenees. Quat Res 49:37–50. https://doi.org/10.1006/qres.1997.1939

Rasmussen SO, Bigler M, Blockley SP, Blunier T, Buchardt SL, Clausen HB, Cvijanovic I, Dahl-Jensen D, Johnsen SJ, Fischer H, Gkinis V, Guillevic M, Hoek WZ, Lowe JJ, Pedro JB, Popp T, Seierstad IK, Steffensen JP, Svensson AM, Vallelonga P, Vinther BM, Walker MJC, Wheatley JJ, Winstrup M (2014) A stratigraphic framework for abrupt climatic changes during the Last Glacial period based on three synchronized Greenland ice-core records: Refining and extending the INTIMATE event stratigraphy. Quat Sci Rev 106:14–28. https://doi.org/10.1016/j.quascirev.2014.09.007

Reille M, Andrieu V (1995) The late Pleistocene and Holocene in the Lourdes Basin, Western Pyrenees, France: new pollen analytical and chronology data. Veg Hist Archaeobot 4:1–21

Reixach T, Delmas M, Calvet M (2021) Climatic conditions between 19 and 12 ka in the eastern Pyrenees, and wider implications for atmospheric circulation patterns in Europe. Quat Sci Rev. https://doi.org/10.1016/j.quascirev.2021.106923

Rodríguez-Rodríguez L, Jiménez-Sánchez M, Domínguez-Cuesta MJ, Rico MT, Valero-Garcés B (2011) Last deglaciation in northwestern Spain: new chronological and geomorphologic evidence from the Sanabria region. Geomorphology 135:48–65. https://doi.org/10.1016/j.geomorph.2011.07.025

Sánchez-Goñi MF, Loutre MF, Crucifix M, Peyron O, Santos L, Duprat J, Malaizé B, Turon JL, Peypouquet JP (2005) Increasing vegetation and climate gradient in Western Europe over the Last Glacial Inception (122–110 ka): data-model comparison. Earth Planet Sci Lett 231:111–130. https://doi.org/10.1016/j.epsl.2004.12.010

Sancho C, Arenas C, Pardo G, Peña-Monné JL, Rhodes EJ, Bartolomé M, García-Ruiz JM, Martí-Bono C (2018) Glaciolacustrine deposits formed in an ice-dammed tributary valley in the south-central Pyrenees: new evidence for late Pleistocene climate. Sediment Geol 366:47–66. https://doi.org/10.1016/j.sedgeo.2018.01.008

Shakun JD, Clark PU, He F, Lifton NA, Liu Z, Otto-Bliesner BL (2015) Regional and global forcing of glacier retreat during the

last deglaciation. Nat Commun 6:1–7. https://doi.org/10.1038/ncomms9059

Sorriaux P, Delmas M, Calvet M, Gunnell Y, Durand N, Edwige P (2016) Relations entre karst et glaciers depuis 450 ka dans les grottes de Niaux-Lombrives-Sabart (Pyrénées ariégeoises) Nouvelles datations U/Th dans la grotte de Niaux. Karstologia 67:3–16

Stange KM, van Balen RT, Kasse C, Vandenberghe J, Carcaillet J (2014) Linking morphology across the glaciofluvial interface: a 10Be supported chronology of glacier advances and terrace formation in the Garonne River, northern Pyrenees, France. Geomorphology 207:71–95. https://doi.org/10.1016/j.geomorph.2013.10.028

Tomkins MD, Dortch JM, Hughes PD, Huck JJ, Stimson AG, Delmas M, Calvet M, Pallàs R (2018) Rapid age assessment of glacial landforms in the Pyrenees using Schmidt hammer exposure dating (SHED). Quat Res (US) 90:26–37. https://doi.org/10.1017/qua.2018.12

Turu V, Peña-Monné JL (2006) Las terrazas fluviales del sistema Segre-Valira (Andorra-La Seu d'Urgell-Organyà, Pirineos Orientales): relación con el glaciarismo y la tectónica activa. Geomorfol. y Territ, pp 113–128

Turu V, Boulton GS, Ros I, Visus X, Peña-Monné JL, Martí-Bono C, Ibern JBI, Serrano-Cañadas E, Sancho-Marcén C, Constante-Orrios A, Pous Fàbregas J, Gonzalez-Trueba JJ, Palomar Molins J, Herrero Simón R, García-Ruiz JM (2007) Structure des grands bassins glaciaires dans le nord de la péninsule ibérique : comparaison entre les vallées d'Andorre (Pyrénées orientales), du Gallego (Pyrénées centrales) et du Trueba (Chaîne cantabrique). Quaternaire. https://doi.org/10.4000/quaternaire.1167

Turu V, Calvet M, Bordonau J, Gunnell Y, Delmas M, Vilaplana J, Jalut G (2016) Did Pyrenean glaciers dance to the beat of global climatic events? Evidence from the Würmian sequence stratigraphy of an ice-dammed palaeolake depocentre in Andorra. Geol Soc Lond Spec Publ 433:111–136. https://doi.org/10.1144/sp433.6

Uppala SM, Kållberg PW, Simmons AJ, Andrae U, da Costa BV, Fiorino M, Gibson JK, Haseler J, Hernandez A, Kelly GA, Li X, Onogi K, Saarinen S, Sokka N, Allan RP, Andersson E, Arpe K, Balmaseda MA, Beljaars ACM, van de Berg L, Bidlot J, Bormann N, Caires S, Chevallier F, Dethof A, Dragosavac M, Fisher M, Fuentes M, Hagemann S, Hólm E, Hoskins BJ, Isaksen L, Janssen PAEM, Jenne R, McNally AP, Mahfouf JF, Morcrette JJ, Rayner NA, Saunders RW, Simon P, Sterl A, Trenberth KE, Untch A, Vasiljevic D, Viterbo P, Woollen J (2005) The ERA-40 re-analysis. Q J R Meteorol Soc 131:2961–3012. https://doi.org/10.1256/qj.04.176

Van der Veen C (1999) Fundamentals of glaciers dynamics, 2nd edn. Balkema, Rotterdam

Vegas Salamanca J (2007) Caracterización de eventos climáticos del Pleistoceno superior-Holoceno mediante el estudio sedimentológico de la Laguna Grande (Sierra Neila, NO Sistema Ibérico). Rev Soc Geol Esp 20:53–70

Wekerle C, Colleoni F, Näslund JO, Brandefelt J, Masina S (2016) Numerical reconstructions of the penultimate glacial maximum Northern Hemisphere ice sheets: Sensitivity to climate forcing and model parameters. J Glaciol 62:607–622. https://doi.org/10.1017/jog.2016.45

Winograd IJ, Coplen TB, Landwehr JM, Riggs AC, Ludwig KR, Szabo BJ, Kolesar PT, Revesz KM (1992) Continuous 500,000-year climate record from vein calcite in Devils Hole, Nevada. Science 258:255–260. https://doi.org/10.1126/science.258.5080.255

# 3. Glacial oscillations during the Bølling–Allerød Interstadial–Younger Dryas transition in the Ruda Valley, Central Pyrenees

Fernandes, M., Oliva, M., Vieira, G., Palacios, D., Fernández-Fernández, J. M., Garcia-oteyza, J., Schimmelpfennig, I., Team, A., & Antoniades, D. (2021). Glacial oscillations during the Bølling–Allerød Interstadial–Younger Dryas transition in the Ruda Valley, Central Pyrenees. *Journal of Quaternary Science*, *37*(1), 42–58. https://doi.org/10.1002/jqs.3379

 ISSN 0267-8179. DOI: 10.1002/jqs.3379

JQS Journal of Quaternary Science QRA Quaternary Research Association

# Glacial oscillations during the Bølling–Allerød Interstadial–Younger Dryas transition in the Ruda Valley, Central Pyrenees

M. FERNANDES,[1]* M. OLIVA,[2] G. VIEIRA,[1] D. PALACIOS,[3] J. M. FERNÁNDEZ-FERNÁNDEZ,[1] J. GARCIA-OTEYZA,[2] I. SCHIMMELPFENNIG,[4] ASTER TEAM[4,5] and D. ANTONIADES[6]
[1]Centre for Geographical Studies, IGOT, Lisbon, Universidade de Lisboa, Portugal
[2]Department of Geography, Universitat de Barcelona, Catalonia, Spain
[3]Department of Geography, Universidad Complutense de Madrid, Madrid, Spain
[4]Aix-Marseille Université, CNRS, IRD, INRAE, Coll. France, UM 34 CEREGE, Aix-en-Provence, France
[5]Consortium: Georges Aumaître, Karim Keddadouche
[6]Department of Geography & Centre for Northern Studies, Université Laval, Quebec, Canada

Received 25 May 2021; Revised 15 September 2021; Accepted 16 September 2021

ABSTRACT: The Upper Garonne Basin included the largest glacial system in the Pyrenees during the last glacial cycle. Within the long-term glacial retreat during Termination-1 (T-1), glacier fluctuations left geomorphic evidence in the area. However, the chronology of T-1 glacial oscillations on the northern slopes of the Central Pyrenees is still poorly constrained. Here, we introduce new geomorphological observations and a 12-sample dataset of $^{10}$Be cosmic-ray exposure ages from the Ruda Valley. This U-shaped valley, surrounded by peaks exceeding 2800 m a.s.l., includes a sequence of moraines and polished surfaces that enabled a reconstruction of the chronology of the last deglaciation. Following the maximum ice extent, warmer conditions prevailing at ~15–14 ka, during the Bølling–Allerød (B–A) Interstadial, favoured glacial retreat in the Ruda Valley. Within the B–A, glaciers experienced two phases of advance/stillstand with moraine formation at 13.5 and 13.0 ka. During the early Younger Dryas (YD), glacial retreat exposed the highest surfaces of the Saboredo Cirque (~2300–2350 m) at 12.7 ka. Small glaciers persisted only inside the highest cirques (~2470 m), such as in Sendrosa Cirque, with moraines stabilising at 12.6 ka. The results of this work present the most complete chronology for Pyrenean glacial oscillations from the B–A to the YD. © 2021 John Wiley & Sons, Ltd.

KEYWORDS: Bølling–Allerød; Central Pyrenees; cosmic-ray exposure dating; deglaciation; Younger Dryas

## Introduction

The present-day landscape of the highest mid-latitude mountain environments is dominated by the glacial dynamics that prevailed during the last glacial cycle and by the post-glacial processes that reshaped glacial landforms during the subsequent deglaciation. Following the end of the Last Glacial Maximum (LGM) at 19–20 ka (Clark *et al.*, 2009), most glaciated mountain regions underwent a rapid deglaciation only interrupted by brief periods of glacial growth. Glacial disappearance favoured paraglacial readjustment and intense periglacial and slope processes, which reshaped the already deglaciated valleys and cirques (Ballantyne, 2008). The current spatial distribution of glacial and periglacial features in the high elevations of most mid-latitude ice-free mountain ranges – such as the Pyrenees, which this research focuses on – results from the climatic shifts during Termination-1 (T-1), the period spanning from 20–19 to 11.7 ka (Denton *et al.*, 2014).

At present, mid-latitude mountains such as those of the Mediterranean region are only sparsely glaciated, with small glaciers located in sheltered cirques (Hughes, 2018). However, there are several other mountain ranges located between 30 and 50° latitude north, such as the Alps or the Himalayas, which are still heavily glaciated and record recent dramatic glacial recession trends (Huss *et al.*, 2021). An accurate comprehension of the climatic sensitivity of current glaciated mountain landscapes can help to understand the timing and magnitude of glacial change during the rapid climate shifts of T-1. The alternation of millennial-scale cold/warm periods during T-1 promoted a temporal pattern of glacial advances and retreats across the Northern Hemisphere (Allard *et al.*, 2021; Rea *et al.*, 2020). Ice core records from the Greenland interior show the following succession of climatic phases in the North Atlantic region during T-1: a cold climate regime during the Oldest Dryas (OD; GS-2.1a: 17.5–14.6 ka), followed by the general warm Bølling–Allerød (B–A) Interstadial (GI-1: 14.6–12.9 ka), with a subsequent intensification of cold conditions during the Younger Dryas (YD; GS-1: 12.9–11.7 ka) (Rasmussen *et al.*, 2014).

In the Iberian mountains, recent advances in constraining the chronology of glacial activity during T-1 using cosmic-ray exposure (CRE) dating have revealed contrasting spatio-temporal patterns (García-Ruiz *et al.*, 2016b; Oliva *et al.*, 2019; Palacios *et al.*, 2017a). Whereas the maximum ice extent occurred asynchronously, glacial oscillations during T-1 show a more synchronous response: colder phases favoured glacial growth, whereas warm periods promoted glacial recession (Oliva *et al.*, 2019) and the evolution from debris-free glaciers to rock glaciers such as those in the Iberian Range (García-Ruiz *et al.*, 2020), Cantabrian Mountains (Rodríguez-Rodríguez *et al.*, 2016) and Central (Palacios *et al.*, 2017a, b) and Eastern Pyrenees (Andrés *et al.*, 2018). To date, there is geomorphic evidence of glacial advances during the OD and YD, as well as of glacial retreat during the B–A and following the YD in the Cantabrian Mountains (Rodríguez-Rodríguez *et al.*, 2017), Central Range (Carrasco *et al.*, 2015; Palacios *et al.*, 2012b) and Sierra Nevada (Gómez-Ortiz *et al.*, 2012; Palacios *et al.*, 2016). However, CRE ages require a careful

*Correspondence: M. Fernandes, as above.
E-mail: marcelo.fernandes@live.com

interpretation and support of geomorphological criteria, as their uncertainty ranges may be greater than the time spanning the T-1 phases (Oliva *et al.*, 2021a).

The Pyrenees were the most extensively glaciated mountain system during the maximum ice extent of the last glaciation in Iberia, hosting ~50% of the peninsula's glacial surface (Oliva *et al.*, 2021b). The chronology of glacier fluctuations during T-1 seems to have followed a similar temporal pattern, although available data are principally derived from the range's southern slope (Andrés *et al.*, 2018; Palacios *et al.*, 2015b, 2017a, b). Pyrenean glaciers readvanced to the valley bottoms during the OD, with ice tongues >15 km long. During the B–A, by 15–14 ka, high temperatures favoured rapid deglaciation and glaciers disappeared from relatively low cirques shaped under peaks of ~2600 m a.s.l. (Oliva *et al.*, 2021a). A subsequent readvance occurred during the YD, with smaller glaciers of only ~4 km length confined within the cirques of the highest massifs above 2200 m (Crest *et al.*, 2017; García-Ruiz *et al.*, 2016a; Jomelli *et al.*, 2020; Palacios *et al.*, 2015a, 2017b; Pallàs *et al.*, 2006). Following both cold periods, glacial retreat triggered intense paraglacial dynamics at ~15–14 ka and ~11–10.5 ka, respectively, which led to the formation of rock glaciers and debris-covered glaciers, particularly in cirques below 2800 m (Andrés *et al.*, 2018; Palacios *et al.*, 2017b).

The timing of glacial oscillations is still poorly constrained on the northern slope of the Pyrenees, such as in the Upper Garonne Basin where this work is focused. Recently, Reixach *et al.* (2021) have summarised the glacial evolution from 19 to 12 ka in the northern Pyrenees, reporting a spatial and temporal pattern for T-1 glacial oscillations similar to that on the southern slopes of the range. Jomelli *et al.* (2020) confirmed glacial growth during the YD in the Ariège Valley, where glaciers persisted in the highest cirques until the early Holocene. Another recent study that focused on the Bacivèr Cirque, near our study area, revealed a rapid deglaciation during the B–A, followed by glacial readvance and the formation of the highest moraines at the B–A/YD transition at ~12.9 ka; subsequently, intense paraglacial readjustment favoured the formation of debris-covered glaciers and rock glaciers inside these moraine systems (Oliva *et al.*, 2021a).

In order to complement our understanding of the glacial history of the Pyrenees, this study uses new data to improve the deglaciation chronology of the Upper Garonne Basin, the largest glacial system in this mountain range, during the local last glacial maximum (lLGM; Fernandes *et al.*, 2017). Glacial retreat in the Ruda Valley, where this work is focused, left widespread geomorphic evidence of glacial and paraglacial origin that can be used to reconstruct the last stages of long-term deglaciation in the Central Pyrenees.

Our study, therefore, has the following objectives:

- To date the glacial landforms of the Upper Garonne Basin.
- To discuss the T-1 deglaciation in the Upper Garonne Basin and its geomorphological implications in the context of the known chronologies from the Pyrenees' southern slopes and from other Iberian and European mountain ranges.
- To examine the palaeoclimatic and palaeoenvironmental significance of the glacial response of the northern slopes of the Pyrenees and compare it with the palaeoclimatic evolution inferred from other records in the North Atlantic region.

## Study area

The Pyrenees stretch east–west over 400 km across north Iberia, with the highest peaks (>3000 m) in the central part of the range. This study focuses on the Ruda Valley, located between latitudes 42°40′ N – 42°42′ N and longitudes 0°57′ E – 1°00′ E (Fig. 1), that constitutes the headwaters of the Upper Garonne Basin. The area is included in the peripheral protection area of the National Park of Aigüestortes and Sant Maurici Lake.

The Upper Garonne Valley shows the typical U-shaped cross-section of glacial valleys, and the Garonne River flows to the north-northwest through the central axis of the Pyrenees. Several tributary rivers drain the glacial valleys descending from glacial cirques carved below peaks from 2800 to 3000 m. Glacial cirques are prevailingly northeast-oriented, with floors generally between 2200 and 2400 m (Lopes *et al.*, 2018).

The U-shaped Ruda Valley, drained by the Ruda River that runs 12 km northwards, constitutes the headwaters of the Upper Garonne Basin. Its catchment encompasses 34 $km^2$, with an elevation range of ~1300 m between Saboredo Peak (2827 m) and the village of Baqueira (~1500 m). The Saboredo Cirque is located in the headwaters of the Ruda Valley; the cirque is north-exposed, extending over 5.7 $km^2$, with its floor at ~2250–2400 m. The Saboredo (2827 m), Sendrosa (2702 m) and Locampo (2658 m) peaks are the highest elevations of the cirque, while its toe is located at ~2250 m.

The present-day mean annual air temperature at Port de la Bonaigua station (2266 m) is 3°C, with the regional 0°C isotherm in the Central Pyrenees estimated to be at 2950 m (López-Moreno *et al.*, 2019). Annual precipitation reaches 1227 mm and falls mostly as snow (mean depth of 1210 mm) from October to May, with a snow duration of 7–8 months on the cirque floor. The combination of low temperatures and abundant snowfall determines the scarce vegetation cover above the treeline (2200–2300 m), where barren rocky terrain is widespread, together with small alpine meadows.

The landscape of the Ruda Valley resulted from the interaction of tectonics and vertical incision, both during Quaternary glaciations and interglacial periods; the latter dominated by alluvial and mass-wasting processes (Fernandes *et al.*, 2017). Glacial and periglacial landforms are preserved on different lithologies across the valley, composed of carboniferous granodiorites and granites in the highest sections, with Cambrian–Devonian metamorphic (hornfels, marbles, slates, quartzites and schists) and sedimentary rocks (limestones, sandstones, conglomerates and lutites) in the lowest parts of the valley (ICGC, 2017; Quesada and Oliveira, 2019). However, despite abundant geomorphic evidence revealing that the Garonne Valley presented the longest glacier in the Pyrenees during the lLGM (*ca.* 80 km; Fernandes *et al.*, 2017), the chronological framework of glacial activity in the entire Upper Garonne Basin is still unknown. The headwaters of the Ruda Valley include a rich sequence of moraine systems and polished bedrock surfaces – as well as relict rock glaciers and protalus lobes (Fernandes *et al.*, 2018) – that can be used to improve the temporal resolution for the chronosequence of the final deglaciation of the upper Garonne Valley.

## Methodology

We reconstructed the last deglaciation chronology of the Ruda Valley in the Upper Garonne Basin by integrating geomorphological and chronological techniques. Fieldwork was conducted during the summer of 2019, when snow cover was limited to the concave and sheltered areas at the highest elevations (>2500 m), which enabled better identification of the glacial landforms, as well as sampling for CRE dating.

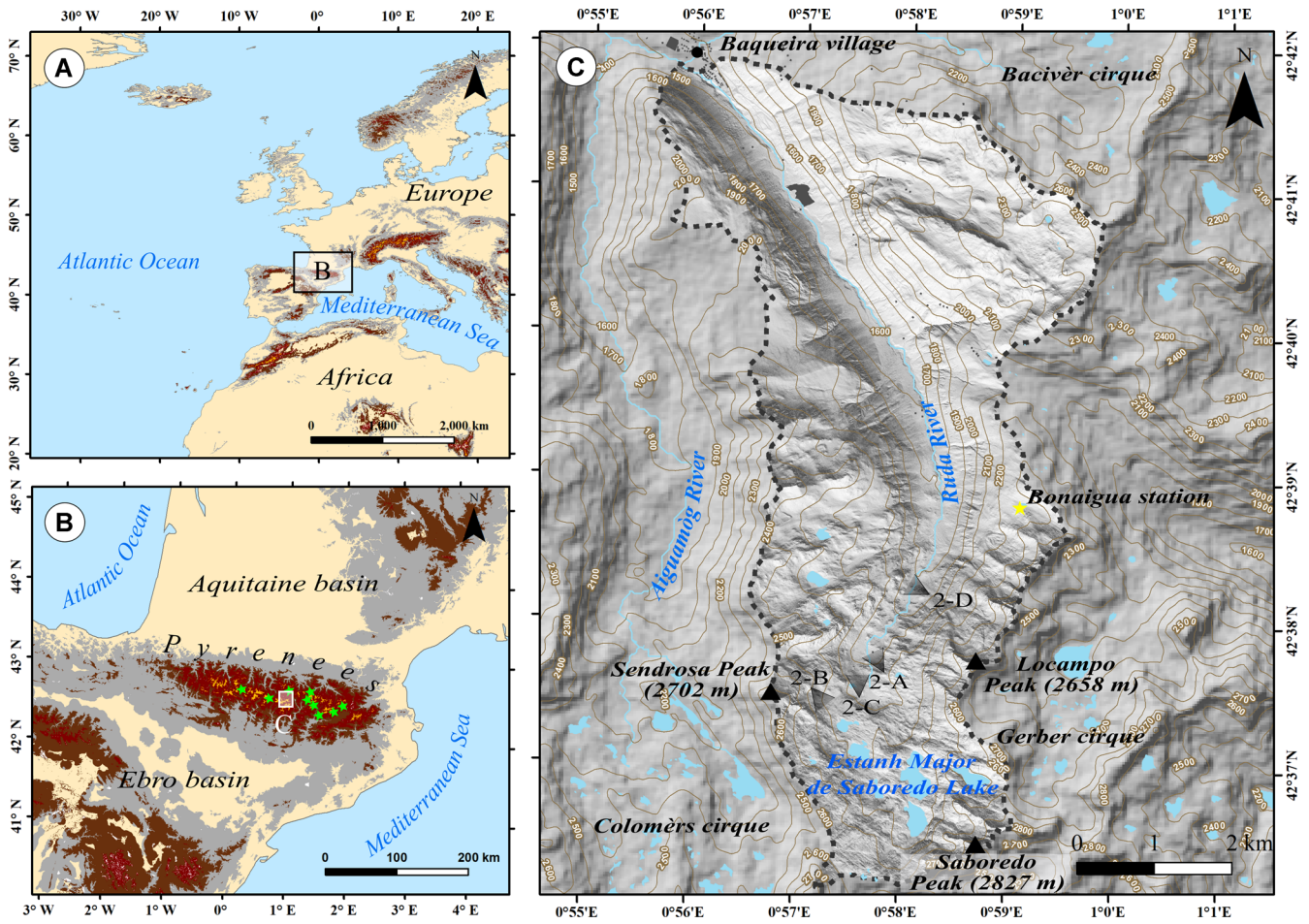


**Figure 1.** Geographical setting of the Ruda Valley. (A) Location in Europe. (B) Location in the Pyrenees with the distribution of the studies mentioned in the discussion (green stars). (C) Limits and topography of the valley with the distribution and view direction of the photos in Figure 2. [Color figure can be viewed at wileyonlinelibrary.com]

## *Geomorphological mapping*

We produced a geomorphological map focusing on glacial and periglacial landforms based on recent general geomorphological maps from the area (Fernandes *et al.*, 2017, 2021). Here we used the same approach based on the combination of aerial orthophotographs (0.25 m cell size) and high-resolution LIDAR digital elevation models (point density of 0.5–2 $m^{-2}$) from the 'Institut Cartogràfic i Geològic de Catalunya' (http://www.icc.cat/appdownloads). The symbology of geomorphological landforms followed Joly (1997).

## *Field strategy and sampling*

We collected 12 granite and granodiorite samples for CRE dating, using a hammer and chisel, from elevations spanning from 1862 to 2470 m (Table 1). To ensure that samples had remained intact since the glacial retreat, we targeted well-anchored moraine boulders and glacially polished bedrock that stood out within their surroundings, which minimises the risk of having been buried under sediment (Fig. 2). To ensure the best cosmic-ray flux reception of the sampling sites, we restricted sample extraction to flat-topped and gentle surfaces, and sampled a thickness of up to 3–5 cm. Corrections for partial shielding due to the surrounding topography were implemented using the ArcGIS toolbox by Li (2018), which applies equations describing the effects of geometric shielding on the sampling sites and a model to predict the nuclide production rate at depth in sloped surfaces (Dunne *et al.* 1999); it required only a point shapefile of the sampling sites including strike/dip of the sampling surfaces and a digital elevation model with a 5 m spatial resolution.

## *Laboratory procedures and exposure age calculation*

Samples were crushed and sieved (>200 g) at the Physical Geography Laboratory of the Universidad Complutense de Madrid (Spain) to the 125–500 µm fraction, which was subsequently processed at the 'Laboratoire National des Nucléides Cosmogéniques' ($LN_2C$) of the 'Centre Européen de Recherche et d'Enseignement des Géosciences de l'Environnement' (CEREGE; Aix-en-Provence, France). In accordance with the quartz-rich lithology of the samples, they were treated for the extraction of the *in situ*-produced cosmogenic nuclide $^{10}$Be.

First, magnetic minerals were discarded through magnetic separation conducted in a Frantz LB-1 magnetic separator. Once the non-magnetic fraction was isolated, it underwent several rounds of chemical attack with a 1:2 mixture of concentrated hydrochloric (HCl) and hexafluorosilicic ($H_2SiF_6$, 2/3) acids to dissolve and discard the non-quartz minerals. The remaining minerals (i.e. non-dissolved feldspar minerals) were subsequently attacked with 4–6 successive partial dissolutions with HF to remove the atmospheric $^{10}$Be and discard the remaining impurities. In order to be sure that the quartz was pure, samples were examined under a binocular microscope. As a result, ~20 g of pure quartz per sample was used to extract the $^{10}$Be (Table 2). After adding ~150 µL of an in-house manufactured (from a phenakite crystal) $^{9}$Be carrier solution

**Table 1.** Geographic location of samples, topographic shielding factor and sample thickness

| Sample name | Landform | Latitude (DD) | Longitude (DD) | Elevation (m a.s.l.)[a] | Topographic shielding factor | Thickness (cm) | Lithology | Size of the boulders largest axis (m) |
|---|---|---|---|---|---|---|---|---|
| *Valley polished surfaces* | | | | | | | | |
| ARAN-40 | Polished surface | 42.6416 | 0.9713 | 1862 | 0.9630 | 3.7 | Granodiorite | |
| ARAN-39 | Polished surface | 42.6393 | 0.9701 | 1900 | 0.9640 | 5.0 | Granodiorite | |
| *Valley external moraines* | | | | | | | | |
| ARAN-38 | Moraine boulder | 42.6296 | 0.9624 | 2079 | 0.9759 | 4.2 | Granite | 3.5 |
| ARAN-37 | Moraine boulder | 42.6299 | 0.9620 | 2075 | 0.9752 | 3.0 | Granite | 3 |
| *Valley internal moraines* | | | | | | | | |
| ARAN-28 | Polished surface | 42.6263 | 0.9593 | 2188 | 1.0000 | 3.5 | Granite | |
| ARAN-27 | Moraine boulder | 42.6257 | 0.9599 | 2184 | 0.9852 | 5.0 | Granite | 4 |
| *Cirque polished surfaces* | | | | | | | | |
| ARAN-36 | Polished surface | 42.6111 | 0.9681 | 2360 | 0.9806 | 3.5 | Granite | |
| ARAN-35 | Polished surface | 42.6152 | 0.9630 | 2316 | 0.9875 | 3.2 | Granite | |
| ARAN-34 | Polished surface | 42.6224 | 0.9596 | 2266 | 0.9901 | 5.0 | Granite | |
| ARAN-31 | Polished surface | 42.6274 | 0.9536 | 2378 | 1.0000 | 3.0 | Granite | |
| *Cirque moraines* | | | | | | | | |
| ARAN-33 | Moraine boulder | 42.6275 | 0.9487 | 2470 | 0.9841 | 3.0 | Granite | 5 |
| ARAN-32 | Moraine boulder | 42.6277 | 0.9480 | 2467 | 0.9789 | 4.0 | Granite | 6 |

[a]Elevations are derived from the 5 m Digital Elevation Model of the Spanish 'Instituto Geográfico Nacional' and are subjected to a vertical accuracy of ±5 m.

(spike, concentration: $3025 \pm 9\ \mu g\ g^{-1}$; Merchel *et al.*, 2008), the purified quartz was dissolved with 48% concentrated HF (3.5 mL per g of quartz + 30 mL in excess). Following total dissolution, the resulting solution was evaporated until dryness, and the residue was recovered with HCl (7.1 molar). Be was then precipitated at pH 8 to beryllium hydroxide ($Be(OH)_2$) by means of ammonia ($NH_3$), and separated from other elements in resin columns: a Dowex 1×8 anionic exchange column to remove elements such as Fe, Mn and Ti, and a Dowex 50 W ×8 cationic exchange column to discard B and separate Be from Al (Merchel and Herpers, 1999). The final eluted Be was again precipitated, dried and oxidised to BeO at 700°C. Finally, the targets for the accelerator mass spectrometer (AMS) measurements were prepared by mixing with niobium powder at an approximate 1:1 proportion and pressing the mixture into copper cathodes.

The targets were analysed at the 'Accelerator pour les Sciences de la Terre, Environnement et Risques' (ASTER) national AMS facility at CEREGE in order to measure the $^{10}Be/^{9}Be$ ratio from which the $^{10}Be$ concentration was later inferred (Table 2). AMS measurements were calibrated against the in-house standard STD-11 with an assigned $^{10}Be/^{9}Be$ ratio of $(1.191 \pm 0.013) \times 10^{-11}$ (Braucher *et al.*, 2015). Based on calibration with the previous ASTER AMS standard NIST-27900 (SRM4325), the new STD-11 is fully compatible with 07KNSTD. The analytical 1σ uncertainties include uncertainties in the AMS counting statistics, an external 0.5% AMS error (Arnold *et al.*, 2010) and the uncertainty related to the chemical blank correction. The $^{10}Be$ half-life considered was $(1.3870 \pm 0.0012) \times 10^{6}$ years (Chmeleff *et al.*, 2010; Korschinek *et al.*, 2010).

We calculated $^{10}Be$ exposure ages by using the CREp online calculator (Martin *et al.*, 2017; available online at: http://crep.crpg.cnrs-nancy.fr/#/), where we selected the following settings: LSD (Lifton-Sato-Dunai) elevation/latitude scaling scheme (Lifton *et al.*, 2014), ERA40 atmospheric model (Uppala *et al.*, 2005) and geomagnetic database based on the LSD framework (Lifton *et al.*, 2014). These settings yielded a worldwide mean sea level high latitude $^{10}Be$ production rate of $3.98 \pm 0.22$ atoms $g^{-1}$ $yr^{-1}$. Exposure ages of the samples with their 1σ full and analytical uncertainties are shown in Table 2. The uncertainties discussed throughout the text include analytical and production rate error unless otherwise stated.

In order to evaluate the potential impact of erosion on the exposure ages, we assumed a steady erosion rate (1 mm $ka^{-1}$) following a conservative maximum value in such a lithological setting according to André (2002). The impact of snow cover was explored assuming that snow currently remains in the area for an annual average of 7.5 months at 2200–2300 m with a mean thickness of 100 cm – and assuming a snow density of 0.2 g $cm^{-3}$ (Styllas *et al.*, 2018) – (Table 3), based on the available data from the Bonaigua weather station (Fig. 1) available since 1997–1998 (Servei Meteorològic de Catalunya; http://www.igc.cat/web/ca/allaus_gruix_neu_v2.php?e=bonaigua%26t=totes). Erosion and snow corrections, as a whole, resulted in ages that were ~9% older (~1% erosion; ~8% snow cover). However, to enable comparisons with other areas, we use the non-corrected ages throughout the text. Moreover, both the thickness and duration of snow cover must have varied significantly since the cirque's deglaciation, given the alternation of cold/warm periods and their associated moisture supplies. Finally, the chi-squared test according to Ward and Wilson (1978) was applied to the samples belonging to each geomorphological unit established on the geomorphological map (Table 1) in order to detect potential exposure age outliers (i.e. 'too old' or 'too young'; Heyman *et al.*, 2011). No outliers were detected (Table 3).

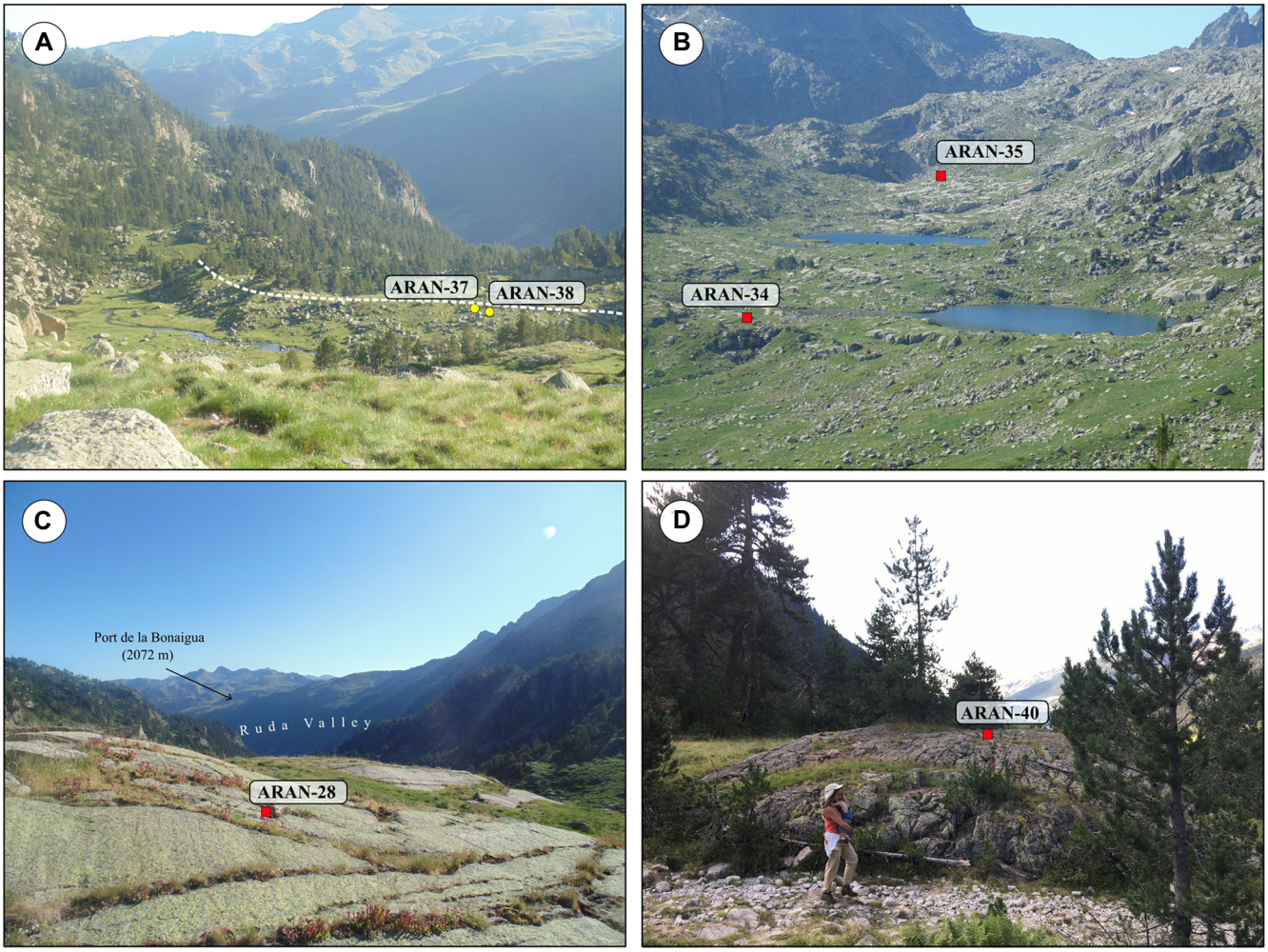


**Figure 2.** Examples of the main geomorphological landforms of glacial origin in the Ruda Valley, together with the location and typology of the dated samples: (A) terminal moraine damming a palaeolake at 2080 m; (B) north–south perspective of the Saboredo Cirque floor showing several lakes distributed in staggered overdeepened basins; (C) polished bedrock surface including striations that reveal the former glacial flow; and (D) *roches moutonnées* located in the forested valley bottom of the valley at 1860 m. [Color figure can be viewed at wileyonlinelibrary.com]

### *Glacier reconstruction and equilibrium-line altitude calculation*

A three-dimensional palaeoglacier reconstruction was performed for the different glacial phases using the 'GLaRe' ArcGIS toolbox devised by Pellitero *et al.* (2016). Former ice thickness was estimated by applying a perfect-plasticity physical-based rheological model along flowlines from the termini to the headwall (Veen Van der, 1999; Benn and Hulton, 2010). Such a toolbox requires only a flowline, a tentative palaeoglacier geometry – approximated from lateral or frontal moraines – and a digital elevation model. Ice thickness was modelled by using a constant shear stress of 100 kPa (Paterson, 1994; Benn and Hulton; 2010). The effect of lateral side drag was corrected by integrating shape factors (F-factor) obtained from cross-sections (Schilling and Hollin, 1981).

Equilibrium-line altitudes (ELAs) were calculated by using the automatic toolbox 'ELA calculation' developed by Pellitero *et al.* (2015). The selected methods were the accumulation area ratio (Porter, 1975; AARs: $0.6 \pm 0.05$) and the area altitude balance ratio (AABR; Osmaston, 2005). We considered two balance ratios for the AABR method: $1.75 \pm 0.71$ (global) and $1.9 \pm 0.81$ (mid-latitude marine glaciers) (Rea, 2009). The mean ELAs were used to discuss the palaeoclimatic implications of the identified glacier advance/stillstand phases.

## Results

The Ruda Valley preserves glacial and periglacial landforms indicative of glacial evolution during the last deglaciation in the Upper Garonne Basin. The chronological framework of this evolution is unveiled by a dataset of 12 $^{10}$Be CRE ages obtained from glacial landforms.

### *Geomorphological evidence*

The wide range of glacial features from the highest sectors to the Ruda Valley floor shows evidence that the entire valley was heavily glaciated during the lLGM and recorded several advances or stillstands within the long-term deglaciation trend. The Ruda Valley is divided into two main geomorphological units (Fig. 3):

(i) The valley floor and mountain slopes follow the typical U-shaped morphology of a glacial valley. The steep slopes, descending from ~2200 to 1800 m, connect the lateral cirques with the valley floor. The hillslopes of the valley start at the upper edge of hanging glacial cirques that define the glacial trimline, marking the uppermost extent of recent glaciations. Hillslopes are concave to rectilinear 300–400 m long sections steeper than 30° that are mostly colonised by forest (i.e. *Pinus nigra)*. The upper part of the valley is defined by two staggered, overdeepened basins filled with peatlands at mean elevations of 2150 and 2070 m. At their margins, two moraine systems

**Table 2.** AMS analytical data and calculated exposure ages. $^{10}Be/^{9}Be$ ratios were inferred from measurements at the ASTER AMS facility. Chemistry blank correction was done by subtracting the number of $^{10}Be$ atoms in the blank from that in the sample. Individual ages are shown with their full uncertainties (including analytical AMS uncertainty and production rate uncertainty) and analytical uncertainty only within brackets. Arithmetic mean ages are given with their full uncertainties (including standard deviation and production rate uncertainty) and standard deviations only in brackets.

| $^{10}Be$ samples analytical AMS data | | | | | | | | |
|---|---|---|---|---|---|---|---|---|
| Sample name | Quartz weight (g) | Mass of carrier ($^{9}Be$ mg) | ASTER AMS cathode number | $^{10}Be/^{9}Be$ ($10^{-14}$) | Blank correction (%) | [$^{10}Be$] ($10^{4}$ atoms $g^{-1}$) | Age (ka) | Mean age (ka) |
| *Valley polished surfaces* | | | | | | | | |
| ARAN-40 | 20.44 | 0.46 | CHBL | 16.34 ± 0.56 | 2.11 | 23.85 ± 0.83 | 15.0 ± 0.9 (0.5) | 14.4 ± 1.2 (0.8) |
| ARAN-39 | 21.32 | 0.45 | CHBK | 15.92 ± 0.49 | 2.18 | 22.15 ± 0.70 | 13.8 ± 0.8 (0.4) | |
| *Valley external moraines* | | | | | | | | |
| ARAN-38 | 21.11 | 0.46 | CHBJ | 17.56 ± 0.54 | 1.95 | 24.99 ± 0.79 | 13.3 ± 0.8 (0.4) | 13.5 ± 0.9 (0.2) |
| ARAN-37 | 21.38 | 0.46 | CHBI | 18.08 ± 0.87 | 1.09 | 25.74 ± 1.25 | 13.7 ± 1.0 (0.6) | |
| *Valley internal moraines* | | | | | | | | |
| ARAN-28 | 20.97 | 0.46 | CHBB | 18.79 ± 0.62 | 1.05 | 27.13 ± 0.91 | 13.0 ± 0.8 (0.4) | 13.0 ± 0.8 (0.1) |
| ARAN-27 | 20.89 | 0.45 | CHBA | 18.64 ± 0.58 | 1.85 | 26.61 ± 0.84 | 13.1 ± 0.8 (0.4) | |
| *Cirque polished surfaces* | | | | | | | | |
| ARAN-36 | 21.51 | 0.46 | CHBH | 21.24 ± 0.65 | 1.62 | 29.53 ± 0.92 | 12.7 ± 0.8 (0.4) | 12.7 ± 0.8 (0.0) |
| ARAN-35 | 21.43 | 0.47 | CHBG | 20.18 ± 0.62 | 1.65 | 29.05 ± 0.91 | 12.8 ± 0.8 (0.4) | |
| ARAN-34 | 20.85 | 0.46 | CHBF | 21.13 ± 0.66 | 1.63 | 30.35 ± 0.96 | 14.0 ± 0.8 (0.4) | |
| ARAN-31 | 21.40 | 0.44 | CHBC | 26.54 ± 0.72 | 1.35 | 35.74 ± 0.98 | 14.8 ± 0.9 (0.4) | |
| *Cirque moraines* | | | | | | | | |
| ARAN-33 | 20.26 | 0.45 | CHBE | 20.30 ± 0.68 | 1.70 | 29.92 ± 1.02 | 11.8 ± 0.7 (0.4) | 12.6 ± 1.3 (1.0) |
| ARAN-32 | 21.63 | 0.45 | CHBD | 24.19 ± 1.26 | 0.85 | 33.15 ± 1.75 | 13.3 ± 1.0 (0.7) | |
| **Chemistry blank details** | | | | | | | | |
| Blank name | Processed with | Mass of carrier ($^{9}Be$ mg) | ASTER AMS cathode number | $^{10}Be/^{9}Be$ ($10^{-14}$) | [$^{10}Be$] ($10^{4}$ atoms) | | | |
| BK-1 | ARAN-27, 31, 33, 34, 35, 36, 38, 39, 40 | 0.46 | CHAT | 0.34 ± 0.04 | 10.30 ± 1.24 | - | - | |
| BK-2 | ARAN-32 | 0.46 | CHBM | 0.20 ± 0.03 | 6.13 ± 0.80 | - | - | |
| BK-3 | ARAN-28, 37 | 0.46 | IGHI | 0.20 ± 0.03 | 5.98 ± 0.93 | - | - | |

**Table 3.** Exposure ages according to erosion and snow cover corrections

| Sample name | Exposure ages (arithmetic mean, in ka) | | | |
|---|---|---|---|---|
| | No correction | Erosion correction | Snow correction | Erosion + snow correction |
| *Valley polished surfaces* | *14.4 ± 1.2* | *14.6 ± 1.2* | *15.5 ± 1.3* | *15.7 ± 1.3* |
| ARAN-40 | 15.0 ± 0.9 (0.5) | 15.2 ± 0.9 (0.5) | 16.1 ± 1.0 (0.5) | 16.4 ± 1.0 (0.6) |
| ARAN-39 | 13.8 ± 0.8 (0.4) | 14.0 ± 0.8 (0.4) | 14.8 ± 0.9 (0.4) | 15.0 ± 0.9 (0.5) |
| *Valley external moraines* | *13.5 ± 0.9* | *13.7 ± 0.9* | *14.5 ± 1.0* | *14.7 ± 1.0* |
| ARAN-38 | 13.3 ± 0.8 (0.4) | 13.5 ± 0.8 (0.4) | 14.4 ± 0.9 (0.4) | 14.6 ± 0.9 (0.4) |
| ARAN-37 | 13.7 ± 1.0 (0.6) | 13.8 ± 1.0 (0.7) | 14.7 ± 1.0 (0.7) | 14.9 ± 1.0 (0.7) |
| *Valley internal moraines* | *13.0 ± 0.8* | *13.2 ± 0.8* | *14.1 ± 0.9* | *14.2 ± 0.9* |
| ARAN-28 | 13.0 ± 0.8 (0.4) | 13.1 ± 0.8 (0.4) | 14.0 ± 0.9 (0.5) | 14.2 ± 0.9 (0.5) |
| ARAN-27 | 13.1 ± 0.8 (0.4) | 13.3 ± 0.8 (0.4) | 14.1 ± 0.8 (0.4) | 14.3 ± 0.9 (0.4) |
| *Cirque polished surfaces* | *12.7 ± 0.8* | *12.9 ± 0.8* | *13.7 ± 0.8* | *13.9 ± 0.8* |
| ARAN-36 | 12.7 ± 0.8 (0.4) | 12.9 ± 0.8 (0.4) | 13.7 ± 0.8 (0.4) | 13.9 ± 0.8 (0.4) |
| ARAN-35 | 12.8 ± 0.8 (0.4) | 12.9 ± 0.8 (0.4) | 13.8 ± 0.8 (0.4) | 14.0 ± 0.8 (0.4) |
| ARAN-34 | 14.0 ± 0.8 (0.4) | 14.2 ± 0.9 (0.4) | 15.1 ± 0.9 (0.5) | 15.3 ± 0.9 (0.5) |
| ARAN-31 | 14.8 ± 0.9 (0.4) | 15.1 ± 0.9 (0.4) | 16.0 ± 0.9 (0.4) | 16.2 ± 0.9 (0.4) |
| *Cirque moraines* | *12.6 ± 1.3* | *12.7 ± 1.4* | *13.5 ± 1.4* | *13.7 ± 1.5* |
| ARAN-33 | 11.8 ± 0.7 (0.4) | 12.0 ± 0.8 (0.4) | 12.7 ± 0.8 (0.4) | 12.9 ± 0.8 (0.4) |
| ARAN-32 | 13.3 ± 1.0 (0.7) | 13.5 ± 1.0 (0.7) | 14.3 ± 1.0 (0.7) | 14.5 ± 1.0 (0.7) |

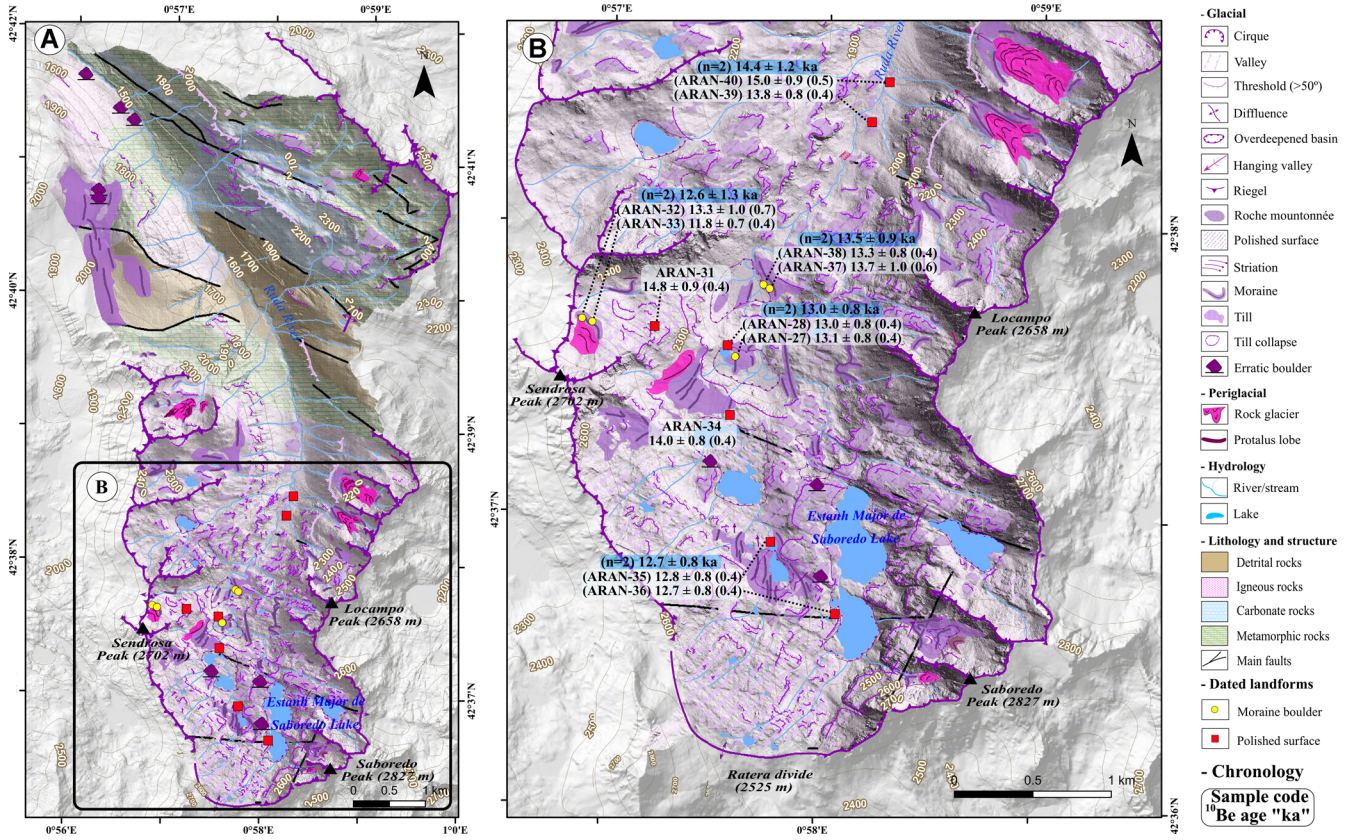


**Figure 3.** (A) Geomorphological map of the study area, with the location of the cosmic-ray exposure samples; and (B) enlargement of the highest parts of the cirque including the location of the $^{10}$Be ages. [Color figure can be viewed at wileyonlinelibrary.com]

occur at 2190 and 2080 m. Two samples were collected from boulders from the external frontal moraine (ARAN-38 and ARAN-37) and the other two were obtained from the internal moraine unit: one from a boulder on the moraine ridge (ARAN-27), and the other from a polished surface with glacial striae (ARAN-28) and moraine boulders (Fig. 4). The lowest part of the valley floor, with a relatively flat slope characteristic of U-shaped glacial valleys and descending from ~1800 to 1500 m, is colonised by alpine meadows and coniferous forests. Isolated *roches moutonnées* are found in the highest section of the valley bottom where granites prevail (>~1800 m), while they are absent in lower areas, where slates and marbles are the dominant lithology. Two samples were collected from polished surfaces at 1900 and 1860 m (ARAN-39 and ARAN-40).

(ii) The highest peaks of the Ruda Valley surrounding the Saboredo Cirque range from 2700–2800 m (Sendrosa and Saboredo peaks) to 2525 m in the mountain divide that may have functioned as a glacial diffluence pass between the Saboredo (Garonne basin) and the Ratera cirques (Noguera

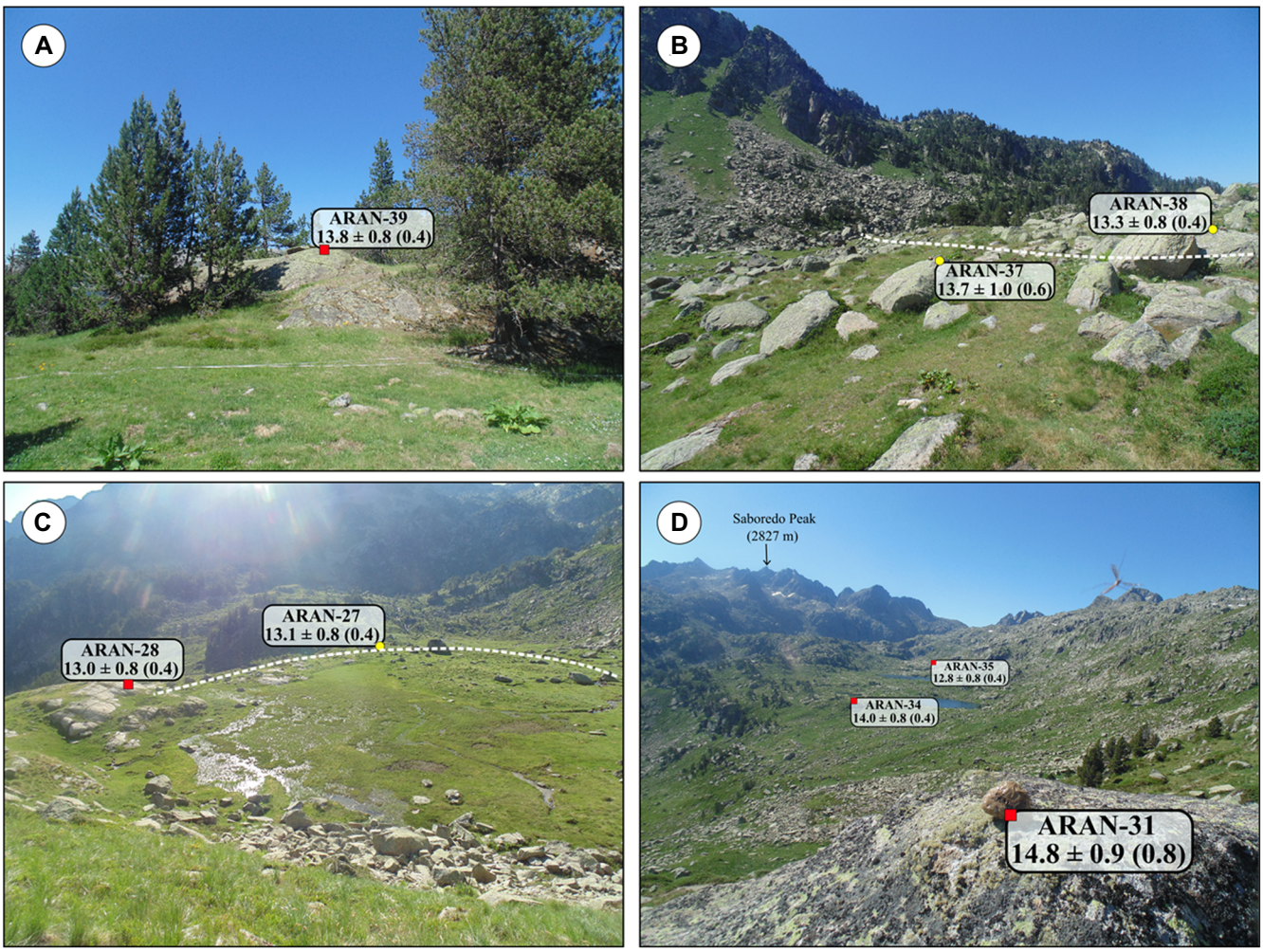


**Figure 4.** Examples of sampled moraines and polished bedrock surfaces, together with cosmic-ray exposure ages (ka). [Color figure can be viewed at wileyonlinelibrary.com]

Pallaresa basin) (Fig. 3). Saboredo is a complex cirque (Barr and Spagnolo, 2015) that includes several minor hollows carved out on the marginal flanks of the peaks. They are separated by truncated spurs with polished surfaces, where one sample (ARAN-31) was collected to examine the timing of glacial thinning at the cirque level. The highest moraines in the Ruda Valley are located at ~2400–2500 m, at the foot of the highest peaks. A prominent cirque moraine at an altitude of 2470 m is located on the eastern slope of the Sendrosa peak; here, we collected two samples (ARAN-33 and ARAN-32). Above the upper moraines, fed by abundant debris supply from the cirque rock walls, rock glaciers and protalus lobes are found. The cirque floors extend between 2200 and 2400 m and preserve features indicative of intense glacial erosion (e.g. overdeepened basins or glacial thresholds) and glacial deposits (e.g. moraines or erratic boulders). In the Saboredo Cirque, glacial abrasion and periglacial processes shaped a large amphitheatre with several overdeepened basins. They are surrounded by polished surfaces and occupied by peatlands and lakes. Three samples were collected from polished surfaces from 2360 to 2270 m (Fig. 3) (ARAN-36; ARAN-35; ARAN-34; Fig. 2; Table 1). Glacial retreat left scattered boulders and till across the area.

## *Geochronological data*

The 12 CRE samples collected from the Ruda Valley returned a chronology spanning from ~15 ± 0.9 to 11.8 ± 0.7 ka, with all ages being consistent with the geomorphological distribution of the dated surfaces (Fig. 4).

Polished surfaces from the highest parts of the Ruda Valley located ~200–250 m below the cirques provided CRE ages of 15.0 ± 0.9 (ARAN-40) and 13.8 ± 0.8 ka (ARAN-39, Fig. 4A) (mean: 14.4 ± 1.2 ka). A similar age was obtained from a sample collected from a truncated spur dividing the Sendrosa and Saboredo cirques, which yielded 14.8 ± 0.9 ka ka (ARAN-31). A sample collected from a polished surface at the edge of the Saboredo Cirque floor (Fig. 3) reported an age of 14.0 ± 0.8 ka (ARAN-34, Fig. 4D).

Moraine boulders from the external moraine located in the lower overdeepened basin yielded ages of 13.3 ± 0.8 (ARAN-38) and 13.7 ± 1.0 ka (ARAN-37) (mean: 13.5 ± 0.9 ka). A boulder from the internal moraine ridge located 110 m above the former moraine provided an age of 13.1 ± 0.8 ka (ARAN-27); this age was compared with a sample from a polished surface which correlates with the internal moraine (Fig. 4C) that returned an age of 13.0 ± 0.8 ka (ARAN-28), which agrees with the latter.

Two samples from polished surfaces of the Saboredo Cirque above 2300 m yielded ages of 12.8 ± 0.8 (ARAN-35) and 12.7 ± 0.8 ka (ARAN-36) (mean: 12.7 ± 0.8 ka). The highest moraines are located inside the highest cirque hollows, such as the Sendrosa hollow. Here, two moraine boulders yielded ages of 11.8 ± 0.7 (ARAN-33) and 13.3 ± 1.0 ka (ARAN-32) (mean: 12.6 ± 1.3 ka).

## *Reconstructed palaeoglaciers and ELAs*

The ELAs of the three reconstructed palaeoglacier extents were calculated for the Ruda catchment. The palaeoglacier existing at

**Table 4.** Reconstructed equilibrium-line altitudes (m a.s.l.) for the middle, late Bølling–Allerød and Younger Dryas moraines using the accumulation area ratio and area altitude balance ratio methods

| Phase | Glacier | AAR(0.6 ± 0.2) | AABR(1.9 ± 0.81) | AABR (1.7 5 ± 0.71) | Mean ELA |
|---|---|---|---|---|---|
| **Valley external moraines (middle B–A; GI-1c)** | **Ruda** | 2481 ± 20 | 2449 −30/+20 | 2454 −30/+15 | 2461 |
| **Valley internal moraines (transition B–A/YD; GI-1b)** | **Ruda** | 2515 −15/+10 | 2498 −25/+15 | 2503 −25/+20 | 2505 |
| **Cirque moraines (early YD)** | **Sendrosa** | 2568 −10/+5 | 2571 −15/+5 | 2576 ± 10 | 2571 |

AABR: area altitude balance ratio; AAR: accumulation area ratio; B–A: Bølling–Allerød; ELA: equilibrium-line altitude; YD: Younger Dryas.

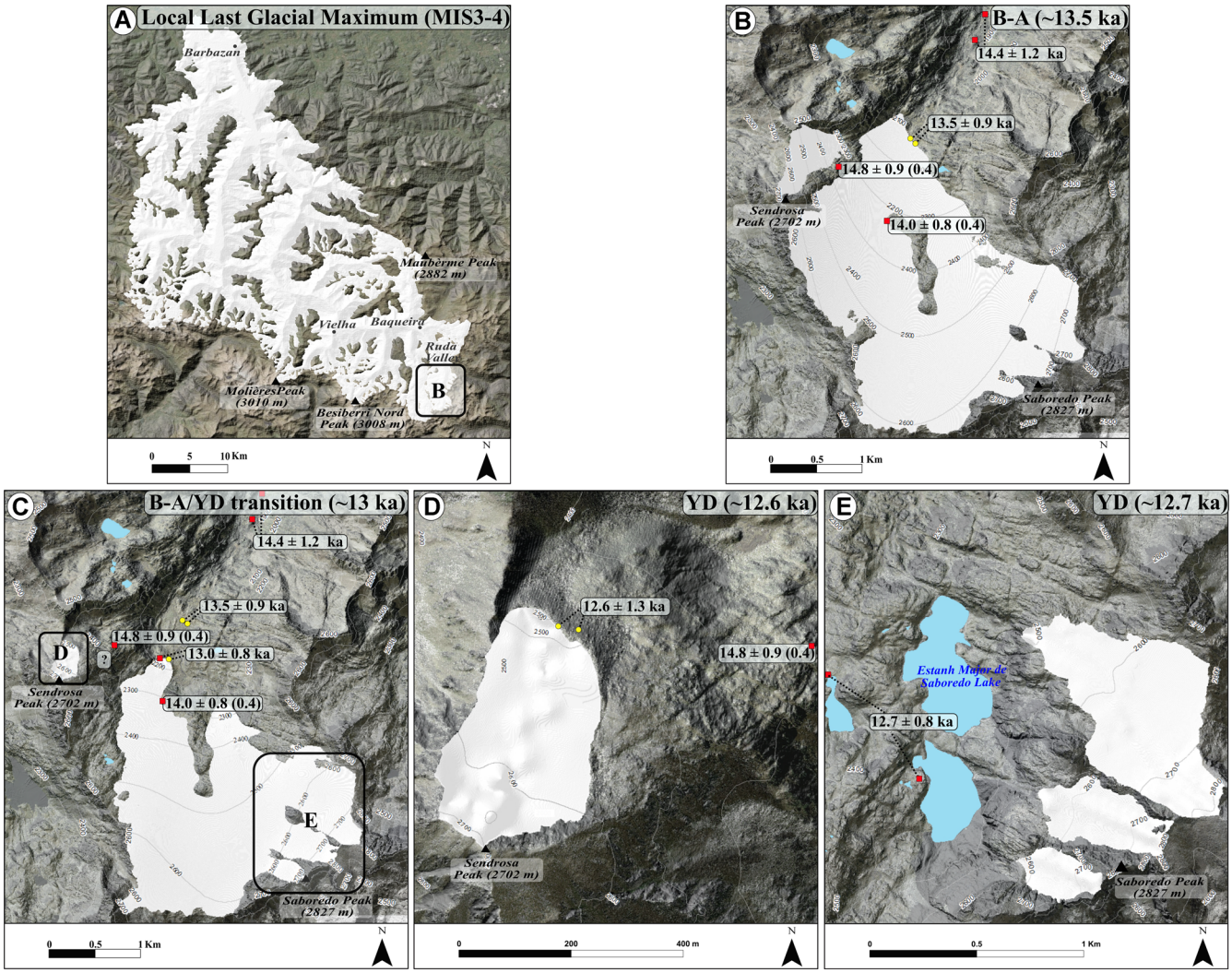


**Figure 5.** Reconstruction of the glacial extent during the different time stages: (A) extensive glaciers occupying the entire Upper Garonne Basin during the local Last Glacial Maximum based on the reconstruction of Fernandes *et al.* (2017); (B) glacial extent during the mid Bølling–Allerød (B–A) at ~13.5 ka in the Ruda Valley; (C) glacier flowing from the Saboredo Cirque during the transition between the late B–A and the early Younger Dryas (YD) at ~13 ka; and (D) small glaciers confined within the highest hollows next to the Sendrosa (D) and Saboredo (E) peaks during the early YD at ~12.7/12.6 ka. [Color figure can be viewed at wileyonlinelibrary.com]

13.5 ± 0.9 ka deposited a moraine system at 2080 m, with a mean ELA located at 2461 m (Table 4). The palaeoglacier at 13.0 ± 0.8 ka formed a moraine at 2190 m, with a mean ELA at 2505 m. Finally, the Sendrosa Cirque moraine located at 2470 m was dated at 12.6 ± 1.3 ka, with an ELA of 2571 m (Table 4).

## Discussion

### *Interpretation of the geomorphological observations and CRE results*

The geomorphological analysis supported by $^{10}$Be dating of glacial landforms show the spatial and temporal patterns of the deglaciation between the B–A and the early YD in the Ruda Valley (Fig. 5). Although the CRE dataset is consistent with sequence of glacial landforms, uncertainty remains in assigning ages either to the late B–A or to the early YD.

The ages of samples from polished surfaces in the valley at 1860–1900 m (ARAN-40 and ARAN-39; 14.4 ± 1.2 ka) suggest that the beginning of glacial retreat in the Ruda Valley took place during the B–A. As glaciers retreated, they became confined within their respective cirques, as revealed by the age of 14.8 ± 0.9 ka (ARAN-31) of a polished surface on the ridge dividing the Sendrosa and Saboredo cirques (Fig. 3). The sample from an outcrop on the lower edge of the cirque (ARAN-34; 14.0 ± 0.8 ka ka) indicates that ice covered the entire Saboredo Cirque floor until ~14 ka ka.

The sampled boulders of the external moraine system (ARAN-38 and ARAN-37) showed statistical coherence based on the chi-squared test following Ward and Wilson (1978) and suggested a glacier advance or stillstand at 13.5 ± 0.9 ka. The age of 13.0 ± 0.8 ka from a moraine boulder (ARAN-27) and an adjacent polished surface (ARAN-28) of the internal moraine system indicate another short advance or stillstand, which is also consistent with the geochronological sequence. These results from staggered moraine systems at ~2080 and ~2190 m provided chronologically consistent mean ages within the B–A, but based on their distinct relative position they have been ascribed to two different stages. Nevertheless, during this period, glaciers flowed from the Saboredo and Sendrosa cirques and generated moraines on the lower overdeepened basins.

According to the ages of samples from the highest surfaces of the Saboredo Cirque floor at 2320–2360 m (ARAN-35 and ARAN-36; 12.7 ± 0.8 ka), the entire cirque floor was deglaciated at the onset of the YD. These ages are consistent with those of the samples from the highest dated moraine cirques in the Sendrosa Cirque at 2460–2470 m (ARAN-32 and ARAN-33), which was also abandoned by the ice by 12.6 ± 1.3 ka. No statistical inconsistency was detected in the exposure ages from this moraine.

## The chronology of deglaciation

During the lLGM, the Garonne glacier flowed ~80 km reaching the Loures-Barousse-Barbazan basin, where it formed a terminal moraine system (Fernandes *et al.*, 2017; Stange *et al.*, 2014). Until the onset of deglaciation, 300–400 m thick ice sat in the Ruda Valley, as shown by the highest lateral moraines between the Ruda and Aiguamòg valleys. This ice thickness must have favoured the occurrence of warm-based glaciers, thus implying basal sliding evidenced by striations on the bedrock surface. Hence, no nuclide inheritance from previous exposure periods is expected at the sampled surfaces.

Samples from polished surfaces from the bottom of the Ruda Valley at 1860–1900 m indicate that by 14.4 ± 1.2 ka, i.e. during the B–A, the glacier was retreating towards the glacial cirque, and was already disconnected from the main Ruda glacier. Consequently, one third of the Ruda Valley was already deglaciated at that time, indicating that by the early B–A the Garonne glacier had only ~5% of the length that it had during the lLGM (Fernandes *et al.*, 2017).

As glaciers retreated and thinned during the B–A, ice masses became individualised within their respective cirques, and the valley glaciers flowing from Sendrosa and Saboredo cirques merged only in the lowest overdeepened basins (Fig. 3). As conditions were less favourable, glaciers receded to higher elevations and the Sendrosa and Saboredo palaeoglaciers became isolated in their respective basins by 14.8 ± 0.9 ka (Fig. 3). The ice covered the entire Saboredo Cirque floor until ~14 ka, as revealed by the sample collected from an outcrop on the edge of the cirque (14.0 ± 0.8 ka), indicating that glacial recession in the Ruda Valley was underway at ~15–14 ka. Similarly, a rapid deglaciation was also recorded at ~15–14 ka in the nearby Bacivèr Cirque, which favoured its complete deglaciation (Fig. 1; Oliva *et al.*, 2021a).

The strong clustering of ages at between ~13.5 and 12.7 ka confirms the dynamic environmental response of the Ruda palaeoglaciers to the abrupt climate transition between the B–A and the early YD. However, our CRE dataset cannot assess the magnitude and patterns of glacial recession during the early B–A in the Ruda Valley, or whether the entire cirque was deglaciated and glaciers reformed and subsequently advanced. Our results suggest, however, that the millennial-scale trend towards glacier recession during the B–A was interrupted by two glacial advances or stillstands with moraine development at 13.5 ± 0.9 and 13.0 ± 0.8 ka (Fig. 5). Samples from moraines located at average elevations of ~2080 and ~2190 m, respectively, indicated the existence of valley glaciers 3.5 and 2.5 km long during the middle of the B–A and during the transition from the B–A to the YD. Indeed, the reconstructed glacial surface for both bases was of 4.4 and 3.8 $km^2$, respectively, with a maximum ice thickness of 300 and 200 m for each of these phases (Fig. 6a, b).

Evidence of glacial recession during the middle of the B–A was also recorded on polished surfaces from the neighbouring Bacivèr Cirque at 13.5 ± 0.8 ka (Oliva *et al.*, 2021a). Local topographical factors, such as the shape of the cirque floor (convex versus concave areas) determined the pattern of glacial flow of thin ice masses during the glacial advances/stillstands that occurred during the B–A. Glaciers flowed downwards from the cirque through concave areas across the western slope, favouring the development of the moraine arcs and crests in lower overdeepened basins (Fig. 3). It is likely that the topography played a major role in determining the process and timing of the deglaciation in both cirques: the accumulation area above 2400 m is larger in the Saboredo Cirque (552 ha) with respect to the Bacivèr Cirque (244 ha) and its prevailing aspect is also more favourable for ice persistence (north vs west).

The Saboredo Cirque floor became ice-free at the beginning of the YD, as revealed by the samples from polished surfaces of the cirque floor at ~2350 m (mean age = 12.7 ± 0.8 ka). The evidence of glacial striations on the rock surface makes the possibility of nuclide inheritance at the sampling sites unlikely. Glaciers might thus also have persisted during the early YD in the highest hollows of the Saboredo Cirque, as was the case in the northern cirque of Sendrosa Peak. Here, the cirque moraine at 2470 m, formed by a 0.4 km long glacier (with a surface of 0.7 $km^2$ and a thickness of 90 m; Fig. 6c), was abandoned at 12.6 ± 1.3 ka. Inside the highest glacial cirques of the Ruda Valley, there are numerous relict rock glaciers and protalus lobes indicative of the past occurrence of permafrost during their formation (Fernandes *et al.*, 2018). As in most of the Pyrenees, these are probably glacier-derived permafrost features associated with the paraglacial phase, when glacial shrinking favoured wall debuttressing, a high debris supply and the subsequent burial of the residual ice masses (Andrés *et al.*, 2018; Oliva *et al.*, 2016).

In short, by the early B–A the Garonne palaeoglacier had receded ~95% of its ~80 km length of the lLGM (Fernandes *et al.*, 2017; Stange *et al.*, 2014). The Ruda palaeoglacier receded 4 km in only ~1.7 ka (~14.4 to ~12.7 ka) from an elevation of ~1800 to >2400–2500 m. This trend towards glacial shrinking before the final ice disappearance was interrupted by three phases of glacier advance or stillstands at 13.5 ± 0.9, 13.0 ± 0.8 and 12.6 ± 1.3 ka, which generated moraines at ~2080, 2190 and 2470 m, respectively.

## Late Quaternary glacial dynamics in the Central Pyrenees and Iberian Peninsula in the context of European glacial evolution

The scientific knowledge on the chronology of the last deglaciation in the Pyrenees has experienced substantial advances over recent years in parallel to progress on glacial chronological constraints in other European and Iberian mountain ranges (García-Ruiz *et al.*, 2010; Palacios and García-Ruiz, 2015). There is increasing evidence that the timing of glacial oscillations during T-1 across Europe followed a similar sequence (Palacios *et al.*, 2021): a significant glacier

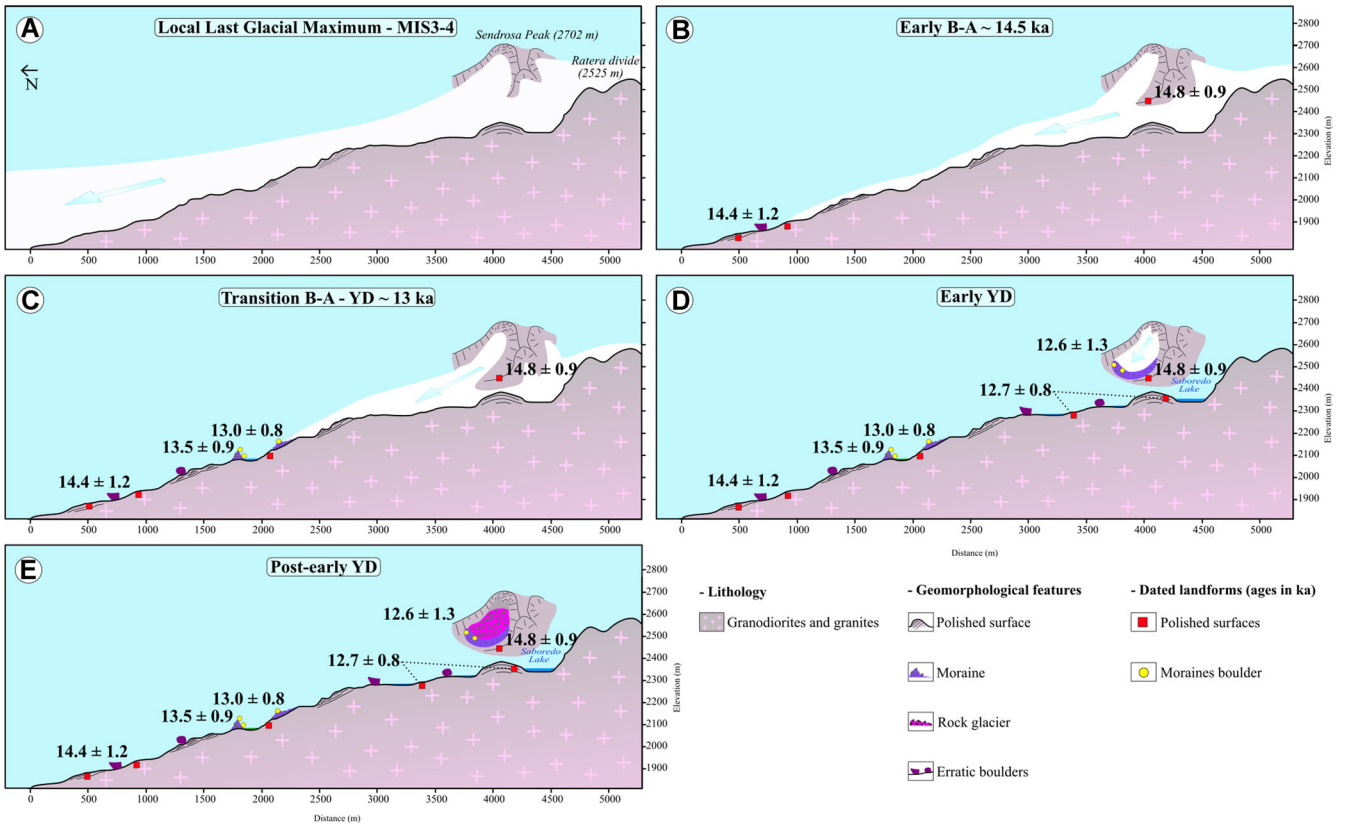


**Figure 6.** Schematic evolution of the glacial phases recorded in the Ruda Valley during the last glacial cycle: (A) extensive and thick glaciers inundated the valley and only a few nunataks protruded the ice during the local Last Glacial Maximum; (B) warm temperatures in the early Bølling–Allerød (B–A) favoured glacial recession, and subsequently the lowest areas of the valley as well as some rock outcrops of the cirque became exposed; (C) glacial advances/stillstands formed moraines during the B–A and at the transition to the Younger Dryas (YD); (D) small glaciers persisted during the early YD in the highest north-facing cirques; and (E) subsequent temperature increases favoured complete deglaciation and triggered paraglacial dynamics, which promoted the formation of rock glaciers in the recently deglaciated ice-free cirques. [Color figure can be viewed at wileyonlinelibrary.com]

advance took place during the OD followed by a rapid retreat during the B–A and a subsequent more limited glacier advance during the YD (Oliva *et al.*, 2019).

Dated evidence of glacial responses in the Pyrenees to Northern Hemisphere cold events during T-1 have mostly focused on the southern slopes (Oliva *et al.*, 2019), although there is an increasing body of new data from the northern slopes of the range that confirms glacial advances and stillstands there during the OD and YD, and glacial shrinking during the B–A (Reixach *et al.*, 2021). The elevation of the peaks as well as the topography of the cirques played a major role in the duration and intensity of the glaciation during T-1 in the high massifs of the Pyrenees. Cirques surrounded by peaks above 2800–2900 m likely included glaciers during most of T-1 until the onset of the Holocene (see e.g. Jomelli *et al.*, 2020; Pallàs *et al.*, 2006; Reixach *et al.*, 2021), while those situated at the foot of lower peaks (i.e. 2500–2600 m) were completely deglaciated during the B–A (Oliva *et al.*, 2021a; Palacios *et al.*, 2017b). Following ice retreat, the slopes were affected by intense readjustments (large, catastrophic rock slope failures, rock slope deformations, rockfalls and rockslides), particularly in areas where the local lithostructure was prone to instability (Fernandes *et al.*, 2020).

In the Central Pyrenees, a period of glacial growth occurred during the OD after the massive deglaciation that took place following the LGM. Moraines dated at 17–15 ka have been reported in the highest valleys of the main massifs, such as in the Ariège (Delmas *et al.*, 2011; Jomelli *et al.*, 2020; Reixach *et al.*, 2021), Ésera (Crest *et al.*, 2017), Gállego (Palacios *et al.*, 2015a), Malniu (Andrés *et al.*, 2018; Palacios *et al.*, 2015b; Pallàs *et al.*, 2010), Têt (Delmas *et al.*, 2008; Tomkins *et al.*, 2018), Aránser (Andrés *et al.*, 2018; Palacios *et al.*, 2015b) and Bassiès (Crest *et al.*, 2017). During that time, glaciers flowed downslope from the headwaters of the highest valleys, with valley glaciers often exceeding 10–15 km (Oliva *et al.*, 2019). Consequently, it is likely that by that time, most of the Ruda Valley was still glaciated, with the ice tongue probably merging with the main Garonne palaeoglacier that was also fed by neighbouring glacier tributaries, such as those descending from the Beret area (Oliva *et al.*, 2021a). Some of the lateral moraine remnants distributed on the left side of the Garonne Valley, *ca.* 20 km from the highest parts of the Saboredo Cirque, formerly attributed to the OD (Fernandes *et al.*, 2017, 2021) may be also correlated with some of the highest moraines and erratic boulders distributed in the Ruda Valley (Fig. 3). Other Iberian mountain ranges include geomorphic evidence of glacial advances during the OD (Palacios *et al.*, 2017a), such as in the Monasterio Valley in the Cantabrian Mountains (Serrano *et al.*, 2016), Peña Negra Valley in the Iberian Range (García-Ruiz *et al.*, 2020), Peñalara massif in the Central Range (Palacios *et al.*, 2012a), San Juan Valley in the Sierra Nevada (Palacios *et al.*, 2016), En Garcia Valley in the Eastern Pyrenees (Reixach *et al.*, 2021) and Gállego and Ésera valleys in the Central Pyrenees (Crest *et al.*, 2017; Palacios *et al.*, 2017b).

No moraine remnants have been found in the lowest and central sections of the Ruda Valley, and the prevailing lithology of slates and marbles in this area is not favourable for the preservation of glacially abraded surfaces. Indeed, the neighbouring Bacivèr Cirque was also completely deglaciated by ~15–14 ka (Oliva *et al.*, 2021a). Thus, our data cannot confirm whether small glaciers persisted in the highest parts of

the Ruda Valley during the B–A, although CRE ages support climatic conditions during the early B–A that were unfavourable for the maintenance of the OD ice masses (Fig. 7). In other valleys of the Pyrenees, glaciers also receded rapidly at ~14.6–14 ka as shown by CRE ages from polished surfaces and scattered erratic boulders in the Ariège (14.4 ± 1.1, 14.1 ± 0.7, 14.0 ± 0.8 ka; Delmas *et al.*, 2011), Gállego (14.6 ± 2.3 ka; Palacios *et al.*, 2015a) and Ésera valleys (14.3 ± 0.5 ka; Crest *et al.*, 2017). Locally, some massifs of the Pyrenees were fully deglaciated during the B–A, with small glaciers persisting only in the highest cirques (Delmas, 2015). A similar pattern was detected in other Iberian ranges, such as in the Sierra Nevada (Palacios *et al.*, 2016), Cantabrian Mountains (Rodríguez-Rodríguez *et al.*, 2017) and the Iberian Range (García-Ruiz *et al.*, 2020), where ice masses shrank significantly by ~15–14 ka. Glacial retreat in the Iberian mountains was triggered by the sudden temperature increase of 3–5°C at the onset of the B–A in western Europe, as inferred from climate models (Renssen and Isarin, 2001). In parallel, significant shifts occurred in the Atlantic Meridional Overturning Circulation (Obase and Abe-Ouchi, 2019). In north Iberia, a maximum increase of the mean annual temperature of 7.5°C at the onset of GI-1 has been estimated in northern Iberia, based on the Ostolo cave speleothem isotopic record (Bernal-Wormull *et al.*, 2021). Marine records from the western Iberian margin also pointed to 5–6°C of warming at the onset of the B–A (Martrat *et al.*, 2007). These warmer conditions also favoured the recession of glaciers across most European mountain ranges, such as in the Alps at 15.9–14.3 cal ka BP (Ivy-Ochs, 2015), Tatra Mountains at 14.8–14.2 ka (Zasadni *et al.*, 2020), Taurus Mountains at 14.6 ± 2.8 ka (Ciner and Sarikaya, 2015), as well as the Scandinavian Ice Sheet, which recorded a shrinking trend starting at 14.6 cal ka BP (Mangerud *et al.*, 2013).

However, the B–A was a climatically unstable period characterised by an alternation of warm and cold temperatures (Rasmussen *et al.*, 2014). The gradual decrease of temperatures from the early to the late B–A was depicted by periods of enhanced cold conditions in the high latitudes of the Northern Hemisphere, which also favoured periods of glacial growth in the Pyrenees (Table 5). Indeed, CRE results indicate the formation of moraines in the Ruda Valley at 13.5 ± 0.9 and 13.0 ± 0.8 ka (Fig. 7). These CRE ages are consistent with the chronostratigraphic sequence but must be taken as approximate due to their uncertainty ranges and the low number of dated samples at each moraine. At that time, small ice tongues ~3 km long flowed downslope from the main Saboredo Cirque as well as from other neighbouring glacial hollows to overdeepened basins, forming moraines at 2080 and 2190 m, respectively. Whereas evidence of phases of glacier advance or stillstands during the transition from the late B–A to the early YD were already found in other cirques in the Central Pyrenees, such as in the Bacivèr Cirque (Oliva *et al.*, 2021a), and in the Cuerpo de Hombre Valley (Sierra de Gredos, Central Range), with moraine stabilisation at 13.1 ka (Carrasco *et al.*, 2015), this is the first study that reports geochronological evidence of a phase with glacial development in the second half of the B–A after the long-term cooling initiated at ~14.5 ka (Fig. 7; Table 5). A few studies in Europe have also found evidence of glacier advances or stillstands during the middle B–A, such as in the Tatra Mountains where moraines stabilised at 13.4 ± 0.5 ka (Engel *et al.*, 2017). By contrast, geomorphic evidence of a period of glacial expansion during the transition between the B–A and the early YD was detected in several regions, such as in the Hardangerfjorden–Herdla area, western Norway, where a till deposit suggested a glacier advance of the Scandinavian Ice Sheet at 13.5–13.0 ka (Mangerud *et al.*, 2016), and in the West Highland and Mull ice fields of the Scottish Highlands, where 18 $^{14}$C dates from organic fragments found in basal tills revealed a glacial readvance from the end of the B–A or earliest YD (Bromley *et al.*, 2018), although these results are considered controversial (Small and Fabel, 2016).

Based on the position of these two moraine ridges, the ELA in the Ruda Valley glacier must have been located at 2461 and 2505 m during the glacial advances of the second part of the B–A and the late B–A or early YD, respectively. Considering that the regional ELA in the Pyrenees currently lies at approximately 3100 m (Jomelli *et al.*, 2020; René, 2011), the ELA must have been located 639–595 m lower than present-day conditions. Assuming an average lapse rate of 0.65°C 100 m$^{-1}$ and no change in precipitation, we infer that summer temperatures must have been 4.2 and 3.9°C lower than the present day during these two phases (Table 4).

The temperature decrease during the early YD favoured the persistence of glaciers inside the highest hollows in the Ruda Valley, depositing moraines at ~2400–2500 m, which were later abandoned by the ice at 12.6 ± 1.3 ka (Fig. 7). The existence of glaciers at high altitudes of the Saboredo Cirque is also confirmed by polished surfaces at elevations of 2200–2300 m that were dated at 12.7 ± 0.8 ka. In the neighbouring Bacivèr Cirque, moraines at 2400 m were abandoned by the ice at 12.8 ka (Oliva *et al.*, 2021a). The elevation difference between the ELA during the YD (2571 m) in the Ruda Valley and present-day values indicates that summer temperatures were ~3.4°C lower during that cold phase (Table 4), which is very similar to the ~3.0°C inferred for the Bacivèr Cirque (Oliva *et al.*, 2021a). Indeed, topoclimatic factors must have played a key role in maintaining small glaciers during the YD at the foot of steep cirque walls, where shading and snow accumulation allowed the longer persistence of reduced ice masses (Boston and Lukas, 2019). In the Pyrenees, YD glacial advances have been detected in cirques of the central (Delmas, 2009; Delmas *et al.*, 2008; García-Ruiz *et al.*, 2016a) and eastern sectors (Crest *et al.*, 2017; Jomelli *et al.*, 2020; Pallàs *et al.*, 2010; Reixach *et al.*, 2021), where 2–3.5 km long glaciers formed at 12.9–11.2 ka. Based on chronostratigraphic data from a variety of sources, evidence of YD glacial advances was also recorded in the highest cirques of other Iberian massifs, although no direct ages are yet available (García-Ruiz *et al.*, 2016a). This is true for the northwestern ranges (Cowton *et al.*, 2009) and the Cantabrian Mountains (Pellitero *et al.*, 2019; Serrano *et al.*, 2015), where moraines above 1800 and 2000 m, respectively, were associated with this cold phase. In the Sierra Nevada, YD moraines dated at 13–12 ka are located in the highest cirques facing east from 2350 (north face) to 2800 m (south face) (Oliva *et al.*, 2014; Palacios *et al.*, 2016). These glacial advances were driven by a temperature cooling quantified at 2–4°C in western Europe that was triggered by a slowdown of the overturning circulation in the North Atlantic (Renssen *et al.*, 2018). In the Pyrenees, the YD was the coldest period of the last deglaciation recorded by a decrease of $^{18}$O in the Ostolo and Seso speleothems that might reflect the temperature decrease of ~5°C (Bartolomé *et al.*, 2015; Bernal-Wormull *et al.*, 2021). Colder conditions also favoured glacial growth in other mountainous regions of Europe, with widespread advances across the Alps between 13.5 and 12 ka (Ivy-Ochs, 2015; Ivy-Ochs *et al.*, 2009), in the Tatra Mountains where moraines stabilised at 11.9 ± 0.5 ka (Engel *et al.*, 2017) and in Turkey where they formed at 12.6 ± 2.3 ka (Ciner and Sarikaya, 2015).

The final deglaciation of the cirques favoured paraglacial dynamics and the formation of the numerous rock glaciers existing today in the Saboredo and Sendrosa cirques, as well as

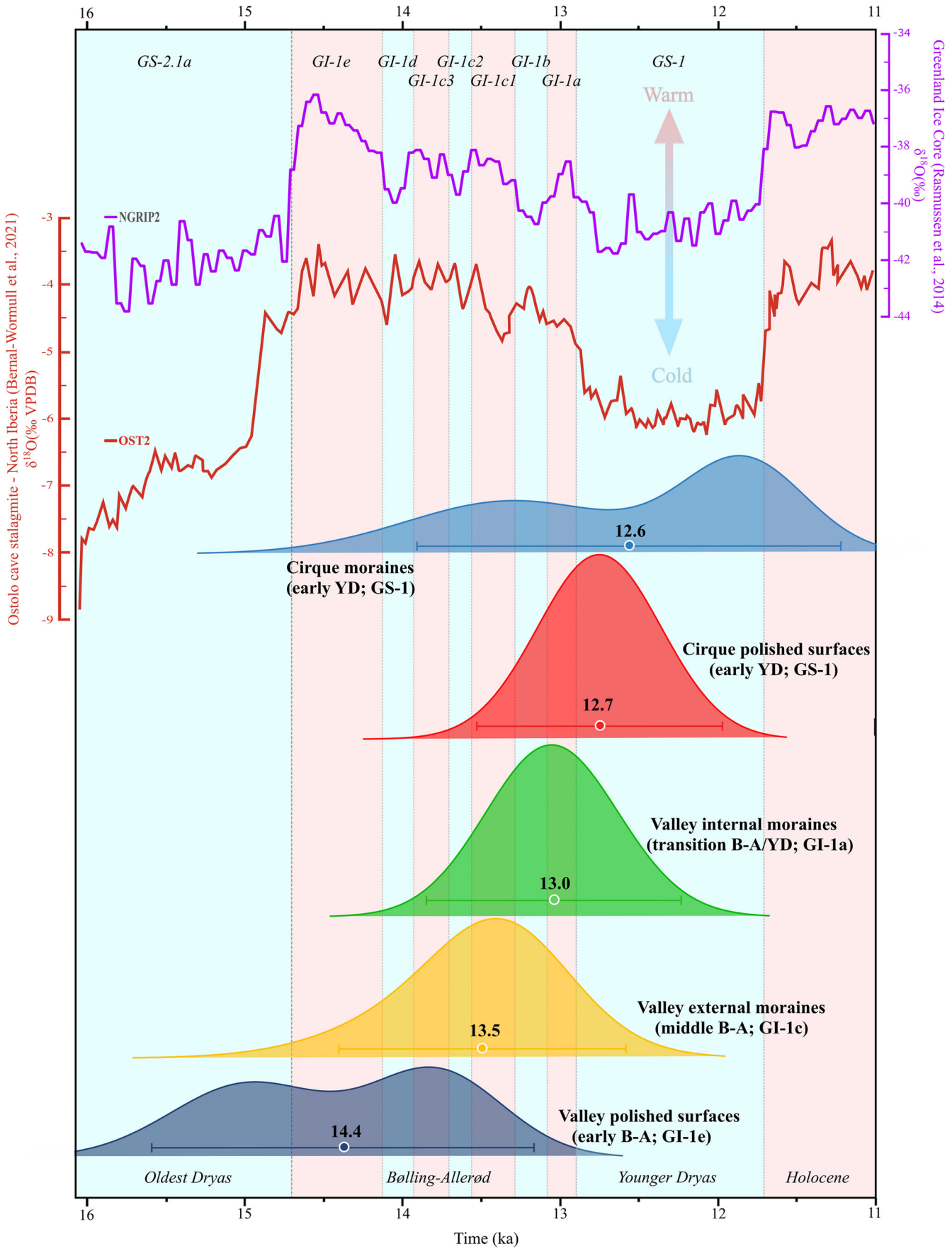


**Figure 7.** Normalised probability distribution functions (PDF) of surface exposure ages vs. temperature evolution from the Oldest Dryas to the early Holocene based on the $\delta^{18}O$ record from the NGRIP ice core from Greenland and the $\delta^{18}O$ record from the speleothem of the Ostolo cave in north Iberia (time periods are defined after Rasmussen *et al.* (2014)). The plots of the units result from the sum of the individual PDF of the samples belonging to them; cold (warm) phases are represented by the blue (red) bands. [Color figure can be viewed at wileyonlinelibrary.com]

**Table 5.** Glacial response in the Ruda Valley during the Bølling–Allerød Interstadial according to the reconstructed climate in Greenland and the Iberian Peninsula

| Phase (ages in ka) | Climate trend in Greenland based on ice core records (Rasmussen *et al.*, 2014) | Glacier response in the Ruda Valley | Climate in the IberianPeninsula based on other independent proxies |
|---|---|---|---|
| GI-1e (14.7–14.1) | Abrupt warming (3–5°C) | Rapid recession at ~15–14 ka | Gradual warming in northern Iberia at 15.4–13.4 cal ka BP (Moreno *et al.*, 2010). Warming conditions in the Pyrenees at 14.7–14.0 cal ka BP (González-Sampériz *et al.*, 2006). |
| GI-1d (14.1–14.0) | Short cold reversal (1–2°C) | | |
| GI-1c (14.0–13.3) | Significant warming at the beginning (2–4°C) followed by a gradual cooling at (~2°C). Intense cold conditions at 13.7–13.6 ka | Glacier advance or stillstand with moraine formation at 13.5 ka | Colder conditions starting at 13.5 cal ka BP in northern Iberia (Moreno *et al.*, 2010). Cold climate in the Pyrenees at 14–13.4 cal ka BP (González-Sampériz *et al.*, 2006). |
| GI-1b (13.3–13.1) | Short cold reversal (1–2°C) | - | Short periods of colder and drier conditions (Moreno *et al.*, 2010). Expansion of cold-climate forest species in the Pyrenees at 13.4–13.1 cal ka BP (González-Sampériz *et al.*, 2006). |
| GI-1a (13.1–12.9) | Early warming followed by a general cooling | Glacier advance or stillstand with moraine formation at 13.0 ka | Cold and dry conditions in the Pyrenees starting at 13.1 cal ka BP (González-Sampériz *et al.*, 2006). |

in the lateral cirques distributed along the Ruda Valley (Fig. 3). These features are currently inactive under the present-day climate regime (Fernandes *et al.*, 2018), with abundant lichen coverage and forest colonisation, particularly on the lowest ridges. In the Pyrenees, as well as in other Iberian ranges, cirque wall readjustment following deglaciation triggered different landforms, such as debris-covered glaciers or rock glaciers, that remained active until the early Holocene (Oliva *et al.*, 2019). This is the case for the Bacivèr Cirque, where the debris-covered glacier that formed inside the highest YD moraines stabilised at 7.2 ± 0.5 ka (Oliva *et al.*, 2021a), and for several other massifs in the Central and Eastern Pyrenees where rock glaciers were active until well into the Holocene (Andrés *et al.*, 2018; García-Ruiz *et al.*, 2016a). A similar pattern was also detected in other Iberian massifs, such as in the Iberian Range (Aumaître *et al.*, 2017) or Sierra Nevada (Palacios *et al.*, 2016), where these paraglacial landforms formed immediately after the deglaciation of the cirques, and remained active until the complete melting of their relict ice during the Holocene Thermal Maximum.

## Conclusions

The Central Pyrenees were extensively glaciated during Quaternary glacial phases and were only slightly transformed by periglacial, nival and slope processes during subsequent interglacial periods such as the Holocene. As a result, the landscape in the Central Pyrenees includes a wide range of geomorphological features that constitutes a prominent natural heritage that contributed to the designation of most protected areas in this mountain range. This is the case for the Ruda Valley, located on the periphery of the National Park of Aigüestortes and Sant Maurici Lake. The valley is one of the most scenic glacial valleys of the Pyrenees, and includes a wide variety of glacial and periglacial landforms, particularly above 1800 m. However, in contrast to the southern slope of the Central Pyrenees where the timing of the glacial evolution has been widely studied, on the northern side there are still temporal and spatial gaps in the chronology of glacial activity. In this work, we determined the magnitude and timing of T-1 glacial oscillations in the Upper Garonne Basin by producing 12 new CRE ages of glacial landforms (moraine boulders and glacially polished surfaces) that provide evidence of the spatio-temporal pattern of glacial oscillations from the B–A to the YD.

The Upper Garonne Basin hosted the largest glacial system of the Pyrenees during the last glacial cycle thanks to its Atlantic-influenced climate and the high altitude of the peaks in the central part of this range. The long-term post-LGM warming favoured glacial recession, particularly during the early B–A, and by 14.4 ± 1.2 ka the Ruda palaeoglacier was already disconnected from the main Garonne palaeoglacier. At that time, the glacier front was located at 1860–1900 m, and some areas of the Saboredo Cirque were already ice-free as a result of ice thinning. The B–A was also a period of great climatic variability, and the small glaciers in the Ruda Valley showed rapid response times with formation of moraines during the coldest B–A phases in northern Iberia. Phases of glacier advance or stillstands promoted the development of moraines at 13.5 ± 0.9 ka, as well as during the transition between the late B–A and the onset of the YD at 13.0 ± 0.8 ka. The YD probably favoured the persistence of small glaciers during an early stage of this cold phase; there is evidence of glacial retreat at the uppermost part of the cirque floor at 12.7 ± 0.8 ka (~2300–2350 m) and moraine abandonment of the highest cirque moraines (2470 m) at 12.6 ± 1.3 ka. Subsequently, glacial disappearance must have promoted paraglacial dynamics and the formation of the (currently relict) rock glaciers existing within these moraines.

Whereas the impact of the B–A deglaciation on the current landscape of the Pyrenean cirques was already known, the sequence of glacial advances and retreats during the B–A and YD presented in this study provides one of the most accurate deglacial histories in southern Europe. This opens new perspectives on the palaeoclimatic evolution in the Iberian Peninsula, in particular, and the Mediterranean region in general. The period from the B–A to the YD has been shown to be a major driver of transformation of the mountain landscapes of the Pyrenees and a key phase to better frame Holocene environmental dynamics in the highest lands of this mountain range. Future studies with new chronological data from other Pyrenean valleys and Iberian mountains will help to better understand T-1 glacier advances and retreats as well as the climate mechanisms behind millennial-scale glacial oscillations in southern Europe.

*Acknowledgements.* This work was funded by the Research Group ANTALP (Antarctic, Arctic, Alpine Environments; 2017-SGR-1102), the Government of Catalonia and the Centro de Estudos Geográficos/IGOT – University of Lisbon (FCT I.P. UIDB/00295/2020 and UIDP/00295/2020). The research topics complement those of the project

PALEOGREEN (CTM2017-87976-P) funded by the Spanish Ministry of Economy and Competitiveness and the project NUNANTAR funded by the Fundação para a Ciência e Tecnologia of Portugal (02/SAICT/2017 – 32002). Marcelo Fernandes holds a PhD fellowship of the Fundação para a Ciência e Tecnologia of Portugal (SFRH/139568/2018); Marc Oliva is supported by the Ramón y Cajal Program (RYC-2015-17597) and José M. Fernández-Fernández is supported by a postdoctoral grant within the NUNANTAR project. $^{10}$Be measurements were performed at the ASTER AMS national facility (CEREGE, Aix-en-Provence), which is supported by the INSU/CNRS and the ANR through the 'Projets thématiques d'excellence' program for the 'Equipements d'excellence' ASTER-CEREGE action and IRD. This research is also framed within the College on Polar and Extreme Environments (Polar2E) of the University of Lisbon. We also thank the National Park of Aigüestortes and Sant Maurici Lake for providing field access to the study sites and the reviewers for their constructive comments that helped to improve the quality of an earlier version of the manuscript.

## References

Allard JL, Hughes P, Woodward JC. 2021. Heinrich Stadial aridity forced Mediterranean-wide glacier retreat in the last cold stage. *Nature Geoscience* **14**: 197–205.

André MF. 2002. Rates of Postglacial rock weathering on glacially scoured outcrops (Abisko-Riksgränsen area, 68°N). *Geografiska Annaler: Series A, Physical Geography* **84**: 139–150.

Andrés N, Gómez-Ortiz A, Fernández-Fernández JM *et al*. 2018. Timing of deglaciation and rock glacier origin in the southeastern Pyrenees: a review and new data. *Boreas* **47**: 1050–1071.

Arnold M, Merchel S, Bourlès DL *et al*. 2010. The French accelerator mass spectrometry facility ASTER: Improved performance and developments. *Nuclear Instruments and Methods in Physics Research Section B: Beam Interactions with Materials and Atoms* **268**: 1954–1959.

Aumaître G, Bourlès D, Keddadouche K *et al*. 2017. Chronological and geomorphological investigation of fossil debris-covered glaciers in relation to deglaciation processes: A case study in the Sierra de La Demanda, northern Spain. *Quaternary Science Reviews* **170**: 232–249.

Ballantyne CK. 2008. After the ice: Holocene geomorphic activity in the Scottish Highlands. *Scottish Geographical Journal* **124**: 8–52.

Barr I, Spagnolo M. 2015. Glacial cirques as palaeoenvironmental indicators: Their potential and limitations. *Earth-Science Review* **151**: 48–78.

Bartolomé M, Moreno A, Sancho C *et al*. 2015. Hydrological change in Southern Europe responding to increasing North Atlantic overturning during Greenland Stadial 1. *Proceedings of the National Academy of Sciences* **112**: 6568–6572.

Benn DI, Hulton NRJ. 2010. An Excel™ spreadsheet program for reconstructing the surface profile of former mountain glaciers and ice caps. *Computers and Geosciences* **36**: 605–610.

Bernal-Wormull JL, Moreno A, Bartolomé M *et al*. 2021. Immediate temperature response in northern Iberia to last deglacial changes in the North Atlantic. *Geology* **XX**: 6–10.

Boston CM, Lukas S. 2019. Topographic controls on plateau icefield recession: insights from the Younger Dryas Monadhliath Icefield, Scotland. *Journal of Quaternary Science* **34**: 433–451.

Braucher R, Guillou V, Bourlès DL *et al*. 2015. Preparation of ASTER in-house 10Be/9Be standard solutions. *Nuclear Instruments and Methods in Physics Research Section B: Beam Interactions with Materials and Atoms* **361**: 335–340.

Bromley G, Putnam A, Borns H *et al*. 2018. Interstadial Rise and Younger Dryas Demise of Scotland's Last Ice Fields. *Paleoceanography and Paleoclimatology* **33**: 412–429.

Carrasco RM, Pedraza J, Domínguez-Villar D *et al*. 2015. Sequence and chronology of the Cuerpo de Hombre paleoglacier (Iberian Central System) during the last glacial cycle. *Quaternary Science Reviews* **129**: 163–177.

Chmeleff J, von Blanckenburg F, Kossert K *et al*. 2010. Determination of the 10Be half-life by multicollector ICP-MS and liquid scintillation counting. *Nuclear Instruments and Methods in Physics Research Section B: Beam Interactions with Materials and Atoms* **268**: 192–199.

Ciner A, Sarikaya MA. 2015. Cosmogenic 36 Cl geochronology of late Quaternary glaciers in the Bolkar Mountains, south central Turkey. In *Quaternary Glaciation in the Mediterranean Mountains*, Hughes PD, Woodward JC (eds). https://doi.org/10.1144/SP433.3

Clark PU, Dyke A, Shakun J *et al*. 2009. The Last Glacial Maximum. *Science* **325**: 710–714.

Cowton T, Hughes P, Gibbard PL. 2009. Palaeoglaciation of Parque Natural Lago de Sanabria, northwest Spain. *Geomorphology* **108**: 282–291.

Crest Y, Delmas M, Braucher R *et al*. 2017. Cirques have growth spurts during deglacial and interglacial periods: Evidence from 10Be and 26Al nuclide inventories in the central and eastern Pyrenees. *Geomorphology* **278**: 60–77.

Delmas M. 2009. Chronologie et impact géomorphologique des glaciations quaternaires dans l'est des Pyrénées. Lab. Rech. en géographie Phys. MEDI-TERRA, Univ. Perpignan. LGP Meudon, Univ. Paris 1 Panthéon Sorbonne Ph.D., 529.

Delmas M. 2015. The last maximum ice extent and subsequent deglaciation of the Pyrenees: an overview of recent research. *Cuadernos De Investigacion Geográfica* **41**: 359.

Delmas M, Gunnell Y, Braucher R *et al*. 2008. Exposure age chronology of the last glaciation in the eastern Pyrenees. *Quaternary Research* **69**: 231–241.

Delmas M, Calvet M, Gunnell Y *et al*. 2011. Palaeogeography and 10Be exposure-age chronology of Middle and Late Pleistocene glacier systems in the northern Pyrenees: Implications for reconstructing regional palaeoclimates. *Palaeogeography, Palaeoclimatology, Palaeoecology* **305**: 109–122.

Dunne J, Elmore D, Muzikar P. 1999. Scaling factors for the rates of production of cosmogenic nuclides for geometric shielding and attenuation at depth on sloped surfaces. *Geomorphology* **27**: 3–11.

Fernandes M, Oliva M, Palma P *et al*. 2017. Glacial stages and postglacial environmental evolution in the Upper Garonne valley, Central Pyrenees. *Science of the Total Environment* **584–585**: 1282–1299.

Fernandes M, Palma P, Lopes L *et al*. 2018. Spatial distribution and morphometry of permafrost-related landforms in the Central Pyrenees and associated paleoclimatic implications. *Quaternary International* **470**: 96–108.

Fernandes M, Oliva M, Vieira G. 2020. Paraglacial slope failures in the Aran valley (Central Pyrenees). *Quaternary International* **566–567**: 24–38.

Fernandes M, Oliva M & Vieira G et al. 2021. Geomorphological map of the Aran valley (Upper Garonne valley, Central Pyrenees). J. Maps.

García-Ruiz JM, Moreno A, González-Sampériz P *et al*. 2010. La cronología del último ciclo glaciar en las montañas del sur de Europa. *Una revisión. Cuaternario y Geomorfol* **24**: 35–46.

García-Ruiz JM, Palacios D, González-Sampériz P *et al*. 2016a. Mountain glacier evolution in the Iberian Peninsula during the Younger Dryas. *Quaternary Science Reviews* **138**: 16–30.

García-Ruiz JM, Palacios D, González-Sampériz P *et al*. 2016b. Evidencias de actividad glaciar durante el Dryas Reciente (12,9-11,7 ka BP) en la Península Ibérica. *Cuaternario y Geomorfol* **30**: 9–21. https://doi.org/10.17735/cyg.v30i1-2.39250

García-Ruiz JM, Palacios D, Fernández-Fernández JM *et al*. 2020. Glacial stages in the Peña Negra valley, Iberian Range, northern Iberian Peninsula: Assessing the importance of the glacial record in small cirques in a marginal mountain area. *Geomorphology* **362**: 107195.

Gómez-Ortiz A, Palacios D, Palade B *et al*. 2012. The deglaciation of the Sierra Nevada (Southern Spain). *Geomorphology* **159–160**: 93–105.

González-Sampériz P, Valero-Garcés BL, Moreno A *et al*. 2006. Climate variability in the Spanish Pyrenees during the last 30,000 yr revealed by the El Portalet sequence. *Quaternary Research* **66**: 38–52.

Heyman J, Stroeven AP, Harbor JM *et al*. 2011. Too young or too old: evaluating cosmogenic exposure dating based on an analysis of compiled boulder exposure ages. *Earth and Planetary Science Letters* **302**: 71–80.

Hughes P. 2018. Little Ice Age glaciers in the Mediterranean mountains: a new analysis. *Cuadernos de Investigación Geográfica* **44**(1): 15–45. http://doi.org/10.18172/cig.3362

Huss M, Bauder A, Linsbauer A *et al*. 2021. More than a century of direct glacier mass-balance observations on Claridenfirn, Switzerland. *Journal of Glaciology* **67**: 697–713.

ICGC. 2017. Base de dades geològiques de Catalunya 1:50.000 v1.0.

Ivy-Ochs S. 2015. Variaciones glaciares en los Alpes europeos al final de la última glaciación. *Cuadernos De Investigacion Geográfica* **41**: 295–315.

Ivy-Ochs S, Kerschner H, Maisch M *et al*. 2009. Latest Pleistocene and Holocene glacier variations in the European Alps. *Quaternary Science Reviews* **28**: 2137–2149.

Joly F. 1997. Glossaire de géomorphologie. Base de donnés sémiologiques pour la cartographie, Masson/Arm. ed. Paris.

Jomelli V, Chapron E, Favier V *et al*. 2020. Glacier fluctuations during the Late Glacial and Holocene on the Ariège valley, northern slope of the Pyrenees and reconstructed climatic conditions. *Mediterranean Geoscience Reviews* **2**: 37–51.

Korschinek G, Bergmaier A, Faestermann T *et al*. 2010. A new value for the half-life of 10Be by Heavy-Ion Elastic Recoil Detection and liquid scintillation counting. *Nuclear Instruments and Methods in Physics Research Section B: Beam Interactions with Materials and Atoms* **268**: 187–191.

Li Y. 2018. Determining topographic shielding from digital elevation models for cosmogenic nuclide analysis: a GIS model for discrete sample sites. *Journal of Mountain Science* **15**: 939–947.

Lifton N, Sato T, Dunai T. 2014. Scaling in situ cosmogenic nuclide production rates using analytical approximations to atmospheric cosmic-ray fluxes. *Earth and Planetary Science Letters* **386**: 149–160.

Lopes L, Oliva M, Fernandes M *et al*. 2018. Spatial distribution of morphometric parameters of glacial cirques in the Central Pyrenees (Aran and Boí valleys). *Journal of Mountain Science* **15**: 2103–2119.

López-Moreno JI, Alonso-González E, Monserrat O *et al*. 2019. Ground-based remote-sensing techniques for diagnosis of the current state and recent evolution of the Monte Perdido Glacier, Spanish Pyrenees. *Journal of Glaciology* **65**: 85–100.

Mangerud J, Goehring BM, Lohne ØS *et al*. 2013. Collapse of marine-based outlet glaciers from the Scandinavian Ice Sheet. *Quaternary Science Reviews* **67**: 8–16.

Mangerud J, Aarseth I, Hughes ALC *et al*. 2016. A major re-growth of the Scandinavian Ice Sheet in western Norway during Allerød-Younger Dryas. *Quaternary Science Review* **132**: 175–205.

Martin LCP, Blard P-H, Balco G *et al*. 2017. The CREp program and the ICE-D production rate calibration database: A fully parameterizable and updated online tool to compute cosmic-ray exposure ages. *Quaternary Geochronology* **38**: 25–49.

Martrat B, Grimalt JO, Shackleton NJ *et al*. 2007. Four climate cycles of recurring deep and surface water destabilizations on the Iberian margin. *Science* **317**: 502–507.

Merchel S, Arnold M, Aumaître G *et al*. 2008. Nuclear Instruments and Methods in Physics Research B Towards more precise 10 Be and 36 Cl data from measurements at the 10 À 14 level: Influence of sample preparation Be/B e. *Nuclear Instruments and Methods in Physics Research Section B: Beam Interactions with Materials and Atoms* **266**: 4921–4926.

Merchel S, Herpers U. 1999. An Update on Radiochemical Separation Techniques for the Determination of Long-Lived Radionuclides via Accelerator Mass Spectrometry. *Radiochimica Acta* **84**: 215–219.

Moreno A, Stoll H, Jiménez-Sánchez M *et al*. 2010. A speleothem record of glacial (25-11.6 kyr BP) rapid climatic changes from northern Iberian Peninsula. *Global and Planetary Change* **71**: 218–231.

Obase T, Abe-Ouchi A. 2019. Abrupt Bølling-Allerød Warming Simulated under Gradual Forcing of the Last Deglaciation. *Geophysical Research Letters* **46**: 11397–11405.

Oliva M, Gómez Ortiz A, Palacios D *et al*. 2014. Environmental evolution in Sierra Nevada (South Spain) since the Last Glaciation, based on multi-proxy records. *Quaternary International* **353**: 195–209.

Oliva M, Serrano E, Gómez-Ortiz A *et al*. 2016. Spatial and temporal variability of periglaciation of the Iberian Peninsula. *Quaternary Science Reviews* **137**: 176–199.

Oliva M, Palacios D, Fernández-Fernández JM *et al*. 2019. Late Quaternary glacial phases in the Iberian Peninsula. *Earth-Science Reviews* **192**: 564–600.

Oliva M, Fernandes M, Palacios D *et al*. 2021a. Rapid deglaciation during the Bølling-Allerød Interstadial in the Central Pyrenees and associated glacial and periglacial landforms. *Geomorphology* **385**: 107735.

Oliva M, Palacios D, Fernández-Fernández JM. 2021b. *Iberia, land of glaciers*. Elsevier.

Osmaston H. 2005. Estimates of glacier equilibrium line altitudes by the Area×Altitude, the Area×Altitude Balance Ratio and the Area×-Altitude Balance Index methods and their validation. *Quaternary International* **138–139**: 22–31.

Palacios D, García-Ruiz JM. 2015. Foreword: Deglaciation in Europe. New insights and questions. *Cuadernos De Investigacion Geográfica* **41**: 257–259.

Palacios D, Andrés N, Marcos J *et al*. 2012a. Maximum glacial advance and deglaciation of the Pinar Valley (Sierra de Gredos, Central Spain) and its significance in the Mediterranean context. *Geomorphology* **177–178**: 51–61.

Palacios D, de Andrés N, de Marcos J *et al*. 2012b. Glacial landforms and their paleoclimatic significance in Sierra de Guadarrama, Central Iberian Peninsula. *Geomorphology* **139–140**: 67–78.

Palacios D, de Andrés N, López-Moreno JI *et al*. 2015a. Late Pleistocene deglaciation in the upper Gállego Valley, central Pyrenees. *Quaternary Research* **83**: 397–414.

Palacios D, Gómez-Ortiz A, Andrés N *et al*. 2015b. Maximum extent of Late Pleistocene glaciers and last deglaciation of La Cerdanya mountains, Southeastern Pyrenees. *Geomorphology* **231**: 116–129.

Palacios D, Gómez-Ortiz A, Andrés N *et al*. 2016. Timing and new geomorphologic evidence of the last deglaciation stages in Sierra Nevada (southern Spain). *Quaternary Science Reviews* **150**: 110–129.

Palacios D, de Andrés N, Gómez-Ortiz A *et al*. 2017a. Evidence of glacial activity during the Oldest Dryas in the mountains of Spain. *Geological Society of London, Special Publications* **433**: 87–110.

Palacios D, García-Ruiz JM, Andrés N *et al*. 2017b. Deglaciation in the central Pyrenees during the Pleistocene–Holocene transition: Timing and geomorphological significance. *Quaternary Science Reviews* **162**: 111–127.

Palacios D, Hughes P, García-Ruiz JM *et al*. 2021. *European Glacial Landscapes*. Elsevier.

Pallàs R, Rodés Á, Braucher R *et al*. 2006. Late Pleistocene and Holocene glaciation in the Pyrenees: a critical review and new evidence from 10Be exposure ages, south-central Pyrenees. *Quaternary Science Reviews* **25**: 2937–2963.

Pallàs R, Rodés Á, Braucher R *et al*. 2010. Small, isolated glacial catchments as priority targets for cosmogenic surface exposure dating of Pleistocene climate fluctuations, southeastern Pyrenees. *Geology* **38**: 891–894.

Paterson WSB. 1994. *The Physics of Glaciers*. 3rd Edition. Elsevier: London.

Pellitero R, Rea BR, Spagnolo M *et al*. 2015. A GIS tool for automatic calculation of glacier equilibrium-line altitudes. *Computers and Geosciences* **82**: 55–62.

Pellitero R, Rea BR, Spagnolo M *et al*. 2016. GlaRe, a GIS tool to reconstruct the 3D surface of palaeoglaciers. *Computers and Geosciences* **94**: 77–85.

Pellitero R, Fernández-Fernández JM, Campos N *et al*. 2019. Late Pleistocene climate of the northern Iberian Peninsula: New insights from palaeoglaciers at Fuentes Carrionas (Cantabrian Mountains). *Journal of Quaternary Science* **34**: 342–354.

Quesada C. 2019. The Geology of Iberia: A Geodynamic Approach: The Variscan Cycle. Springer. Cham, 544 pp. https://doi.org/10.1007/978-3-030-10519-8

Rasmussen SO, Bigler M, Blockley SP *et al*. 2014. A stratigraphic framework for abrupt climatic changes during the Last Glacial period based on three synchronized Greenland ice-core records: Refining and extending the INTIMATE event stratigraphy. *Quaternary Science Reviews* **106**: 14–28.

Rea BR. 2009. Defining modern day Area-Altitude Balance Ratios (AABRs) and their use in glacier-climate reconstructions. *Quaternary Science Reviews* **28**: 237–248.

Rea BR, Pellitero R, Spagnolo M *et al*. 2020. Atmospheric circulation over Europe during the Younger Dryas. *Science Advances* **6**(50): 1–14. https://doi.org/10.1126/sciadv.aba4844

Reixach T, Delmas M, Calvet M. 2021. Climatic conditions between 19 and 12 ka in the eastern Pyrenees, and wider implications for atmospheric circulation patterns in Europe. *Quaternary Science Reviews* **260**: 106923.

René P. 2011. Régression des glaciers pyrénéens et transformation du paysage depuis le Petit Âge Glaciaire. *Sud-Ouest Européen* **32**: 5–19.

Renssen H, Goosse H, Roche M *et al*. 2018. The global hydroclimate response during the Younger Dryas event. *Quaternary Science Reviews* **193**: 84–97.

Renssen H, Isarin RFB. 2001. The two major warming phases of the last deglaciation at 14.7 and 11.5 ka cal BP in Europe. *Global and Planetary Change* **30**: 117–153.

Rodríguez-Rodríguez L, Jiménez-Sánchez M, Domínguez-Cuesta MJ *et al*. 2017. Timing of last deglaciation in the Cantabrian Mountains (Iberian Peninsula; North Atlantic Region) based on in situ-produced 10Be exposure dating. *Quaternary Science Reviews* **171**: 166–181.

Rodríguez-Rodríguez L, Jiménez-Sánchez M, Domínguez-Cuesta MJ *et al*. 2016. Chronology of glaciations in the Cantabrian Mountains (NW Iberia) during the Last Glacial Cycle based on in situ-produced 10Be. *Quaternary Science Reviews* **138**: 31–48.

Schilling DH, Hollin JT. 1981. Numerical reconstructions of valley glaciers and small ice caps. In *The Last Great Ice Sheets*, Denton GH, Hughes TJ (eds). Wiley: New York; 207–220.

Serrano E, Gómez-Lende M, Pellitero R *et al*. 2015. Deglaciación en la Cordillera Cantábrica: Modelo y evolución. *Cuadernos De Investigacion Geográfica* **41**: 389–408.

Serrano E, González-Trueba JJ, Pellitero R *et al*. 2016. Quaternary glacial history of the Cantabrian Mountains of northern Spain: a new synthesis. *Geological Society of London, Special Publications* **433**: 55–85.

Small D, Fabel D. 2016. Was Scotland deglaciated during the Younger Dryas? *Quaternary Science Reviews* **145**: 259–263.

Stange KM, van Balen RT, Kasse C *et al*. 2014. Linking morphology across the glaciofluvial interface: A 10Be supported chronology of glacier advances and terrace formation in the Garonne River, northern Pyrenees, France. *Geomorphology* **207**: 71–95.

Styllas MN, Schimmelpfennig I, Benedetti L *et al*. 2018. Late-glacial and Holocene history of the northeast Mediterranean mountains - New insights from in situ-produced 36Cl-based cosmic ray exposure dating of paleo-glacier deposits on Mount Olympus, Greece. *Quaternary Science Reviews* **193**: 244–265.

Tomkins MD, Dortch JM, Hughes P *et al*. 2018. Rapid age assessment of glacial landforms in the Pyrenees using Schmidt hammer exposure dating (SHED). *Quaternary Research* **90**: 26–37.

Uppala SM, Kållberg PW, Simmons AJ *et al*. 2005. The ERA-40 reanalysis. *Quarterly Journal of the Royal Meteorological Society* **131**: 2961–3012.

Veen Van der, C. 1999. Fundamentals of Glaciers Dynamics, Second Edi. ed. Balkema, Rotterdam.

Ward GK, Wilson SR. 1978. Procedures for Comparing and Combining Radiocarbon Age Determinations: a Critique. *Archaeometry* **20**: 19–31.

Zasadni J, Piotr K, Bro E *et al*. 2020. Latest Pleistocene glacier advances and post-Younger Dryas rock glacier stabilization in the Mt. Kriváň group, High Tatra Mountains, Slovakia. *Geomorphology* **358**: 107093.

# 4. Rapid deglaciation during the Bølling-Allerød Interstadial in the Central Pyrenees and associated glacial and periglacial landforms

Oliva, M., Fernandes, M., Palacios, D., Fernández-Fernández, J. M., Schimmelpfennig, I., Team, A., & Antoniades, D. (2021). Rapid deglaciation during the Bølling-Allerød Interstadial in the Central Pyrenees and associated glacial and periglacial landforms. *Geomorphology*, *385*, 107735. https://doi.org/10.1016/j.geomorph.2021.107735

Geomorphology 385 (2021) 107735

Contents lists available at ScienceDirect

Geomorphology

journal homepage: www.elsevier.com/locate/geomorph

# Rapid deglaciation during the Bølling-Allerød Interstadial in the Central Pyrenees and associated glacial and periglacial landforms

M. Oliva [a,*], M. Fernandes [b], D. Palacios [c], J.-M. Fernández-Fernández [b], I. Schimmelpfennig [d], D. Antoniades [e], ASTER Team: [d]

Georges Aumaître, Didier Bourlès, Karim Keddadouche

[a] Department of Geography, Universitat de Barcelona, Catalonia, Spain
[b] Centre for Geographical Studies, IGOT, Universidade de Lisboa, Lisbon, Portugal
[c] Department of Geography, Complutense University of Madrid, Madrid, Spain
[d] Aix-Marseille Université, CNRS, IRD, INRAE, Coll. France, UM 34 CEREGE, Aix-en-Provence, France
[e] Department of Geography & Centre for Northern Studies, Université Laval, Quebec, Canada

ARTICLE INFO

*Article history:*
Received 26 February 2021
Received in revised form 1 April 2021
Accepted 1 April 2021
Available online 9 April 2021

*Keywords:*
Central Pyrenees
Bølling-Allerød
Deglaciation
Cosmic-Ray Exposure dating
Moraines
Polished bedrock
Paraglacial processes

ABSTRACT

The Central Pyrenees hosted a large ice cap during the Late Pleistocene. The cirques under relatively low-altitude peaks (2200–2800 m) include the greatest variety of glacial landforms (moraines, fossil debris-covered glaciers and rock glaciers), but their age and formation process are poorly known. Here, we focus on the headwaters of the Garonne River, namely on the low-altitude Bacivèr Cirque (highest peaks at ~2600 m), with widespread erosive and depositional glacial and periglacial landforms. We reconstruct the pattern of deglaciation from geomorphological observations and a 17-sample dataset of $^{10}$Be Cosmic-Ray Exposure (CRE) ages. Ice thickness in the Bacivèr Cirque must have reached ~200 m during the maximum ice extent of the last glacial cycle, when it flowed down towards the Garonne paleoglacier. However, by ~15 ka, during the Bølling-Allerød (B-A) Interstadial, the mouth of the cirque was deglaciated as the tributary glacier shrank and disconnected from the Garonne paleoglacier. Glacial retreat was rapid, and the whole cirque was likely to have been deglaciated in only a few centuries, while paraglacial processes accelerated, leading to the transformation of debris-free glaciers into debris-covered and rock glaciers in their final stages. Climate conditions prevailing at the transition between the B-A and the Younger Dryas (YD) favored glacial growth and the likely development of small moraines within the slopes of the cirque walls by ~12.9 ka, but the dating uncertainties make it impossible to state whether these moraines formed during the B-A or the YD. The melting of these glaciers favored paraglacial dynamics, which promoted the development of rock glaciers as well as debris-covered glaciers. These remained active throughout the Early Holocene until at least ~7 ka. Since then, the landscape of the Bacivèr Cirque has seen a period of relative stability. A similar chronological sequence of deglaciation has been also detected in other cirques of the Pyrenees below 3000 m. As in other mid-latitude mountain regions, the B-A triggered the complete deglaciation of the Garonne paleoglacier and promoted the development of the wide variety of glacial and periglacial landforms existing in the Bacivèr cirque.



## 1. Introduction

Termination-1 (T-1), the period spanning from the end of the Last Glacial Maximum (LGM, 19–20 ka; Clark et al., 2009) to the onset of the Holocene (11.7 ka; Denton et al., 2014), saw a massive worldwide glacial retreat that favored a large-scale reorganisation of oceanic and atmospheric circulation patterns, global sea level rise, redefinition of coastlines, shifts in land cover and ecosystems, and changes in greenhouse gas concentrations. An accurate comprehension of the spatial and temporal patterns of environmental change that occurred during the last major deglacial period, particularly glacial oscillations, can provide insights into rapid landscape readjustment, which allows the significance of recent trends due to warming climates to be assessed in a longer-term context (Oliva et al., 2019; Oliva et al., 2021). A better understanding of the sensitivity of glaciers in mid-latitude mountains to rapidly changing past climates can thus help to assess the magnitude of future changes and the fate of mountain glaciers in these regions.

* Corresponding author at: Department of Geography, Universitat de Barcelona, Catalonia, Spain.
*E-mail address:* marcoliva@ub.edu (M. Oliva).

https://doi.org/10.1016/j.geomorph.2021.107735
0169-555X/

Whereas the long-term, global-scale glacial retreat that occurred during T-1 was favored by greenhouse gas increases, regional glacial advances and retreats followed forcings at smaller scales (Denton et al., 2014). In the Northern Hemisphere, ice core records from Greenland reveal a sequence of alternating colder and warmer periods during T-1: the cold period, the Oldest Dryas (OD; 17.5–14.6 ka), was followed by the much warmer Bølling-Allerød (B-A) Interstadial (14.6–12.9 ka) and a subsequent return to colder conditions during the Younger Dryas (YD; 12.9–11.7 ka) (Rasmussen et al., 2014). In mid-latitude regions, such as the Iberian Peninsula, glaciers shrank in response to the long-term warming that was recorded during T-1, although colder millennial-scale phases favored re-expansion and warmer periods triggered accelerated shrinking (Oliva et al., 2019). While local maximum ice extents during the last glacial cycle occurred asynchronously in different mountain ranges in Iberia (Oliva et al., 2019), glacial oscillations during T-1 followed very similar patterns in response to changing climate in the North Atlantic region (Buizert et al., 2018; Rea et al., 2020). For areas where chronological data are available, such as the Central Range (Carrasco et al., 2015; Palacios et al., 2012), Pyrenees (Andrés et al., 2018; Palacios et al., 2017b, 2017a, 2015b), Cantabrian Mountains (Rodríguez-Rodríguez et al., 2017), and Sierra Nevada (Gómez-Ortiz et al., 2012; Palacios et al., 2016), glaciers generally advanced during the OD and YD, and retreated during the B-A and after the YD during the Early Holocene.

In the Pyrenees, where the present work focuses, glacial records in several valleys (Gállego, Ésera, Noguera Ribargoçana, Ariège) have shown evidence of two periods with glacial expansion during T-1 (Crest et al., 2017; Jomelli et al., 2020; Palacios et al., 2017b, 2015a; Pallàs et al., 2006). The first phase of glacial advance after the massive retreat of the LGM took place during the OD, with ice tongues up to 15 km long reaching the mountain fronts. The second phase, in the late Pleistocene, occurred during the YD with the presence of small glaciers up to 4 km long which developed from north-facing cirques of the highest massifs, above 2200 m (García-Ruiz et al., 2016). In between, the B-A saw a rapid glacial retreat, with the ice disappearing from most of the highest massifs by 15–14 ka and the formation of rock glaciers and debris-covered glaciers in many cirques in response to intense paraglacial readjustment, mainly in relatively low-altitude cirques below 2800 m (Andrés et al., 2018; Palacios et al., 2017b). By the end of the YD at 11–10.5 ka, almost all YD glaciers had disappeared and a new generation of rock glaciers formed in the recently deglaciated cirques (Oliva et al., 2016).

Despite recent advances in our understanding of climatic and environmental consequences during T-1, the spatial and temporal patterns of glacial response in some European mountains is still poorly known, particularly in the Mediterranean region. In this sense, the Pyrenees, located in the transitional area between Atlantic and Mediterranean climatic influence, and between the southern and northern European mountains, constitute a mountain range of great glacial and climatic relevance. However, the chronology of glacial oscillations in several valleys of the Central Pyrenees is still uncertain, particularly for T-1. In addition, the origin of the great variety of glacial and periglacial landforms, especially in relatively low-altitude cirques, is unknown, as is the chronology of their formation. Data from this area and this period is therefore needed to shed light on the prevailing paleoclimatic conditions, as well as the atmospheric configuration driving glacial oscillations during T-1. To this end, we had the following specific objectives:

- To provide new data on glacial oscillations during T-1 for the Upper Garonne Basin, where absolute deglaciation ages are still lacking.
- To compare results from the Upper Garonne Basin with the timing of deglaciation as well as the age of formation and stabilization of the different glacial and periglacial landforms that exist in many of the cirques at lower altitudes in the Pyrenees.
- To compare glacial evolution in this mountain range with that which occurred in the Iberian mountains as well as other southern European ranges, and contrast their spatio-temporal patterns. This is needed to frame the glacial response within the paleoclimatic evolution of Europe during deglaciation, as inferred from natural archives and climate models.

## 2. Study area

The Pyrenees are the largest mountain range in the Iberian Peninsula, spanning a 400 km W-E transect. The central part of the range contains the highest massifs, with peaks exceeding 3000 m a.s.l., such as the Maladeta (3404 m), Monte Perdido (3355 m) and Posets (3371 m). This research focuses on the Bacivèr Cirque, located in the upper Garonne valley (Fig. 1), at latitudes 42°40′ N–42°42′ N and longitudes 0°57′ E–1°00′ E.

The relief is structured by the U-shaped Garonne valley that drains towards the N-NW, receiving inflow from tributary rivers that drain adjacent glacial valleys with headwaters in peaks ranging from 2800 to 3000 m. Glacial cirques in the Upper Garonne valley are predominantly NE-exposed and the altitude of their floors ranges between 2200 and 2400 m (Lopes et al., 2018). The floor of the Bacivèr Cirque, where this study focuses, is located at similar altitudes but faces W; it extends over 10 $km^2$ with the highest altitudes exceeding 2600 m at the Marimanya (2675 m; 42°42′33″N 1°00′44″E), La Llança (2658 m) and Bacivèr (2642 m) peaks and the lowest at 1850–1900 m at the Beret Plateau (Fig. 1). This area represents the hydrological divide between rivers draining to the Atlantic via the Garonne River and those flowing to the Mediterranean Sea via the Noguera Pallaresa.

At present, the mean air annual temperature (MAAT) at the nearby Bonaigua station (2266 m) is 3 °C whereas the annual precipitation totals 1227 mm, mostly in the form of snow that falls during the cold months of the year. Snow on the ground generally persists for 7–8 months of the year. The treeline lies between 2200 and 2300 m, where *Pinus nigra* is replaced at higher elevations by alpine meadows on the cirque floor and barren rocky terrain elsewhere. The lithology of the area is mainly composed of Carboniferous granodiorites and granites, but there are also Silurian marbles at the lower margins of the Bacivèr Cirque and limestones intercalated with Devonian slates on the Beret Plateau (Institut Cartogràfic i Geològic de Catalunya, 2017).

The landscape of the Bacivèr Cirque includes a wide range of glacial and periglacial landforms that are inherited from the last Pleistocene glacial cycle and the subsequent deglaciation (Fernandes et al., 2017). The W-NW aspect of this compound cirque and the high elevation of its floor (2200–2400 m) resulted in abundant snowfall accumulation and its subsequent transformation into ice during the cold Pleistocene phases. However, the chronology of the local maximum ice extent of the last glacial cycle is not yet known, although recent studies encompassing the entire Garonne paleoglacier show evidence that the entire cirque was largely covered by ice during that phase (Fernandes et al., 2017). This is confirmed by the existence of glacially polished surfaces ~200 m above the Bacivèr Cirque floor. Post-LGM warming favored the shrinking of that glacier, which receded and lost thickness during the last deglaciation. This is confirmed on the Beret Plateau, where glacial striae on polished surfaces show different directions which suggest that the glacier descending from the Bacivèr Cirque, among others, diverged either to the main Garonne Glacier (SW) or the Noguera Pallaresa Glacier (N). Within the Bacivèr Cirque, there is a variety of erosive and depositional landforms, including moraine complexes indicative of multiple readvances within the final stages of the long-term deglaciation. As observed in other neighboring valleys, the melting of the last glaciers favored the development of rock glaciers during the paraglacial stage (Knight, 2019; Knight et al., 2019), although they are inactive under present-day climate conditions (Fernandes et al., 2018). The southern fringe of the Bacivèr Cirque is included in the Baqueira-Beret ski resort domain, which has altered some slopes to expand winter sports facilities.

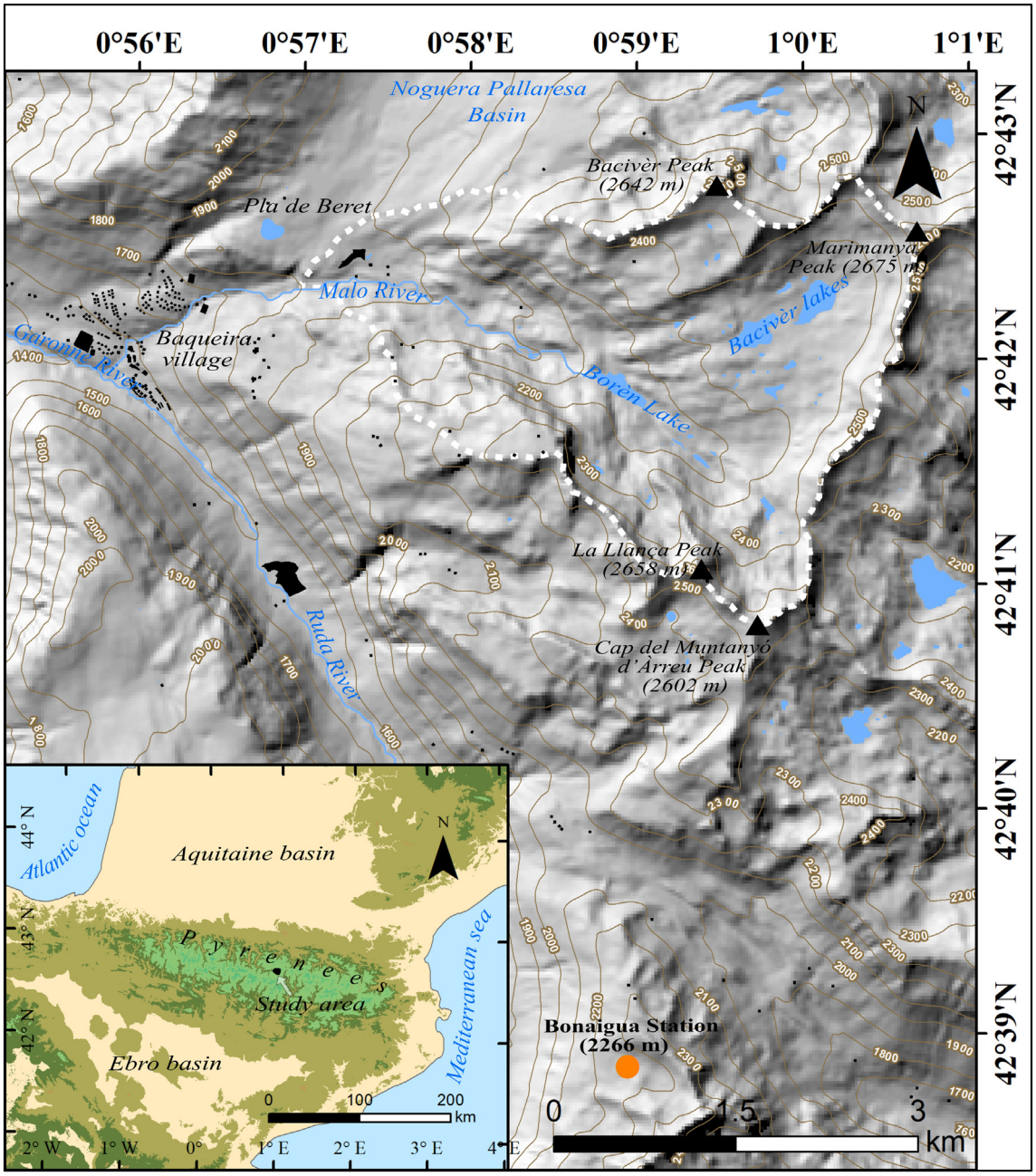


**Fig. 1.** Location of (a) the Central Pyrenees; and (b) the Bacivèr Cirque within this range.

## 3. Methodology

In order to reconstruct past glacial oscillations since the onset of deglaciation in the Bacivèr Cirque, we used an integrated geomorphological and geochronological approach. Field work was conducted in June 2016, when the absence of snow cover enabled the identification of different geomorphic features and collection of samples for Cosmic-Ray Exposure (CRE) dating.

### 3.1. Geomorphological mapping

We produced a geomorphological map at 1:20000 scale by using an ArcGIS 10.7 (ESRI) database. The map was based on: (i) stereoscopic photo-interpretation though out the Iberpix 4 online anaglyph map viewer (https://www.ign.es/iberpix2/visor/); (ii) visual inspection of satellite imagery from Google Earth; and (iii) the combination of orthophotomaps (0.25 m cellsize) and high-resolution LIDAR digital elevation models (density points of 0.5–2 $m^{-2}$) obtained from the 'Institut Cartogràfic i Geològic de Catalunya' (http://www.icc.cat/appdownloads). Special attention was paid to glacial landforms and related features, which were outlined and symbolized according to Joly (1997). The generated geomorphological map was then validated in the field, as we surveyed the entire area with a focus on glacial and periglacial landforms.

### 3.2. Field strategy and sampling

We collected a total of 17 samples for CRE dating using a hammer and a chisel. We targeted boulders belonging to moraines, a debris-covered glacier and glacially polished outcrops of granites and

granodiorites. We aimed to ensure the optimal exposure of the sampling sites to the cosmic-ray flux, and thus selected flat-topped and gentle surfaces (<20°) of rock outcrops rather than steep slopes or sharp crests. The thickness of the extracted samples ranged from 2 to 4.5 cm (Table 1). To account for any shielding due to the surrounding topography, the topographic shielding factor was calculated for all sampling sites by means of the ArcGIS toolbox devised by Li (2018) that implements well-known routines explained in Dunne et al. (1999), and only needs a point shapefile of the sampling sites, including the strike and the dip of the sampled surfaces, and a digital elevation model (DEM).

### 3.3. Laboratory procedures and exposure age calculation

Before the chemical processing of the samples, they were crushed and sieved to the 0.25–0.8 mm fraction at the Physical Geography Laboratory (Universidad Complutense de Madrid, Spain). Thereafter, we treated the rock samples at the Laboratoire National des Nucléides Cosmogéniques ($LN_2C$) of the Centre Européen de Recherche et d'Enseignement des Géosciences de l'Environnement (CEREGE; Aix-en-Provence, France). In accordance with the quartz-rich lithology of the samples, they were processed for the extraction of the in situ produced cosmogenic nuclide $^{10}$Be.

In order to remove magnetic minerals, we conducted a magnetic separation through a "Frantz LB-1" separator. Once the non-magnetic fraction was isolated, it underwent several rounds of chemical attacks with a concentrated mixture of hydrochloric (1/3 HCl) and hexafluorosilicic (2/3 $H_2SiF_6$) acids to dissolve and discard the non-quartz minerals. Subsequently, four successive partial dissolutions of the remaining minerals with concentrated hydrofluoric acid (HF) helped dissolve the remaining impurities (e.g. non-dissolved feldspar minerals) and removed atmospheric $^{10}$Be. As a result, samples yielded from 8 to 22 g of purified quartz (Table 2). Just before the total dissolution of quartz, 150 μL of an in-house manufactured (from a phenakite crystal) $^{9}$Be carrier solution (spike, concentration: 3025 ± 9 μg $g^{-1}$; Merchel et al., 2008) were added to the samples. The purified quartz was subsequently dissolved by acid leaching with 48% concentrated HF (3.6 mL per g of quartz + 30 mL in excess). Following the total dissolution, we evaporated the resulting solutions until dryness, and recovered samples with HCl (7.1 M). The Be samples were then precipitated at PH = 9 to beryllium hydroxide ($Be(OH)_2$) by means of ammonia ($NH_3$), and separated from other elements in resin columns: an Dowex 1 × 8 anionic exchange column to remove elements such as Fe, Mn and Ti, and a Dowex 50WX8 cationic exchange column to discard B and recover Be (Merchel and Herpers, 1999). The final eluted Be was precipitated again, and the Be precipitate was dried and oxidized to BeO at 700 °C. Finally, the targets for accelerator mass spectrometer (AMS) measurements were prepared by mixing the niobium powder with the BeO keeping an approximate 1:1 proportion and pressing the mixture into copper cathodes.

The targets were analysed at the Accelerator pour les Sciences de la Terre, Environnement et Risques (ASTER) national AMS facility at CEREGE in order to measure the $^{10}$Be/$^{9}$Be ratio from which the $^{10}$Be concentration was later inferred (Table 2). The AMS measurements were calibrated against the in-house standard STD-11 with an assigned $^{10}$Be/$^{9}$Be ratio of (1.191 ± 0.013) × $10^{-11}$ (Braucher et al., 2015). The analytical 1σ uncertainties include uncertainties in the AMS counting statistics and an external 0.5% AMS error (Arnold et al., 2010) and the uncertainty related to the chemical blank correction. The $^{10}$Be half-life considered was (1.387 ± 0.0012) × $10^{6}$ years (Chmeleff et al., 2010; Korschinek et al., 2010).

We calculated $^{10}$Be exposure ages by using the CREp online calculator (Martin et al., 2017; available online at: http://crep.crpg.cnrs-nancy.fr/#/), where we selected the following settings: LSD (Lifton-Sato-Dunai) elevation/latitude scaling scheme (Lifton et al., 2014), ERA40 atmospheric model (Uppala et al., 2005) and geomagnetic database based on the LSD framework (Lifton et al., 2014). These settings yielded a world-wide mean $^{10}$Be production rate at sea level high latitude (SLHL) of 3.98 ± 0.22 atoms $g^{-1}$ $yr^{-1}$. Exposure age results of the samples are shown in Table 2, together with their full 1σ uncertainties (derived from analytical and production rate uncertainties) and their analytical uncertainties only. The uncertainties discussed throughout the text are given with their analytical uncertainties only, for internal comparison. Due to the high analytical uncertainty, arising from low

**Table 1**
Geographic location of samples, topographic shielding factor, sample thickness and vertical distance from the summit.

| Sample name | Landform | Latitude (DD) | Longitude (DD) | Elevation (m a.s.l.)[a] | Topographic shielding factor | Thickness (cm) |
|---|---|---|---|---|---|---|
| *Mouth of the cirque* | | | | | | |
| ARAN-16 | Polished surface | 42.7017 | 0.9717 | 1998 | 0.9748 | 3.0 |
| ARAN-17 | Polished surface | 42.7033 | 0.9700 | 1949 | 0.9626 | 3.2 |
| *Central lower polished bedrock* | | | | | | |
| ARAN-14 | Polished surface | 42.6968 | 0.9880 | 2215 | 1.0000 | 3.7 |
| ARAN-15 | Polished surface | 42.6946 | 0.9879 | 2179 | 0.9897 | 3.5 |
| *Central higher erratic boulder* | | | | | | |
| ARAN-10 | Erratic boulder | 42.6980 | 0.9956 | 2322 | 0.9972 | 3.3 |
| *Highest polished surfaces* | | | | | | |
| ARAN-3 | Polished surface | 42.6950 | 1.0047 | 2436 | 0.9718 | 4.0 |
| ARAN-4 | Polished surface | 42.6948 | 1.0046 | 2438 | 0.9688 | 4.0 |
| ARAN-8 | Polished surface | 42.6961 | 1.0031 | 2371 | 0.9801 | 4.5 |
| ARAN-9 | Polished surface | 42.6967 | 1.0023 | 2353 | 0.9859 | 3.5 |
| ARAN-13 | Polished surface | 42.7034 | 1.0063 | 2371 | 0.9849 | 3.0 |
| *Highest moraines* | | | | | | |
| ARAN-1 | Moraine boulder | 42.6959 | 1.0052 | 2431 | 0.9671 | 3.0 |
| ARAN-2 | Moraine boulder | 42.6959 | 1.0052 | 2431 | 0.9659 | 2.2 |
| ARAN-11 | Moraine boulder | 42.7034 | 1.0062 | 2371 | 0.9856 | 3.0 |
| ARAN-12 | Moraine boulder | 42.7067 | 1.0083 | 2437 | 0.9746 | 4.0 |
| *Debris-covered glacier* | | | | | | |
| ARAN-5 | Moraine boulder | 42.6945 | 1.0042 | 2437 | 0.9732 | 3.0 |
| ARAN-6 | Moraine boulder | 42.6943 | 1.0043 | 2435 | 0.9598 | 3.0 |
| ARAN-7 | Moraine boulder | 42.6945 | 1.0041 | 2434 | 0.9705 | 3.2 |

[a] Elevations are derived from the 5 m Digital Elevation Model of the Spanish "Instituto Geográfico Nacional" and are subjected to a vertical accuracy of ±5 m.

**Table 2**
AMS analytical data and calculated exposure ages. $^{10}Be/^{9}Be$ ratios were inferred from measurements at the ASTER AMS facility. Individual ages are shown with their full uncertainties (including analytical AMS uncertainty and production rate uncertainty) and analytical uncertainty only within brackets. Arithmetic mean ages are given with their full uncertainties (including standard deviation and production rate uncertainty) and standard deviations only in brackets. Ages in grey italics correspond to potential outliers and thus are rejected and excluded from the interpretation and discussion.

$^{10}Be$ samples analytical AMS data

| Sample name | Quartz weight (g) | Mass of carrier ($^{9}Be$ mg) | ASTER AMS cathode number | $^{10}Be/^{9}Be$ ($10^{-14}$) | Blank correction (%) | [$^{10}Be$] ($10^{4}$ atoms $g^{-1}$) | Age (ka) | Mean age (ka) |
|---|---|---|---|---|---|---|---|---|
| *Mouth of the cirque* | | | | | | | | |
| A-16 | 18.0 | 0.461 | IGHY | 15.042 ± 0.420 | 1.32 | 25.370 ± 0.719 | 14.2 ± 0.8 (0.4) | 14.2 ± 0.8 (0.4) |
| *A-17* | *21.3* | *0.458* | *IGHZ* | *22.411 ± 1.490* | *0.89* | *31.913 ± 2.141* | *18.6 ± 1.5 (1.2)* | |
| *Central lower polished bedrock* | | | | | | | | |
| A-14 | 21.7 | 0.458 | IGHW | 20.693 ± 0.654 | 0.97 | 28.838 ± 0.922 | 13.5 ± 0.8 (0.4) | 13.8 ± 0.9 (0.4) |
| A-15 | 20.5 | 0.456 | IGHX | 19.694 ± 0.543 | 1.02 | 29.035 ± 0.810 | 14.1 ± 0.8 (0.4) | |
| *Central higher erratic boulder* | | | | | | | | |
| A-10 | 20.5 | 0.469 | IGHS | 23.563 ± 0.877 | 0.81 | 35.806 ± 1.345 | 15.4 ± 1.0 (0.6) | 15.4 ± 1.0 (0.6) |
| *Highest polished surfaces* | | | | | | | | |
| A-3 | 20.0 | 0.456 | IGHL | 25.889 ± 0.768 | 0.78 | 39.034 ± 1.168 | 16.0 ± 1.0 (0.5) | 14.8 ± 1.3 (0.9) |
| A-4 | 12.5 | 0.462 | IGHM | 14.033 ± 0.560 | 1.38 | 34.125 ± 1.382 | 14.1 ± 0.9 (0.5) | |
| A-8 | 14.7 | 0.465 | IGHQ | 16.711 ± 0.861 | 1.15 | 34.993 ± 1.826 | 15.0 ± 1.1 (0.7) | |
| A-9 | 21.3 | 0.464 | IGHR | 22.311 ± 0.733 | 0.86 | 32.122 ± 1.065 | 13.8 ± 0.8 (0.4) | |
| A-13 | 7.9 | 0.450 | IGHV | 9.718 ± 0.414 | 2.10 | 36.223 ± 1.578 | 15.2 ± 1.0 (0.6) | |
| *Highest moraines* | | | | | | | | |
| A-1 | 21.0 | 0.457 | IGHJ | 21.479 ± 0.758 | 0.93 | 30.905 ± 1.102 | 12.7 ± 0.8 (0.5) | 12.9 ± 0.9 (0.3) |
| A-2 | 20.9 | 0.457 | IGHK | 21.561 ± 0.703 | 0.93 | 31.225 ± 1.028 | 12.8 ± 0.8 (0.4) | |
| A-11 | 20.8 | 0.454 | IGHT | 16.955 ± 0.596 | 1.19 | 24.419 ± 0.869 | 13.3 ± 0.9 (0.5) | |
| *A-12* | *21.6* | *0.456* | *IGHU* | *22.450 ± 0.885* | *0.87* | *31.457 ± 1.252* | *10.0 ± 0.7 (0.4)* | |
| *Debris-covered glacier* | | | | | | | | |
| A-5 | 20.7 | 0.461 | IGHN | 25.426 ± 1.110 | 0.76 | 37.513 ± 1.652 | 15.2 ± 1.0 (0.6) | – |
| A-6 | 21.6 | 0.462 | IGHO | 12.470 ± 0.599 | 1.55 | 17.537 ± 0.856 | 7.2 ± 0.5 (0.3) | |
| A-7 | 21.7 | 0.454 | IGHP | 24.384 ± 0.754 | 0.83 | 33.718 ± 1.052 | 13.8 ± 0.8 (0.4) | |

Chemistry blank details

| Blank name | Processed with | mass of carrier ($^{9}Be$ mg) | ASTER AMS cathode number | $^{10}Be/^{9}Be$ ($10^{-14}$) | [$^{10}Be$] ($10^{4}$ atoms) | [$^{10}Be$] ($10^{4}$ atoms $g^{-1}$) | Age (ka) | Mean age (ka) |
|---|---|---|---|---|---|---|---|---|
| BK-2 | A- 1, 2, 3, 7, 11, 13, 14, 15, 16, 17 | 0.456 | CHBM | 0.201 ± 0.026 | 6.127 ± 0.795 | – | – | – |
| BK-3 | A- 4, 5, 6, 8, 9, 10, 12 | 0.458 | IGHI | 0.195 ± 0.03 | 5.978 ± 0.927 | – | – | – |

AMS currents and counting statistics, sample A-17 was discarded from the discussion.

In order to evaluate the impact of potential erosion on the exposure ages, we assumed a steady erosion rate (1 mm $ka^{-1}$) with a conservative maximum value according to André (2002). The impact of snow cover was estimated by extrapolating the current snow duration in the area, with an annual average of 7.5 months at 2200–2300 m and a mean thickness of 100 cm based on the data series of Bonaigua station (Fig. 1) available since 1997–1998 (Servei Meteorològic de Catalunya; http://www.igc.cat/web/ca/allaus_gruix_neu_v2.php?e=bonaigua&t=totes) (Table 3). We applied eq. 3.76 in Gosse and Phillips (2001) to calculate the snow correction factor (Gosse and Phillips, 2001). Erosion and snow corrections as a whole resulted in ages older by ~9%, with a minor contribution from the erosion correction (<2%). However, throughout the text we use the uncorrected ages in order to enable comparison with other areas, and considering that past snow cover thickness and duration are unknown. It must have changed significantly since the cirque's deglaciation, with an alternation of colder/warmer periods associated with changing moisture conditions.

### 3.4. Paleoglacier reconstruction and Equilibrium-Line Altitude (ELA) calculation

Paleoglaciers were reconstructed to model their spatial extent and paleotopography during the considered time periods. Three-dimensional glacier reconstruction was produced using the 'GLaRe'

**Table 3**
Exposure ages according to erosion and snow cover corrections.

| Sample name | Exposure ages (ka) | | | |
|---|---|---|---|---|
| | No correction | Erosion correction | Snow correction | Erosion + snow correction |
| *Mouth of the cirque* | | | | |
| A-16 | 14.2 ± 0.8 (0.4) | 14.4 ± 0.8 (0.4) | 15.3 ± 0.9 (0.4) | 15.5 ± 0.9 (0.4) |
| A-17 | 18.6 ± 1.5 (1.2) | 18.9 ± 1.5 (1.2) | 20.0 ± 1.6 (1.2) | 20.3 ± 1.6 (1.2) |
| *Central lower polished bedrock* | | | | |
| A-14 | 13.5 ± 0.8 (0.4) | 13.7 ± 0.8 (0.4) | 14.5 ± 0.9 (0.4) | 14.7 ± 0.9 (0.5) |
| A-15 | 14.1 ± 0.8 (0.4) | 14.3 ± 0.8 (0.4) | 15.1 ± 0.9 (0.4) | 15.3 ± 0.9 (0.4) |
| *Central higher erratic boulder* | | | | |
| A-10 | 15.4 ± 1.0 (0.6) | 15.6 ± 1.0 (0.6) | 16.6 ± 1.1 (0.6) | 16.9 ± 1.1 (0.6) |
| *Highest polished surfaces* | | | | |
| A-3 | 16.0 ± 1.0 (0.5) | 16.2 ± 1.0 (0.5) | 17.2 ± 1.0 (0.5) | 17.5 ± 1.0 (0.5) |
| A-4 | 14.1 ± 0.9 (0.5) | 14.3 ± 0.9 (0.6) | 15.1 ± 1.0 (0.6) | 15.3 ± 1.0 (0.6) |
| A-8 | 15.0 ± 1.1 (0.7) | 15.2 ± 1.1 (0.8) | 16.1 ± 1.2 (0.8) | 16.4 ± 1.2 (0.8) |
| A-9 | 13.8 ± 0.8 (0.4) | 14.0 ± 0.9 (0.5) | 14.8 ± 0.9 (0.5) | 15.0 ± 0.9 (0.5) |
| A-13 | 15.2 ± 1.0 (0.6) | 15.4 ± 1.0 (0.6) | 16.4 ± 1.1 (0.7) | 16.6 ± 1.1 (0.7) |
| *Highest moraines* | | | | |
| A-1 | 12.7 ± 0.8 (0.5) | 12.9 ± 0.8 (0.5) | 13.7 ± 0.9 (0.5) | 13.9 ± 0.9 (0.5) |
| A-2 | 12.8 ± 0.8 (0.4) | 13.0 ± 0.8 (0.4) | 13.8 ± 0.8 (0.4) | 14.0 ± 0.9 (0.4) |
| A-11 | 13.3 ± 0.9 (0.5) | 13.4 ± 0.9 (0.5) | 14.3 ± 0.9 (0.5) | 14.5 ± 0.9 (0.5) |
| A-12 | 10.0 ± 0.7 (0.4) | 10.1 ± 0.7 (0.4) | 10.8 ± 0.7 (0.4) | 10.9 ± 0.7 (0.4) |
| *Debris-covered glacier* | | | | |
| A-5 | 15.2 ± 1.0 (0.6) | 15.4 ± 1.0 (0.7) | 16.4 ± 1.1 (0.7) | 16.6 ± 1.1 (0.7) |
| A-6 | 7.2 ± 0.5 (0.3) | 7.3 ± 0.5 (0.3) | 7.8 ± 0.5 (0.4) | 7.8 ± 0.5 (0.4) |
| A-7 | 13.8 ± 0.8 (0.4) | 14.0 ± 0.8 (0.4) | 14.9 ± 0.9 (0.4) | 15.1 ± 0.9 (0.4) |

ArcGIS toolbox devised by Pellitero et al. (2016). It estimates past ice thickness along a flowline by applying the perfect-plasticity physical-based numerical model of Van der Veen (1999) following the calculation routines later proposed by Benn and Hulton (2010). The toolbox only requires a flowline, a tentative paleoglacier geometry (approached as a basin whose boundaries are defined by the position of lateral and/or frontal moraines) and a digital elevation model. Ice thickness was modelled by using an average shear stress of 100 kPa (Paterson, 1994; Benn and Hulton, 2010). Ice thicknesses were corrected based on shape factors (F-factor) obtained from a number of representative cross-sections in order to reduce the error of modelled values to <10% (Pellitero et al., 2016). From these procedures, we produced DEMs of the paleoglaciers during different stages. Later, from those DEMs, ELAs were calculated by using the automatic toolbox developed by Pellitero et al. (2015). The selected methods were the Accumulation Area Ratio (Porter, 1975) and the Area Altitude Balance Ratio (AABR; Osmaston, 2005). When applying the AABR, we considered two BR, namely: 1.75 ± 0.71 (global) and 1.9 ± 0.81 for mid-latitude maritime glaciers (Rea, 2009). We selected the latter, given the location of the study area in the mid-latitudes and the local influence of the Atlantic air masses. Conversely, for the AAR, the ratio 0.6 ± 0.05 (Porter, 1975) has been applied.

## 4. Results

The spatial distribution of glacial and periglacial landforms across the Bacivèr Cirque suggests the occurrence of a sequence of periods during the deglaciation of the cirque. The timing of these phases is constrained by 17 $^{10}$Be CRE ages inferred from glacial and periglacial records (Table 2).

### 4.1. Geomorphological evidence and CRE sampling strategy

Bacivèr is a large amphitheatre-shaped cirque (5 km long, 3.8 km wide) that forms the headwaters of the Malo River, which drains towards the Beret Plateau and flows into the Garonne River 6 km below. This complex cirque can be divided in three large geomorphological units (Fig. 2): (i) the peaks and walls that form the head of the amphitheatre, (ii) the set of glacial, periglacial and paraglacial landforms distributed at the foot of the walls, and (iii) the large flat floor, composed of polished bedrock surfaces with small depressions and scattered erratic boulders. The cirque was heavily glaciated during the last glacial cycle, and the deglaciation following the LGM left widespread glacial and periglacial records (Fig. 3):

(i) The cirque floor shows traces of intense glacial abrasion, with very scarce glacial deposits, mostly in the form of small, vegetated moraine ridges and some sparse erratic boulders. The short vertical distance between the cirque's walls and its floor implied low debris supply, which may explain the relatively small size of the moraine systems distributed across the cirque. Glacial erosion on the cirque floor generated several staggered, over-deepened basins that were occupied by lakes following deglaciation. From the central-lower part of the cirque, we collected three samples for CRE dating, two from polished surfaces (A-14, A-15) and one from an erratic boulder (A-10). The cirque gradually narrows downstream, becoming a steep U-shaped glacial valley until the confluence with the Beret Plateau at 1860 m. This lowest section mainly includes polished surfaces, with few remnants of moraine deposits due to the topographical setting, which favors intense erosion processes that have destroyed glacial accumulations. Here, we collected two samples from a polished bedrock surface (A-16, A-17) that is indicative of the onset of deglaciation of the bottom of the Bacivèr valley.

(ii) The Bacivèr Cirque constitutes a compound cirque (Barr and Spagnolo, 2015) composed of five smaller cirques with NW, N, E, SE and SW aspects (Fig. 3). Depending on the deepening of the individual cirques, distinct geomorphological sequences are present: (a) in steep and heavily carved out landforms (e.g. SE- and SW-exposed cirques), there are several generations of rock glaciers distributed in the upper part of the cirque basins that still show well-preserved furrows and ridges, with vegetation colonizing the lowest crests that reflects their current inactivity; in addition, some moraine ridges surround these landforms and enclose these small cirques distributed above the cirque floor; in the E cirque, there is also a small, collapsed, debris-covered glacier with longitudinal ridges and furrows; (b) elongated moraine ridges

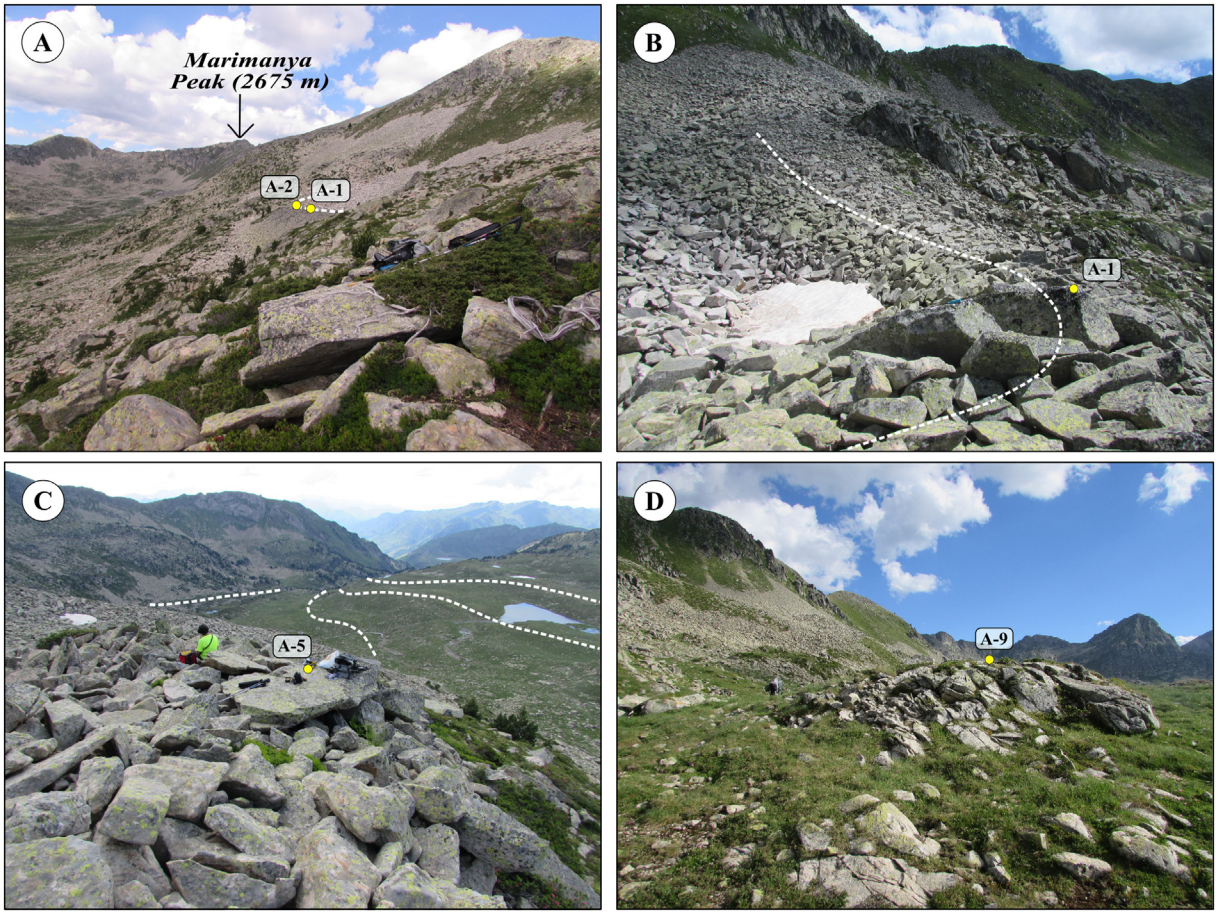


**Fig. 2.** Examples of the main geomorphological units in the Bacivèr Cirque, together with the location of the dated samples: (a) peaks and cirque walls; (b) moraine generated by the debris-covered glacier at the foot of the cirque walls; (c) view of the cirque floor (with minor moraine ridges marked in the picture) from the highest moraines; and (d) polished bedrock surfaces distributed in the cirque floor.

fill the depressions in small glacial hollows at the contact between the cirque floor and the steep but short rock slopes (e.g. NW and E units).

The chronological study focused particularly on the eastern side of the main Bacivèr Cirque, at the foot of the summit ridge stretching N—S between Tuc de Marimanya and Cap del Muntanyó d'Àrreu (2602 m), where the main glacial and periglacial deposits are distributed. The northern side forms a 1 km-long, straight profile with peaks ranging from 2630 to 2530 m, and an elongate moraine, parallel to the wall at a distance of only 200 m, stretching over 800 m at altitudes between 2410 and 2460 m; here, we collected samples for CRE dating (A-11, A-12) from two moraine boulders. The southern hollow is more excavated by glacial and periglacial processes, including four small tongue-shaped moraines filling the hollows with polished surfaces among them. We collected two samples from the northernmost moraine ridge only 180 m from the wall (A-1, A-2), two samples from the central part of the polished bedrock 180 m from the wall (A-3, A-4), two samples from the external moraine of a debris-covered glacier 160 m from the wall (A-5, A-7), and one sample from a boulder located on a ridge inside this moraine 120 m from the wall (A-6). Moreover, we collected three samples from polished bedrock surfaces at distances of ~100–200 m from the moraines and ~ 300–400 from the wall, in both areas (A-8, A-9, A-13).

(iii) The peaks surrounding the cirque have relatively homogeneous altitudes ranging from 2500 to 2650 m, with small elevation differences of 150–200 m with respect to the base of the cirque floor. The cirque walls are steep and covered by a thick debris mantle generated by the intense frost shattering of the upper rock outcrops.

### 4.2. Geochronological data

The 17 samples collected for CRE dating yielded ages spanning from the B-A to the Mid-Late Holocene (Fig. 4). Glacial retreat during the last deglaciation in the Bacivèr valley started following the LGM according to the lowermost samples, which yielded ages of 18.6 ± 1.2 (A-17) and 14.2 ± 0.4 ka (A-16), respectively. Sample A-17 is considered an outlier because it is 3–4 ka older and its analytical uncertainty is significantly higher compared to the remaining samples of the dataset, and therefore is not further discussed.

Post-LGM glacial shrinking exposed the central-lowest part of the cirque floor, as revealed by the samples collected from the polished bedrock that yielded ages of 13.5 ± 0.4 (A-14) and 14.1 ± 0.4 ka (A-15) (13.8 ± 0.4 ka; $n = 2$) as well as from a scattered erratic boulder 15.4 ± 0.6 ka (A-10). The samples collected from polished bedrock in the upper part of the cirques show ages very similar to those of the central-lower sector. The sample from the northern side yielded an age of 15.2 ± 0.6 ka (A-13), whereas the samples from the southern sector of the Bacivèr Cirque were aged 15–14 ka (A-8 and A-9, respectively).

The two sampled boulders from the moraine of the northern side of the cirque returned ages of 10.0 ± 0.4 (A-12) and 13.3 ± 0.5 ka (A-11), although the former is not consistent with the chronostratigraphic sequence and thus was rejected. By contrast, the more robust chronology of the southern cirque unit gave slightly older ages of 12.7 ± 0.5 (A-1) and 12.8 ± 0.4 ka (A-2) (12.8 ± 0.5 ka; n = 2) for the boulders of the northernmost moraine. Samples from the polished bedrock dividing

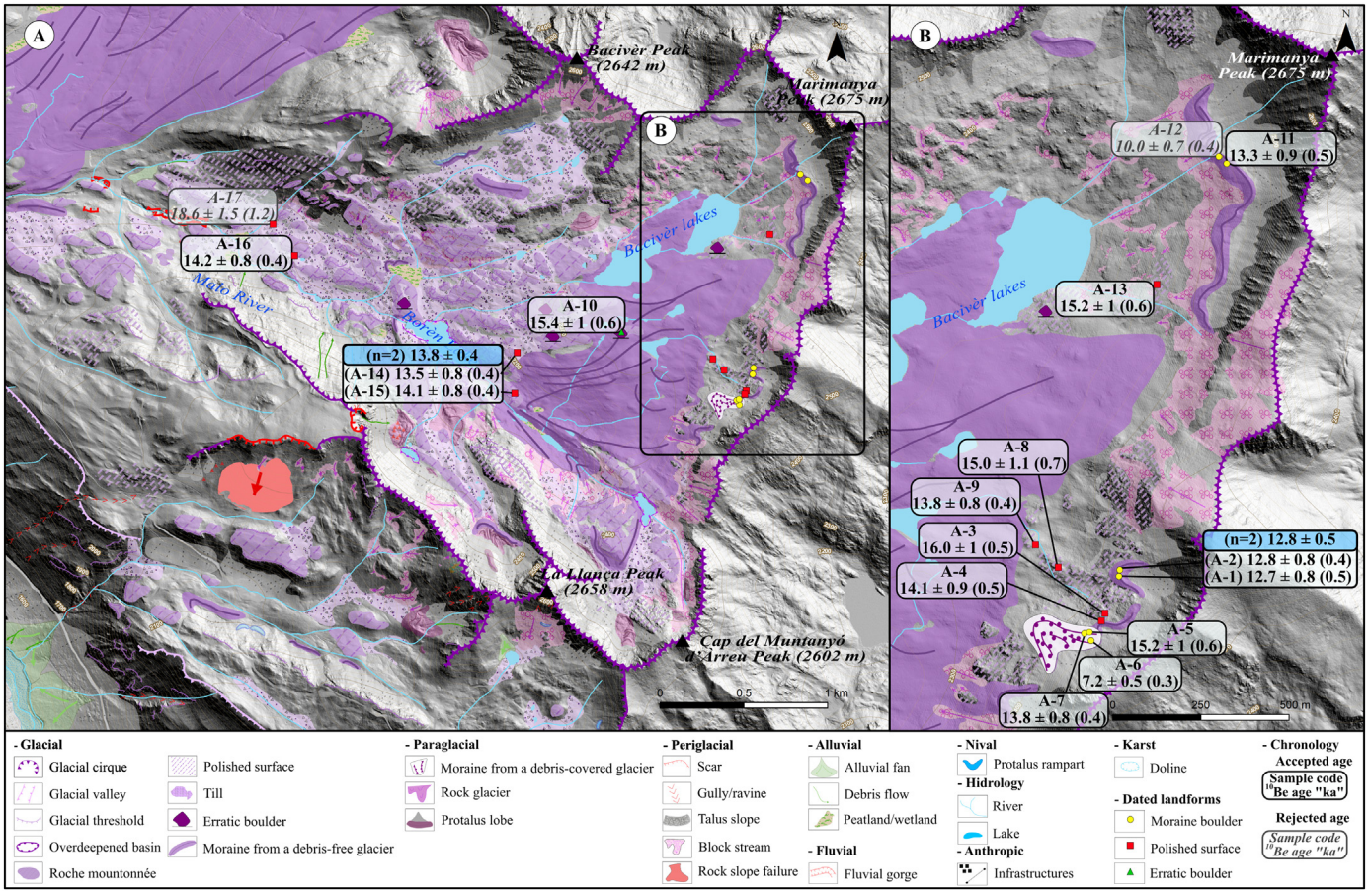


**Fig. 3.** (a) Geomorphological map of the study area, with CRE results of the dated landforms; and (b) enlargement of the eastern part of the cirque where a larger number of samples were collected.

the moraine ridges within the cirque yielded an age range of ~16–14 ka (A-3 and A-4, respectively). These are slightly older than the ages of boulders on the external moraine of a debris-covered glacier that were dated at 15–14 ka (A-5 and A-7, respectively). Finally, one sample from the external ridge inside this landform was dated at 7.2 ± 0.3 ka (A-6).

## 5. Discussion

The combination of geomorphological observations with $^{10}$Be-dated glacial features distributed across the Bacivèr Cirque enabled us to infer space-time patterns of deglaciation in the cirque since the Late Glacial. In addition, this chronology also indicates the timing of formation of a debris-covered glacier located on the highest slopes of the cirque:

### *5.1. Chronology of the deglaciation and geomorphological significance*

The age of polished glacial surfaces indicated that the deglaciation of the mouth of the cirque - where it gradually turns into a narrow U-shaped glacial valley - had occurred by 14.2 ± 0.8 ka, and consequently that the Bacivèr tributary glacier was disconnected from the main Garonne paleoglacier flowing from the upper Beret Plateau downslope through the Aran valley prior to this time (A-16; Fig. 5).

Glacial retreat was a very rapid process during the B-A as the entire cirque was deglaciated by ~15–14 ka, according to polished surfaces from the central-lowest part of the cirque floor. These surfaces yielded a deglaciation age (13.8 ± 0.4 ka) that overlaps with that inferred from samples collected from the highest areas of the cirque, both from the eastern (~15–14 ka) and northern sides (15.0 ± 0.7 ka). There are minor inconsistencies between the CRE dataset (see Table 2) and the geomorphological stratigraphy, as some boulders are slightly older than the ages of the polished bedrock surfaces on which they rest. This may be due to nuclide inheritance: (i) the boulder may have fallen on the glacier during a period of glacial shrinking that exposed the highest section of the cirque walls, and it was subsequently transported supraglacially a few hundred meters prior to deposition on the cirque floor (Çiner et al., 2017); or (ii) the boulder was not reworked enough (inefficient erosion) given its closeness to the cirque headwall and the subsequent limited bearing and transport distance (see García-Ruiz, 1979). Also, variations in the local snow cover, which is much thicker on bedrock surfaces than on boulders that protrude considerably from the ground, might be responsible for the age differences. We therefore consider that within the geomorphological and analytical uncertainties of the CRE dating, the exposure of erratic boulders and related polished bedrock started roughly at the same time. Ice-moulded surfaces within the individual glacial cirques provided similar deglaciation ages (Fig. 3; ~16–14 ka). This phase, however, is compatible with the occurrence of periods of relative glacial stability, which may have generated the small moraine ridges distributed on the main cirque floor (Fig. 3), as well as the small debris-covered glacier located in the eastern hollow of the Bacivèr Cirque. Here, two boulders returned slightly younger ages (~15–14 ka; see Table 2) than the neighboring polished bedrock (~16–14 ka). These exposure ages from the highest surfaces suggest that the rapid glacial shrinking recorded during the B-A probably favored the disappearance of glaciers in the cirque by ~15–14 ka, with some stagnant ice masses in favorable topographical settings under the protection of the wall and with an intense debris supply.

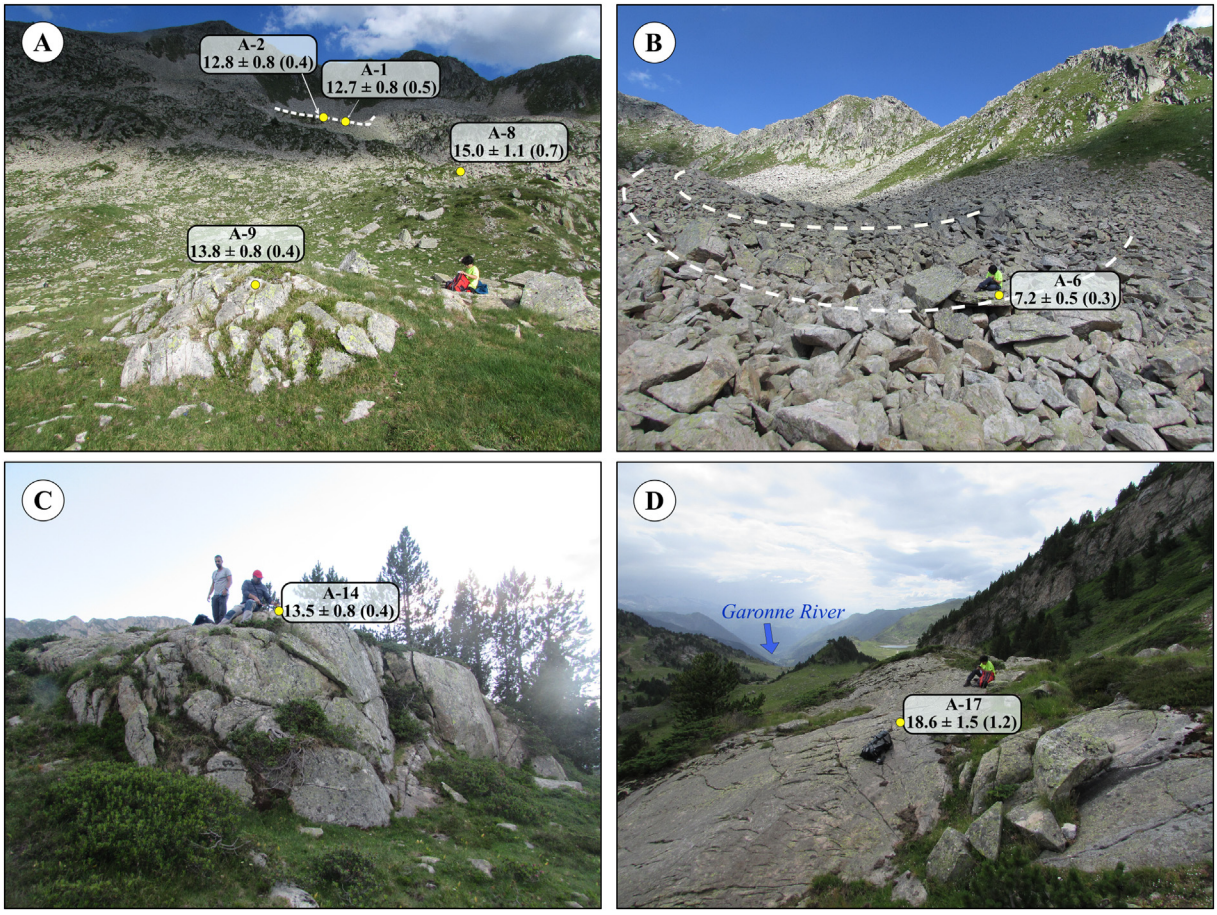


**Fig. 4.** Examples of sampled moraines and polished bedrock, together with CRE ages (ka).

In short, the considerable homogeneity of the CRE results in the area seems to indicate a rapid retreat of 3 km of the glacier at the beginning of B-A, with only small glaciers (200–300 m long) sheltered by the wall surviving, and under an intense paraglacial activity. This abundant debris supply caused the residual glaciers to evolve towards a range of typologies, including debris-covered glaciers in some cirques, and rock glaciers in others. These landforms are widespread features in deglacierizing mountains that transition from glaciated into paraglacial landscapes (Knight et al., 2019). The coincidence of the ages of the boulders belonging to these formations and those of the rock platforms where they rested indicates the short time elapsed between the general deglaciation and the collapse of these residual small glaciers, which determined the stabilization of their deposits (Fig. 3).

Exposure ages of moraine boulders revealed that the highest moraine was abandoned and finally stabilized at 12.8 ± 0.5 ka, whereas one sample from the northernmost dated landform (Fig. 3) yielded a

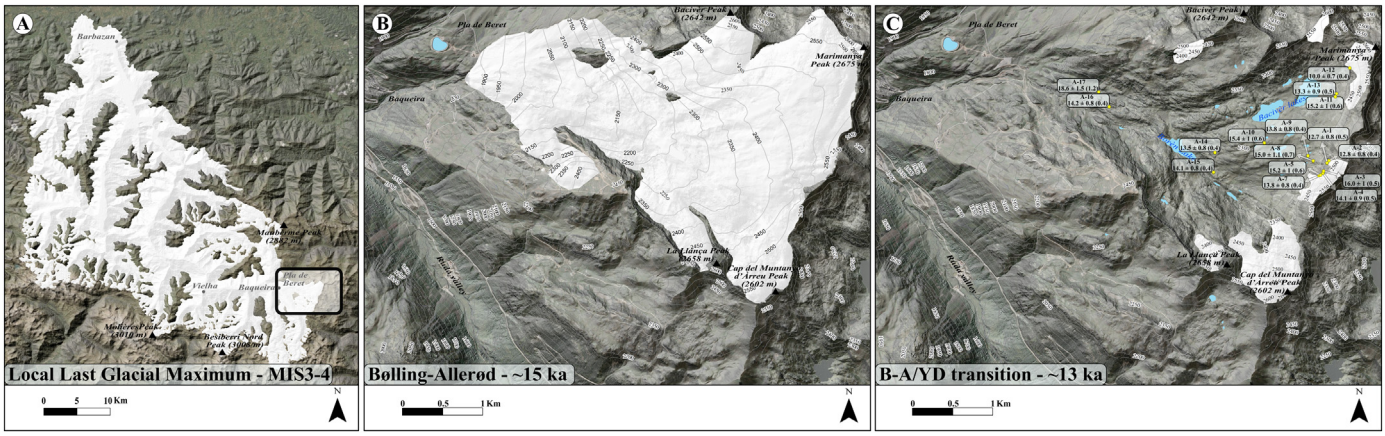


**Fig. 5.** Glacial extent and ice thickness in the Bacivèr Cirque during different time stages: (a) ice thickness in the cirque adapted from the reconstruction of Fernandes et al. (2017) for the entire Upper Garonne Basin; (b) ice extent prior to the OD deglaciation in the lower part of the cirque (the limits of the glaciers during that phase are not yet determined); and (c) ice masses that existed in the cirque during the YD.

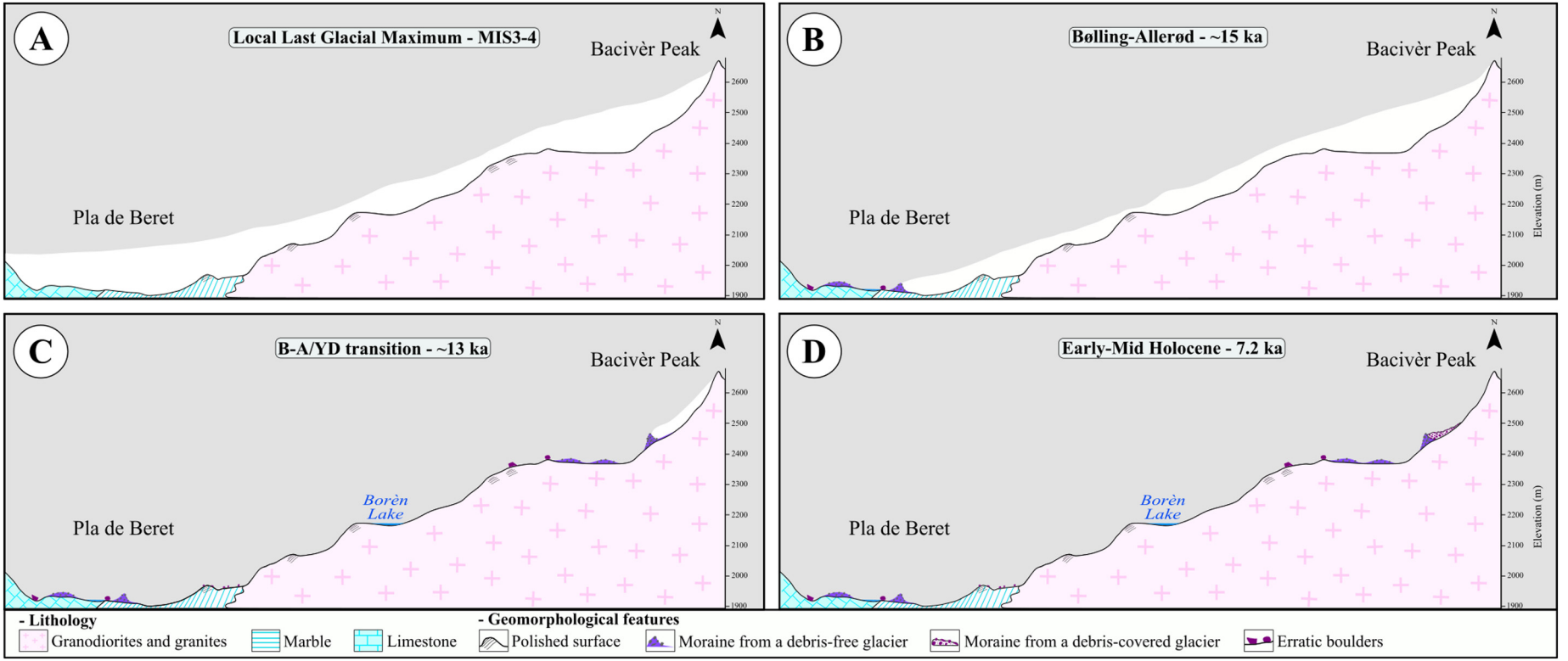


**Fig. 6.** Schematic evolution of the formation of the moraine system and rock glaciers in the Bacivèr Cirque during the last deglaciation: (a) the cirque was covered by a thick ice cover during the maximum ice extent of the last glacial cycle; (b) at the end of the OD, glaciers receded towards the highest valleys and left widespread small moraine ridges and glacial boulders across the Beret Plateau; (c) during the B-A, deglaciation was a very rapid process and the entire Bacivèr Cirque was ice free by ~14–15 ka; and (d) ice expansion during the YD favored the formation of small glaciers at the foot of the highest peaks of the cirque.

**Table 4**
Glacial activity during the main cold and warm periods following the LGM in different Iberian mountains.

| Mountain range | Massif/area | Oldest Dryas | Bølling-Allerød | Younger Dryas | Early to mid-Holocene | References |
|---|---|---|---|---|---|---|
| Pyrenees | Eastern | The existence of frontal moraines generated at 17–15.5 ka demonstrates the existence of glacial advances in Puigpedrós-Tossa Plana de Lles massifs, Carlit massif and in the Têt valley (lengths 2–3 km). These moraines were relatively close to the headwalls of the valleys at 2200–2300 m. | CRE ages show a rapid retreat of glaciers towards the interior of the cirques in the Puigpedrós-Tossa Plana de Lles massifs and Ariège valley, sometimes coetaneous with the formation of rock glaciers, which stabilized shortly after their formation | Moraines formed at 13–11.5 ka have been dated in the Puigpedrós-Tossa Plana de Lles massifs and Ariège valley. These complexes are located at 2300–2400 m, and at 1–1.5 km from the headwalls in the highest and north-facing cirques | The last glaciers disappeared during the mid-Holocene and gave rise to the formation of rock glaciers in the Ariège | Delmas et al. (2008), Pallàs et al. (2010), Palacios et al. (2015a, 2015b), Delmas (2015), Tomkins et al. (2018), Andrés et al. (2018), Jomelli et al. (2020) |
| Pyrenees | Central | Lateral and frontal moraines have been dated in the Gállego Valley at ~16 ka (length 11 km). Moraines within the cirques have been also dated at ~16 ka in lower cirques (e.g. Piniecho) at 2400 m (length 0.3 km). | CRE ages evidence a rapid retreat of the glaciers towards the interior of the cirques in Noguera Ribagorçana, Ésera and Gállego valleys | Glaciers formed during the YD generated moraines at the end of this period in the highest valleys of the Noguera Ribagorçana and Gállego basins at distances of 2–6 km from the cirque headwalls. Once they melted, rock glaciers developed in the interior of many cirques | Some rock glaciers stabilized during the mid-Holocene in cirques of the Gállego valley | Pallàs et al. (2006), Crest et al. (2017), Palacios et al. (2017a, 2017b), Tomkins et al. (2018) |
| Cantabrian Mountains | Central Massif and Montaña Palentina | A frontal moraine was dated at ~15 ka and other arches suggest front stagnations and/or minor re-advances at 17.5 ka in the Monasterio valley. Evidence of glacial advances, with formation of moraines at 17–16 ka also reported in the Montaña Palentina. Rock glaciers were active by 16 ka in the Porma catchment | Glacial retreat and formation of rock glaciers in some cirques such as the Monasterio catchment during the B-A | Possible presence of glaciers in the higher north-facing cirques | No evidence of glacial activity has been found in this range | Rodríguez-Rodríguez et al. (2016), Rodríguez-Rodríguez et al. (2017), Pellitero et al. (2019) |
| Central Range | Sierra de Guadarrama | Moraines from 16 to 17 ka very close to the LGM ones. Rock glacier stabilization at 15 ka | Glacial retreat and definitive disappearance of most of the glaciers | Possible existence of small glacierets in Peñalara. Definitive disappearance of the ice at 11.7 ka | No evidence of glacial activity | Palacios et al. (2012), Carrasco González et al. (2016) |
| | Sierra de Gredos | Glacial readvances in many valleys left several push moraines at 17.5–16 ka, a few hundred meters behind LGM moraines | Rapid retreat of the glaciers to the interior of the cirques, at the foot of the headwalls | Small glaciers in the interior of the north facing and higher cirques | Retreat at 10 ka as the last evidence of glacial activity | Palacios et al. (2011), Carrasco et al. (2015) |
| Iberian Range | Demanda, Cebollera and Urbión | Glacial recovery and readvance at ~17 ka in the San Lorenzo cirque, with a small ice tongue (300 m long) at 1950 m that deposited the highest moraine. Formation of a rock glacier at ~15 ka in the Peña Negra cirque | Glacial retreat and development of rock glaciers inside some cirques and onset of the collapse of some debris-covered glaciers (San Lorenzo cirque) | Chronological evidence of glacial advances is not yet available, although the presence of glaciers during this period is likely in the Demanda, Mencilla and Urbión massifs | Evidence of glacial activity in the Iberian Range during the Early Holocene is limited to the remnants of a small debris-covered ice mass in the San Lorenzo and Mencilla cirques although they remained active until mid-Holocene | Vegas (2007), Fernández-Fernández et al. (2017), García-Ruiz et al. (2020) |
| Betic Range | Sierra Nevada | Glacial readvance at ~17 ka with ice tongues occupying the valley bottoms at 2500–2800 m (lengths 2–3 km). Formation of moraines close to the LGM moraine systems | Rapid glacial recession at ~15 to 14.5 ka as revealed by CRE dates of polished bedrock surfaces. Glaciers were probably only confined within the northern highest cirques | Glacier expansion at ~13 to 12 ka in the cirques and headwaters of the highest valleys at 2800–3000 m, namely in east-facing slopes (lengths ~1 km). Few glaciers existed on the southern slope and only in the westernmost valleys | Small glaciers persisted at the foot of the highest peaks at ~3000 m until ~10 to 9 ka. Their melting favored paraglacial processes with the development of rock glaciers that stabilized ~7 to 6 ka | Gómez-Ortiz et al. (2015), Gómez-Ortiz et al. (2012), Oliva et al. (2020), Oliva et al. (2014), Palacios et al. (2016) |

slightly older age of 13.3 ± 0.5 ka; the average of the three moraine samples results in an age of 12.9 ± 0.3 ka. Remarkably, we highlight that these are minimum ages that do not include erosion and snow corrections (Table 3). The uncertainty range of CRE dating and the small number samples makes it difficult to differentiate whether the moraine stabilized at the end of the B-A or at the beginning of the YD.

The absence of further glacial landforms at higher elevations suggests that the Bacivèr Cirque has not accumulated glacial ice since ~12.9 ka. However, the degradation of these glaciers enhanced paraglacial dynamics and the persistence of small ice masses as small debris-covered glaciers. A sample collected from a ridge of one such landform yielded an exposure age of 7.2 ± 0.3 ka. We interpret this as the age of stabilization of the boulder once the inner ice melted away and mobility ceased, which might be representative of the collapse/final melting of the inner sector of the debris-covered glacier (Fig. 6). The location of the sample on a ridge 100 m distant from the wall

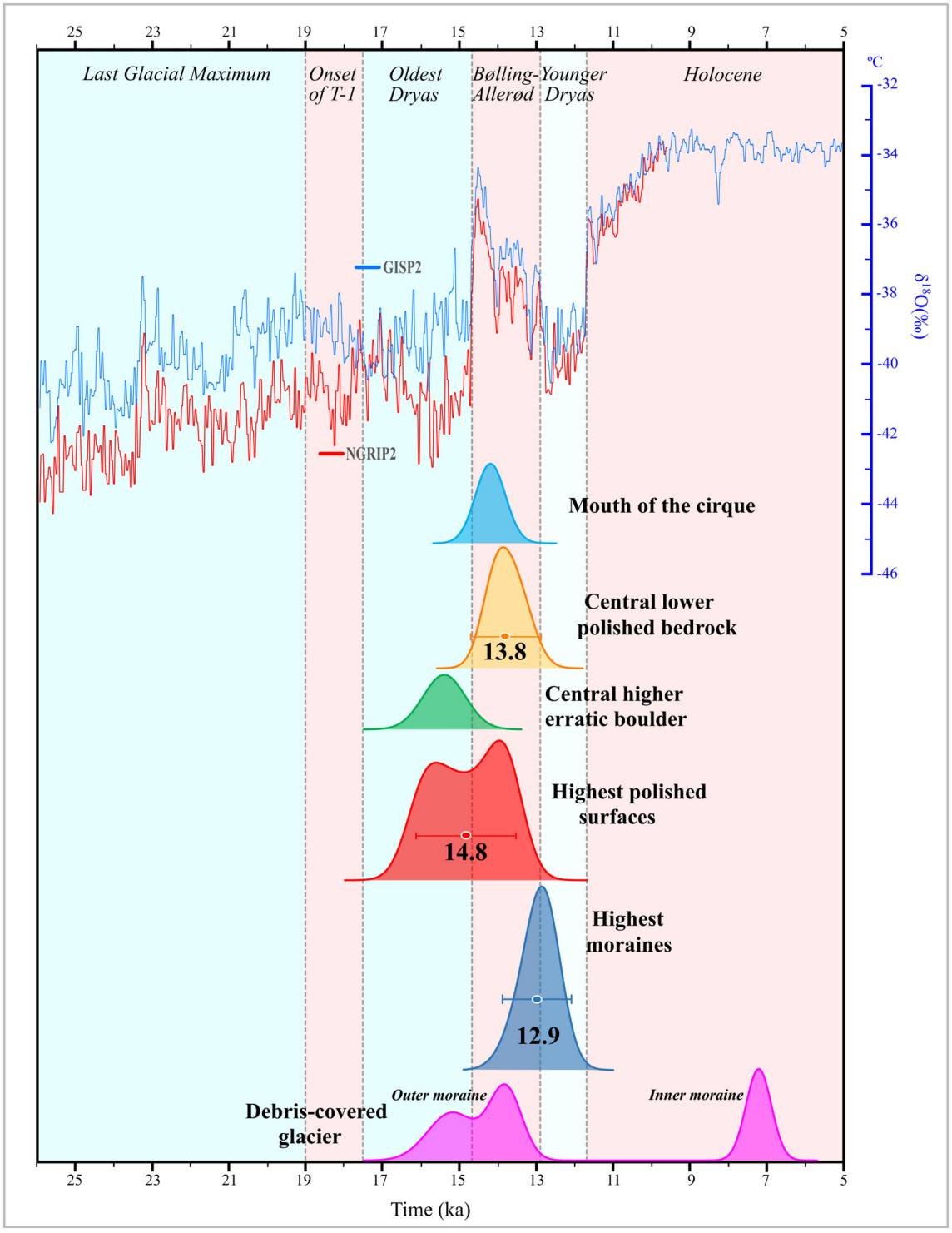


**Fig. 7.** Normalized probability distribution functions (PDF) of exposure ages vs. temperature evolution since the LGM based on the $\delta^{18}O$ record from the NGRIP ice core from Greenland (time periods are defined after Rasmussen et al. (2014)). The plots of the units result from the sum of the individual PDF of the samples belonging to them.

rules out the possibility of the boulder having fallen from the wall and supports this interpretation. Our data suggests that this debris-covered glacier formed under intense paraglacial dynamics following the deglaciation and stabilizing during the Early Holocene. Debris-covered and rock glaciers located in other small hollows of this valley and in similar relative positions may also have followed a similar pattern to that observed in other Pyrenean valleys (Andrés et al., 2018; García-Ruiz et al., 2016; Palacios et al., 2017b).

### *5.2. Late Quaternary glacial dynamics in the Central Pyrenees and Iberian Peninsula*

The Iberian ranges are among the mountains where knowledge about Pleistocene glacial evolution has most improved in the last decade (Oliva et al., 2019). New chronological information about their glacial history from recent years has been complemented with a better knowledge of the spatial and temporal dynamics of periglacial processes that

reshaped the landscape fashioned by Quaternary glaciers, particularly during the Holocene (Oliva et al., 2018, 2016).

In this Iberian context, together with the Sierra Nevada massif and the Cantabrian Mountains, the Pyrenees stand out as the mountain ranges where the numerous glacial studies have produced the best chronologies of glacial oscillations (Table 4). There is still an open debate and divergent information with regards to the timing of the maximum glacial advance during the last glacial cycle on both the northern and southern slope of the Pyrenees (Delmas et al., 2021). There is more consensus, and much more homogeneous information, about the timing of glacial advances and retreats during colder and warmer periods during T-1. However, most research has been conducted in the major glacial valleys and highest mountain cirques, whereas lower-altitude catchments remain poorly investigated. To shed light on the role of altitude and topographical conditions controlling glacial oscillations during T-1, we reconstructed the deglaciation process in the upper Garonne Basin focusing on one valley of its headwaters, the Bacivèr Cirque. The fact that its cirque summits reach only 2600–2650 m determined a pattern of deglaciation similar in both extent and timing to some of the tributaries of the Gállego Valley (Palacios et al., 2017b) or the Ariège Valley (Jomelli et al., 2020) - where summits are around 2600–2700 m - rather than that reported for glaciers developed at the foot of summits around 3000 m (García-Ruiz et al., 2016; Palacios et al., 2017b; Pallàs et al., 2006).

In the Pyrenees, the highest peaks exceeding 2900 m remained covered by extensive, thick and strongly erosive ice caps during the Late Quaternary, while in lower ranges between 2400 and 2800 m glaciers were much thinner. Consequently, many of these ridges emerged above the glaciers as nunataks (Delmas et al., 2021). This is of great importance for understanding the local geomorphological evolution during T-1, especially on substrates of crystalline rocks. The cirques of the highest peaks were intensely eroded by glacial processes, which removed the entire weathering mantle. As such, when glaciers retreated, paraglacial dynamics were less intense in these areas. By contrast, in lower-altitude massifs, the weathered mantle has been partially preserved on the walls (less affected by glacial erosion) and when glaciers retreated, paraglacial processes were comparatively more intense. For this reason, a greater diversity of glacial and periglacial sedimentary landforms, which can provide a detailed picture of the environmental evolution during deglaciation, is found in the interior of low-altitude crystalline cirques. This geomorphological pattern has also been identified in other mid-altitude cirques of the Central Pyrenees, such as Catieras, Piniecho and Brazato (Palacios et al., 2017b), as well as in other relatively high cirques in the Eastern Pyrenees, including Malniu and Perafita (Andrés et al., 2018).

The cold conditions that prevailed during the OD favored the reoccupation of the valley floors by glaciers at ~17–16 ka (Fig. 7), as occurred in several valleys in the Central and Eastern Pyrenees (Palacios et al., 2017a) (Table 4). At this time, the upper Garonne Basin must still have been extensively glaciated, with moraine systems located in the main valley also fed by the glacier descending from the Bacivèr Cirque that contributed ice to the Garonne paleoglacier (Fernandes et al., 2017). However, this phase was reconstructed based on the identification of moraine systems alone, and no direct ages are yet available for the upper Garonne valley.

**Table 5**
Reconstructed ELAs (m) for the YD moraines using the AAR and AABR methods.

| Glacier | AAR = 0.6 ± 0.05 | AABR = 1.9 ± 0.81 | AABR = 1.75 ± 0.71 | Average ELA |
|---|---|---|---|---|
| Malo | 2486 + 10/−5 | 2484 ± 10 | 2484 + 10/−5 | 2485 |
| Rosari | 2499 ± 5 | 2507 ± 10 | 2507 + 10/−5 | 2504 |

As temperatures rose by 3–5 °C in western Europe during the B-A Interstadial (Clark et al., 2012), the Garonne paleoglacier receded rapidly and several small alpine or cirque glaciers remained, individualized within the headwaters of the highest valleys. CRE dates of the lowest sections of the Bacivèr valley suggest that the disconnection between the Beret Plateau (i.e. Garonne paleoglacier) and the Bacivèr paleoglaciers took place prior to 14.2 ± 0.8 ka. At that time, the glacier had a length of 3.8 km and had shrunk significantly since the maximum ice expansion of the last glacial cycle, when the Garonne paleoglacier reached a length of 89 km (Fernandes et al., 2017). In fact, the overlapping between the samples collected from the cirque floor and the polished bedrock surfaces of the higher glacial thresholds suggests that deglaciation was a very rapid process and that the entire cirque (~10 $km^2$) was ice-free by ~15–14 ka. The presence of small (undated) moraine ridges distributed across the Bacivèr Cirque (Figs. 2c and 3) reveals the occurrence of short periods of glacial advance or standstills during the B-A. However, as small moraines, these ridges must have formed during short periods favoring shifts in glacier mass balance that resulted in stabilization or even very limited glacier growth within an overall trend of warming and accelerated retreat (see e.g. Chandler et al., 2016). The partial overlapping of the CRE uncertainty ranges impedes precise constraints of particular events within the cirque's deglaciation chronology, which has also occurred in other massifs in the Pyrenees where the transition between different T-1 cold/warm periods cannot be detected with high precision (e.g. Pallàs et al., 2006). In any case, glaciers in the Pyrenees during the B-A may only have persisted in the highest northern cirques of the highest massifs whereas low-altitude catchments must have been ice-free during this period (Oliva et al., 2019), as most of the glaciated massifs were during the OD in the Mediterranean region (Palacios et al., 2017b, 2017a). In the Alps, glacial extents were significantly reduced during the B-A and glaciers only persisted in the highest sectors of the highest valleys (Ivy-Ochs, 2015).

The cooling from the B-A to the YD in Western Europe has been quantified at 5–10 °C (Clark et al., 2012), although it might have been lower in the Iberian Peninsula: terrestrial records suggest a temperature decrease of 2.5 °C (Iriarte-Chiapusso et al., 2016) whereas marine records from the Alborán Sea (Cacho et al., 2002) and the Portuguese coast (Rodrigues et al., 2010) point to temperatures lower by 4–5 °C. In parallel to the lower temperatures that generally prevailed during the YD, significant hydrological shifts were recorded (Bartolomé et al., 2015; Cheng et al., 2020; Rea et al., 2020) that must have affected the ELA in the Central Pyrenees. In the case of the Bacivèr cirque, we assume that these small glaciers readvanced or stabilized at the transition between the B-A and the YD, probably due to the protection of a thick debris cover on a glacier that did not reach the cirque floor. These cirque glaciers were small (Fig. 5), with lengths of 0.2–0.3 km and surface extents of 13–18 ha, and with their fronts at elevations of ~2400 m. These glaciers represented only ~0.3% of the length of the Garonne paleoglacier during the maximum ice extent of the last glacial cycle (Fernandes et al., 2017). This pattern is similar to that in in the Upper Gállego Valley (Catieras and Piniecho cirques) where the B-A frontal moraines are located 0.4–0.6 km from the headwall, at 2300–2350 m, in cirques where the maximum elevations are ~2700 m, slightly higher than in the Bacivèr Cirque (Palacios et al., 2017a). Similar to the Bacivèr cirque, in the Alps, glacial expansion during the B-A/YD transition left two moraine systems that were dated between ~13.5 and ~12 ka (Ivy-Ochs, 2015); in the highest mountains in Greece on Mount Olympus moraines stabilized at ~13.5–11.7 ka (Styllas et al., 2018) and on Mount Chelmos at ~13.1–10.5 ka (Pope et al., 2017); and in Anatolian mountains two phases occurred at ~13 and ~ 11.5 ka, both in the Kaçkar Mountain range (Akçar et al., 2007) and Uludağ Mountain (Zahno et al., 2010).

Based on the reconstruction of the two dated moraine ridges, during the transition between the B-A and the YD, the ELA in the Bacivèr Cirque must have been at 2485 and 2504 m, respectively (average 2495 m; Table 5). The current regional 0 °C isotherm in the Central Pyrenees lies at ~2950 m (López-Moreno et al., 2019), which roughly coincides with the ELAs in some still glaciated massifs such as Monte Perdido and

Maladeta (Chueca et al., 2005). Therefore, assuming an ELA depression of 455 m with respect to the current regional estimate of 2950 m, an average lapse rate of 0.65 °C 100 $m^{-1}$ and no change in precipitation – as inferred for some areas in the Mediterranean region, such as the Maritime Alps (Spagnolo and Ribolini, 2019) – summer temperatures must have been ~3.0 °C lower than at present during the transition between the B-A and the YD to allow the formation or stabilization of such small glaciers. Mass balance models suggest slightly lower temperatures in the Ariège Valley, ranging from 3.9 and 5.1 °C, based on the reconstruction of glaciers from the moraine systems of two cirques (Jomelli et al., 2020).

Overall, our results and those from other studies in the Pyrenees show that the time spanning from the early B-A to the YD was a major driver of landscape change in the high sectors of the Pyrenees as: (i) prevailing warm conditions promoted the definitive disappearance of glaciers in most cirques, particularly in low-to mid-altitude cirques, (ii) glacial shrinking favored the formation of debris-covered glaciers that extend over the cirque floors, and (iii) glacial retreat was followed by very intense paraglacial dynamics that favored the formation of permafrost-related landforms such as rock glaciers and protalus lobes (Fernandes et al., 2018) as well as abundant slope failures in formerly glaciated areas (Fernandes et al., 2020).

The temperature increase of ~4 °C in western Europe recorded at the onset of the Holocene (Clark et al., 2012) favored the disappearance of YD glaciers. However, as detected in some cirques at the foot of the highest peaks, at ~2900–3000 m in the Central and Eastern Pyrenees (Table 4), intense paraglacial adjustment following glacial shrinking led to the formation of rock glaciers (Andrés et al., 2018; Oliva et al., 2016). Indeed, the deep glacial hollows excavated in steep slopes surrounding the Bacivèr Cirque included well-developed rock glaciers. Interestingly, in an east-facing hollow that was less excavated by glacial and periglacial erosion, a debris-covered glacier formed once climate conditions became unfavorable for glacial activity. According to the exposure age of the sampled boulder (sample A-6) suggesting its geomorphic stabilization, this landform must have contained glacial ice until at least ~7.2 ka, when it finally melted away during the Holocene Thermal Maximum (Renssen et al., 2009). This timing is very similar to the stabilization of rock glaciers in the Central and Eastern Pyrenees (Andrés et al., 2018; García-Ruiz et al., 2016; Palacios et al., 2015a), as well as to the final collapse of the debris-covered glaciers that existed in the Sierra de la Demanda, Iberian Range, that persisted until 7–6 ka (Fernández-Fernández et al., 2017). As revealed by present-day analogs, these landforms can undergo significant morphodynamic changes in deglacierizing mountains and may have a long residence time in the landscape (Knight et al., 2019). Ice can thus persist protected beneath the debris cover in sheltered areas, little affected by atmospheric temperatures, as also detected in Iceland (Campos et al., 2019; Fernández-Fernández et al., 2020; Tanarro et al., 2019).

However, recent research has also shown that debris-covered glaciers can be more sensitive to climate variability than initially thought, as some features may respond rapidly to changes in temperature and precipitation (Charton et al., 2020). Therefore, when interpreting past glacial oscillations both climate changes as well as paraglacial processes must be taken into account. This means that the great intensity of the paraglacial readjustment in these cirques, under relatively low-altitude peaks in crystalline rocks and where the rock walls retain most of the weathered mantle, interferes with the effects of climate on glacier dynamics. In any case, it should be highlighted that the same chronological pattern for the deglacial period was also observed in cirques with similar characteristics in the Central (Palacios et al., 2017b) and Eastern Pyrenees (Andrés et al., 2018). The new debris cover on the glacier surface, supplied by paraglacial processes, can promote glacier advance or long-term stability by drastically reducing the ablation and shifting mass balance (Herreid and Pellicciotti, 2020). As such, paraglacial processes can interrupt the deglaciation process to some extent even without climatic influence (Hambrey et al., 2019, 2008; Jones et al., 2019; Rowan et al., 2015). The factors controlling the advances/retreats of debris-covered glaciers, as well as their collapse, are not fully understood, and further research is needed to clarify their response to short- and long-term climate trends. This is particularly important in the current global warming scenario, where glacier shrinking is accelerating and paraglacial processes are delivering large amounts of sediment to the surface of glaciers, considering that 7.3% of the area of mountain glaciers is debris-covered and this percentage is expected to increase in response to increasing temperatures (Herreid and Pellicciotti, 2020).

Since the inferred disappearance of glacial ice of the cirque at ~7.2 ka, the natural evolution of the landscape of the Bacivèr Cirque has been driven mainly by nival processes and periglacial dynamics (Fernandes et al., 2017). Current morphodynamics are associated with the occurrence of a seasonal frost ground thermal regime, as permafrost conditions are only found extensively in areas above 2900 m in the Central Pyrenees (Serrano et al., 2019), much higher than the highest summits of the Bacivèr Cirque.

In summary, the reconstructed temporal pattern of deglaciation of the Bacivèr Cirque during T-1 is fully consistent with the timing reported in other sectors of the Pyrenees (Andrés et al., 2018; Palacios et al., 2017b) and other Iberian mountains (see summary in Oliva et al., 2019) with accelerated glacier retreat during the B-A, and the subsequent activation of paraglacial processes and a minor glacial re-expansion during the B-A/YD transition. No disparity in timing of maximum ice extent across the Mediterranean mountains is observed during the last deglaciation. The ages of glacial advances and retreats in Iberia during T-1 are similar to those that occurred in central-northern Europe, such as Iceland (Fernández-Fernández et al., 2020), the British Isles (Barth et al., 2016), and the Alps (Ivy-Ochs, 2015; Moran et al., 2016). The chronology is also similar to that reported in other temperate European mountains, such as the Anatolian Peninsula (Köse et al., 2019; Sarıkaya et al., 2017), the Carpathians (Gheorghiu et al., 2015; Makos et al., 2018), the southern Balkans (Styllas et al., 2018), the Dinaric Alps (Žebre et al., 2019), and Atlas Mountains (Hughes et al., 2018). Indeed, the timing of oscillations resembles the past evolution of the Scandinavian Ice Sheet, which retreated considerably during the B-A and regrew and advanced tens of km as temperatures declined during the transition towards the YD (Greenwood et al., 2015; Hughes et al., 2016; Mangerud et al., 2016). All in all, the data seems to indicate that deglaciation followed very homogeneous climatic patterns throughout Europe, with minor differences imposed by local topoclimatic conditions.

## 6. Conclusions

One of the main attractions of the natural heritage of the Central Pyrenees is its glacial landscape. During Quaternary colder phases, glaciers have fashioned the valleys and cirques, which were subsequently reshaped by periglacial conditions during the warmer interglacial periods. Despite the fact that the highest massifs of the Central Pyrenees are some of the mid-latitude mountain areas where glacial evolution has been studied in the greatest detail, the timing of development of glacial phenomena remains poorly investigated for cirques at lower altitudes. This is the case of the Bacivèr Cirque, from where we introduced CRE ages of glacial landforms that are indicative of glacial oscillations during T-1 in the upper Garonne valley.

The Atlantic-influenced upper Garonne Basin favored the development of the longest glacier in the entire range (~90 km) despite having its headwaters at elevations of 2600–2650 m, 600–800 m lower than the highest peaks in the Pyrenees. The chronology of deglaciation of one of the cirques in the headwaters of the Garonne paleoglacier also contributes to a better understanding of glacial oscillations on the northern slope of the Pyrenees. The Bacivèr Cirque, with its wide cirque floor located at 2200–2400 m, was located above the regional ELA during the maximum ice extent of the last glacial cycle. As temperatures increased following the LGM, glaciers rapidly retreated to the headwaters of the highest

valleys and the glacier flowing downvalley from the Bacivèr Cirque became disconnected from the Garonne Glacier prior to ~15–14 ka, when the lowest part of the cirque became ice free. Glacial recession was enhanced during the B-A at ~15–14 ka, with the cirque likely being fully deglaciated. Small cirque glaciers formed or remained at the foot of the wall during the transition between the B-A and the YD. These small glaciers were affected by paraglacial readjustment of the slopes, which triggered their transformation into rock glaciers and a debris-covered glacier. Their fronts collapsed almost immediately, but in some cases, their upper sections remained active during the Early Holocene, until at least ~7 ka; since then, periglacial slope processes and nival activity have shaped the highest parts of the massif. The chronology of glacial advances and retreats during T-1 reconstructed from the Bacivèr Cirque is similar to that reported from other lower Pyrenean glaciers. Therefore, the period spanning from the early B-A to the transition towards the YD dramatically transformed the mountain landscape of the Pyrenees and favored the development of the great geomorphological diversity of glacial and periglacial landforms that exists today in many cirques of this mountain range.

The glacial and periglacial landscape of the Bacivèr Cirque inherited from past periods and slightly reshaped during the current interglacial is also being intensely transformed by human activities. The expansion of the neighboring ski resort, with the ski slopes and associated infrastructure, has already destroyed geomorphic evidence. The findings presented in this study are thus clear evidence of the richness of crucial information that this cirque contains, and of the need to preserve its landscape for future generations.

## Declaration of competing interest

The authors of this manuscript declare that they have no known competing financial interests or personal relationships that could have appeared to influence the work reported in this paper.

## Acknowledgements

This research was funded by the Research Group ANTALP (Antarctic, Arctic, Alpine Environments; 2017-SGR-1102) funded by the Government of Catalonia and by the Research Group ZEPHYRUS (Climate Change and Environmental Systems) of the Universidade de Lisboa. The study topics complement those of the project PALEOGREEN (CTM2017-87976-P) funded by the Spanish Ministry of Economy and Competitiveness and the NUNANTAR project funded by the Fundação para a Ciência e Tecnologia of Portugal (02/SAICT/2017 - 32002). Marc Oliva is supported by the Ramón y Cajal Program (RYC-2015-17597). José María Fernández-Fernández is supported by a postdoctoral grant within the NUNANTAR project, whereas Marcelo Fernandes holds a PhD fellowship of the Fundação para a Ciência e Tecnologia of Portugal (FCT - UIDB/00295/2020). The $^{10}$Be and $^{36}$Cl measurements were performed at the ASTER AMS national facility (CEREGE, Aix en Provence), which is supported by the INSU/CNRS and the ANR through the "Projets thématiques d'excellence" program for the "Equipements d'excellence" ASTER-CEREGE action and IRD. This research is also supported and framed within the College on Polar and Extreme Environments (Polar2E) of the University of Lisbon. We thank Jesús Ruiz-Fernández and María Palacios for their support in the field. We also thank Matteo Spagnolo and an anonymous reviewer for their comments on a draft of this paper.

## References

Akçar, N., Yavuz, V., Ivy-Ochs, S., Kubik, P.W., Vardar, M., Schlüchter, C., 2007. Paleoglacial records from Kavron Valley, NE Turkey: field and cosmogenic exposure dating evidence. Quat. Int. 164–165, 170–183. https://doi.org/10.1016/j.quaint.2006.12.020.

André, M.F., 2002. Rates of Postglacial rock weathering on glacially scoured outcrops (Abisko-Riksgränsen area, 68°N). Geogr. Ann. Ser. A Phys. Geogr. 84, 139–150. https://doi.org/10.1111/j.0435-3676.2002.00168.x.

Andrés, N., Gómez-Ortiz, A., Fernández-Fernández, J.M., Tanarro, L.M., Salvador-Franch, F., Oliva, M., Palacios, D., 2018. Timing of deglaciation and rock glacier origin in the southeastern Pyrenees: a review and new data. Boreas 47, 1050–1071. https://doi.org/10.1111/bor.12324.

Arnold, M., Merchel, S., Bourlès, D.L., Braucher, R., Benedetti, L., Finkel, R.C., Aumaître, G., Gottdang, A., Klein, M., 2010. The French Accelerator Mass Spectrometry Facility ASTER: Improved Performance and Developments. 268, pp. 1954–1959. https://doi.org/10.1016/j.nimb.2010.02.107.

Barr, I.D., Spagnolo, M., 2015. Glacial cirques as palaeoenvironmental indicators: their potential and limitations. Earth Sci. Rev. 151, 48–78. https://doi.org/10.1016/j.earscirev.2015.10.004.

Barth, A.M., Clark, P.U., Clark, J., McCabe, A.M., Caffee, M., 2016. Last Glacial Maximum cirque glaciation in Ireland and implications for reconstructions of the Irish Ice Sheet. Quat. Sci. Rev. 141, 85–93. https://doi.org/10.1016/j.quascirev.2016.04.006.

Bartolomé, M., Moreno, A., Sancho, C., Stoll, H.M., Cacho, I., Spötl, C., Belmonte, Á., Edwards, R.L., Cheng, H., Hellstrom, J.C., 2015. Hydrological change in Southern Europe responding to increasing North Atlantic overturning during Greenland Stadial 1. Proc. Natl. Acad. Sci. 112, 6568–6572. https://doi.org/10.1073/pnas.1503990112.

Benn, D.I., Hulton, N.R.J., 2010. An ExcelTM spreadsheet program for reconstructing the surface profile of former mountain glaciers and ice caps. Comput. Geosci. 36, 605–610. https://doi.org/10.1016/j.cageo.2009.09.016.

Braucher, R., Guillou, V., Bourlès, D.L., Arnold, M., Aumaître, G., Keddadouche, K., Nottoli, E., 2015. Preparation of ASTER In-house 10Be/9Be Standard Solutions. 361 pp. 335–340.

Buizert, C., Keisling, B.A., Box, J.E., He, F., Carlson, A.E., Sinclair, G., DeConto, R.M., 2018. Greenland-wide seasonal temperatures during the Last Deglaciation. Geophys. Res. Lett. 45, 1905–1914. https://doi.org/10.1002/2017GL075601.

Cacho, I., Grimalt, J.O., Canals, M., 2002. Response of the Western Mediterranean Sea to rapid climatic variability during the last 50,000 years: a molecular biomarker approach. J. Mar. Syst. 33–34, 253–272. https://doi.org/10.1016/S0924-7963(02)00061-1.

Campos, N., Tanarro, L.M., Palacios, D., Zamorano, J.J., 2019. Slow dynamics in debris-covered and rock glaciers in Hofsdalur, Tröllaskagi Peninsula (northern Iceland). Geomorphology 342, 61–77. https://doi.org/10.1016/j.geomorph.2019.06.005.

Carrasco, R.M., Pedraza, J., Domínguez-Villar, D., Willenbring, J.K., Villa, J., 2015. Sequence and chronology of the Cuerpo de Hombre paleoglacier (Iberian Central System) during the last glacial cycle. Quat. Sci. Rev. 129, 163–177. https://doi.org/10.1016/j.quascirev.2015.09.021.

Carrasco González, R., Pedraza Gilsanz, J., Willenbring, J., Karampaglidis, T., Soteres García, R., Martín Duque, J., 2016. Morfología glaciar del Macizo de Los Pelados-El Nevero (Parque Nacional de la Sierra de Guadarrama). Nueva interpretación y cronología. Boletín la Real Soc. Española Hist. Nat. Sección Geológica 110, 49–64.

Chandler, B.M.P., Evans, D.J.A., Roberts, D.H., 2016. Recent retreat at a temperate Icelandic glacier in the context of the last ~80 years of climate change in the North Atlantic region. Arktos 2. https://doi.org/10.1007/s41063-016-0024-1.

Charton, J., Jomelli, V., Schimmelpfennig, I., Verfaillie, D., Favier, V., Mokadem, F., Gilbert, A., Brun, F., Aumaître, G., Bourlès, D.L., Keddadouche, K., 2020. A debris-covered glacier at Kerguelen (49°S, 69°E) over the past 15 000 years. Antarct. Sci. 13, 1–13. https://doi.org/10.1017/S0954102020000541.

Cheng, H., Zhang, H., Spötl, C., Baker, J., Sinha, A., Li, H., Bartolomé, M., Moreno, A., Kathayat, G., Zhao, J., Dong, X., Li, Y., Ning, Y., Jia, X., Zong, B., Brahim, Y.A., Pérez-Mejiás, C., Cai, Y., Novello, V.F., Cruz, F.W., Severinghaus, J.P., An, Z., Edwards, R.L., 2020. Timing and structure of the Younger Dryas event and its underlying climate dynamics. Proc. Natl. Acad. Sci. U. S. A. 117, 23408–23417. https://doi.org/10.1073/pnas.2007869117.

Chmeleff, J., von Blanckenburg, F., Kossert, K., Jakob, D., 2010. Determination of the 10Be half-life by multicollector ICP-MS and liquid scintillation counting. Nucl. Instrum. Methods Phys. Res. B Beam Interact. Mater. Atoms 268, 192–199. https://doi.org/10.1016/j.nimb.2009.09.012.

Chueca, J., Julián, A., Saz, M.A., Creus, J., López-Moreno, J.I., 2005. Responses to climatic changes since the Little Ice Age on Maladeta Glacier (Central Pyrenees). Geomorphology 68, 167–182. https://doi.org/10.1016/j.geomorph.2004.11.012.

Çiner, A., Sarıkaya, M.A., Yıldırım, C., 2017. Misleading old age on a young landform? The dilemma of cosmogenic inheritance in surface exposure dating: moraines vs. rock glaciers. Quat. Geochronol. 42, 76–88. https://doi.org/10.1016/j.quageo.2017.07.003.

Clark, P.U., Dyke, A.S., Shakun, J.D., Carlson, A.E., Clark, J., Wohlfarth, B., Mitrovica, J.X., Hostetler, S.W., McCabe, A.M., 2009. The Last Glacial Maximum. Science (80-. ) 325, 710–714. https://doi.org/10.1126/science.1172873.

Clark, P.U., Shakun, J.D., Baker, P.A., Bartlein, P.J., Brewer, S., Brook, E., Carlson, A.E., Cheng, H., Kaufman, D.S., Liu, Z., Marchitto, T.M., Mix, A.C., Morrill, C., Otto-Bliesner, B.L., Pahnke, K., Russell, J.M., Whitlock, C., Adkins, J.F., Blois, J.L., Clark, J., Colman, S.M., Curry, W.B., Flower, B.P., He, F., Johnson, T.C., Lynch-Stieglitz, J., Markgraf, V., McManus, J., Mitrovica, J.X., Moreno, P.I., Williams, J.W., 2012. Global climate evolution during the last deglaciation. Proc. Natl. Acad. Sci. 109, E1134–E1142. https://doi.org/10.1073/pnas.1116619109.

Crest, Y., Delmas, M., Braucher, R., Gunnell, Y., Calvet, M., 2017. Cirques have growth spurts during deglacial and interglacial periods: evidence from $^{10}$Be and $^{26}$Al nuclide inventories in the central and eastern Pyrenees. Geomorphology 278, 60–77. https://doi.org/10.1016/j.geomorph.2016.10.035.

Delmas, M., 2015. La última máxima extensión del hielo y posterior deglaciación de los Pirineos: revision de la investigación reciente. Cuad. Investig. Geogr. 41, 359–387. https://doi.org/10.18172/cig.2708.

Delmas, M., Gunnell, Y., Braucher, R., Calvet, M., Bourlès, D., 2008. Exposure age chronology of the last glaciation in the eastern Pyrenees. Quat. Res. 69, 231–241. https://doi.org/10.1016/j.yqres.2007.11.004.

Delmas, M., Gunnell, Y., Calvet, M., Reixach, T., Oliva, M., 2021. The Pyrenees: glacial landforms from the Last Glacial Maximum. In: Palacios, D., Hughes, P., García-Ruiz, J.M., Andrés, N. (Eds.), European Glacial Landscapes. Elsevier.

Denton, G.H., Anderson, R.F., Toggweiler, J.R.R., L Edwards, R., Schaefer, J.M., Putnam, A.E., Jiménez-Amat, P., Zahn, R., Bentley, M.J., Ocofaigh, C.Ó., Anderson, J.B., Conway, H., Davies, B.J., Graham, A.G.C., Hillenbrand, C.D., Hodgson, D.A., Jamieson, S.S.R., Larter, R.D., Mackintosh, A., Smith, J.A., Verleyen, E., Ackert, R.P., Bart, P.J., Berg, S., Brunstein, D., Canals, M., Colhoun, E.A., Crosta, X., Dickens, W.A., Domack, E.W., Dowdeswell, J.A., Dunbar, R., Ehrmann, W., Evans, J., Favier, V., Fink, D., Fogwill, C.J., Glasser, N.F., Gohl, K., Golledge, N.R., Goodwin, I., Gore, D.B., Greenwood, S.L., Hall, B.L., Hall, K., Hedding, D.W., Hein, A.S., Hocking, E.P., Jakobsson, M., Johnson, J.S., Jomelli, V., Jones, R.S., Klages, J.P., Kristoffersen, Y., Kuhn, G., Leventer, A., Licht, K., Lilly, K., Lindow, J., Livingstone, S.J., Massé, G., McGlone, M.S., McKay, R.M., Melles, M., Miura, H., Mulvaney, R., Nel, W., Nitsche, F.O., O'Brien, P.E., Post, A.L., Roberts, S. J., Saunders, K.M., Selkirk, P.M., Simms, A.R., Spiegel, C., Stolldorf, T.D., Sugden, D.E., van der Putten, N., van Ommen, T., Verfaillie, D., Vyverman, W., Wagner, B., White, D.A., Witus, A.E., Zwartz, D., Buizert, C., Gkinis, V., Severinghaus, J.P., He, F., Lecavalier, B.S., Kindler, P., Leuenberger, M., Carlson, A.E., Vinther, B.M., Masson-Delmotte, V., White, J.W.C., Liu, Z., Otto-Bliesner, B.L., Brook, E.J., Bentley, M.J., Fogwill, C.J., Kubik, P.W., Sugden, D.E., Hodgson, D.A., Roberts, S.J., Smith, J.A., Verleyen, E., Sterken, M., Labarque, M., Sabbe, K., Vyverman, W., Allen, C.S., Leng, M. J., Bryant, C., Glasser, N.F., Davies, B.J., Carrivick, J.L., Rodés, A., Hambrey, M.J., Smellie, J.L., Domack, E.W., Müller, J., Stein, R., Miettinen, A., Divine, D.V., Husum, K., Koç, N., Jennings, A., Levy, L.B., Kelly, M.A., Lowell, T.V., Hall, B.L., Hempel, L.A., Honsaker, W.M., Lusas, A.R., Howley, J.A., Axford, Y.L., Schaefer, J.M., Finkel, R.C., Goehring, B.M., Alley, R.B., Denton, G.H., Håkansson, L., Briner, J.P., Alexanderson, H., Aldahan, A., Possnert, G., Tabone, I., Blasco, J., Robinson, A., Alvarez-Solas, J., Montoya, M., Bennike, O., Björck, S., Schaefer, J.M., Finkel, R.C., Balco, G., Alley, R.B., Caffee, M.W., Briner, J.P., Young, N.E., Gow, A.J., Schwartz, R., Bevis, M., Harig, C., Khan, S.A., Brown, A., Simons, F.J., Willis, M., Fettweis, X., van den Broeke, M.R., Madsen, F.B., Kendrick, E., Caccamise, D.J., van Dam, T., Knudsen, P., Nylen, T., Arndt, J.E., Jokat, W., Dorschel, B., Bradley, S.L., Reerink, T.J., Van De Wal, R.S.W., Helsen, M.M., Stokes, C.R., Margold, M., Clark, C.D., Tarasov, L., Kelly, M.A., Lowell, T.V., Hall, B.L., Schaefer, J.M., Finkel, R.C., Goehring, B.M., Alley, R.B., Denton, G.H., Davies, B.J., Hambrey, M.J., Smellie, J.L., Carrivick, J.L., Glasser, N.F., Bentley, M.J., Fogwill, C.J., Kubik, P.W., Sugden, D.E., Ocofaigh, C.Ó., Davies, B.J., Livingstone, S.J., Smith, J.A., Johnson, J.S., Hocking, E.P., Hodgson, D.A., Anderson, J.B., Bentley, M.J., Canals, M., Domack, E.W., Dowdeswell, J.A., Evans, J., Glasser, N.F., Hillenbrand, C.D., Larter, R. D., Roberts, S.J., Simms, A.R., Cofaigh, C.Ó., Davies, B.J., Livingstone, S.J., Smith, J.A., Johnson, J.S., Hocking, E.P., Hodgson, D.A., Anderson, J.B., Bentley, M.J., Canals, M., Domack, E.W., Dowdeswell, J.A., Evans, J., Glasser, N.F., Hillenbrand, C.D., Larter, R. D., Roberts, S.J., Simms, A.R., Buizert, C., Gkinis, V., Severinghaus, J.P., He, F., Lecavalier, B.S., Kindler, P., Leuenberger, M., Carlson, A.E., Vinther, B.M., Masson-Delmotte, V., White, J.W.C., Liu, Z., Otto-Bliesner, B.L., Brook, E.J., Jiménez-Amat, P., Zahn, R., Mcgehee, R., Schaefer, J.M., Finkel, R.C., Balco, G., Alley, R.B., Caffee, M.W., Briner, J.P., Young, N.E., Gow, A.J., Schwartz, R., Sinclair, G., Carlson, A.E., Mix, A.C., Lecavalier, B.S., Milne, G.A., Mathias, A., Buizert, C., DeConto, R., Jomelli, V., Schimmelpfennig, I., Favier, V., Mokadem, F., Landais, A., Rinterknecht, V., Brunstein, D., Verfaillie, D., Legentil, C., Aumaitre, G., Bourlès, D.L., Keddadouche, K., Martinson, D.G., Miettinen, A., Divine, D.V., Husum, K., Koç, N., Jennings, A., Bentley, M.J., Hodgson, D.A., Smith, J.A., Cofaigh, C.Ó., Domack, E.W., Larter, R.D., Roberts, S.J., Brachfeld, S., Leventer, A., Hjort, C., Hillenbrand, C.D., Evans, J., Jackson, R., Carlson, A.E., Hillaire-Marcel, C., Wacker, L., Vogt, C., Kucera, M., Peck, V.L., Allen, C.S., Kender, S., McClymont, E.L., Hodgson, D.A., Bentley, M.J., Ocofaigh, C.Ó., Anderson, J. B., Conway, H., Davies, B.J., Graham, A.G.C., Hillenbrand, C.D., Hodgson, D.A., Jamieson, S.S.R., Larter, R.D., Mackintosh, A., Smith, J.A., Verleyen, E., Ackert, R.P., Bart, P.J., Berg, S., Brunstein, D., Canals, M., Colhoun, E.A., Crosta, X., Dickens, W.A., Domack, E.W., Dowdeswell, J.A., Dunbar, R., Ehrmann, W., Evans, J., Favier, V., Fink, D., Fogwill, C.J., Glasser, N.F., Gohl, K., Golledge, N.R., Goodwin, I., Gore, D.B., Greenwood, S.L., Hall, B.L., Hall, K., Hedding, D.W., Hein, A.S., Hocking, E.P., Jakobsson, M., Johnson, J.S., Jomelli, V., Jones, R.S., Klages, J.P., Kristoffersen, Y., Kuhn, G., Leventer, A., Licht, K., Lilly, K., Lindow, J., Livingstone, S.J., Massé, G., McGlone, M. S., McKay, R.M., Melles, M., Miura, H., Mulvaney, R., Nel, W., Nitsche, F.O., O'Brien, P. E., Post, A.L., Roberts, S.J., Saunders, K.M., Selkirk, P.M., Simms, A.R., Spiegel, C., Stolldorf, T.D., Sugden, D.E., van der Putten, N., van Ommen, T., Verfaillie, D., Vyverman, W., Wagner, B., White, D.A., Witus, A.E., Zwartz, D., Müller, J., Stein, R., Hodgson, D.A., Roberts, S.J., Smith, J.A., Verleyen, E., Sterken, M., Labarque, M., Sabbe, K., Vyverman, W., Allen, C.S., Leng, M.J., Bryant, C., Levy, L.B., Kelly, M.A., Lowell, T.V., Hall, B.L., Hempel, L.A., Honsaker, W.M., Lusas, A.R., Howley, J.A., Axford, Y.L., Martinson, D.G., Stammerjohn, S.E., Iannuzzi, R.A., Smith, R.C., Vernet, M., McCave, I.N., Crowhurst, S.J., Kuhn, G., Hillenbrand, C.D., Meredith, M.P., Bennike, O., Björck, S., Lecavalier, B.S., Fisher, D.A., Milne, G.A., Vinther, B.M., Tarasov, L., Huybrechts, P., Lacelle, D., Main, B., Zheng, J., Bourgeois, J., Dyke, A.S., Arndt, J.E., Jokat, W., Dorschel, B., Winsor, K., Carlson, A.E., Caffee, M.W., Rood, D.H., Bevis, M., Harig, C., Khan, S.A., Brown, A., Simons, F.J., Willis, M., Fettweis, X., van den Broeke, M.R., Madsen, F.B., Kendrick, E., Caccamise, D.J., van Dam, T., Knudsen, P., Nylen, T., S-hakun, J.D., Clark, P.U., He, F., Lifton, N.A., Liu, Z., Otto-Bliesner, B.L., R. Rintoul, S., W. Hughes, C., Olbers, D., Glasser, N.F., Davies, B.J., Carrivick, J.L., Rodés, A., Hambrey, M. J., Smellie, J.L., Domack, E.W., Larsen, N.K., Levy, L.B., Carlson, A.E., Buizert, C., Olsen, J., Strunk, A., Bjørk, A.A., Skov, D.S., Håkansson, L., Briner, J.P., Alexanderson, H., Aldahan, A., Possnert, G., Putnam, A.E., Edwards, R.L., Toggweiler, J.R.R., Schaefer, J. M., Anderson, R.F., Denton, G.H., Tabone, I., Blasco, J., Robinson, A., Alvarez-Solas, J., Montoya, M., Lecavalier, B.S., Fisher, D.A., Milne, G.A., Vinther, B.M., Tarasov, L., Huybrechts, P., Lacelle, D., Main, B., Zheng, J., Bourgeois, J., Dyke, A.S., Stokes, C.R., Margold, M., Clark, C.D., Tarasov, L., Jackson, R., Carlson, A.E., Hillaire-Marcel, C., Wacker, L., Vogt, C., Kucera, M., Mcgehee, R., Davies, B.J., Hambrey, M.J., Smellie, J.L., Carrivick, J.L., Glasser, N.F., Golledge, N.R., Keller, E.D., Gomez, N., Naughten, K.A., Bernales, J., Trusel, L.D., Edwards, T.L., Jomelli, V., Schimmelpfennig, I., Favier, V., Mokadem, F., Landais, A., Rinterknecht, V., Brunstein, D., Verfaillie, D., Legentil, C., Aumaitre, G., Bourlès, D.L., Keddadouche, K., McCave, I.N., Crowhurst, S.J., Kuhn, G., Hillenbrand, C.D., Meredith, M.P., Martinson, D.G., R. Rintoul, S., W. Hughes, C., Olbers, D., Peck, V.L., Allen, C.S., Kender, S., McClymont, E.L., Hodgson, D.A., Martinson, D.G., Stammerjohn, S.E., Iannuzzi, R.A., Smith, R.C., Vernet, M., Bradley, S.L., Reerink, T.J., Van De Wal, R.S.W., Helsen, M.M., Denton, G.H., Anderson, R.F., Toggweiler, J.R.R., Edwards, R.L., Schaefer, J.M., Putnam, A.E., Shakun, J.D., Clark, P.U., He, F., Lifton, N.A., Liu, Z., Otto-Bliesner, B.L., 2014. The Last Glacial Termination. Quat. Sci. Rev. 100, 1652–1656. https://doi.org/10.1126/science.1184119.

Dunne, J., Elmore, D., Muzikar, P., 1999. Scaling factors for the rates of production of cosmogenic nuclides for geometric shielding and attenuation at depth on sloped surfaces. Geomorphology 27, 3–11. https://doi.org/10.1016/S0169-555X(98)00086-5.

Fernandes, M., Oliva, M., Palma, P., Ruiz-Fernández, J., Lopes, L., 2017. Glacial stages and postglacial environmental evolution in the Upper Garonne valley, Central Pyrenees. Sci. Total Environ. 584–585, 1282–1299. https://doi.org/10.1016/j.scitotenv.2017.01.209.

Fernandes, M., Palma, P., Lopes, L., Ruiz-Fernández, J., Pereira, P., Oliva, M., 2018. Spatial Distribution and Morphometry of Permafrost-related Landforms in the Central Pyrenees and Associated Paleoclimatic Implications. 470, pp. 96–108. https://doi.org/10.1016/j.quaint.2017.08.071.

Fernandes, M., Oliva, M., Vieira, G., 2020. Paraglacial slope failures in the Aran valley (Central Pyrenees). Quat. Int. 566-567, 24–38.

Fernández-Fernández, J.M., Palacios, D., García-Ruiz, J.M., Andrés, N., Schimmelpfennig, I., Gómez-Villar, A., Santos-González, J., Álvarez-Martínez, J., Arnáez, J., Úbeda, J., Léanni, L., Aumaître, G., Bourlès, D., Keddadouche, K., 2017. Chronological and geomorphological investigation of fossil debris-covered glaciers in relation to deglaciation processes: a case study in the Sierra de La Demanda, northern Spain. Quat. Sci. Rev. 170, 232–249. https://doi.org/10.1016/j.quascirev.2017.06.034.

Fernández-Fernández, J.M.J.M., Palacios, D., Andrés, N., Schimmelpfennig, I., Tanarro, L.M. L.M., Brynjólfsson, S., López-Acevedo, F.J., Sæmundsson, Þ., Team, A.S.T.E.R.S.T.E.R, 2020. Constraints on the timing of debris-covered and rock glaciers: an exploratory case study in the Hólar area, northern Iceland. Geomorphology 361, 107196. https://doi.org/10.1016/j.geomorph.2020.107196.

García-Ruiz, J.M., 1979. El glaciarismo cuaternario en la Sierra de la Demanda (Logroño-Burgos, España). Cuad. Investig. Geogr. Hist. 5, 325.

García-Ruiz, J.M., Palacios, D., González-Sampériz, P., de Andrés, N., Moreno, A., Valero-Garcés, B., Gómez-Villar, A., 2016. Mountain glacier evolution in the Iberian Peninsula during the Younger Dryas. Quat. Sci. Rev. 138, 16–30. https://doi.org/10.1016/j.quascirev.2016.02.022.

García-Ruiz, J.M., Palacios, D., Fernández-Fernández, J.M., Andrés, N., Arnáez, J., Gómez-Villar, A., Santos-González, J., Álvarez-Martínez, J., Lana-Renault, N., Léanni, L., 2020. Glacial stages in the Peña Negra valley, Iberian Range, northern Iberian Peninsula: assessing the importance of the glacial record in small cirques in a marginal mountain area. Geomorphology 362, 107195. https://doi.org/10.1016/j.geomorph.2020.107195.

Gheorghiu, D.M., Hosu, M., Corpade, C., Xu, S., 2015. Deglaciation constraints in the Parâng Mountains, Southern Romania, using surface exposure dating. Quat. Int. 388, 156–167. https://doi.org/10.1016/j.quaint.2015.04.059.

Gómez-Ortiz, A., Palacios, D., Palade, B., Vázquez-Selem, L., Salvador-Franch, F., 2012. The deglaciation of the Sierra Nevada (Southern Spain). Geomorphology 159–160, 93–105. https://doi.org/10.1016/j.geomorph.2012.03.008.

Gómez-Ortiz, A., Oliva, M., Palacios, D., Salvador-Franch, F., Vázquez-Selem, L., Salvà-Catarineu, M., De Andrés, N., 2015. The deglaciation of Sierra Nevada (Spain), synthesis of the knowledge and new contributions. Cuad. Investig. Geográfica 41, 409. https://doi.org/10.18172/cig.2722.

Gosse, J.C., Phillips, F.M., 2001. Terrestrial in situ cosmogenic nuclides:theory and application. Quat. Sci. Rev. 20, 1475–1560. https://doi.org/10.1016/S0277-3791(00)00171-2.

Greenwood, S.L., O'Regan, M., Swärd, H., Flodén, T., Ananyev, R., Chernykh, D., Jakobsson, M., 2015. Multiple re-advances of a Lake Vättern outlet glacier during Fennoscandian Ice Sheet retreat, south-central Sweden. Boreas 44, 619–637. https://doi.org/10.1111/bor.12132.

Hambrey, M.J., Quincey, D.J., Glasser, N.F., Reynolds, J.M., Richardson, S.J., Clemmens, S., 2008. Sedimentological, geomorphological and dynamic context of debris-mantled glaciers, Mount Everest (Sagarmatha) region, Nepal. Quat. Sci. Rev. 27, 2361–2389. https://doi.org/10.1016/j.quascirev.2008.08.010.

Hambrey, M.J., Quincey, D.J., Glasser, N.F., Reynolds, J.M., Richardson, S.J., Clemmens, S., Jones, D.B., Harrison, S., Anderson, K., Korschinek, G., Bergmaier, A., Faestermann, T., Gerstmann, U.C., Knie, K., Rugel, G., Wallner, A., Dillmann, I., Dollinger, G., von Gostomski, C.L., Kossert, K., Maiti, M., Poutivtsev, M., Remmert, A., Žebre, M., Sarıkaya, M.A., Stepišnik, U., Yıldırım, C., Çiner, A., Barth, A.M., Clark, P.U., Clark, J., McCabe, A.M., Caffee, M., Gheorghiu, D.M., Hosu, M., Corpade, C., Xu, S., Greenwood, S.L., O'Regan, M., Swärd, H., Flodén, T., Ananyev, R., Chernykh, D., Jakobsson, M., Knight, J., Harrison, S., Jones, D.B., Makos, M., Rinterknecht, V., Braucher, R., Tołoczko-Pasek, A., Arnold, M., Aumaître, G., Bourlès, D., Keddadouche, K., Mangerud, J., Aarseth, I., Hughes, A.L.C., Lohne, Ø.S., Skår, K., Sønstegaard, E., Svendsen, J.I., Rowan, A.V., Egholm, D.L., Quincey, D.J., Glasser, N.F., Sarıkaya, M.A., Çiner, A., Yıldırım, C., Styllas, M.N., Schimmelpfennig, I., Benedetti, L., Ghilardi, M., Aumaître, G., Bourlès, D., Keddadouche, K., 2019. Late-glacial and Holocene history of the northeast Mediterranean mountains - New insights from in situ-produced 36 Cl-based cosmic ray exposure dating of paleo-glacier deposits on Mount Olympus, Greece. Quat. Sci. Rev. 39, 14–24. https://doi.org/10.1016/j.quascirev.2015.11.013.

Herreid, S., Pellicciotti, F., 2020. The state of rock debris covering Earth's glaciers. Nat. Geosci. 13, 621–627. https://doi.org/10.1038/s41561-020-0615-0.

Hughes, A.L.C., Gyllencreutz, R., Lohne, Ø.S., Mangerud, J., Svendsen, J.I., 2016. The last Eurasian ice sheets - a chronological database and time-slice reconstruction, DATED-1. Boreas 45, 1–45. https://doi.org/10.1111/bor.12142.

Hughes, P.D., Fink, D., Rodés, Á., Fenton, C.R., Fujioka, T., 2018. Timing of Pleistocene glaciations in the High Atlas, Morocco: new 10Be and 36Cl exposure ages. Quat. Sci. Rev. 180, 193–213. https://doi.org/10.1016/j.quascirev.2017.11.015.

Institut Cartogràfic i Geològic de Catalunya, 2017. Base de dades geològiques de Catalunya 1:50.000 v1.0.

Iriarte-Chiapusso, M.J., Muñoz Sobrino, C., Gómez-Orellana, L., Hernández-Beloqui, B., García-Moreiras, I., Fernández Rodriguez, C., Heiri, O., Lotter, A.F., Ramil-Rego, P., 2016. Reviewing the Lateglacial-Holocene transition in NW Iberia: a palaeoecological approach based on the comparison between dissimilar regions. Quat. Int. 403, 211–236. https://doi.org/10.1016/j.quaint.2015.09.029.

Ivy-Ochs, S., 2015. Variaciones glaciares en los Alpes europeos al final de la última glaciación. Cuad. Investig. Geogr. 41, 295–315. https://doi.org/10.18172/cig.2750.

Joly, F., 1997. Glossaire de géomorphologie. Base de donnés sémiologiques pour la cartographie. Masson/Arm. ed, Paris.

Jomelli, V., Chapron, E., Favier, V., Rinterknecht, V., Braucher, R., Tournier, N., Gascoin, S., Marti, R., Galop, D., Binet, S., Deschamps-Berger, C., Tissoux, H., Aumaitre, G., Bourlès, D.L., Keddadouche, K., 2020. Glacier fluctuations during the Late Glacial and Holocene on the Ariège valley, northern slope of the Pyrenees and reconstructed climatic conditions. Mediterranean Geosci. Rev. 2, 37–51. https://doi.org/10.1007/s42990-020-00018-5.

Jones, D.B., Harrison, S., Anderson, K., 2019. Mountain glacier-to-rock glacier transition. Glob. Planet. Chang. 181, 102999. https://doi.org/10.1016/j.gloplacha.2019.102999.

Knight, J., 2019. A new model of rock glacier dynamics. Geomorphology 340, 153–159. https://doi.org/10.1016/j.geomorph.2019.05.008.

Knight, J., Harrison, S., Jones, D.B., 2019. Rock glaciers and the geomorphological evolution of deglacierizing mountains. Geomorphology 324, 14–24. https://doi.org/10.1016/j.geomorph.2018.09.020.

Korschinek, G., Bergmaier, A., Faestermann, T., Gerstmann, U.C., Knie, K., Rugel, G., Wallner, A., Dillmann, I., Dollinger, G., von Gostomski, C.L., Kossert, K., Maiti, M., Poutivtsev, M., Remmert, A., 2010. A new value for the half-life of 10Be by heavy-ion elastic recoil detection and liquid scintillation counting. Nucl. Instrum. Methods Phys. Res. B Beam Interact. Mater. Atoms 268, 187–191. https://doi.org/10.1016/j.nimb.2009.09.020.

Köse, O., Sarıkaya, M.A., Çİner, A., Candaş, A., 2019. Late Quaternary glaciations and cosmogenic 36 Cl geochronology of Mount Dedegöl, south-west Turkey. J. Quat. Sci. 34, 51–63. https://doi.org/10.1002/jqs.3080.

Li, Y., 2018. Determining topographic shielding from digital elevation models for cosmogenic nuclide analysis: a GIS model for discrete sample sites. J. Mt. Sci. 15, 939–947. https://doi.org/10.1007/s11629-018-4895-4.

Lifton, N., Sato, T., Dunai, T.J., 2014. Scaling in situ cosmogenic nuclide production rates using analytical approximations to atmospheric cosmic-ray fluxes. Earth Planet. Sci. Lett. 386, 149–160. https://doi.org/10.1016/J.EPSL.2013.10.052.

Lopes, L., Oliva, M., Fernandes, M., Pereira, P., Palma, P., Ruiz-Fernández, J., 2018. Spatial distribution of morphometric parameters of glacial cirques in the Central Pyrenees (Aran and Boí valleys). J. Mt. Sci. 15. https://doi.org/10.1007/s11629-018-4873-x.

López-Moreno, J.I., Alonso-González, E., Monserrat, O., Del Río, L.M., Otero, J., Lapazaran, J., Luzi, G., Dematteis, N., Serreta, A., Rico, I., Serrano-Cañadas, E., Bartolomé, M., Moreno, A., Buisan, S., Revuelto, J., 2019. Ground-based remote-sensing techniques for diagnosis of the current state and recent evolution of the Monte Perdido Glacier, Spanish Pyrenees. J. Glaciol. 65, 85–100. https://doi.org/10.1017/jog.2018.96.

Makos, M., Rinterknecht, V., Braucher, R., Tołoczko-Pasek, A., Arnold, M., Aumaître, G., Bourlès, D., Keddadouche, K., 2018. Last Glacial Maximum and Lateglacial in the Polish High Tatra Mountains - revised deglaciation chronology based on the 10Be exposure age dating. Quat. Sci. Rev. 187, 130–156. https://doi.org/10.1016/j.quascirev.2018.03.006.

Mangerud, J., Aarseth, I., Hughes, A.L.C., Lohne, Ø.S., Skår, K., Sønstegaard, E., Svendsen, J.I., 2016. A major re-growth of the Scandinavian Ice Sheet in western Norway during Allerød-Younger Dryas. Quat. Sci. Rev. 132, 175–205. https://doi.org/10.1016/j.quascirev.2015.11.013.

Martin, L.C.P., Blard, P.-H., Balco, G., Lavé, J., Delunel, R., Lifton, N., Laurent, V., 2017. The CREp program and the ICE-D production rate calibration database: A fully parameterizable and updated online tool to compute cosmic-ray exposure ages. Quat. Geochronol. 38, 25–49. https://doi.org/10.1016/J.QUAGEO.2016.11.006.

Merchel, S., Herpers, U., 1999. An update on radiochemical separation techniques for the determination of long-lived radionuclides via accelerator mass spectrometry. Radiochim. Acta 84, 215–219. https://doi.org/10.1524/ract.1999.84.4.215.

Merchel, S., Arnold, M., Aumaître, G., Benedetti, L., Bourlès, D.L., Braucher, R., Alfimov, V., Freeman, S.P.H.T., Steier, P., Wallner, A., 2008. Towards more precise 10 Be and 36 Cl data from measurements at the 10 À 14 level: influence of sample preparation Be / B e. Nucl. Inst. Methods Phys. Res. B 266, 4921–4926. https://doi.org/10.1016/j.nimb.2008.07.031.

Moran, A.P., Ivy Ochs, S., Vockenhuber, C., Kerschner, H., 2016. Rock glacier development in the Northern Calcareous Alps at the Pleistocene-Holocene boundary. Geomorphology 273, 178–188. https://doi.org/10.1016/j.geomorph.2016.08.017.

Oliva, M., Gómez Ortiz, A., Palacios, D., Salvador-Franch, F., Salvà-Catarineu, M., 2014. Environmental evolution in Sierra Nevada (South Spain) since the last Glaciation, based on multi-proxy records. Quat. Int. 353, 195–209. https://doi.org/10.1016/j.quaint.2014.02.009.

Oliva, M., Serrano, E., Gómez-Ortiz, A., González-Amuchastegui, M.J., Nieuwendam, A., Palacios, D., Pérez-Alberti, A., Pellitero, R., Ruiz-Fernández, J., Valcárcel, M., Vieira, G., Antoniades, D., 2016. Spatial and temporal variability of periglaciation of the Iberian Peninsula. Quat. Sci. Rev. 137, 176–199. https://doi.org/10.1016/j.quascirev.2016.02.017.

Oliva, M., Žebre, M., Guglielmin, M., Hughes, P.D., Çiner, A., Vieira, G., Bodin, X., Andrés, N., Colucci, R.R., García-Hernández, C., Mora, C., Nofre, J., Palacios, D., Pérez-Alberti, A., Ribolini, A., Ruiz-Fernández, J., Sarıkaya, M.A., Serrano, E., Urdea, P., Valcárcel, M., Woodward, J.C., Yıldırım, C., 2018. Permafrost conditions in the Mediterranean region since the Last Glaciation. Earth Sci. Rev. 185, 397–436. https://doi.org/10.1016/j.earscirev.2018.06.018.

Oliva, M., Palacios, D., Fernández-Fernández, J.M., Rodríguez-Rodríguez, L., García-Ruiz, J.M.M., Andrés, N., Carrasco, R.M.M., Pedraza, J., Pérez-Alberti, A., Valcárcel, M., Hughes, P.D.D., 2019. Late Quaternary glacial phases in the Iberian Peninsula. Earth Sci. Rev. 192, 564–600. https://doi.org/10.1016/j.earscirev.2019.03.015.

Oliva, M., Sarikaya, A., Hughes, P., 2020. Holocene and earlier glaciations in the Mediterranean mountains. Mediterranean Geosci. Rev. 2 (1), 1–4.

Oliva, M., Palacios, D., Fernández-Fernández, J.M., 2021. Iberia, Land of Glaciers. Elsevier.

Osmaston, H., 2005. Estimates of glacier equilibrium line altitudes by the Area × Altitude, the Area × Altitude Balance Ratio and the Area × Altitude Balance Index methods and their validation. Quat. Int. 138–139, 22–31. https://doi.org/10.1016/j.quaint.2005.02.004.

Palacios, D., de Marcos, J., Vázquez-Selem, L., 2011. Last Glacial Maximum and deglaciation of Sierra de Gredos, central Iberian Peninsula. Quat. Int. 233, 16–26. https://doi.org/10.1016/j.quaint.2010.04.029.

Palacios, D., de Andrés, N., de Marcos, J., Vázquez-Selem, L., 2012. Glacial landforms and their paleoclimatic significance in Sierra de Guadarrama, Central Iberian Peninsula. Geomorphology 139–140, 67–78. https://doi.org/10.1016/j.geomorph.2011.10.003.

Palacios, D., de Andrés, N., López-Moreno, J.I., García-Ruiz, J.M., 2015a. Late Pleistocene deglaciation in the upper Gállego Valley, central Pyrenees. Quat. Res. (United States) 83, 397–414. https://doi.org/10.1016/j.yqres.2015.01.010.

Palacios, D., Gómez-Ortiz, A., Andrés, N., Vázquez-Selem, L., Salvador-Franch, F., Oliva, M., 2015b. Maximum extent of Late Pleistocene glaciers and last deglaciation of La Cerdanya mountains, Southeastern Pyrenees. Geomorphology 231, 116–129. https://doi.org/10.1016/j.geomorph.2014.10.037.

Palacios, D., Gómez-Ortiz, A., Andrés, N., Salvador, F., Oliva, M., 2016. Timing and new geomorphologic evidence of the last deglaciation stages in Sierra Nevada (southern Spain). Quat. Sci. Rev. 150, 110–129. https://doi.org/10.1016/j.quascirev.2016.08.012.

Palacios, D., de Andrés, N., Gómez-Ortiz, A., García-Ruiz, J.M., 2017a. Evidence of glacial activity during the Oldest Dryas in the mountains of Spain. Geol. Soc. Spec. Publ. 433, 87–110. https://doi.org/10.1144/SP433.10.

Palacios, D., García-Ruiz, J.M., Andrés, N., Schimmelpfennig, I., Campos, N., Léanni, L., Aumaître, G., Bourlès, D.L., Keddadouche, K., 2017b. Deglaciation in the central Pyrenees during the Pleistocene–Holocene transition: timing and geomorphological significance. Quat. Sci. Rev. 162, 111–127. https://doi.org/10.1016/j.quascirev.2017.03.007.

Pallàs, R., Rodés, Á., Braucher, R., Carcaillet, J., Ortuño, M., Bordonau, J., Bourlès, D., Vilaplana, J.M., Masana, E., Santanach, P., 2006. Late Pleistocene and Holocene glaciation in the Pyrenees: a critical review and new evidence from 10Be exposure ages, south-central Pyrenees. Quat. Sci. Rev. 25, 2937–2963. https://doi.org/10.1016/j.quascirev.2006.04.004.

Pallàs, R., Rodés, Á., Braucher, R., Bourlès, D., Delmas, M., Calvet, M., Gunnell, Y., 2010. Small, isolated glacial catchments as priority targets for cosmogenic surface exposure dating of pleistocene climate fluctuations, southeastern Pyrenees. Geology 38, 891–894. https://doi.org/10.1130/G31164.1.

Paterson, W.S.B., 1994. The Physics of Glaciers. 3rd Editio. ed. Elsevier, London https://doi.org/10.1016/C2009-0-14802-X.

Pellitero, R., Rea, B.R., Spagnolo, M., Bakke, J., Hughes, P., Ivy-Ochs, S., Lukas, S., Ribolini, A., 2015. A GIS tool for automatic calculation of glacier equilibrium-line altitudes. Comput. Geosci. 82, 55–62. https://doi.org/10.1016/j.cageo.2015.05.005.

Pellitero, R., Rea, B.R., Spagnolo, M., Bakke, J., Ivy-Ochs, S., Frew, C.R., Hughes, P., Ribolini, A., Lukas, S., Renssen, H., 2016. GlaRe, a GIS tool to reconstruct the 3D surface of palaeoglaciers. Comput. Geosci. 94, 77–85. https://doi.org/10.1016/j.cageo.2016.06.008.

Pellitero, R., Fernández-Fernández, J.M., Campos, N., Serrano, E., Pisabarro, A., 2019. Late Pleistocene climate of the northern Iberian Peninsula: new insights from palaeoglaciers at Fuentes Carrionas (Cantabrian Mountains). J. Quat. Sci. 34, 342–354. https://doi.org/10.1002/jqs.3106.

Pope, R.J., Hughes, P.D., Skourtsos, E., 2017. Glacial history of Mt Chelmos, Peloponnesus, Greece. Geol. Soc. Spec. Publ. 433, 211–236. https://doi.org/10.1144/SP433.11.

Porter, S.C., 1975. Equilibrium-line altitudes of late quaternary glaciers in the Southern Alps, New Zealand. Quat. Res. 5, 27–47. https://doi.org/10.1016/0033-5894(75)90047-2.

Rasmussen, S.O., Bigler, M., Blockley, S.P., Blunier, T., Buchardt, S.L., Clausen, H.B., Cvijanovic, I., Dahl-Jensen, D., Johnsen, S.J., Fischer, H., Gkinis, V., Guillevic, M., Hoek, W.Z., Lowe, J.J., Pedro, J.B., Popp, T., Seierstad, I.K., Steffensen, J.P., Svensson, A.M., Vallelonga, P., Vinther, B.M., Walker, M.J.C., Wheatley, J.J., Winstrup, M., 2014. A stratigraphic framework for abrupt climatic changes during the Last Glacial period based on three synchronized Greenland ice-core records: refining and extending the INTIMATE event stratigraphy. Quat. Sci. Rev. 106, 14–28. https://doi.org/10.1016/j.quascirev.2014.09.007.

Rea, B.R., 2009. Defining modern day area-altitude balance ratios (AABRs) and their use in glacier-climate reconstructions. Quat. Sci. Rev. 28, 237–248. https://doi.org/10.1016/j.quascirev.2008.10.011.

Rea, B.R., Pellitero, R., Spagnolo, M., Hughes, P., Ivy-Ochs, S., Renssen, H., Ribolini, A., Bakke, J., Lukas, S., Braithwaite, R.J., 2020. Atmospheric circulation over Europe during the Younger Dryas. Sci. Adv. 6, eaba4844. https://doi.org/10.1126/sciadv.aba4844.

Renssen, H., Seppä, H., Heiri, O., Roche, D.M., Goosse, H., Fichefet, T., 2009. The spatial and temporal complexity of the holocene thermal maximum. Nat. Geosci. 2, 411–414. https://doi.org/10.1038/ngeo513.

Rodrigues, T., Grimalt, J.O., Abrantes, F., Naughton, F., Flores, J.-A., 2010. The last glacial–interglacial transition (LGIT) in the western mid-latitudes of the North Atlantic: abrupt sea surface temperature change and sea level implications. Quat. Sci. Rev. 29, 1853–1862. https://doi.org/10.1016/j.quascirev.2010.04.004.

Rodríguez-Rodríguez, L., Jiménez-Sánchez, M., Domínguez-Cuesta, M.J., Rinterknecht, V., Pallàs, R., Bourlès, D., 2016. Chronology of glaciations in the Cantabrian Mountains (NW Iberia) during the Last Glacial Cycle based on in situ-produced10Be. Quat. Sci. Rev. 138, 31–48. https://doi.org/10.1016/j.quascirev.2016.02.027.

Rodríguez-Rodríguez, L., Jiménez-Sánchez, M., Domínguez-Cuesta, M.J., Rinterknecht, V., Pallàs, R., 2017. Timing of last deglaciation in the Cantabrian Mountains (Iberian Peninsula; North Atlantic Region) based on in situ-produced 10Be exposure dating. Quat. Sci. Rev. 171, 166–181. https://doi.org/10.1016/j.quascirev.2017.07.012.

Rowan, A.V., Egholm, D.L., Quincey, D.J., Glasser, N.F., 2015. Modelling the feedbacks between mass balance, ice flow and debris transport to predict the response to climate change of debris-covered glaciers in the Himalaya. Earth Planet. Sci. Lett. 430, 427–438. https://doi.org/10.1016/j.epsl.2015.09.004.

Sarıkaya, M.A., Çiner, A., Yıldırım, C., 2017. Cosmogenic 36Cl glacial chronologies of the Late Quaternary glaciers on Mount Geyikdağ in the Eastern Mediterranean. Quat. Geochronol. 39, 189–204. https://doi.org/10.1016/j.quageo.2017.03.003.

Serrano, E., Lende, M.G., Ignacio, J., Moreno, L., Pisabarro, A., Fernández, A.M., de Sanjosé-Blasco, J.J., Gómez-Lende, M., López-Moreno, J.I., Pisabarro, A., Martínez-Fernández, A., 2019. Periglacial environments and frozen ground in the central Pyrenean high mountain area : ground thermal regime and distribution of landforms and processes. Permafr. Periglac. Process. 30, 292–309. https://doi.org/10.1002/ppp.2032.

Spagnolo, M., Ribolini, A., 2019. Glacier extent and climate in the Maritime Alps during the Younger Dryas. Palaeogeogr. Palaeoclimatol. Palaeoecol. 536, 109400. https://doi.org/10.1016/j.palaeo.2019.109400.

Styllas, M.N., Schimmelpfennig, I., Benedetti, L., Ghilardi, M., Aumaître, G., Bourlès, D., Keddadouche, K., 2018. Late-glacial and Holocene history of the northeast Mediterranean mountains - new insights from in situ-produced36Cl-based cosmic ray exposure dating of paleo-glacier deposits on Mount Olympus, Greece. Quat. Sci. Rev. 193, 244–265. https://doi.org/10.1016/j.quascirev.2018.06.020.

Tanarro, L.M., Palacios, D., Andrés, N., Fernández-Fernández, J.M., Zamorano, J.J., Sæmundsson, Þ., Brynjólfsson, S., 2019. Unchanged surface morphology in debris-covered glaciers and rock glaciers in Tröllaskagi peninsula (northern Iceland). Sci. Total Environ. 648, 218–235. https://doi.org/10.1016/j.scitotenv.2018.07.460.

Tomkins, M.D., Huck, J.J., Dortch, J.M., Hughes, P.D., Kirbride, M.P., Barr, I.D., 2018. Schmidt Hammer exposure dating (SHED): calibration procedures, new exposure age data and an online calculator. Quat. Geochronol. 44, 55–62. https://doi.org/10.1016/j.quageo.2017.12.003.

Uppala, S.M., Kållberg, P.W., Simmons, A.J., Andrae, U., da Costa Bechtold, V., Fiorino, M., Gibson, J.K., Haseler, J., Hernandez, A., Kelly, G.A., Li, X., Onogi, K., Saarinen, S., Sokka, N., Allan, R.P., Andersson, E., Arpe, K., Balmaseda, M.A., Beljaars, A.C.M., van de Berg, L., Bidlot, J., Bormann, N., Caires, S., Chevallier, F., Dethof, A., Dragosavac, M., Fisher, M., Fuentes, M., Hagemann, S., Hólm, E., Hoskins, B.J., Isaksen, L., Janssen, P.A.E.M., Jenne, R., McNally, A.P., Mahfouf, J.F., Morcrette, J.J., Rayner, N.A., Saunders, R.W., Simon, P., Sterl, A., Trenberth, K.E., Untch, A., Vasiljevic, D., Viterbo, P., Woollen, J., 2005. The ERA-40 re-analysis. Q. J. R. Meteorol. Soc. 131, 2961–3012. https://doi.org/10.1256/qj.04.176.

Van der Veen, C.J., 1999. Fundamentals of Glacier Dynamics. Balkema, Rotterdam.

Vegas, J., 2007. Caracterización de eventos climáticos del Pleistoceno Superior- Holoceno mediante el estudio sedimentológico de la Laguna Grande (Sierra de Neila, NO Sistema Ibérico). Rev. de la Soc. Geol. de Espana 20 (1-2), 53–70.

Zahno, C., Akçar, N., Yavuz, V., Kubik, P.W., Schlüchter, C., 2010. Chronology of Late Pleistocene glacier variations at the Uludağ Mountain, NW Turkey. Quat. Sci. Rev. 29, 1173–1187. https://doi.org/10.1016/j.quascirev.2010.01.012.

Žebre, M., Sarıkaya, M.A., Stepišnik, U., Yıldırım, C., Çiner, A., 2019. First 36 Cl cosmogenic moraine geochronology of the Dinaric mountain karst: Velež and Crvanj Mountains of Bosnia and Herzegovina. Quat. Sci. Rev. 208, 54–75. https://doi.org/10.1016/j.quascirev.2019.02.002.

# 5. Paraglacial slope failures in the Aran valley (Central Pyrenees)

Fernandes, M., Oliva, M., & Vieira, G. (2020). Paraglacial slope failures in the Aran valley (Central Pyrenees). *Quaternary International*, *566–567*, 24–38. https://doi.org/10.1016/j.quaint.2020.07.045

Quaternary International 566-567 (2020) 24–38

Contents lists available at ScienceDirect

Quaternary International

journal homepage: www.elsevier.com/locate/quaint

# Paraglacial slope failures in the Aran valley (Central Pyrenees)

M. Fernandes [a,*], M. Oliva [b], G. Vieira [a]

[a] Centre for Geographical Studies – IGOT, Universidade de Lisboa, Portugal
[b] Department of Geography, University of Barcelona, Spain

ARTICLE INFO

*Keywords:*
Aran valley
Central pyrenees
Glaciation
Paraglacial dynamics
Slope failures

ABSTRACT

Slope failures are widespread phenomena in mid-latitude mountain environments that were glaciated during the Last Glacial Cycle. This is the case of the Aran valley, in the Upper Garonne catchment, Central Pyrenees, that included glaciers several hundred meters thick. Following postglacial warming and ice thinning, the recently deglaciated slopes were subject to intense stress readjustments - the so-called paraglacial dynamics. We have identified up to 135 major slope failures in the Aran valley, with only 10 units occurring outside the glaciated domain of the maximum ice extent of the Last Glacial. The presence of polished bedrock surfaces, till and moraine ridges next to some of these features evidence a close connection between glacial and slope processes. We have detected different types of slope failures affecting both bedrock (12 large catastrophic rock slope failures, 16 rock-slope deformation, 34 rockfalls, and 49 rockslides) and unconsolidated glacial sediments (14 slope readjustments on drift-mantled slopes). The average altitude of rock slope failures oscillates between 1551 and 1991 m, with a mean length ranging from 147 to 905 m and a width between 247 and 513 m. The affected surface is also highly variable, oscillating between 0.02 and 126.2 ha. Slope failures occur in different lithological settings, but they are most frequent in slate, lutite and limestone bedrocks. We conclude that most of the failures show a paraglacial origin, though other factors (i.e. lithology and topography) promoted slope instability.

## 1. Introduction

Landscape transition from glacial to non-glacial periods results in major changes in the geomorphological setting of mountain areas and polar regions (Serrano et al., 2018; Ruiz-Fernández et al., 2019). This shift implies a geomorphic readjustment to the new environment, which is know as the paraglacial phase (Slaymaker, 2011; Oliva et al., 2019a). The intensity of the paraglacial response decreases with time and affects deglaciated areas at timescales ranging from years to several millennia (Church and Ryder, 1972; Ballantyne, 2002). The timescale of paraglacial dynamics is debatable, though it is generally accepted that, at least, as long as glacial material is available, deglaciated areas are in the paraglacial phase (Ballantyne, 2002). Following glacial retreat, paraglacial processes are more intense on slopes from recently deglaciated cirques and valleys (Ballantyne, 2002). In these newly exposed ice-free environments, slope debuttressing triggers very active slope processes reworking both glacial sediments and affecting the stability of bedrock outcrops.

Slope response to paraglacial adjustment encompasses distinct geomorphological processes. Rock slope failures (RSF) are one of the main drivers in dismantling recently deglaciated areas and mobilizes a large amount of sediments from the high areas to the valley floors (Feuillet and Mercier, 2012; Cossart et al., 2013). This process is enhanced by the presence of permafrost increasing the activity of rock slope failures, particularly during rapid warming periods when permafrost degrades (Krautblatter et al., 2012; Etzelmüller, 2013). RSF is a general term that includes several types of displacements in bedrock, such as large catastrophic rock slope failures (large rockslides and rock avalanches), paraglacial rock-slope deformation (deep-seated gravitational slope deformations) and rapid rockfalls (Ballantyne, 2002). Rockslides can be also considered as RSF events (Jarman, 2006). Paraglacial dynamics does not only affect the bedrock, but also reworks drift-mantled slopes that can be efficiently eroded by postglacial processes (Ballantyne, 2002).

Since the Maximum Ice Extent of the Last Glacial Cycle (MIE), mid-latitude mountains such as the Pyrenees have been affected by a long-term deglaciation process and small periods of glacial readvance (Oliva et al., 2019b) that have resulted in a variety of paraglacial phenomena. This study focuses on the mapping and spatial characterization of paraglacial slope processes that reshaped the landscape of the Upper

* Corresponding author. Centre for Geographical Studies – IGOT, University of Lisbon, Rua Branca Edmée Marques, 1600-276, Lisbon, Portugal.
*E-mail address:* marcelo.fernandes@campus.ul.pt (M. Fernandes).

https://doi.org/10.1016/j.quaint.2020.07.045
Received 14 February 2020; Received in revised form 22 July 2020; Accepted 24 July 2020
Available online 25 September 2020

Garonne catchment since the MIE.

To date, in Iberian mountain ranges, few works have examined the spatial distribution and geographical characteristics of paraglacial adjustments following MIE glacial retreat. In the Sierra Nevada, the deglaciation of cirques promoted the development of rock glaciers during the paraglacial phase at the end of the Younger Dryas and the onset of the Holocene (Oliva et al., 2016; Palacios et al., 2016). Currently, at ca. 3000–3100 m, paraglacial dynamics is very intense in this massif, occurring in cirques that were glaciated during the Little Ice Age (LIA), with a variety of processes and landforms (rockfalls, mudflows, debris flows, development of rock glaciers and protalus lobes, etc.) subject to permafrost degradation (Gómez-Ortiz et al., 2014). In the Iberian Central Range, Last Glacial Maximum (LGM) moraines present in steep slopes are currently being eroded by water erosion, landslides and debris flows suggesting that these areas are still in the paraglacial readjustment phase (Palacios et al., 2011, 2012; Campos et al., 2018). In the Cantabrian Mountains, paraglacial dynamics following the LGM was examined through the analysis of several deposits in deglaciated slopes and glacial cirques (alluvial, drift-mantled slopes, landslides, etc.), and results revealed an intense landslide activity occurring after the glacial retreat prior to 16.1 ka (Alonso and Corte, 1992; Rodríguez-Rodríguez et al., 2018; Santos-González et al., 2018). Evidence of contemporary paraglacial dynamics has been also described in the Cantabrian Mountains, namely in the cirque bottoms that were glaciated during the LIA at elevations of 2100 m, where a wide range of processes are observed, such as pattern ground, ice mounds, debris flows, etc. (González-Trueba, 2007; Ruiz-Fernández, 2015; Serrano et al., 2018).

In the Pyrenees, glaciers during the MIE reached the piedmont in the northern valleys (Goron, 1941; Taillefer, 1953; Stange et al., 2014; Fernandes et al., 2017) but stayed within the valleys in its southern slope (Calvet, 2004; Delmas, 2015). The long-term deglaciation following the LGM was interrupted by several glacial advances (García-Ruiz et al., 2003, 2013, 2015; González-Sampériz et al., 2006; Delmas, 2015; Palacios et al., 2015b; Oliva et al., 2019b). Therefore, the spatial patterns of paraglacial adjustment are constrained by the different glacial phases. Following the deglaciation, a wide range of rock failures occurred on slopes of the Eastern Pyrenees and were categorized as catastrophic, rockslides or rock-slope deformation (Jarman et al., 2014). Glacial retreat favoured rockslope deformation during the Late Glacial and Holocene (Gutiérrez et al., 2005; McCalpin and Corominas, 2019). Catastrophic failures also occurred following the deglaciation, and some sites still record small surface displacements (Corominas et al., 2015). In addition, the distribution of some slope deposits in the Pyrenees such as debris accumulations, drift-mantled slopes and alluvial fans were also associated with paraglacial dynamics (García-Ruiz et al., 1988, 2007; Palacios et al., 2015; Fernandes et al., 2017). Rock glaciers are very abundant permafrost-related features inside the cirques in the Pyrenees, and their origin has been associated with a rapid deglaciation, having thus a paraglacial origin (Fernandes et al., 2018; Palacios et al., 2015a, 2015b; Serrano et al., 2011). Paraglacial dynamics is currently active in the Central Pyrenees approximately above 2700 m (González-García, 2014).

Taking into account the knowledge gap on the relationship of major slope processes and the paraglacial readjustment in the Central Pyrenees, this paper aims to better understand the geomorphological evidence and the patterns of paraglacial response in the Upper Garonne valley, namely the Aran valley. To do so, we target at three specific goals:

(i) Map the diversity of the major slope failures.
(ii) Examine the spatial distribution of those failures and its relationship with the formerly glaciated area.
(iii) Discuss the variety of paraglacial slope phenomena with its controlling factors of the mid-latitude mountains ranges.

## 2. Study area

The Aran valley is located in the Central Pyrenees between latitudes 42°36′ and 42°51′N and longitudes 0°40′ and 1°00′E and constitutes the headwaters of the Upper Garonne basin (Fig. 1). The Aran valley encompasses 553 km$^2$, with elevations exceeding 3000 m a.s.l., in the Besiberri Nord and Molières peaks, and minimum elevations of ca. 600 m in the northern Spanish border. In 2019, the total population of the valley is 9971 inhabitants distributed in 9 municipalities that are mostly located in the main valley floor and neighbouring margins.

The geological formation of the axial part of the Pyrenees is associated with the Hercynian orogeny and the reactivation of the folding system during the Alpine uplift (Zwart, 1979; Beaumont et al., 2000). The Upper Garonne valley represents an important lithological sequence to describe the geological history of the Pyrenees (Kleinsmiede, 1960). Based on its lithology and morphostructure, the Aran valley can be divided in three units:

(i) The Dome of Garonne is composed by subhorizontal flatlying structures (Kleinsmiede, 1960; García-Sansegundo, 1996) and materials from the Cambrian and the Ordovician. Outcrops from this group are schists, marbles, slates, quartzite, but also sandstones and lutites (Sitter and Zwart, 1962; García-Sansegundo, 2004). The southern boundary of this unit lies between Liat and Bossòst faults (Fig. 1). Comparing with the other group morphologies, this one is defined by narrow U-shaped valleys and the lowest glacial peaks (Maubèrme - 2882 m).
(ii) The Sinclinorium of the Aran valley is a highly folded and faulted syncline structure (E-W oriented) from the Devonian and Silurian (Kleinsmiede, 1960; Zwart, 1979). It is composed of intercalated limestones, lutites, sandstones and black slates (Kleinsmiede, 1960). The area is flanked by the Liat and Bossòst faults in the northern part and by the Maladeta batholith in its southern fringe (Fig. 1). Morphologically, the relief of this group is characterized by wide valleys, mainly oriented E-W and with large plateaus in the upper parts.
(iii) The Maladeta batholith is associated to the central axis of the Pyrenees, which intruded at the end of Hercynian orogeny, in the Carboniferous (Kleinsmiede, 1960) and is composed essentially of granodiorites with a dense joint network, but scarce faulting (García-Sansegundo, 2004) (Fig. 1). This group includes the widest U-shaped valleys mostly oriented S–N and the highest peaks (Molières −3010 m).

In addition to lithological constraints, the modern-day landscape of the valley is largely determined by the impact of Pleistocene glaciations. The Aran valley includes several U-shaped tributaries converging into the main Garonne valley. During the coldest phases of the Last Glacial Cycle, glaciers flowed downvalley to the Garonne valley reaching the piedmont of the Central Pyrenees at the terminal Loures-Barouse-Barbazan basin (Goron, 1941; Taillefer, 1966; Stange et al., 2014). The MIE of the Last Glacial Cycle is estimated to have occurred during the MIS 4 (50–70 ka) (Delmas, 2015), when glaciers showed thicknesses exceeding 800 m in the Aran valley and 600 m in the tributaries (Bordonau, 1992; Fernandes et al., 2017). Following the last MIE, several phases of glacier advance and stabilization occurred during Termination-1, as revealed by the existence of different moraine systems within the valleys (Bordonau, 1992; Martí-Soler, 1988; Fernandes et al., 2017). Although there is still no chronological framework for those glacial oscillations, it is likely that they followed a similar timing than in other Pyrenean valleys, with glacial advances documented during the Oldest and Younger Dryas, as well as during the coldest periods of the Holocene (García-Ruiz et al., 2014, 2016; Palacios et al., 2017; Oliva et al., 2019b).

After the glaciers retreated, paraglacial readjustment triggered intense sediment redistribution from the upper slopes to the valley

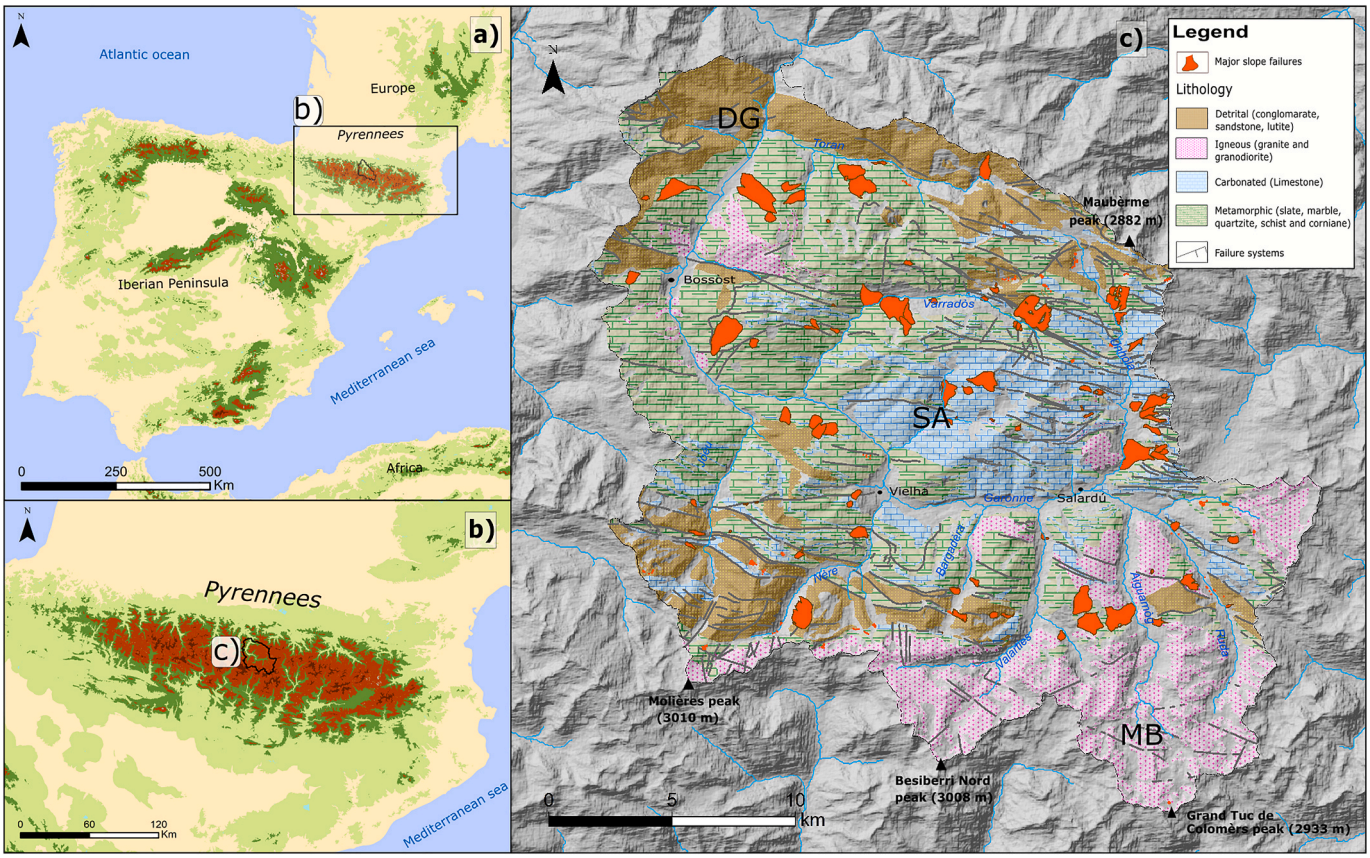


**Fig. 1.** Location of the Aran valley within the Iberian Peninsula (A) and the Pyrenees (B), including also the lithological setting (C), where (DG) represents the Dome of Garonne, (SA) corresponds to the Sinclinorium of the Aran valley, and (MB) shows the Maladeta batholith.

floors. In the valley slopes and glacial cirques, there are superficial and deep RSF, as well as detrital accumulations that constitute the primary sources of the sediment cascade (Serrat et al., 1994; Martí-Soler, 1988; Fernandes et al., 2017). This also includes the drift-mantled slopes that were initially assumed to be completely washed (Kleinsmiede, 1960), although more recent studies identified the existence of till deposits on the slopes of the Aran valley (Martí-Soler, 1988). Paraglacial sediment stores were also identified in small glacial basins down to 1900 m, infilled with lacustrine and peat deposits during the paraglacial phase (Martí-Soler, 1988; Serrat et al., 1994). Similarly, flatter areas between ca. 650 and 1400 m were interpreted as overdeepened basins infilled by proglacial sediments (Serrat et al., 1994). Within the deglaciated cirques above 1700 m, there are permafrost-related landforms, such as rock glaciers that must have formed during the paraglacial phase (Fernandes et al., 2018).

The Aran valley is located in a climatic transition zone between the Atlantic and the Mediterranean climates. At 2266 m (Bonaigua station), the mean annual air temperature (MAAT) is 3 °C and precipitation totals 1225 mm (2007–2018).

## 3. Methodology

The study of the major slope failures and of their relationship with the paraglacial phase was examined using different approaches. Firstly, we conducted a detailed geomorphological mapping of the study area using remote sensing data and GIS tools in ArcGIS 10.6.1 with subsequent *in situ* validation. Later, quantitative data was obtained on their topographical distribution and morphology, as well as on the lithological setting and prevailing morphostructure.

### 3.1. Geomorphological mapping

The geomorphological mapping of the study area was carried out in GIS environment using the orthophotomaps of 25 × 25 cm resolution from the *Institut Cartogràfic i Geològic de Calatunya* (ICGC) and the digital elevation model at 1 × 1 m resolution generated from LiDAR data and provided by the same institution. The digital stereo viewer of the *Instituto Geográfico Nacional* was also used for the interpretation and mapping of the landforms. The geomorphological map was subsequently validated with field observations.

The map analysis was complemented with the modelling of the glacier surface for the MIE in the Aran valley published in Fernandes et al. (2017) to evaluate the distribution of the major slope landforms within the area formerly occupied by the glaciers. Slope failures were classified and mapped following the paraglacial mass movements classification by Ballantyne (2002). Four different types of paraglacial slope failure were identified in bedrock areas that were under ice during the Last Glacial Cycle (Fig. 2):

(i) Large catastrophic rock slope failures (CRF), characterized by the presence by fan-shaped accumulation with wider toe and well-defined upslope scars. These also show concavities and convexities in body of the deposit (Ballantyne, 2002).
(ii) Rock-slope deformation (RSD) include failures affecting most of the slope, with the presence of trenches, double ridges, tension cracks, scarps, antiscars, benches, bulges and characterized by poorly defined boundaries and failure surfaces (McCalpin and Corominas, 2019).
(iii) Rockfalls (RF) are chaotic accumulations of large boulders associated with cirque walls, overdeepened basins or valley margins (Ballantyne, 2002). Rockfalls are one of the most widespread

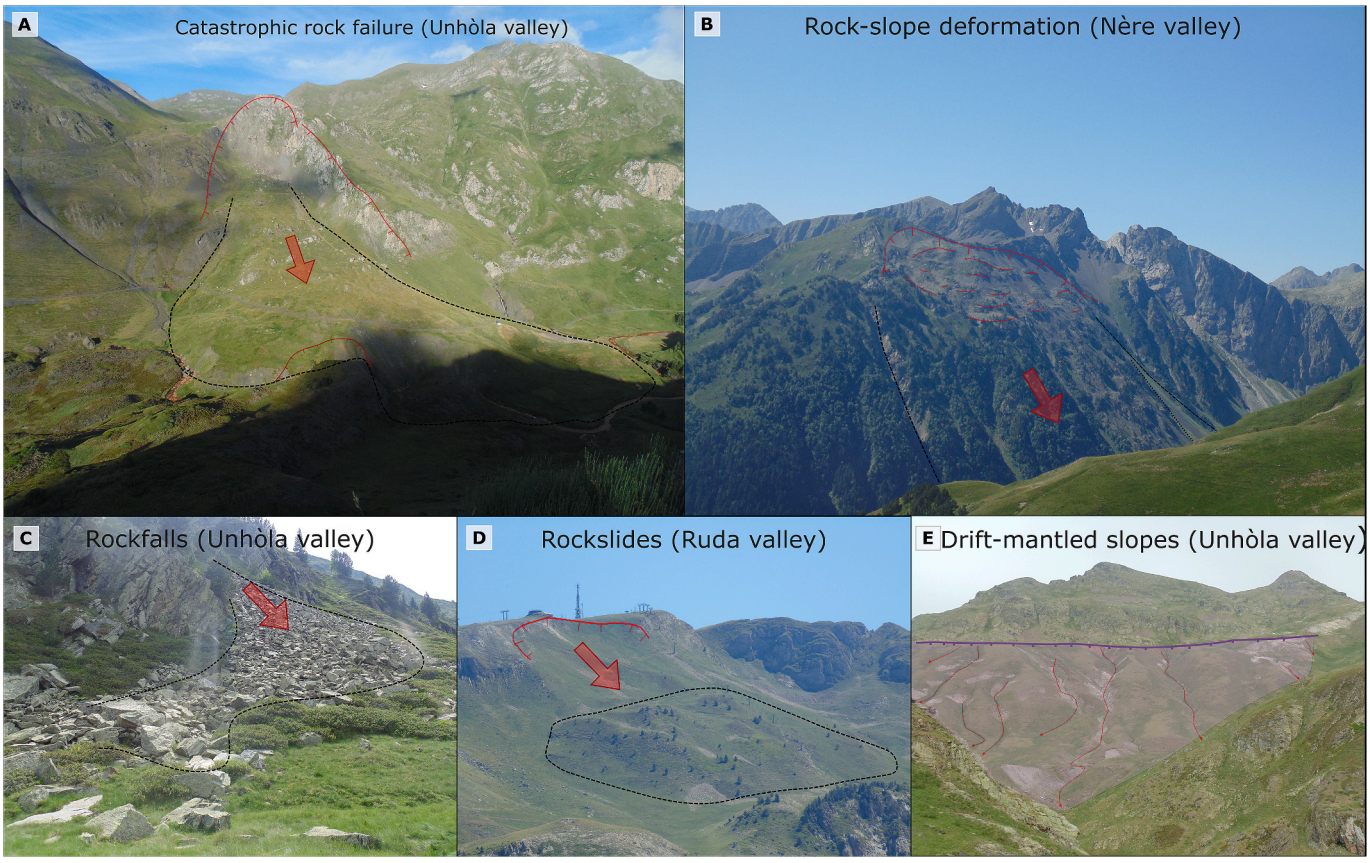


**Fig. 2.** Examples of major slope failures.

geomorphological process in mountain areas and is a very active process in the current periglacial belt of mid-latitude mountains. In this study, we only examine the major rockfalls deposits as events that may have occurred during the paraglacial phase (Wilson, 2009).

(iv) Rockslides (RS) are rotational landslides with one or a few main scars and well-defined boundaries. Upslope there is usually a concave surface of rupture and an elongated cohesive body flowing short distances downslope with a lobated front (Jarman, 2006; Highland and Bobrowsky, 2008).

In addition, we have also identified slope readjustments on drift-mantled slopes (DMS). These processes are interpreted as a result of paraglacial dynamics following deglaciation. DMS are particularly prone to postglacial erosion in steep slopes covered by till deposits (Ballantyne, 2002). In this group, we include two types of weathering features:(i) traces of superficial erosional landforms (gullies), and (ii) transversal scars on unconsolidated glacial deposits affected by deformation.

### 3.2. Quantification of spatial controls of major slope failures

With the purpose of characterizing the morphometry and the topographical distribution of slope failures in the Aran valley, using a digital elevation model at 1 × 1 m resolution in a GIS environment, we obtained the minimum, mean, and maximum values of width, length, size and altitude as well as the mode of slope and aspect for each unit. The lithology and morphostructure also determine the stress release during the paraglacial phase (Augustinus, 1996). Therefore, the 1:50000 lithological map from ICGC allowed to identify rock type and the distance to the nearest fault from the main scar, as well as the morphostructural group (Sinclinorium of the Aran valley, Dome of Garonne, Maladeta batholith) of each landform.

## 4. Results

A total of 135 major slope failures were identified in Aran valley (Fig. 3), with only 10 features distributed outside the glaciated environment during the Last Glacial Cycle. The rest of the landforms occur within an elevation range between 636 and 2606 m across the slopes of the main Garonne valley, as well as across the hillsides of the tributaries, overdeepened basins, and glacial cirque walls. Together, they extend over an area of 3012 ha, which represents almost ca. 5% of the entire the Aran valley.

### 4.1. Typology and organization of slope phenomena

In the Aran valley, we distinguished five different groups of major slope movements, four in bedrock and one in the deposits: 12 CRF, 16 RSD, 34 RF, 49 RS and 14 DMS (Fig. 2).

These failures occur at a wide range of altitudes, with an average elevation difference between the top and the lowest limits of the landforms of ca. 300 m. However, some large events, such as that next to Bossòst village (Fig. 3), can reach an elevation range of 1120 m. In most cases, failures affected only sections of the slopes, whereas in others affected the entire hillside. Most of these landforms are concentrated in slopes between 20 and 30° (40%). The prevailing aspects of are W (31%) and N oriented (27%), followed by E (24%) and S exposures (18%). The surface occupied by rock failures in the Aran valley is highly variable, ranging from 0.02 to 126.2 ha, with a mean of 23.8 ha. The average of length and width is 510 m and 329 m, respectively, with a length/width ratio of 1.6 (Table 1).

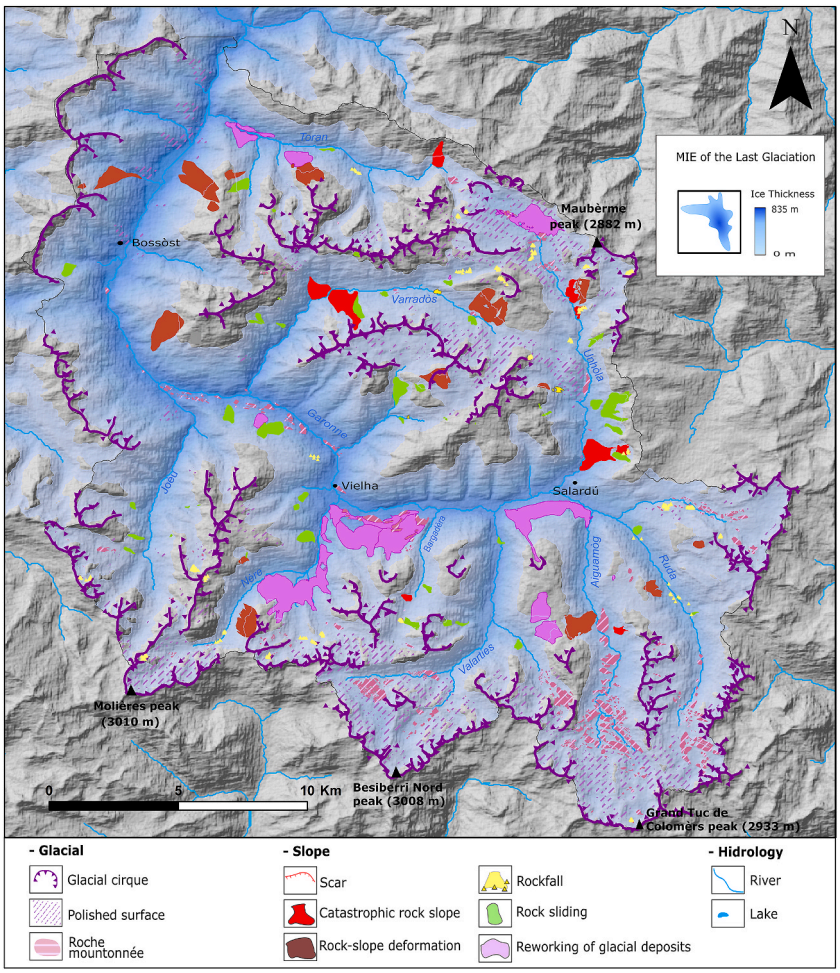


**Fig. 3.** Distribution of the major slope failures in the Aran valley together with the ice thickness modelled for the MIE of the Last Glacial Cycle by Fernandes et al. (2017).

*4.1.1. Catastrophic rock failures (CRF)*

CRF in the Aran valley occurred mainly on the slopes of the tributaries next to the Garonne main valley floor. These failures follow the type of Bagergue village unit (A/B, Fig. 4), where a large mass movement originated from a glacial cirque at 2200 m and is currently being intensively reworked by alluvial dynamics. Surrounding the cirque, there are successive parallel deep scars seated on fault contacts between slates and limestones, with dammed lakes between the ridges. In the lower part of the landform there are concavities and convexities with well-defined lobate fronts. There are other cases that fit within the CRF group (C/D, Fig. 4), although with smaller dimensions. A CRF may be subsequently affected by other slope processes: this is the case of the Bargadèra valley (C/D, Fig. 4), where the presence of lobate ridges composed of fine sediments suggests that were mobilized by viscous events, such as earth-flows.

The average mean altitude of the CRF failures is 1551 m. They are distributed along an altitudinal range from 769 m to 2214 m. With regards to the slope, CRF are found in relatively gentle hillsides with an average of 26.3°. This type of landforms is manly exposed to the S (33%). The surface covered by the CRF averages 24.7 ha. Landforms tends to show more elongated shape with averages of 742 m (length) and 359 m (width), respectively. The average length/width ratio is 2.2 (Table 1).

*4.1.2. Rock-slope deformation (RSD)*

RSD are distributed on the slopes of the main valley and tributaries, as well as inside glacial cirques. Main transversal scars and antiscars are widespread. The main body can be segmented in sub-units normally flanked by scarps. The lateral boundaries and the toe of RSD landforms are usually defined by streams. In some landforms included in this RSF group, transversal antiscars showing the deep-seated deformation are also found. Other features can be also indicators of this deformation, such as sparse debris deposits on slopes. A typical example of this group is found in the Varradòs valley, where the complex main body of the landform shows transversal scars and antiscars with double ridges, tension cracks, scarps and bulges, and is locally affected by talus cones, screes, rockfalls and gullies (A/B, Fig. 5).

The mean altitudes of the RSD in the Aran valley is 1716 m. These failures are distributed along an elevation range from 636 to 2485 m, with an average slope of 26°. The prevailing aspect is W (38%), followed by W and N orientations. The RSD failures show an average area of 33.8 ha and show elongated bodies, with averages of 905 m (length) and 513 m (width). Therefore, the average length/width ratio is 1.8 (Table 1).

*4.1.3. Rockfalls (RF)*

RF are the most abundant slope failure phenomena in the Aran valley, occurring next to the cirque walls, steep valleys sides and rockfaces of overdeepened basins. This category includes all landforms with source at a deglaciated rockwall, although the accumulation zones can be diverse, including talus cones, glacial deposits, rock glaciers, rock failures or bedrock surfaces. The Unhòla valley shows an excellent study case (B, Fig. 6), where the fault contact between lutites and limestone with slates, exposes a vertical 170 m high limestone scarp that favours rock fall activity. The difference in size of the boulders between the large

**Table 1**
Main topographical and morphometrical characteristics of RSF in the Aran valley.

| | Units | Topography | | | | | | | | Morphometry | | | | | | | | | |
|---|---|---|---|---|---|---|---|---|---|---|---|---|---|---|---|---|---|---|---|
| | | Altitude (m) | | | Slope (°) | | | Aspect (°) | | | Area (ha) | | | Length | | | Width | | | L/W ratio | | |
| | | min | mean | max | min | mode | max | 1st | 2nd | 3rd | min | mean | max | min | mean | max | min | mean | max | min | mean | max |
| **CRF** | 12 | 769 | 1551 | 2014 | 0.4 | 26.3 | 68.3 | S | W/E | N | 1.0 | 24.7 | 113.6 | 157 | 742 | 1895 | 84 | 359 | 925 | 1.3 | 2.2 | 3.8 |
| **RSD** | 16 | 636 | 1716 | 2485 | 0.0 | 26 | 69.6 | W | E | N/S | 2.0 | 33.8 | 126.2 | 192 | 905 | 2155 | 130 | 513 | 1127 | 1.2 | 1.8 | 2.5 |
| **RF** | 34 | 1070 | 1991 | 2606 | 1.6 | 21.1 | 54.9 | W | N/E | S | 0.02 | 4.4 | 63.3 | 3.29 | 147 | 1288 | 26 | 247 | 1475 | 0.0 | 0.8 | 2.8 |
| **RS** | 49 | 928 | 1793 | 2482 | 1.6 | 28.7 | 67.5 | W | N | E | 0.3 | 16.4 | 123.6 | 95.4 | 577 | 1535 | 59 | 318 | 1180 | 1.2 | 2.1 | 4.7 |
| **Total** | 111 | 636 | 1817 | 2606 | 0.0 | 25.8 | 86 | W | N | E | 0.02 | 16.1 | 126.2 | 3 | 510 | 2155 | 26 | 329 | 1475 | 0.0 | 1.6 | 4.7 |

rocks from the rockfall deposit (with boulders up to 50 $m^2$) and the smaller ones from the surrounding debris talus covered by vegetation, demonstrates that periglacial dynamics are no longer active at 1850 m, and the large boulders must therefore be associated to other geomorphic triggers.

The average altitude of the RF shows the highest values of all studied slope phenomena, with a mean of 1991 m. These failures are distributed along an altitudinal range from 1070 m to 2606 m, and the accumulation area of the deposits shows an average slope of 21.1°. Concerning aspect, no clear control is observed (Table 1). The average area is 4.4 ha and boulder accumulations are wide and sparse than debris talus landforms, extending in average along 147 m (length) and 247 m (width). The average length/width ratio is 0.8 (Table 1).

#### 4.1.4. Rockslides (RS)

RS are distributed across the slopes of the main Garonne valley, tributaries as well as in the glacial cirques. This type of RSF includes cohesive mass gravitational slope movements with bedrock outcrops in the surface of rupture or/and in the main scar. It is also common to find relatively small deformations on top of the slide, with lobate and convex shapes (A/B, Fig. 7), related to viscous earth flows (creep) on unconsolidated glacial sediments. A clear example is located in the Varicauva forest, close to the Pònt d'Arròs village (C/D, Fig. 7). Here, the main scar of a rotational rockslide shows a surface of rupture exposing sandstones and lutites. The variations of the vegetation cover are indicative of the area affected by rock sliding and the limits of the prominent toe. On the landslide surface, sparse granite boulders can also be found showing evidence of a drift-mantled slope cover.

RS show the lowest mean altitudes, with an average of 1793 m. These failures are distributed along an altitudinal range between 928 m and 2482 m. Rockslides show a steep slope average of 28.7° and are preferentially distributed in W exposures (38.7%). RS failures have an average area of 16.4 ha and are elongated landforms with averages of 577 m (length) and 318 m (width). The average length/width ratio is 2.1 (Table 1).

#### 4.1.5. Drift-mantled slopes (DMS)

The presence of glacial sediments on slopes favours their reshaping following deglaciation. Geomorphic evidence of postglacial erosion processes is mainly found in the most recently deglaciated areas, such as glacial cirques and plateau margins. In the Aran valley, this type of slope adjustment is expressed in two ways: (i) subsuperficial and large deformed till failures in relatively gentle areas such as the margins of the plateau of Monto-romies (A/B, Fig. 8) where the main body includes well-developed transversal and superficial scars; (ii) superficial erosion, which is widespread in moraines, such as in the lateral moraine at the Unhòla glacial cirque at 2200–2300 m (C/D, Fig. 8). This moraine shows coalescent and intersected gullies mobilizing sediments downslope onto the accumulation areas, where debris cones and alluvial fans are found.

### 4.2. Lithological and morphostructural controls of slope processes

Together with the impact of past glaciations, the diversity and distribution of lithologies and fault systems in the Aran valley constrains the geomorphological dynamics. This group of analysis shows the lithostructural variability on the four types of RSF (Table 3). There are 19 lithological groups in the Aran valley, being sandstones and lutites the most widespread lithology occupying 84 $km^2$ (19.7% of the area). Failures are more abundant in slates, representing 25.2% of the total number, whereas in lutites and limestones, they represent 18.9%, 14.4% in sandstones and lutites, 9.9% in marbles, and 9% in schists. Within these major groups, marble shows the highest ratio with 0.7 event per $km^2$ followed by lutites and limestones (0.44) and slates (0.40). This first five classes represent 77.5% of all failures despite extending over only 64% of the Aran valley. Failures that occur in metamorphic bedrock concentrate 55% of all events within an area of only 45.8% of the Aran

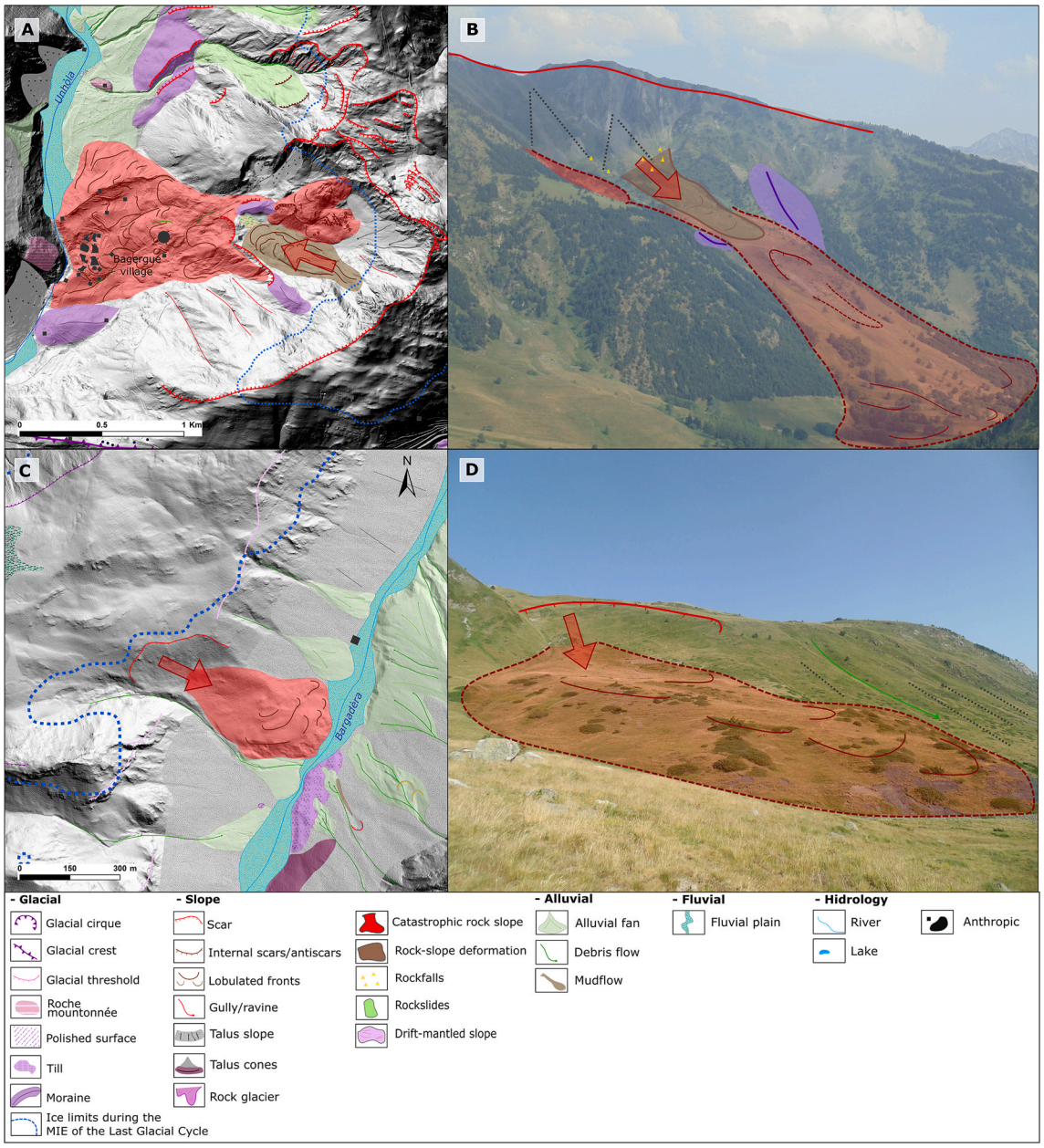


**Fig. 4.** Examples of large catastrophic rock slope failures: the Bagergue village in the Unhòla valley (A, B) and the Bargadèra valley (C, D).

valley (0.3 occurrences per km$^2$). In contrast, only 2.7% of the rock failures occur in granodiorite, that extends over 50 km$^2$ of the Aran valley (12.1%) (Table 2). In terms of morphostructure, 77.5% of the failures are distributed in the Sinclinorium of the Aran valley, 18.9% in the Dome of Garona and 3.6% in the Maladeta batholith (Table 3). The distance between the nearest fault to the slope scar shows an average value of 363 m, ranging from 0 to 2113 m.

#### 4.2.1. *Catastrophic rock failures (CRF)*

The CRF occur mostly (91.7%) in the Synclinorium of the Aran valley. In most of this group, failures occur in slates (50%), with a minor proportion distributed on schist, marble, limestone, and hornfels. In 4 of the 12 failures, the main scar is connected to faults (Table 3).

#### 4.2.2. *Rock-slope deformation (RSD)*

The RSD are found in the Sinclinorium of the Aran valley (56.3%) and in the Dome of Garona (43.9%). Therefore, they occur in a wide range of lithological settings including schist, slate, sandstone and lutite, slate and marble. Up to 31.2% of the failures occur precisely on schists. More than one third of the RSD (7 of 16) occurred next to the main faults existing in the Aran valley (Table 3).

#### 4.2.3. *Rockfalls (RF)*

The RF in the Aran valley are found in the Sinclinorium of the Aran valley (61.8%) but also in the Dome of Garona (29.4%) and Maladeta batholith (8.8%). The majority of the falls occur in sandstones and lutites (20.6%) although other lithologies are also affected, such as lutite and limestone, marble, sandstone and lutite, limestone and slate. A low number of RF (7 of 34) are connected to faults (Table 3).

#### 4.2.4. *Rockslides (RS)*

The RS are distributed in the three morphostructural groups: in the Sinclinorium of the Aran valley with 91.8%, in the Dome of Garona with 6.1%, and in the Maladeta batholith with 2%. The prevailing lithology of the rockslides is slates (36.7%) although other bedrocks are also affected, such as lutite and limestone, schist, sandstone and lutite,

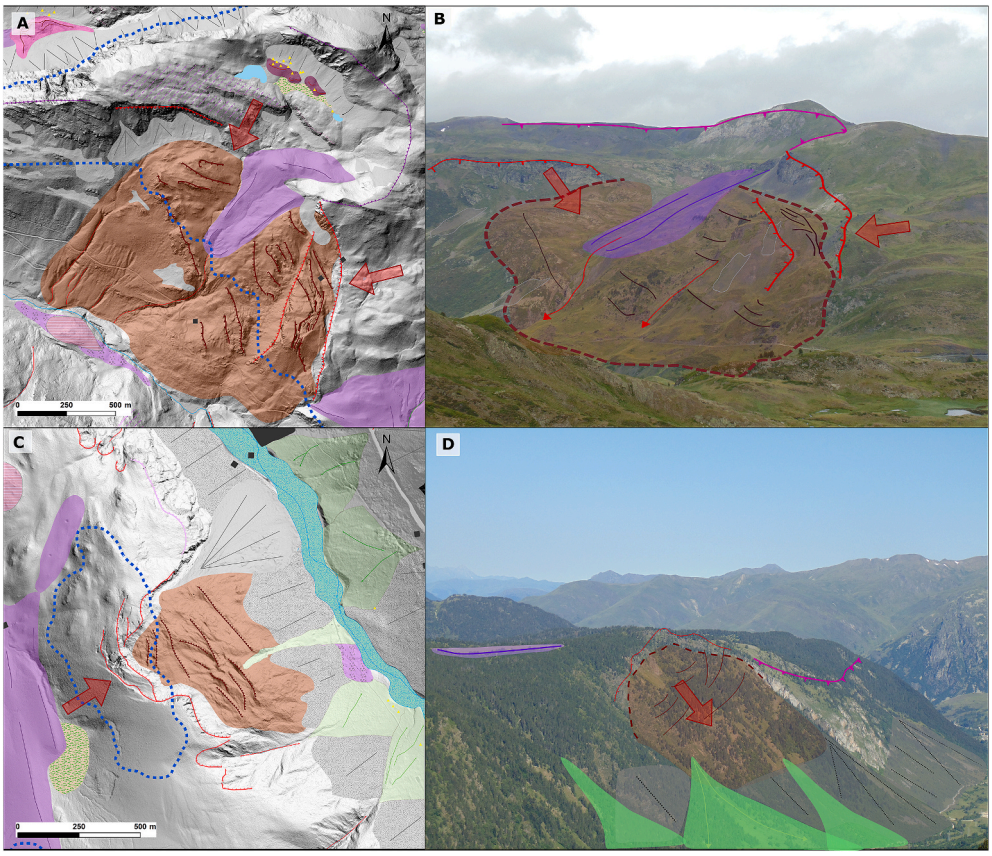


**Fig. 5.** Examples of rock-slope deformation: the Vadarròs valley (A, B) and the Ruda valley (C, D) (same legend than in Fig. 4).

marble, quartzite and lutite, granodiorite, sandstone, slate and marble, granodiorite. From the 49 RS, 25 show the main scars next to faults (Table 3).

#### 4.2.5. *Drift-mantled slopes (DMS)*

The reworking of drift-mantled slopes depends on the distribution of glacial deposits. There does not seem to be a lithological or morphostructural control on this group since this are essentially sedimentary cover deposits.

### 4.3. *Spatial connection of slope failures and the glaciated domain during the Last Glacial cycle*

During the Last Glacial Cycle, the Aran valley was heavily glaciated as revealed by the widespread geomorphic evidence of glacial erosional and depositional features distributed across the landscape. Glaciers carved S–N overdeepened basins in the valley floors that have been infilled by postglacial sediments. Polished bedrock surfaces are also found in the main valley floor at elevations from 650 to 1200 m, such as near the Bossòst and Vielha villages (Figs. 2 and 9), as well as in valley slopes, where glacial striations and 20–30 cm deep grooves are also found – such as those next to the Pònt d'Arròs village – and are indicative of the E-W flow of glaciers. Glacial erratics are abundant along the hillsides up to ca. 800 m from the valley bottom, which reflects the minimum ice thickness during the MIE. Following glacial thinning, till was deposited along the slopes, including some moraine ridges in the valley floors. Glaciers disappeared in the Aran valley probably during the Early Holocene (Fernandes et al., 2017) and, since then, environmental dynamics has been mostly shaped by periglacial, nival, alluvial and slope processes, together with soil formation and vegetation colonization.

The slope failures of the Aran valley show a close connection with the glaciated area, as they are located within the limits of the ice during the Last Glacial Cycle that reached a thickness between 189 and 777 m (Fernandes et al., 2017) (Figs. 3 and 10). The failures are distributed in the hillsides of U-shaped glacial valleys, margins of overdeepened basins, and rock walls of glacial cirques. The average values of the minimum altitudes of the slope failures range from 1380 to 1958 m, well below the ice surface during the maximum glacial expansion, and therefore affected by intense glacial erosion.

## 5. Discussion

The current landscape of the Aran valley is a consequence of the strong impact of Quaternary glaciations as well as postglacial environmental dynamics that reshaped the valleys through a wide range of processes, including periglacial, nival and alluvial dynamics as well as slope processes. A detailed geomorphological study of the major slope failures existing in the formerly glaciated area in the Aran valley resulted in the identification of 125 features corresponding to different type of processes (Fig. 3). These features show a wide range of morphologies and dimensions, covering an extent of ca. 5% of the entire Aran valley.

### 5.1. *Why are most slope failures of paraglacial origin?*

In contrast to other neighbouring valleys of the Central (Palacios et al., 2015a, 2017b) and Eastern Pyrenees (Palacios et al., 2015b; Jomelli et al., 2020), there are still no available chronological data about Late Pleistocene glacial phases in the Upper Garonne basin and the subsequent postglacial slope readjustment. Our knowledge of the glacial evolution is still limited to geomorphological observations and a relative glacial chronology (Fernandes et al., 2017). Therefore, it is difficult to assess the importance of the paraglacial phase in the development of the

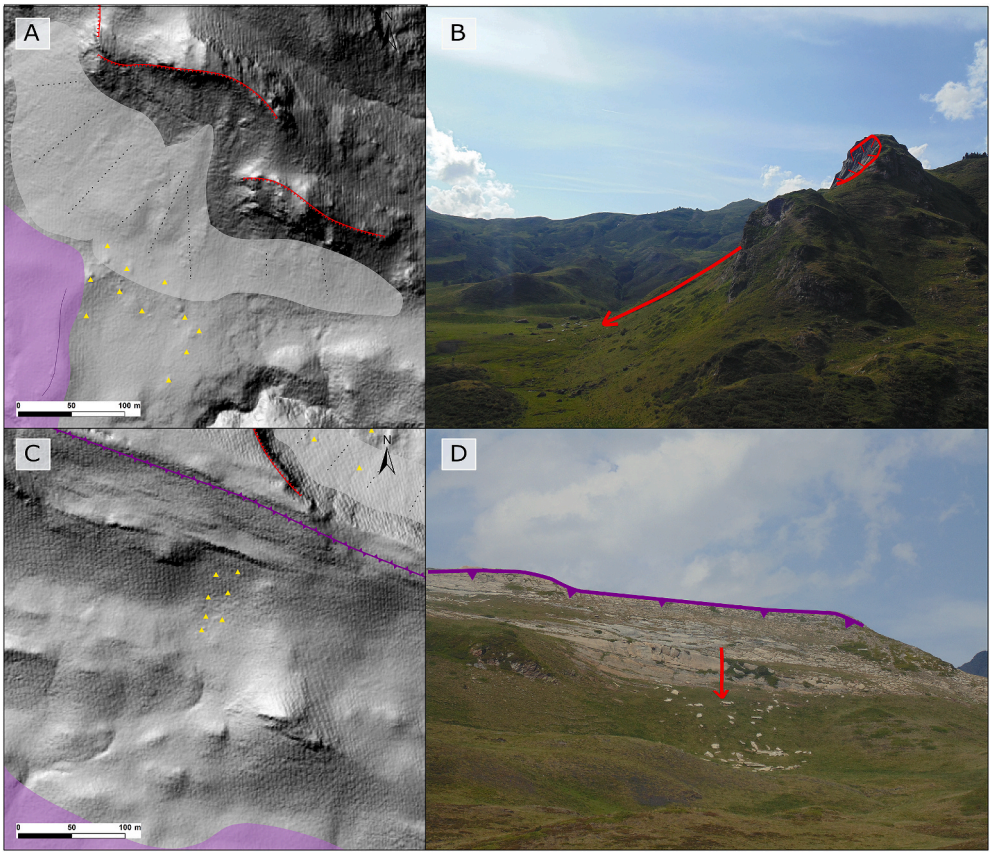


**Fig. 6.** Examples of rockfalls: the Unhòla valley at 1800 m (A, B) and at 2200 m (C, D) (same legend than in Fig. 4).

major slope failures in the Aran valley as this needs a robust chronology of glacial oscillations, as well as of the timing of generation of the different type of slope features. However, the spatial connection between glacial landforms and deposits and slope failures is indicative of a close interaction between them. Indeed, the abundance of unconsolidated glacial and periglacial deposits on slopes enhances the potential of slope susceptibility with the resulting danger for human infrastructures and settlements distributed across the valley floor.

The occurrence of a wide range of glacial phenomena showed evidence that the area was heavily glaciated during the Last Glacial Cycle (Bordonau, 1992; Serrat et al., 1994; Martí-Soler, 1988). Erratic boulders point to the maximum ice thickness reached by the glaciers, whereas moraines are indicative of phases of stabilization or glacial advance within the long-term glacial retreat. Glacial modelling based on the different sets of moraine fronts suggest four different stages: at the piedmont (400–500 m), within the main valley floor (1000–1850 m), inside the high valleys (2050–2200 m), and in the glacial cirques (2260–2590 m) (Fernandes et al., 2017). During the MIE of the Last Glacial Cycle, 76% (420 $km^2$) of the Aran valley was covered by ice, developing a complex glacial system with several diffluence and transfluences filled with ice most of the headwaters of the Upper Garonne basin, including the cirques, valleys and high plateaus. The very thick ice cover in the valley floors as well as along the hillsides produced very intense erosion and abrasion processes. The topography and the pre-glacial geomorphological setting determined the characteristics of the glaciated environments as well as the erosional and depositional glacial processes (Benn and Evans, 2010). In turn, once the glacier disappeared, the new exposed terrain was affected by the debuttstressing effect and slopes adjusted to the new conditions during the paraglacial phase (Oliva and Ruiz-Fernández, 2015). Then, slopes were prone to release the geomorphic stress through a wide range slope processes, both in bedrock areas as well as in unconsolidated glacial terrain.

The fact that most failures occurred in glaciated areas during the Last Glacial Cycle is indicative that they must have formed following the deglaciation as glacial erosion would have eroded all traces of previous slope failures. The different type of slope failures is a consequence of the local topographical setting, lithological properties as well as the geomorphological context with regards to past glaciation. The existence of glacial polished surfaces, erratic boulders, sparse till deposits and moraine systems in the surroundings of slope failures also confirm a close connection with past glacial activity (Figs. 4, 5, 7 and 8).

In addition, it is likely that permafrost may have enhanced slope dynamics during the paraglacial phase. The presence of various permafrost-related landforms, namely rock glaciers and protalus lobes, at elevations ranging from 1745 to 2725 m (Fernandes et al., 2018) confirms the occurrence of permanently frozen ground conditions in the recently deglaciated slopes of the periglacial mountain belt during several millennia following the deglaciation. Colder phases during Termination-1, such as the Oldest and Younger Dryas, must have promoted the development of several generations of permafrost features associated with paraglacial dynamics in the Central Pyrenees (Oliva et al., 2016). Present-day and Early Holocene analogues from Scandinavia confirm the potential of permafrost for triggering major paraglacial slope failures in steep areas, namely in the form of rockslides (Böhme et al., 2019).

The global chronological review of McColl (2012) showed that large paraglacial failures can occur some thousands of years after the ice retreats. Several dated failures reported ages between 16 until 1 ka in deglaciated slopes of the European Alps and other mid-latitude ranges, such as the Arroumd village (High Atlas) where a catastrophic event was dated at 4.5 ± 0.5 $^{10}$Be ka (Hughes et al., 2014). McColl (2012) therefore considers that slope failures in formerly glaciated areas, even in recent times, result from the paraglacial relaxation of the landscape to non-glacial conditions. Similarly, in the Pyrenees slope failures occurred

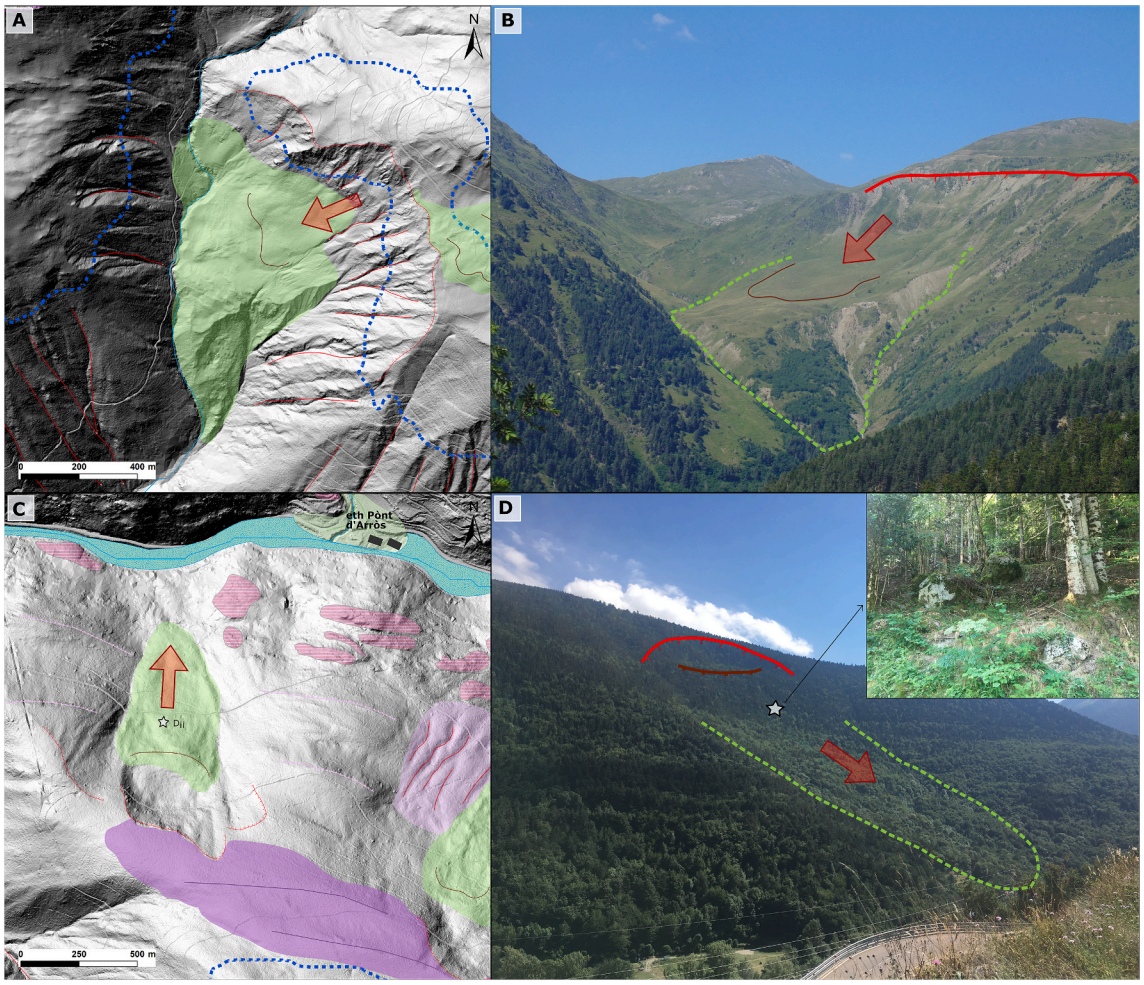


**Fig. 7.** Examples of rockslides: the Salient valley (S of the Vadarròs; A, B) and the Varicauva forest in the Garonne valley (C, D) (same legend than in Fig. 4).

following the deglaciation as shown by several examples: the RSD in Encampanada (Andorra) was dated at 15.3 ± 1.1 ka cal BP (McCalpin and Corominas, 2019), a very similar age than in the Ubago (Eséra Valley) that yielded a minimum age of 15.1–14.9 ka cal BP (Gutiérrez et al., 2008).

There are, however, several RSF that formed more recently. Some RSD developed during the Holocene, such as in Estós (Eséra valley) with an age of ca. 7.7 ka cal BP (Gutiérrez et al., 2005), and in Cristallere (Aspe valley) that resulted in AD 1380 (Lebourg et al., 2014). Other RSD generated during the paraglacial phase reactivated in several events during the Holocene (Gutiérrez et al., 2005, 2008; McCalpin and Corominas, 2019). In some cases, despite not having chronological data yet, the presence of highly weathered scars, organic-rich soil layers and dense vegetation cover can be indicative of older origin, whereas fresh scars, clear morphologies and unvegetated terrain can be associated with a recent formation. Geomorphic evidence of recent dynamics can be observed in the Bagergue CRF that shows a similar fan morphology than the Canillo event (Andorra), which started after the deglaciation and still records displacement rates of 4 cm $yr^{-1}$ (Corominas et al., 2015). The monitoring of recent scar movement rates from other RSF, such as post-LIA RSD suggested its gradual trend to stabilization on the Vénéon valley (Western Alps) (Duvillard et al., 2018). Despite the apparent inactivity of these RSD, the potential reactivation of these features can not be excluded by future perturbations (Kellerer-Pirklbauer et al., 2010).

### 5.2. *Controlling factors of paraglacial slope failures in the Aran valley*

The massive deglaciation occurred in the Pyrenees, as well as across most mountain ranges of the Northern Hemisphere at 19–20 ka (Clark et al., 2012) triggered a large vertical reorganization of geoecological processes in mountain environments, and slope dynamics became one of the major drivers of the recently deglaciated landscape as part of the paraglacial response. Apart from the impact of retreating glaciers, the intensity and spatial extent of slope failures was also determined by the topographical setting, the lithological characteristics and network of faults existing in the area, as well as by climate conditions (Fig. 11).

Slope failures are more abundant in steep slopes than in gentle hillsides, which must have been affected by other periglacial slope processes during the paraglacial phase, such as solifluction, debris flows, mudflows, etc. (Oliva et al., 2016). Slope failures in the Aran valley showed average slopes between 21 and 29°, which are of similar magnitude to those described for RSF in other mid-latitude mountain environments such as in RSD in Central Pyrenees (Gutiérrez et al., 2005), Scottish Highlands (Jarman, 2006), and the European Alps (Agliardi et al., 2012; Ostermann and Sanders, 2017). Moderate slopes (ca. 24°) can favour large RSD, while steeper faces can trigger catastrophic events such as RS (Agliardi et al., 2012).

The lithological setting is also a major constraint for large slope failure events. The Aran valley includes several lithologies, and the boundaries between them favour the occurrence of instabilities that trigger slope processes. In fact, 96% of the failures occur within the Dome of Garonne and the Sinclinorium of the Aran valley where the summits reach ca. 2500–2800 m whereas in the Madaleta batholith with

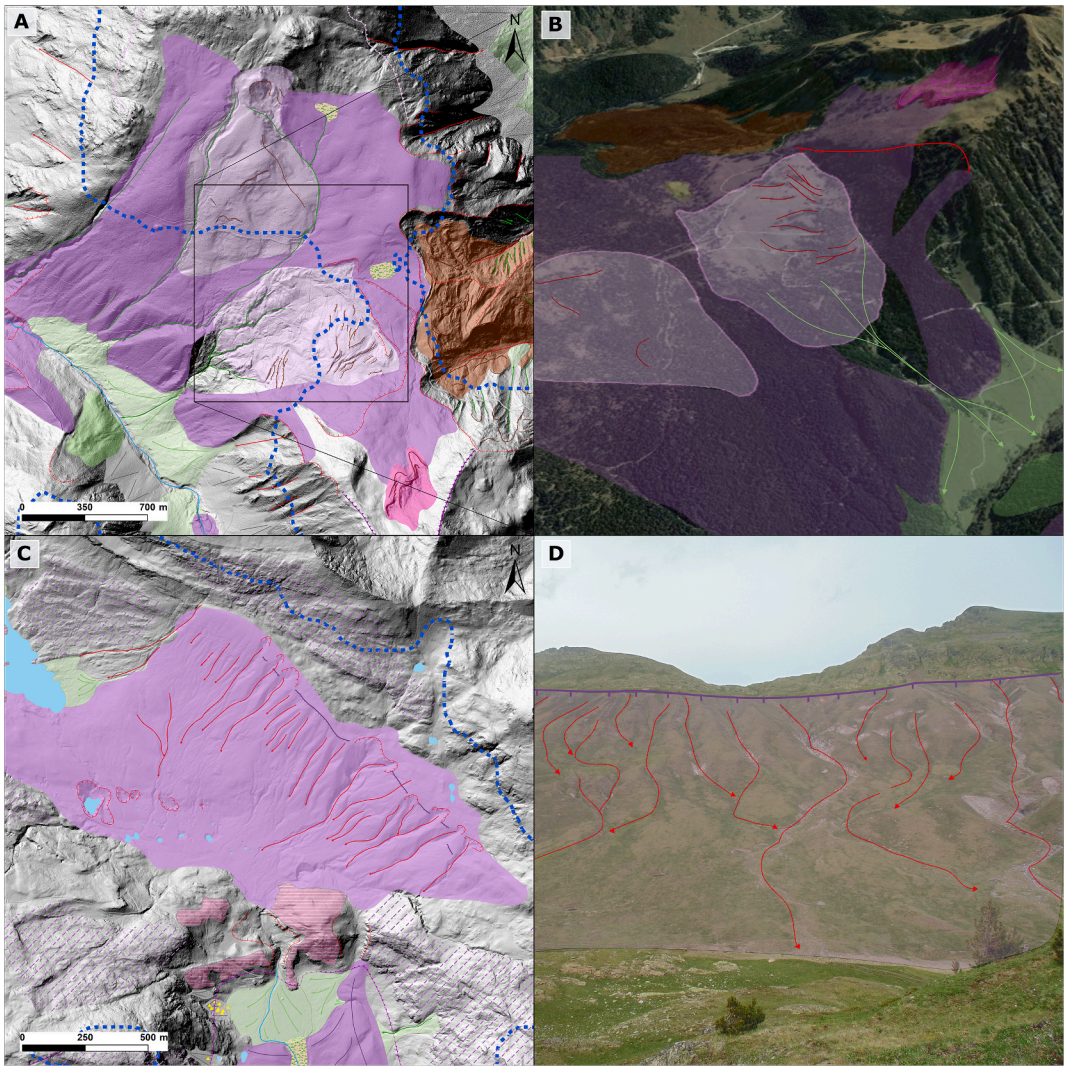


**Fig. 8.** Examples of drift-mantled slopes: the Mont-Romies plateau in the Valarties valley (A, B) and in the glacial cirque of the Unhòla valley (C, D) (same legend than in Fig. 4).

**Table 2**
Lithology of RSF in the Aran valley. Note that there are 19 lithological classes and two are not presented because they have no failures occurrence (lutite, and marble and slate).

| | Failures | | Lithological unit | | |
|---|---|---|---|---|---|
| | Number | % | Area (km$^2$) | % | Ratio |
| Slate | 28 | 25.2 | 70.2 | 16.5 | 0.40 |
| Lutite and limestone | 21 | 18.9 | 48.3 | 11.4 | 0.44 |
| Sandstone and lutite | 16 | 14.4 | 83.9 | 19.7 | 0.19 |
| Marble | 11 | 9.9 | 15.8 | 3.7 | 0.70 |
| Schist | 10 | 9.0 | 54.8 | 12.9 | 0.18 |
| Limestone | 8 | 7.2 | 24.6 | 5.8 | 0.32 |
| Limestone and slate | 4 | 3.6 | 4.7 | 1.1 | 0.84 |
| Granodiorite | 3 | 2.7 | 51.2 | 12.1 | 0.06 |
| Quartzite and lutite | 3 | 2.7 | 15.9 | 3.7 | 0.19 |
| Slate and marble | 1 | 0.9 | 17.9 | 4.2 | 0.06 |
| Quartzite | 1 | 0.9 | 7.4 | 1.7 | 0.13 |
| Granite | 1 | 0.9 | 18.3 | 4.3 | 0.05 |
| Quartzite and slate | 1 | 1.0 | 5.9 | 1.4 | 0.17 |
| Hornfels | 1 | 0.9 | 2.1 | 0.5 | 0.49 |
| Sandstone | 1 | 0.9 | 1.0 | 0.2 | 1.05 |
| Slate and limestone | 1 | 0.9 | 0.1 | 0.0 | 16.04 |
| Total | 111 | 100 | 422.0 | 76.7 | 0.26 |

**Table 3**
Rock slope failure distribution by lithological and morphostructural units of the in Aran valley. Note that the 11 (10.5%) features from DMS are excluded from the table.

| | Morphostructural units | | | Number of failures close to faults (‘50 m) | Main lithology | Total |
|---|---|---|---|---|---|---|
| | SA | GD | MB | | | |
| **CRF** | 91.7 | 8.3 | 0.0 | 4 (33%) | Slate (50%) | 12 (10.8%) |
| **RSD** | 56.3 | 43.8 | 0.0 | 7 (44%) | Schist (31.2%) | 16 (14.4%) |
| **RF** | 61.8 | 29.4 | 8.8 | 7 (21%) | Sandstone and lutites (20.6%) | 34 (30.6%) |
| **RS** | 91.8 | 6.1 | 2.0 | 25 (51%) | Slate (36.7%) | 49 (44.1%) |
| **Total** | 77.5 | 18.9 | 3.6 | 25 (39%) | Slate (25.2%) | 111 |

the highest peaks of the study area (exceeding 3000 m) there are only 4% of the failures. This is visible in the Nère valley in the boundary between sandstones and lutites where a RSD occurred (B, Fig. 2) or in the Ruda valley where a RS took place in the fault contact between slates with lutites and limestones (C, D Fig. 5). However, no RSD was detected in the granodiorite bedrock suggesting that stress release was not

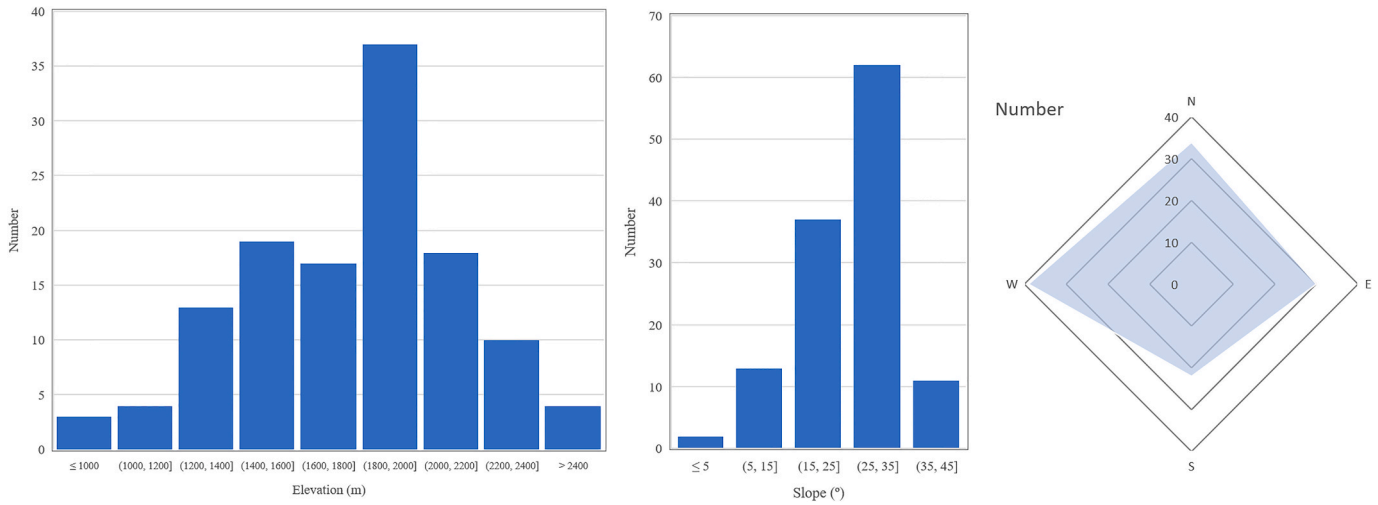


**Fig. 9.** Distribution of RSF based on altitude, slope and aspect.

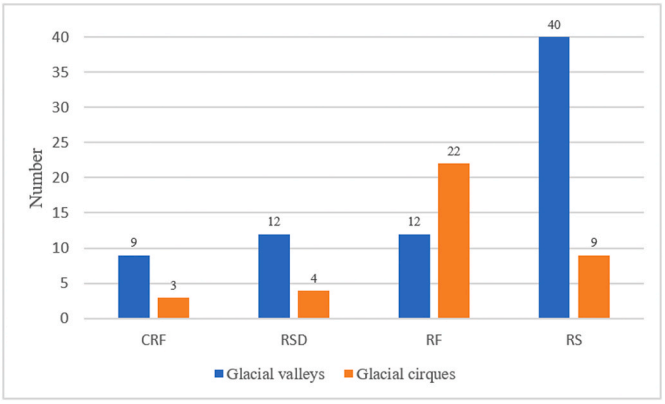


**Fig. 10.** Distribution of RSF based on their former glaciated setting.

enough to affect the stability in these rocks. Deep and surficial slope processes are strongly determined by the prevailing bedrock, as it is shown by the higher occurrence of RF in limestones and CRF and RS in slates (Table 3). In addition, the different types of RSF are clearly favoured by certain lithology's: slates (CRF and RS), schists (RSD) and limestones (RF). The lithological control on paraglacial processes has been also observed in several valleys from Ariège, Andorra, Carlit and Puigmal regions (Central-Eastern Pyrenees), where RSF are strongly associated with metasedimentary terrain (Jarman et al., 2014). In other Iberian mountain regions, such as in the Cantabrian Mountains, RS are mostly distributed on sandstones in contact with shales (Santos-González et al., 2018). The major role of lithology on the occurrence of RSD has been also detected in the European Alps, where the distribution of RSF and RS mostly develop on metamorphic rocks (Agliardi et al., 2012), as in the Scottish Highlands, where paraglacial RSF also occur mostly on metamorphic bedrocks (Jarman, 2006).

The presence of major faults also explains the occurrence of some RSF. Up to 43 events out of 111 (39%) have been detected very close to a fault (Fig. 1), a pattern that is more pronounced in the case of the Ruda or Nère valleys. This is the case of the deep gravitational movements (i.e. RSD) generated in structural discontinuities defined by dipping slips. Faults as a major driver of slope instability have been also described in other formerly glaciated mountain environments, such as in the Italian (Ambrosi and Crosta, 2006) and Eastern Alps (Agliardi et al., 2009), Scotland and NW Ireland (Ballantyne et al., 2014). The presence of faults enhances the weathering of parent rock material and may also trigger earthquakes. Although the Pyrenees are a low to moderate seismic zone (Ruiz et al., 2006; Quesada and Oliveira, 2019), instrumental seismicity data associated with the North Maladeta fault shows evidence that it can be the epicenter of destructive earthquakes, such as the earthquake of 1373 (Ribagorça) and 1923 (Vielha) (Ortuño Candela, 2008). Seismicity has been also appointed as a potential trigger of some large landslides in the northern slope of the Pyrenees; this is the case of the RSD event in the Aspe valley due to the Lavedan earthquake of AD 1380 (Lebourg et al., 2014) or in the Central Pyrenees where the RSD of the Ésera valley probably occurred after the Vielha earthquake of AD 1923 (Gutiérrez et al., 2008). Therefore, we can not discard that some RSF identified in the Aran valley could be triggered by seismic events.

The climate regime must have been a direct and indirect agent triggering slope processes. Whereas centennial to millennial-scale climate changes during Termination-1 promoted glacial advances and retreats with the associated implications for slope instability, extreme weather events may have also triggered slope failures as it currently occurs in mountain regions through a wide range of phenomena: heavy and persisting rains, rain-on-snow events, snow melt, etc. (Borgatti and Soldati, 2013; Robinson et al., 2017). Climate also affects the intensity of physical and weathering processes in cold-climate environments (Hall et al., 2002; French, 2007). Recently deglaciated environment are subjected to very intense cryogenic conditions with active periglacial processes in poorly vegetated environments (Oliva et al., 2011). Consequently, the exposed bedrock is therefore intensely affected by subaerial weathering and more prone to rock falls. As temperature rises, vegetation spreads and soil formation is more intense, which enhances geomorphic stability (Oliva et al., 2009). This is particularly effective for unconsolidated glacial sediments, including moraines and drift-mantled slopes.

Paraglacial rock slope processes are thus influenced by a variety of factors acting synchronously as part of a system that favours sediment redistribution from the upper parts to the valley floors. In turn, some failures can also trigger other slope processes; in the Aran valley, the RSD in the upper Unhòla valley includes antiscars dipping below a CRF, which suggests that the RSD occurred first than the CRF. Similar paraglacial slope processes were described in the Italian Alps where four of the five CRF were associated to RSD (Ostermann and Sanders, 2017). The sediments generated by these RSF will be used by future geomorphological dynamics to reshape the present-day landscape through a range of processes (glacial, periglacial, aeolian, alluvial and fluvial) to enlarge valleys, initiate cirques, reduce ridges, breach watersheds or sharpen horns (Wilson et al., 2004).

In addition, there are other processes not related to paraglacial dynamics that trigger slope instability in the Aran valley, such as certain human activities. Historically, most activities were confined in the

lowlands, and thus were not susceptible of generating mass movements. However, over the last millennia deforestation in the alpine belt (>2200 m) of the Central Pyrenees for transhumance purposes led to the activation of certain geomorphic processes at very local scale, particularly shallow landslides, soil erosion, solifluction, etc (García-Ruiz et al., 2020).

## 6. Conclusions

The Aran valley is a highly populated mountain environment visited annually by thousands of tourists attracted by the beauty of its landscape and the quality of its snow resorts. However, this mountain area is susceptible of being affected by several natural hazards, among which slope processes are one of the most important. Therefore, a better understanding of the spatial distribution of these processes can be used by local authorities to assess territorial planning issues.

The current landscape of mid-mountain environments is highly determined by the impact of Quaternary glaciations. Past glaciers shaped the highest peaks, as well as the surrounding valleys, but its disappearance also favoured postglacial environmental dynamics. These paraglacial processes were particularly intense during the millennia following deglaciation and result in a wide range of periglacial, slope and alluvial features. Glacial debuttstressing and consequent stress release from the last deglaciation in mountain areas are intimately related with paraglacial failures.

In the Aran valley, the timing of glacial oscillations during the Last Glacial Cycle, and thus of paraglacial dynamics, is still unknown. In this study, we characterized the typology and geographical setting of the major slope landforms existing in this valley that show a strong connection with the areas that were glaciated during the Late Pleistocene. Up to 125 major slope failures mapped in this valley correspond to areas occupied by the ice during the Last Glacial Cycle, namely in hillsides of U-shaped glacial valleys, margins of overdeepened glacial basins and rock walls of glacial cirques. In some areas, there seems to be also a control of lithology and morphostructure on the occurrence of slope failures: vertical rock walls next to faults favoured rockfalls, schist terrain favoured rock-slope deformation landforms and slates promoted catastrophic rock failures. Therefore, the action of Quaternary glaciers in this highly variable geological setting enhanced the potential for slope activity.

Some of these paraglacial slope failures are still active and others might be susceptible to future potential readjustment. Therefore, a deeper knowledge of their spatial distribution as well as the mechanisms involved in their development is needed to better assess their future dynamics and reduce potential damage to local settlements and infrastructures. To that purpose, a more robust database of the major slope failures as well as its current and past activity must be developed in the forthcoming years.

## Declaration of competing interest

The authors declare that they have no known competing financial interests or personal relationships that could have appeared to influence the work reported in this paper.

## Acknowledgements

Marcelo Fernandes is funded by a PhD fellowship (SFRH/139569/2018) from the Fundação para a Ciência e Tecnologia of Portugal. Marcelo Fernandes and Gonçalo Vieira are funded also by the Centro de Estudos Geográficos - University of Lisbon (FCT - UIDB/00295/2020). Marc Oliva is supported by the Ramón y Cajal Program (RYC-2015-17597) and the Research Group ANTALP (Antarctic, Arctic, Alpine Environments; 2017-SGR-1102) funded by the Government of Catalonia through the AGAUR agency. This work complements the PALEOGREEN (CTM2017-87976-P) project of the Ministry of Economy of Spain.

## References

Agliardi, F., Crosta, G.B., Frattini, P., 2012. Slow rock-slope deformation. In: Clague, J.J., Stead, D. (Eds.), Landslides: Types, Mechanisms and Modeling. Cambridge University Press, pp. 207–221.

Agliardi, F., Zanchi, A., Crosta, G.B., 2009. Tectonic vs. gravitational morphostructures in the central Eastern Alps (Italy): constraints on the recent evolution of the mountain range. Tectonophysics 474, 250–270. https://doi.org/10.1016/j.tecto.2009.02.019.

Alonso, V., Corte, A.E., 1992. Postglacial fracturing in the cantabrian cordillera (NW Spain). Z. Geomorphol. 36, 479–490.

Ambrosi, C., Crosta, G.B., 2006. Large sackung along major tectonic features in the Central Italian Alps. Eng. Geol. 83, 183–200. https://doi.org/10.1016/j.enggeo.2005.06.031.

Augustinus, P., 1996. Rock mass strength and the stability of some glacial valley slopes. In: International Journal of Rock Mechanics and Mining Sciences and Geomechanics Abstracts, pp. 28A–29A.

Ballantyne, C.K., 2002. Paraglacial geomorphology. Encycl. Quat. Sci. Second Ed. 21, 553–565. https://doi.org/10.1016/B978-0-444-53643-3.00089-3.

Ballantyne, C.K., Sandeman, G.F., Stone, J.O., Wilson, P., 2014. Rock-slope failure following Late Pleistocene deglaciation on tectonically stable mountainous terrain. Quat. Sci. Rev. 86, 144–157. https://doi.org/10.1016/j.quascirev.2013.12.021.

Beaumont, C., Muñoz, J.A., Hamilton, J., Fullsack, P., 2000. Factors controlling the Alpine evolution of the central Pyrenees inferred from a comparison of observations and geodynamical models. J. Geophys. Res. Solid Earth 105, 8121–8145. https://doi.org/10.1029/1999jb900390.

Benn, D.I., Evans, D.J.A., 2010. Glaciers and Glaciation, second. Hodder Education, London. https://doi.org/10.5860/CHOICE.35-6240.

Böhme, M., Hermanns, R.L., Gosse, J., Hilger, P., Eiken, T., Lauknes, T.R., Dehls, J.F., 2019. Comparison of monitoring data with paleo–slip rates: cosmogenic nuclide dating detects acceleration of a rockslide. Geology 47, 339–342.

Bordonau, J., 1992. Els Complexos Glàcio-Lacustres Relacionats Amb El Darrer Cicle Glacial Als Pirineus. Universitat de Barcelona.

Borgatti, L., Soldati, M., 2013. Hillslope processes and climate change. Treatise Geomorphol. 7, 306–319. https://doi.org/10.1016/B978-0-12-374739-6.00180-9.

Calvet, M., 2004. The quaternary glaciation of the pyrenees. Dev. Quat. Sci. 2, 119–128. https://doi.org/10.1016/S1571-0866(04)80062-9.

Campos, N., Tanarro, L.M., Palacios, D., 2018. Geomorphology of glaciated gorges in a granitic massif (Gredos range, central Spain). J. Maps 14, 321–329. https://doi.org/10.1080/17445647.2018.1468829.

Church, M., Ryder, J., 1972. Paraglacial sedimentation: a consideration of fluvial processes conditioned by glaciation. Geol. Soc. Am. Bull. 83, 1–30.

Clark, P., Shakun, J., Baker, P., Bartlein, P., Brewer, S., Brook, E., Carlson, A., Cheng, H., Kaufman, D., Liu, Z., Marchitto, T., Mix, A., Morrill, C., Otto-Bliesner, B., Pahnke, K., Russell, J.M., Whitlock, C., Adkins, J., Blois, J., Clark, J., Colman, S., Curry, W., Flower, B., He, F., Johnson, T., Lynch-Stieglitz, J., Markgraf, V., McManus, J., Mitrovica, J., Moreno, P., Williams, J., 2012. Global climate evolution during the last deglaciation. Proc. Natl. Acad. Sci. Unit. States Am. 109, 1134–1142. https://doi.org/10.1073/pnas.1116619109.

Corominas, J., Iglesias, R., Aguasca, A., Mallorquí, J.J., Fàbregas, X., Planas, X., Gili, J.A., 2015. Comparing satellite based and ground based radar interferometry and field observations at the Canillo landslide (pyrenees). In: Engineering Geology for Society and Territory - Volume 2. Springer International Publishing, Cham, pp. 333–337. https://doi.org/10.1007/978-3-319-09057-3_51.

Cossart, E., Mercier, D., Decaulne, A., Feuillet, T., 2013. An overview of the consequences of paraglacial landsliding on deglaciated mountain slopes: typology, timing and contribution to cascading fluxes. Quaternaire 24, 13–24. https://doi.org/10.4000/quaternaire.6444.

Delmas, M., 2015. The last maximum ice extent and subsequent deglaciation of the Pyrenees: an overview of recent research. Cuadernos Invest. Geogr. 41, 359. https://doi.org/10.18172/cig.2708.

Duvillard, P.A., Ravanel, L., Deline, P., Dubois, L., 2018. Paraglacial rock slope adjustment beneath a high mountain infrastructure—the pilatte hut case study (Écrins mountain range, France). Front. Earth Sci. 6, 1–14. https://doi.org/10.3389/feart.2018.00094.

Etzelmüller, B., 2013. Recent advances in mountain permafrost research. Permafr. Periglac. Process. 24, 99–107. https://doi.org/10.1002/ppp.1772.

Fernandes, M., Oliva, M., Palma, P., Ruiz-Fernández, J., Lopes, L., 2017. Glacial stages and post-glacial environmental evolution in the Upper Garonne valley, Central Pyrenees. Sci. Total Environ. 584–585, 1282–1299. https://doi.org/10.1016/j.scitotenv.2017.01.209.

Fernandes, M., Palma, P., Lopes, L., Ruiz-Fernández, J., Pereira, P., Oliva, M., 2018. Spatial distribution and morphometry of permafrost-related landforms in the Central Pyrenees and associated paleoclimatic implications. Quat. Int. 470, 96–108. https://doi.org/10.1016/j.quaint.2017.08.071.

Feuillet, T., Mercier, D., 2012. Post-little ice age patterned ground development on two pyrenean proglacial areas: from deglaciation to periglaciation. Geogr. Ann. Ser. A Phys. Geogr. 94, 363–376. https://doi.org/10.1111/j.1468-0459.2012.00459.x.

French, H., 2007. The Periglacial Environment, third. ed. John Wiley & Sons, Ltd, London.

García-Ruiz, J., Alvera, B., Barrio, G. Del, Puigdefabregas, J., 2007. Geomorphic processes above timberline in the Spanish pyrenees. Mt. Res. Dev. 10, 201. https://doi.org/10.2307/3673600.

García-Ruiz, J., Valero-Garcés, B., González-Sampériz, P., Lorente, A., Martí-Bono, C., Beguería, S., Edwards, L., 1988. Stratified scree in the Central Spanish Pyrenees: paleoenvironmental implications. Tep. Apx. 60, 27–30.

García-Ruiz, J.M., Palacios, D., de Andrés, N., Valero-Garcés, B.L., López-Moreno, J.I., Sanjuán, Y., 2014. Holocene and 'little ice age' glacial activity in the marboré cirque, monte perdido massif, central Spanish pyrenees. Holocene 24, 1439–1452. https://doi.org/10.1177/0959683614544053.

García-Ruiz, J.M., Palacios, D., González-Sampériz, P., de Andrés, N., Moreno, A., Valero-Garcés, B., Gómez-Villar, A., 2016. Evidencias de actividad glaciar durante el Dryas Reciente (12,9-11,7 ka BP) en la Península Ibérica. Cuaternario Geomorfol. 30, 9–21. https://doi.org/10.17735/cyg.v30i1-2.39250.

García-Ruiz, J.M., Tomás-Faci, G., Diarte-Blasco, P., Montes, L., Domingo, R., Sebastián, M., Lasanta, T., González-Sampériz, P., López-Moreno, J.I., Arnáez, J., Beguería, S., 2020. Transhumance and long-term deforestation in the subalpine belt of the central Spanish Pyrenees: an interdisciplinary approach. Catena 195, 104744. https://doi.org/10.1016/j.catena.2020.104744.

García-Sansegundo, J., 2004. Estructura varisca de los Pirineos. In: Geologia de España, pp. 254–258.

García-Ruiz, J., Valero-Garcés, B., Martí-Bono, C., González-Sampériz, P., 2003. Asynchroneity of maximum glacier advances in the central Spanish Pyrenees. J. Quat. Sci. 18, 61–72. https://doi.org/10.1002/jqs.715.

García-Sansegundo, J., 1996. Hercynian structure of the axial zone of the pyrenees: the Aran valley cross-section (Spain-France). J. Struct. Geol. 18, 1315–1325. https://doi.org/10.1016/S0191-8141(96)00050-8.

Gómez-Ortiz, A., Oliva, M., Salvador-Franch, F., Salvà-Catarineu, M., Palacios, D., De Sanjosé-Blasco, J.J., Tanarro-García, L.M., Galindo-Zaldívar, J., Sanz De Galdeano, C., 2014. Degradation of buried ice and permafrost in the Veleta cirque (Sierra Nevada, Spain) from 2006 to 2013 as a response to recent climate trends. Solid Earth 5, 979–993. https://doi.org/10.5194/se-5-979-2014.

González-García, M., 2014. La alta montaña periglaciar en el Pirineo Central español: procesos, formas y condiciones ambientales. Universidad de Málaga.

González-Sampériz, P., Valero-Garcés, B., Martí-Bono, C., Moreno, A., Dedoubat, J., Delgado-Huertas, A., García-Ruiz, J., Jalut, G., Otto, T., Navas, A., 2006. Climate variability in the Spanish Pyrenees during the last 30,000 yr revealed by the El Portalet sequence. Quat. Res. 66, 38–52. https://doi.org/10.1016/j.yqres.2006.02.004.

González-Trueba, J., 2007. La Pequeña Edad de Hielo en los Picos de Europa: Análisis y reconstrucción del avance glaciar histórico (s. XIX). Santander Serv. Publicaciones la Univ. Cantab. Fund. Marcelino Botín.

Goron, L., 1941. Les vallums morainiques et les terrasses des dernières glaciations dans la région prépyrénéenne et son avant-pays (suite et fin). Rev. Geogr. Pyren. Sud. Ouest. 12, 147–226. https://doi.org/10.3406/rgpso.1941.4499.

Gutiérrez, F., Acosta, E., Ríos, S., Guerrero, J., Lucha, P., 2005. Geomorphology and geochronology of sackung features (uphill-facing scarps) in the Central Spanish Pyrenees. Geomorphology 69, 298–314. https://doi.org/10.1016/j.geomorph.2005.01.012.

Gutiérrez, F., Ortuño, M., Lucha, P., Guerrero, J., Acosta, E., Coratza, P., Piacentini, D., Soldati, M., 2008. Late Quaternary episodic displacement on a sackung scarp in the central Spanish Pyrenees. Secondary paleoseismic evidence? Geodin. Acta 21, 187–202. https://doi.org/10.3166/ga.21.187-202.

Hall, K., Thorn, C.E., Matsuoka, N., Prick, A., 2002. Weathering in cold regions: some thoughts and perspective. Prog. Phys. Geogr. 26, 577–603. https://doi.org/10.1191/0309133302pp353ra.

Highland, L., Bobrowsky, P., 2008. Introduction the landslide handbook-A guide to understanding landslides. Landslide Handb. - A Guid. to Underst. Landslides 4–42.

Hughes, P.D., Fink, D., Fletcher, W.J., Hannah, G., 2014. Catastrophic rock avalanches in a glaciated valley of the High Atlas, Morocco: 10Be exposure ages reveal a 4.5 ka seismic event. Geol. Soc. Am. Bull. 126, 1093–1104. https://doi.org/10.1130/B30894.1.

Jarman, D., 2006. Large rock slope failures in the Highlands of Scotland: characterisation, causes and spatial distribution. Eng. Geol. 83, 161–182. https://doi.org/10.1016/j.enggeo.2005.06.030.

Jarman, D., Calvet, M., Corominas, J., Delmas, M., Gunnell, Y., 2014. Large-scale rock slope failures in the eastern pyrenees: identifying a sparse but significant population in paraglacial and parafluvial contexts. Geogr. Ann. Ser. A Phys. Geogr. 96, 357–391. https://doi.org/10.1111/geoa.12060.

Jomelli, V., Chapron, E., Favier, V., Rinterknecht, V., Braucher, R., Tournier, N., Gascoin, S., Marti, R., Galop, D., Binet, S., Deschamps, C., Tissoux, H., Aumaitre, G., Bourlès, D.L., Keddadouche, K., 2020. Glacier fluctuations during the Late Glacial and Holocene on the Ariège valley , northern slope of the Pyrenees and reconstructed climatic conditions. Mediterr. Geosci. Rev. https://doi.org/10.1007/s42990-020-00018-5.

Kellerer-Pirklbauer, A., Proske, H., Strasser, V., 2010. Paraglacial slope adjustment since the end of the Last Glacial Maximum and its long-lasting effects on secondary mass wasting processes: hauser Kaibling, Austria. Geomorphology 120, 65–76. https://doi.org/10.1016/j.geomorph.2009.09.016.

Kleinsmiede, W.F.J., 1960. Geology of the valle d'Aran (central pyrenees). Leidse Geol. Meded. 25, 129–245.

Krautblatter, M., Funk, D., Günzel, F.K., 2012. Why permafrost rocks become unstable: a rock-ice-mechanical model in time and space. Earth Surf. Process. Landforms 38, 876–887. https://doi.org/10.1002/esp.3374.

Lebourg, T., Zerathe, S., Fabre, R., Giuliano, J., Vidal, M., 2014. A Late Holocene deep-seated landslide in the northern French Pyrenees. Geomorphology 208, 1–10. https://doi.org/10.1016/j.geomorph.2013.11.008.

Martí-Soler, M., 1988. Estudi geomorfològic del massis central de la Vall d'Aran (Pirineu Central). Bachelor thesis. University of Barcelona.

McCalpin, J.P., Corominas, J., 2019. Postglacial deformation history of sackungen on the northern slope of Pic d'Encampadana, Andorra. Geomorphology 337, 134–150. https://doi.org/10.1016/j.geomorph.2019.04.007.

McColl, S.T., 2012. Paraglacial rock-slope stability. Geomorphology 153–154, 1–16. https://doi.org/10.1016/j.geomorph.2012.02.015.

Oliva, M., Mercier, D., Ruiz-Fernández, J., McColl, S., 2019a. Paraglacial processes in recently deglaciated environments. Land Degrad. Dev. 1–6 https://doi.org/10.1002/ldr.3283.

Oliva, M., Palacios, D., Fernández-Fernández, J.M., Rodríguez-Rodríguez, L., García-Ruiz, J., Andrés, N., Carrasco, R.M., Pedraza, J., Pérez-Alberti, A., Valcárcel, M., Hughes, P., 2019b. Late quaternary glacial phases in the iberian Peninsula. Earth Sci. Rev. 192, 564–600. https://doi.org/10.1016/j.earscirev.2019.03.015.

Oliva, M., Ruiz-Fernández, J., 2015. Coupling patterns between para-glacial and permafrost degradation responses in Antarctica. Earth Surf. Process. Landforms 40, 1227–1238. https://doi.org/10.1002/esp.3716.

Oliva, M., Schulte, L., Ortiz, A.G., 2011. The role of aridification in constraining the elevation range of Holocene solifluction processes and associated landforms in the periglacial belt of the Sierra Nevada (southern Spain). Earth Surf. Process. Landforms 36, 1279–1291. https://doi.org/10.1002/esp.2116.

Oliva, M., Schulte, L., Ortiz, A.G., 2009. Morphometry and late holocene activity of solifluction landforms in the sierra Nevada, southern Spain. Permafr. Periglac. Process. 20, 369–382. https://doi.org/10.1002/ppp.645.

Oliva, M., Serrano, E., Gómez-Ortiz, A., González-Amuchastegui, M.J., Nieuwendam, A., Palacios, D., Pérez-Alberti, A., Pellitero, R., Ruiz-Fernández, J., Valcárcel, M., Vieira, G., Antoniades, D., 2016. Spatial and temporal variability of periglaciation of the Iberian Peninsula. Quat. Sci. Rev. 137, 176–199. https://doi.org/10.1016/j.quascirev.2016.02.017.

Ortuño Candela, M., 2008. Deformación activa en el Pirineo Central: La falla Norte de la Maladeta y otras fallas activas. University of Barcelona.

Ostermann, M., Sanders, D., 2017. The Benner pass rock avalanche cluster suggests a close relation between long-term slope deformation (DSGSDs and translational rock slides) and catastrophic failure. Geomorphology 289, 44–59. https://doi.org/10.1016/j.geomorph.2016.12.018.

Palacios, D., Andrés, N., Marcos, J., Vázquez-Selem, L., 2012. Maximum glacial advance and deglaciation of the Pinar Valley (Sierra de Gredos, Central Spain) and its significance in the Mediterranean context. Geomorphology 177–178, 51–61. https://doi.org/10.1016/j.geomorph.2012.07.013.

Palacios, D., de Andrés, N., Gómez-Ortiz, A., García-Ruiz, J.M., 2017a. Evidence of glacial activity during the Oldest Dryas in the mountains of Spain. Geol. Soc. Lond. Spec. Publ. 433, 87–110. https://doi.org/10.1144/SP433.10.

Palacios, D., de Andrés, N., López-Moreno, J., García-Ruiz, J., 2015a. Late Pleistocene deglaciation in the upper gállego valley, central pyrenees. Quat. Res. (United States) 83, 397–414. https://doi.org/10.1016/j.yqres.2015.01.010.

Palacios, D., de Marcos, J., Vázquez-Selem, L., 2011. Last glacial maximum and deglaciation of sierra de Gredos, central iberian Peninsula. Quat. Int. 233, 16–26. https://doi.org/10.1016/j.quaint.2010.04.029.

Palacios, D., García-Ruiz, J., Andrés, N., Schimmelpfennig, I., Campos, N., Léanni, L., Aumaître, G., Bourlès, D.L., Keddadouche, K., 2017b. Deglaciation in the central pyrenees during the pleistocene–holocene transition: timing and geomorphological significance. Quat. Sci. Rev. 162, 111–127. https://doi.org/10.1016/j.quascirev.2017.03.007.

Palacios, D., Gómez-Ortiz, A., Andrés, N., Salvador, F., Oliva, M., 2016. Timing and new geomorphologic evidence of the last deglaciation stages in Sierra Nevada (southern Spain). Quat. Sci. Rev. 150, 110–129. https://doi.org/10.1016/j.quascirev.2016.08.012.

Palacios, D., Gómez-Ortiz, A., Andrés, N., Vázquez-Selem, L., Salvador-Franch, F., Oliva, M., 2015b. Maximum extent of late Pleistocene glaciers and last deglaciation of La cerdanya mountains, southeastern pyrenees. Geomorphology 231, 116–129. https://doi.org/10.1016/j.geomorph.2014.10.037.

Quesada, C., Oliveira, J., 2019. The Geology of Iberia: A Geodynamic Approach, Regional Geology Reviews. Springer International Publishing, Cham. https://doi.org/10.1007/978-3-030-11190-8.

Robinson, J.D., Vahedifard, F., Aghakouchak, A., 2017. Rainfall-triggered slope instabilities under a changing climate: comparative study using historical and projected precipitation extremes. Can. Geotech. J. 54, 117–127. https://doi.org/10.1139/cgj-2015-0602.

Rodríguez-Rodríguez, L., González-Lemos, S., Ballesteros, D., Valenzuela, P., Domínguez-Cuesta, M.J., Llana-Fúnez, S., Jiménez-Sánchez, M., 2018. Timing of paraglacial rock-slope failures and denudation signatures in the cantabrian mountains (North iberian Peninsula). Land Degrad. Dev. 29, 3159–3173. https://doi.org/10.1002/ldr.3012.

Ruiz-Fernández, J., 2015. Las formas de modelado glaciar, periglaciar y fluviotorrencial del Macizo Occidental de los Picos de Europa (Cordillera Cantábrica). Bol. Asoc. Geógrafos Esp. 581–587.

Ruiz-Fernández, J., Oliva, M., Nývlt, D., Cannone, N., García-Hernández, C., Guglielmin, M., Hrbáček, F., Roman, M., Fernández, S., López-Martínez, J., Antoniades, D., 2019. Patterns of spatio-temporal paraglacial response in the Antarctic Peninsula region and associated ecological implications. Earth Sci. Rev. 192, 379–402. https://doi.org/10.1016/j.earscirev.2019.03.014.

Ruiz, M., Gallart, J., Díaz, J., Olivera, C., Pedreira, D., López, C., González-Cortina, J.M., Pulgar, J.A., 2006. Seismic activity at the western Pyrenean edge. Tectonophysics 412, 217–235. https://doi.org/10.1016/j.tecto.2005.10.034.

Santos-González, J., González-Gutiérrez, R.B., Santos, J.A., Gómez-Villar, A., Peña-Pérez, S.A., Redondo-Vega, J.M., 2018. Topographic, lithologic and glaciation style influences on paraglacial processes in the upper Sil and Luna catchments, Cantabrian Mountains, NW Spain. Geomorphology 319, 133–146. https://doi.org/10.1016/j.geomorph.2018.07.019.

Serrano, E., González-Trueba, J., Sanjosé, J., 2011. Dynamic, evolution and structure of Pyrenean rock glaciers. Cuadernos Invest. Geogr. 37 https://doi.org/10.18172/cig.1260.

Serrano, E., Oliva, M., González-García, M., López-Moreno, J.I., González-Trueba, J., Martín-Moreno, R., Gómez-Lende, M., Martín-Díaz, J., Nofre, J., Palma, P., 2018. Post-little ice age paraglacial processes and landforms in the high Iberian mountains: a review. Land Degrad. Dev. 29, 4186–4208. https://doi.org/10.1002/ldr.3171.

Serrat, D., Martí, M., Bordonau, J., 1994. Geologia, Geomofologia e Risques, em: Geografia Física, em: Atlas comarcau de Catalunya-Val d'Aran. Inst. Cart. Catalunya. General. Catalunya.

Sitter, L.U., Zwart, H.J., 1962. Geological map of the paleozoic of the central pyrenees. Leidse Geol. Meded. 33, 191–254.

Slaymaker, O., 2011. Criteria to distinguish between periglacial, proglacial and paraglacial environments. Quaest. Geogr. 30, 85–94. https://doi.org/10.2478/v10117-011-0008-y.

Stange, K.M., van Balen, R.T., Kasse, C., Vandenberghe, J., Carcaillet, J., 2014. Linking morphology across the glaciofluvial interface: a 10Be supported chronology of glacier advances and terrace formation in the Garonne River, northern Pyrenees, France. Geomorphology 207, 71–95. https://doi.org/10.1016/j.geomorph.2013.10.028.

Taillefer, F., 1966. Quaternaire et géomorphologie sur le versant nord des Pyrénées centrales, d'après H. Alimen. Rev. Geogr. Pyren. Sud. Ouest. 37, 47–57. https://doi.org/10.3406/rgpso.1966.4814.

Taillefer, F., 1953. La morphologie de la Moyenne Garonne et les données pédologiques. [d'après Albert Cavallié, Formation, évolution et classification des sols au département de Tarn-et-Garonne]. Rev. Geogr. Pyren. Sud. Ouest. 24, 159–162. https://doi.org/10.3406/rgpso.1953.1373.

Wilson, P., 2009. Rockfall talus slopes and associated talus-foot features in the glaciated uplands of Great Britain and Ireland: periglacial, paraglacial or composite landforms? Geol. Soc. Lond. Spec. Publ. 320, 133–144. https://doi.org/10.1144/SP320.9.

Wilson, P., Clark, R., Smith, A., 2004. Rock-slope failures in the Lake District: a preliminary report. Proc. - Cumberl. Geol. Soc. 7, 13–36. https://doi.org/10.4324/9780203416402.

Zwart, H.J., 1979. The geology of the central pyrenees. Leidse Geol. Meded. 1–75.

# 6. Geomorphological record of the glacial to periglacial transition in the Central Pyrenees: the Lòcampo Cirque in the regional context

The following chapter was submitted as a research paper in Geomorphology on January 2nd of 2023 with the reference GEOMOR-12408.

# Geomorphological record of the glacial to periglacial transition in the Central Pyrenees: the Lòcampo cirque in the regional context

Fernandes, M.[1], Oliva, M.[2], Fernández-Fernández, J. M.[3], Vieira, G.[1,4], Palacios, D.[3], García-Oteyza, J.[4], Ventura, J.[2], Schimmelpfennig, I.[5] & ASTER Team[5]

[1]Centre of Geographical Studies, Institute of Geography and Spatial Planning, Universidade de Lisboa, Lisbon, Portugal

[2]Department of Geography, Universitat de Barcelona, Catalonia, Spain

[3]Department of Geography, Universidad Complutense de Madrid, Madrid, Spain

[4]Associated Laboratory Terra, Portugal

[5]Aix-Marseille Université, CNRS, IRD, INRAE, Coll. France, UM 34 CEREGE, Aix-en-Provence, France

**Corresponding author**

Marcelo Fernandes, marcelo.fernandes@campus.ul.pt

Edifício IGOT, Cidade Universitária

Rua Branca Edmée Marques, 1600-276 Lisboa

**Highlights**

- The glacial to periglacial transition is reconstructed in the Lòcampo Cirque, Pyrenees
- A wide range of glacial and periglacial landforms are preserved at 2200-2300 m a.s.l.
- Last glacial advance represented by the moraine abandonment by 13.2 ± 1.1 ka
- Glacial-to-periglacial transition occurred at 13.6 ± 0.9 ka
- A rock glacier stabilized at 11.9 ± 0.7 ka, or afterwards

**Abstract**

In the highest tributaries of the Upper Garonne Basin, Central Pyrenees, cirques up to ca. 2600 m a.s.l. were already deglaciated by 15-14 ka. The long-term deglaciation during Termination-1 (T-1) was interrupted by glacial advances within the cirques during the Bølling–Allerød (B-A) interstadial and the Younger Dryas (YD) stadial. The cirques preserve a variety of glacial and periglacial landforms whose chronologies are poorly known. This study is focused on the Lòcampo cirque (42º38'06'' N and 0º59'10''E), Upper Garonne Basin, where a detailed geomorphological map and $^{10}$Be terrestrial cosmic ray exposure (CRE) dating allowed us to constrain the chronosequence between the glacial and periglacial domains. In the small Lòcampo cirque, a glacier formed a cirque moraine between 2200 and 2300 m a.s.l, which surrounds a relict rock glacier encompassing several transversal ridges. Additionally, longitudinal ridges typically observed in debris-covered glaciers are preserved between the moraine and the rock glacier. The 8-sample dataset of CRE ages indicates the formation of the cirque moraine during the second half of the B-A, by 13.2 ± 1.1 ka. Exposure ages from the rock glacier boulders show a range between 13.6 ± 0.9 and 11.9 ± 0.7 ka, which did not allow to chronologically constrain its formation. Therefore, the environmental evolution following the moraine stabilisation could follow the formation of a debris-covered glacier at the bottom of the Lòcampo cirque, with the subsequent formation of the rock glacier. After the rock glacier formation, its front rapidly ceased at 13.6 ± 0.9 ka, while the upper ridges gradually stabilized during ca. 2-3 ka until it became definitively relict at 11.9 ± 0.7 ka – or afterwards. These results show evidence of the complex glacial to periglacial transition in the relatively low altitude cirques of the Central Pyrenees during the T-1. More robust chronological datasets are needed to better understand the role of climate forcings and local topography during the deglaciation in mid-latitude mountain environments.

**Keywords:** Central Pyrenees, Termination-1, $^{10}$Be CRE dating, cirques, moraines, rock glaciers

## 1. Introduction

Millennial-scale warming events throughout the last deglaciation promoted glacier recession towards the upper catchments in mid-latitude mountain ranges, such as those of the Mediterranean basin (e.g. Hughes et al., 2006a, 2006b; Palacios et al., 2022). The end of the Last Glacial Cycle (Termination-1; T-1) spans from the culmination of the Last Glacial Maximum (LGM) at 26-19 ka to the beginning of the Holocene at 11.7 ka (Clark et al., 2009; Vázquez-Riveiros et al., 2022). During this phase, the increase of summer insolation and unstable marine-based ice sheet margins in the northern hemisphere triggered the release of a considerable amount of icebergs (Denton et al., 2010). As a result of an important freshwater input delivered into the North Atlantic Ocean, the Atlantic Meridional Overturning Circulation (AMOC) weakened and favoured the occurrence of cold spells such as the Oldest Dryas or Heinrich Stadial-1 (HS-1 ca. 18.2-14.6 ka; Toucanne et al., 2015) and Younger Dryas (YD: 12.9-11.7 ka; Rasmussen et al., 2014). On the contrary, a possible intensification of the AMOC forced an abrupt warm period between these stadials (14.6 and 12.9 ka), known as Bølling–Allerød (B-A; Rasmussen et al., 2014; Obase & Abe-Ouchi, 2019; Capron et al., 2021).

These large climatic variations during T-1 promoted the accelerated glacial recession in high mountains of the Mediterranean basin interrupted by minor advances during millennial and centennial-scale cold-climate events. These oscillations have been spatially reconstructed and chronologically constrained in some locations based on geomorphological evidence (e.g. García-Ruiz et al., 2016; Palacios et al., 2017a; Allard et al., 2021). As glaciers retreated, ice-free terrain became gradually covered by non-glacial deposits through periglacial, slope and alluvial processes, which were particularly intense during the paraglacial phase (Ballantyne, 2002; Oliva et al., 2019). This landscape adjustment implied a new slope morphology, since the debuttressing of the rock and sediment slopes contributed to a complex sediment cascade (Ballantyne, 2002; McColl, 2012). In highland permafrost areas from mid-latitude mountains, the enhanced warming favoured widespread rock slope failures (Krautblatter et al., 2012; Hilger et al., 2019; Oliva et al., 2019).

In mountain regions, a wide range of glacial and periglacial features resulted from the gradual recession of glaciers during the last stages of the deglaciation. Most of those are still preserved in the highest areas and provide valuable paleoclimatic and paleoenvironmental data to understand the timing and associated geomorphological dynamics of the paraglacial phase (Hughes & Woodward, 2009). Within the cirques, the shrinking glaciers abandoned frontal moraines and triggered a massive debris-supply onto the slopes and bottom of the cirques that promoted the formation of rock glaciers, most of them of glacigenic origin (Knight, 2019; Knight et al., 2019). However, depending on the relief configuration, the deglaciation process favoured a more or less intense paraglacial activity, which resulted in different degree of occupation of debris across the cirque floor and slopes. In any case, the chronological framework of this is still poorly known (Oliva et al., 2016).

In the Pyrenees, the spatial distribution of cirque floors shows a north-south and east-west elevation gradient. In the Eastern Pyrenees, cirque floors are located between 1300 and 2300 m a.s.l. (Delmas et al., 2015), whereas in the Central Pyrenees they are higher, between 1600-2800 m a.s.l. in the northern slope and 1800-3000 m a.s.l. in the southern side of the range (Lopes et al., 2018; García-Ruiz et al., 2020). The chronology of the cirque deglaciation was constrained by cosmic-ray exposure (CRE) dating and suggests that most cirques below 2800-3000 m a.s.l. were completely deglaciated by the onset of the Holocene (Palacios et al., 2015a; 2015b; 2020; Crest et al., 2017; Jomelli et al., 2020; Oliva et al., 2021; Reixach et al., 2021). In the highest cirques, glacial evidence preserved in the form of cirque moraines originated in several glacial advances or standstills during HS-1, B-A and YD (Palacios et al., 2015a, 2015b; 2017; Jomelli et al., 2020; Fernandes et al., 2021a; Oliva et al. 2021; Reixach et al., 2021). Glacier recession following these glacial advances probably under a continental climate allowed the formation of rock glaciers in the deglaciated areas (Fernandes et al., 2018). Rock glaciers in the Central Pyrenees are mainly dispersed between 2100 and 2400 m a.s.l. in the northern face (e.g. Aran Valley) and between 2300 and 2600 m a.s.l. in the southern side of the range (e.g. Boí and Noguera Pallaresa valleys; Fernandes et al., 2018; Ventura, 2020). Considering the present-day lower limit of the permafrost belt in the Pyrenees, the few active rock glaciers are located above 2600 m a.s.l. (northern face) and 2800 m a.s.l. (southern face; Serrano et al., 2001, 2006, 2011; González-García, 2014). Therefore, most rock glaciers in the Pyrenees are relict, although their chronological evolution remains poorly known.

The scarce studies that tried to understand the period of stabilization or stagnation of rock glaciers by applying CRE methods on its boulders showed a considerable variation of the ages (Moran et al., 2016; Steinemann et al., 2020; Amschwand et al., 2021; Lehmann et al., 2022;). For example, in the most representative large rock glaciers composed of a succession of ridges and furrows, the oldest ages have been found in the lower part of the landform and the most recent in the highest ridges, suggesting the time of rock glacier activity (Frauenfelder et al., 2005; Rode & Kellerer-Pirklbauer, 2012; Scapozza et al., 2014; Winkler & Lambiel, 2018). On the other hand, present-day monitoring of inactive (or transitional; Delaloye & Echelard, 2021) rock glaciers reports frequent boulder adjustments as the internal frozen mass shrinks in response to current warming (Gómez-Ortiz et al., 2019). This pattern occurred also in the past as revealed by CRE ages in relict rock glaciers yielding a wide range of ages that show the transition towards the relict state can take several thousands of years (Fernández-Fernández et al., 2020; Tanarro et al., 2021). In any case, the youngest age in a CRE dataset from rock glaciers is indicative of its final stabilization. In the Pyrenees, the first studies on rock glaciers from the Eastern and Central parts of the range indicate that they became stable during the transition from cold to warm periods, such as from the HS-1 to the B-A and from the YD to the Holocene (Andrés et al., 2018; Jomelli et al., 2020). During the B-A, the stabilization of frontal lobes between 2100 and 2400 m a.s.l. occurred at 14-13 ka in the Aràser and Duran valleys, Eastern Pyrenees (Palacios et al., 2015b;

Andrés et al., 2018) and in the Gállego Valley, southern face of the Central Pyrenes (Palacios et al., 2015a; Palacios et al., 2017b). Similarly, during the YD / Holocene transition, evidence of frontal lobe stabilization at elevations of 2200-2400 m a.s.l. by 12-11 ka was detected in the Aràns er and Gállego valleys (Palacios et al., 2015b; 2017b). Throughout the Mid-Holocene, stabilization of boulders in the frontal lobes of rock glaciers at ca. 2400 m a.s.l. occurred by 7 ka in the Ariège Valley and by 6-5 ka in the Gállego Valley (Palacios et al., 2017b; Jomelli et al., 2020). Finally, the stagnation of boulders from the upper lobes above 2400 m a.s.l. occurred essentially during the Mid-Late Holocene; this is the case of rock glaciers that ceased activity by 8-7 ka in the Aràns er valley (Andrés et al., 2018) and by 1 ka in the Ariège valley (Jomelli et al., 2020).

Despite this limited knowledge of some areas of the Pyrenees, little is known about the timing, process and asynchronies of rock glacier formation in the northern slope of the Pyrenees. In order to fill in this gap, the objectives of this work are:

i) To reconstruct the chronology of the last glacial advance in the Lòcampo cirque, Central Pyrenees.
ii) To constrain the chronology of the stabilization in a rock glacier located at 2200-2300 m a.s.l.
iii) To shed light on the factors, triggers and mechanisms that supported the glacial-to-periglacial conditions during the last phase of the last deglaciation.

## 2. Study area

The Pyrenees are a mountain range dividing the Iberian Peninsula from the rest of the European continent. They stretch from the Mediterranean Sea to the Atlantic Ocean along ca. 400 km, with ca. 100 km of width. The highest peaks are located in the central axis of the range, where many rise above 3000 m a.s.l. (e.g. Aneto Peak, 3404 m a.s.l.), and become gradually lower towards the W and E regions.

The Upper Garonne Basin is located in the Central Pyrenees and is administratively divided into two districts by the French and Spanish border. Whereas la Pique River drains the western French territory, the main Garonne River drains in the Eastern Spanish part articulated by the Aran Valley. Both flow northwards along typical U-shaped valleys carved out by glaciers during Quaternary glaciations. The highest interfluves show mainly NE-exposed cirques stretching from 2100-2400 m a.s.l. in the floors to over 3000 m a.s.l. to peaks above their headwalls (e.g. Molières Peak, 3009 m a.s.l.; Besiberri Nord Peak, 3007 m a.s.l.).

This study focuses on the eastern margin of the Ruda Valley – headwaters of the Garonne Basin – where the Lòcampo cirque is located, at 42º38’06’’-42º38’27’’N latitude and 0º58’36’’-0º59’10’’E longitude. It extends over 800 m a.s.l. in length and 500 m a.s.l. in width between 2200 and 2644 m a.s.l. at the

highest peak (Tuc de Lòcampo; Figure 1). The bedrock is hornblende granodiorite and porphyritic granite from the Maladeta Batholith that intruded the Pyrenean Palaeozoic basement during the Carboniferous, at ca. 300 Ma (Cochelin, 2017). In contact with granitoids, the older Ordovician slates, marbles and hornfels are well marked, forming the concave slopes (>30º) of the Ruda Valley and the relatively flat area of the Bonaigua divide (ca. 2000 m a.s.l.). This valley was shaped by glacial abrasion during, at least, the last two glaciations (129 ka and before 24-21 ka) when large glaciers reached the Pyrenean foreland (Fernandes et al., 2021b). During and following the LGM, glacial retreat was massive and reached the cirque level by 15-14 ka, as shown by CRE dating in the Bacivèr cirque, next to Lòcampo cirque (Oliva et al., 2021). At the Bonaigua meteorological station (2266 m a.s.l.; Servei Meteorológic de Catalunya), the mean annual air temperature (MAAT) between 2000 and 2020 was 3 ºC and the annual precipitation reached ca. 1200 mm. On the cirque bottom, snow lasts from October to June, recording frequently >200 cm of depth in late winter and early spring (Bonsoms et al., 2021). The Lòcampo cirque contains a large moraine system and a well-developed relict rock glacier that constitute a representative study case to explore their origin and the chronological sequence of the transition between the glacial to periglacial domains in the Central Pyrenees (Fernandes et al., 2022; Figure 1).

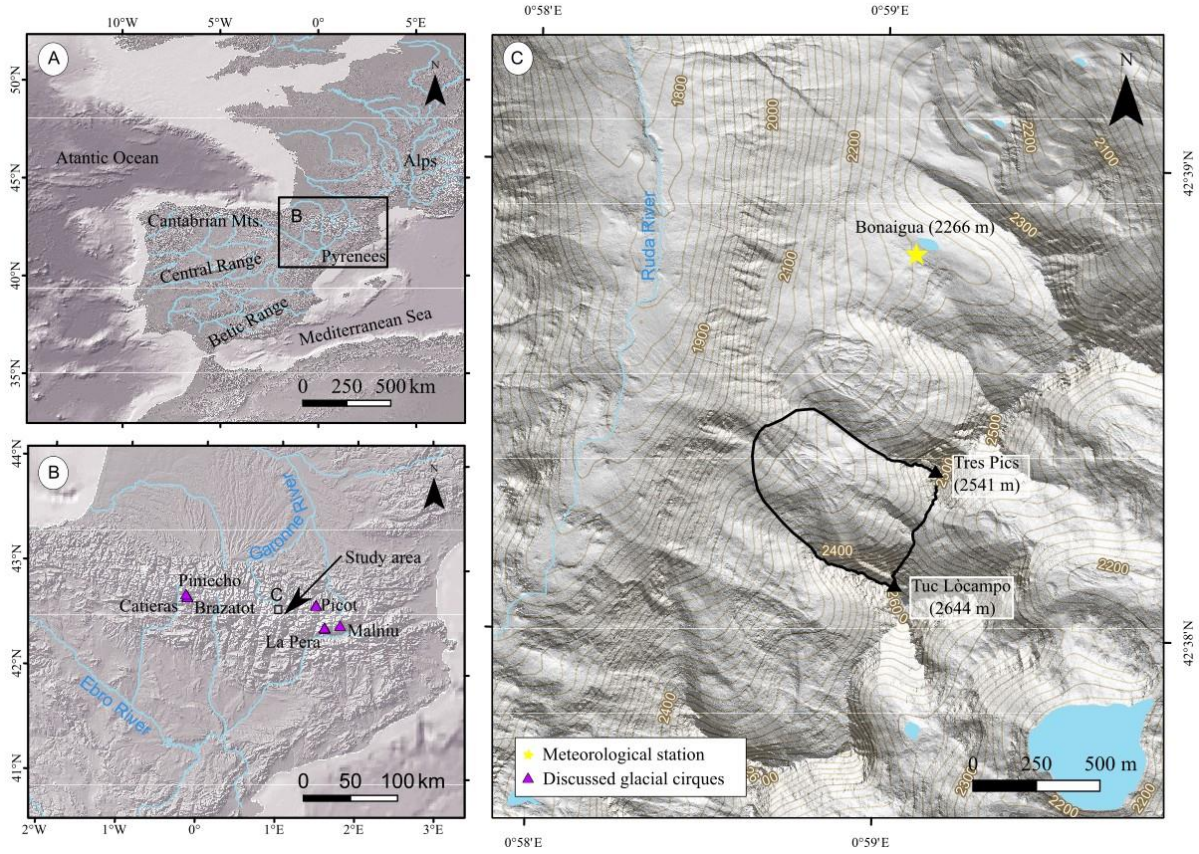


Figure 1. Geographical setting of the Lòcampo cirque highlighted by the back line (C) within the Pyrenees (B) and within Western Europe (A).

## 3. Methodology

The reconstruction of the glacial and postglacial dynamics at the Lòcampo cirque was based on complementary geomorphological and geochronological approaches. Fieldwork was conducted during the summer of 2020, when the terrain was snow-free and allowed the best identification of the glacial and periglacial features and the collection of rock samples for CRE.

### 3.1. Geomorphology and sampling strategy

A detailed geomorphological map at 1:5,000 scale was adapted from Fernandes et al. (2022) and prepared using ArcMap (ESRI). Mapping was based on the interpretation of 1-m resolution orthophotomaps and 1-m resolution LiDAR-derived digital elevation models (DEM) from the 'Institut Cartogràfic i Geològic de Catalunya', supported by field work.

Glacial and periglacial features were targeted for dating based on the geomorphological map, with 8 granodiorite rock samples collected with a hammer and chisel (Table 1). The criterion for the boulder sampling was limiting the risk of postglacial reworking (i.e. overturning) or burial. Hence, we sampled boulders well-anchored in the moraine, far from the talus and on top of the ridges of the rock glacier, with the longest axis ranging between 2 and 9 m (Figure 2). Rock splits 3-5 cm thick were extracted from flat and gentle surfaces at the top of the selected boulders. 5 samples were collected from the cirque moraine (ARAN-47, ARAN-48, ARAN-49, ARAN-53 and ARAN-54) and 1 from the top of each of the three highest ridges of a rock glacier (ARAN-50, ARAN-51 and ARAN-52).

Table 1. Geographic location, topographic shielding factor and sample thickness of samples from boulders.

| Sample name | Latitude (DD) | Longitude (DD) | Elevation (m a.s.l.)[a] | Topographic shielding factor | Thickness (cm) |
|---|---|---|---|---|---|
| *Glacial cirque moraine* | | | | | |
| ARAN-47 | 42.6399 | 0.9802 | 2236 | 0.9614 | 3.9 |
| ARAN-48 | 42.6398 | 0.9802 | 2236 | 0.9708 | 2.3 |
| ARAN-49 | 42.6397 | 0.9805 | 2240 | 0.9628 | 3.0 |
| ARAN-53 | 42.6385 | 0.9836 | 2334 | 0.9238 | 4.5 |
| ARAN-54 | 42.6385 | 0.9836 | 2332 | 0.9269 | 4.0 |
| *Rock glacier* | | | | | |
| ARAN-50 | 42.6396 | 0.9797 | 2224 | 0.9714 | 3.8 |
| ARAN-51 | 42.6393 | 0.9803 | 2236 | 0.9530 | 3.1 |
| ARAN-52 | 42.6391 | 0.9818 | 2266 | 0.9501 | 4.0 |

[a] Elevations are derived from the 5 m Digital Elevation Model of the Spanish "Instiuto Geográfico Nacional" and are subjected to a vertical accuracy of ±5 m.

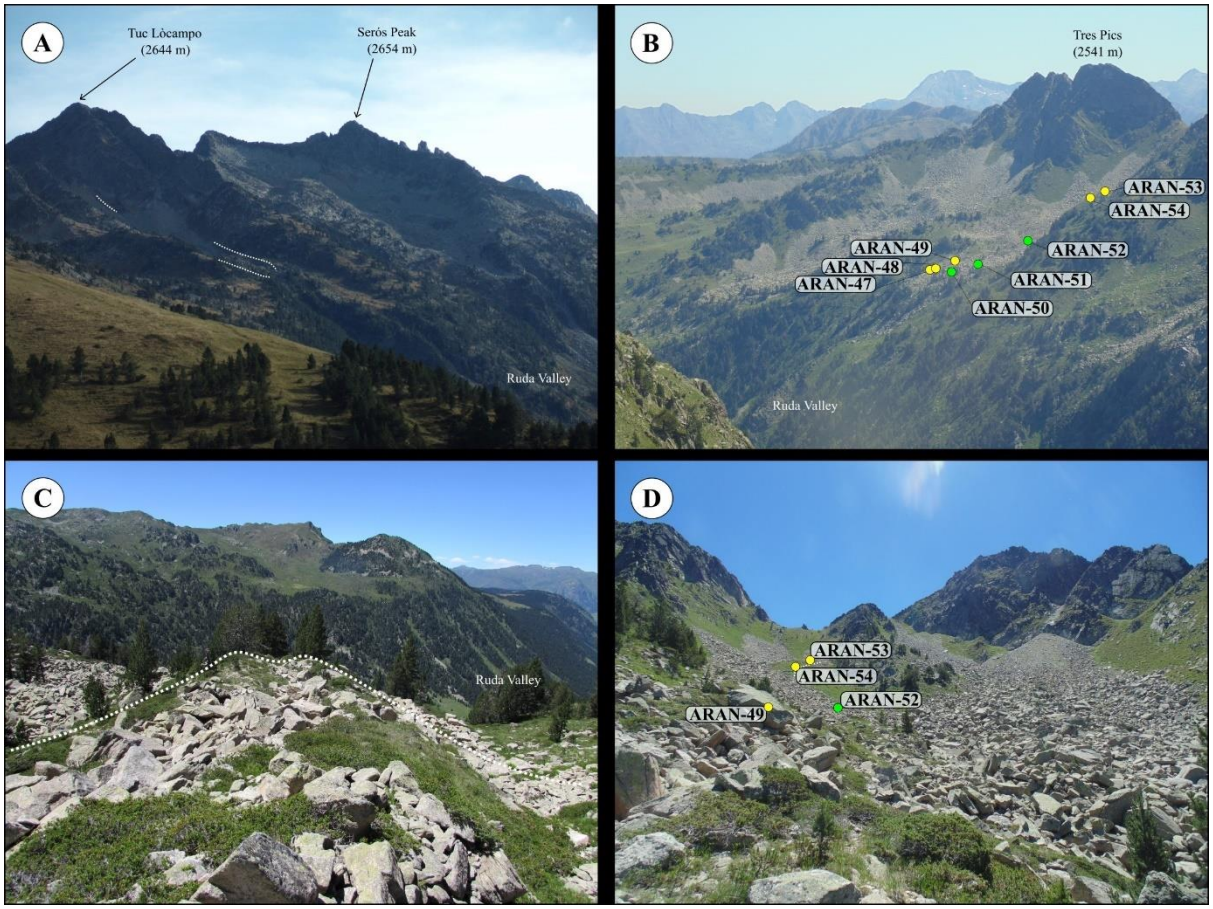


Figure 2. Pictures of the Lòcampo cirque looking south (A) and north (B), as well as from the right ridge of the cirque moraine (C) and the rock glacier (D). Collected samples from moraine (yellow dots) and rock glacier (green dots) boulders are plotted in the pictures b and c.

### 3.2. Sample processing and exposure age calculation

The quartz-richness of the granodiorites from the Lòcampo cirque allowed the extraction of the *in situ*-produced cosmogenic nuclide $^{10}$Be. Samples were crushed and sieved to the 125-500 µm fraction at the laboratory of Physical Geography of the Universidad Complutense de Madrid (Spain). Further physical and chemical sample processing was conducted at the 'Laboratoire National des Nucléides Cosmogéniques' ($LN_2C$) of the 'Centre Européen de Recherche et d'Enseignement des Geosciences de l'Environnement' (CEREGE; Aix-en-Provence, France). The final physical procedures focused on the removal of the magnetic minerals by using a 'Frantz LB-1' magnetic separator.

In order to discard the remaining non-quartz minerals (e.g. feldspar), the non-magnetic fraction underwent several consecutive leachings of concentrated mixture of hydrochloric (1/3 HCl) and hexafluorosilicic (2/3 $H_2SiF_6$) acids and after that, atmospheric $^{10}$Be was removed by successive partial dissolutions with concentrated hydrofluoric (HF). Subsequently, about 20 g of each sample were spiked with 150 µL on an in-house manufactured $^{9}$Be carrier solution (3025 ± 9 µg $^{9}$Be; Merchel et al., 2008).

Finally, samples were totally dissolved in HF and Be was isolated using ion exchange columns and recovered as BeO (Merchel & Herpers, 1999; Dunai, 2010).

BeO targets were mixed with niobium powder and loaded in copper cathodes for $^{10}Be/^{9}Be$ ratio measurements (Table 2) at the national accelerator mass spectrometer (AMS) facility ASTER at the CEREGE. AMS measurements were calibrated against the in-house standard STD-11 with an assigned $^{10}Be/^{9}Be$ ratio of $1.191 \pm 0.013 \times 10^{-11}$ (Braucher et al., 2015).

Table 2. AMS analytical data and exposure ages. 10Be/9Be ratios were inferred from measurements at the ASTER AMS facility. Individual ages are shown with their full uncertainties (including analytical AMS uncertainty and production rate uncertainty) and analytical uncertainty only within brackets. Arithmetic mean ages are given with their full uncertainties and standard deviations within brackets

| **$^{10}$Be samples analytical AMS data** | | | | | | | | |
|---|---|---|---|---|---|---|---|---|
| **Sample name** | **Quartz weight (g)** | **Mass of carrier ($^{9}$Be mg)** | **ASTER AMS cathode number** | **$^{10}$Be/$^{9}$Be ($10^{-14}$)** | **Blank correction (%)** | **[$^{10}$Be] ($10^{4}$ atoms g$^{-1}$)** | **Age (ka)** | **Mean age (ka)** |
| *Glacial cirque moraine* | | | | | | | | |
| ARAN-47 | 20.10 | 0.44 | IGNM | 18.09 ± 0.57 | 1.07 | 26.25 ± 0.83 | 12.6 ± 0.8 (0.4) | |
| ARAN-48 | 19.43 | 0.44 | IGNN | 18.21 ± 0.64 | 1.06 | 27.33 ± 0.97 | 12.9 ± 0.8 (0.5) | |
| ARAN-49 | 20.38 | 0.44 | IGNO | 20.70 ± 0.86 | 9.36 | 29.60 ± 1.24 | 14.1 ± 0.9 (0.6) | 13.7 ± 1.5 (0.5) |
| *ARAN-53* | *20.63* | *0.44* | *IGNS* | *12.90 ± 4.97* | *1.52* | *18.01 ± 7.05* | *8.4 ± 3.2 (3.2)*[a] | |
| *ARAN-54* | *20.01* | *0.44* | *IGNT* | *22.62 ± 0.74* | *8.61* | *32.77 ± 1.08* | *15.2 ± 0.9 (0.4)* | |
| *Rock glacier* | | | | | | | | |
| ARAN-50 | 21.01 | 0.44 | IGNP | 20.29 ± 0.81 | 9.51 | 28.28 ± 1.14 | 13.6 ± 0.9 (0.5) | |
| ARAN-51 | 21.03 | 0.44 | IGNQ | 17.71 ± 0.59 | 1.09 | 24.55 ± 0.83 | 11.9 ± 0.7 (0.4) | 12.7 ± 1.4 (0.4) |
| ARAN-52 | 20.50 | 0.44 | IGNR | 18.83 ± 0.59 | 1.04 | 26.50 ± 0.83 | 12.7 ± 0.8 (0.4) | |

| **Chemistry blank details** | | | | | | |
|---|---|---|---|---|---|---|
| Blank name | Mass of carrier ($^{9}$Be mg) | ASTER AMS cathode number | $^{10}$Be/$^{9}$Be ($10^{-14}$) | [$^{10}$Be] ($10^{4}$ atoms) | | |
| ARAN BK | 0.44 | IGNV | 0.20 ± 0.03 | 5.65 ± 0.84 | - | - |

[a] The exposure age in grey and italics was identified as outliers based on low measurement currents and high analytical uncertainty. The exposure age is therefore not included in the interpretation.

The partial shielding of the surrounding reliefs was geometrically corrected by implementing a topographic shielding factor (Dunne et al., 1999), obtained from the ArcGIS toolbox developed by Li (2018). It requires the location of the sampling sites (point shapefile), the strike/dip angles of the sampled surfaces and a DEM (a 5-m cell size was used for an efficient geoprocessing and calculation).

Exposure ages were calculated in the CREp online calculator (univ-lorraine.fr; Martin et al., 2017) with the Lifton-Sato-Dunai (LSD) elevation/latitude scaling scheme (Lifton et al., 2014), ERA40 atmospheric model (Uppala et al., 2005), the geomagnetic database based on the LSD framework (Lifton et al., 2014), and the world wide mean production rate of 3.98 ± 0.22 atoms to $^{10}$Be g$^{-1}$ yr$^{-1}$ at sea level high-latitude (Martin et al., 2017) to enable the full comparison with the updated glacial chronology in Iberian mountains (Oliva et al., 2022). Calculated exposure ages are shown in Table 2 together with the respective 1σ full and analytical uncertainties. Full error is presented with the ages unless otherwise is stated.

Erosion correction was implemented through a conservative rate of 1 mm ka$^{-1}$, representative of biotite-rich crystalline rock type (André, 2002). The snow shielding correction is also included in Table 3, considering 100 cm snow depth with 0.2 g cm$^{-3}$ density and lasting for 7-8 months according to data from nearby areas of the Central Pyrenees (see Oliva et al., 2021). Both corrections resulted in ca. 9% older ages with ca. 1% from erosion and ca. 8% from snow cover. However, as most of the published ages from other areas do not consider any correction, we used non-corrected ages. The chi-squared test was applied according with the Ward and Wilson (1978) in the moraine units and the sample ARAN-54 was (15.2 ± 3.2 ka) was detected as an outlier. The high internal errors of the sample ARAN-53 (8.4 ± 3.2 ka) due to the low current during the AMS measurements implied rejecting this age.

Table 3. Exposure ages according to different erosion and snow cover correction scenarios.

| **Sample name** | **Exposure ages (arithmetic mean, in ka)** | | | |
|---|---|---|---|---|
| | **No correction** | **Erosion correction** | **Snow correction** | **Erosion + snow correction** |
| *Glacial cirque moraine* | *13.2 ± 11 (0.5)* | *13.3 ± 1.2* | *14.2 ± 1.2* | *14.4 ± 1.2* |
| ARAN-47 | 12.6 ± 0.8 (0.4) | 12.8 ± 0.8 (0.4) | 13.6 ± 0.8 (0.4) | 13.8 ± 0.8 (0.4) |
| ARAN-48 | 12.9 ± 0.8 (0.5) | 13 ± 0.8 (0.5) | 13.9 ± 0.9 (0.5) | 14.1 ± 0.9 (0.5) |
| ARAN-49 | 14.1 ± 0.9 (0.6) | 14.2 ± 0.9 (0.6) | 15.1 ± 1 (0.6) | 15.3 ± 1 (0.6) |
| ARAN-53 | *8.4 ± 3.2 (3.2)* | *8.5 ± 3.3 (3.2)* | *9.1 ± 3.5 (3.5)* | *9.2 ± 3.5 (3.5)* |
| ARAN-54 | *15.2 ± 0.9 (0.4)* | *15.4 ± 0.9 (0.5)* | *16.4 ± 1 (0.5)* | *16.6 ± 1 (0.5)* |
| *Rock glacier* | *12.7 ± 1.4 (0.4)* | *12.9 ± 1.2* | *13.7 ± 1.2* | *13.9 ± 1.3* |
| ARAN-50 | 13.6 ± 0.9 (0.5) | 13.8 ± 0.9 (0.5) | 14.6 ± 0.9 (0.6) | 14.8 ± 0.9 (0.6) |
| ARAN-51 | 11.9 ± 0.7 (0.4) | 12 ± 0.8 (0.4) | 12.8 ± 0.8 (0.4) | 12.9 ± 0.8 (0.4) |
| ARAN-52 | 12.7 ± 0.8 (0.4) | 12.8 ± 0.8 (0.4) | 13.6 ± 0.8 (0.4) | 13.8 ± 0.8 (0.4) |

## 4. Results

The geomorphological mapping revealed a significant variety of glacial and periglacial landforms in the Lòcampo cirque. Exposure ages provided the chronological framework of the moraine and rock glacier stabilization during the final phases of the last deglaciation (Figure 3).

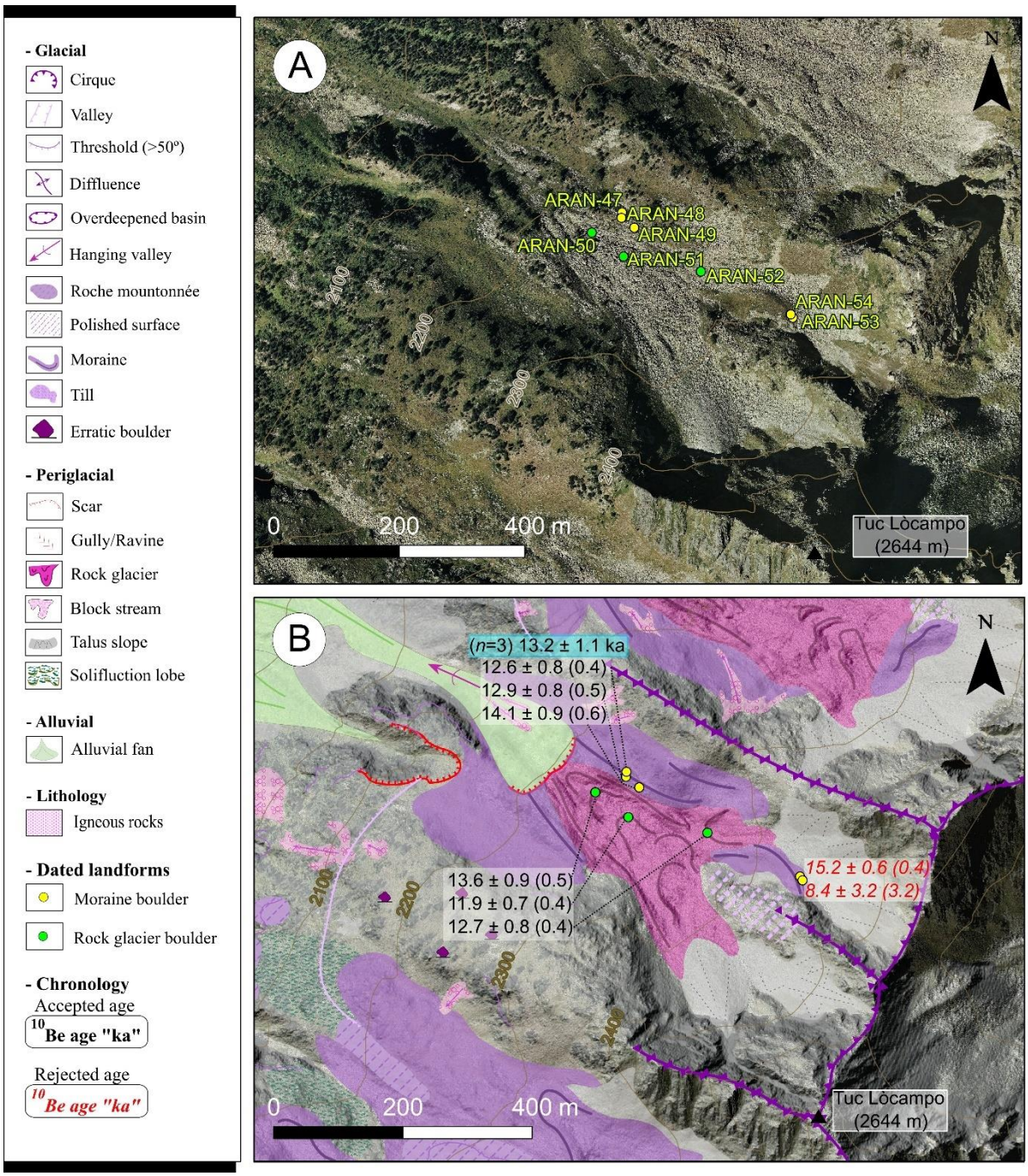


Figure 3. Above, an orthophotomap from the Lòcampo cirque with the distribution of the samples and below, the geomorphological map with the distribution of the CRE ages.

### 4.1. Geomorphological evidence

The Lòcampo glacial cirque is oriented towards NW and is relatively small (38 ha) compared to those in the rest of the Aran Valley (62 ha on average; Lopes et al., 2018). It is located on the western face of the arête dividing the Ruda and Gerber valleys. The steep headwall of the cirque is composed of 100-300 m rock walls (from ca. 2600 on the ridge to 2300 m a.s.l. at the foot) and includes two glacial overdeepenings separated by a rock ridge. On the sides of the Lòcampo cirque, interfluves at 2360-2200 m a.s.l. separating the adjacent cirques show glacially abraded surfaces with scattered erratic boulders. These interfluves become steeper towards the cirque floor where the rock walls are covered by talus debris and block streams. On the bottom of the cirque, an overdeepened depression (ca. 300-m-long, ca. 200-m-wide) extends between 2300 and 2200 m a.s.l. where a moraine system is preserved. The Lòcampo cirque connects with the main Ruda Valley through a steep slope (>30º) of 400 m.

A frontal moraine closes the cirque between 2290 and 2220 m a.s.l.. The moraine is composed of meter-sized subangular to subrounded boulders embedded in a sandy matrix forming an elongated 5-m high ridge on the northern and southern margins of the cirque. On this moraine, a sequence of two 2-m high ridges oblique to the main one and composed of large subrounded boulders with no matrix are interpreted as push moraines. On the forefront of the frontal moraine, the till is affected by a scar that cuts the moraine evidencing that this section of the moraine was eroded by gravitational processes. Finally, on the north side of the rock ridge dividing the two glacial hollows there is another moraine ridge at 2340-2280 m a.s.l., which is composed of anchored boulders. As this moraine stretches westwards towards the centre of the cirque, it is likely that is a remnant of a medial moraine belonging to the same system of the cirque moraine (Figure 3).

At the bottom of the cirque, a 5-ha rock glacier, extends from 2330 to 2210 m a.s.l. and has 410 m-length and 150 m-width. It includes >5-m high ridges perpendicular to the slope and divided by furrows. All ridges are composed of 1-9 m-long angular to subangular boulders - that tend to be larger in the lower ridges -, with a lack of fine-grained sediments. This NW-oriented rock glacier shows no signs of activity; it is located under the present day lower limit of active rock glaciers (ca. 2650 m; e.g. Serrano et al., 2011) and below the lower elevation of continuous permafrost in the Pyrenees (ca. 2800-3000 m; Serrano et al., 2019), and with trees also occur revealing lack of movement. In the upper sector of the rock glacier, two ridges are distributed (ca. 5-12 m-high) at ca. 2267-2280 m a.s.l. and are individualised at each of the glacial hollow of the cirque. The following well-defined ridge (ca. 4-5 m-high) is located at 2235-2240 m and lies in the central part of the rock glacier. Further down, at 2220-2230 m, another ridge (ca. 5-6 m-high) narrows as it gets closer to the front of the rock glacier. Finally, at 2215-2208 m a.s.l., the last ridge (ca. 7-8 m-high) is almost connected with the cirque moraine (Figure 3).

Between the margins of the cirque moraine and the rock glacier, there are longitudinal ridges that stretch parallelly to both northern and southern moraine ridges. These elongated ridges encompass angular to surrounded boulders embedded on fine matrix. Besides, thick debris cover the area between these ridges and the rock glacier, with no visible depression in between. Therefore, this moraine features might suggest a deposition during a phase of transition between the debris-free and the rock glacier, likely from a debris-covered glacier (Fernández-Fernández et al., 2017).

### 4.2. Geochronological data

The 8 samples dataset from the Lòcampo cirque yielded ages covering a 3-ka period representative of the final phases of the deglaciation in the Aran Valley, between 14.1 ± 0.9 ka and 11.9 ± 0.7 ka (Table 2; Figure 4).

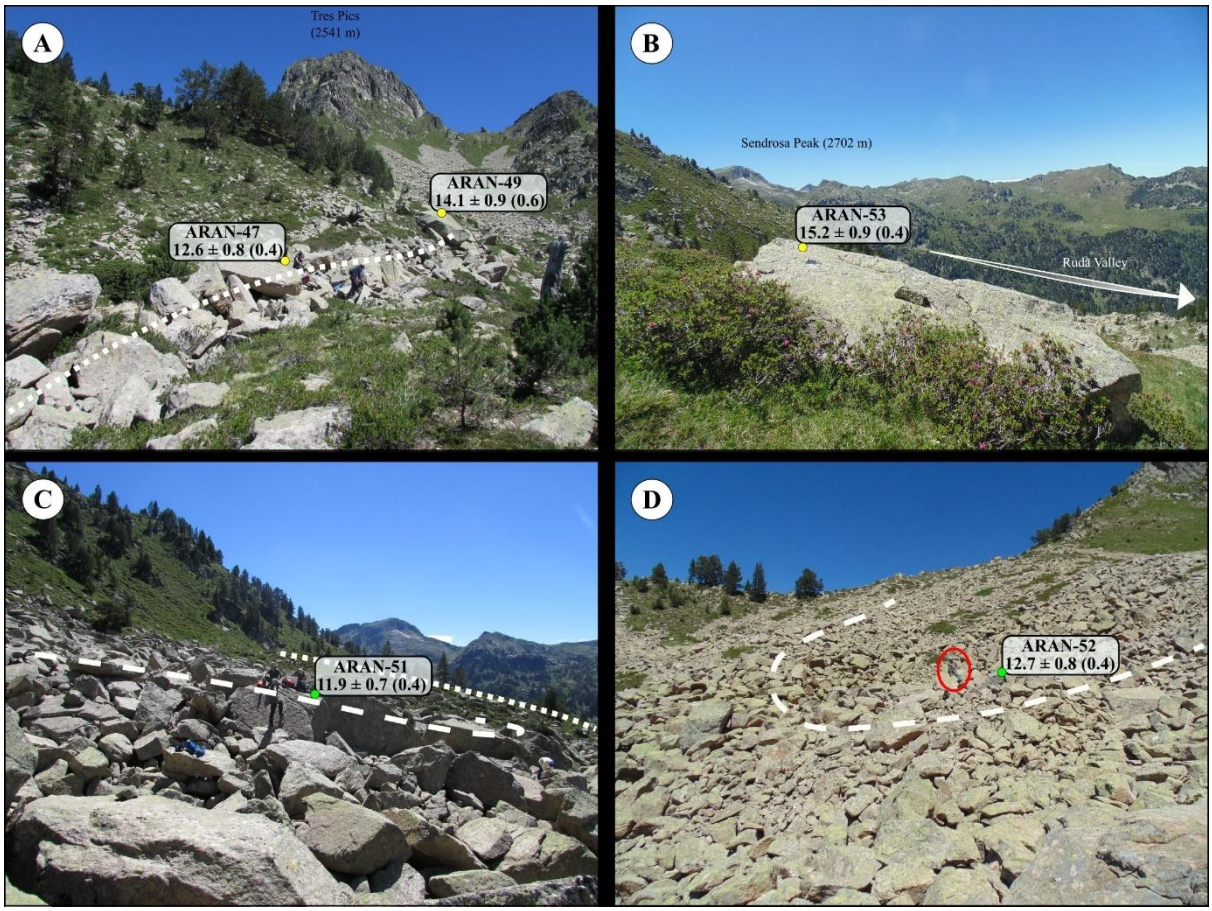


Figure 4. Examples of landforms with the respective CRE ages: A) Northern ridge of the cirque moraine; B) upper unit of the moraine system; C) internal lobe of the rock glacier with the left ridge of the cirque moraine; D) upper lobe of the rock glacier with the graphic scale of men size (black circle).

At the northern margin of the glacial cirque, the three samples from the cirque moraine (ARAN-47, ARAN-48 and ARAN-49) reported chronostratigraphically and statistically consistent ages: 12.6 ± 0.8, 12.9 ± 0.8 and 14.1 ± 0.9 ka, which yield a mean age of 13.2 ± 1.1 ka.

The three samples obtained from stable boulders of the highest ridges of the rock glacier (ARAN-50, ARAN-51 and ARAN-52) showed a geomorphologically consistent sequence of ages of 13.6 ± 0.9, 11.9 ± 0.7 and 12.7 ± 0.8 ka, considering the long-lasting stabilization of the rock glacier (Lehmann et al., 2022).

## 5. Discussion

The $^{10}$Be CRE age dataset supported on the detailed geomorphological mapping allowed to develop a model of the glacial to periglacial transition in the Lòcampo cirque. The sampled boulders yielded ages spanning the second half of T-1.

### 5.1. Geomorphological interpretation and hypotheses construction

This study underpins the nonlinear long-term deglaciation in the Upper Garonne Basin during the T-1 that has been proposed in earlier studies (Fernandes et al., 2017, 2021a, 2022; Oliva et al., 2021). The cirque moraine was likely formed by a debris-free glacier as it is significantly higher (ca. 12-15 m) than the rock glacier ridges. Using radar sound surveys, Haeberli (1985) determined that debris-free glaciers are much thicker features than the debris-covered ones, and therefore can form more prominent moraine features. The CRE ages from the cirque moraine in the Lòcampo cirque showed a mean of 13.2 ± 1.1 ka. In datasets with relatively high scattered ages, the average provides a reasonable estimate for the true age of the moraine formation (Applegate et al., 2012). This moraine age suggests the moment when the it was abandoned and became stable, after the glacier advance that occurred during the second half of the B-A.

The rock glacier located within the limits of the cirque moraine of the Lòcampo cirque indicates that periglacial conditions compatible with the occurrence of permafrost occurred between 13.6 ± 0.9 and 11.9 ± 0.7 ka and substituted the cirque glacier that formed that aforementioned moraine. This chronological range is interpreted as the transition period until the rock glacier became definitively relict. However, the exact timing of formation of the rock glacier can not be inferred due to the overlapping of the exposure ages of the moraine (13.2 ± 1.1 ka) and the rock glacier (frontal ridge = 13.6 ± 0.9 ka).

Therefore, we understand that the formation of the rock glacier took place after the development of a debris-covered glacier as revealed by the presence of longitudinal crests in contact with the internal margins of the moraine (Clark et al., 1994). The debris-covered glacier occurred between

the moraine stabilization and the subsequent rock glacier formation. In addition, the overlap of CRE ages between the cirque moraine and the rock glacier might underline that those boulders were already emplaced on top of the glacier surface during the moraine stabilization. This would support the idea that the ice mass hosted in the Lòcampo cirque was a debris-covered glacier before the rock glacier was formed. Since then, the intense debris supplied by the surrounding slopes during the paraglacial phase as well as the abundant material left by the debris-covered glacier favoured the development of the rock glacier. However, we can not exclude that the rock glacier could have formed directly after the stabilization of the moraine (Figure 5). Such evolution could have occurred during the late B-A / early YD, as suggested by the similar ages from the cirque moraine and the oldest age of the rock glacier (see e.g. Fernández-Fernández et al., 2020; Tanarro et al., 2021). However, these scenarios need to be validated with further CRE dating in future studies.

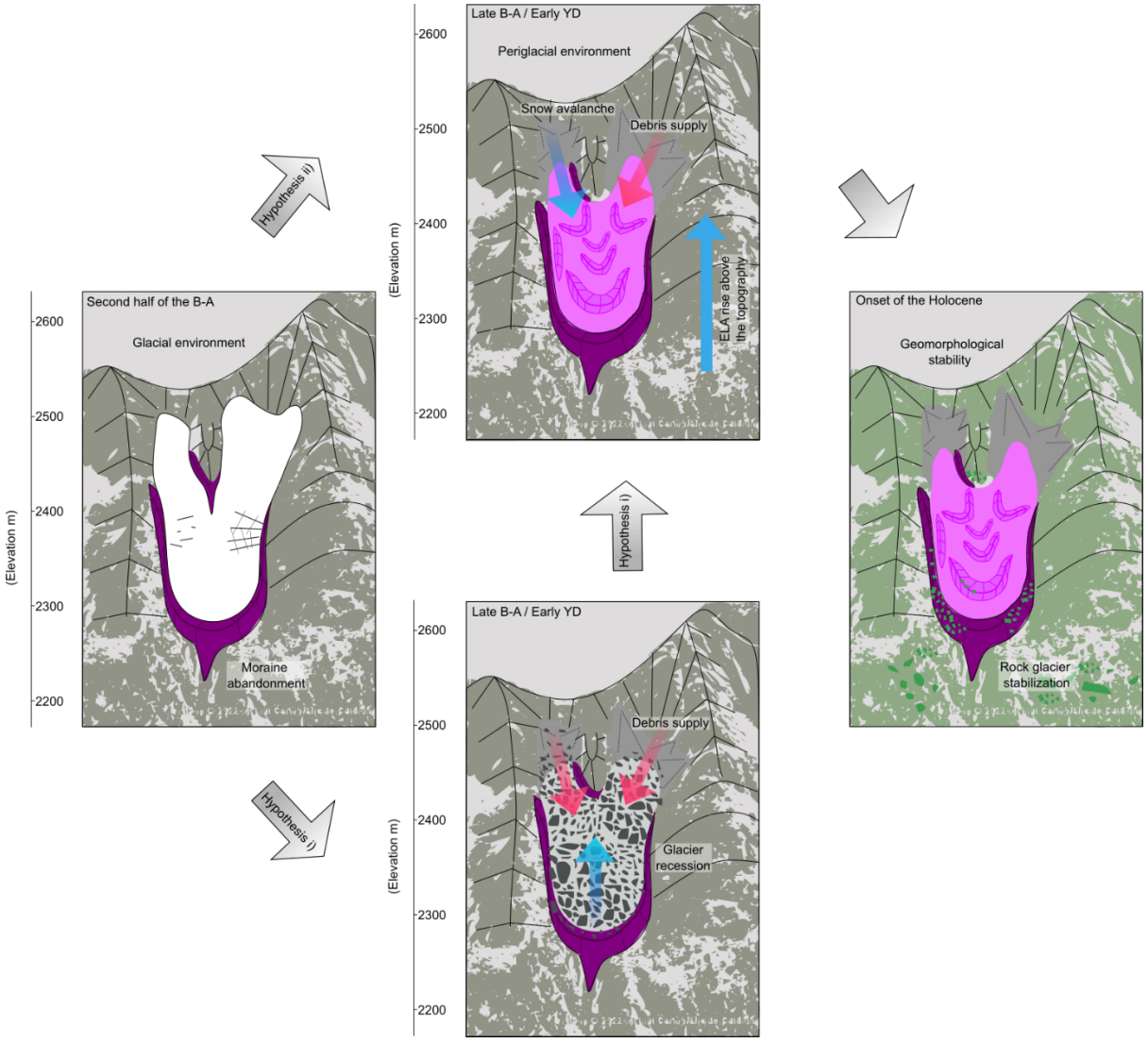


Figure 5. Evolution model of the Lòcampo cirque with the possible scenarios. Development of the cirque moraine from a debris-free glacier during the second half of the B-A which was then

substituted either by a debris-covered one or by a rock glacier during the Late B-A / early YD. Finally, during the onset of the Holocene, or afterwards, the whole rock glacier became relict.

The fact that the oldest CRE age coincides with the frontal rock glacier ridge suggests that the rock glacier toe ceased activity right after its development. However, it is likely that the transitional period between the rock glacier became inactive (with the presence of a frozen body) and finally relict (with its final melting) could have last for 2-3 ka, as the boulder that lies in the centre of the rock glacier yielded a much younger age (11.9 ± 0.7 ka) that does not overlap with the oldest one (13.6 ± 0.9 ka). This period is probably indicating the subsequent phase of boulder readjustments or displacements triggered by the degradation of buried ice and subsequent their sinking that potentially persisted longer in the centre and thicker part of the rock glacier. In this sense, the youngest age suggests the moment when the rock glacier became definitively relict at 11.9 ± 0.7 ka or afterwards.

Finally, we cannot exclude the possibility that some boulders may have provided older ages due to the retaining of an unknown amount of nuclide inheritance or even a more complex history considering the time of transport on the glacier surface after detachment from the rock walls (Anderson et al., 2018; Scherler & Egholm, 2020).

### 5.2. Glacial and periglacial evolution of the Upper Garonne Basin

During the Late Pleistocene glaciations, the Lòcampo cirque was fully glaciated and intensely shaped by glacial processes, as demonstrated by the paleoglacier reconstruction of the entire Garonne catchment (Fernandes et al., 2017; 2021b). The Garonne paleoglacier reached ca. 80 km-long, with a maximum ice thickness of ca. 800 m, probably during, at least, the last two glacial cycles, as revealed by absolute dating applied to the glacial landforms and glaciolacustrine sediments in the terminal basin, at 420-440 m a.s.l. (Andrieu, 1991; Fernandes et al., 2021b). During the LGM, the terminal basin was already deglaciated as suggested by two $^{10}$Be ages from polished surfaces obtained at 18 km from the cirque moraine system (24.2 ± 2.1 and 20.7 ± 1.2 ka; Fernandes et al., 2021b). After the onset of the deglaciation, as in the rest of the Pyrenees, the Garonne paleoglacier retreated to the highest valleys. In fact, the deglaciation of the Garonne catchment was underway until ca. 15-14 ka, when cirque floors under peaks of 2600-2700 m a.s.l. became entirely deglaciated, such as in Bacivèr cirque (Oliva et al., 2021). Similarly, in the surroundings of the Lòcampo cirque, the lowest polished bedrock surfaces in the Ruda Valley (1860 and 1900 m a.s.l.) showed similar $^{10}$Be exposure ages of 15.0 ± 0.9 and 13.8 ± 0.8 ka (Fernandes et al., 2021a). The horizontal glacial retreat was parallel to ice thinning: polished surfaces between 140 and 30 m (2380-2260 m a.s.l.) above the Saboredo cirque floor reported ages of 14.8 ± 0.9 and 14.0 ± 0.8 ka. Therefore, considering the similar altitude of the cirque floor

(2200-2300 m a.s.l.) and the prevailing aspect (W) of the Lòcampo cirque with respect to Bacivèr cirque, it is reasonable to think that it was also probably ice-free at 15-14 ka.

Following the period of glacier recession until the first half of the B-A, glacial advances or standstills occurred during short-lived cold periods favouring glacier inception on the Lòcampo cirque floor, as shown by the samples from the cirque moraine that yielded a stabilization age of 13.2 ± 1.1 ka. At the highest tributaries of the Upper Garonne Basin, glacial advances during the second half of the B-A have already been reported: in the Ruda Valley, glacial advances formed a moraine system with external (at 2080 m a.s.l.) and internal ridges (at 2190 m a.s.l.), dated at 13.5 ± 0.9 and 13.0 ± 0.8 ka, respectively (Fernandes et al. 2021a). To date, no other evidence of glacial activity during this period has been reported in the Upper Garonne Basin.

Following the moraine stabilization within the Lòcampo cirque, a transition from debris-free to debris-covered glacier occurred likely during a very short period during the late B-A / early YD, however, we need more CRE ages to confirm the exact timing of this process. In fact, transitional landforms from debris-free to debris-covered glaciers have been shown to have formed in a few hundred years, as revealed by previous studies based on CRE (Fernández-Fernández et al., 2020; Palacios et al., 2020) and numerical simulations (Anderson et al., 2018). Similar results have been obtained in the Bacivèr cirque, where the evolution of a debris-free to debris-covered glacier could have occurred during the B-A / YD transition, becoming definitively stable during the Mid-Holocene (Oliva et al., 2021).

The cirque moraine closes a relict rock glacier in the Lòcampo cirque with CRE ages ranging from 13.6 ± 0.9 to 11.9 ± 0.7 ka in three different ridges at 2280-2267, 2240-2235 and 2230-2220 m. The thick debris mantle forming the Lòcampo rock glacier must have favoured a long preservation of the inner ice/permafrost, which delayed its complete stabilization that finally occurred during the onset of the Holocene, or afterwards. This wide range of CRE ages of the rock glacier may also indicate the prevailing climate in North Iberia during the YD (Oliva et al., 2016). In fact, the cold and dry conditions may have favoured the persistence of permafrost within the rock glacier and boulder readjustment until its final stabilization at 11.9 ± 0.7 ka. Further CRE dates should confirm if this chronological pattern presented for rock glacier stabilization in the Upper Garonne Basin represents a widespread pattern for the entire range.

Similar geomorphological evidence and geochronological data have been also reported in the neighbouring cirques suggesting that during the late B-A / early YD glaciers were confined within the highest areas of the Upper Garonne Basin. However, depending on the local topography and the intensity of the paraglacial adjustment of the slopes, the deglaciation process followed different patterns:

i) In wider cirques of the main valleys of the Garonne catchment with highest peaks of ca. 2700-2800 m a.s.l., glacial advances during the second half of the B-A have been reported: in the N-exposed Ruda Valley, glacial advances formed a moraine system with external (at 2080 m a.s.l.) and internal ridges (at 2190 m a.s.l.), dated at 13.5 ± 0.9 and 13.0 ± 0.8 ka, respectively (Fernandes et al. 2021a). However, determining the chronology of glacial advances during these centennial-scale events could be very challenging when using CRE and its associated uncertainties (Naughton et al., 2022). After such advances, glaciers completely vanished from the bottom of the cirques and left no periglacial features, as suggested by two polished surfaces above the moraine ridges (at 2310 and 2350 m a.s.l.) that yielded CRE ages of 12.7 ± 0.8 and 12.8 ± 0.8 ka (Fernandes et al., 2021a).

ii) In sheltered and lateral cirques with peaks at ca. 2600-2700 m a.s.l., small glaciers persisted or readvanced at the foot of the cirque walls forming moraines at ca. 2400 m a.s.l. during the onset of the YD. This is the case of the NE cirque of the Sendrosa Peak (2702 m) where a moraine yielded a mean CRE age of 12.6 ± 1.3 ka (Fernandes et al., 2021a), or at the foot of the western rock wall of the Rosari Peak (2606 m a.s.l.), Bacivèr cirque, where a small cirque moraine was dated at 12.8 ± 0.5 ka (Oliva et al., 2021). Within these moraines, cirque floors are covered with large chaotic deposits that suggest a gradual evolution towards periglacial conditions: a) longitudinal ridges and furrows suggest the existence of former debris-covered glaciers before its final deglaciation, such as in the Bacivèr cirque; b) transversal ridges and furrows suggest the occurrence of rock glaciers, as it occurs in the Sendrosa and Lòcampo cirques.

### 5.3. Chronology of the debris-free glacier to rock glacier transition in the Iberian Peninsula

During the second half of the B-A, glaciers of the Iberian Peninsula only persisted in the highest valleys of the Pyrenees (Oliva et al., 2022), where topoclimatic conditions were more favourable to glacial maintenance (Fernandes et al., 2021a; Reixach et al., 2021). This is the case of the glacier in the Lòcampo cirque where the moraine was abandoned by the glacier (650 m long) and became stable by 13.2 ± 1.1 ka. These glacial standstills or advances can also correlate with short-lived cold reversals during the B-A interstadial recorded in Greenland ice cores (i.e. GI-1c and GI.1a; Rasmussen et al., 2014). However, due to the intrinsic limitations of the CRE dating on the uncertainty range, other dating techniques with higher precision are needed to support this linkage. The current available CRE ages in the Pyrenees show two periods of moraine formation during the second half of the B-A, where the oldest glacial advance has been reported in the Central and Eastern parts of the range at ca. 13.8-13.5 ka (Fernandes et al., 2021a; Reixach et al., 2021). This has been observed in moraines surrounding the glacial cirque in the Aränser Valley, Eastern Pyrenees, at 2200 m a.s.l. that reported a mean age of 13.6 ± 0.9 ka (*n*=3; Palacios et al.,

2015b; Andrés et al., 2018; Reixach et al., 2021). Similar ages were recalculated from moraines in the Têt Valley at 2150 m a.s.l., 13.8 ± 0.6 ka (*n*=2; Delmas et al., 2008; Reixach et al., 2021). In the Central Pyrenees, a moraine from the Noguera Ribagorçana Valley (1560 m a.s.l.) yielded exposure ages of 13.7 ± 0.9 ka (*n*= 3; Pallàs et al., 2006), and in the abovementioned Ruda Valley (2080 m a.s.l.) at 13.5 ± 0.9 ka (*n*=2; Fernandes et al., 2021a). On the other hand, the youngest glacial advance during that phase was constrained at ca. 13.2-12.8 ka in the Têt Valley (*n*=2: 13.1 ± 0.6 ka; Reixach et al., 2021), Bacivèr cirque (*n*=2: 12.8 ± 0.5 ka; Oliva et al., 2021), Ruda Valley (*n*=2: 13.0 ± 0.8 ka; Fernandes et al., 2021a) and in the Soulcen Valley (*n*=2: 13.2 ± 0.3 ka; Jomelli et al., 2020). However, in the Lòcampo cirque, we have only found evidence of the second glacial phase (13.2-12.9 ka).

The abandonment of such features was also favoured the formation of periglacial features in deglaciating cirques of the Pyrenees, as likely occurred in the Lòcampo cirque. These shrinking glaciers became progressively covered with debris supply enhanced by periglacial or even paraperiglacial conditions (Mercier, 2008). Past shifts in prevailing climate can determine the evolution of glaciers into debris-covered or rock glaciers (Anderson et al., 2018). Following glacial retreat during the second half of the B-A, enhanced debris supply would support the development of either debris-covered glaciers or rock glaciers during the late B-A / early YD. However, it is likely that the deglaciation of the cirque in the Lòcampo cirque must have been different in each scenario. Longer deglaciation of the cirque would be expected for the formation of the debris-covered glacier compared to a rock glacier, as the ice content below the debris mantle is usually higher (85-45%; Janke et al., 2015). In fact, during the late B-A / early YD, sheltered cirques favoured glacier persistence next the foot of rock walls from where boulders fed the debris-cover glacier (Fernandes et al., 2021b).

In the Iberian Peninsula, the application of CRE dating on moraine boulders from debris-free and debris-covered glaciers revealed a scattered age distribution. This suggests an almost synchronous stabilization of the front with the recently abandoned (debris-free glacier) moraines and by contrast, the upper sectors of the debris-covered glaciers became stable some millennia later. This delay might be related to the long period of boulder displacement triggered by the degradation of buried ice/permafrost that can persist for millennia trapped below the surface (Fernández-Fernández et al., 2017). In fact, the insulating effect of a debris mantle over buried ice can reduce ca. 40 times glacial ablation (Bosson & Lambiel, 2016). This long-term stabilization has been detected in the deglaciated cirques during the T-1 (Fernández-Fernández et al., 2017; Oliva et al., 2021). In the Sierra de la Demanda, Iberian Range, the transition from a debris-free to a debris-covered glacier was reconstructed in the Mencilla cirque through CRE ages from boulders belonging to moraines and a debris mantle located in less than 500 m from each other (1600-1700 m a.s.l.). The results showed synchronous stabilization during the Holocene Thermal Maximum

(HTM), by 8-6 ka (Fernández-Fernández et al., 2017). As shown in the same study, a debris-covered glacier developed in the San Lorenzo cirque at 1800-1900 m a.s.l., between moraines attributed to the LGM and the HS-1; in this case, authors proposed that activity definitively ceased by 8.7 ± 0.8 ka (Fernández-Fernández et al., 2017). This pattern was also detected at the Bacivèr cirque, where a small debris-covered glacier at 2400-2500 m a.s.l. likely stopped moving by 7.2 ± 0.5 ka (Oliva et al., 2021).

The onset of the YD in Europe was a period of abrupt temperature decrease with an N-S gradient of 2-5 ºC (Cacho et al., 2001; Moreno et al., 2014; Naughton et al., 2016) and a precipitation reduction of ca. 20% (Renssen et al., 2018). In Iberia, the decrease of ca. 5 ºC inferred from $\delta^{18}O$ values in the Ostolo Cave during this stadial showed severe conditions that, on the one hand, were sufficient to maintain glaciers only at the highest mountain ranges (Oliva et al., 2022). On the other hand, it favoured periglacial activity under permafrost conditions in many Pyrenean cirques (Oliva et al., 2016). The chronological data derived from the application of CRE dating in rock glaciers is increasingly showing that most of the rock glaciers in the Iberian Peninsula had a paraglacial origin and became stable soon after their formation during the B-A interstadial (Palacios et al., 2012, 2015a, 2016, 2017b; Andrés et al., 2018; Jomelli et al., 2020; Santos-González et al., 2022). Indeed, buried ice could have eventually been preserved in transitional rock glaciers due to the reduced ablation rate and nourishment of ice by snow avalanches (Bosson & Lambiel, 2016; Anderson et al., 2018). This persistence of permafrost conditions could also happen to the rock glacier in the Lòcampo cirque.

During the onset of the Holocene, SST in Western Europe increased by about 2 ºC in the Atlantic margin and >6 ºC in the Mediterranean basin (Cacho et al., 2001). These warmer conditions led to a general rise of the periglacial belt in the highest mountain ranges of the Iberian Peninsula (Oliva et al., 2016). Higher temperatures must have favoured the gradual melting of the frozen masses – possibly buried glacial ice and permafrost layers – existing beneath the rock glacier of the Lòcampo cirque, which became relict. In fact, several rock glaciers in other Iberian ranges stabilized during the Holocene (Oliva et al., 2016). In the southern Central Pyrenees, some rock glaciers ceased their movement during the YD / Holocene transition. This occurred in the Piniecho and Catieras cirques (Gállego Valley), where stabilization of frontal lobes from different rock glaciers at ca. 2200-2400 m a.s.l. occurred at 12.6 ± 1.6-11.1 ± 1.3 ka and 12.5 ± 1.3-11.6 ± 1.4 ka, respectively (Palacios et al., 2015b; Table 4). In the Eastern Pyrenees, CRE was also applied on the frontal lobe of an E-facing rock glacier at ca. 2400-2500 m a.s.l. in the La Pera cirque (Aránser Valley), which stabilized by 12.6 ± 1.7 ka (Andrés et al., 2018). Finally, in Sierra Nevada, most rock glaciers stabilized at the end of the YD, such as in the Dílar Valley, where the north-facing rock glacier front (2600-3000 m a.s.l.) became stable by 11.4 ± 1.0 ka (Palacios et al., 2016).

## 6. Conclusions

Glacial and periglacial landforms are widespread features across the cirques of the Central Pyrenees, constituting the geomorphological record of environmental evolution during the last deglaciation. The present work brings a new 8-sample CRE dataset from moraine and rock glacier boulders. The small Lòcampo cirque hosts a cirque moraine at ca. 2200-2300 m a.s.l. that was abandoned by a debris-free glacier during the second half of the B-A, at 13.2 ± 1.1 ka. These ages agree well with other studies in the Pyrenees that report glacial advances/standstills during the second half of the B-A. The CRE ages of 13.6 ± 0.9 to 11.9 ± 0.7 ka reported in the rock glacier do not allow to constrain its formation chronologically and therefore, we interpret the following evolution: after the moraine stabilization, an intermediate phase of a debris-covered glacier formation occurred, which was followed by the rock glacier development and subsequent stabilization. Therefore, the stabilization of the rock glacier front occurred soon after its formation (13.6 ± 0.9 ka) and became definitively relict during the onset of the Holocene (11.9 ± 0.7 ka), or afterwards. The scattered rock glacier ages spanning ca. 2-3 ka are indicative of the transition period towards its relict state, which was possibly delayed during the cold and dry YD, when boulders readjusted due to the presence of buried ice (and permafrost) until its complete melting (and thawing). This is a first attempt to constrain the evolutionary model of a debris-free glacier – debris-covered glacier – rock glacier in the Pyrenees and needs to be assessed with more precise chronological data to validate and extrapolate this model to other deglaciated mountain areas.

## Acknowledgements

This work was funded by the Research Group ANTALP (Antarctic, Arctic, Alpine Environments; 2017-SGR-1102), the Government of Catalonia and the Centro de Estudos Geográficos/IGOT - University of Lisbon (FCT I.P. UIDB/00295/2020 and UIDP/00295/2020). The research topics complement those of the project PALEOGREEN (CTM2017-87976-P) funded by the Spanish Ministry of Economy and Competitiveness and the project NUNANTAR funded by the Fundação para a Ciência e Tecnologia of Portugal (02/SAICT/2017 - 32002). Marcelo Fernandes holds a PhD fellowship of the Fundação para a Ciência e Tecnologia of Portugal (FCT - SFRH/139568/2018); Marc Oliva is supported by the Ramón y Cajal Program (RYC-2015-17597). $^{10}$Be measurements were performed at the ASTER AMS national facility (CEREGE, Aix-en-Provence), which is supported by the INSU/CNRS and the ANR through the "Projets thématiques d'excellence" program for the "Equipements d'excellence" ASTER-CEREGE action and IRD. This research is also framed within the College on Polar and Extreme Environments (Polar2E) of the University of Lisbon. We also thank the National Park of Aigüestortes and Sant

Maurici Lake for providing field access to the study sites and the reviewers for their constructive comments that helped to improve the quality of an earlier version of the manuscript.

## 7. References

Allard, J. L., Hughes, P. D., & Woodward, J. C. (2021). Heinrich Stadial aridity forced Mediterranean-wide glacier retreat in the last cold stage. *Nature Geoscience*. https://doi.org/10.1038/s41561-021-00703-6

Amschwand, D., Ivy-Ochs, S., Frehner, M., Steinemann, O., Christl, M., & Vockenhuber, C. (2021). Deciphering the evolution of the Bleis Marscha rock glacier (Val d'Err, eastern Switzerland) with cosmogenic nuclide exposure dating, aerial image correlation, and finite element modeling. *Cryosphere*, *15*(4), 2057–2081. https://doi.org/10.5194/tc-15-2057-2021

Anderson, R. S., Anderson, L. S., Armstrong, W. H., Rossi, M. W., & Crump, S. E. (2018). Glaciation of alpine valleys: The glacier – debris-covered glacier – rock glacier continuum. *Geomorphology*, *311*, 127–142. https://doi.org/10.1016/j.geomorph.2018.03.015

André, M. F. (2002). Rates of Postglacial rock weathering on glacially scoured outcrops (Abisko-Riksgränsen area, 68°N). *Geografiska Annaler, Series A: Physical Geography*, *84*(3–4), 139–150. https://doi.org/10.1111/j.0435-3676.2002.00168.x

Andrés, N., Gómez-Ortiz, A., Fernández-Fernández, J. M., Tanarro, L. M., Salvador-Franch, F., Oliva, M., & Palacios, D. (2018). Timing of deglaciation and rock glacier origin in the southeastern Pyrenees: a review and new data. *Boreas*, *47*(4), 1050–1071. https://doi.org/10.1111/bor.12324

Andrieu, V. (1991). *Dynamique du paléoenvironnement de la vallée montagnarde de la Garonne (Pyrénées Centrales, France) dela fin des temps glaciaires à l'actuel*. University of Toulouse.

Applegate, P. J., Urban, N. M., Keller, K., Lowell, T. V., Laabs, B. J. C., Kelly, M. A., & Alley, R. B. (2012). Improved moraine age interpretations through explicit matching of geomorphic process models to cosmogenic nuclide measurements from single landforms. *Quaternary Research*, *77*(2), 293–304. https://doi.org/10.1016/j.yqres.2011.12.002

Ballantyne, C. K. (2002). Paraglacial Geomorphology. *Encyclopedia of Quaternary Science: Second Edition*, *21*(December 2001), 553–565. https://doi.org/10.1016/B978-0-444-53643-3.00089-3

Bonsoms, J., Gonzalez, S., Prohom, M., Esteban, P., Salvador-Franch, F., López-Moreno, J. I., &

Oliva, M. (2021). Spatio-temporal patterns of snow in the Catalan Pyrenees. *International Journal of Climatology*, *41*(12), 5676–5697. https://doi.org/10.1002/joc.7147

Bosson, J., & Lambiel, C. (2016). Internal Structure and Current Evolution of Very Small Debris-Covered Glacier Systems Located in Alpine Permafrost Environments. *Frontiers in Earth Science*, *4*(April). https://doi.org/10.3389/feart.2016.00039

Braucher, R., Guillou, V., Bourlès, D. L., Arnold, M., Aumaître, G., Keddadouche, K., & Nottoli, E. (2015). Preparation of ASTER in-house 10Be/9Be standard solutions. *Nuclear Instruments and Methods in Physics Research Section B: Beam Interactions with Materials and Atoms*, *361*, 335–340. https://doi.org/https://doi.org/10.1016/j.nimb.2015.06.012

Cacho, I., Grimalt, J. O., Canals, M., Sbaffi, L., Shackleton, N. J., Schönfeld, J., & Zahn, R. (2001). Variability of the western Mediterranean Sea surface temperature during the last 25,000 years and its connection with the Northern Hemisphere climatic changes. *Paleoceanography*, *16*(1), 40–52. https://doi.org/10.1029/2000PA000502

Capron, E., Rasmussen, S. O., Popp, T. J., Erhardt, T., Fischer, H., Landais, A., Pedro, J. B., Vettoretti, G., Grinsted, A., Gkinis, V., Vaughn, B., Svensson, A. M., Vinther, B., & White, J. W. C. (2021). The anatomy of past abrupt warmings recorded in Greenland ice. *Nature Communications*, *2021*. https://doi.org/https://doi.org/10.1038/s41467-021-22241-w

Clark, D., Clark, M. M., & Gillespie, A. R. (1994). Debris-covered glaciers in the sierra nevada, california, and their implications for snowline reconstructions. In *Quaternary Research* (Vol. 41, Issue 2, pp. 139–153). https://doi.org/10.1006/qres.1994.1016

Clark, P. U., Dyke, A., Shakun, J. D., Carlson, A. E., Wohlfarth, B., Mitrovica, J., Hostetler, S., & McCabe, A. (2009). The Last Glacial Maximum. *Science*, *325*(5941), 710–714. https://doi.org/10.1126/science.1172873

Cochelin, B. (2017). *Champ de déformation du socle paléozoïque des Pyrénées* [University of Toulouse 3]. https://tel.archives-ouvertes.fr/tel-01467202v2

Crest, Y., Delmas, M., Braucher, R., Gunnell, Y., & Calvet, M. (2017). Cirques have growth spurts during deglacial and interglacial periods: Evidence from 10Be and 26Al nuclide inventories in the central and eastern Pyrenees. *Geomorphology*, *278*, 60–77. https://doi.org/10.1016/j.geomorph.2016.10.035

Delaloye, R., & Echelard, T. (2021). Towards standard guidelines for inventorying rock glaciers: baseline concepts (version 4.2). In *IPA Action Group Rock glacier inventories and kinematics (Ed.)*.

Delmas, M., Gunnell, Y., Braucher, R., Calvet, M., & Bourlès, D. L. (2008). Exposure age

chronology of the last glaciation in the eastern Pyrenees. *Quaternary Research*, *69*(2), 231–241. https://doi.org/10.1016/j.yqres.2007.11.004

Delmas, M., Gunnell, Y., & Calvet, M. (2015). A critical appraisal of allometric growth among alpine cirques based on multivariate statistics and spatial analysis. *Geomorphology*, *228*, 637–652. https://doi.org/10.1016/j.geomorph.2014.10.021

Denton, G. H., Anderson, R. F., Toggweiler, J. R., Edwards, R. L., Schaefer, J. M., & Putnam, A. E. (2010). The Last Glacial Termination. *Science*, *328*(5986), 1652–1656. https://doi.org/10.1126/science.1184119

Dunai, T. J. (2010). *Cosmogenic Nuclides: Principles, Concepts and Application in the Earth Surface Sciences*. Cambridge University Press. https://doi.org/10.1016/ j.quageo.2009.1004.1003 B.1

Dunne, J., Elmore, D., & Muzikar, P. (1999). Scaling factors for the rates of production of cosmogenic nuclides for geometric shielding and attenuation at depth on sloped surfaces. *Geomorphology*, *27*(1–2), 3–11. https://doi.org/10.1016/S0169-555X(98)00086-5

Etzelmüller, B., Patton, H., Schomacker, A., Czekirda, J., Girod, L., Hubbard, A., Lilleøren, K. S., & Westermann, S. (2020). Icelandic permafrost dynamics since the Last Glacial Maximum – model results and geomorphological implications. *Quaternary Science Reviews*, *233*, 106236. https://doi.org/10.1016/j.quascirev.2020.106236

Fernandes, M., Oliva, M., Palma, P., Ruiz-Fernández, J., & Lopes, L. (2017). Glacial stages and post-glacial environmental evolution in the Upper Garonne valley, Central Pyrenees. *Science of The Total Environment*, *584–585*, 1282–1299. https://doi.org/10.1016/j.scitotenv.2017.01.209

Fernandes, M., Oliva, M., Vieira, G., & Lopes, L. (2022). Geomorphology of the Aran Valley (Upper Garonne Basin, Central Pyrenees). *Journal of Maps*, 1–13. https://doi.org/10.1080/17445647.2022.2035266

Fernandes, M., Oliva, M., Vieira, G., Palacios, D., Fernández-Fernández, J. M., Garcia-oteyza, J., Schimmelpfennig, I., Team, A., & Antoniades, D. (2021)a. Glacial oscillations during the Bølling–Allerød Interstadial–Younger Dryas transition in the Ruda Valley, Central Pyrenees. *Journal of Quaternary Science*, *37*(1), 42–58. https://doi.org/10.1002/jqs.3379

Fernandes, M., Oliva, M., Vieira, G., Palacios, D., Fernández-Fernández, J. M., Delmas, M., García-Oteyza, J., Schimmelpfennig, I., Ventura, J., & ASTER, team. (2021)b. Maximum glacier extent of the Penultimate Glacial Cycle in the Upper Garonne Basin (Pyrenees): new chronological evidence. *Environmental Earth Sciences*, *80*(24), 796.

https://doi.org/10.1007/s12665-021-10022-z

Fernandes, M., Palma, P., Lopes, L., Ruiz-Fernández, J., Pereira, P., & Oliva, M. (2018). Spatial distribution and morphometry of permafrost-related landforms in the Central Pyrenees and associated paleoclimatic implications. *Quaternary International*, *470*. https://doi.org/10.1016/j.quaint.2017.08.071

Fernández-Fernández, J. M., Palacios, D., Andrés, N., Schimmelpfennig, I., Tanarro, L. M., Brynjólfsson, S., López-Acevedo, F. J., Sæmundsson, Þ., & Team, A. (2020). Constraints on the timing of debris-covered and rock glaciers: An exploratory case study in the Hólar area, northern Iceland. *Geomorphology*, *361*, 107196. https://doi.org/10.1016/j.geomorph.2020.107196

Fernández-Fernández, J. M., Palacios, D., García-Ruiz, J. M., Andrés, N., Schimmelpfennig, I., Gómez-Villar, A., Santos-González, J., Álvarez-Martínez, J., Arnáez, J., Úbeda, J., Léanni, L., & Team, A. (2017). Chronological and geomorphological investigation of fossil debris-covered glaciers in relation to deglaciation processes: A case study in the Sierra de La Demanda, northern Spain. *Quaternary Science Reviews*, *170*(August), 232–249. https://doi.org/10.1016/j.quascirev.2017.06.034

Frauenfelder, R., Laustela, M., & Kääb, A. (2005). Relative age dating of Alpine rockglacier surfaces. *Zeitschrift Für Geomorphologie*, *49*(2), 145–166. http://www.schweizerbart.de//papers/zfg/detail/49/64937/Relative%5C_age%5C_dating%5C_of%5C_Alpine%5C_rockglacier%5C_surfaces

García-Ruiz, J. M., Palacios, D., Fernández-Fernández, J. M., Andrés, N., Arnáez, J., Gómez-Villar, A., Santos-González, J., Álvarez-Martínez, J., Lana-Renault, N., & Léanni, L. (2020). Glacial stages in the Peña Negra valley, Iberian Range, northern Iberian Peninsula: Assessing the importance of the glacial record in small cirques in a marginal mountain area. *Geomorphology*, *362*, 107195. https://doi.org/10.1016/j.geomorph.2020.107195

García-Ruiz, J. M., Palacios, D., González-Sampériz, P., De Andrés, N., Moreno, A., Valero-Garcés, B. L., & Gómez-Villar, A. (2016). Mountain glacier evolution in the Iberian Peninsula during the Younger Dryas. *Quaternary Science Reviews*, *138*, 16–30. https://doi.org/10.1016/j.quascirev.2016.02.022

Gómez-Ortiz, A., Oliva, M., Salvador-Franch, F., Palacios, D., Tanarro, L. M., Sanjosé-Blasco, J. J., & Salvà-Catarineu, M. (2019). Monitoring permafrost and periglacial processes in Sierra Nevada (Spain) from 2001 to 2016. *Permafrost and Periglacial Processes*, *30*(4), 278–291. https://doi.org/10.1002/ppp.2002

González-García, M. (2014). *La alta montaña periglaciar en el Pirineo Central español: procesos, formas y condiciones ambientales* [Universidad de Málaga]. http://hdl.handle.net/10630/6973

Haeberli, W. (1985). Creep of Mountain Permafrost: Internal Structure and Flow of Alpine Rock Glaciers. *Mitteilungen Der Versuchsanstalt Fur Wasserbau, Hydrologie Und Glaziologie an Der Eidgenossischen Technischen Hochschule Zurich*, *77*.

Hilger, P., Etzelmüller, B., Myhra, K. S., Hermanns, R. L., Jacobs, B., Krautblatter, M., Magnin, F., & Westermann, S. (2019). Permafrost is a crucial factor for paraglacial landscape modifications in glaciated mountain regions. *Geophysical Research Abstracts*, *21*.

Janke, J. R., Bellisario, A. C., & Ferrando, F. A. (2015). Classification of debris-covered glaciers and rock glaciers in the Andes of central Chile. *Geomorphology*, *241*, 98–121. https://doi.org/10.1016/j.geomorph.2015.03.034

Jomelli, V., Chapron, E., Favier, V., Rinterknecht, V., Braucher, R., Tournier, N., Gascoin, S., Marti, R., Galop, D., Binet, S., Deschamps, C., Tissoux, H., Aumaître, G., Bourlès, D. L., & Keddadouche, K. (2020). Glacier fluctuations during the Late Glacial and Holocene on the Ariège valley, northern slope of the Pyrenees and reconstructed climatic conditions. *Mediterranean Geoscience Reviews*, *0123456789*. https://doi.org/10.1007/s42990-020-00018-5

Knight, J. (2019). A new model of rock glacier dynamics. *Geomorphology*, *340*, 153–159. https://doi.org/10.1016/j.geomorph.2019.05.008

Knight, J., Harrison, S., & Jones, D. B. (2019). Rock glaciers and the geomorphological evolution of deglacierizing mountains. *Geomorphology*, *324*, 14–24. https://doi.org/10.1016/j.geomorph.2018.09.020

Krautblatter, M., Funk, D., & Günzel, F. K. (2012). Why permafrost rocks become unstable: A rock-ice-mechanical model in time and space. *Earth Surface Processes and Landforms*, *38*(8), 876–887. https://doi.org/10.1002/esp.3374

Lehmann, B., Anderson, R. S., Bodin, X., Cusicanqui, D., Valla, P. G., & Carcaillet, J. (2022). Alpine rock glacier activity over Holocene to modern timescales (western French Alps). *Earth Surface Dynamics*, *10*(3), 605–633. https://doi.org/10.5194/esurf-10-605-2022

Li, Y. (2018). Determining topographic shielding from digital elevation models for cosmogenic nuclide analysis: a GIS model for discrete sample sites. *Journal of Mountain Science*, *15*(5), 939–947. https://doi.org/10.1007/s11629-018-4895-4

Lifton, N. A., Sato, T., & Dunai, T. J. (2014). Scaling in situ cosmogenic nuclide production rates

using analytical approximations to atmospheric cosmic-ray fluxes. *Earth and Planetary Science Letters*, *386*, 149–160. https://doi.org/10.1016/j.epsl.2013.10.052

Lopes, L., Oliva, M., Fernandes, M., Pereira, P., Palma, P., & Ruiz-Fernández, J. (2018). Spatial distribution of morphometric parameters of glacial cirques in the Central Pyrenees (Aran and Boí valleys). *Journal of Mountain Science*, *15*(10). https://doi.org/10.1007/s11629-018-4873-x

Martin, L. C. P., Blard, P.-H., Balco, G., Lavé, J., Delunel, R., Lifton, N. A., & Laurent, V. (2017). The CREp program and the ICE-D production rate calibration database: A fully parameterizable and updated online tool to compute cosmic-ray exposure ages. *Quaternary Geochronology*, *38*, 25–49. https://doi.org/10.1016/j.quageo.2016.11.006

McColl, S. T. (2012). Paraglacial rock-slope stability. *Geomorphology*, *153–154*, 1–16. https://doi.org/10.1016/j.geomorph.2012.02.015

Merchel, S., Arnold, M., Aumaître, G., Benedetti, L., Bourlès, D. L., Braucher, R., Alfimov, V., Freeman, S. P. H. T., Steier, P., & Wallner, A. (2008). Towards more precise 10Be and 36Cl data from measurements at the 10-14 level: Influence of sample preparation. *Nuclear Instruments and Methods in Physics Research, Section B: Beam Interactions with Materials and Atoms*, *266*(22), 4921–4926. https://doi.org/10.1016/j.nimb.2008.07.031

Merchel, S., & Herpers, U. (1999). An Update on Radiochemical Separation Techniques for the Determination of Long-Lived Radionuclides via Accelerator Mass Spectrometry. *Radiochimica Acta*, *84*(4), 215–219. https://doi.org/10.1524/ract.1999.84.4.215

Mercier, D. (2008). Paraglacial and paraperiglacial landsystems: concepts, temporal scales and spatial distribution. *Géomorphologie : Relief, Processus, Environnement*, *14*(4), 223–233.

Moran, A. P., Ivy-Ochs, S., Vockenhuber, C., & Kerschner, H. (2016). Rock glacier development in the Northern Calcareous Alps at the Pleistocene-Holocene boundary. *Geomorphology*, *273*, 178–188. https://doi.org/10.1016/j.geomorph.2016.08.017

Moreno, A., Svensson, A. M., Brooks, S. J., Connor, S., Engels, S., Fletcher, W. J., Genty, D., Heiri, O., Labuhn, I., Perşoiu, A., Peyron, O., Sadori, L., Valero-Garcés, B. L., Wulf, S., & Zanchetta, G. (2014). A compilation of Western European terrestrial records 60-8kaBP: Towards an understanding of latitudinal climatic gradients. *Quaternary Science Reviews*, *106*, 167–185. https://doi.org/10.1016/j.quascirev.2014.06.030

Naughton, F., Sánchez-Goñi, M. F., Landais, A., Rodrigues, T., Vázquez-Riveiros, N., & Toucanne, S. (2022). The Bølling-Allerød Interstadial. In D. Palacios (Ed.), *European Glacial Landscapes* (pp. 0–7). https://doi.org/https://doi.org/10.1016/B978-0-323-91899-

2.00015-2

Naughton, F., Sánchez-Goñi, M. F., Rodrigues, T., Salgueiro, E., Costas, S., Desprat, S., Duprat, J., Michel, E., Rossignol, L., Zaragosi, S., Voelker, A. H. L., & Abrantes, F. (2016). Climate variability across the last deglaciation in NW Iberia and its margin. *Quaternary International*, *414*, 9–22. https://doi.org/10.1016/j.quaint.2015.08.073

Obase, T., & Abe-Ouchi, A. (2019). Abrupt Bølling-Allerød Warming Simulated under Gradual Forcing of the Last Deglaciation. *Geophysical Research Letters*, *46*(20), 11397–11405. https://doi.org/10.1029/2019GL084675

Oliva, M., Fernandes, M., Palacios, D., Fernández-Fernández, J. M., Schimmelpfennig, I., Team, A., & Antoniades, D. (2021). Rapid deglaciation during the Bølling-Allerød Interstadial in the Central Pyrenees and associated glacial and periglacial landforms. *Geomorphology*, *385*, 107735. https://doi.org/10.1016/j.geomorph.2021.107735

Oliva, M., Mercier, D., Ruiz-Fernández, J., & McColl, S. (2019). Paraglacial processes in recently deglaciated environments. *Land Degradation & Development*, *November 2018*, 1–6. https://doi.org/10.1002/ldr.3283

Oliva, M., Palacios, D., & Fernández-Fernández, J. M. (2022). *Iberia, land of glaciers: How The Mountains Were Shaped By Glaciers* (M. Oliva, D. Palacios, & J. M. Fernández-Fernández (eds.)). Elsevier.

Oliva, M., Serrano, E., Gómez-Ortiz, A., González-Amuchastegui, M. J., Nieuwendam, A., Palacios, D., Pérez-Alberti, A., Pellitero, R., Ruiz-Fernández, J., Valcárcel, M., Vieira, G., & Antoniades, D. (2016). Spatial and temporal variability of periglaciation of the Iberian Peninsula. *Quaternary Science Reviews*, *137*, 176–199. https://doi.org/10.1016/j.quascirev.2016.02.017

Palacios, D., Andrés, N., López-Moreno, J. I., & García-Ruiz, J. M. (2015)a. Late Pleistocene deglaciation in the upper Gállego Valley, central Pyrenees. *Quaternary Research (United States)*, *83*(3), 397–414. https://doi.org/10.1016/j.yqres.2015.01.010

Palacios, D., Gómez-Ortiz, A., Andrés, N., Vázquez-Selem, L., Salvador-Franch, F., & Oliva, M. (2015)b. Maximum extent of Late Pleistocene glaciers and last deglaciation of La Cerdanya mountains, Southeastern Pyrenees. *Geomorphology*, *231*, 116–129. https://doi.org/10.1016/j.geomorph.2014.10.037

Palacios, D., de Andrés, N., de Marcos, J., & Vázquez-Selem, L. (2012). Glacial landforms and their paleoclimatic significance in Sierra de Guadarrama, Central Iberian Peninsula. *Geomorphology*, *139–140*, 67–78. https://doi.org/10.1016/j.geomorph.2011.10.003

Palacios, D., de Andrés, N., Gómez-Ortiz, A., & García-Ruiz, J. M. (2017)a. Evidence of glacial activity during the Oldest Dryas in the mountains of Spain. *Geological Society, London, Special Publications*, *433*(1), 87–110. https://doi.org/10.1144/SP433.10

Palacios, D., García-Ruiz, J. M., Andrés, N., Schimmelpfennig, I., Campos, N., Léanni, L., Aumaître, G., Bourlès, D. L., & Keddadouche, K. (2017)b. Deglaciation in the central Pyrenees during the Pleistocene–Holocene transition: Timing and geomorphological significance. *Quaternary Science Reviews*, *162*, 111–127. https://doi.org/10.1016/j.quascirev.2017.03.007

Palacios, D., Gómez-Ortiz, A., Andrés, N., Salvador-Franch, F., & Oliva, M. (2016). Timing and new geomorphologic evidence of the last deglaciation stages in Sierra Nevada (southern Spain). *Quaternary Science Reviews*, *150*(October), 110–129. https://doi.org/10.1016/j.quascirev.2016.08.012

Palacios, D., Hughes, P. D., García-Ruiz, J. M., & Andrés, N. (2022). *European Glacial Landscapes: Maximum extent of glaciations* (D. Palacios, P. Hughes, J. M. García-Ruiz, & N. Andrés (eds.)). Elsevier.

Palacios, D., Oliva, M., Gómez-Ortiz, A., Andrés, N., Fernández-Fernández, J. M., Schimmelpfennig, I., Léanni, L., & Team, A. S. T. E. R. (2020). Climate sensitivity and geomorphological response of cirque glaciers from the late glacial to the Holocene, Sierra Nevada, Spain. *Quaternary Science Reviews*, *248*. https://doi.org/10.1016/j.quascirev.2020.106617

Pallàs, R., Rodés, Á., Braucher, R., Carcaillet, J., Ortuño Candela, M., Bordonau, J., Bourlès, D. L., Vilaplana, J. M., Masana, E., & Santanach, P. (2006). Late Pleistocene and Holocene glaciation in the Pyrenees: a critical review and new evidence from 10Be exposure ages, south-central Pyrenees. *Quaternary Science Reviews*, *25*(21–22), 2937–2963. https://doi.org/10.1016/j.quascirev.2006.04.004

Rasmussen, S. O., Bigler, M., Blockley, S. P., Blunier, T., Buchardt, S. L., Clausen, H. B., Cvijanovic, I., Dahl-Jensen, D., Johnsen, S., Fischer, H., Gkinis, V., Guillevic, M., Hoek, W. Z., Lowe, J., Pedro, J. B., Popp, T., Seierstad, I. K., Steffensen, J. P., Svensson, A. M., … Winstrup, M. (2014). A stratigraphic framework for abrupt climatic changes during the Last Glacial period based on three synchronized Greenland ice-core records: Refining and extending the INTIMATE event stratigraphy. *Quaternary Science Reviews*, *106*, 14–28. https://doi.org/10.1016/j.quascirev.2014.09.007

Reixach, T., Delmas, M., & Calvet, M. (2021). Climatic conditions between 19 and 12 ka in the eastern Pyrenees, and wider implications for atmospheric circulation patterns in Europe.

*Quaternary Science Reviews*, *260*. https://doi.org/10.1016/j.quascirev.2021.106923

Renssen, H., Goosse, H., Roche, M., & Sepp, H. (2018). *The global hydroclimate response during the Younger Dryas event*. https://doi.org/10.1016/j.quascirev.2018.05.033

Rode, M., & Kellerer-Pirklbauer, A. (2012). Schmidt-hammer exposure-age dating (SHD) of rock glaciers in the Schöderkogel-Eisenhut area, Schladminger Tauern Range, Austria. *Holocene*, *22*(7), 761–771. https://doi.org/10.1177/0959683611430410

Scapozza, C., Lambiel, C., Bozzini, C., Mari, S., & Conedera, M. (2014). Assessing the rock glacier kinematics on three different timescales: A case study from the southern Swiss Alps. *Earth Surface Processes and Landforms*, *39*(15), 2056–2069. https://doi.org/10.1002/esp.3599

Scherler, D., & Egholm, D. L. (2020). Production and Transport of Supraglacial Debris: Insights From Cosmogenic 10 Be and Numerical Modeling, Chhota Shigri Glacier, Indian Himalaya. *Journal of Geophysical Research: Earth Surface*, *125*(10), 1–26. https://doi.org/10.1029/2020JF005586

Serrano, E., Agudo, C., Delaloye, R., & González-Trueba, J. J. (2001). Permafrost distribution in the Posets massif, Central Pyrenees. *Norsk Geografisk Tidsskrift*, *55*(4), 245–252. https://doi.org/10.1080/00291950152746603

Serrano, E., de Sanjosé-Blasco, J. J., Gómez-Lende, M., López-Moreno, J. I., Pisabarro, A., & Martínez-Fernández, A. (2019). Periglacial environments and frozen ground in the central Pyrenean high mountain area: Ground thermal regime and distribution of landforms and processes. *Permafrost and Periglacial Processes*, *30*(4), 292–309. https://doi.org/10.1002/ppp.2032

Serrano, E., González-Trueba, J. J., & Sanjosé-Blasco, J. J. (2011). Dynamic, evolution and structure of Pyrenean rock glaciers. *Cuadernos de Investigacion Geografica*, *37*(2). https://doi.org/https://doi.org/10.18172/cig.1260

Serrano, E., San José, J. J., & Agudo, C. (2006). Rock glacier dynamics in a marginal periglacial high mountain environment: Flow, movement (1991–2000) and structure of the Argualas rock glacier, the Pyrenees. *Geomorphology*, *74*(1–4), 285–296. https://doi.org/10.1016/j.geomorph.2005.08.014

Steinemann, O., Reitner, J. M., Ivy-Ochs, S., Christl, M., & Synal, H. A. (2020). Tracking rockglacier evolution in the Eastern Alps from the Lateglacial to the early Holocene. *Quaternary Science Reviews*, *241*, 106424. https://doi.org/10.1016/j.quascirev.2020.106424

Tanarro, L. M., Palacios, D., Fernández-Fernández, J. M., Andrés, N., Oliva, M., Rodríguez-Mena, M., Schimmelpfennig, I., Brynjólfsson, S., Sæmundsson, Þ., Zamorano, J. J., Úbeda, J., Aumaître, G., Bourlès, D. L., & Keddadouche, K. (2021). Origins of the divergent evolution of mountain glaciers during deglaciation: Hofsdalur cirques, Northern Iceland. *Quaternary Science Reviews*, *273*. https://doi.org/10.1016/j.quascirev.2021.107248

Toucanne, S., Soulet, G., Freslon, N., Silva Jacinto, R., Dennielou, B., Zaragosi, S., Eynaud, F., Bourillet, J. F., & Bayon, G. (2015). Millennial-scale fluctuations of the European Ice Sheet at the end of the last glacial, and their potential impact on global climate. *Quaternary Science Reviews*, *123*, 113–133. https://doi.org/10.1016/j.quascirev.2015.06.010

Uppala, S. M., Kållberg, P. W., Simmons, A. J., Andrae, U., da Costa Bechtold, V., Fiorino, M., Gibson, J. K., Haseler, J., Hernandez, A., Kelly, M. A., Li, X., Onogi, K., Saarinen, S., Sokka, N., Allan, R. P., Andersson, E., Arpe, K., Balmaseda, M. A., Beljaars, A. C. M., … Woollen, J. (2005). The ERA-40 re-analysis. *Quarterly Journal of the Royal Meteorological Society*, *131*(612), 2961–3012. https://doi.org/10.1256/qj.04.176

Vázquez-Riveiros, N., Toucanne, S., Rodrigues, T., Landais, A., Naughton, F., & Sánchez-Goñi, M. F. (2022). Definition of the Last Glacial Cycle marine stages and chronology. In D. Palacios, P. Hughes, J. M. García-Ruiz, & N. Andrés (Eds.), *European Glacial Landscapes* (pp. 171–173). Elsevier B.V. https://doi.org/https://doi.org/10.1016/B978-0-12-823498-3.00023-6

Ventura, J. (2020). Spatial and temporal distribution of glaciers, debris-covered glaciers and rock glaciers during the last deglaciation in the Valley of the Bonaigua (Central Pyrenees). *Cuadernos de Investigación Geográfica*, *46*(2), 413–446. https://doi.org/http://doi.org/10.18172/cig.4395

Ward, G. K., & Wilson, S. R. (1978). Procedures for comparing and combining radiocarbon age determination: a critique. *Archaeometry*, *20*(1), 19–31. https://doi.org/10.1111/j.1475-4754.1978.tb00208.x

Winkler, S., & Lambiel, C. (2018). Age constraints of rock glaciers in the Southern Alps/New Zealand – Exploring their palaeoclimatic potential. *Holocene*, *28*(5), 778–790. https://doi.org/10.1177/0959683618756802

# Section 3: Conclusions

# Conclusions

The identification of the typology and an accurate survey of the spatial distribution of landforms and deposits in high mountain ranges have highly contributed to tracking Late Quaternary environmental and climate change. In the Pyrenees, glacial evidence is widespread across the range, and recent research has demonstrated that during the Late Pleistocene and Holocene, glaciers responded synchronously to global temperature oscillations and asynchronously to precipitation. The W-E alignment of the mountain range between the Atlantic and Mediterranean and the rough relief configuration determined different spatial and temporal patterns of glacial oscillations within the range. To better understand the impact of past glaciations on the landscape of the Central Pyrenees, this dissertation uses geomorphological mapping, geochronology and palaeoglacier modelling to reconstruct the Late Pleistocene glaciations in the Upper Garonne basin.

The main outcomes of this dissertation are: i) the detailed mapping of the glacial and periglacial landforms and deposits in the Aran Valley, ii) the identification of the MIE of the PGC in the Pyrenees, which occurred at ca. 130 ka, iii) the demonstration of the early glacier retreat during the GLGM, by 24-21 ka, iv) the identification of the several glacial advances during the deglaciation, namely between the late B-A and the early YD (13-12 ka), v) the identification of the major role of paraglacial dynamics in the current landscape organization, as large landslides and rock glaciers developed within the mountain slopes and cirques following glacial retreat, and vi) the proposal of a geochronological and geomorphological model for the glacial to periglacial transition period, including the timing of rock glacier stabilisation.

The analysis of the distribution of glacial and periglacial phenomena in the Upper Garonne basin confirmed the widespread occurrence of cold-climate geomorphological processes during the Late Pleistocene. Indeed, very large glaciers expanded during glacial cycles, as confirmed by external (420-720 m a. s. l.) and internal moraine systems (460-820 m) in the LBBB (Table 3.1). The Garonne palaeoglacier started a long-term shrinking that was interrupted by several glacial readvances or standstills. These are demonstrated by moraines located on mountain slopes (1000-1850 m) and high valley floors (2000-2100 m). Following these glacial advances, glaciers retreated from the valley floors leaving an open landscape with unconsolidated sediments transported into these ice-free depressions. The glacial recession was interrupted by a new glacial phase within the cirques, characterised by two glacial advances that formed moraines at 2400-2500 m and at above 2500 m (Paper 1; Fernandes et al., 2022). As glaciers retreated from the low-altitude cirques, a transition towards the periglacial domain was recorded by the formation of numerous rock glaciers at the foot and bottom of the rock walls. Lastly, glaciers retreated to the highest cirques under peaks above 3000 m, such as the Perdiguero and Maupas peaks, where they

persist nowadays above 2750 m, while active rock glaciers occur above 2600 m. The current position of the ELA at 3139 m under the ongoing warming threatens their stability.

**Table 3.1. Geographic distribution of the glacial phases across the Upper Garonne basin.**

| Glacial phase | Glacier system | Glacier type | Elevation of the moraines (m) | Distance from the headwaters (km) | Phase | ELA (m)* |
|---|---|---|---|---|---|---|
| Phase 1 | M-1a | Piedmont | 420-720 | 80 | Maximum | 1704 |
| | M-1b | Piedmont | 460-820 | 79 | Maximum | ? |
| Phase 2 | M-2a | Alpine | 1000-1850 | 23-2 | Deglaciation | 1982 |
| | M-2b | Alpine | 2000-2100 | 4.5-0.5 | Deglaciation | 2461-2505 |
| Phase 3 | M-3a | Cirque | 2400-2500 | 2-0.4 | Deglaciation | 2504-2571 |
| | M-3b | Cirque | >2590 | 0.7-0.1 | Holocene | >2971 |

*ELA elevation resulted from the AABR and AAR mean values for the glacial advances during the maximum and deglaciation and for the Holocene, ELA was collected from Serrano (2022).

The timing of formation of the moraine systems that were mapped in the Upper Garonna basin was still unknown. The application of CRE dating on glacial features showed that suitable boulders and age results are mainly controlled by the exposure time and their geomorphological setting. Indeed, despite the robust CRE dataset in the LBBB, the weathered state of the moraines and the intense human occupation made it challenging to find adequate boulders for exposure dating and, during the age interpretation, 50% of the results were excluded because of lack of coherence, likely associated to post-glacial dynamics (e.g. exhumation of boulders). By contrast, in the upper tributaries, the dataset was based on a set of boulders with well-preserved surfaces and where glacial striations were still often observed. There, ages yielded a suitable chronological sequence, and no significant problems arose from the age interpretation. The full dataset allowed us to date glacial evidence from the last two glacial cycles until the onset of the current interglacial.

One of the current biggest challenges in Quaternary Sciences is to achieve and constrain the glaciations chronologically since the Mid-Pleistocene. In the Pyrenees, glaciers responded to the global cold forcing during the MIS-6, i.e. MIE of the PGC (Fig. 3.1). This finding in supported by the CRE ages from boulders on the external moraine system from the LBBB that showed an exposure age of 129 ka, constituting the first and the most solid chronological record of the PGC in the Pyrenees (Paper 2; Fernandes et al., 2021a). During this phase, the 80 km-long Garonne palaeoglacier reached the foreland of the range, with 800 m of maximum ice thickness in the main valley. The preservation of the PGC evidence indicates that the largest glacier of the Pyrenees during the MIE was bigger than during the MIE of the LGC. During the MIE of the PGC, the palaeoELA was at 1700 m, and summer temperatures were 9.3 ºC lower than the current ones.

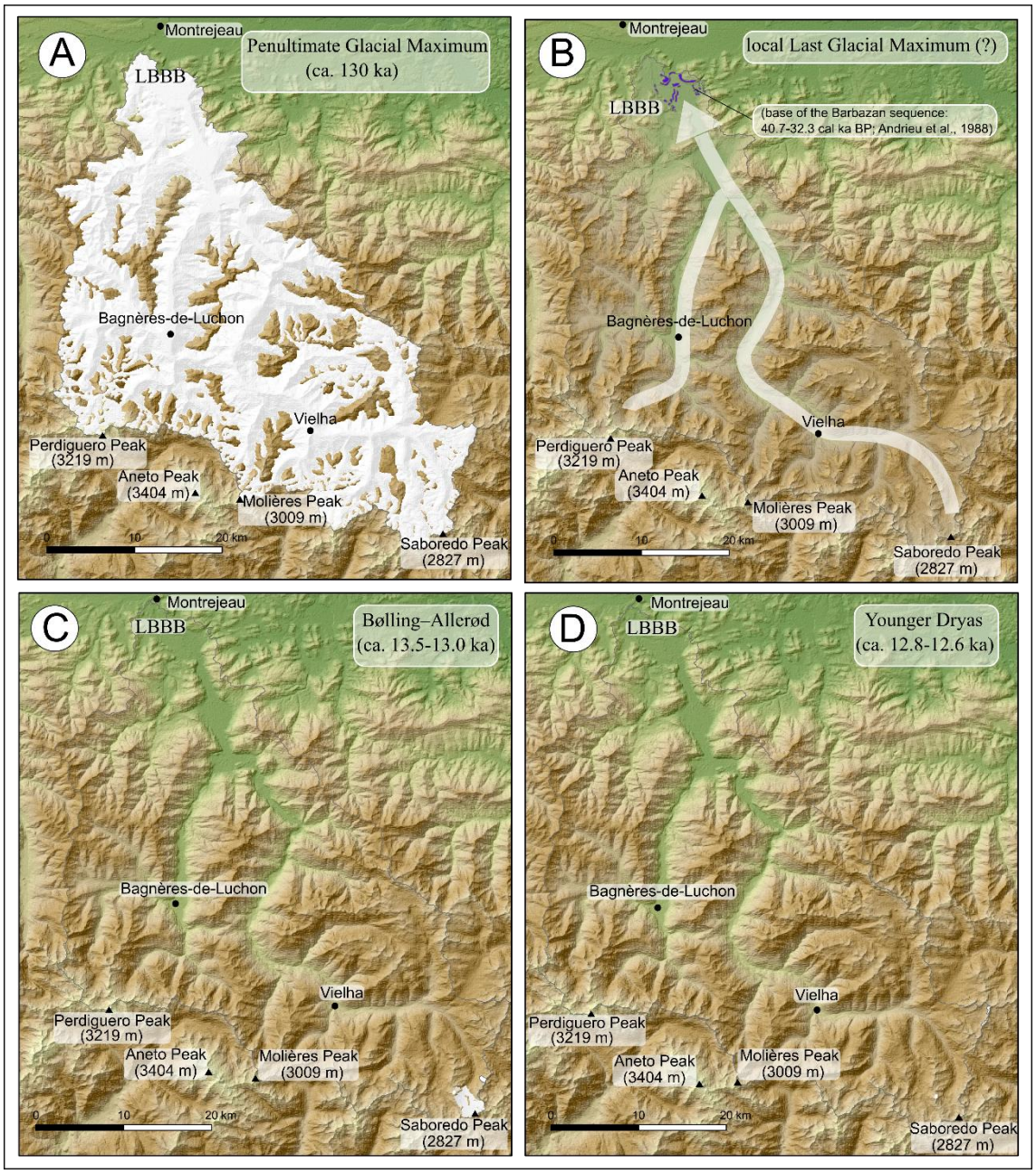


Figure 3.1. Dated glacial advances during the Mid to Late Pleistocene in the Upper Garonne valley: A) glaciers in the main valleys during the Penultimate Glacial Maximum; B) Distribution of the internal moraine system in the LBBB indicating that the glacier was close to the PGC position; C) glaciers during in the Ruda Valley during the second half of the B-A; D) Glaciers in the Sendrosa and Bacivèr cirques during the YD.

During the LGC, while glaciers were still growing in Northern Europe or at their maximum extent by the GLGM, in the Atlantic-influenced valleys of the Pyrenees, they were already retreating (Delmas et al., 2022a). This pattern could result from prevailing dry conditions in the Atlantic facade of the European continent that forced glaciers to starvation on the Atlantic-influenced valleys of the Pyrenees during the GLGM. In this period, the glacier retreat in the Garonne catchment is demonstrated by two polished surfaces located 7 km upvalley from the LBBB at the Marignac basin that yielded ages of 24 and 21 ka (Paper 2; Fernandes et al., 2021a).

These ages suggest that the deglaciation in the Upper Garonne basin was already ongoing during the GLGM, which correlates with the initial sedimentation of silts and organic matter by 29.9-27.2 cal ka BP in the Barbazan Lake (Andrieu et al., 1988; Delmas et al., 2022b).

The massive glacier recession during and after the GLGM in the Pyrenees was interrupted by several glacial advances during the deglaciation. During the first of these glacial readvances or standstills, moraines on mountain slopes were built by 2 to 23 km long glaciers on the lateral basins and high valleys, respectively. However, no boulders were suitable to be dated in the moraines of the main Garonne Valley. Following this phase, warm conditions prevailed during the second half of the B-A, forcing glaciers to retreat up valley. This retreat is supported by the solid dataset of 14 CRE ages in polished surfaces and erratic boulders with exposure ages of 15-14 ka (Papers 3 and 4; Fernandes et al., 2021; Oliva et al., 2021).

During the centennial cold spells of the second half of the B-A, conditions favoured glacier growth or maintenance in high valleys and low-altitude cirques (>2600 m). This glacial advance was confirmed by several dated moraines that showed exposure ages of 13.5, 13.2 and 13 ka (Papers 3 and 6; Fernandes et al., 2021b; Fernandes et al., submitted). These 0.5 to 4.5-km-long had palaeoELAs at 2461 and 2505 m and summer palaeotemperatures of 4.2 and 3.9 ºC lower than the current days. Such cold climate conditions agree with the other moraines from the Central Pyrenees that yielded similar ages (e.g. Noguera Ribagorçana and Gállego) and thus confirm a period favourable for the presence of glaciers in the Pyrenees during the late B-A.

During the cold YD stadial, climate conditions were favourable to glacier advance or standstill in the small and sheltered glacial cirques in the Garonne (Table 3.2). These glaciers developed frontal moraines that yield an exposure age of 12.8 and 12.6 ka (Papers 3 and 4; Fernandes et al., 2021b; Oliva et al., 2021). These moraines were formed by 0.4-2 km-long glaciers and had palaeoELAs at 2504 and 2571 m with summer palaeotemperatures of 3 and 3.4 ºC lower than today, respectively. However, the dry climate associated with this period was not favouring glaciers maintenance resulting in their recession from large floors in cirques with peaks below 2900 m. This has been proposed by two exposure ages of 12.8 and 12.7 ka from the polished surfaces in the cirque floor.

**Table 3.2. Chronological reconstruction of the glacial phases across the Upper Garonne basin.**

| Glacial phase | Glacier system | Glacial type | Elevation of the moraines (m) | Summer temp. (ºC)* | Chronology |
|---|---|---|---|---|---|
| Phase 1 | M-1a | Piedmont | 420-720 | 9.3 | MIS-6: 130 ka |
| | M-1b | Piedmont | 460-820 | ? | <LLGM (?) |
| Phase 2 | M-2a | Alpine | 1000-1850 | ? | OD (?) |
| | M-2b | Alpine | 2000-2100 | 4.2-3.9 | B-A: 13.5-13.0 ka |
| Phase 3 | M-3a | Cirque | 2400-2500 | 3.4-3 | YD: 12.8-12.6 ka |
| | M-3b | Cirque | >2590 | ? | Neoglaciation (?) |

* Lower summer temperatures than the current ELA at 3139 m (Campos et al., 2021)

Following the deglaciation of the mountain slopes and glacial cirques, the landscape suffered a rapid transformation during the paraglacial phase, as demonstrated by the widespread distribution of slope failures and rock glaciers associated to glacial retreat (Fig. 3.2). In the mountain slopes of the Upper Garonne basin, four types of rock slope failures were documented within the glaciation limits: large catastrophic rock slope failures, rock slope deformations, rockfalls and landslides. The rock slope failures were highly controlled by lithology as they tend to be distributed in slates and lutites with limestones (Paper 5; Fernandes et al., 2020). Instability also occurred in glacial cirques as after the deglaciation, rock glaciers formed largely in granitic terrain. The rock glaciers within the glacial cirques also evidence that these formerly glaciated areas evolved to periglacial environments. This transition was very rapid or even synchronous to the deglaciation during the second half of the B-A, as demonstrated by the exposure ages from the moraine to rock glacier sequence at the Lòcampo cirque. Right after the moraine abandonment by 13.2 ± 1.1 ka, a rock glacier front became stable by 13.6 ± 0.9 ka. However, the insulation effect of the debris mantle on interstitial ice delayed the final disappearance of ice from the rock glaciers that only occurred 2-3 ka later, at the onset of the Holocene. The exposure ages from the same rock glacier showed that it became definitively relict by 11.9 ka (Paper 6; Fernandes et al., submitted).

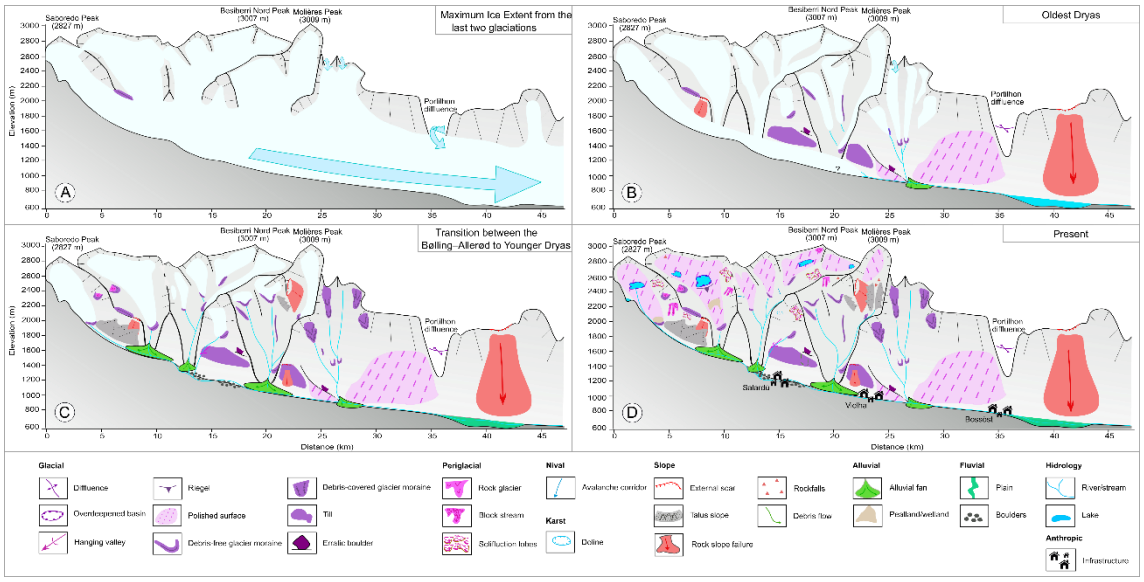


Figure 3.2. Glacial evolution and post-glacial geomorphological dynamics in the high valleys of the Upper Garonne basin during the Late Pleistocene (adopted from Fernandes et al., 2022): A) maximum ice extent of the two glacial cycles; B) glacial tongues flowing downvalleys within the long-term glacial retreat of the Garonne paleoglacier that favoured also intense slope readjustment; C) alpine and cirque glaciers (B-A and YD) with very intense postglacial slopes dynamics, including the occurrence of permafrost that promoted the formation of rock glaciers; D) final deglaciated cirques with periglacial processes prevailing at higher elevations (inactive rock glaciers), and slope, alluvial and fluvial processes at lower elevations.

The results presented here improved the knowledge about the Late Pleistocene glaciations in the largest of the Pyrenean glaciers, as well as the glacial to periglacial transition implications in the glacial cirques. Several problems have raised, represent new scientific questions:

- Is the preglacial relief of the Central Pyrenees – where high flat areas occur in smooth interfluves, poorly carved cols or plateaus – a new potential setting to date glacial deposits from the Mid to Late Pleistocene? These areas might be suitable for preservation of glacial evidence during thousands or millions of years, as fluvial, alluvial and slope processes were not as intense as in the lowlands';

- When were the moraines from the mountain slopes (e.g. Nere valley) and lateral basins deposited? The first glacial advance phase of the deglaciation is still missing in the Upper Garonne basin. According to the sequence of glacial advances in the Upper Garonne basin, these deposits could show OD stadial age by applying the CRE dating technique;

- Is applying CRE dating on polished surfaces across the main valley appropriate to reconstruct the gross rate of recession in the Garonne palaeoglacier? The glacial recession from the GLGM to the OD can be possibly unveiled in the polished surfaces from the lower sector of the basin;

- Methodological limitations from CRE uncertainties and Greenland $^{18}O_{ice}$ insensibility and lack of correlation between the European and Greenland palaeorecords preclude the link between the glacial advances and the centennial-scale cold spells of the B-A. i) Can we solve CRE uncertainties by incrementing CRE-datasets robustness in these moraines? ii) Can we better

constrain these glacial phases by combining CRE-datasets with other more precise absolute dating techniques ($^{14}C$)? iii) Can we find a better correlation between the B-A glacial advances and other high-resolution continental proxies from the mid-latitudes of the Northern Hemisphere? iv) Will the local cosmogenic production rate in the Iberian Peninsula reduce the CRE-uncertainties?;

- Can we unveil the age of the moraine above 2500 m in the Central Pyrenees by applying CRE dating? This study will possibly show the age of glacial advances from the Early Holocene or Neoglaciation. This question has been addressed only in very few studies;
- When did the large rock slope failures occur, and what is the period of response of the slopes to the glacial retreat in the Upper Garonne basin? The application of CRE, OSL or radiocarbon dating will likely constrain these processes;
- How many generations of rock glaciers exist in the Central Pyrenees? The rock glacier formation and stabilisation below and above the 2200-2300 m level is still unknown in the Upper Garonne basin, and the application of CRE dating will probably show and help to reconstruct the evolution of permafrost in the Central Pyrenees;
- What is the age of the debris-covered glaciers and their transition to rock glaciers in the Central Pyrenees? Complex periglacial landforms where features from debris-covered and rock glaciers are distinguished should be selected to date and assess the glacial to periglacial evolution.

# Section 4: Appendix

# Geomorphological map of the Aran Valley